INTEGRATED EVALUATION OF AIR FLOW AND GAS DISPERSION FOR UNDERGROUND STATION SAFETY STRATEGIES BASED ON SUBWAY CLIMATOLOGY

A thesis submitted for the degree of

Doctor of Philosophy

Zi Qian

SCHOOL OF MECHANICAL AND SYSTEMS ENGINEERING

NEWCASTLE UNIVERSITY

March 2017

ABSTRACT

Rail underground systems are seen as a way to overcome traffic congestion in city environments. Many new subways are being built in China and developing countries. Recent studies have however shown that the ventilation of subway systems is poorly understood. There is significant danger to life if a fire occurs or toxins such as chemical or biological agents are released in a subway. Understanding the air flow inside a subway and how this is affected by the local environment is key in establishing effective evacuation strategies.

A series of tracer gas experiments conducted as part of this research have been carried out. To expand the subway climatology from an experimental framework into a virtual and simulation environment, 3D Computational Fluid Dynamic models have been developed, which include the simulation of local microclimate and air movement inside the station respectively. The station CFD model has allowed the analysis of the air flow inside the station under the prevailing external weather condition.

Results show promising links between external climatic factors, the subway climatology and the ability to predict the dispersal of smoke/toxins. The local weather pattern has a large influence on the background airflow inside a station and dominated the flow direction at station exits which is been used to evaluate the efficiency of pedestrian evacuation and also determine the safer evacuation route and exit. The possibilities of integrating these findings will allow for a more holistic safety assessment to be carried out that could reduce the loss of life or mitigate harmful effects on public health. It also fills a knowledge gap in design guidelines from a safety perspective underground station construction and ventilation.

ACKNOWLEDGEMENTS

The completion of this thesis would not have been possible without the support of my supervisors Dr. Roberto Palacin and Professor Brian Agnew of the School of Mechanical and Systems Engineering, Newcastle University. I am deeply grateful for their immense knowledge, valuable suggestions, kindly guidance and encouragement that drove me to complete this thesis.

I would like to thank the Ruhr University Bochum and Nexus (Tyne and Wear Passenger Transport Executive) for the resources provided.

I would like to extend my appreciation to Dr. Emine Mine Thompson and Dr. James Charlton from University of Northumbria at Newcastle for the support.

Finally, I would like to thanks my parents Mr. Qian Jinhua and Mdm. Dong Qiao for their love throughout my life.

TABLE OF CONTENTS

LIST OF FIGURES

LIST OF TABLES

Glossary of terms

Abbreviation	Definition
3D	Three-dimensional
CFD	Computational Fluid Dynamics
DBT	Dry-Bulb temperature
EW	East-West
k-ε	K-epsilon
mb	Millibars
NS	North-South
^{o}C	Celsius
ppb	Parts per billion
ppm	Parts per million
RANS	Reynolds-averaged Navier–Stokes
rh	Relative humidity
SF_6	Sulfur hexafluoride
VNG	Virtual Newcastle Gateshead
VR	Virtual Reality
WBT	Wet-Bulb temperature

Chapter 1. Introduction

The purpose of this thesis is to expand the concept of Subway Climatology to gain a better understanding of how air mixes between the subterranean levels and the local external airflow of a subway station. Linking local weather data with the natural background airflow in the station allows identification of the main air flow pattern responsible for driving the dispersion of toxic agents or smoke in an emergency situation through a given station. Such air flow pattern and speed can be evaluated using Computational Fluid Dynamics (CFD) simulation which when coupled with pedestrian movement modelling will assist in identifying the correct evacuation procedures to reduce fatalities from exposure to the toxic gases. The outcomes of this research can be used to inform the decision making process with regard to the initiation of effective measures to minimize the impact of dangerous substances within the subway system. This thesis has additional significance in that it can also support the development of guidelines for the structural design of subway systems to improve air quality and reduce the danger to passengers in an emergency situation.

1.1 Background

The first underground urban railway line, the Metropolitan line in London, was opened on 10th January, 1883 to cope with the rapid population growth and increasing traffic congestion in London at that time. Shortly after, other major cities worldwide, (Moscow, Glasgow, Paris, Brussels, New York, Stockholm, Berlin) developed their own systems, which have now become an essential part of urban transport systems across the globe. More than 60 countries and nearly 200 cities have developed subway systems (Chu, 2004) with an accumulated track length greater than 6,000 km. Many new subways are being constructed worldwide and it is predicted that by the year 2050 China alone will be operating over 2,000 km of railways carrying 50-80% of total urban passenger traffic (Zhou, 2006). The subway can be therefore seen as principal for urban development.

The increase in densely populated urban settlements combined with the economic and social needs for mobility make underground mass rapid transport systems an important feature of life in the developed and developing world. However, underground environments bring their own risks. Since the 1920s subways have accounted for 38% of all terrorist attacks on transport (Jenkins, 2001). Most infamously, in March 1995, the Aum Shinrikyo (Japan) cult released sarin nerve gas on five converging subway

trains at the height of the morning commute hour in Tokyo (Metraux, 1995). This attack still has a deleterious effect on the Japanese people. It is the most well-known attack on a subway system although more recently there have been successful or planned incidents in Sydney (1999) (Jenkins, 2001), Düsseldorf and Berlin (2002) (Litman, 2005), Manila (2000) (Banlaoi, 2009), Madrid (2004) (Rose *et al.,* 2007), Moscow (2004 and 2010) (Loukaitou-Sideris *et al*., 2006; Monaghan, 2010). London (2005) (Murphy, 2006). In addition, the subway commuter is subject to the risk of accident as witnessed by the recent fire in Washington in which one person died and 84 were hospitalised. These incidents show a real and present danger for subways systems. It is now considered that subway systems are uniquely vulnerable to a terrorist attack with a likely scenario being the release of chemical or biological agents (Policastro and Coke, 1998). The problem is compounded by the lack of understanding of the nature of air flow in subway systems. The majority of subways are however, over 75 years old and were built at a time when analytical tools were not available to fully understand the impact of the internal building structure on the system ventilation. Health and safety aspects of passenger movement within a station or evacuation strategies were also not considered to be of prime importance (Network Rail, 2011). Many systems are coping with passenger numbers far in excess of their initial design capacity which can lead to difficulties at peak times.

It is clear from these incidents that the subway operators and other stakeholders might not have robust enough evacuation strategies in place and the infrastructure of the subway system does not facilitate rapid evacuation. Any evacuation strategy related to gaseous substance or smoke should consider the dispersion of the smoke or toxic agents in directing the passengers to safety. Understanding how these elements are distributed in a station or tunnel system is key to establishing effective evacuation strategies. However, it is clear from these initial studies that the understanding of the behaviour of the air flow in a subway is poorly understood. Over 60% of deaths in fires are caused either wholly or partially by inhalation of smoke or toxic gases (Woolley and Raftery, 1975). As in these events, the main danger to passengers' health and life is the inhalation of smoke and toxic gases as these are released in almost complete enclosed areas (Hu *et al.,* 2014). Thus evacuation strategies that provide routes which reduce the exposure time of individuals to a toxic environment could potentially reduce the loss of life or effects on an evacuee's health. The strategy "take the nearest exit with the shortest path to the over ground" might not be the best response.

An initial approach to understand the air flow in subway systems stems from work performed in natural cave systems at the Ruhr University in Bochum where subways have been compared to cave systems be they barometric or thermal in nature by Pflitsch (2003), Pflitsch and Piasecki (2003) and Pflitsch *et al.* (2005). The authors described how climatologic differences of both cave types are mainly based on the different driving forces of air flow that occur in the entrance area and also in the interior of the cave. In thermal caves density differences of unequal temperature air masses lead to compensating air flows while in barometric caves pressure variations of the atmosphere enforce a temperature independent compensating air flow. The different genesis of air flows has far-reaching consequences for the climatic character of the caves and hence the subway system. Subways that behave like thermal caves typically contain large public spaces with wide corridors and passages and very strong chimney effects, they exhibit relatively low air flow velocity (0.2-0.5 m/s). Within barometric systems however air flow of several m/s can be measured, at least close to the openings, and sometimes further in. The internal air flow of thermal systems has a strong seasonal characteristic, with clear differences between summer and winter and stronger oscillations of direction during spring and autumn. Barometric systems show small differences between summer and winter; this effect is due to the seasonal variability and stability of passing pressure systems. In an ideal barometric type, air exchange takes place through all openings and across the whole profile in the same direction (inwards or outwards) at the same time. In contrast to this, air flow into and out of thermal systems usually takes place at the same time (inflow in one, outflow at another entrance), but through different openings. Single openings show a vertical differentiation in air exchange. Another small but important difference is the effect of the inward and outward flowing air on the pressure conditions inside the system. The pressure drop in thermal systems, caused by the out flowing air to the upper entrance in winter and the lower entrance in summer, is equalized quickly by air flowing into the other entrance. So, the internal pressure is more or less in equilibrium with the outside pressure at all times. In a barometric system a steady air movement is set up in order to equalize the air pressure with the outer atmosphere. This is only accomplished for short time periods which leads to flow oscillations. The variable flow conditions lead to differences regarding the thermal conditions of subway systems. In the case of Thermal systems, the upper surface opening is influenced by the passing of air masses. In summer, relatively warm air from the outside flows into the opening, while in winter the air from the subway that is warmer than the outside atmosphere flows outwards. A

lower surface opening however is characterised by the discharge of cool air masses. In winter the cold air of the outside atmosphere flows inwards while in summer the relatively cool internal air flows outwards. This leads to the formation of a relatively cool area in the lower level, while the upper parts of a thermal system are warmer compared to the annual mean. In this respect a thermal vertical gradient of the atmosphere has to be taken into account. This means that the absolute temperature values have to be reduced accordingly in order to be able to note the described effects. The temperature gradient between the two openings should point in the same direction provided that there are no further influences. Thereby the gradients near the opening will be high and temperature equilibrium is reached after a few metres for low air flow rates, or several hundred metres for large flow rates. The thermal appearance of barometric systems turns out to be entirely different. At all surface openings there is a constant change between incoming and out flowing air throughout the year. Thus in summer relatively warm air (compared to the air inside) and in winter relatively cold air masses penetrate into all openings from the outside. Therefore, the temperature gradient observed between the openings and the inner parts should run similarly from every surface opening into the interior. The above considerations are useful theoretical concepts as this clear difference between the two types of driving mechanisms does not exist in reality. However, there is evidence that thermal and barometric effects can exist inside a single system and even close to each other. The situation becomes more complicated in subways when internal energy sources such as escalator motors and forced ventilation systems have to be taken into consideration.

It is self-evident that the natural background air current caused by the air exchange between the underground station and the outside, has an important influence on the dispersion of smoke and/or toxic agents within a subway system and should be considered when ventilation systems are being designed and evacuation strategies formulated. The ventilation systems of subways have been the subject of much research in the past mainly focused on providing a comfortable environment than an understanding of the spread of smoke or other toxic agents through the system. Unfortunately two basic assumptions that are commonly made regarding the nature of the air flow in these structures are fundamentally wrong.

The first discredited assumption is that the airflow in subways is uniform and unidirectional. The work by Pflitsch *et al*. (2012) has shown the presence of a background air current that is independent of the train movements or active ventilation

systems. Moreover, this current does not consist of simple, continuous and equally distributed air movements; it is, on the contrary, a highly complex system of currents with spatial and temporal variations that can be regarded as an independent current. This background air movement was found to be re-established 3 to 5 minutes after the passage of a train and the complex metastable system of air currents that exists in subway tunnels is influenced by numerous factors, chiefly by the outside weather conditions (Pflitsch *et al*., 2012). The weather dependant variability is in complete contrast to the current modelling approach which assumes a permanent uniform air current. Results from a long term study in Dortmund indicate that the differences in air temperature within the subway and between the subway and the outer environment, respectively, exert the main influence on the air flow system (Pflitsch *et al*., 2012). These temperature differences can show marked changes, especially in the winter months, as the tunnel air temperature lags behind the temperature changes in the outer atmosphere. A high temperature gradient usually leads to increased flow velocities within the subway tunnels by a factor of 4, with a stabilized flow direction. In the summer months, temperature differences are much more localized and can result in flow reversals with weak velocities in the tunnels. Periods of extreme cold or warm weather lead to a stabilization of a whole section for a short time as strong temperature gradients between the inside and outside air temperatures produce compensational exchange fluxes.

The second long held assumption is that ingress or exhaust of air at tunnel portals aerates the whole system. This has also been challenged by studies in Dortmund and Newcastle that show that the influence of the outside air is confined to a small region close to the tunnel openings by Pflitsch *et al*. (2012). The underground stations also influence the tunnel air flow as the temperature differences between two levels in a station can also lead to strong exchange currents which will also affect the whole subway system. This lack of understanding of the nature of the air flow in subways has led to ventilation systems being wrongly specified and in some cases fighting against the background air flow.

A modern approach to subway system design would use Computational Fluid Dynamics (CFD) to predict the air flow and other associated features such as energy consumption at an early stage in the design process as is being done for large buildings. Unfortunately, the vast majority of subways were constructed long before CFD was available and for many systems the architectural drawings are now longer available to

assist in the development of the CFD models. All is not lost however because modern Virtual Reality (VR) technology has provided a new tool that can make the modelling of all subway systems possible and also enable more detailed simulation activities to take place. Virtual Reality allows three dimensional images of objects to be created by way of laser scanning. This has been used for several years to create images of buildings for conservation purposes, for evacuation simulation (using Legion software) and training purposes. The laser scanning of a building generates a series of points called a “point cloud” which can then be texturized with photographic information to create the three dimensional virtual environment images. The point cloud can also be used to produce CFD mesh files to allow calculations to take place. This represents a relatively straightforward method of developing CFD models of a building or subway system which can be used for the prediction of air flow, and with appropriate packages the dispersion of smoke in a fire and the resulting reduction in visibility due to the smoke. A pedestrian simulation software called Legion that has been developed to examine evacuation instances in sports stadia can also be interfaced with the point data to enable evacuation routes in subways to be evaluated. The Virtual three-dimensional (3D) environment can also act as a training tool for fire and rescue personnel to prepare them for an incident and will be helpful to maintenance crews to allow them to practice an operation remote from the subway. The potential for the use of virtual environment model in this situation is large and technologically feasible.

1.2 Research purpose

This research is intended to establish a virtual environment based analysis procedure to develop an integrated approach to modelling air flow, toxic gas or smoke dispersion, evacuation strategies, energy management and resilience. The use of virtual environment model can overcome the problem that many existing subway systems were constructed before the advent of CAD systems and it is most likely that the architect drawings, which could be used to develop the CFD images no longer exist.

It is proposed to build virtual environment models of the Monument Metro Station and thence to use these in simulation of air flow to then be in a position to predict the dispersion of dangerous substances (chemical or biological agents) and to overlay these on evacuation simulation models. This research has significance in that it aims to firstly support the development of guidelines for the structural design of subway systems minimizing the dispersion of dangerous substances. This work is timely because several existing subway systems in Europe have reached the age at which

they need to be refurbished and there is also a pressing need in some regions for the construction of new subways and tunnels. This has been pointed out by The European Rail Research Advisory Council (ERRAC, 2009) “at the time of the elaboration of this research 391 km of metro system network extension were under construction in 28 European cities and municipalities and 23 cities are planning to create new metro system or to extend their metro network by creating new lines or extensions with a total length of 396km”. The development potential of metro system worldwide is large as the International Association of Public Transport recognized. Since the first underground line opened in London in 1890, 116 conurbations in Europe, America, Asia and the Middle East and North Africa have built their own metro systems and there are 560 cities with populations of over one million that are considering the development of new of metro systems (ERRAC, 2009).

1.2.1 *Justification of Monument Station for Research*

The Monument Metro Station is the principal station on the underground section of the Tyne and Wear Metro system used by almost 6 million passengers per year (NEXUS, 2013). The Tyne and Wear Metro was opened in 1980. At the time of writing is operated by DB Regio (a subsidiary of German railway Deutsche Bahn) on behalf of the local transport authority Nexus and is one of only three underground metro systems in the UK outside London, along with Liverpool and the Glasgow Subway (Pflitsch *et al.,* 2013). The Monument Metro station is the only metro station on the Tyne and Wear Metro that accommodates both lines as show in the Figure 1.

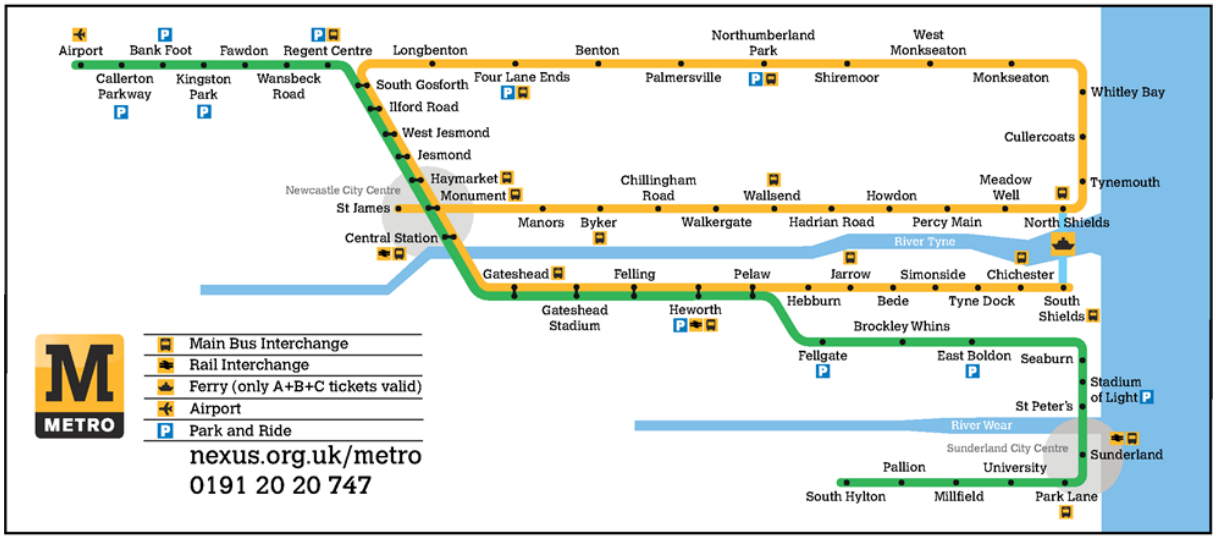

Figure 1: Schematic Map of the Tyne and Wear Metro System (NEXUS, 2013)

The Tyne and Wear Metro section across Newcastle city centre is fully underground, as highlighted in red in Figure 2. It has a total length of 4km encompassing six stations. The underground tunnel starts on the North-South line at Jesmond station and extends to the Central Station. The East-West line begins at Manors and ends at St James. The two lines cross at the Monument interchange.

Figure 2: Underground Stations at Newcastle City Centre

The monument Metro station is situated fully underground with the highest level being the ticket hall area and it has four platforms on two tracks that cross at different levels. The platforms are accessed by escalators or by lift from the ticket hall and there is a connecting stair well between the different platform levels. The station has an entrance to the Eldon Square shopping centre and two others at Grey Street and Blackett Street. Being a station with such high importance and locality within the town centre, it is widely used by commuters travelling to work or shopping. An additional factor to support the choice of the Monument Station is that it was the subject of some initial air flow studies in 2008 by Pflitsch *et al.* (2012), which provides valuable lessons for the purpose of this research.

The authors Pflitsch *et al.* (2012) indicated that the airflow in the tunnels is dominated by a strong background flow that is independent of the train movement. The authors also indicated that the airflow was found to be very complicated with stratification and reversals being observed. The impact of the ventilation system on the natural airflow also indicated a lack of understanding of subway climatology when the system was constructed. It is proposed that a full and extensive monitoring of the Monument station be undertaken over a prolonged period to facilitate a full understanding of the internal air flow and its interaction with the over ground climate. This approach will contribute to remove risk to passengers and emergency service personal in the event of the

release of a toxic agent or the presence of a fire in the subway. More specifically, the measurements from an ultrasonic anemometer installed in the tunnel indicated that the bulk air flow in the lower level of the Monument station (Platform 1 and 2) is dominated by a northerly flowing air stream of relatively high velocity (for subway tunnels) and by an easterly flowing airstream on the middle level (Platform 3 and 4). This is independent of any train movements, which distorts this strong background flow for only one or two minutes following the passage of a train. The direction and strength of the air velocity is indicated in Figure 3 showing positive values of airflow speed are in the westerly directions and negative values in northerly directions. So that the flow direction on platform 1 is from the Central station to the Monument station. The strong flow velocity is mainly due to a chimney effect produced by the steady incline of the tracks rising from the Tyne crossing in the south to emerge at ground level at Jesmond in the north. It is also clearly shown in Figure 3 that the airflow is influenced by the operation of the ventilation fans. The south-north air stream is adversely affected by operation of the ventilation system as this becomes stronger when the fans are not in service. This behaviour is also reflected in the temperature measurements in the tunnels shown in Figure 4 and Figure 5. The overall trends of air flow and temperature follow those exhibited in barometric cave systems as reported by Pflitsch (2003) and Pflitsch *et al*. (2010).

The measurements taken during operation break (night) at 2008 conducted by Pflitsch (2012) provide a preliminary understanding of the background air temperature, velocity and the effect of the ventilation fans and gate operation which is demonstrated from Figure 3 to 7. The mechanical ventilation system has been decommissioned after 2009 before this research was started. Figure 8, 9 and 10 show the thermal images that indicate heat gain and loss in the station taken by Pflitsch (Pflitsch, 2012) at 9th December 2008.

This research has extend the subway climatology research experiments conducted by Pflitsch (2012) at 2008 in length and variation. In research method, this research has developed the subway climatology research from an experimental research work into a simulation environment research method. It has been develop into an analytical methodology for the analysis of air movement and ventilation of subway systems to evaluate ventilation efficiency and inform the decision making process to improve the efficiency of evacuation and also support early stage design for new subway systems.

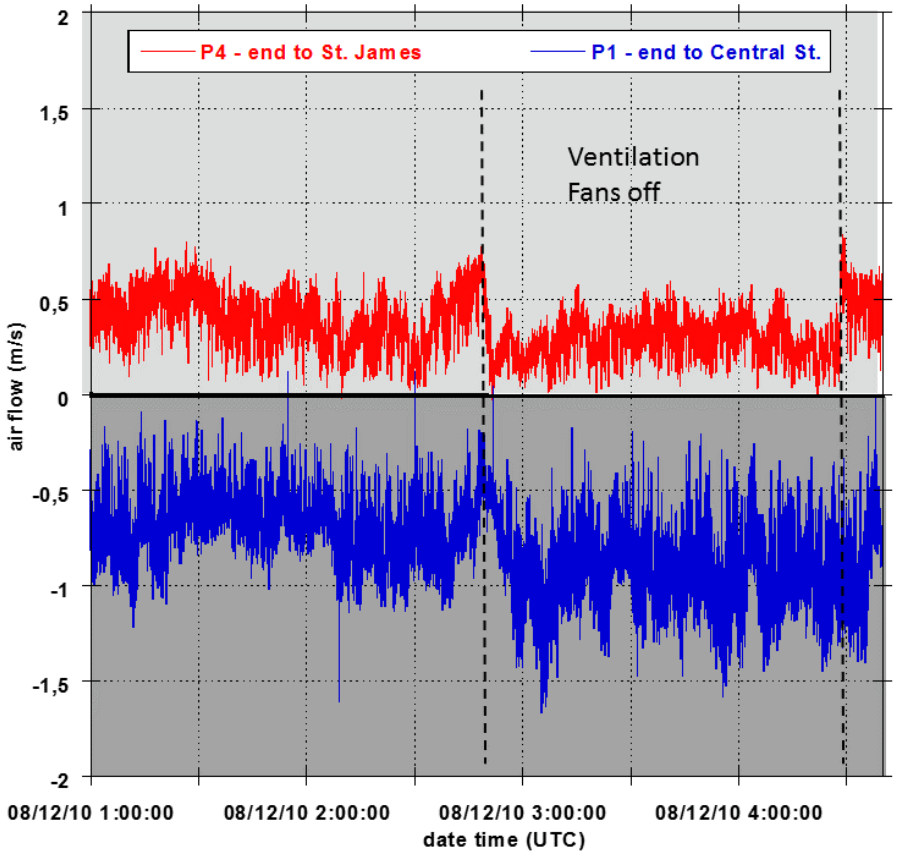

Figure 3: Air Flow at Monument Station platforms (tunnel flow) for different working conditions of the ventilation fans (Pflitsch *et al.,* 2012).

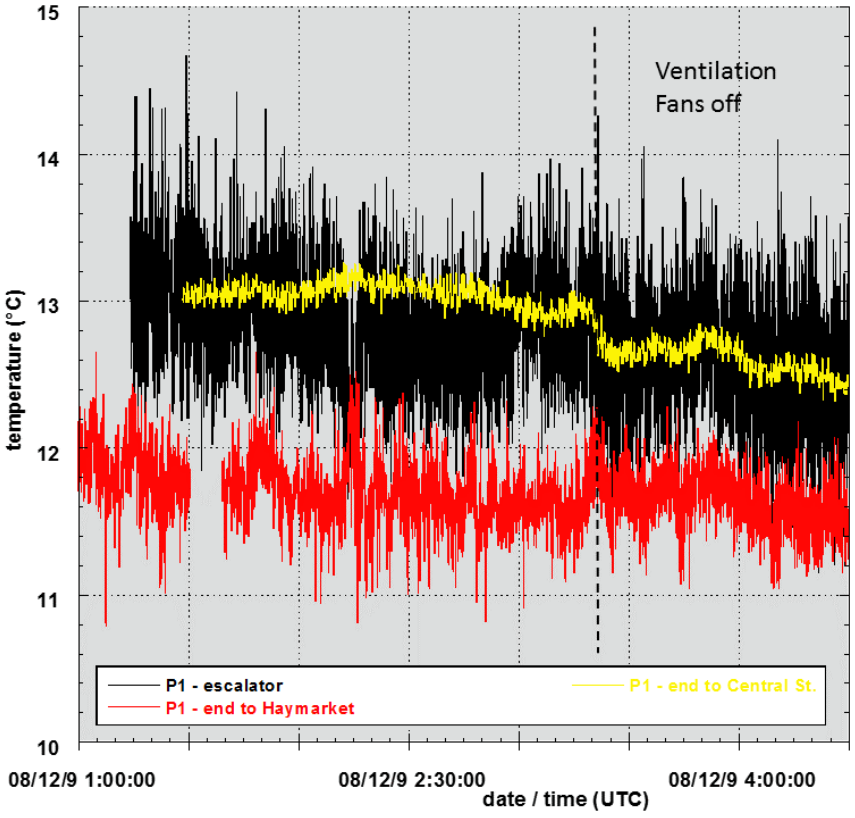

Figure 4: Variation of Air Temperature at Monument station lower level platform 1 and 2 for different working conditions of the ventilation fans (Pflitsch *et al.,* 2012).

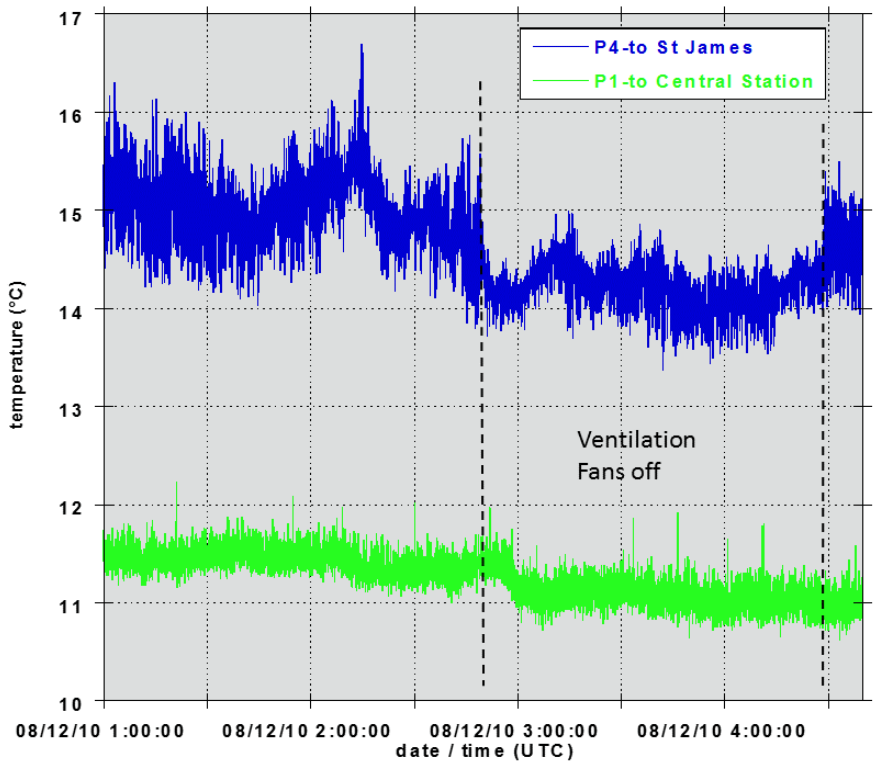

Figure 5: Variation of air temperature at platforms 1 and 4 for different working conditions of the ventilation fans (Pflitsch *et al.,* 2012).

The unsteady nature of the air flow over the three and a half hour measurement period is evident in Figure 6 and 7. The measurement error of the ultrasonic anemometer as specified by the manufacturer is ±1.5 m/s which is large compared with the magnitude of the measured velocities but other observations at the time taken with a hand held anemometer indicated flows of a similar magnitude and the same direction. This correlation provides confidence that the measured results do reflect the true nature of the air flow. A sample of the anemometers were calibrated in a wind tunnel against a pito-static probe after the measurements and showed errors of no more than 0.1 m/s. Irrespective of the measurement accuracy the trends in the air flow are indisputable, the influences of the ventilation fans and the gates are real effects. These results are also supported by the temperature measurements that have a greater degree of accuracy than the anemometers.

The main feature of the situation in the Monument station is a positive variation in temperature from the platforms to the upper concourse area. The analysed data from ultrasonic sensors installed in the tunnel indicate a clear daily variation with the lower platforms (1 and 2) being colder than the upper platforms (2 and 3) as shown in Figure 6. This is the normal variation that is to be expected in thermal driven chimney effect produced by changes in air buoyancy that occurs due to local differences in

temperature and moisture and is a much more stable phenomenon than that which would occur if a temperature inversion were to develop. This has been noted elsewhere by Pflitsch (Pflitsch *et al.,* 2012).

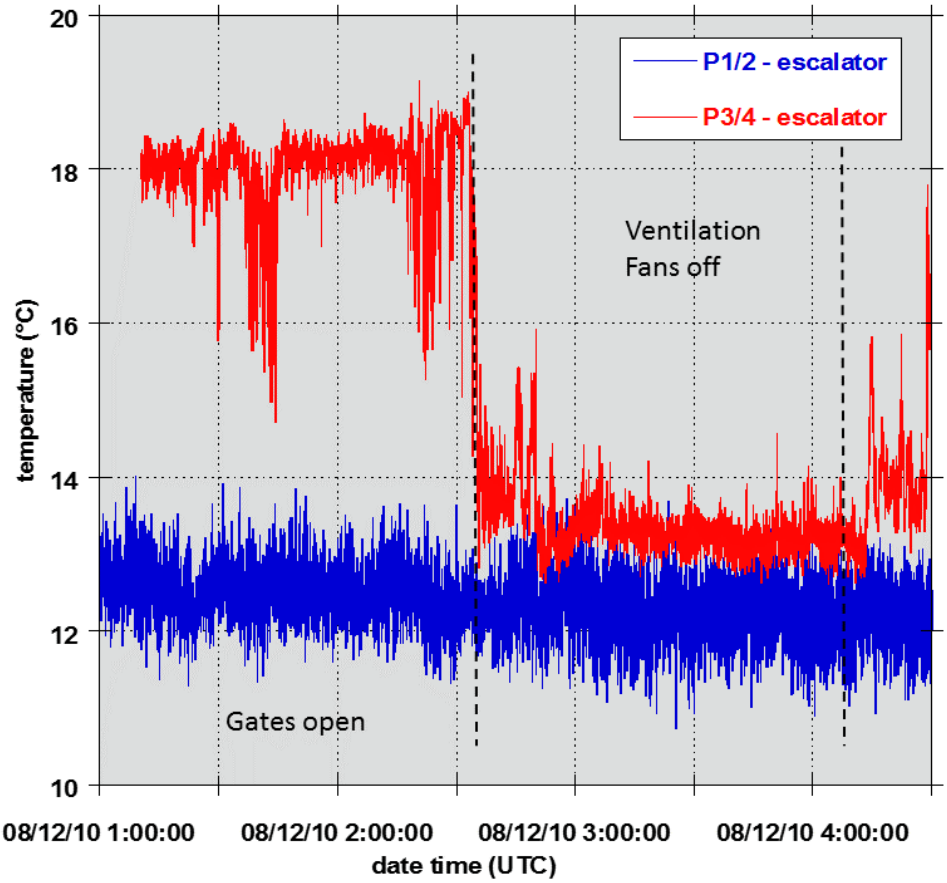

Figure 6: Variation of air temperature at Monument Station escalators for different working conditions of the ventilation fans and exit gate ways (Pflitsch *et al.,* 2012).

Underground stations with a high vertical extent facilitate the formation of an unstable inversion layer between the middle and lower levels station that inhibits the normal air flow. Of particular interest is the relatively steady and higher velocity of airflow without significant changes of the direction in both the lower level platforms and escalators. The positive direction of the escalator air flow signifies that it is ascending the escalator. The effect of the ventilation fans and the station gates is also apparent. Operation of the ventilation fans is seen to inhibit the natural background air flow in the escalators with a significant flow reversal occurring in the higher level escalator linking platforms 3 and 4 to the concourse. This is clearly shown in Figure 7 which also shows the opening of the Exit 1 (Blackett Street) doors.

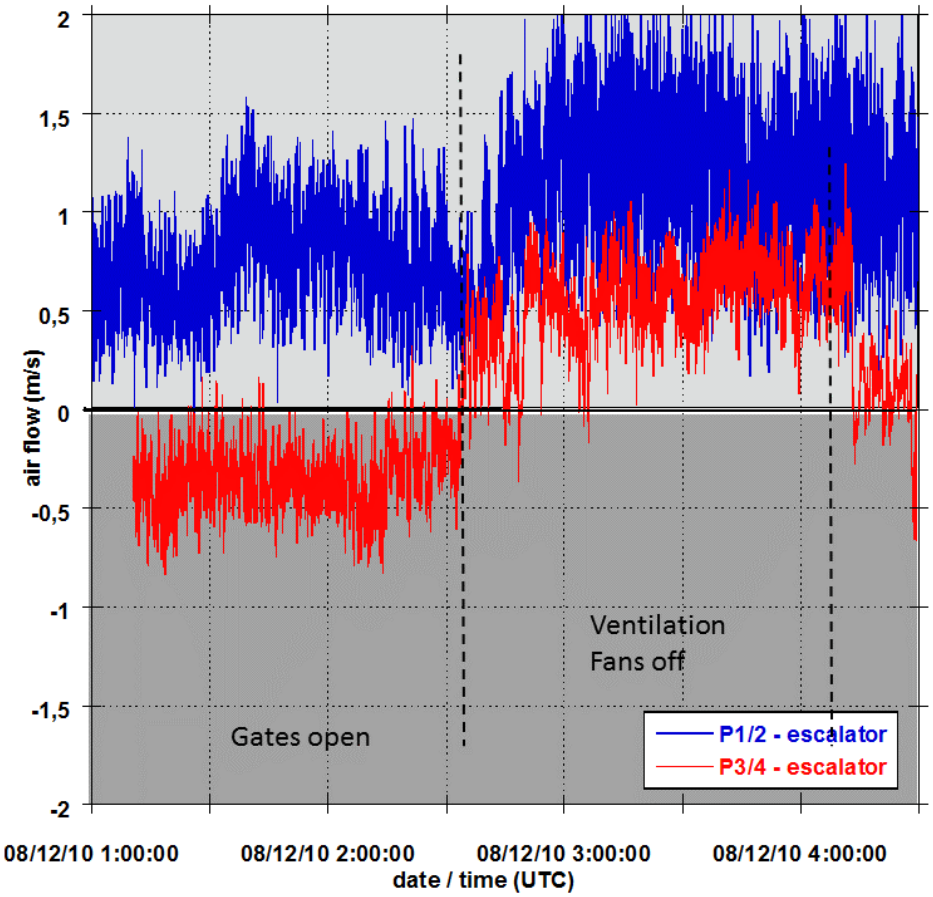

Figure 7: Variation of air velocity at the Monument Station escalators for different working conditions of the ventilation fans and exit gate ways (Pflitsch *et al.,* 2012).

This allows ingress of cold outside air into the concourse area which is then drawn down the upper level escalator without significant mixing with the original air in the concourse. It is quite possible that the sensors are reacting to flow stratification in this region which is a feature of the night time and may not be typical of flow patterns that would occur during the day time when the ambient air temperature is greater than that in the station and the air flow is mixed by the movement of passengers. The air would normally be energised by thermal currents set up by the energy supplied to the escalators. The temperature of the escalators in different phases of operation can be appreciated from thermal camera images reproduced in Figure 8. The left side set is in full load operation, the middle is stopped and the right side is on light load setting. This energy variation would also lead to flow stratification and varying degrees of chimney effect within the escalator wells.

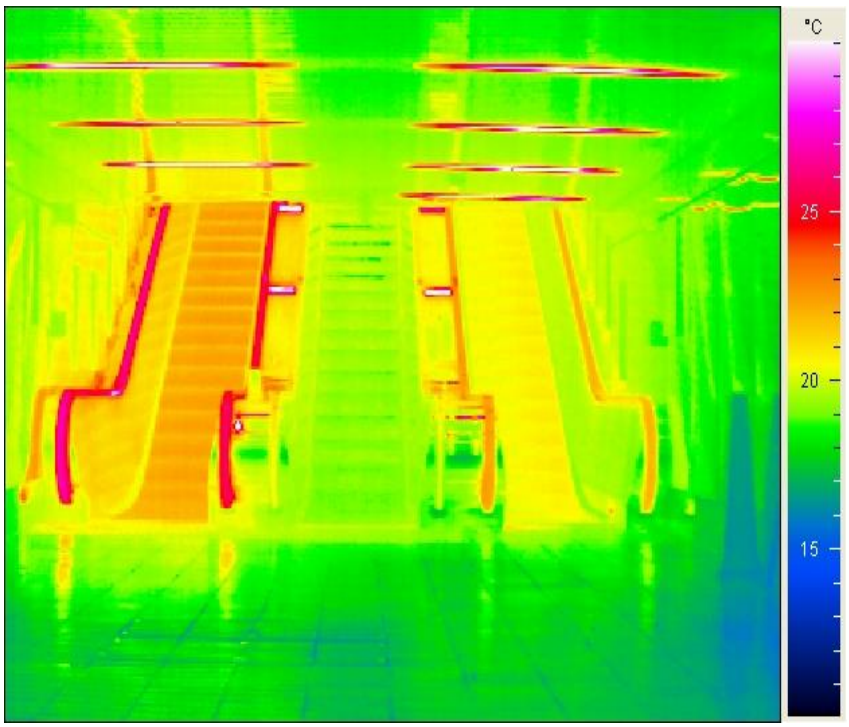

Figure 8: Thermal Images of Monument Station escalators (left: high velocity, middle: not working, right: slow velocity) (Pflitsch *et al.,* 2012).

The thermal images of the Jesmond Station tunnel portal, Figure 9, clearly show the spatial variation of temperature in the station with the strip lighting (shown as red) being the most energetic elements in the station. The cold outside air can be seen through the tunnel portal as the coldest (blue) region.

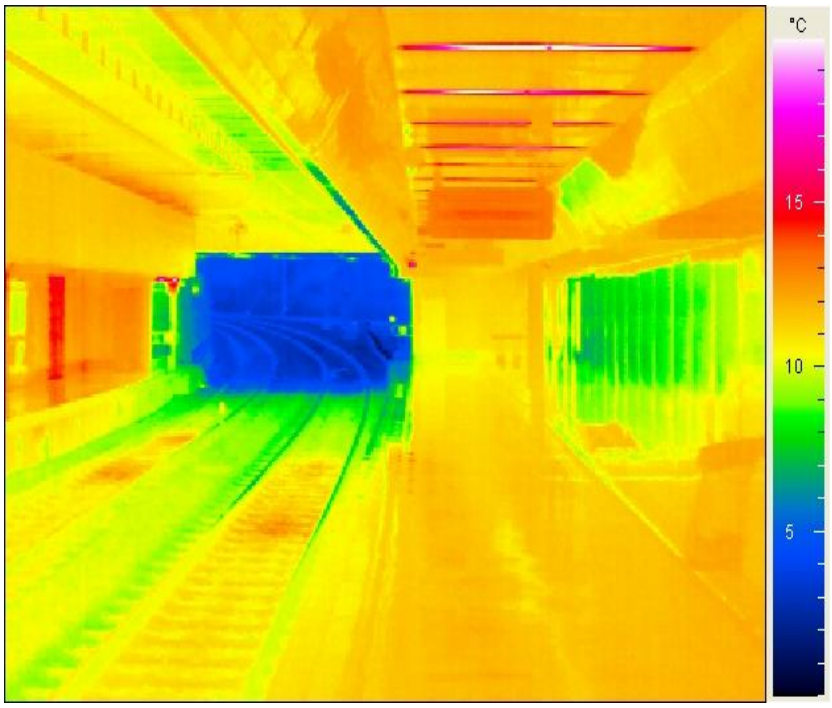

Figure 9: Thermal Image of Jesmond Station Portal at 11.00 pm (Pflitsch *et al.,* 2012).

A series of time lapse photographs of the same image is shown in Figure 10 taken from 11.30 pm to 5.00 pm at intervals of 30 minutes. The natural inclusion of cold air is demonstrated by the extension of the blue zone along the train lines. Other parts of the station were unaffected by the penetration of cold air along the track and this had very little influence on the bulk air movement in the portal. Measurements indicated that the very strong northerly air flow was maintained but was attenuated by 0.5 m/s locally and this had no effect on the flow in parts of the system located away from the portal.

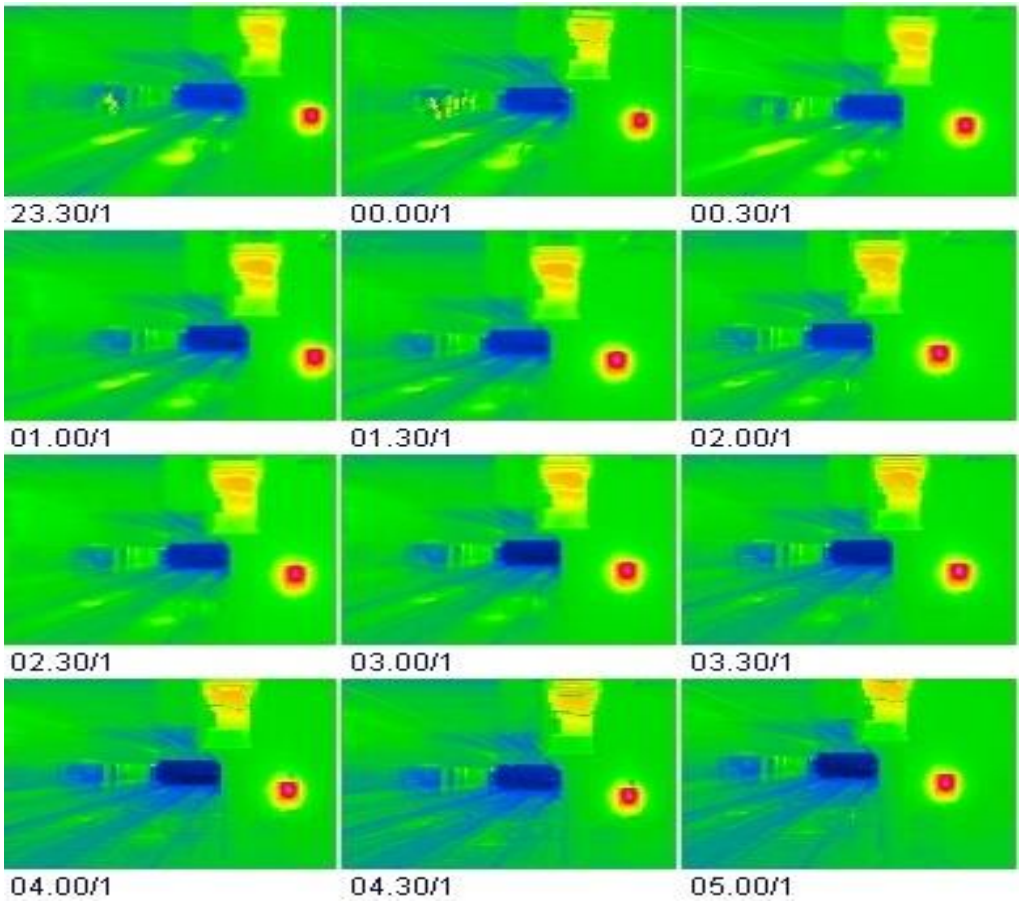

Figure 10: Time lapse thermal images of Jesmond Station portal (Pflitsch *et al.,* 2012).

The measurements taken courtesy of Nexus (Pflitsch *et al.,* 2012) in the tunnels of the Newcastle upon Tyne Metro have shown the presence of a strong background air flow that is driven by a chimney effect produced by the incline of the tracks. This is independent of any train movement and is quickly re-established after the passing of a train. The direction of the air streams at the time of the measurements was northerly on the line connecting the Tyne crossing to Jesmond and easterly in the line connecting St James to Manners. A seasonality of background flow has been noted in other underground rail system that is driven by the over ground climate but in this case the

background flow is so strong that this may not occur. A seasonally stable flow simplifies the decision process with regard to predicting the spread of a toxin in the tunnels but this needs to be verified by continuous monitoring. The performance of the forced ventilation system indicates that the impact this would have on the natural ventilation in the tunnels was poorly understood when installed. It is clear that this is not needed and that significant operational savings could be made by dispensing with this all together.

The influence of the tunnel portals on the flow characteristics is much localised, having no effect on the direction and velocity of the bulk background air flow. The development of a stratified inflow at ground level can be seen at the Jesmond portal but this is extremely localised and requires a long time to become established. This would have little effect on the spread and distribution of a toxin from the tunnel portal into the surrounding urban area.

The behaviour of the air in the Monument station concourse is much more complicated. This is influenced by several factors that can promote instabilities and flow reversals. These factors are the condition of the escalators, the tunnel ventilation and the position of the station gates. It is also likely that an aspect of seasonality will also have some influence here. It will be very difficult to predict the spread of a toxin in this region with any certainty given the present low level of understanding of the interaction of the various parameters that play a role in behaviour of the air migration. This is a worrying situation for the Police and Fire and Rescue personal who have to deploy their staff safely and to the best effect.

The limited measurements taken have shown that the airflow in the underground section of the Tyne and Wear metro system is much more complicated than hitherto thought. It exhibits flow reversals and stratification and is influenced by several operational factors. This indicates a high level of risk for passengers and the rescue personal in the event of the release of a toxic agent in the railway. These results reflect the low level of knowledge in subway climatology when the system was constructed, a situation that is probably repeated in other subways around the world. Further long term and extensive measurements need to be undertaken to gain a comprehensive understanding airflow in the subway.

As this research is conducted primarily on airflow patterns within the subway station, Monument station has additional factors that would facilitate this research. It is vitally

important to take into consideration all possible factors that may influence the experimental data. The first factor to be considered is the locality and surrounding buildings near the station. As mentioned earlier, chimney effects play a significant role in determining the air exchange in a subway. The Monument Metro station is situated directly beneath busy streets and retail shops. The airflow to and from the subway and the street level is critical in managing, controlling and maintaining the station climate and understanding the dispersion of toxins within the station. The advantage however of this being a fully underground and enclosed station is that all air flow patterns can be monitored and simulated for the entire station with little influence from the outside.

1.3 Research aims and objectives

The aim of the proposed research is to gain a further understanding of subway climatology and develop a robust methodology for the simulation and analysis of the air flow pattern in the Monument Metro Station that can be used to establish the flow pattern that drives the movement of toxic agents in the event of an emergency and the extent this is influenced by the local microclimate. This will provide a foundation to produce a simulation of the dispersion of toxic agents or smoke and the evacuation of passengers in a virtual environment that will inform the decision making process in the event of an emergency incident and/or support the development of early stage design guidelines for subway systems.

The question behind this and underpinning the research is how to understand the air flow pattern in a subway system and to account for the numerous factors influencing it, such as local weather conditions, station and tunnel layout and design, the ventilation system and train operational. This ultimately will lead to efficient and sustainable evacuation strategies and minimise the impact of an emergency event in terms of loss of life and generally improve the environment of subways.

To address this research question, the following five objectives have been defined:

1. To conduct a preliminary study and extensive literature review to establish an understanding of the cave mica climate and subway climatology.

2. Investigate the micro-climate of Newcastle City centre using measured data and weather station data to meet the requirement of modelling the subway climatology for the Monument Station.

3. To strengthen the understanding of details and sensitivity of airflow speed and pattern by conducing field measurements and tracer gas experiments

4. To perform detailed and accurate modelling of airflow patterns within the Monument station using a Computational Fluid Dynamics (CFD) package and utilising measured input data.

5. To empirically validate CFD simulated results with measured data and further simulated sensitivity scenarios to external conditions and train movement variables.

6. To integrate and evaluate the pedestrian evacuation simulation with the air flow and gas dispersion speed and patterns.

1.4 Contribution to knowledge

This research is understood to be the first in which an entire subway station has been monitored and measured to produce a CFD simulation of the airflow in operational and non-operational conditions. The simulation has taken into account local seasonal weather conditions, the station and tunnel design, the ventilation system and train operation factors. The air flow pattern has been established as a base to overlay the dispersion route of toxic gasses and to examine the effectiveness of evacuation strategies. The virtual environment platform developed for the CFD analysis has been used with a pedestrian movement simulation software package to evaluate an existing evacuation strategy and to make suggestions about an alternative strategy. This research outcome can be used to support the decision making process with regard to the initiation of effective measures to minimize the impact of the release of toxins within a subway and the most effective deployment of available resources.

In addition, this research has been nationally and internationally recognised, presented and published as follows:

Best Academic Research Award on the Rail Category at 6th European Transport Research Conference held at Warsaw, Poland, 18-21 April 2016.

Second prize at Railway Division Young Engineers Presentation Competition 2015 The Institution of Mechanical Engineers, UK, 14 January 2015.

Second prize for Best Academic Presentation competition at Next Generation Rail conference, 1-3 July 2015, Coventry, UK.

Qian, Z., Agnew, B., Thompson, E. M. (2014) 'Simulation of Air flow, Smoke Dispersion and Evacuation of the Monument Metro Station based on Subway Climatology', Fusion - 32nd eCAADe Conference - Volume 1, Newcastle upon Tyne, UK, 10-12 September 2014, pp. 119-128.

Qian, Z., Agnew, B., and Palacin R. (2016) 'Towards an integrated evaluation smoke or toxic gas dispersion and the pedestrian evacuation of subway station', *14th World Conference on Transport Research Society (WCTRS)*, SHANGHAI (CHINA), 10-15 July 2016.

Qian, Z., Charlton, J., Agnew, B. and Thompson, E., (2015) 'Towards an integrated evaluation of the effects on health from smoke or toxic gas dispersion in the evacuation of subway tunnels'. *Journal of Transport & Health*, 2(2), ppS10-S11.

Spiegel, J., Brüne, M., Dering, N., Pflitsch, A., Qian, Z., Agnew, B., Palacin, R. and Irving, M. (2014) 'Propagation of tracer gas in a subway station controlled by natural ventilation'. *Journal of Heat Island Institute International*. Vol, 9, p.2.

1.5 Structure of the thesis

This thesis consists of ten chapters supported by two appendices. One of these chapters is the current introductory chapter which outlines the aims and the motivations of this work while the other chapters are arranged as follows:

Chapter 2 presents a literature review covering topics and latest published research work related to this study. This includes Subway Climatology, Laser scanning for 3D modelling, Fire Safety in Tunnels, Pedestrian simulation and evacuation, Computational Fluid Dynamics (CFD) simulation and virtual environment model.

Chapter 3 is devoted to the research methodology that is divided into experimental and computational analysis of the subway station. In particular, it covers the 3D modelling, Experimental Measurements, Computational Fluid Dynamics (CFD) and the interfacing with virtual environment model.

Chapter 4 presents the development process of 3D modelling based on a virtual environment model produced by laser scanning. Relevant software selection is discussed and the procedure of converting point cloud data from laser scanning to produce files for CFD modelling is described.

Chapter 5 is concerned with the execution of the air flow and temperature measurements aspects of this project. This includes some result from earlier findings about mechanical ventilation and gate operation affects, weather data of Newcastle upon Tyne, the measurement of the air flow in and around the station and temperature variation along the tunnel.

Chapter 6 presents the details of different tracer gas experiments that were carried out together with an analysis and a discussion of the results. The experimental data from both Chapter 5 and Chapter 6 were developed to provide a further understanding of the air flow condition in the tunnels, outside and inside the station in order to validate the CFD simulation results.

Chapter 7 is concerned with examining the characteristics of the weather conditions outside the station and the influence this has on the station internal air flow. This is particularly concerned, through modelling the local micro-climate, with the impact variations in the local wind direction and speed have on the air flow through the station and at the station openings (entrance/exit).

Chapter 8 describes the CFD simulation of the air flow in the station. It begins by discussing the basic principles of CFD modelling, the development of the computational grid and boundary conditions. It is also concerned with the validation of the CFD modelling by the measurements and experiments.

Chapter 9 is devoted to further CFD analysis of the air flow to recreate the tracer gas experiment conditions. The effect of train movement is examined and the sensitivity of the station to different internal and external air flow patterns is investigated. Finally, the resulting air flow is combined with an evacuation simulation using the software package Legion to assess the evacuation strategy of the statin.

Chapter 10 presents the conclusion of this work and makes recommendations for further work.

Chapter 2. Literature Review

2.1 Introduction

Public transportation systems are used by millions of people every day. The large number of individuals in the confined space of a Metro system, especially during rush hours, makes these systems vulnerable to terrorist attacks (Pflitsch *et al.,* 2013) and other emergency situations as has been illustrated in for example Tokyo 1995 (Murakami, 2010; Coke *et al.,* 2000), London 2005 (Murphy, 2006) or Moscow 2010 (Levy, 2010). Moreover, fire safety is a major concern because of the large number of serious tunnel fires which have occurred in Europe since 1995. As a result the European Parliament commissioned a study of tunnel safety in 2008 with a view to produce a set of recommendations and guidelines to be implemented in the European Union (Beard and Cope, 2007). That research was intended to enable the stakeholders to take more reliable and informed decisions which may possibly save passenger lives. The uncertainty prior to this was due to a lack of understanding about the diffusion paths of smoke and/or toxins and an understanding of the dilution of toxic substances. Furthermore the extent to which escape routes for the passengers would be compromised by the spread of the smoke or toxic agents was and is poorly understood (Pflitsch *et al.,* 2010).

The scope of this chapter ranges from Subway Climatology to CFD modelling of a subway and evacuation simulation and is divided into several sections that are linked through virtual environment as this is considered to be an appropriate platform to disseminate the findings of this work to a non-technical audience. This chapter is intended to discuss the current state of the art related to the understanding of air flow and dispersion of toxins in subway systems, providing the basis and context for the remainder of this thesis.

2.2 Subway Climatology

Subway Climatology is a new research field for the management of possible catastrophes in subway-systems that has been proposed by Pflitsch *et al.* (2003). From the early 70s, subway evacuation and tunnel safety in emergency situations in the event of fire or terrorist attack have aroused great concern but it is only relatively recently following fires and terrorist attacks in subway systems that efforts have been

made to understand the nature of the air flow in a subway system and the relationship this has with the outside atmospheric condition.

An understanding of airflows in subway systems and tunnels stems from work performed in natural cave systems be the barometric or thermal in nature. The climatologic differences of both cave types are mainly based on the different driving forces of airflow that occur in the entrance area and also in the interior of the cave. In thermal caves density differences of unequal temperature air masses lead to compensating air flows (Moore and Sullivan**,** 1964; Palmer, 2007) while in barometric caves pressure variations of the atmosphere enforce a temperature independent compensating air flow (Pflitsch and Piasecki**,** 2003; Pflitsch *et al.,* 2005). The different genesis of airflows has far-reaching consequences for the climatic character of subway systems. The most important differences between thermal and barometric systems are based upon the character of the airflow. Systems that contain large public spaces with wide corridors and passages and very strong chimney effects exhibit relatively low air flow velocity (0.2-0.5 m/s) (Boes, 1997). Research of Jewel and Wind Cave the two big barometric cave systems in South Dakota, USA by Pflitsch *et al.* (2010) found within barometric systems airflow of several m/s can be measured, at least close to the openings, and sometimes within the cave. The internal airflow of thermal systems has a strong seasonal characteristic, with clear differences between summer and winter and stronger oscillations of direction during spring and autumn. Barometric systems show small differences between summer and winter; this effect is due to the seasonal variability and stability of passing pressure systems. In an ideal barometric type, air exchange takes place through all openings and across the whole profile in the same direction (inwards or outwards) at the same time. In contrast to this, air flow into and out of thermal systems usually takes place at the same time (inflow in one, outflow at another entrance), but through different openings. Single openings show a vertical differentiation in air exchange. Another small but important difference is the effect of the inward and outward flowing air on the pressure conditions inside the system. The pressure drop in thermal systems, caused by the out flowing air to the upper entrance in winter and the lower entrance in summer, is equalized quickly by air flowing into the other entrance. So, the internal pressure is more or less in equilibrium with the outside pressure at all times (this is an idealised assumption and a theoretical concept). In a barometric system a steady air movement is set up in order to equalize the air pressure with the outer atmosphere. This is only accomplished for a short time period which leads to flow oscillations. The variable flow conditions lead to differences regarding the

thermal conditions of subway systems. In the case of Thermal systems, the upper surface opening is influenced by the passing of air masses. In summer, relatively warm air from the outside flows into the opening, while in winter the air from the subway that is warmer than the outside atmosphere flows outwards. A lower surface opening however is characterised by the discharge of cool air masses. In winter the cold air of the outside atmosphere flows inwards while in summer the relatively cool internal air flows outwards. This leads to the formation of a relatively cool area in the lower level, while the upper parts of a thermal system are warmer compared to the annual mean. In this respect a thermal vertical gradient of the atmosphere has to be taken into account. This means that the absolute temperature values have to be reduced accordingly in order to be able to note the described effects. The temperature gradient between the two openings should point in the same direction provided that there are no further influences. Thereby the gradients near the opening will be high and temperature equilibrium is reached after a few metres for low airflow rates, or several hundred metres for large flow rates. The thermal appearance of barometric systems turns out to be entirely different. At all surface openings there is a constant change between incoming and out flowing air throughout the year. Thus in summer relatively warm air (compared to the air inside) and in winter relatively cold air masses penetrate into all openings from the outside. Therefore, the temperature gradient observed between the openings and the inner parts should run similarly from every surface opening into the interior.

The above considerations are useful theoretical concepts as this clear difference between the two types of driving mechanisms does not exist in reality. However, there is evidence that thermal and barometric effects can exist inside a single system and even close to each other, which is described Kato *et al.* (1995). The situation becomes more complicated however when internal heat (energy) sources such as escalator motors and forced ventilation systems have to be taken into consideration.

Before the several studies in the USA which stated the general existence of a train independent background airflow done by Policastro and Coke (1998); Pflitsch (2001a; 2001b) and Pflitsch and Flick (2000) it was thought that the ‘piston effect’ which is the airflow induced by train movements, was the main factor determining the airflow regime and directed the airflow direction and dispersal of a subway system (Brown, 1966; Rasmus and Brock, 1944; Rudolf, 1997). Several studies with sufficient data collection in the subways of New York City (U.S.A.) and Dortmund (Germany) proved instead the

existence of a traffic independent natural background airflow that is temporally and spatially variable regarding its velocity and its direction (Pflitsch and Geppert, 2000; Pflitsch *et al.,* 2000). During operation hours the train service generally is the controlling factor for the dispersal events; nevertheless the natural airflow always influences the dispersal in the background. During normal operation times after the passage of a train and after the train service ends the background airflow restores very quick and becomes dominant (Pflitsch, 2001a). These research showed the natural background airflow of a station to be very stable but may show a seasonal variation.

The aim of the Subway Climatology, aspects of this thesis is to gain a better understanding of how air mixes between the subterranean levels and street-level (regional airflow) in a subway station and to identify the main driving forces for the dispersion of smoke or toxic agents throughout the station. The ventilation systems of subways have been the subject of much research in the past (Fletcher *et al.,* 1994; Kim and Kim, 2007; Li *et al.,* 2003). Understanding the influence of the background air flow on the ventilation of the subway system is important given its significant influence on the direction and strength of the internal air flow and air exchange within the station. This air exchange is strongly influenced by chimney effects within the underground buildings (for instance in escalator wells). A recent study by Pflitsch *et al.* (2013) has shown that, in the event of a disaster, airborne toxins in subway systems are dispersed mainly by air movements caused by natural ventilation and chimney effects that are produced by the pressure differential between station levels and street levels. Warm air within a station naturally flows upwards towards the over ground entrances by way of stairs and escalators. The addition of energy to the air from the escalator motors enhances the buoyancy effect of the air accelerating the dispersion. However flow reversals or recirculation have been noticed between different levels in a station due to the interaction of the natural air flow with the station ventilation system (Pflitsch *et al.,* 2012). This can lead to a blocking of normal exit routes making them unsafe and in the worst case they become death traps. As a consequence the influence of natural ventilation should be included in the disaster planning in order to develop effective strategies for the reaction to fires and the dispersal of toxic gases.

2.3 Virtual Reality Model

Metro and subway system construction is on the increase world-wide with longer tunnels being built, often as part of ever more complex transport systems. Every metro system is unique in terms of method of construction and layout of the stations. This

has been pointed out by Beard (2009). Due to the fact, that subway systems operate mostly underground, they have special conditions during any emergency situation. The behaviour of a subway system should be considered together with the over ground climatology. The background air flow is very complex but recent advances in computing power and developments in programming have made it possible to explore flows using computational methods. Unfortunately, the presentation of the air flow data is very difficult for non-experts (such as the metro operators) to understand so it is essential that a better means of displaying this information is also developed. It is considered that Virtual Reality is a possible means of displaying this information in an easily understood format. The information about the subway station building used to produce a virtual environment is provide by laser scanning the station interior, so the characteristics of the air flow (which will also be accommodated in the virtual environment images) will be obtained by computer simulation. This approach is discussed in the sections below. Virtual Reality is now recognised as a very important tool within the built environment for enabling the decision process for City Planners, Architects (Greenwood *et al.,* 2008; Horne *et.al,* 2008) and Builders but also health and safety training simulations, for fire fighters and rescue personnel (Yuan *et al.,* 2012). The use of virtual environment model within the construction industry is seen by many as holding great potential for increasing effectiveness as well as improving the democratization of the building process and urban planning (Greenwood *et al.,* 2008). The Built Environment Visualisation Centre at Northumbria University is one of the Virtual Reality Centres in the UK and has set the benchmark for this type of activity by hosting the Virtual Newcastle Gateshead (VNG) research project. This is a joint venture between Northumbria University, Newcastle City Council and Gateshead Council to create a three-dimensional digital model of the urban core areas of both Newcastle and Gateshead covering 30km^2 at present, with a view to extend the coverage approximately to 102km^2. A recent research paper (Morton *et al.,* 2012) highlighted the fact that VNG model offers a unique opportunity by providing developers, architects and planners with the means to accurately assess the impact of design proposals within their urban context.

As part of the urban planning process the VNG model is providing a more effective and efficient communication. The model also supports VNG's host partner, Northumbria University, in their research activities into city modelling and spatial data management and manipulation. The full potential of VR can be taken much further as, by engaging with the scientific community, it can be developed for noise mapping, wind modelling,

pedestrian simulation and thermal imagery. In order to do this, it is necessary to interface the virtual environment with CFD modelling to accurately represent, in real time, the air flow and dispersion of agents in a subway systems and tunnels and in the over ground urban environment. Ren *et al.* (2006) presented a virtual reality system developed using texture mapping and particle systems to implement vivid visualization of flames and smoke for the simulation of occupant evacuation in an underground station. The simulation of a fire and an evacuation process in a virtual environment which can be used for trainings in a virtual environment can be done cheaply, easily and safely. This has been demonstrated by Ren *et al.* (2008) who developed a virtual reality system to illustrate the spreading of flame and smoke to simulate an emergency evacuations during a fire. This was a multi-grid, multi-base-state database model and was used to overcome the disadvantages of traditional smoke spreading simulations.

The benefits of linking building planning with virtual environment representation are many and can be summarised as:

• For architects, designers and planners it can be used as an early stage design tool to assess the functionality of proposed new tunnels and station designs and examine the result of proposed changes in the layout of existing stations, as well as the impact on the surrounding urban.

• For psychologists and resilience planners it provides a means of assessing the behaviour of people of all ages and state of health in an emergency situation in a subway.

• For subway operator it can be used as a training tool to familiarize maintenance workers with details of the tunnels and it can also be used to simulate emergency incidents.

• For Emergency Services it will assist in operational planning for a possible incident.

The data obtained for this thesis through the CFD and virtual environment modelling of the urban environment provide easily understood information to the operational planners of emergency incidents (police, subway operator, fire and rescue) and can also be available to architects, designers and planners as input to a future application contributing in the early design stage.

2.4 Laser scanning for 3D modelling

A necessary starting point of any virtual environment study of an existing building is the creation of the data files that contain the information about the building geometry, internal and external, the surface topography and texture. This can be done by creating a Point Cloud of geometrical points from a 3D laser scan of an existing building. All of this data can then be used to generate the geometry of the building (Hamil, 2011). In June of 2011 Existing Building Information Modelling (eBIM) company were commissioned to fully laser scan and produce a Building Information Model (Revit) of the Monument Mall shopping centre which is adjacent to the Monument Metro Station concourse in Newcastle upon Tyne (eBIM, 2011a). By far the greatest advantage of being able to directly insert the point cloud information into Revit is the accuracy of the information. Another positive effect this can bring is the speed at which a model can be built, with the 'tracing surface' provided by the point cloud being available to draw over in three dimensions, precisely relative to all other elements of data in the entire surveyed cloud – the cloud itself lending itself perfectly to the practice of 3D viewing and working (eBIM, 2011b).

The next step after generating the point cloud data is to convert this to a three dimensional model. According to the study conducted by Kimpton *et al.,* (2010) in which a section of a wall on a complex heritage building, the Black Gate in Newcastle upon Tyne, was recoded, there are many commercial software packages that are able to convert point cloud data into a triangulated mesh model. All of the software packages evaluated in this report can export a triangulated mesh to a variety of 3D file formats so they can be used by all of the major 3D modelling and CAD packages. Table 1 shows some of those available and in Table 2 the time it took to convert the same point cloud data into a triangulated mesh is shown.

Software	Website
VRMesh Studio	www.vrmesh.com
3D Reshaper	www.3dreshaper.com
Rapidform XOS/Scan	www.rapidform.com
Geomagic Studio	www.geomagic.com
Silverlining	www.farfieldtechnology.com
3D Reconstructor 2	www.reconstructor.it
Polycloud	www.menci.com
PolyWorks	www.innovmetric.com
Leios	www.egsolutions.com

Table 1: Point Cloud to Mesh Software (Kimpton *et al.,* 2010)

Software	Time taken	Triangles
3D Reshaper	14 mins	4,159,653
VRMesh Studio	6 mins	3,881,740
Rapidform	3 mins 30 secs	2,542,186
Geomagic Studio	1 min 20 secs	4,127,064

Table 2: Point Cloud Conversion Results (Kimpton *et al.,* 2010)

The results of this test showed that Geomagic Studio processed the data in the fastest time and produced a mesh with almost the same number of triangles as the slowest performing piece of software. This then has the potential of making the VR technique an effective early design tool for investigating ventilation in large building and the associated spread of smoke, dust or chemical or biological agents released in a terrorist incident.

2.5 CFD simulation application in tunnel and Subway Stations studies

CFD has some important advantages compared to wind tunnel testing. Wind tunnel measurements are generally only performed at a few selected points in the urban model, and do not provide a whole image of the flow field. CFD on the other hand provides whole-flow field data, i.e. data on the relevant parameters in all points of the computational domain. Unlike wind tunnel testing, CFD does not suffer from potentially incompatible similarity requirements because simulations can be conducted at full scale. This is particularly important for extensive urban areas. (Blocken et al., 2012) CFD modelling of the air flow within and around buildings and related thermal and dispersal phenomena play an essential role in determining the urban environment. The flow regimes can broadly be divided into internal and external flows. Internal flows are low speed and often strongly buoyancy influenced (Patel *et al.,* 1985). These features offer particular challenges for CFD simulation. A further problem within the built environment is the wide range of length scales that can vary from room size down to the details and dimensions of ventilation grills and boundary layers. The cornerstone of CFD is the Navier-Stokes equation set expressed for turbulent flows in suitable averaged velocity and pressures to make them amenable to numerical solution without excessive computing time. The conventional approach is time averaging in which the dependent variables take their time-averaged values and the equations are then referred to as the Reynolds-Averaged Navier-Stokes (RANS) standard k-3 turbulence model (Jones and Launder, 1972).

Buoyancy and viscous effects in both the near-wall and bulk flow regions have proved to be particularly difficult to capture correctly in turbulence models and have seen some significant advances. Much research deals with a comparative study of LES and RANS (k-ε model) for a typical bluff-body flow, namely the flow around a surface mounted cubical obstacle placed in a plane channel. A comparison of the capability of the different methods is demonstrated with the work of Breuer *et al.,* (1996). However, in the case of near-wall flows these often require direct calculation of boundary layers rather than use of wall functions, which can be excessively expensive computationally. Because there is no clearly superior model which works well over a wide range of applications, commercial CFD codes tend to offer a number of options. Unfortunately, and as a reflection of the state of the art, the only reliable guide to selection from these for a particular application is previous experience on a similar problem. Certain types of application appear to defy accurate solution by the available RANS models. A notable example is the flow around buildings, where the pressure distributions, wake structures and turbulence characteristics on or near some surfaces are not well captured by any RANS model (Murakami *et al.,* 1993; Fureby and Grinstein, 1998).

In the last 10-15 years, Large Eddy Simulation (LES) (Ferziger, 1985), an alternative turbulence modelling approach, has shown increasing promise to overcome the limitations and deficiencies of Reynolds averaging (Lin, 2010). Computational fluid dynamics are applied to simulate the smoke movement in a ventilated tunnel fire through LES by Gao *et al.* (2004). In the study by Chow *et al*. (2006), the LES technique was applied to predict the spread of smoke and fire in a public underground car park through fire dynamics simulator. In LES, spatial averaging is performed on the scale of the computational grid spacing, with the result that modelling is only required of the pseudo-stress terms that represent turbulent motions below this scale. LES is much better suited to prediction of unsteady effects than the RANS, since it computes directly all but the small-scale, high-frequency components. Although LES is at a much earlier stage of development than RANS modelling, there are already applications where it is proving to be superior in the example of the flow around a building. Advances in CFD methodology and computer hardware have, nevertheless, made it feasible to apply LES to industrial problems and it is an option in commercial CFD codes (Murakami *et al.,* 1993; Park *et al.,* 1997; Borth, 1990).

Many flow-related problems in the built environment also involve simultaneous heat and/or mass transfer e.g. heating and air conditioning; fire and smoke spread; and

gaseous pollution. In the case of heat transfer, all three modes, convection, conduction and radiation, often need to be taken into account (Park *et al.,* 1997). The basic equations governing these processes are the differential set for conservation of energy and mass of individual chemical components. In the case of heat conduction and radiation, these can be formulated without approximation (although for radiation simplified forms are sometimes used for economy) and are incorporated in most general-purpose CFD codes. The issues and approaches are similar to those for the flow field modelling with some additions:

• Accurate prediction of the relevant flow field features is a prerequisite to good heat/mass transfer modelling.

• Surface heat transfer is particularly sensitive to details of the wall boundary layers, including their turbulence structure - ironically often more than the flow itself. Thus, predictions of heat transfer coefficients may be less accurate than friction factors. This is sometimes compensated for pragmatically, by employing empirical heat transfer coefficient correlations in the CFD model (Borth, 1990).

• Buoyancy-influenced flows are particularly challenging to model due to the strong interactions between the flow and density fields, which can either augment or diminish the turbulence, according to whether the flow is unstably or stably stratified, respectively. Stable stratification can lead to locally low Reynolds numbers and additional associated modelling difficulties (Breuer *et al.,* 1996; Murakami *et al.,* 1996).

• Pollutant dispersion modelling from localised sources involves similar issues as heat transfer, including sensitivity to turbulence anisotropy, even in simple boundary layer flows (Gosman, 1999).

• Many of these issues and developments are at the leading edge of turbulence research and therefore may not all be reflected in current commercial CFD codes.

• On the other hand, it should also be recognised that even the existing models in these codes often give useful results and acceptable accuracy, particularly in relation to comfort requirements.

Fundamental studies like those reported from Fureby and Grinstein (1998) and Gosman (1999) show quite clearly the limitations of RANS models in predicting the wind-generated flows around building. Research by Gousseau *et al.* (2011), evaluated the performance of two different modelling approaches, the RANS standard k-e and

Large Eddy Simulation (LES) for high-resolution CFD simulation using Fluent 6.3. The status of the modelling of turbulence, heat and mass transfer was briefly reviewed and developments in computer solution methodology were outlined, with emphasis on geometry-handling and mesh-generation capabilities and parallel computing. The software has now reached the stage that the achievable level of accuracy is viewed as acceptable for some purposes and has led to CFD being used in a variety of applications such as for wind engineering and environmental comfort and safety research. The level of prediction accuracy is already sufficient for the purposes of this research area.

Early studies such as that of Tahry and Gosman (1981) have focused on relatively simple situations like the spread of a chimney plume over flat terrain or escaped gas dispersal behind a single building. The software has now developed to the stage that a complete underground metro station had been modelled by Mendonca and Drake (1996) including the ticket hall, which has two substantial covered ground-level entrances, the tunnels and escalators leading to the train platforms and a train. In this case the flexibility of unstructured meshing was required by the irregular topology and use was made of arbitrary interfacing to allow different styles of entrance structure to be tried. CFD studies have also been performed of the induced flows within metro train tunnels and platforms caused by the train motion. Studies of very specific features of subway systems such as stair wells have produced some very interesting characteristic and scaling laws (Ergin-Ozkan *et al.,* 1995; Reynolds, 1986) that can be utilised in the CFD modelling. Wind-induced pollutant dispersion is another area of application of CFD. Commercial codes such as SIRANE are now being used to study somewhat more complex situations, for instance the pollutant spread in ‘street canyons', i.e. city streets bounded by relatively tall buildings (Soulhac and Salizzoni, 2010). The three-dimensional flow in a subway tunnel caused by the passage of a train has been analysed by Kim and Kim (2007). This was done with a 1/20 scale model tunnel with pressure and air velocity variations together with computational numerical analysis based on RANS and used the sharp interface method for the moving boundary of an immersed solid. The predicted numerical model results showed good agreement with the experimental results. As mentioned earlier the piston effect has a strong impact during operation in Subway Stations. The piston effect refers to the forced-air flow inside a tunnel or shaft caused by moving vehicles. This has been examined by Pan *et al.* (2013) who showed that it has a great effect on the temperature, wind speed, and air quality in subway stations, introducing fresh air and discharging foul air through

the subway ventilation system influence the subway station thermal environment. Wang *et al.* (2010) and He *et al.* (2007) concluded that the tunnel area and length, the one-way resistance coefficient, the local resistance coefficient, and various other factors such as train speed and length plus the tunnel blockage ratio, influence the piston wind speed. Tao (2005) also conducted research to control the air velocity in a station by limiting the train speed, changing the size of the tunnel, changing the exhaust system and the station layout. Han *et al.* (2010) simulated the effect of different forms of piston ventilations on the tunnel ventilation and pointed out that a direct airshaft was superior to an inclined airshaft.

2.5.1 CFD Simulation of fires

CFD codes have also been developed to predict the outcome of a fire in a tunnel or a subway system. Simcox *et al*. (1992) examined the effect of varying heat release rates, heat release area, and different boundary conditions through simulations investigating the King's Cross fire. Further research by Woodburn and Britter (1996a; 1996b) was concerned with investigating and quantifying several sensitive factors between CFD simulation and experimental measurements of a fire in a tunnel. They found that the naive use of a CFD simulations code is likely to cause large uncertainties. Errors between simulation and experiment were up to 60%. They established the need for the precise specification of ventilation velocity profile, natural convective, radiative heat transfer, wall roughness, boundary condition, turbulence model and heat input rate for the simulation.

In the early research, Chow (1996) predicted five fires that would have a high likelihood of occurring in a tunnel from a self-developed fire field model for studying the aerodynamic and smoke movement in a tunnel. Further, experimental data collected in a smaller tunnel from an abandoned copper mine in Norway was used to justify the prediction. Those experiment were validated the numerical simulating tunnel fires in different scenarios. A study by Lee and Ryou (2006) modified and developed CFD models to predict the effect of the aspect ratio on smoke movement in tunnel fires using FDS 3.0. Fire Dynamics Simulator (FDS) is a large-eddy simulation (LES) code for low-speed flows, with an emphasis on smoke and heat transport from fires. Their results were compared with a full scale experiment. Their numerical simulation showed the predicted temperature distribution under the ceiling was in good agreement with experimental values within 10^{o}C. Results from varying the aspect ratio showed good agreement with experimental data. The temperature near the fire source decreased

with the increase of the aspect ratio but the rate of the temperature decrease was reduced by a decrease of the heat loss in the slantwise direction. This work confirmed the possibility of the application of FDS code to predict the smoke movement in tunnel fires. Subsequently it has been used to predict the temperature and smoke distribution of a tunnel fire (Wen *et al.,* 2007) and a simulation of temperature and smoke distribution of a tunnel fire were performed by Xiaojun (2008). In this study some modifications to the model were presented including the governing equations, radiation heat transfer models and flow rate through openings.

A review of several papers indicated that a station ventilation system is the most important component of the subway systems when events involving heavy smoke occur. Research by Teodosiu *et al*. (2016) analysed the efficiency of a mid-tunnel fan mechanical ventilation system when a train on fire and stopped at a platform. This work was performed using the CFD modelling software ANSYS Fluent 15.0. The results showed that a good ventilation strategy can lead to the safe evacuation of passengers once they have left the train. In a similar study by Meng *et al.* (2014) used CFD simulations to study the effectiveness of different ventilation modes in case of a train fire in a subway station. Results showed that appropriate activation of the air supply system can improve the efficiency of the ventilation system in smoke control, and vice versa. It was better to activate a lobby air supply system and meanwhile close the platform air supply system. The additional smoke barrier, smoke propagation in a subway station can controlled by optimal use of the ventilation system. Zhou and Zhang (2012) also evaluated the effectiveness of an air curtain to improve the ventilation in the subway station fires using CFD simulations. This research of Chen, *et al.* (2003) of three-dimensional smoke flow fields under various kinds of fires were computed by CFD modelling to investigate the effectiveness of the smoke control scheme of the Gong-Guan subway station (GGSS) which is a typical subway station of the Taipei Rapid transport system. The results indicate that the stack effect plays a deterministic role in smoke control when a fire occurs near the stairwell and no mechanical smoke control is necessary. When a fire occurs in other places, such as at the end or the centre of the platform, the current mechanical control schemes are effective which is controlled smoke confined to a small region or is evacuated from the station, leaving the four exits free of smoke so that the passengers can escape through them. This research also investigated the effectiveness of the smoke control system and proposed an innovative smoke control scheme for fires occurring on the chassis of a train with the smoke control on platform edge door. This study provides both

valuable information for the design of passenger evacuation routes in fires as well as criteria for the design of a smoke control system for subway stations.

2.5.2 Validation

The tunnel ventilation systems typically consist of ventilation shafts located at each end of station and/or between two stations to provide longitudinal forced ventilation for the control and extraction of smoke from a fire in the tunnels, to maintain tolerable conditions in the non-incident tunnel, and to control and extract smoke in the event of fire on a train at a station platform (Ting *et al.,* 2012). The CFD simulations are traditionally validated by detailed wind-tunnel experiments or in field measurements. Order-of-accuracy verification is necessary to ensure that software correctly solves a given set of equations and experimental results are required to set up accurate boundary conditions. For example, Apte *et al.* (1991) who investigated the effects of varying ventilation velocities and fuel pan size on the spread of smoke in a tunnel compared their simulation results with experiments performed in a large scale wind tunnel. The dispersion of a pollutant emitted from a roof stack in the wake of a tower, in a two-building configuration was examined by numerical simulation (CFD) by Stathopoulos (2004) and validated by experiments in which sulfur-hexafluoride (SF_6) tracer gas was released on the roof of building and concentrations were measured at several locations on this roof and on the facade of a neighbouring high-rise building. Lateb *et al.* (2011) validated his LES simulation of pollutant dispersion in an actual building group in downtown Montreal. A comparison of numerical simulations and experimental tests of ventilation in tunnels has been performed by Ingason *et al.* (1999) who evaluated the effects and influence of longitudinal ventilation on the smoke spread in tunnels when using thermal and mechanical point exhaust ventilation. Ribot *et al.* (1999) performed a numerical simulation of smoke extraction by roof ventilation in a tunnel by using CFX Fluent and compared it with experimental results.

Experimental validation of CFD results can be done in several ways. For small and relatively simple tests which do not involve high velocities wind tunnel tests can be performed based on Reynolds number scaling. This is adequate for architectural elements such as stair wells for instance but will be very difficult to undertake for a complete station. Direct measurements of the airflow can be undertaken with sensors placed at discrete locations within a station (Pflitsch *et al.,* 2010) measuring airflow in subway system. This requires robust sensors if they are to be kept in place for any length of time but the use of ultra-sonic anemometers has proved to be a reliable and

successful means of obtaining air flow data from subway systems. A more detailed understanding of the airflow in a building can be obtained by the application of tracer gas tests. In this a tracer gas is released inside a building and sensors placed in the building that have been synchronised to the gas release time record the time and concentration of the tracer gas. In recent tests in Berlin, the Cave and Subway Climatology group at the Ruhr-University released sulphur hexafluoride (SF_6) as a tracer gas to evaluate the efficiency of evacuation routes. SF_6 is a well-established tracer gas that is used in mines and to detect for leaks in electrical switch gear. It behaves like normal air, it is colourless, odourless and non-flammable and normally exists in very small quantities in air as it is entirely man made (Turk *et al.,* 1968; Pflitsch *et al.,* 2012, Brune *et al.,* 2016). In these series of measurements air samples were taken in syringes at different locations in the station. The time after the release time of the SF_6 was recorded and the sample was then taken to a laboratory for analysis. This sampling rate was inevitable slow involving a large number of student volunteers to take the measurements. Analysis of the results reflected the trajectories of toxic airborne agents from a source to the exits of the station and pointed out the safest escape routes. The tracer gas experiments plus air flow measurements can give answers to the spreading of toxic agents in subway stations but they can also be used to provide boundary conditions for CFD analysis of complete buildings and also validate the subsequent CFD results. They are also very useful tool for examining the dynamic interaction of the background air flow and the train induced flows in a subway system.

Pedestrian simulations were used to calculate evacuation times for possible escape routes. Designated evacuation routes in a multi agent simulation show the importance of a dynamic guiding system on the evacuation process. Combining these methods, an empirical investigation for different evacuation strategies can be analysed and assessed in respect to safety.

2.6 Evacuation of an underground station and evacuation simulation

An understanding of pedestrian movements is of major importance in the planning and design of subway systems for two main reasons. The first is that the highly directional movement of pedestrians can itself cause disturbances in the air flow; this effect has never been studied in detail. The second is the understanding of the response of pedestrians during emergency situations. Since the first quantitative approaches to pedestrian movement in the 1950s reported by Batty (2003), a considerable work has

been done in the field, from traffic like models (Blue, 1998) to queuing behaviour (Barnes, 1998). The Traffic Models have been criticised for excessive simplification of the environment and the motivation and goals of pedestrians.

An early example of the study of the evacuation of a subway station was performed by Proulx (1991) who used video recordings and observations to analyse the behaviour of passengers. Following the development of computer systems, VR and the interest in the built environment the simulation of pedestrian evacuation process in underground space has developed rapidly (Thompson and Marchant, 1995; Gwynne *et al.,* 1999; Chen and Zhan, 2008; Kuligowski, 2016). Two unfortunate incidents at Kings Cross station, a fire in 1987 and a terrorist bomb in 2005 which both resulted in loss of life stimulated interest in developing resilient evacuation strategies in subways. Models have been developed to assess preparedness measures for the emergency services to limit the loss of life and damage to property, and to improve the response phase of an incident in existing station (Castle, 2006). This has been further extended, (Junfeng, 2010; Shi *et al.,* 2012), as a method to evaluate station design from a safety and resilience aspect at the design stage.

Recent studies (Charlton, 2011; Giddings *et al.,* 2011; Horne *et al.,* 2014) have identified the commercially available software “Legion” as the ideally software for pedestrian simulation. Legion is the leader in this niche market. It can model pedestrian movement in detail to account for the impact of age, gender; health or industrial standard flow rate assumptions can be used.

Legion SpaceWorks simulates and analyses the movement of pedestrians within CAD defined environments and designed to reproduce the complex dynamics of multi-directional movement. The combination of intelligent entities and the richness of the modelling environment ensures that the collective behaviour of a crowd within a modelled venue emerges realistically from the activities of individuals. The software has an impressive track record of projects around the world and outputs have been validated against real-life measurements by customers and independent third parties (Legion Limited). Legion simulation model has been calibrated and validated using empirical data collected from around the world (Berrou *et al.,* 2007). It has been used to assess safety and security issues in rail and metro stations, for safety certification and to test evacuation scenarios analysis by several workers (Junfeng, 2010; Le Glatin *et al.,* 2014). Legion can also be interfaced with other software as has been shown by Liying (2010) who created a series of evacuation simulations by combining Legion with

the Fire Dynamic Simulator (FDS) when evaluating an evacuation of the Lingangxincheng atrium metro station of Shanghai.

2.7 Conclusion of Literature Review

This literature review has shown that it is possible to use virtual environment as a platform to pursue research into the dynamics of the airflow in subway systems. The utility of virtual environment lies in the fact that it can be used to display the results of complicated mathematical modelling to any audience but it can also be used as an information source or carrier for other simulation software. The point cloud generated by laser scanning a station can be used for developing CFD simulations of airflow and smoke dispersion and pedestrian evacuation simulations. This can be done for existing stations for which detailed drawings are not available but it could be developed at an early stage in the station design to inform designers and architects of the nature of the airflow in a subway station or system.

The behaviour of the airflow in a subway system can be likened to that in a cave system following the work of the Bochum group. This is perhaps a first step in understanding the temperature and velocity fields within and around a station can be to achieve better subway environments but there remain several key questions relating to the effect the background air flow, ventilation systems and train piston have on the temperature, wind speed, and air quality in subway stations. To proceed further and address some of these issues a program of study has been devised involving CFD modelling of the air flow in and around the Monument Station at Newcastle. These simulations on their own are insufficient to completely understand the situation in the station so the proposed research also includes tracer gas experiments in order to validate the CFD plus indicating how toxic agents would spread in the station and through the accompanying tunnels. This has been integrated with pedestrian simulations using the software Legion allowing to calculate evacuation times and exposure times for possible escape routes. The delivery of the pedestrian movement information by virtual environment will allow decision makers not conversant with normal computer graphic type displays, to comprehend key elements of design, safety, operations and security and be in a position to make decisions in an informed and objective manner. The speedy and safe evacuation of the subway system through the recognition of the most endangered places, an understanding of pedestrian behaviour and the directing of the rescue personnel to the most important places will be an important deliverable of this project.

The modelling of a subway station and adjoining tunnels has not been attempted prior to this work in this detail. This will be the first step in the development of an integrated simulation platform that may be developed into an early stage design tool for planners and architects responsible for subway system design.

Chapter 3. Research Methodology

3.1 Research design

The objectives of this thesis are addressed by providing a platform that promotes shared understanding, transfer of knowledge and expertise advancing the development of Subway Climatology. Of extreme importance is the presentation of information in a format that can be understood by non-experts as it is the subway system operatives that will have to make operational decisions in the event of an incident. It is important then that any information that is produced in this research is presented in a comprehensible format that will allow quick and accurate responses to be made. This is a natural extension of the OrgGaMIR (Pflitsch, 2010) project that showed the existence of the variable back ground air flow in a subway system but was not able to develop a method of enabling operatives to make decisions based on real time events. Also it could not be applied to additional stations without a great deal of extra work nor could it be used to predict the airflow in a station in real time or as a design tool for architects and station designers.

It can be appreciated from the above that this is a complicated and ambitious task. To put this into perspective the flow chart in Figure 11 has been produced to show how the different parts of this project are inter related.

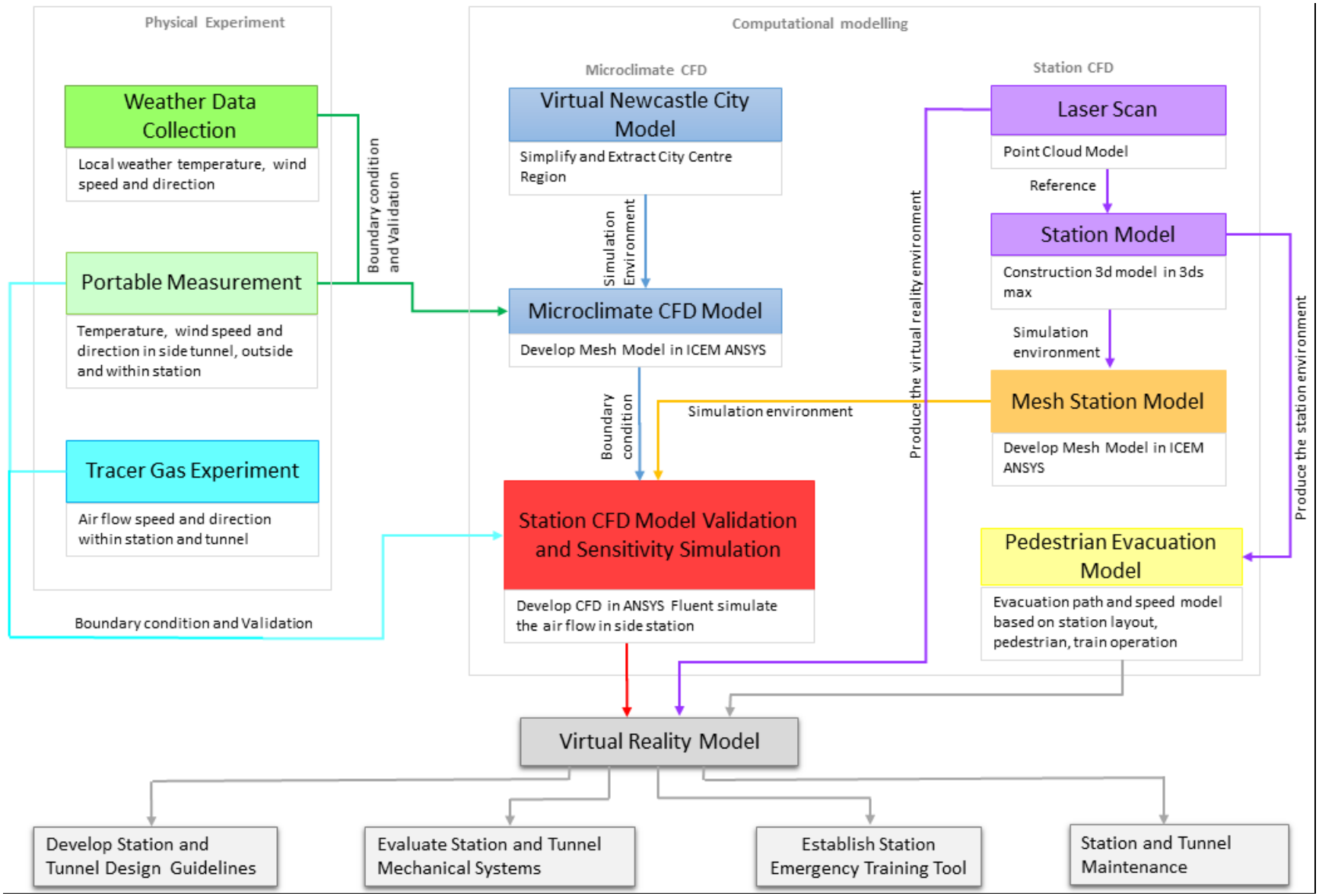

Figure 11: Research Method flow chart

This research has been divide to three parts which are brought together to produce an integrated design tool that will be useful to the key stakeholders in station design and subway operation improving the safety of the travelling public. The first part is the experimental measurements, shown in the left hand column of Figure 11. These physical experiments include an assessment of Newcastle city weather data collected from a nearby weather station (the top item in the column), the taking of measurements inside the station and at locations just outside the station exits using portable instruments (the second item in the column) and finally a series of experiments in which a tracer gas was released in the station, in a train passing through the station and at different locations in the subway system (the third item in the column). The tracer gas experiments were done in collaboration with the Cave and Subway Research Group of the Ruhr University at Bochum who provided the equipment and technical support for the correct running of the experiments. The main outcomes from this physical experimental part of the thesis are shown in Figure 11 underneath the boxes in the column appropriate to the activity and they are used as inputs to the next phase of the work as indicated by the labels on the connecting arrows. These experimental parts of the project furnished a preliminary understanding of the air flow in and around the station and provide data for use in the CFD simulation.

The second part was the virtual model development which is shown as the middle column in Figure 11. A modelling environment was created from the Newcastle Gateshead City Model to enable a CFD model of the local microclimate in the vicinity of the station. This was intended to investigate the impact of the buildings surrounding the station on air flow strength and direction at the station exits and provide data to inform a CFD model of the station created to examine the internal airflow. The development of the CFD model is shown in the right hand column. In the absence of and computer aided drawings of the station (which will be the same for the vast majority of existing subway station elsewhere) an efficient and straightforward means of generating a model environment was required. This was achieved by laser scanning the station and converting the point cloud thus created into a three dimensional model using the package 3ds Max and then into a CFD mesh that could be used in a CFD package. These steps are shown as the yellow boxes in Figure 11. The main elements of the three columns were then brought together to create a CFD model of the station using the CFD package ANSYS-Fluent. Information from the experimental measurements provided the input data for the CFD boundary conditions and enabled

the CFD output to be validated. An important part of this work was the creation of the CFD mesh in a quick and efficient manner and the establishment that the CFD results were not mesh sensitive. The output of this part which integrated all the aspects mentioned previously was the modelling of the air flow in the station to understand the nature of the airflow and the impact the outside climate has upon it. A sensitivity analysis was performed that established ways of controlling the airflow in the station. Finally, a Virtual model of the station was created which formed the link between the highly technical features developed so far and the subway operators and the Fire and Rescue personnel. This is shown as the main output of this project in Figure 11 as the horizontal box at the bottom of the figure from which are emerging boxes indicating additional tasks such as pedestrian evacuation, Fire and Safety training and the development of evacuation strategies which will all be of use to the Subway operating companies, station designers and architects and the Fire and Rescue personnel.

3.2 The research environment

To meet this end, the Monument Station at Newcastle served as a working laboratory in which air flow, temperature and humidity data were recorded continuously at specific places and other tests were performed to validate the CFD predictions. As discussed in section 1.2.1 the Monument Station was chosen because it is the largest station in Newcastle containing four platforms serving two tracks that are one above the other. The lowest track is the north–south track that serves the Central station in the south and the Haymarket station in the north. The east-west track serves St. James football ground in the west and Manors station in the east. The rails are all underground in this region of the rail system emerging over-ground at Jesmond Station in the north, on the Tyne valley crossing at the south and at Manors in the east with St James being a terminus, as shown in Figure 1.

The lower platforms are connected to the east west platforms by a pedestrian stair case and both sets of platforms are connected to the station concourse by means of escalators. The station concourse is situated underground around the base of the Grey's Monument at the top of Grey Street. Two exits from the concourse to the over ground streets are in place in Grey street and in Blackett Street. A third internal corridor links the station concourse to the nearby Eldon Square shopping centre.

The modelling of the airflow in the station will use a CFD platform in this work but the workers are mindful that this may not be the best platform to use with ongoing

advances in other platforms such as are used for computer games. As the Monument Station and many others that may be of interest were designed and built before the digital age and because the available drawings are insufficiently detailed a significant part of the work has been the creation of the files to perform CFD analysis. The CFD model will need to be validated by other measurements both in the station and over ground and boundary conditions were to be established.

The utility of virtual environments for this project became apparent through discussions with the personnel of the Northumbria University Visualisation Suite. Producing a laser scan of the station produces sufficient data that can be converted to the type of data files that can be used to develop the computational grid for the CFD analysis. Texturising the point cloud developed from the scans will also produce a virtual image that can be used for performing tests in virtual reality. For instance, the virtual model representations can be used as a training tool to familiarise the emergency services with the station layout prior to a rescue or it can be used to prepare maintenance crews to work in the tunnels. The data files can also be interfaced with other software, for instance, the Legion suite which is used to simulate evacuation situations in large buildings such as sports stadiums can be used to assess evacuation routes in a subway. Finally, the files can be interfaced with CFD modelling to consider the spread of smoke or toxic gas. The modelling environment for CFD analysis is shown in Chapter 6

To support this internal flow analysis, 3D Computational Fluid Dynamic models have been developed to simulate the local over ground microclimate in the vicinity of the station. The local weather pattern around the station portals has been examined and correlated to the readings of a local weather station. In addition, it was necessary to validate the CFD models by comparing the predicted results with local internal flows obtained from direct measurements of the air flow and from tests involving the release of a tracer gas SF_6 in the station.

The results from the tracer gas tests can also be combined with pedestrian movement simulation to assess the effectiveness of the current evacuation procedure of the station. In the wider context, this will produce information for architects and designers and metro system operators that will enhance the decision making process with regard to the initiation of effective measures to minimize the impact of smoke or the release of a toxic agent within the subway system. It will develop guidelines for the structural

design of subway systems to minimize the dispersion of dangerous substances and promote safe and effective evacuation strategies. The tool developed can be deployed to assess existing stations but can also be applied to create new designs, based upon modern CAD files, so that elements that can hinder evacuation routes or put the travelling public in danger can be removed before the construction begins. A further application in the wider context it will be useful for energy audits of the station buildings.

3.3 Methodology Boundaries and Limitations

Prior to conducting this research, it is important to identify the boundaries and limitations that the local environment imposes on the research. This will produce a clear awareness on the scope of research, allowing the focus and boundaries of the research to be established at an early stage.

This research aims to develop a method to evaluate and model the air flow in and around an underground station. Thus the model has been designed specifically for air flow simulations and using appropriate CFD packages with associated turbulence models to deliver quick solutions with an appropriate degree of accuracy for this problem. The modelling of the air flow in the station is the main objective of this work. The modelling of fires and smoke dispersion have been considered in terms of this being a natural development of this work but not been undertaken here. A necessary condition however is that the computer platform that is used need to be compatible with fire simulation packages.

The use of Computational Fluid Dynamics (CFD) to study physically complex built environments requires models to be validated by experimental data (van Hooff and Blocken, 2012). CFD studies of natural ventilation of stations in a city centre should consider both the wind flow pattern around the station and the airflow within the station driven by tunnel and buoyancy effects. Experimental validation of the CFD is problematic because of a limited number of measurement points and the high variability of the data due to the changing local meteorological conditions. The validation has used an averaged value within period of measurement time (within 1 minutes/within 10 minutes). The CFD simulation detail of city centre and station has been discussed in Chapter 7 and Chapter 8 respectively.

The accuracy of the experimental measurements taken in and around the station was limited to the accuracy of the measurement instruments employed. Also the number of

data sets obtained were restricted by time and the data was not collected fully in a synchronous manner. Thus the data is time averaged but considering the time constants and the length scales of the station and the surrounding buildings it is considered that this is a valid appropriate method of data collection enabling the response of the station to external factors to be understood.

This chapter has provided an overview of the methods and approaches adopted to achieve the research objectives and the overall aim of this research. Justifications and reasoning for the selected methods have been reviewed and discussed. The following chapters cover these areas in greater detail.

Chapter 4. Development of Station Model

4.1 Introduction

The experimental work carried out in this research performed during this project served two purposes both connected to the CFD modelling. The first purpose was the generation of the data files through the laser scanning of the station to establish a three-dimensional model of the station. To provide a model environment to enable the CFD modelling of the internal airflow to take place. The second purpose was the measurement of airflow inside the station and in the surrounding locality in order to create the input data files for the CFD modelling and also to validate the CFD results which are presented in Chapters 5 and 6. These pieces of work included direct measurement of the airflow in the station, measurement of the airflow characteristics in the vicinity of the station surrounds and the comparison of this data with information recorded in a nearby weather station. A very detailed study of the internal airflow was also conducted by the release of a tracer gas in the station. The objective behind this test was to provide input data to support the CFD modelling but also to consider the residence time and concentration of a toxin in the station and examine the impact this has on the evacuation of passengers from the station. The following sections of this chapter provided details of this experimental work. The remainder of this chapter demonstrates the laser scanning of the station and the process required to develop this into a polygon model for the CFD modelling.

4.2 Laser scanning

A full laser scan of the public areas of the Monument Metro Station which contains 68 scans has been produced in two nights in September 2014. The regions scanned included the four platforms and tunnels in two different levels, the concourse area, the escalators linking the platforms to the concourse, the stairs between the different platform levels and part of the surrounding building in the vicinity of the station entrances and exits.

A FARO Focus3D scanner was chosen to do this work. This is a high-speed Terrestrial Laser Scanner (TLS) offering the most efficient method for 3D measurement and 3D image documentation. Multiple scans from different positions can then be automatically placed to create a cohesive point cloud, resembling an exact measureable copy of even the most complex and large scale geometries. The scanner has an accuracy of

± 2mm and a measurement speed of 976,000 points/second. A reference of single scan using FARO Focus 3D in 1/8 resolution which contain 10.9 million points, 12,272 mm/10m point distance takes 3:44 minutes.

Compared to other available scanners the FARO Focus provides the most efficient method for 3D measurement and 3D image documentation for the range within 40m which is most suitable for scanning the interiors of building. This 3D laser scanner produces dense point clouds containing millions of points that provide detailed 3D colour images. The accompanying software “FARO SCENE” processed and managed the scanned data and automatically placed and registered multiple scans from different positions to produce the point cloud data, which was then used for 3D visualization or as a reference for modelling, meshing and exporting into various formats.

An example of the textured point cloud data of the passageway between platform 1 and 2 is shown in Figure 12 and Figure 13. The white sphere in the centre of the picture is for registration purposes.

Figure 12: The scans are register and positioning by recognition the reference objects placed during the scanning

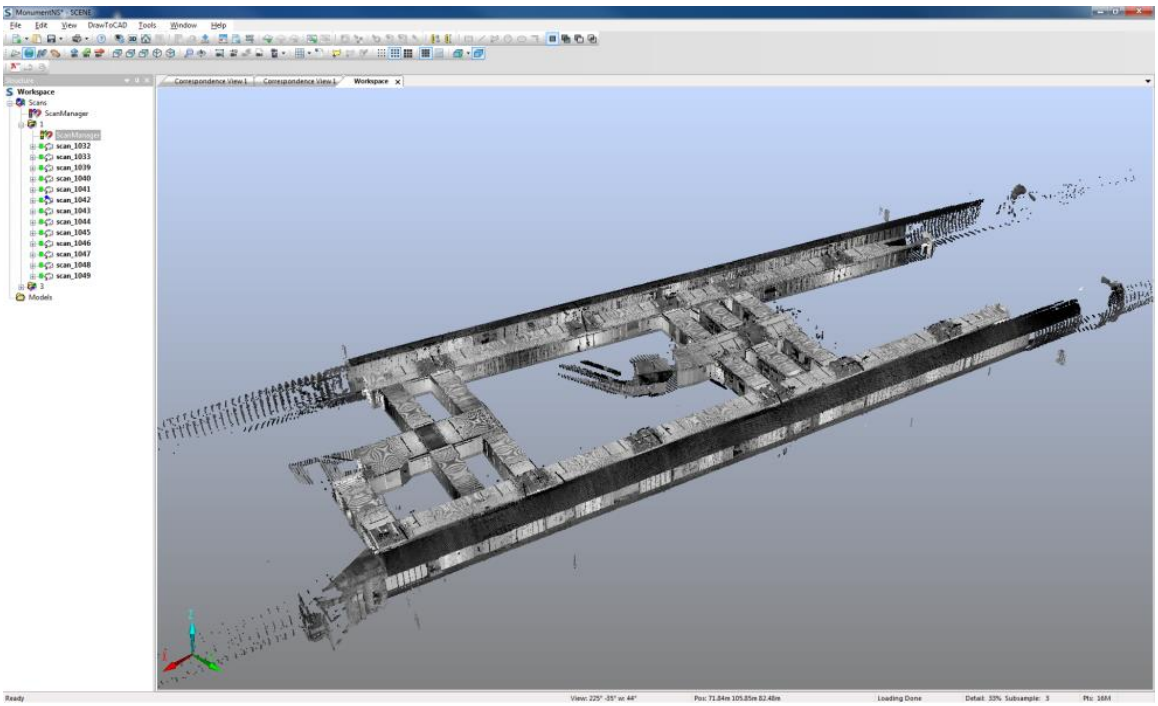

Figure 13: SCENE the documentation software for FARO's 3D laser scanner

4.3 Process point cloud data

The full laser scan of the Monument Metro Station was processed FARO SCENE which is the documentation software for FARO's 3D laser scanner (Faro.com, 2013). This point-cloud data based software takes data from simple measurements converting it to 3D visualizations that can be exported into various point cloud and other modelling based formats. Once SCENE has registered the scan data, it can commence evaluation and further processing right away as shown in Figure 14 and Figure 15 which show the complete station point cloud model. Figure 16 is a perspective view of Monument Metro station on the city centre map which shows the position of the underground structure.

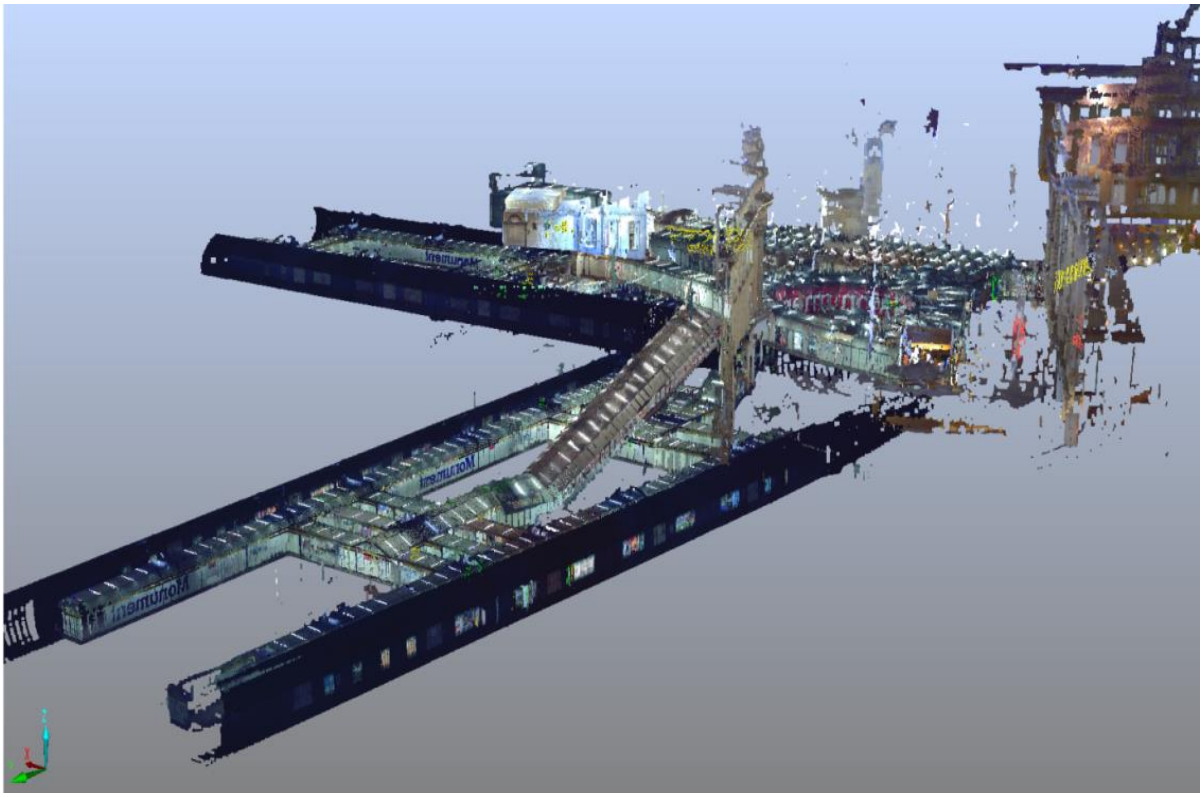

Figure 14: Registered Point Cloud model of Monument Metro Station (1)

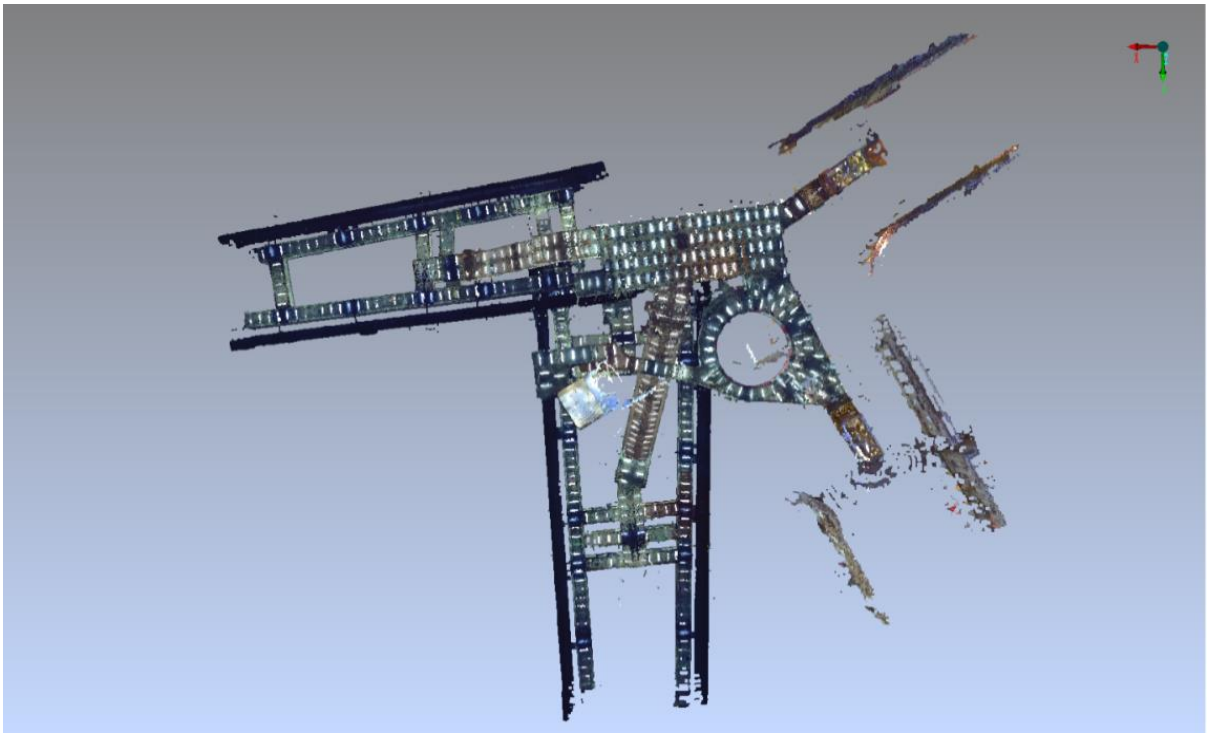

Figure 15: Registered Point Cloud model of Monument Metro Station (2)

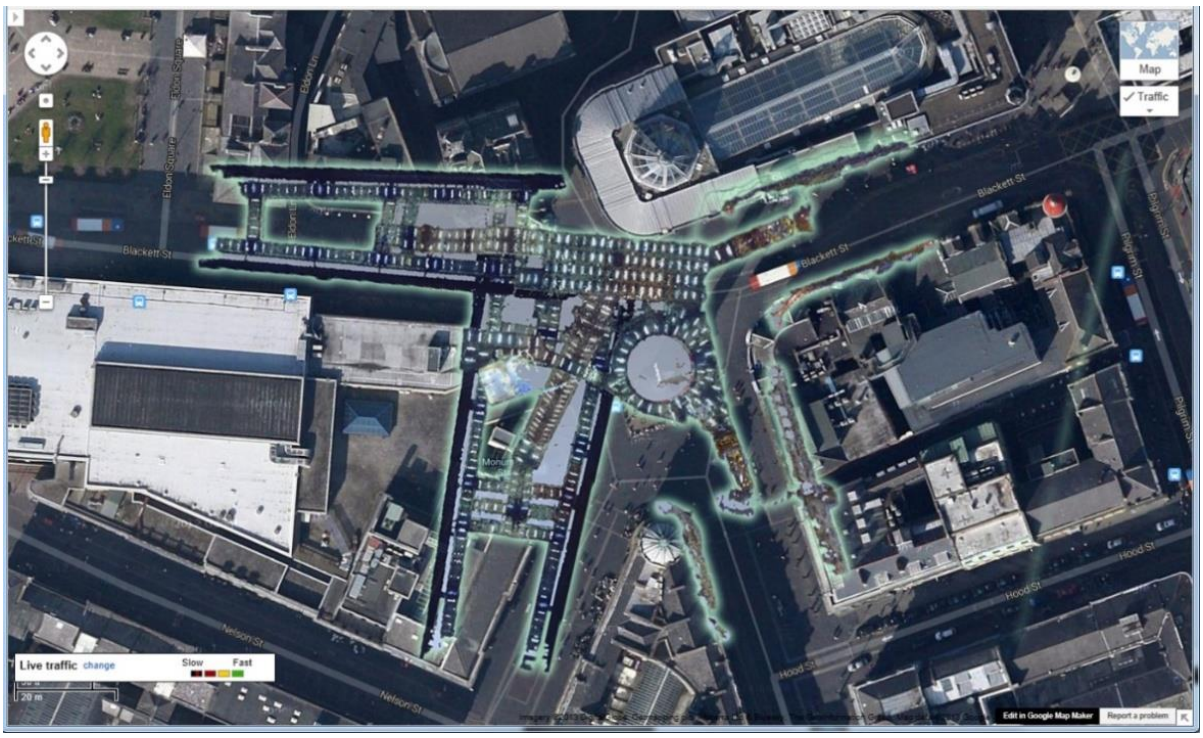

Figure 16: Perspective view of Monument Metro station on the map (GoogleMaps, 2013)

4.4 Development of station 3D model

The polygon models of Monument station were developed by referencing the point cloud station model. There are several software programs that could be used to achieve conversion from point cloud to polygon models such as 3ds Max (Autodesk.co.uk, 2013), Geomagic Studio (Geomagic.com, 2013), VR Mesh (Vrmesh.com, 2003), CATIA (Systèmes, 2002-2014), Certainty 3D (Certainty3d.com, 2013) and Mesh Lab (Cignoni, P., 2013). A review of these software packages indicates that there are two main methods to achieve the modelling. These are automatic and manual operation. Geomagic Studio is an automated complete toolbox for transforming 3D scanned data into highly accurate surface, polygon and Native CAD models. However, a test of transforming one 3D scan required 1 hour to complete one scan which would require an excessive amount of time to process the complete station scans. The automate model convert method could produce a highly accurate model but the degree of detail is unnecessary for this research so this approach was not adopted.

An alternative manual operation was conducted using the package 3ds max which contains a point cloud plugin called Clouds2Max which provides a simple solution for importing point cloud data into 3ds Max. This method produced polygon models with

low noise which can satisfy the accuracy requirements of CFD models and avoid unnecessary calculations. An exercise in which 10 scans were processed in this way showed that this manual method was much quicker than the automatic method using Geomagic Studio. Comparing the output accuracy the manual model give a similarly accurate polygon model in a shorter time. A simple polygon model in 3ds Max of two tunnels and platforms located on the same level is show in Figure 17 and Figure 18. The whole station construction line modelled by the point cloud is shown in Figure 19, Figure 20 and Figure 21.

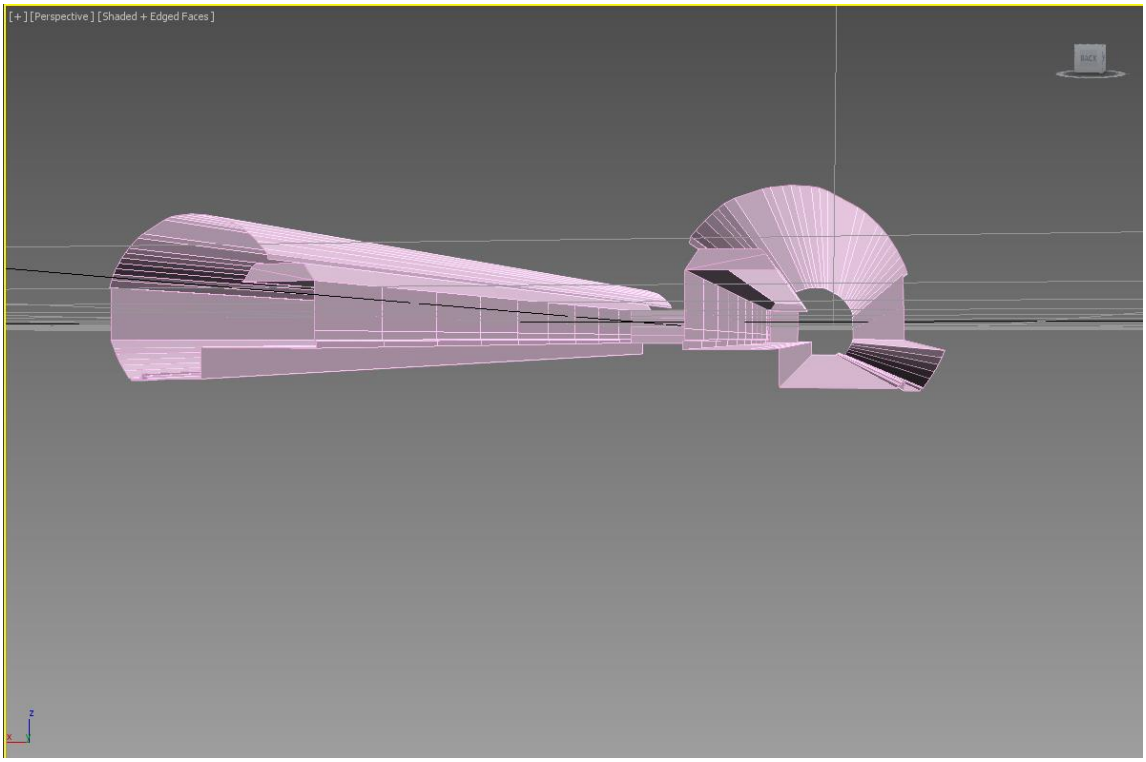

Figure 17: Model of two tunnels and platforms located in 3ds Max (1)

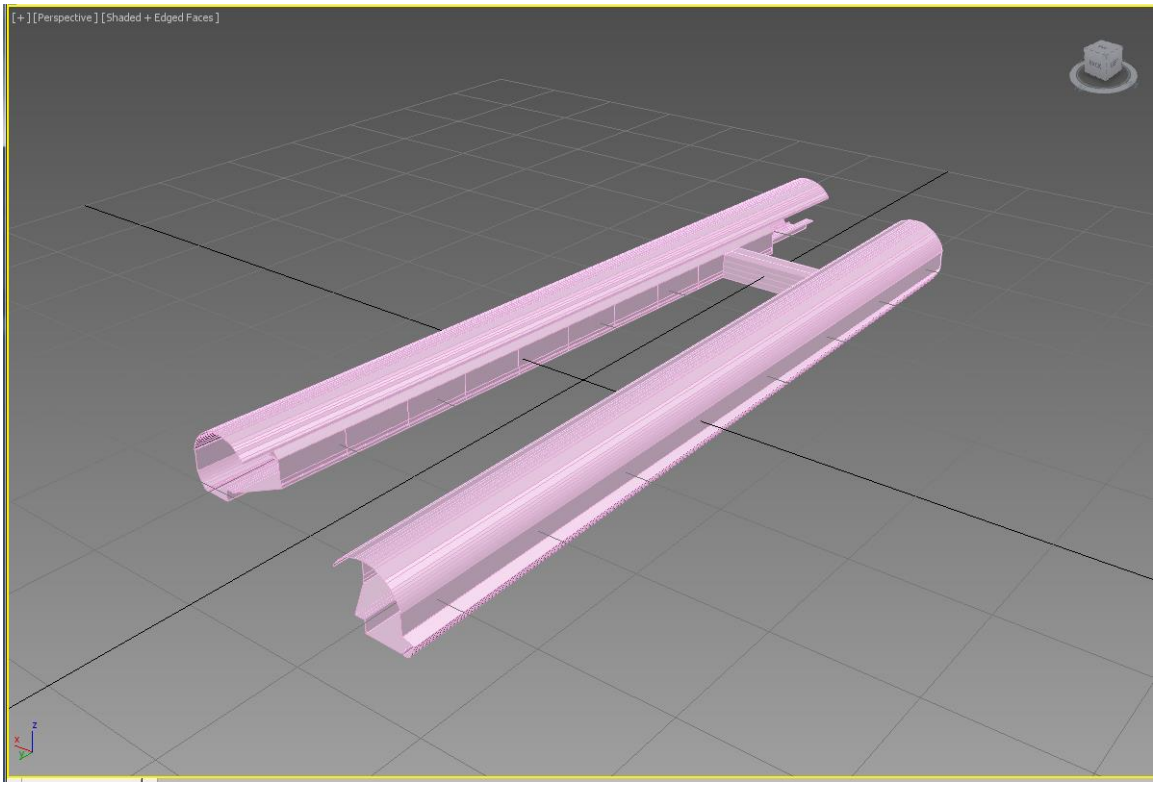

Figure 18: Model of two tunnels and platforms located in 3ds Max (2)

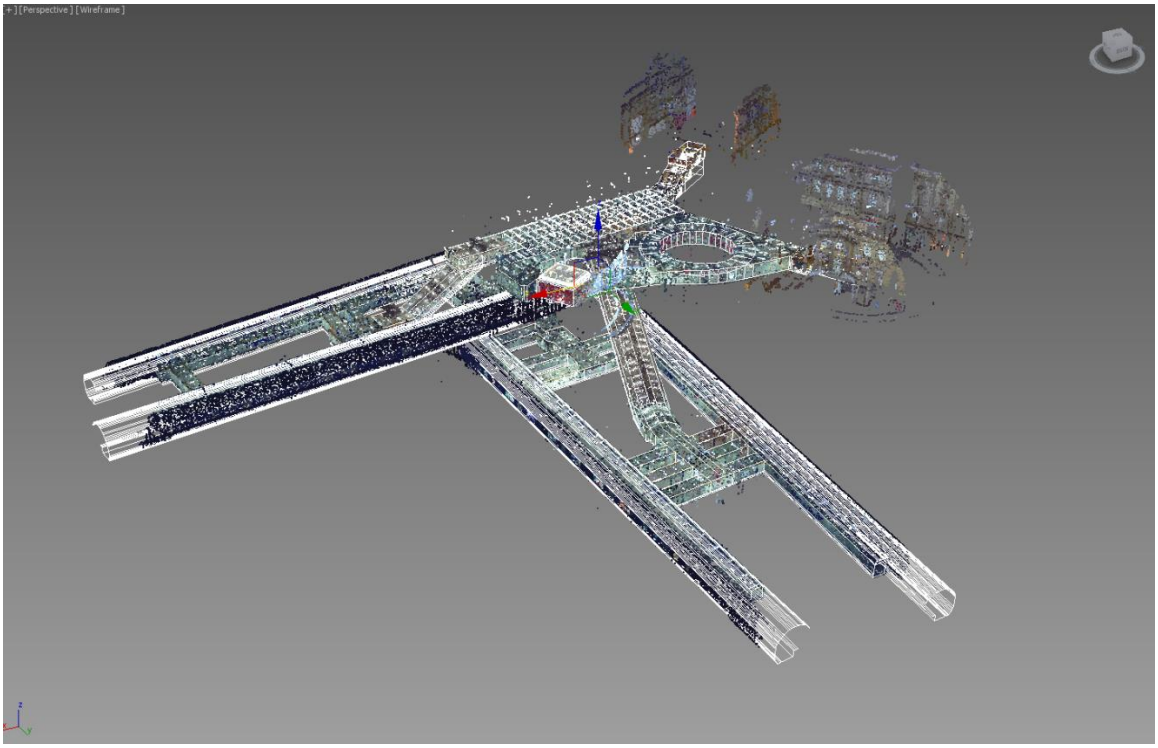

Figure 19: 3D model develop from laser scan and laser scan model of Monument Metro Station

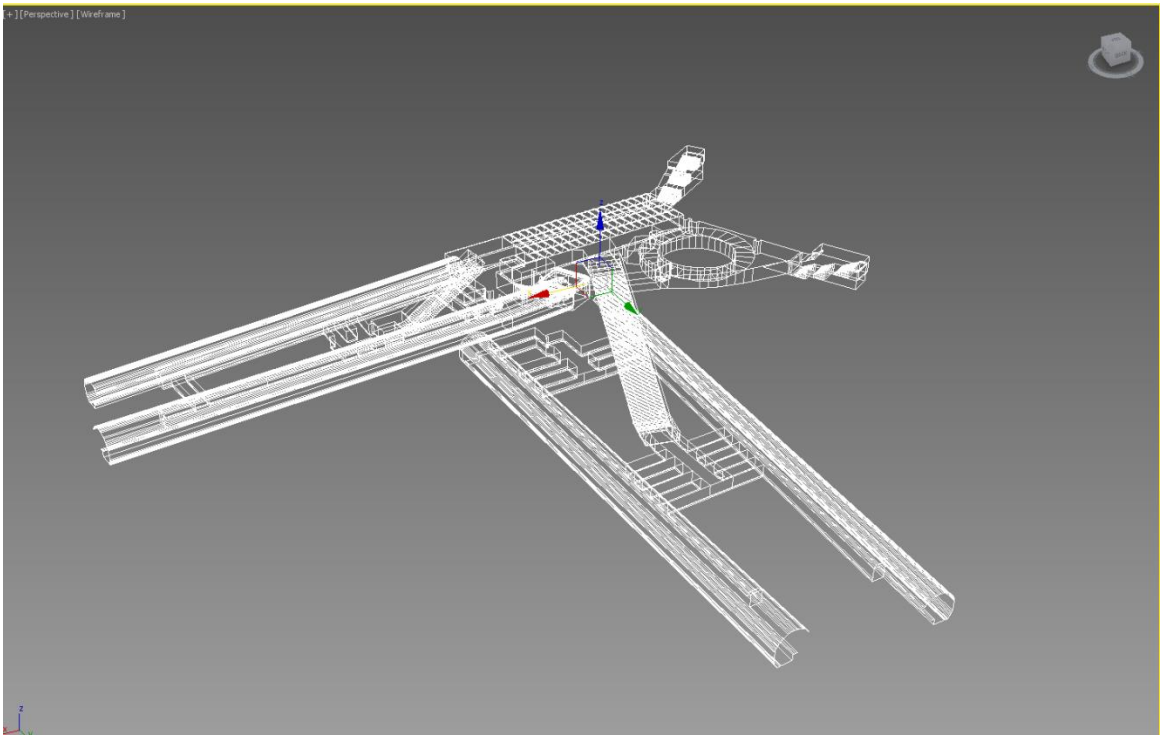

Figure 20: Completed 3D model develop of Monument Metro Station (1)

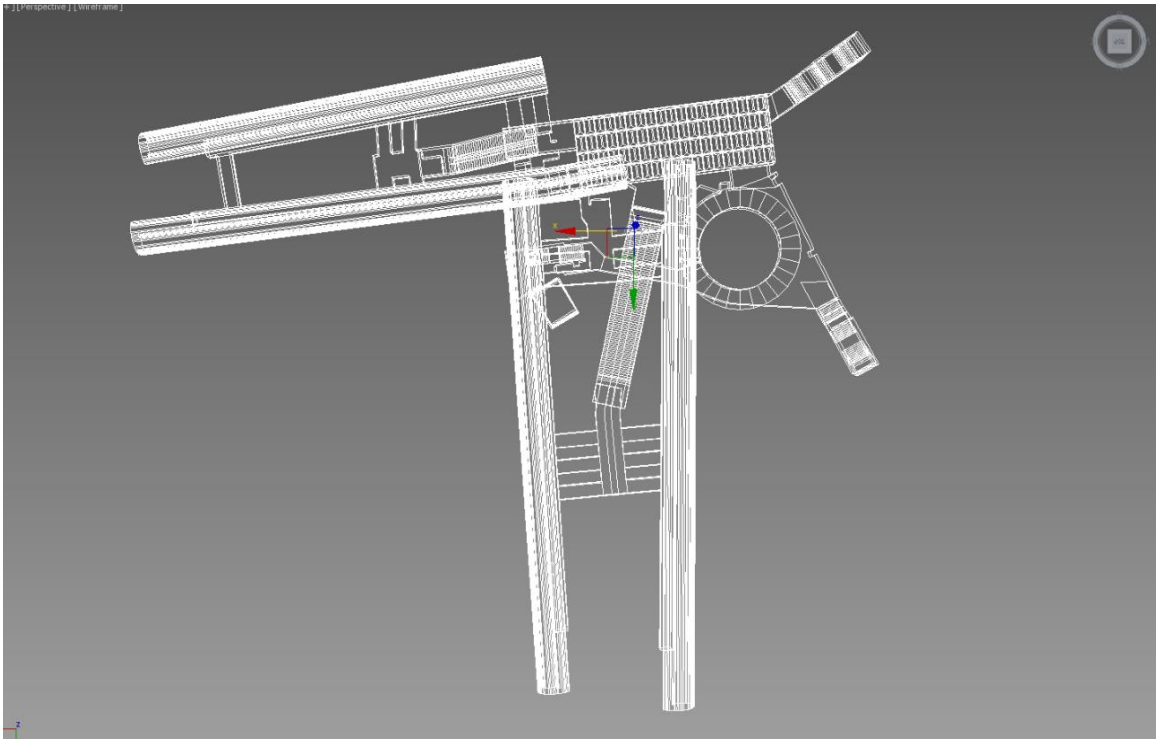

Figure 21: Completed 3D model develop of Monument Metro Station (2)

The point cloud model and polygon model in 3ds max could be rendered as a walkthrough animation or further virtual reality purposes such as pedestrian modelling using the Legion software. The polygon model in 3ds max can be exported as IGES (*.igs) and SAT (*.sat) format models which can be interfaced to ANASYS as input data for generating the CFD mesh models. In this respect it is a very useful piece of software

as far as this research is concerned and forms the backbone of the CFD modelling elements of this work.

4.5 Conclusion

Laser scanning is a well-established technique in many different activities and it is a multitude of visualization, animation, rendering and mass customization applications. A polygon model of the Monument station has been successfully produced by adapting a point cloud model produced from laser scans. This in an effective method to produce an accurate and smooth polygon model which will satisfy the accuracy required of CFD modelling. This is also a very effective method to produce a visual environment for further analysis or work. This is a technique that can readily be used for existing stations when architectural drawings or CAD files are not available to be used to develop the CFD model. This model environment enables the CFD modelling of the internal air flow and pedestrian evacuation simulation to take place as described in Chapter 8.

Chapter 5. Air Flow and Temperature Measurement

5.1 Introduction

The measurement results described in this chapter has used three types of measurements i.e. those taken from instruments that had been installed in the station for several years collecting long term data (Pflitsch, 2012), direct measurements using hand-held portable instruments and measurement taken by temporary installed loggers collecting air flow and temperature characteristics of the station surroundings. All these three types of measurements were taken inside the Monument station and at adjoining stations with the external environmental conditions being obtained from data recorded in a nearby weather station.

This chapter discusses the air flow and temperature measurements carried out in the tunnel, outside station and inside station to investigate the existing conditions in these locations. The previous study of the mechanical ventilation and gate operation effect to the background airflow and temperature using ultrasonic anemometers installed inside the tunnel to the Monument Station is described in Section 5.2. The weather data collection mothed and partial data at the period coinciding of tracer gas will then carried out in Chapter 6 are demonstrate in section 5.3. The weather data related to experiment air flow outside Monument Station and measured by portable instrument is described in Section 5.4.1. While the internal air flow measured using the same procedure is described in Section 5.4.2. Finally, section 5.5 analyses the temperature variation at each side of the underground station in the entire North–South tunnel and each side of Monument Station in the East-West tunnel.

5.2 Long Term Air Flow Measurements in Tunnel

This measurement result has been analysed by Pflitsch *et al.* (2012) as part of a preliminary study of the station background current and factors such as mechanical ventilation, entrance gate operation and train operation that could have an impact on temperature and air flow as discussed in Chapter 1. Ultrasonic anemometers have been installed inside the tunnel at Monument Station, central station and Haymarket Station since 2009 to record long term measurements of the wind speed inside the tunnel as shown in Figure 22. This data was used for establishing the initial starting and boundary condition of the station CFD modelling. The specification information of

the Ultrasonic Anemometers installed inside the tunnel at Monument Station listed in Table 3.

Figure 22: Ultrasonic anemometers install in the tunnel

More data representing the air temperature and flow can be seen in Figure 23, Figure 24 and Figure 25. In addition, measurements have been made with hand held instruments at specific times and locations in the station. These included measurements of humidity, wind speed and direction at 15 different locations (as shown in Figure 29) inside the Monument Station. These measurements were taken at regular 2-3 day intervals from October 2013 to January 2014.

Measuring Range	
Wind velocity	0 - 45 m/s
Wind Components	- 45 - + 45 m/s
Wind Direction	0 – 359 ^{o}
Temperature Range	- 30 ^{o}C to + 50 ^{o}C
Accuracy	±3% fsd ±1.35 m/s
Measuring Resolution	
Velocity	+/- 0.01 m/s
Components	+/- 0.01 m/s
Wind direction	+/- 1 ^{o}
Temperature	+/- 0.01 K
Time Resolution	
Sampling Rate	0.004 to 25 Hz
Averaging Interval	1 to 65535 samples

Table 3: Specification of the Ultrasonic Anemometers

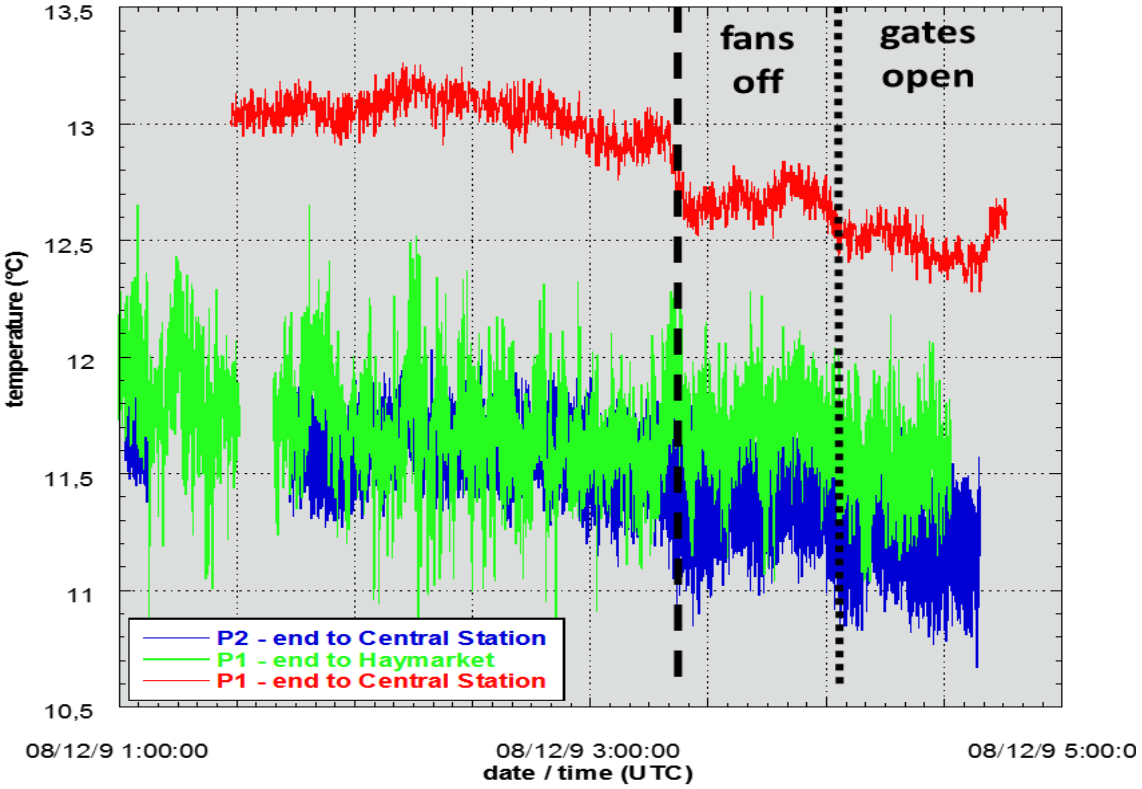

Figure 23: Temperature graph impact by fan and gate operation (Pflitsch *et al.*, 2012)

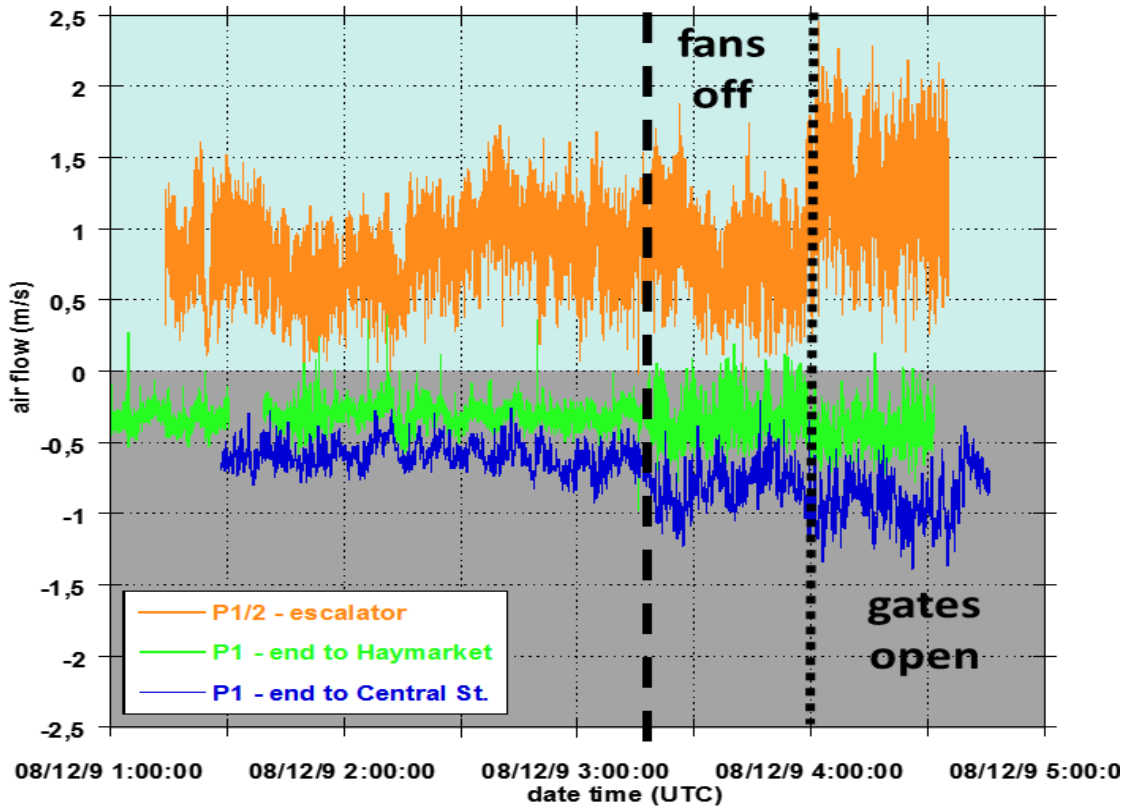

Figure 24: Air flow speed graph impact by fan and gate operation 1 (Pflitsch *et al.*, 2012)

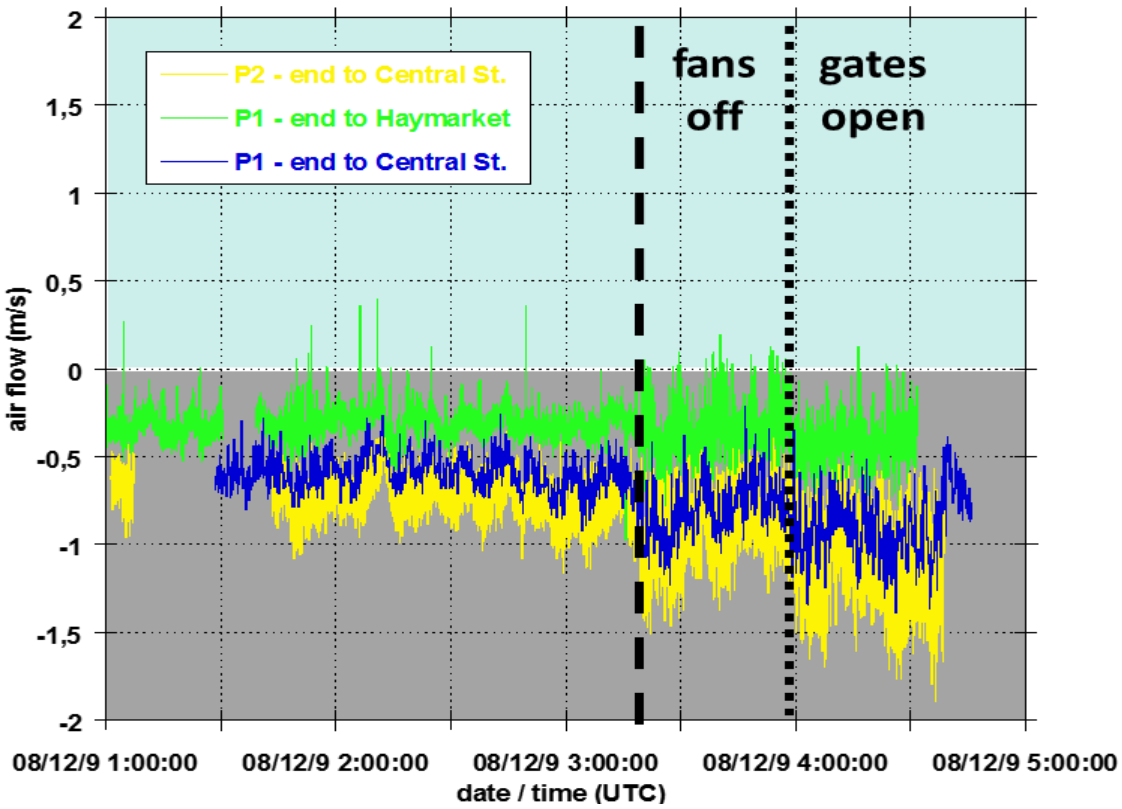

Figure 25: Air flow speed graph impact by fan and gate operation 2 (Pflitsch *et al.,* 2012)

5.3 Weather Data Collection

In order to produce an accurate CFD model of the station a simulation of the local micro-climate in the vicinity of the station is required. To this end city centre weather data was collected and used as an input. The data was obtained from a weather station located at the roof of the Ellison Building situated at a distance of approximately 600 meters from the station. In the following this is designated as data 'C003'. The weather station 'C003' has been operational since August 2008 but a complete set of recordings from that time is not available. The data includes temperature, pressure, humidity, wind speed and direction measured every 10 mins. The exits of Monument Station are located at street level and are influenced by human activity and the so called urban heat island effect so a calculation is required to factor in these features to determine the micro-climate at this location.

The primary source of energy in the urban environment is the sun but energy can be increased by human activity intensifying the urban heat island effect. This heat comes from activities such as transport, industrial processes and air conditioning. A further minor contributing factor to the urban heat island is air pollution. This is due to heavily

polluted atmosphere that may act to produce a local greenhouse effect. The maximum effect of the urban heat island causative factors described above is achieved in calm clear conditions during very warm periods with a plentiful supply of solar radiation during the day (Greater London Authority, 2006). An example of this is shown in Figure 26 which shows the distribution of surface temperature for London at 21:30 hrs on August 7, 2003. The elevated temperature of the centre of the city above the surrounding countryside by 4 to 5^{o}C is clearly illustrated.

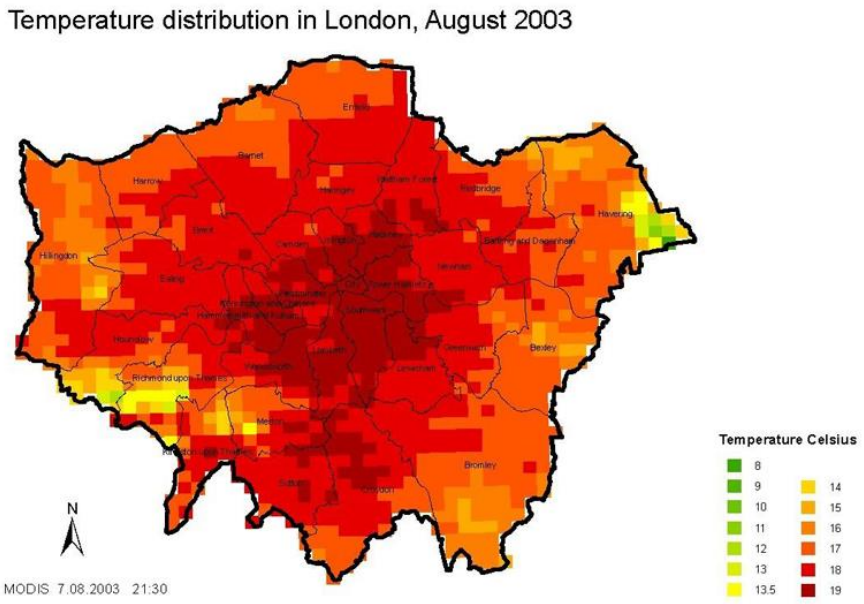

Figure 26: Distribution of surface temperature for 1km2 grid squares across London at 21:30hrs on August 7, 2003 (Greater London Authority, 2006)

Research performed by Wilby (2005) suggests that the most intense heat island effect develops in summer. He recorded an average peak temperature difference of 3^{o}C over the summer of 1999. It is therefore necessary in this work to recognise that a temperature difference will exist between the weather station and the Monument Station and to take this into account.

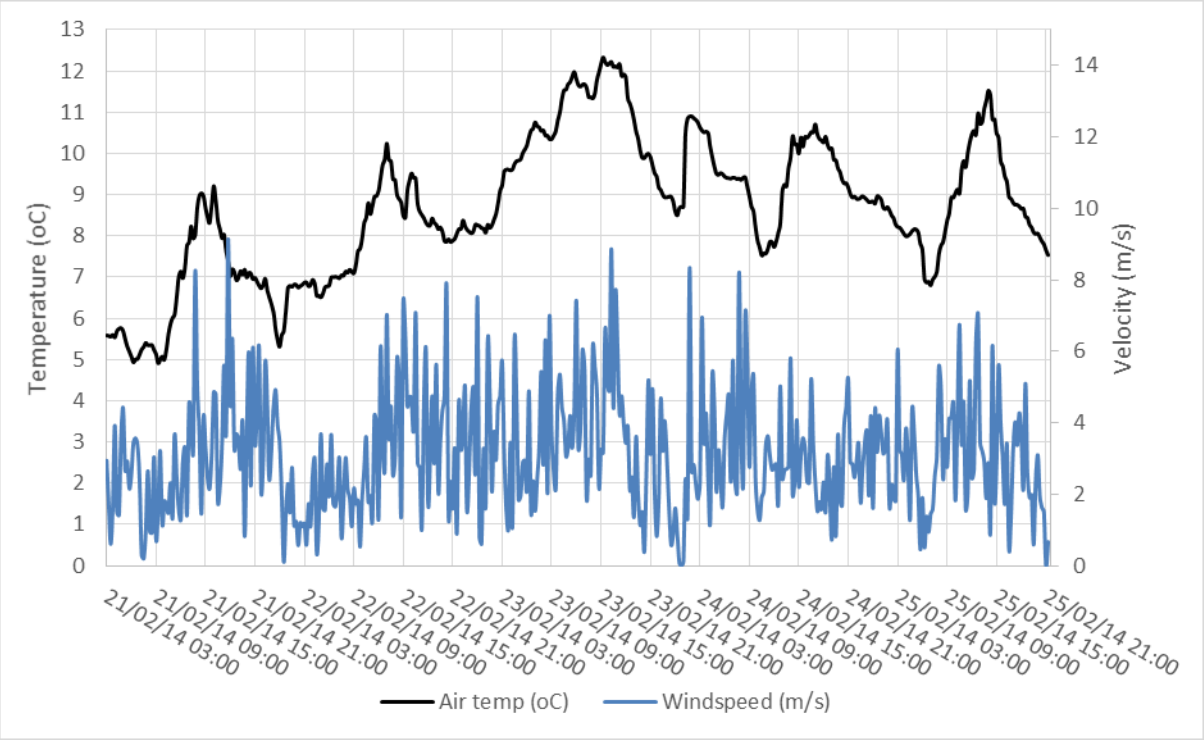

Figure 27: The local weather profile at the tracer gas experiment.

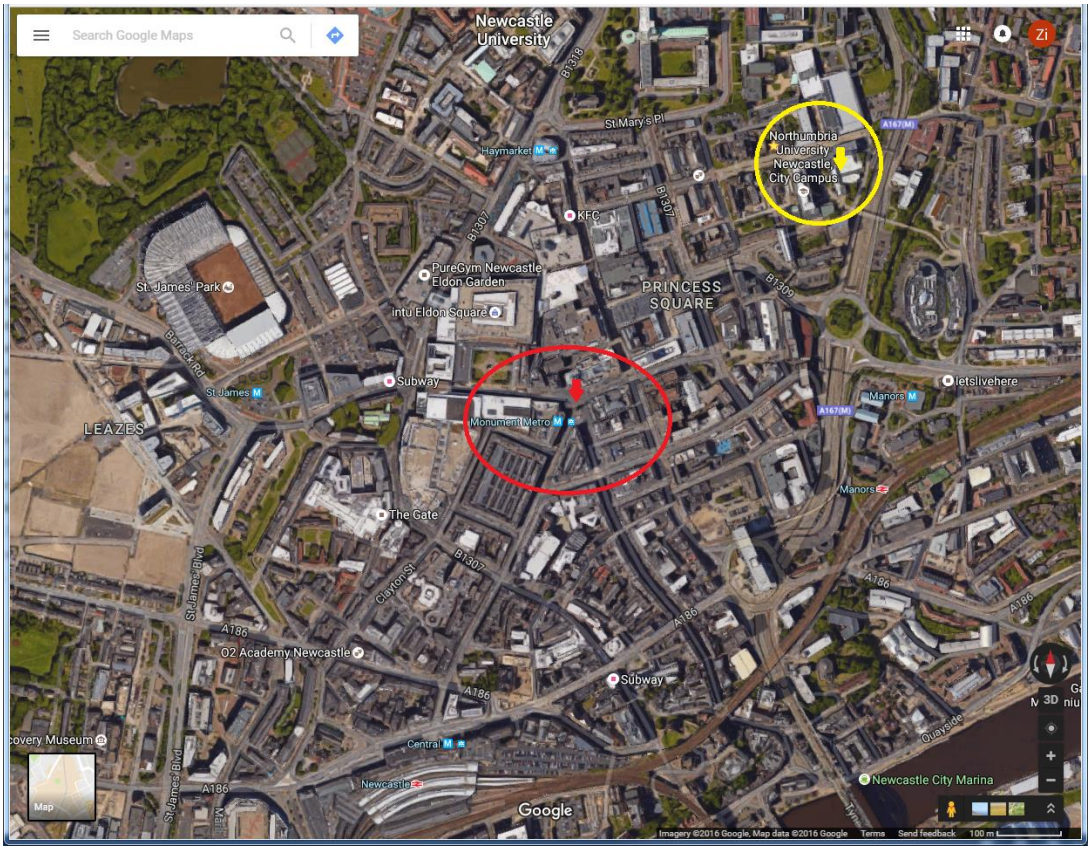

Figure 28: Location of the Monument station and weather station (GoogleMaps, 2013)

A sample of the data collected from the weather station is shown in Figure 27. This weather station location is shown as a yellow probe and Monument station is the red probe in Figure 28. The data shown in Figure 28 corresponds with the period when measurements were also being taken in the tunnel (described in section 5.4) and the tracer gas experiment conducted in the station (described in section 5.5). It can be observed that the temperature and wind velocity is higher in the daytime than at night. The weather data collected was compared with the external airflow outside the station exits taken with portable equipment. The weather data and the external air flow measurements were used to verify the microclimate CFD model described in Chapter 6.

5.4 Portable Air Flow Measurements

In order to investigate the air flow pattern and speed inside the station and at the exits to the surrounding urban landscape, measurements were taken using portable devices. Specifically temperature, air flow speed and direction at the station platforms, corridors, escalators and stairs, the concourse area and Exit/Entrances were measured for three months during different times of the day. The measurements were taken at the location shown as a red point in Figure 29. These portable measurements also provided information about the piston effect of the trains when they arrived and departed the station and provided a valuable insight into the speed and sensitivity of the flow pattern.

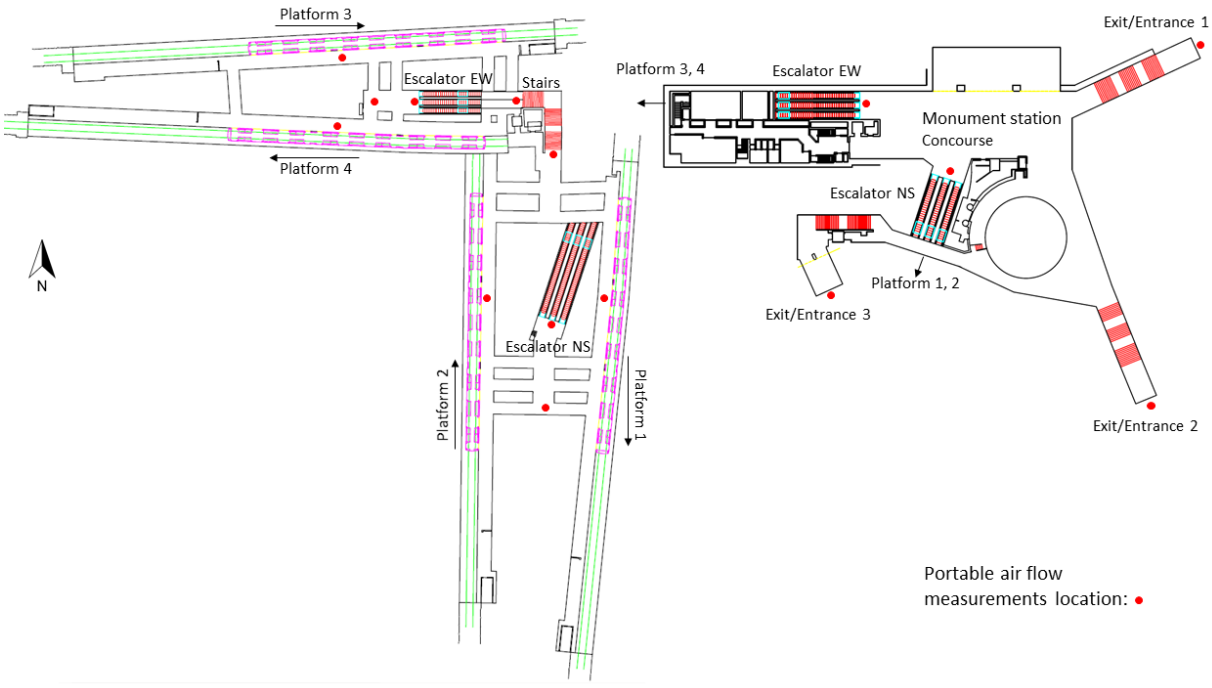

Figure 29: Location of the measurement point around the Monument Metro Station

Three measurement points were chosen at street level just outside the three exit/entrances as shown in Figure 30. The red rectangle indicates the Exit 1 location, which is in the middle of an East-West street that was busy with traffic. The triangle is showing the location of Exit 2 which was located at a north-south pedestrianised street. The cross shows the location of Exit 3 which was at a junction with the shopping centre and is covered by the shopping centre entrance. The measurements indicated that the air flow at these points was very variable so minimum and maximum values were recorded.

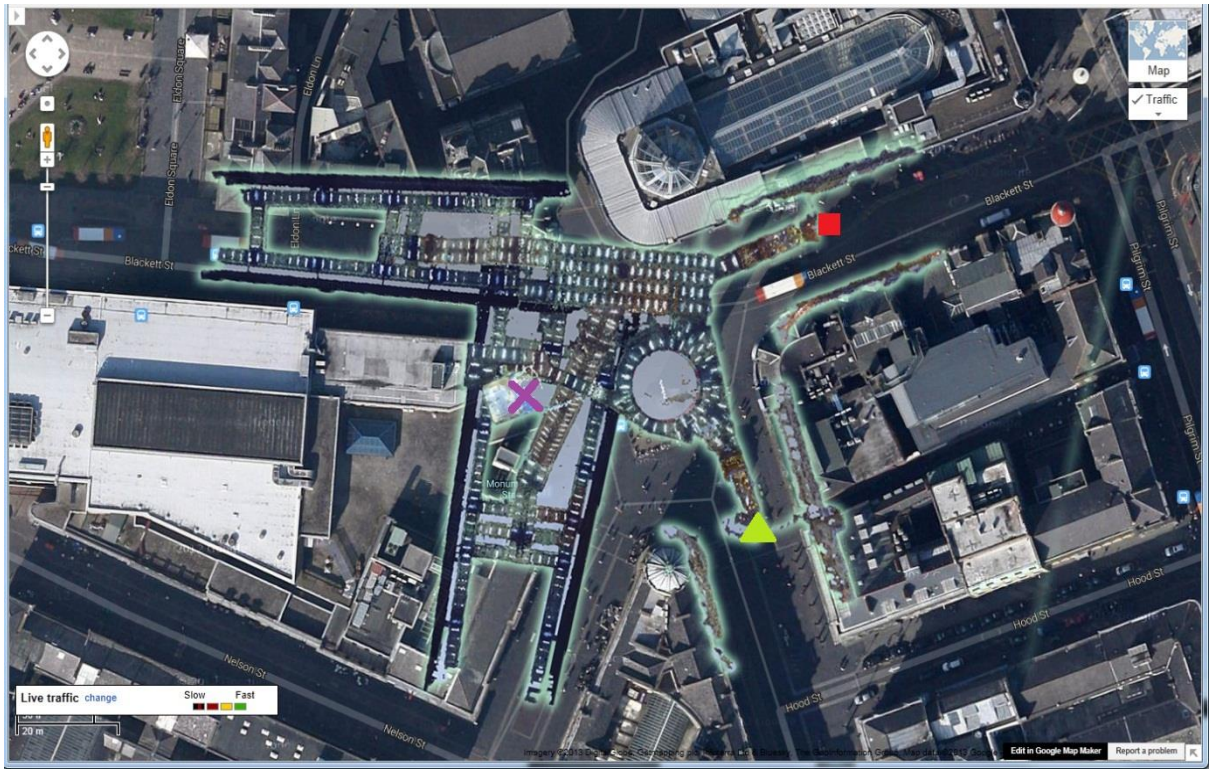

Figure 30: Location of the three measurement points at the street level (GoogleMaps, 2013)

5.4.1 External air flow

Figure 31 to Figure 36 show the weather data collected from the Ellison building compared with the external airflow measurements taken at the three Exit/Entrance at Monument station using portable equipment in October and November 2013. The data from the weather station was recorded at 10 minute intervals. Figure 31 and Figure 32 show that the temperature at the weather station is always lower than that at the station exits from 0.2ºC up to 2.5ºC. These two graphs show a strong correlation between the weather station data and the recorded data.

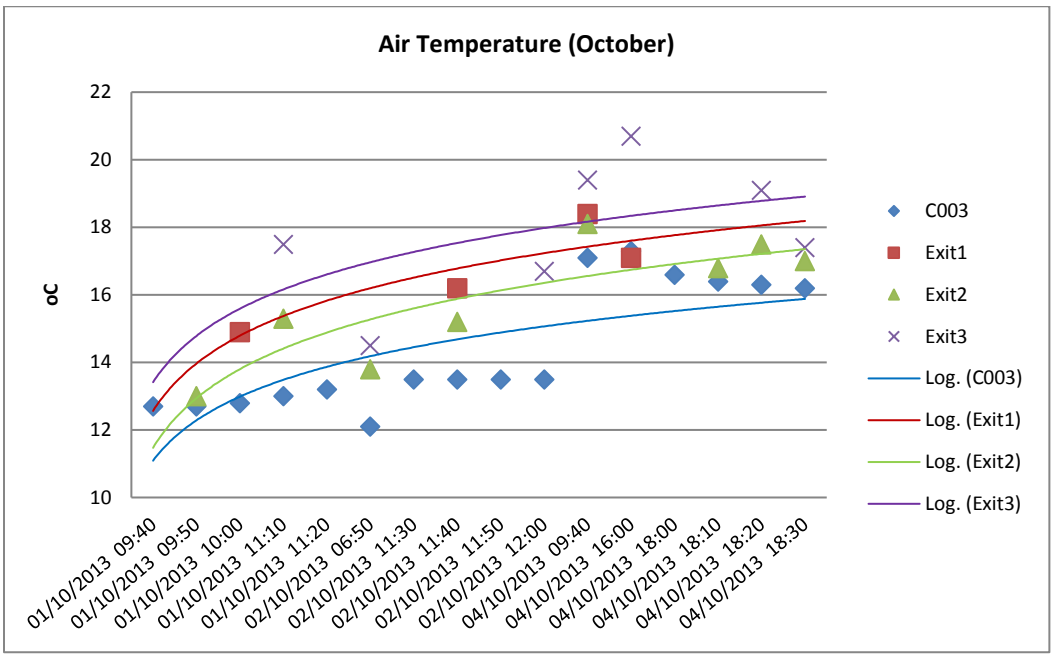

Figure 31: Measurement temperature, weather station data and trend line in October 2013

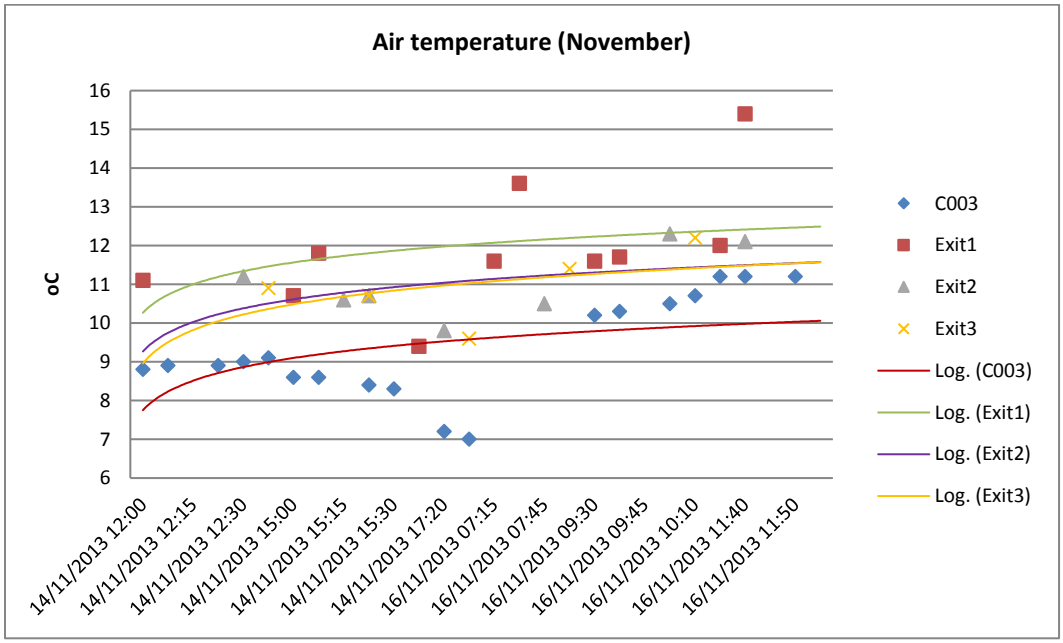

Figure 32: Measurement temperature, weather station data and trend line in November 2013

The graphs in Figure 33, Figure 34, Figure 35 and Figure 36 show the wind speed correlation between the weather station data and the three exits of the station, the wind speed at the weather station is generally higher than air flow at the station exits. However, this only shows the correlation of the recorded speed. Wind direction and wind pressure also play an important role if the airflow is outwards or inwards to the station. Further analysis of microclimate modelling has been discussed in Chapter 7.

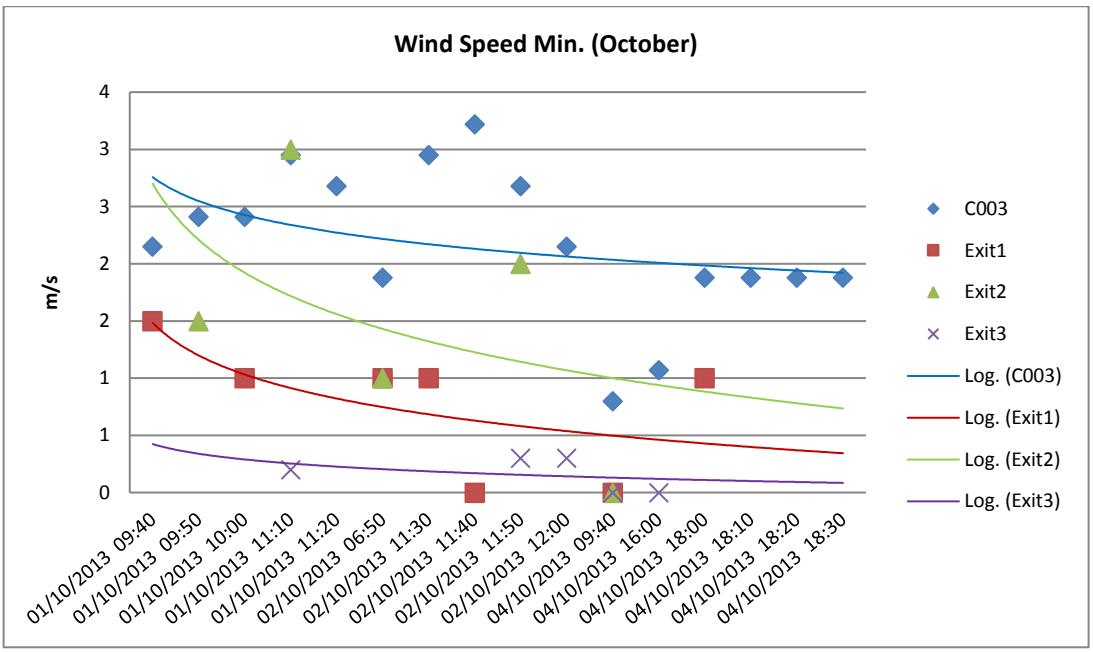

Figure 33: Measurement of minimum wind speed and trend line at October 2013

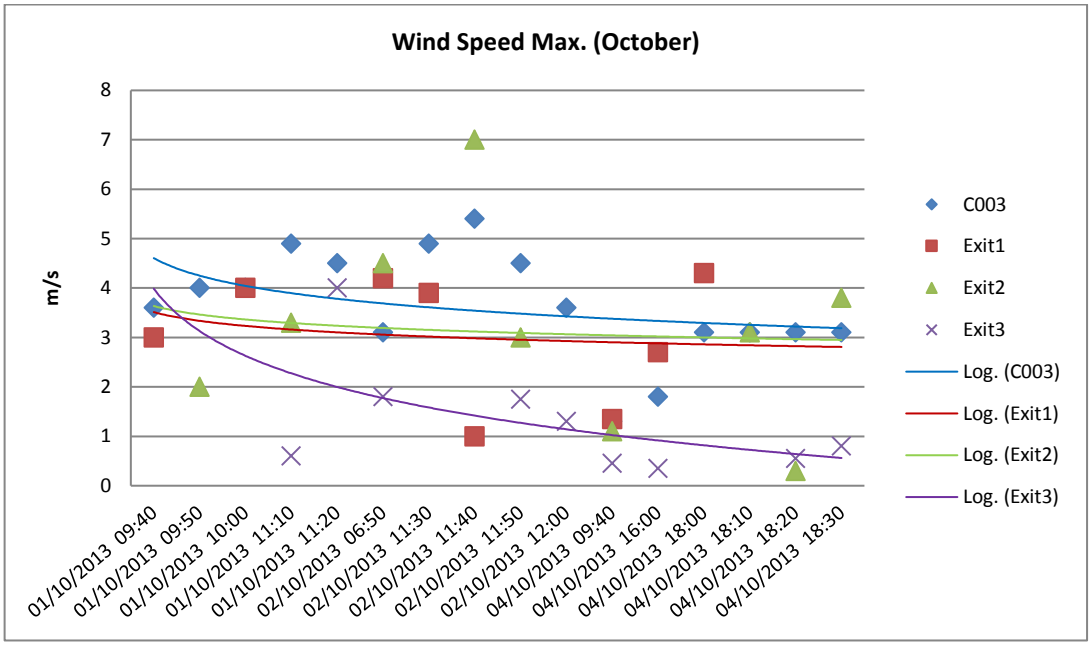

Figure 34: Measurement of maximum wind speed and trend line at October 2013

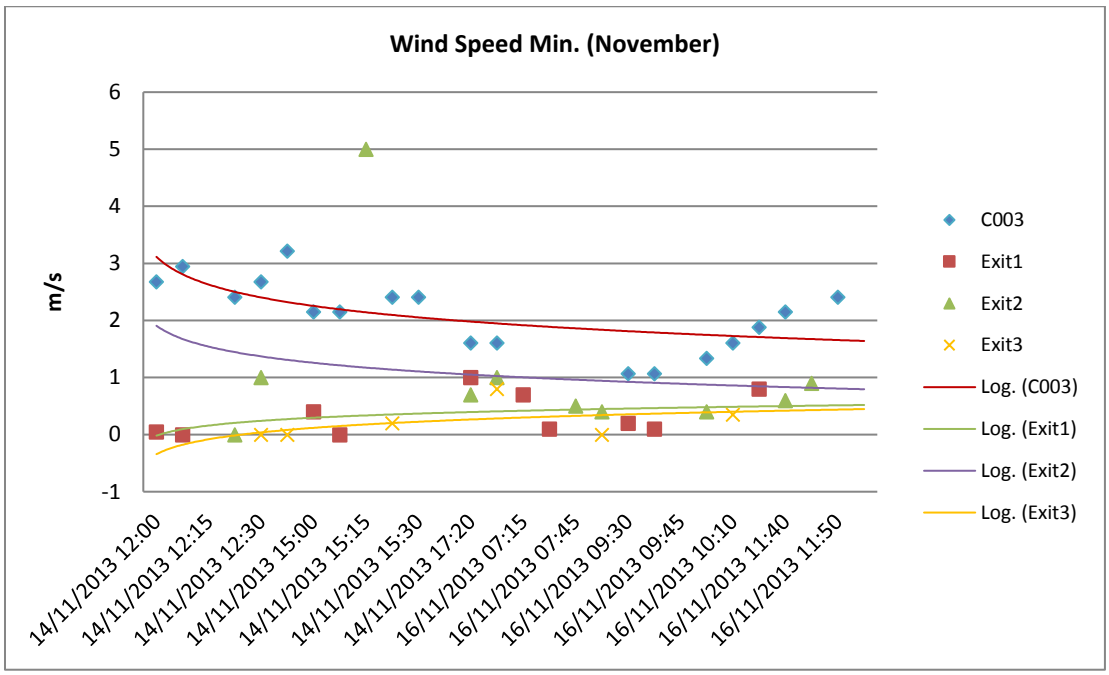

Figure 35: Measurement of minimum wind speed and trend line at November 2013

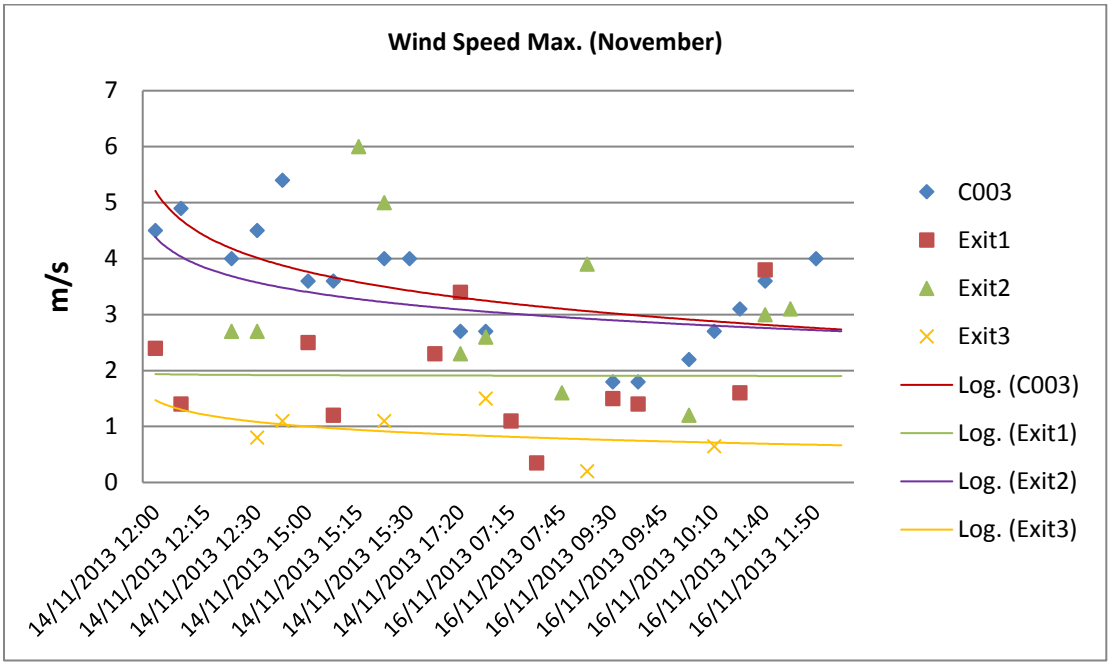

Figure 36: Measurement of maximum wind speed and trend line at November 2013

5.4.2 Internal air flow

The internal air flow speed, direction and temperature have been recorded inside the station at locations shown in Figure 29. These measurements were taken at different intervals over a period of two days in October 2013. A sample of the readings is shown in the Table 4 to Table 15. All the portable measurements readings can be found in Appendix A.

Table 4 displays a sample of readings taken at platform 1 in the North-South tunnel. It can be seen that the air flow was very variable when the trains were operating. The flow field consisted of the natural background air flow on which was superimposed the impact of train motion. The strong background air flow was from south to north but train motion from the north caused the air flow direction to reverse and the speed increased rapidly up to 5.2 m/s. When the train emerged from the tunnel the peak speed then rapidly reduced to a very small flow speed of 0.2 m/s or even to zero when the train arrived at the platform. This air flow rapidly reversed when the train left the platform.

Location: NS Tunnel, Platform 1. Train direction: N to S						
Date	Time	Air flow speed min. m/s	Air flow speed max. m/s	Air flow Direction	WBT ^{o}C	DBT ^{o}C
01/10/2013	10:45		0.1	S to N No train	13.5	19
	10:46		3	N to S train arriving pf 2		
	10:48		1.5	N to S pf1 train leaving pf 2 train arriving	13.8	19
	13:17		0.45	N to S train arrived pf 2		
	13:18		0.9	N to S train leaving pf 2		
	13:19	0.45	0.7	N to S train left pf 2	13.4	18.3
	13:21	0.1	0.3	N to S train arriving pf 1		
	13:22		2.2	N to S train arriving pf 1		
	13:23		1.2	S to N train arriving pf 1		
	13:25	0.45	0.7	S to N No train continue for 1 mins		
	13:27		5.2	N to S train arriving pf 1		
	13:29		0.6	N to S pf1 train leaving pf 2 train arriving		
	13:31		0	Keep for 10 sec		
	13:31:30	0.55	0.65	N to S train arriving pf 1		
	13:32		4.5	N to S train arriving pf 1		
	13:33	0	0.2	N to S train arrived pf 1		
	13:34		1	S to N train leaving pf 1		

	13:35-13:36	0.45	0.65	N to S train left pf 1		
02/10/2013	09:43		2	N to S train arriving pf 1		
	09:44	0	0.2	N to S train arrived pf 1		
	09:45		2.7	S to N train leaving pf 1		
	9:45:30	0.4	0.55	N to S train arriving pf 2		
	09:46		0.6	N to S train arriving pf 2		
	09:46:30		0.87	N to S train leaving pf 2		
	09:47	0.1	0.2	S to N after train left pf 2		
	14:13	0.35	0.45	N to S train arriving pf 2	14.7	18.5
	14:14		2	N to S train arriving pf 2		
	14:15		0.5	S to N train into pf 2		
	14:16		1.3	N to S train arrived at pf 2		
	14:17		0.8	N to S train leaving pf 2		
	14:19		0.5	N to S train arriving pf 2		
	14:20		0	train arrived pf 2		
	14:21		0.9	N to S train leaving pf 2		
	14:22		0	after train left pf 2		

Table 4: Internal airflow at Platform 1 from portable airflow measurements

The airflow at the corridors between platform 1 and 2 is highly dependent on the train activity. The airflow direction was from the active platform to the other platform when a train entered the station and reversed when the train left the platform. For example, referring to Table 5 on the 02/10/2013 at 09:56 airflow was from platform 2 to platform 1 when the train entered the platform but at 09:57 when the train left the platform 2 the airflow reversed. This effect was seen to increase when a train was active at both platforms this can be seen to have occurred at 13:58:30 when the airflow speed from platform 2 to platform 1 increased to 4.4 m/s when a train was leaving platform 1 and a second train was arriving at platform 2.

Location: NS Tunnel, between pf 1 and pf 2						
Date	Time	Air flow speed min. m/s	Air flow speed max. m/s	Air flow Direction	WBT ^{o}C	DBT ^{o}C
01/10/2013	10:44		0	No train	13.5	19
	13:57		0	No train		
	13:58		1.4	pf1 to pf2 train arriving at pf1		
	13:58:30		4.4	pf2 to pf1 train leaving at pf1 train arriving at pf2		
	13:59		1.4	pf1 to pf2 train leaving at pf2		
	14:00		0	No train	13.4	18.6
02/10/2013	09:51		0.4	pf1 to pf2 train through EW line		
	09:52		0	No train		
	09:53		2.6	pf2 to pf1 train arriving at pf2		
	09:53:30	0.3	0.5	pf2 to pf1 train arrived pf2		
	09:54		4	pf1 to pf2 train leaving at pf2 train arriving at pf1		
	09:55	0.35	0.45	pf1 to pf2 train leaving at pf1		
	09:56		2	pf2 to pf1 train arriving at pf2		
	09:57		1.5	pf1 to pf2 train leaving at pf2		
	10:00		2.9	pf1 to pf2 train arriving at pf1		
	14:22		1.9	pf1 to pf2 train arriving at pf1 &pf2 pf1 earlier than pf2		
	14:23	0.7	0.8	pf1 to pf2 two train at both pf		
	14:24	0.7	0.8	pf2 to pf1 train leaving at pf1		
	14:25		1.35	pf1 to pf2 train leaving at pf2		
	14:26	0	0.1	Reserve but less than 0.1		
	14:28		3.7	pf1 to pf2 train arriving at pf1		
	14:29		0.7	pf2 to pf1 train leaving at pf1		
	14:31		2.2	pf2 to pf1 train arriving at pf2		
	14:32		0.6	pf1 to pf2 train leaving at pf2		

Table 5: Internal air flow between platform 1 and 2 from portable air flow measurements

A measurement sample at platform 2 in the North-South tunnel is shown in Table 6. The background airflow from south to north is enhanced by the train operation in the same direction. Only a few seconds of data was recorded when the train started to leave the platform but it can be seen that the background airflow was restored very quickly.

Location: NS Tunnel, Platform 2. Train direction: S to N						
Date	Time	Air flow Speed min. m/s	Air flow Speed max. m/s	Air flow Direction	WBT ^{o}C	DBT ^{o}C
01/10/2013	10:38		0.4	S to N No train	13.9	18
	10:39		1.2	S to N train from pf1		
	10:40		0.9	S to N after train left pf1		
	10:43		2.5	S to N train arriving at pf1		
	10:44		1	S to N train leaving pf1		
	13:39		1.5	S to N train leaving pf2		
	13:40		2.5	S to N train arriving at pf2	13	18
	13:41	0.8	1	S to N train leaving pf2		
	13:45	0.4	0.55	S to N No train		
	13:46		1.5	S to N train arriving at pf1		
	13:47		2.5	S to N train arriving at pf2		
	13:48		1.4	S to N train leaving pf2		
	13:49	0.85	0.9	S to N No train		
02/10/2013	10:04		0	No train		
	10:05		0.95	S to N train arriving at pf1		
	10:06		0.3	S to N train leaving pf1		
	10:06:30	0.2	0.3	S to N No train		
	10:07		0.1	S to N Reverse		
	10:08		2.8	S to N train arriving at pf2		
	10:08	0.3	1	S to N train arrive pf2		
	10:10	0.5	0.7	N to S when the train start to leave at pf 2		
	10:11		1.4	S to N train left pf1		
	10:12		2.8	S to N train arriving at pf2	13.7	17.6
	10:13	0.5	0.7	N to S when the train leaving but still in the pf 2		
	10:13:30		1.8	S to N train left pf2		
	14:33	0.8	0.9	S to N No train		
	14:35		2.8	S to N train arriving at pf2		

	14:36		1.2	S to N train arrived pf2 train arriving at pf1		
	14:36:30		0.4	N to S when the train leaving but still in the pf 2 (few seconds)		
	14:37		1.75	S to N train leaving pf1		
	14:38	0.3	0.4	S to N No train		

Table 6: Internal airflow at platform 2 from portable airflow measurements

Two measurements were taken at the staircase linking the different platform levels in the station. Measurements at the lower level NS tunnel are shown in Table 7 and data measured from the higher level at EW tunnel level is shown in Table 8. The airflow at the both lower and higher level of the stair are highly dependent on the train motion in of both tunnels and the train activity at all the platforms. The airflow was rarely measured with no train operation. The airflow direction reversed frequently and the airflow speed was at a high level with train activity.

The measurements taken at the North-South lower tunnel, when a train was at platform 1 and 2 indicated that the air flow direction is always towards the stair from the platform. The speed could be up to 4.4m/s into the stair as can be seen for the measurements taken at 09:17 02/10/2013 when a train entered platform 2. On the other hand, the highest speed measured at the East-West tunnel at the top of the stairs was 3m/s as measured at 12:48 on 02/10/2013. This phenomenon was similar with the train operating at platform 3 and 4 but with the air flow direction reversed.

Location: Stairs, at NS tunnel level (Platform 1 and 2)						
Date	Time	Air flow Speed min. m/s	Air flow Speed max. m/s	Air flow Direction	WBT ^{o}C	DBT ^{o}C
01/10/2013	10:34	0.5	0.6	into stair No train	14.8	19.2
	10:35		0.8	into stair NS train arriving	13.3	18.6
	12:57	1.2	3.4	into stair Train arriving at pf 2		
	12:59	1	2	into stair Train arriving at pf 1		
	13:00		0.7	from stair		
	13:01	0	0.1	Reversed		
	13:02		1.2	from stair train through EW		
	13:03		1.5	into stair Train arriving at pf 1		
	13:04		4.2	from stair Train arriving at pf 1		
	13:05		1.8	from stair train through EW and NS		
	13:07	0.7	0.9	into stair		
	13:09		2.9	into stair Train arriving at pf 1		
	13:11		0.8	into stair Train arriving at pf 2		
	13:12		1.7	from stair Train leaving pf 2		
02/10/2013	08:59		3	into stair Train arriving at pf 2		
	09:00			from stair Train arrived pf 2		
	09:01		0.9	into stair Train leaving at pf 2		
	09:02		0.8	from stair train arriving pf 1		

	09:03		2	from stair Train leaving pf 1		
	09:04		2.1	from stair train come through EW pf 3& 4		
	09:06		4.4	into stair Train arriving at pf 1		
	09:07		2.1	from stair Train leaving pf 1		
	09:08	0.4	0.55	from stair No train		
	09:09	0.35	0.5	into stair		
	09:10		0.95	into stair		
	09:11		3.4	into stair Train arriving at pf 2		
	09:11:30	0.1	0.2	from stair Train leaving pf 2		
	09:12		2.2	into stair Train arriving pf 1		
	09:12:30		0.9	from stair	14	18.4
	09:13		1.5	from stair Train leaving pf 1		
	09:17		4.4	into stair Train arriving at pf 2		
	09:19		1.8	from stair Train leaving pf 2		
	13:59		3.7	into stair Train arriving pf 1		
	14:00	0.4	0.5	into stair Train arrived pf 1		
	14:01		2.2	from stair Train leaving pf 2		
	14:02	0.5	0.8	from stair No train		
	14:02:30	0.25	0.35	from stair No train		
	14:03		1.8	from stair train come through EW line		
	14:04		2.2	into stair		
	14:05		3	into stair train leaving EW line		
	14:06		2	from stair train arriving through EW line & pf 2		
	14:07		1.4	Rev from stair train leaving NE line		
	14:08	0	0.1	Reverse into stair		
	14:08-14:09	0	2	No train		
	14:11	0.8	0.9	into stair No train		

Table 7: Internal air flow at North-South tunnel level stair from portable air flow measurements

Location: Stairs, at EW tunnel level (Platform 3 and 4)						
Date	Time	Air flow Speed min. m/s	Air flow Speed max. m/s	Air flow Direction	WBT ^{o}C	DBT ^{o}C
01/10/2013	10:30		2.5	into stairs train leaving from EW line		
	10:31	0.3	0.4	from stair No train	13.4	18.5
	10:32		1.2	from stair Train arriving at NS line		
	10:33		0.3	Reversed		
	12:48	2	3	into stairs train leaving from EW line		
	12:50	1.6	2.2	into stair Train arriving at NS line		
	12:52		1.7	into stair Train arriving at pf 4		
	12:53	1.6	2.7	into stair Train leaving at pf 4		
	12:54	1	3.3	into stair Train arriving at pf 4		
	12:55		0.3	No train		
02/10/2013	08:47		0.5	into stair		
	08:48		1.7	from stair	13.8	18.9
	08:52		2.2	into stair Train arriving at pf 3		
	08:53		2.5	from stair Train leaving pf 3		
	08:53:30		0	Reversed		
	08:54		2.5	into stairs train leaving from pf 4		
	08:55	0.3	0.55	into stair No train		
	08:56		1.6	from stair Train arriving at NS line		
	08:57		0.6	in to stair		
	13:51		2.95	into stair Train arriving at pf 3		
	13:52		0.9	from stair Train arrived pf 3		
	13:53		3.3	Reversed from stair Train leaving pf3		
	13:53:30		0	Reversed		
	13:54		3.3	Reversed. To stair Train arriving at pf 4		
	13:55		1	from stair		
	13:56		0.45	into stair		
	13:57-13:58		0	No train		

Table 8: Internal air flow at East-West tunnel level stairs from portable air flow measurements

Table 9 is showing a sample of measurement taken at platform 3 in the East-West tunnel. It can be seen that the background airflow without train operation could be up to 0.9 m/s from east to west as measured at 13:14 on 02/10/2013. The airflow reversed quickly by the piston effect of a train entering the platform from the west tunnel with a speed up to 1.8 m/s. The train operation has a strong and instant effect on the background airflow. The background airflow was quick to restore after the passage of the train.

Location: EW Tunnel, Platform 3. Train direction: W to E						
Date	Time	Air flow Speed min. m/s	Air flow Speed max. m/s	Air flow Direction	WBT ^{o}C	DBT ^{o}C
01/10/2013	10:27		1.2	W to E Train arriving at pf 3	13.4	18.3
	12:20	0.45	0.6	E to W No train		
	12:26	1	1.5	W to E Train arriving at pf 3		
	12:26:30		0.5	W to E Train arrived at pf 3		
	12:27	1	1.5	W to E Train leaving at pf 3		
	12:28	0		No train		
	12:29		0.3	Train through pf 4		
02/10/2013	07:58	0	0.3	No train		
	07:59		0.52	E to W No train	13.8	17.4
	08:03		0.9	E to W Train through pf4		
	08:04		1.2	W to E Train arriving at pf 3		
	08:05		0.85	W to E Train arrived at pf 3		
	08:06		1.8	W to E Train leaving at pf 3		
	13:07		0	No train		
	13:08-13:09	0.35	0.5	E to W NO train	13.7	18
	13:11	0.7	0.8	E to W Train cross NS line		
	13:14		0.9	E to W No train		
	13:15		1	W to E Train arriving at pf 3		
	13:16		0.35	E to W Train arrived at pf 3		
	13:17		1.4	W to E Train leaving at pf 3		
	13:19	0.12	0.3	E to W Very small Reverse		
	13:21	0	0	No train		

Table 9: Internal air flow at Platform 3 from portable air flow measurements

The airflow pattern at the corridors between platform 3 and 4, shown in Table 10, is similar to those shown in Table 5. This is also highly dependent on the train activity. The airflow direction is from the active platform when the train arrived and reversed when the train left.

Location: EW Tunnel. Between pf 3 and pf 4						
Date	Time	Air flow Speed min. m/s	Air flow Speed max. m/s	Air flow Direction	WBT ^{o}C	DBT ^{o}C
01/10/2013	10:17		0.8	pf 3 to pf 4 train arriving at pf 3		
	10:18		0.2	No train		
	10:30		2.2	pf 4 to pf 3 train arriving at pf 4		
	12:18		1.5	pf 4 to pf 3 train arriving at pf 4		
02/10/2013	08:08	0	0.6	pf 4 to pf 3 No train	14.3	19
	08:33		0.4	pf 4 to pf 3	13.6	18
	08:37		3.4	pf 4 to pf 3 train arriving at pf 4		
	08:40	0	0.4	pf 4 to pf 3 train arrived pf 4		
	08:41		0.5	pf 3 to pf 4 train leaving pf 4		
	13:22		0.3	pf 3 to pf 4 train left pf 4		
	13:24	0.2	0.6	No train		
	13:25	0.1	0.3	pf 3 to pf 4		
	13:25-13:27	0	0.1	pf 4 to pf 3		
	13:28	0	0.5	pf 4 to pf 3		
	13:29		2.2	pf 3 to pf 4 train arriving at pf 3		
	13:30	0.4	0.5	pf 3 to pf 4 train arrived pf 3		
	13:31		1.1	pf 4 to pf 3 train leaving pf 3		
	13:32		0.5	pf 3 to pf 4 after train left pf 3		
	13:35	0	0	No train		
	13:36	0.5	0.6	pf 4 to pf 3 train arriving at pf 4		
	13:36:30	0	0.1	pf 4 to pf 3 train arrived pf 4		
	13:37		0.5	pf 3 to pf 4 train leaving pf 4		
	13:37:30	0.4	0.5	No train		

Table 10: Internal air flow between Platform 3 and 4 from portable air flow measurements

The measurement taken at platform 4 in East-West tunnel are shown in Table 11. These are similar to the results from platform 2 in the NS tunnel. The background airflow is enhanced by the train operation in the same direction. The background airflow direction from east to west was 0.9 m/s with no train operation and varied from 0.2 m/s to 4.5 m/s within 1 minute when a train entered the platform as shown at 12:40 on 01/10/2013. The background airflow quickly restored after the train left the platform.

Location: EW Tunnel, Platform 4. Train direction E to W.						
Date	Time	Air flow Speed min. m/s	Air flow Speed max. m/s	Air flow Direction	WBT ^{o}C	DBT ^{o}C
01/10/2013	10:15		0.35	E to W	0.7	19.4
	12:34	0.2	0.35	E to W No train	12.5	16.8
	12:35	0.15	0.2	E to W No train		
	12:39		0.1	E to W No train		
	12:40		4.5	E to W Train arriving at pf 4		
	12:41	0.2	0.5	E to W Train arrived pf 4		
	12:42		1.3	E to W Train leaving pf 4		
	12:43	0.8	1.3	E to W 1 mins continuously		
02/10/2013	08:43		3.4	E to W Train arriving at pf 4		
	08:44		0.7	E to W Train leaving pf 4		
	08:45		1.1	E to W Train arriving at pf 3		
	08:46		0.75	E to W Train leaving pf 3		
	13:38	0.8	0.9	E to W No train		
	13:43		0.2	E to W Train arriving at pf 3 out of pf		
	13:43:30	0.6	0.7	E to W Train leaving pf 3 when the train close to pf		
	13:44		2	E to W Train arriving at pf 4		
	13:45	0	0.1	E to W Train arrived pf 4		
	13:46	0	0.1	W to E Then the train stop at pf 4		
	13:47		1.05	E to W Train leaving pf 4		
	13:47:30	0.8	0.9	E to W No train		
	13:48		0.6	E to W No train		

Table 11: Internal air flow at Platform 4 from portable air flow measurements

Two series of measurements were taken for each of the escalators. The escalator NS connected the NS tunnel, platforms 1 and 2, with the concourse area and the escalator EW connected the East-West tunnel, platform 3 and 4, with the concourse area. Measurements were taken at platform level and the concourse level. Generally, the airflow at the escalators was highly affected by the train operation as was the stair mentioned earlier. The difference is that the stairs were affected by the train operation in both tunnels which resulted in the airflow being reversed at the stair. The airflow at the escalators was more stable than that at the stair. The concourse area had an impact on the airflow at the escalators.

The airflow velocity at the bottom of the escalators was strongly influenced by the train operation. When a train entered the NS platforms the airflow at the bottom of the NS escalator was measured to be 3.5m/s at 10:51 01/10/2013 as shown in Table 12. A similar situation was recorded for the EW escalator with an air speed of 3 m/s being recorded at 11:53 on 01/10/2013 as shown in Table 14.

A similar result was observed at the concourse level at the top of the escalators. This is shown in Table 13 and Table 15. Without the train operation, the peak airflow measured from the escalator to the concourse area at the top of the NS escalator was 1.1m/s at 14:55 on 02/10/2013. The peak airflow measured at the top of the escalator EW was 0.35 m/s at 12:08 on 02/10/2013 but the EW escalator measurements showed a high degree of instability and flow reversals at the interface with the concourse area. This airflow at the EW escalator was generally weaker than the NS escalator.

Location: Escalator NS (down). Platform level						
Date	Time	Air flow Speed min. m/s	Air flow Speed max. m/s	Air flow Direction	WBT ^{o}C	DBT ^{o}C
01/10/2013	10:51		3.5	pf to escalator train arriving	13.9	19.5
	10:51:30		1	pf to escalator train arrived pf		
	10:52		2	escalator to pf train leaving		
	10:53	0	0.3	No train		
	10:54		1.5	escalator to pf train leaving		
	11:40	2.5	3	pf to escalator train arriving		
	11:41	0.1	0.6	No train		
	11:43	0.1	1	escalator to pf train leaving	14.7	21.2
02/10/2013	10:20	0.5	0.65	pf to escalator		
	10:21	0.2	0.3	pf to escalator	14.2	18.8
	10:22		2	pf to escalator train arriving		
	10:23		0.8	pf to escalator		
	10:24	0.1	0.2	escalator to pf train leaving		
	10:25		0.4	pf to escalator		
	10:26		2.5	pf to escalator train arriving at pf 1		
	10:27	0	0.2	pf to escalator train arrived pf 1		
	10:28		2	escalator to pf train leaving pf1		
	10:29		0.6	pf to escalator		
	14:42	0.3	0.55	escalator to pf		
	14:43	0	0.1	Reserved		
	14:44	0.4	0.7	pf to escalator		
	14:45		1.7	pf to escalator train arriving at pf 1		
	14:46		1	pf to escalator train arrived pf 1		
	14:47		1.3	escalator to pf train leaving pf1		
	14:48	0.3	0.5	pf to escalator		
	14:50	0.3	0.9	escalator to pf		

Table 12: Internal air flow at Escalator NS (down) from portable air flow measurements

Location: Escalator NS (up), Concourse level						
Date	Time	Air flow Speed max. m/s	Air flow Speed max. m/s	Air flow Direction	WBT ^{o}C	DBT ^{o}C
01/10/2013	10:07	0.5	1	from escalator No train		
	10:58		2.7	from escalator train arriving		
	11:00	2.7	3	from escalator train arriving		
	11:01	0.6	0.7	from escalator train left		
	11:02		0.2	no train		
	11:29		0.5	concourse to escalator		
02/10/2013	10:31	0	0.3	come up from escalator		
	10:32		1.5	concourse to escalator		
	10:34	0	0.1	from escalator		
	10:35		2.7	from escalator train arriving		
	10:37		1.9	concourse to escalator	14.9	20.3
	10:38	0.2	0.35	concourse to escalator No train		
	10:39		0.4	concourse to escalator		
	14:55		1.1	concourse to escalator No train	15.6	21
	14:56-14:57	0	0.3	Reversing		
	14:57	0.3	0.9	from escalator		
	14:58		2.8	from escalator train arriving		
	14:59	0.4	0.9	from escalator train arrived		
	15:00		2.45	concourse to escalator train leaving		
	15:01		0.35	from escalator		
	15:03	0	0.95	Reversing		
	15:04		2	from escalator train arriving		
	15:05		1.9	concourse to escalator train leaving		
	15:06	0.4	0.5	concourse to escalator train left and arriving same time		

Table 13: Internal air flow at Escalator NS (up) from portable air flow measurements

Location: Escalator EW (down), Platform level						
Date	Time	Air flow Speed min. m/s	Air flow Speed max. m/s	Air flow Direction	WBT ^{o}C	DBT ^{o}C
01/10/2013	10:09	0.4	0.9	pf to escalator	1.35	19.4
	11:48	0.6	0.8	escalator to pf	13.8	19.9
	11:49	0.1	0.3	escalator to pf		
	11:50	0.1	0.8	escalator to pf		
	11:53	2.5	3	escalator to pf train leaving at pf 3		
	11:54	0.4	0.5	pf to escalator train arriving at pf 4		
	11:55		0.8	escalator to pf train leaving at pf 4		
	11:57	0	0.3	escalator to pf		
02/10/2013	07:43		0.65	pf to escalator		
	07:44	0	2.2	pf to escalator train arriving at pf 4		
	07:45	0	0	when train arrived	15.2	21.2
	12:22	0.3	0.8	escalator to pf		
	12:23	0	0.5	Reversed pf to escalator		
	12:24	0	0.2	Reverse every 5 seconds keeping 2 mins		
	17:29		1.65	escalator to pf		
	17:30	0	0.1	escalator to pf		
	17:31	0	0	when train arrived		
	17:31	0	0.4	escalator to pf train leaving		
	17:32	0.4	0.6	Reversed pf to escalator		
	17:34	0.2	0.7	pf to escalator		
	17:35	0	0	No train		

Table 14: Internal air flow at Escalator EW (down) from portable air flow measurements

Location: Escalator EW (up), Concourse level						
Date	Time	Air flow Speed min. m/s	Air flow Speed max. m/s	Air flow Direction	WBT ^{o}C	DBT ^{o}C
01/10/2013	10:05	0.5	2.5	from escalator train arriving EW	14.5	21.5
	11:26	0.4	1.3	from escalator		
	11:27		2.3	concourse to escalator train leaving EW	13.8	21.3
02/10/2013	07:39		2.3	from escalator train arriving EW		
	07:42		2.7	concourse to escalator train leaving EW	14.7	20.2
	12:08	0.15	0.35	from escalator No train		
	12:10		1.3	concourse to escalator	15.6	20.9
	12:11	0.3	0.9	concourse to escalator		
	12:13	0.4	0.65	concourse to escalator		
	12:16	0	0.1	from escalator		
	12:17		1.3	from escalator train arriving EW		
	12:18		1.6	from escalator train arriving EW		
	12:19		2.65	concourse to escalator train leaving EW		

Table 15: Internal air flow at Escalator EW (up) from portable air flow measurements

5.5 Temperature Measurements in the Tunnels

In the past, air currents in underground systems have been widely described as unsteady, alternating and unpredictable but this refers to the piston effect induced by train motion (Rasmus and Brock, 1944; Chen *et al.,* 2003; Pan *et al.,* 2013). However this is only one part of the complex system of air currents in the underground. It is now accepted that there is a steady natural ventilation current in subway systems which is independent of train movement and mechanical ventilation. This has been observed in several subway systems (Pflitsch, 2001). This natural ventilation, as a background airflow, is a highly complex system of air currents with spatial and temporal variation, which can be defined as an independent airflow system. This background air flow is modified by movement of trains and quickly re-establishes in a short time after the passage of a train or the termination of traffic (about 1-3 minutes) (Pflitsch *et al.,* 2011). It is generally considered but not fully established that this background air flow is mainly influenced by the outside weather conditions and station structure and condition.

The temperature differences within the subway system and between subway and outside atmosphere have a strong influence on underground air currents. It has been thought that subway systems behave like cave systems in that large temperature

differences between inside and outside, notable during periods of extreme cold or heat leads to strong compensating airflows between the inside and the outside (Pflitsch *et al.,* 2013). High temperature gradients usually lead to stronger and more stable airflows in the tunnel system. This effect can be observed in caves especially in winter months when the temperature inside the system lags behind the changing of the outside temperature. The situation is however much more complicated in a subway. During conventional operation, an underground railway will gain heat from many sources including the train propulsion and braking systems, carriage accessories, carriage air-conditioning and third rail losses (Bendelius, 1976). The braking system can contribute up to 85% of the tunnel's heat-load, while the passengers contribute nearly 75% of the heat load in the train under peak-loading conditions (Ampofo *et al.,* 2004). This is shown in Figure 37. The heat gain of the train and the tunnel in the typical underground railway system without air conditioning system is shown in Figure 37 and Figure 38.

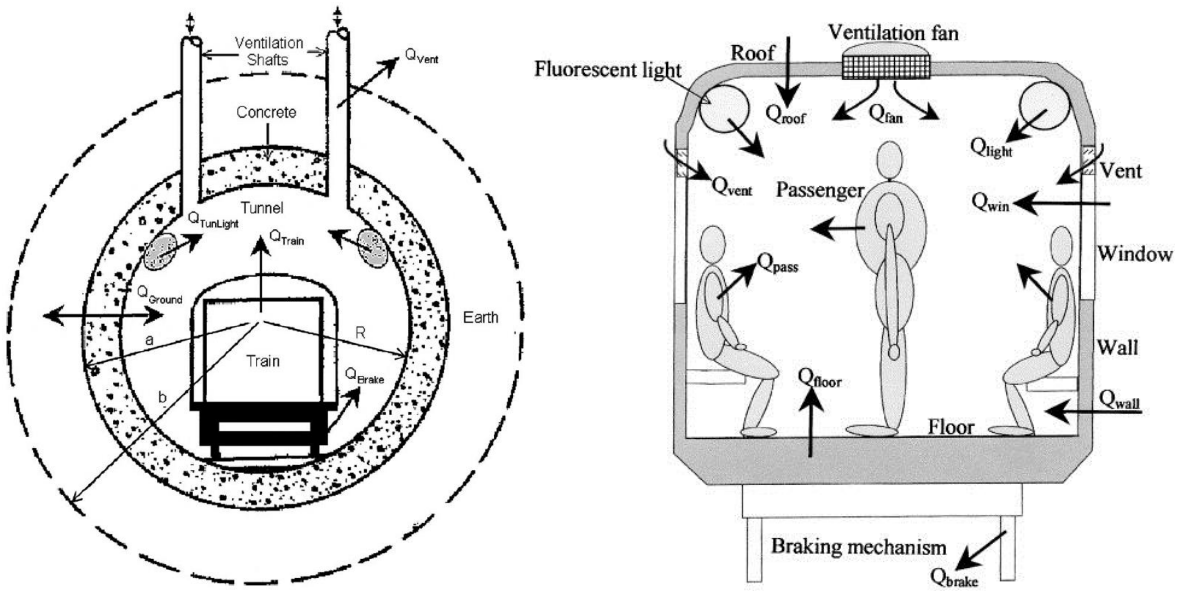

Figure 37: Heat load in the train carriage and underground rail way tunnel (Ampofo *et al.,* 2004)

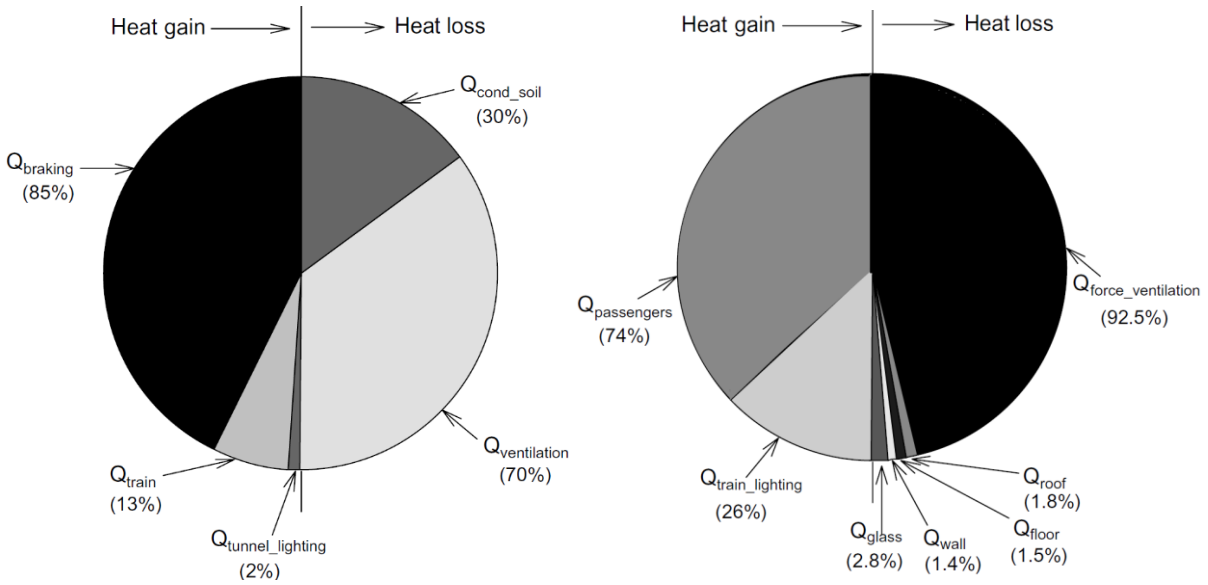

Figure 38: Heat balance for a train carriage and underground rail way tunnel (Ampofo *et al.,* 2004)

In addition, subway systems are designed with pressure relief shafts (Hagenah *et al.,* 2006; Crossrail, 2007) which are required between stations to allow access for the fire and rescue services in the event of an emergency underground and to allow control of smoke in the event of a fire in the tunnel; It is also thought that they are required to maintain the tunnel air quality and temperature within prescribed limits during periods of train service congestion. In the Tyne and Wear metro system ventilation shafts were fitted with fans capable of supplying or extracting large volumes of air and controlling the environment in both the stations and the tunnels. There were in total three ventilation shafts located just beyond the end of the platforms of each underground station. The draught relief shafts were constructed at both ends of each underground station with ducts connecting to the running tunnels just beyond the headwall at the end of the platforms to relieve the piston effect of the train movement. There was only one draught relief shaft in the middle of the North-South tunnel which was located at the end of the Haymarket station platform 1. Recent work by Pflitsch (2012) shows that the interaction of the forced ventilation system with the background air flow produced unexpected flow reversals within the Monument station when the fans were running compared when they were still. This could lead to the public being placed in danger in the event of an emergency evacuation due to a toxic gas release because of uncertainty about the dispersion path of the toxin. This illustrates how poorly understood subway ventilation systems were when these elements were installed in the 1960s. The situation is further complicated by the so called heat island effect which

has been observed in many city environments. Any seasonal temperature variation has been observed to be slight but may not be sufficient to produce any seasonal reverse of the back ground air flow pattern in the cold-climate. Strong chimney effects have been observed in some subway systems during cold weather conditions, when the outside air is much colder than the air in the subway (Spiegel *et al.,* 2014) but the seasonal variability of the airflow in the subways of the major UK cities has not been fully established.

The general method for numerical simulations of station ventilation modelling tends to use a uniform boundary condition for the tunnel based on the flow induced by the train piston effect (Huang *et al.,* 2012). Only recently have modellers been aware of the weather related air flow and have begun to use the background airflow as the boundary condition. In an emergency situation when the trains have stopped running it is this air flow that forms the correct boundary condition. This aspect is an important part of this work and this chapter presents the measurement of temperature and airflow speed inside the Monument Station and the North South tunnel crossing it and the connections to other stations. These measurement results will be used to establish the pattern of the natural airflow in the system and lead to a practical method for simulating underground air flow dynamics.

5.5.1 Data logger measurement instrument and set up

The natural back ground airflow in the subway is driven by changes in the elevation of the track and by chimney effects induced by temperature variations in the system. The tunnel geometry is shown in Figure 39 which indicates that the tunnel raises from the Tyne crossing to Jesmond station in a south north direction which is the direction of the natural air flow.

In order to measure the temperatures in the tunnels from the Central station through to the Monument, Haymarket and to Jesmond station, wireless mini data loggers produced by GEO PRECISION were installed in the tunnel between 20/02/2014 and 25/02/2014. This was also the period when tracer gas experiments were conducted. The data loggers were installed in the tunnel at each side of the platform to record temperature, relative humidity, atmospheric pressure, hydraulic pressure, CO_2 concentration and metric potential but for this research only the temperature data was utilised. In the future if it is possible to consider air quality in the subway then relative humidity and CO_2 concentration would be important and relevant factors.

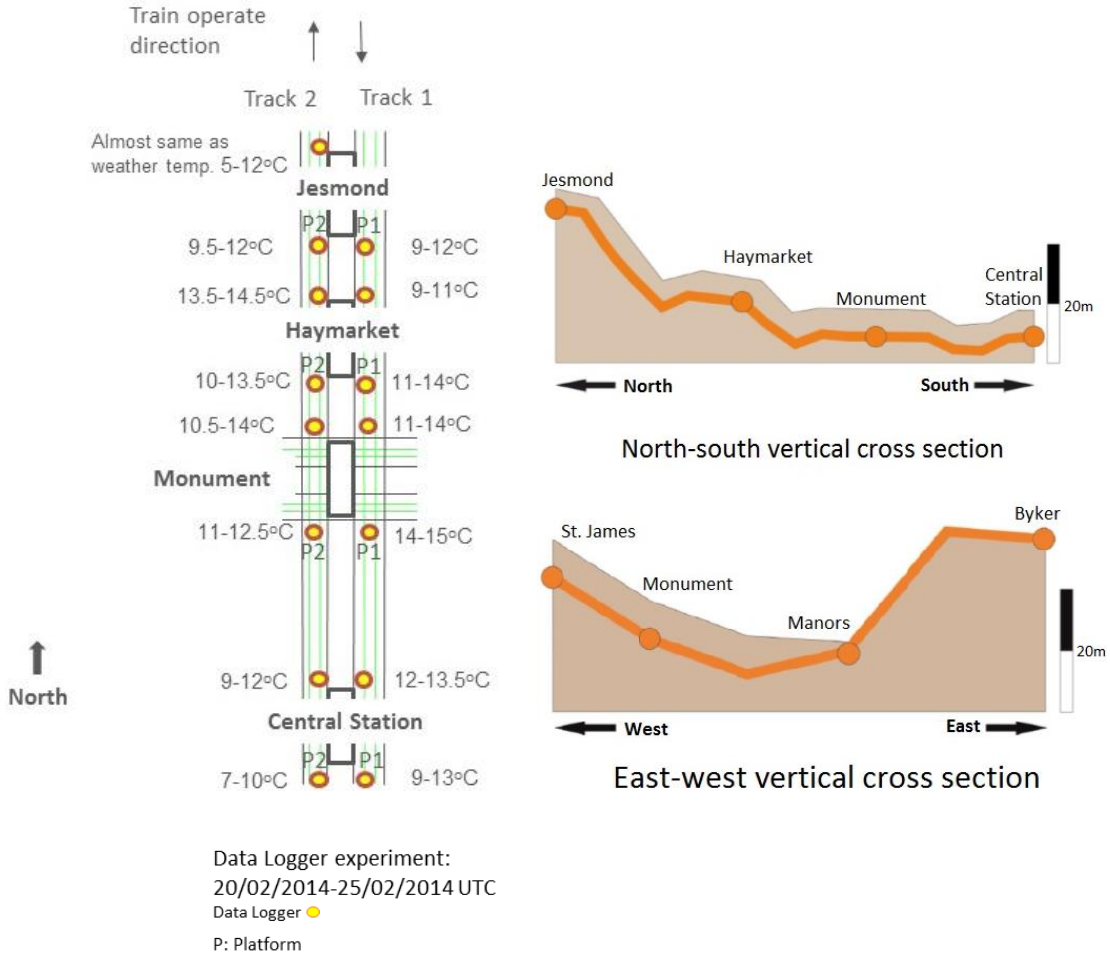

Figure 39: Location of instruments at Jesmond, Haymarket, Monument and Central Station and Tunnel geometry

5.5.2 Temperature from Data logger placed along track 1

The following section presents the results from the data logger measurements. An overview of all the data is presented in Figure 40 and Figure 41 which also show the local external weather temperature. Following the temperatures in the south to north direction in the direction of the background airflow the first measurement was taken at the tunnel portal at the Central Station (purple line). Comparing track 1 and 2 with the weather temperature (black line) in Figure 40 and Figure 41 it can be seen that the temperature during the day time was higher than at night and the temperature trend indicates a strong correlation with the external environmental weather temperature but the tunnel temperature was more stable showing less variability. The temperature at the Central station south of platform 1 was up to 4°C higher than the weather temperature (black line) as shown in Figure 40. In the operational time there were

significant temperature variations which was the effect of the air flow constantly reversing due to the piston effect of the trains entering the station from the north.

On the other track (Figure 41) the temperature is very close to the weather temperature. During the daytime the temperature was even lower than the weather temperature. There was a 2ºC to 3ºC temperature difference between track 1 and 2 at the Central station which may be caused by local geography outside the tunnel entrance.

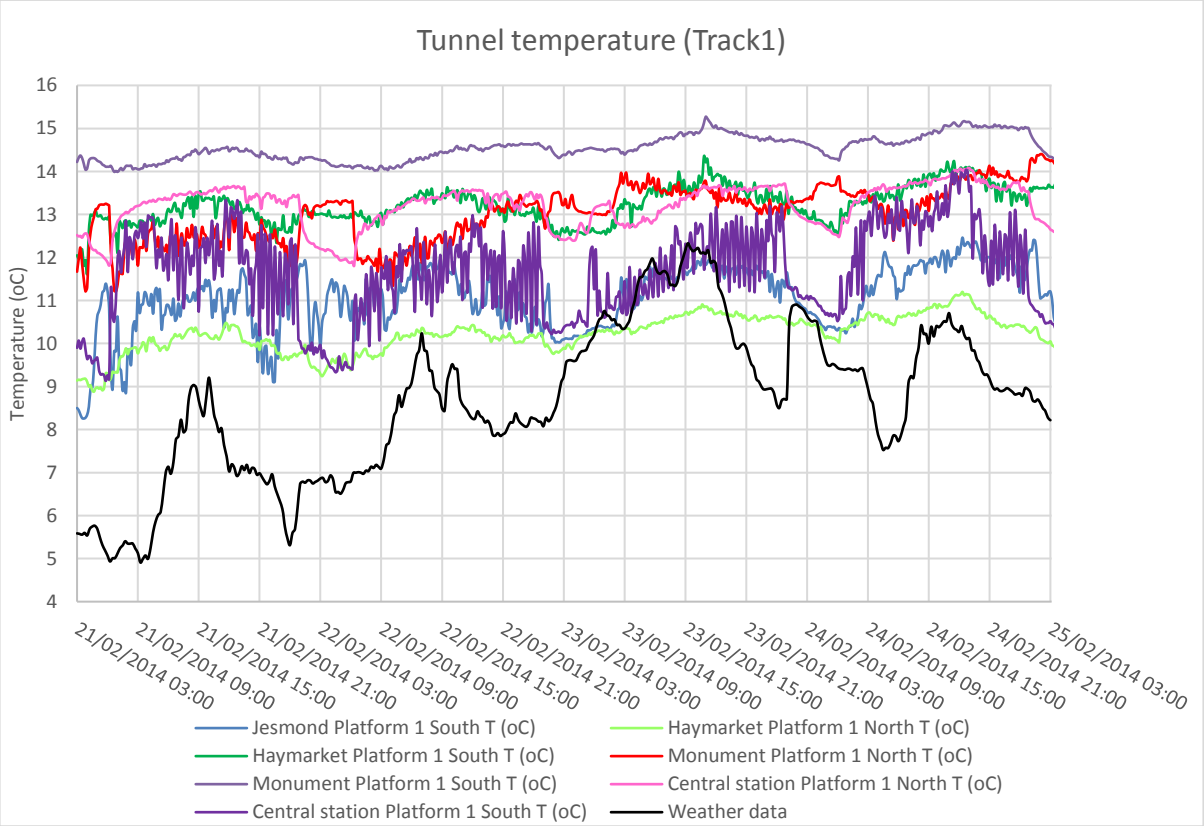

Figure 40: The temperature graph of loggers placed at track 1 with local weather

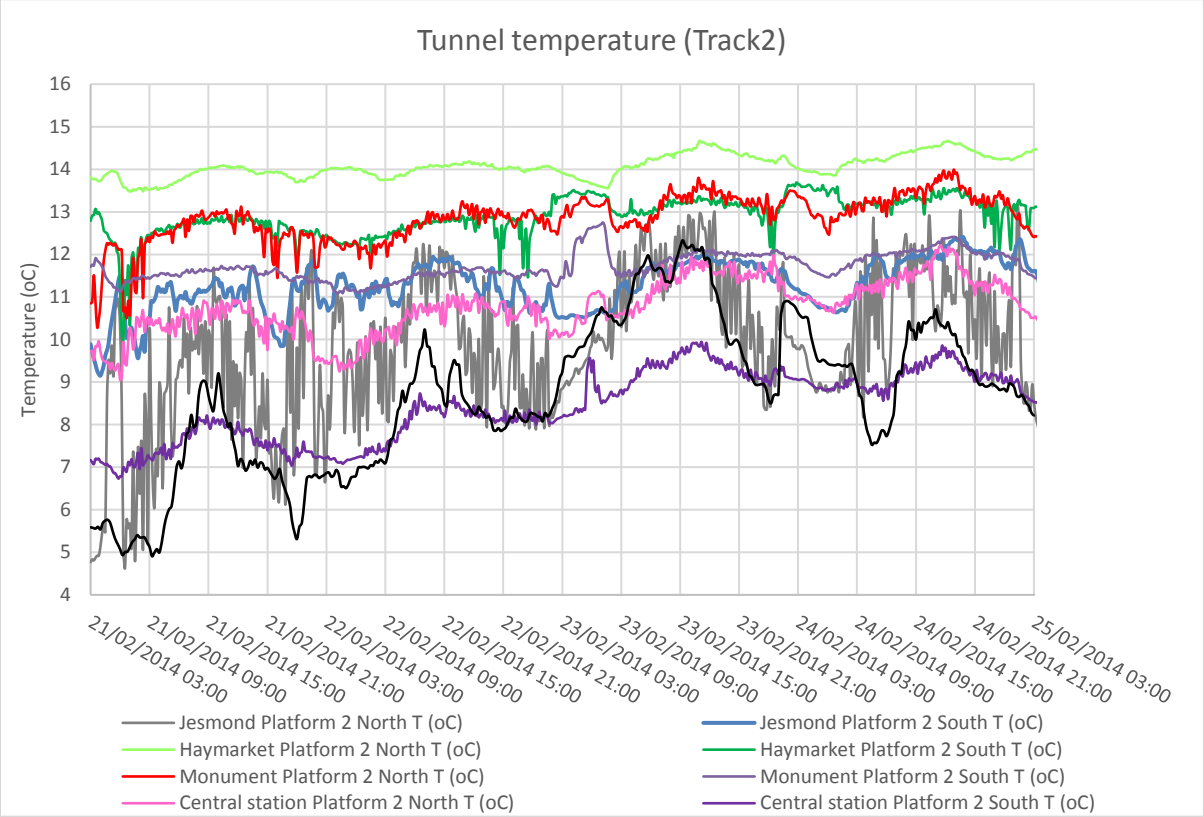

Figure 41: The temperature graph of loggers placed at track 2 with local weather

For a better comparison of the temperature variations between the stations in each tunnel, the data has been broken down to consider individual stations as shown in Figure 42 to Figure 49. In both tunnels the air temperature increased by around 2ºC as it passed through the Central station and around a further 1ºC as it passed through the tunnel to the south of the Monument station.

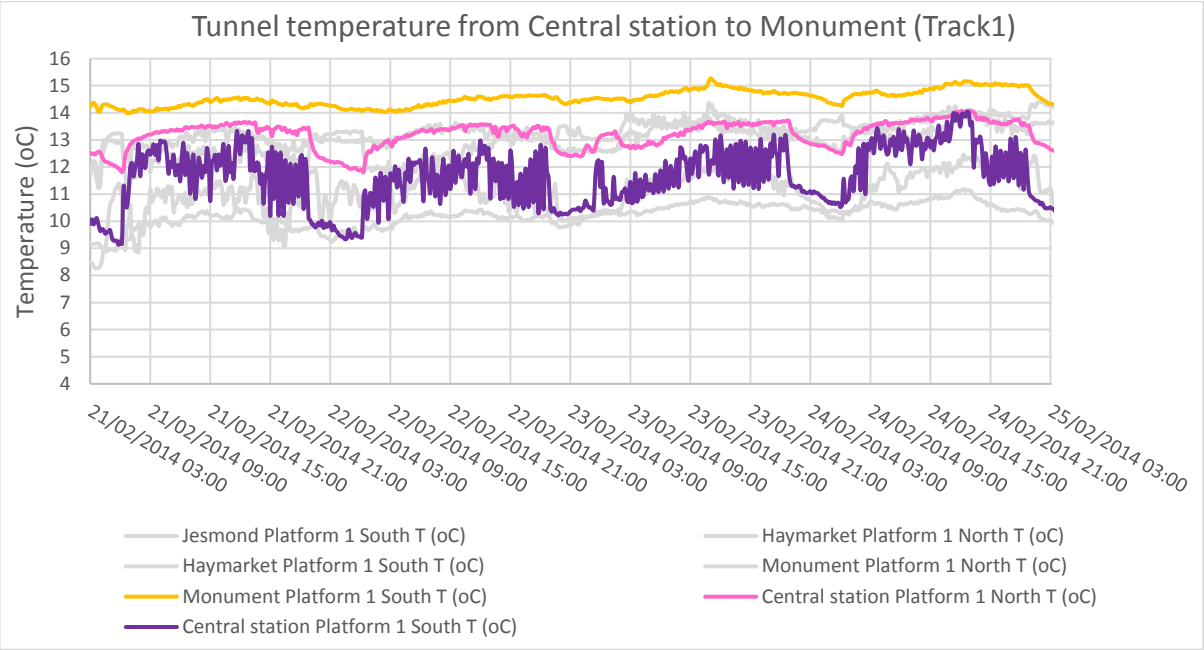

Figure 42: The logger temperatures at track 1 (Each side of the Central Station and south of Monument station)

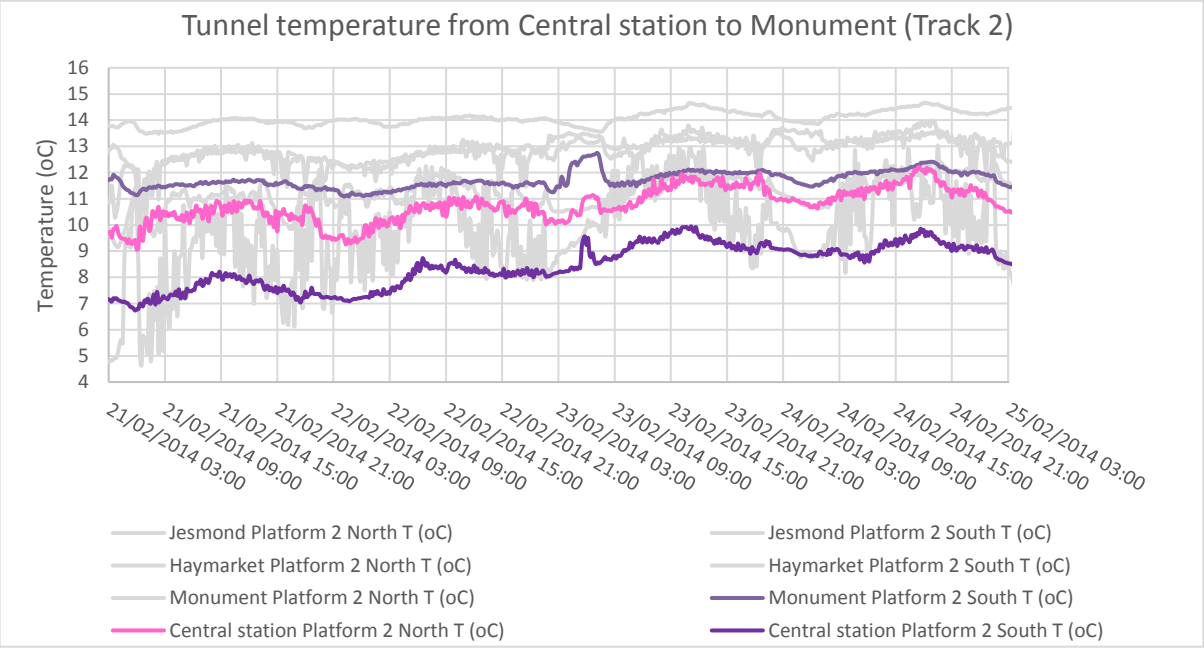

Figure 43: The logger temperatures at track 2 (Each side of the central station and south of Monument station)

The temperature at track 1 dropped by 1°C to 2°C and track 2 raised by around 1°C as the air passed through the Monument station. There was a 3°C difference between the temperature entering the Monument station at platform 1 and that at the north end of platform 2 as shown by the yellow line in Figure 44 and Figure 45. The airflow appears to have mixed better in this station than in the other underground stations because of

the connection corridors between the two platforms. This station was originally constructed for the largest pedestrian volume as the main station in the city centre. The tunnel temperatures at the Monument station for both track 1 and 2 are shown in Figure 46. It can be seen that the air temperature leaving the station at the north of the platforms is very close and in the middle of the temperature range of the south platform. The temperature fluctuation is miniscule from the North Monument station to Haymarket station and the temperatures of both tracks were very similar.

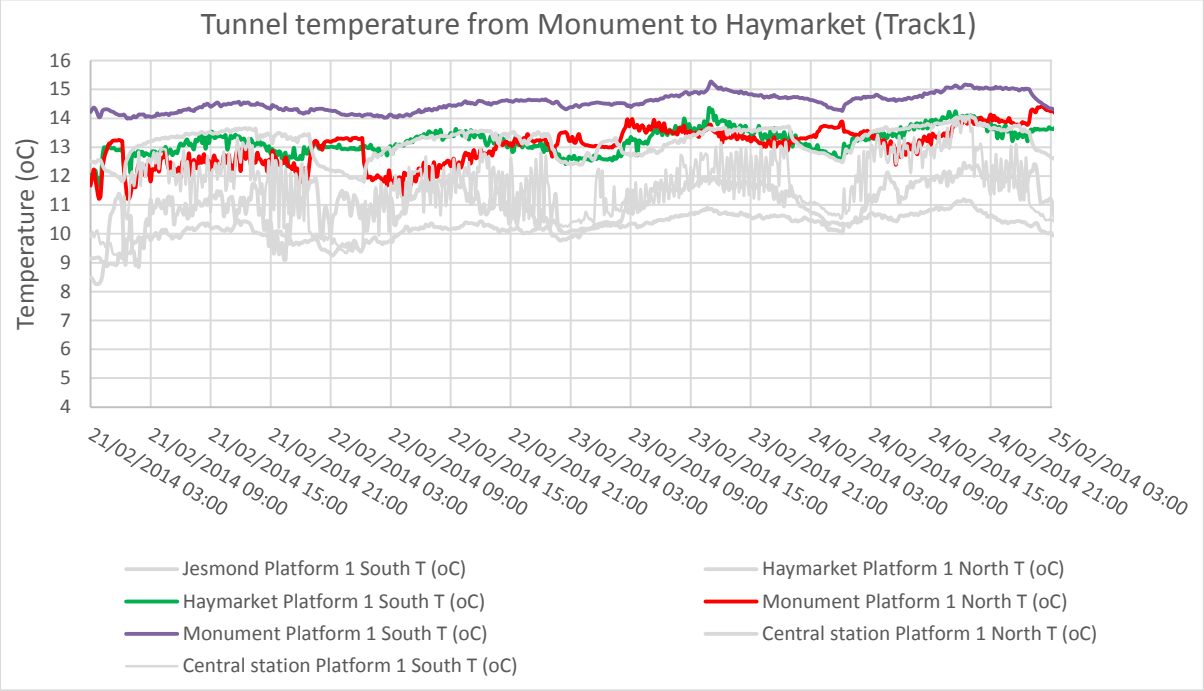

Figure 44: The logger temperatures at track 1 (Each side of the Monument station and south of Haymarket Station)

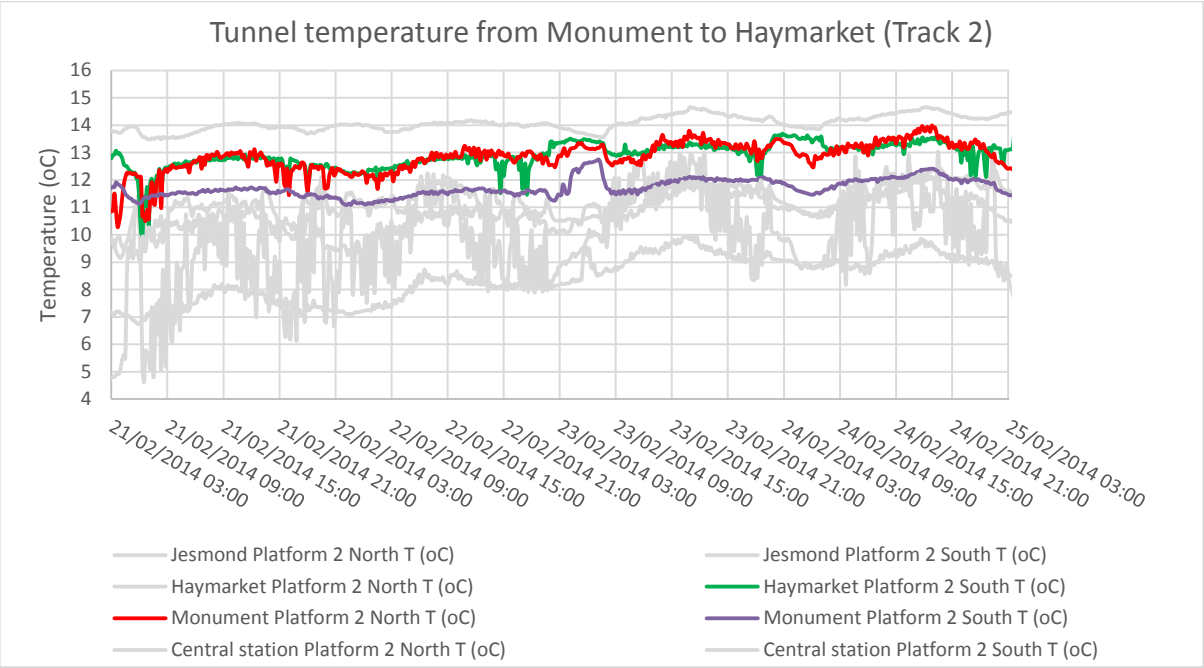

Figure 45: The logger temperatures at track 2 (Each side of the Monument station and south of Haymarket station)

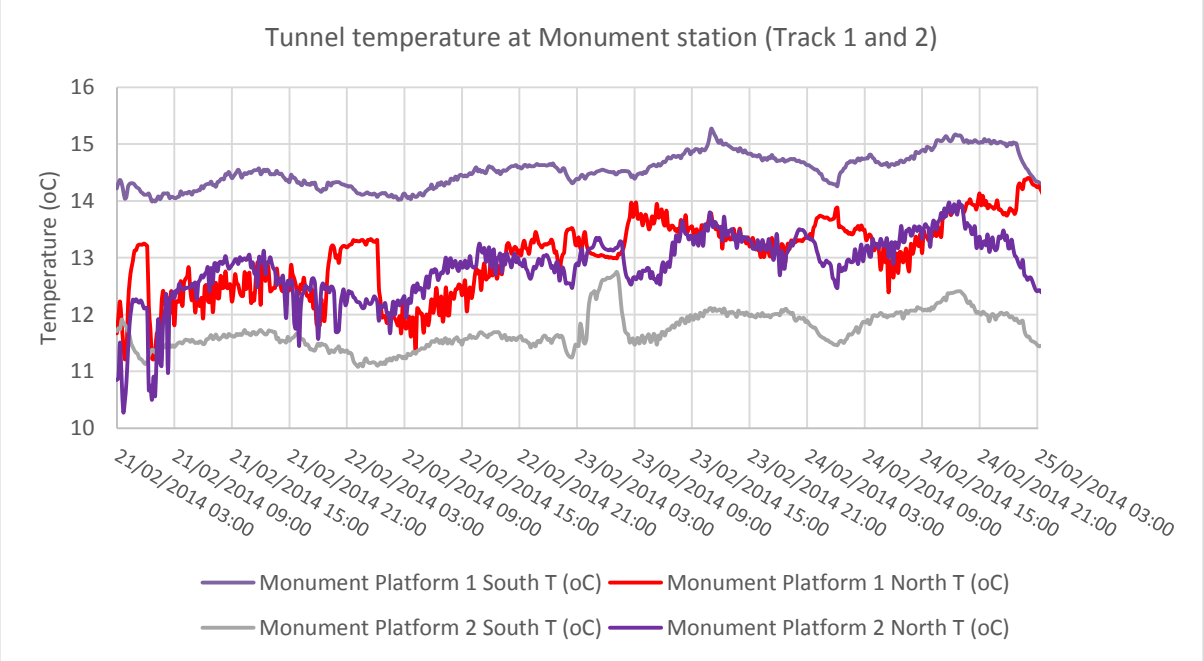

Figure 46: The logger temperatures at the Monument station for both track 1 and 2

The temperature entering the Haymarket station was around 13^{o}C (dark green line) at both tracks as shown in Figure 47 and Figure 48. The temperature was raised 1^{o}C at the north of the Haymarket station on platform 2, but the temperature at the north of the Haymarket station on platform 1 dropped 2^{o}C to 3^{o}C due to the presence of a relief

shaft north of Haymarket platform 1 that allowed cool air to enter the tunnel. This is shown in Figure 40.

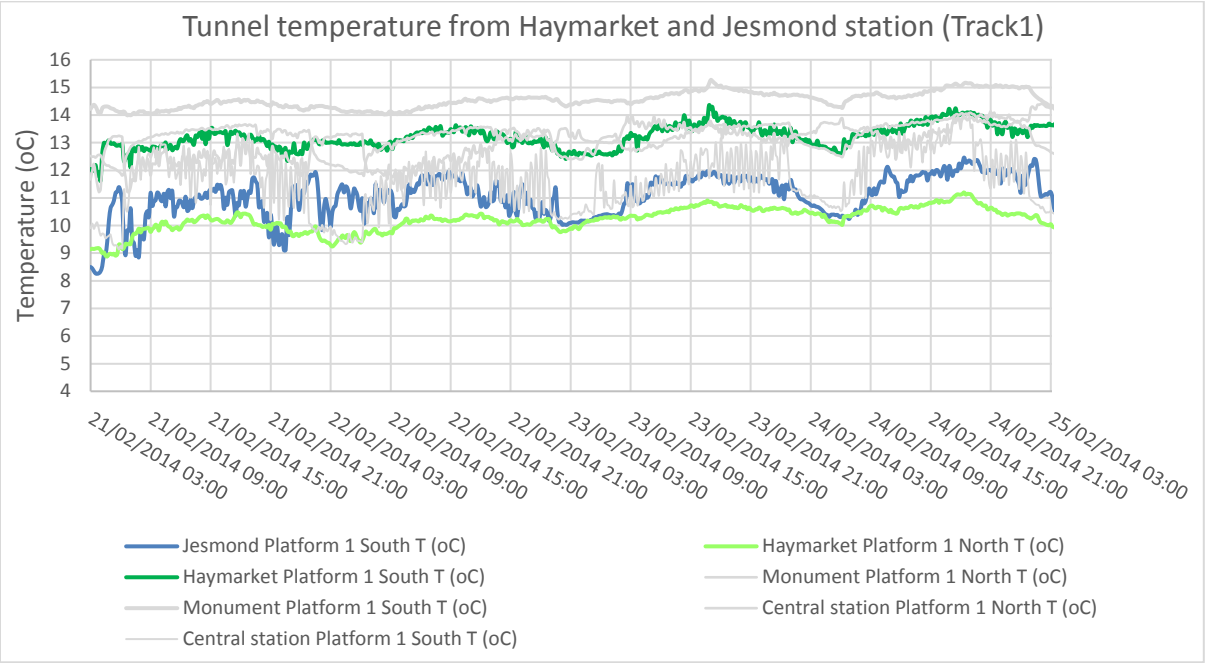

Figure 47: The logger temperatures at track 1 (Each side of the Haymarket Station and south of Jesmond Station)

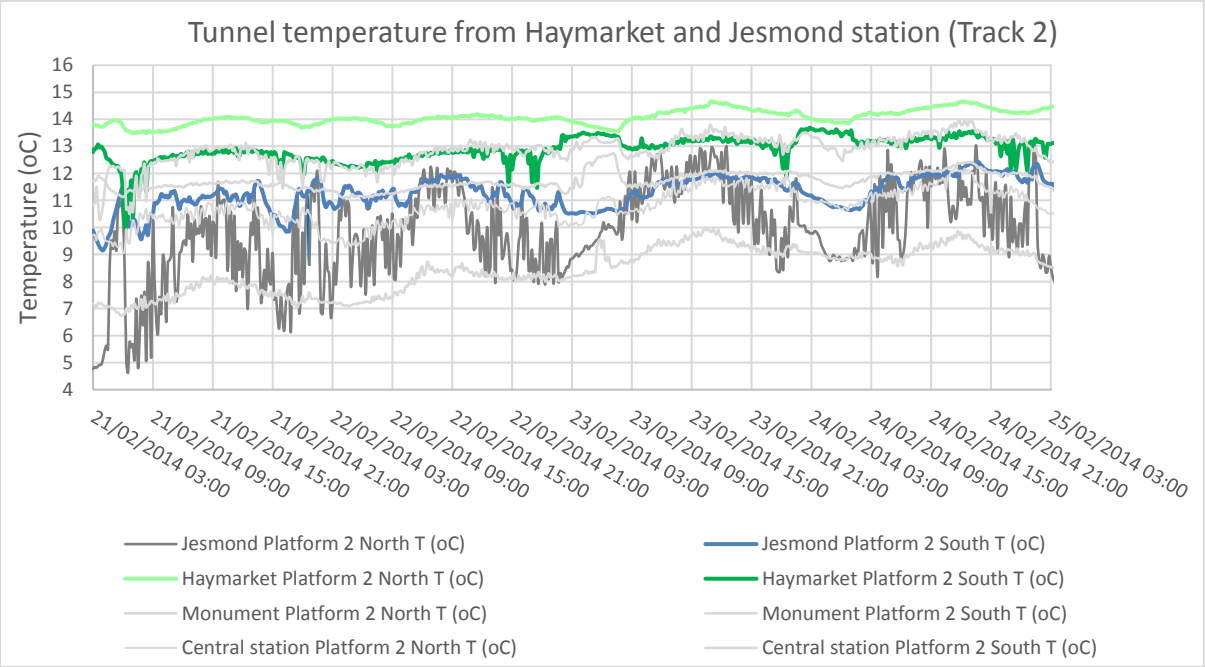

Figure 48: The logger temperatures at track 2 (Each side of the Haymarket station and south of Jesmond station)

The measurements taken at Jesmond station located at the north end of the tunnel showed that the temperature was very close to the weather temperature as shown in Figure 49.

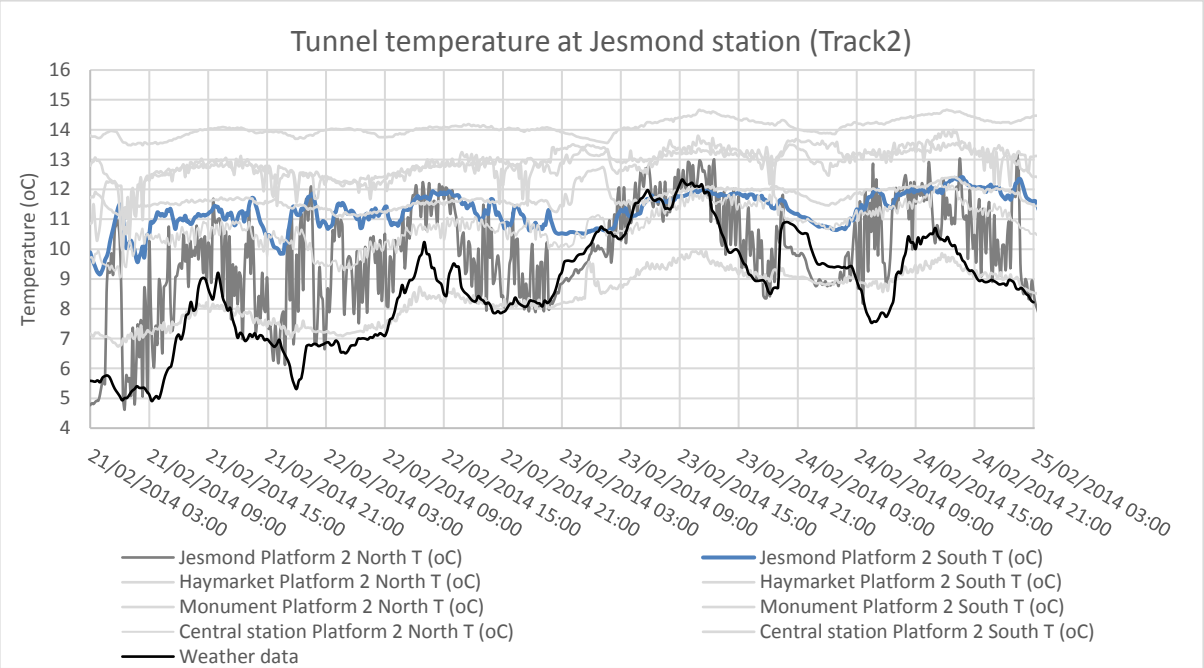

Figure 49: The logger temperatures at track 2 (Each side of the Jesmond station)

5.5.3 Summary of data logger measurement results

Temperature variations in the tunnel can be highly variable. They tend to follow the local ambient temperature but are highly affected by the heat generated within the system. The air temperature tended to increase as it flowed through the tunnels but was also affected by the varying airflow from ventilation shafts and draught relief shafts. In this system, the ventilation shafts had less effect on the tunnel environment compare to the draught relief shaft as the ventilation fans had not been used since 2009. The temperature difference between the local external ambient temperature and the tunnel could up to 9^{o}C as measured at the Monument station platform 1 south at 9:00 on 21/02/2014. It is these temperature differences together with the tunnel geometry elevation that drives a stable background airflow in the tunnel.

5.6 Conclusion

This chapter has presented, described and discussed the air flow and temperature variation inside the station, in the immediate environment outside the station and in the subway tunnels. The findings of a previous study that showed that the mechanical ventilation and gate operation have an immediate and substantial effect on the background air flow and temperature were discussed. Furthermore, very detailed and sensitive measurement were taken using portable instruments and correlations between the weather station data and external weather condition outside the station exits established. These station external condition are the key influencing factor to the air flow inside the station through the exits. This data has also have been used for modelling and validating the microclimate CFD modelling described in Chapter 7. The data measured using portable instrumentation inside the station has shown a very high variation and sensitivity of the air movement within the station leading to a better understanding about the air movements inside the station. In addition, this measurement have been very valuable complimenting data obtained from the ultrasonic anemometers permanently located in the subway especially during operational hours. Lastly, the temperature measurements in the entire tunnel shows the temperature differences between the tunnel and the local weather could be up to 9^{o}C. This has a strong influence on underground air currents as it is this differential that creates the chimney effect driving the air flow through the station which in turn strengthens and stabilises the airflows in the tunnel system.

Chapter 6. Tracer Gas Experiments

6.1 Introduction

The weather data, portable measurement data and air flow and temperature data measured (Chapter 5) together with the tracer gas experiments provide further understanding of the air flow pattern outside and within the station and in the vicinity of the station exits. These very detailed measurements showed the main factors that affected the air flow at different locations inside and outside the station exits. Due to the limitation of taking portable measurements this set of data was unsynchronized at different locations. Therefore, a further detailed study of the internal airflow was conducted by measuring the dispersion of a tracer gas, SF_6, in the station. The objective behind these tests were to provide input data for the CFD model boundary condition and validating it as shown in the research method flow chart Figure 11 (Chapter 3). The experiments also allowed consideration of the residence time and concentration of a toxin in the station and examination of the impact these factors have on the evacuation of passengers from the station. The following sections of this chapter provided details of this experimental work and the results.

6.2 Background

The release of tracer gas for detecting airflows in buildings, mines and many industrial applications is a well-established (Leonard *et al.,* 1984). A commonly used tracer gas is sulphur hexafluoride (SF_6) as it is an extremely stable gas produced entirely anthropogenically so any concentration in the atmosphere is entirely from human activity. A discussion of the atmospheric history of SF_6 is provided in Bullister *et al.* (2006).

Sulphur hexafluoride is used as it is nontoxic, odourless, invisible and easily detectable due to its very low occurrence in the atmosphere of > 0.005 ppb. The safe threshold exposure limit of SF_6 is 1,000ppm (parts per million) for an average eight hour exposure period so experiments can be done in public spaces without any risk for the public. SF_6 is six times heavier than air, but previous experiments proved that it mixed very rapidly with and mimics the behaviour of air (Pflitsch *et al.,* 2010). Shaw (1984) suggested that in tests that are designed to measure the air tightness of buildings it is important to ensure that the SF_6 is evenly distributed in the measuring volume which requires care being given to the mode of dispersion. In this case however such

considerations are not warranted as it is the spatial and temporal concentration of SF_6 that is of interest for this thesis. The method of distribution is of less significance than the dispersion pattern so the tracer gas was released from a gas cylinder containing liquefied SF_6. Two types of tests were designed and undertaken. Experiments 1, 2 and 3 involved releasing the gas inside the station at the lowest platform during the train operational time and during an operation break. SF_6 sensors were distributed throughout the station and in adjoining stations to detect the gas dispersion rate and concentration. Some SF_6 sensors were combined with anemometers as shown in Figure 52. The locations of the SF_6 sensors and ultrasonic anemometers for each experiment are show in section 6.4, 6.5 and 6.6.

The measurements taken previously indicated that the air flow would be northwards along the platform driven by the background air flow but it was also expected that there would be some migration towards the upper platforms but the extent of this was unknown. The aim of the tracer gas experiments in which the gas was released at the platform has been to examine how fast dispersion of hazardous substances could contaminate a whole subway station, which parts of the station were affected and which parts stayed free of contamination. Similar experiments in other subway systems showed that within 5 minutes nearly most evacuation routes were contaminated (Spiegel *et al.,* 2014)

Experiments 4 and 5 involved the release of the tracer gas inside operational trains. These tests mimicked the Sarin gas attack on the Tokyo underground. Two tests were conducted, in the first the gas was released in a train as it travelled from Gateshead station to Ilford Road station. SF_6 sensors were located in the train, as well as in the train following behind and along the underground platforms and stations the train passed through. A second experiment was also conducted in a train travelling in the opposite direction. The aim of these experiments was to examine how fast and over what area a hazardous substances could contaminate stations along the track and to examine the possibility of contamination of a following train.

The tracer gas experiments carried out in this research can be summarised as follows:

	Operational time	Ultrasonic anemometer used	SF_6 sensors used	SF_6 gas released location	SF_6 sensors located
Tracer gas experiment 1:		✓	✓	P1	Monument station
Tracer gas experiment 2:	✓		✓	Between P1 and P2	Monument and neighbouring stations
Tracer gas experiment 3:		✓	✓	Between P1 and P2	Monument and neighbouring stations
Tracer gas experiment 4:	✓		✓	Inside train	Stations the train passed through
Tracer gas experiment 5:	✓		✓	Inside train	Stations the train passed through

Tracer gas experiment 1:

- SF_6 gas released at Monument station lower platform 1 at operation break.
- SF_6 sensors located at Monument station.
- Ultrasonic anemometer located at Monument station (each platform, stairs, escalators and 2 exits/entrance).

Tracer gas experiment 2:

- SF_6 gas released between Monument Station lower Platform 1 and 2 during operational time.
- SF_6 sensors located at Monument station platforms and neighbouring stations.
- No ultrasonic anemometer were used.

Tracer gas experiment 3:

- SF_6 gas released between Monument Station lower Platform 1 and 2 during operation break.

- SF_6 sensors located at Monument Station platforms and neighbouring stations.
- Ultrasonic anemometer located at Monument station platforms.

Tracer gas experiment 4:

- SF_6 gas released inside an operating train on platform 2 track from Felling to Ilford Road
- SF_6 sensors located in the train in which the gas was released, on a following train and on underground station platforms that the train passed through.

Tracer gas experiment 5:

- SF_6 gas released inside an operating train at platform 1 track from Ilford Road to Central station
- SF_6 sensors located in the train in which the gas was released, on a following train and on underground station platforms that the train passed through.

6.3 Monitoring system

The traditional method of monitoring atmospheric concentrations of SF_6 relies mainly on gas chromatography using an electron capture detector, a Shimadzu GC-8AIE is an example (Law *et al.,* 1994; Brüne *et al.,* 2016). These types of instruments provide an analysis of a given sample but are not suitable for providing real time analysis and recording of continuous samples. In the recent past, studies in the Berlin metro system (Pflitsch *et al.,* 2013) relied on air samples being captured in syringes at strategic points in the subway. The samples were then later analysed in a laboratory. This method was labour intensive and suffered from a low sample rate because of the time taken to prepare and load the syringe. Pflitsch *et al.* (2013) indicated that new sensor platforms were developed and deployed. The new sensors were based on the principle of infrared absorption in which an integrated gas sensor consisting of a modular blackbody radiator and an interference filter tuned to the absorption frequency of SF_6 of 10.6 µm as shown in Figure 50 (Brüne *et al.,* 2016). They are able to measure concentrations of 0.05 ppm to 50 ppm (optical measurement range) of SF_6 (Potje-Kamloth, 2014).

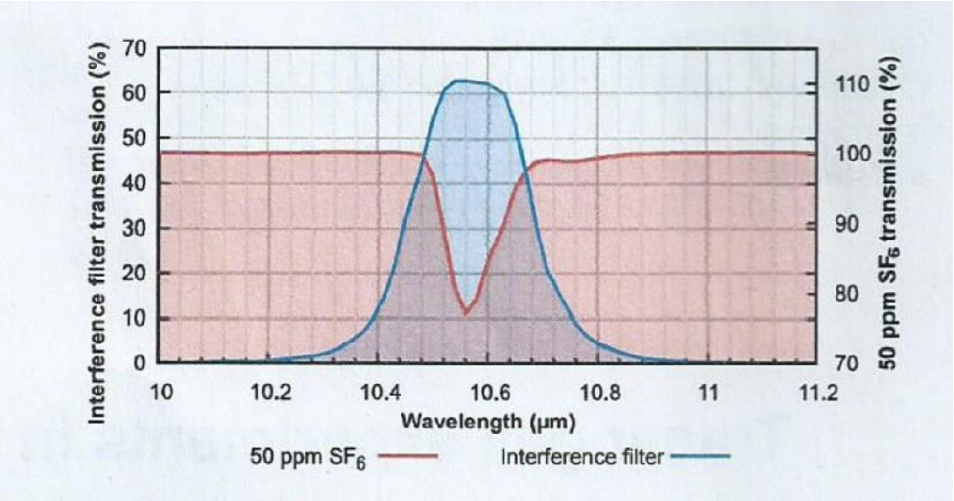

Figure 50: Transmission of the interference filter and absorption bands of SF_6. (Brüne *et al.,* 2016)

The detector units employed a novel amplifying and signal conditioning software that used a map-correlation algorithm, which decoupled the sensor from ambient temperature and pressure fluctuations. These results in a very low nonlinearity in the sub ppm range for a temperature range of -10°C to 40°C as shown in Figure 51. Figure 52 shows the release of the SF_6 at the platform, the portable SF_6 sensors and the ultrasonic anemometers employed as part of the experiments related to this thesis. The detector units were designed to be interfaced with air flow and temperature sensors.

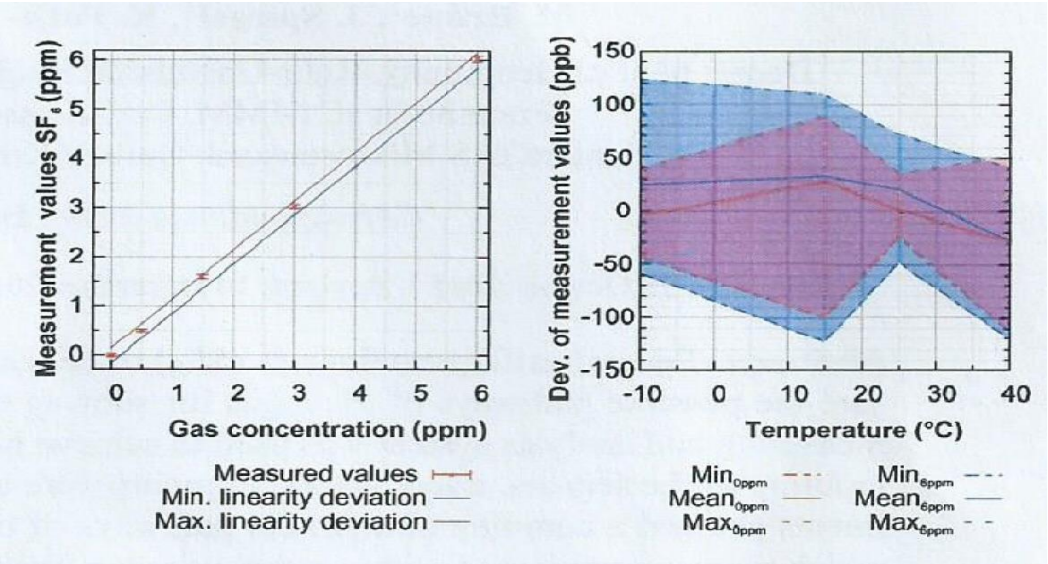

Figure 51: Representation of the nonlinearity in the sub-ppm range of the SF_6 detector over a temperature range -10°C to 40°C (Brüne *et al.,* 2016)

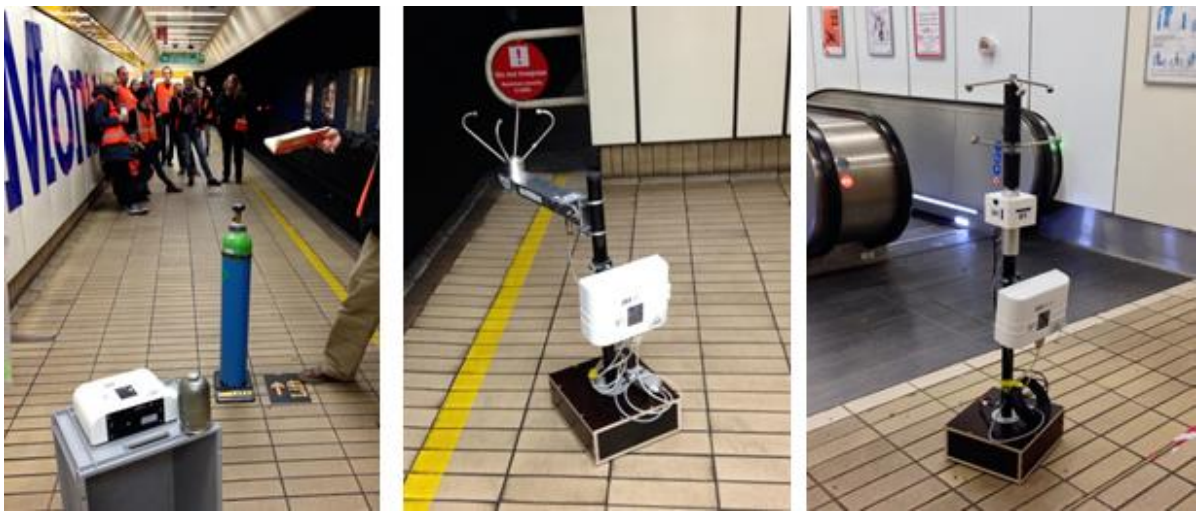

Figure 52: Photos of release SF_6 at platform, SF_6sensors and ultrasonic anemometers

6.4 Tracer Gas Experiment 1

6.4.1 Tracer Gas Experiment 1 setup and map

In tracer gas experiment 1, the release point of the tracer gas was at the lowest level in the middle of platform 1 north of the corridor to the escalator but before the staircase linking to platforms 3 and 4. A gas sensor was placed at every tunnel portal, at the connections to the main concourse and the other platform level and at two places in the middle of platform 1 adjacent to the gas bottle. This was repeated on the other level. Platform 3 and 4 were equipped with gas sensors at each end and ultrasonic anemometers were used to measure the air velocity at the same time. The position of the velocity sensors can be seen as the blue circles in Figure 53. SF_6 sensors were also placed at the top of the escalators in the station concourse and adjacent to the exits to Blackett Street and Grey Street as shown in Figure 53.

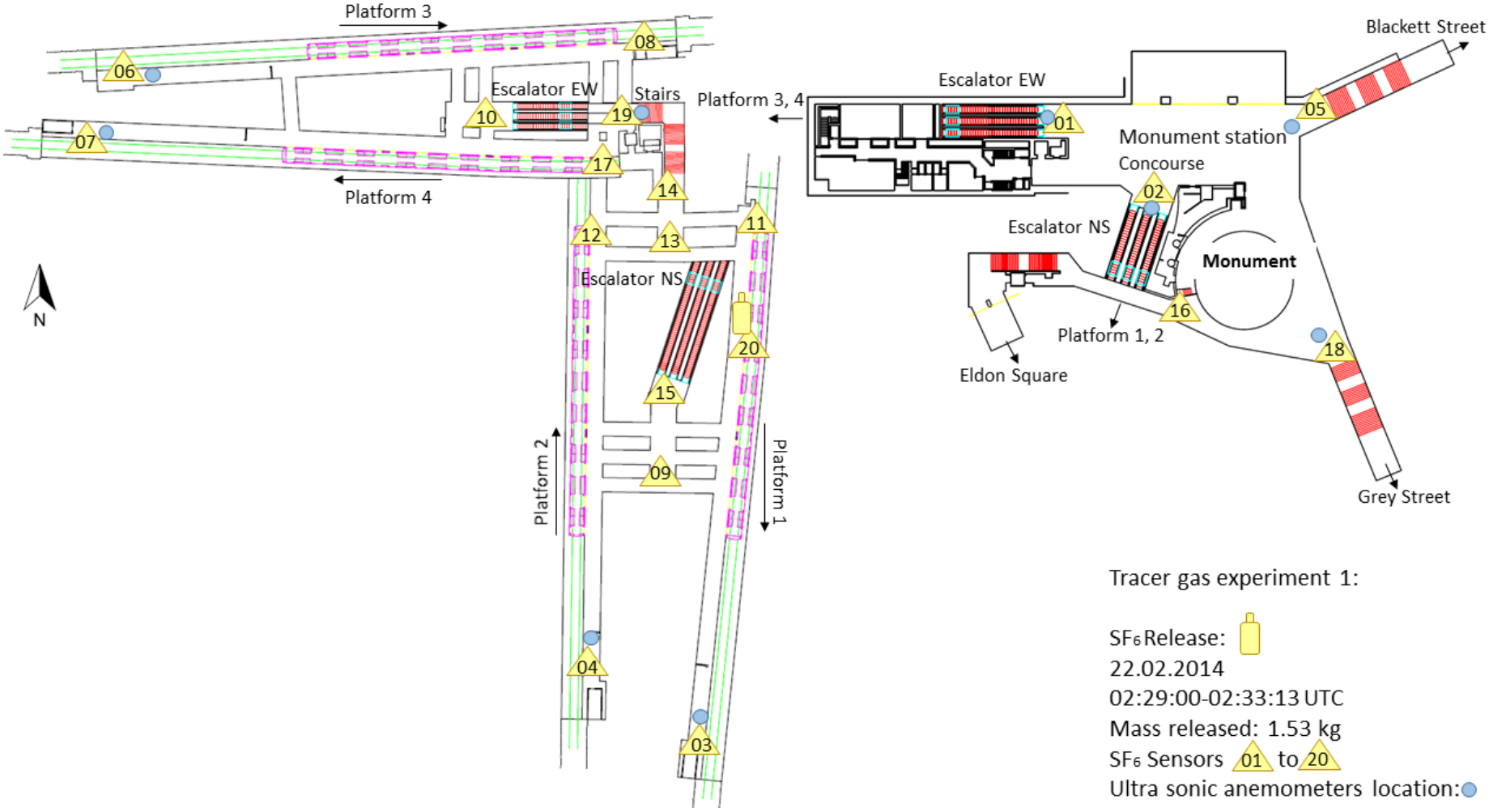

Figure 53: Location of the measurement instruments in Monument Station for Tracer Gas Experiment 1

6.4.2 Tracer Gas Experiment 1 ultrasonic anemometer result

This experiment was conducted from 02:29:00 to 02:33:13 on the night of 22/02/2014 during the nightly operational break. One and a half kg of SF_6 were released into the station. This was intended to indicate the nature of the natural background air flow within the station. The ultrasonic anemometer simultaneously measured the air flow, temperature and humidity at the blue points indicated in Figure 53. The graph below shows the velocity data over the time period from 02:20 to 03:10. It is customary when showing the output from an ultrasonic anemometer to designate one direction as positive and flow in the opposite direction as negative. The air flow speed displayed in Figure 54 to Figure 56 are in 50 minutes and 7 minutes time range respectively of each platform level during the gas release time. However in Figure 54 (NS tunnel) and Figure 55 (EW tunnel) all the flows on the platforms are in the same direction and in Figure 56 the flow at the escalator is upwards towards the concourse area. The flow at the staircase linking the lower and upper platforms is shown as negative but in this case the flow is from the lower to the higher platforms not in the opposite direction to the platform air flow. This has been done for clarity as otherwise the graphs would have overlapped and been very difficult to read.

From the measurement results at the NS tunnel level, it can be seen that the velocities are stable with a small degree of variability. The average velocity at platform 1 was 0.4m/s which is lower than the platform 2 average velocity of 1m/s. The direction in both cases was from south to north. The air flow at platform 1 shows a larger variation than platform 2, it is thought this is due to the presence of a ventilation shaft located close to platform 1. The velocity at the escalator is upwords from the platforms to the concoures level at an average speed of 1m/s. The air flow at the connecting stair case between the lower and upper platforms varied between 0.4 m/s and 1.5 m/s from the lower to the higher platforms.

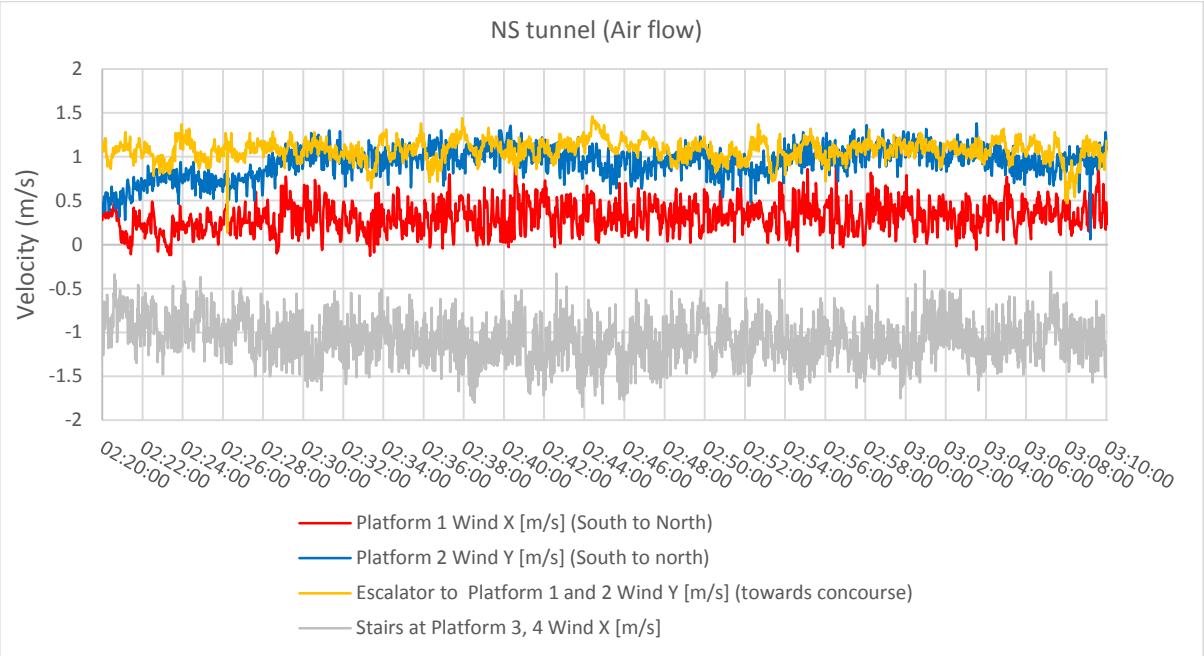

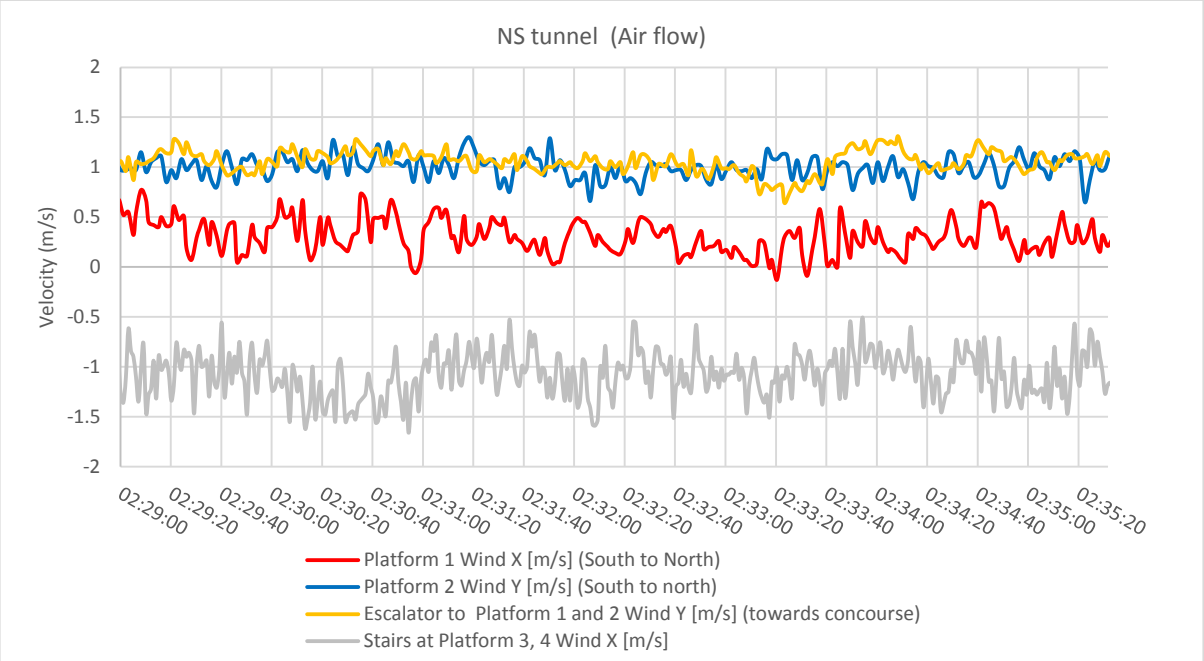

Figure 54: Tracer gas experiment 1 ultrasonic anemometer air flow result at the North-South tunnel platforms 1 and 2

The air flow results in the EW tunnel at platform 3 and 4 indicate a lower airflow velocity from east to west. The strongest air flow at this level is from the stair well linking the different levels. The escalator airflow indicated a large degree of variability with frequent flow reversals that correlate to the unsteady air flow behaviour at the concourse Exit 1.

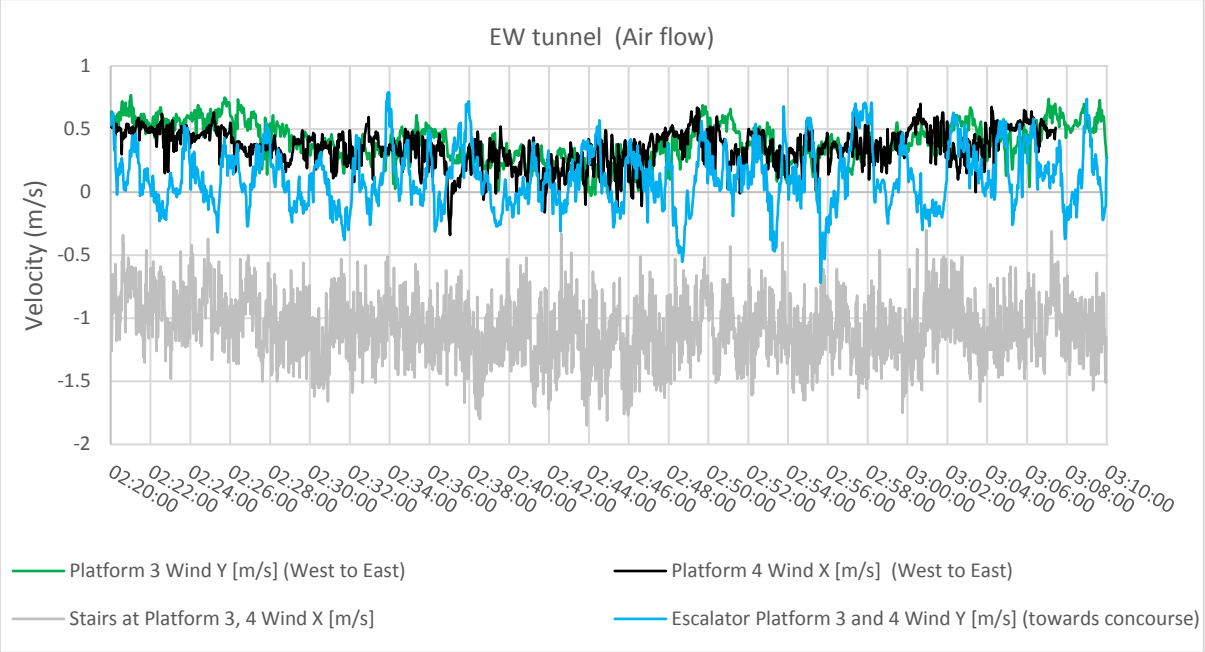

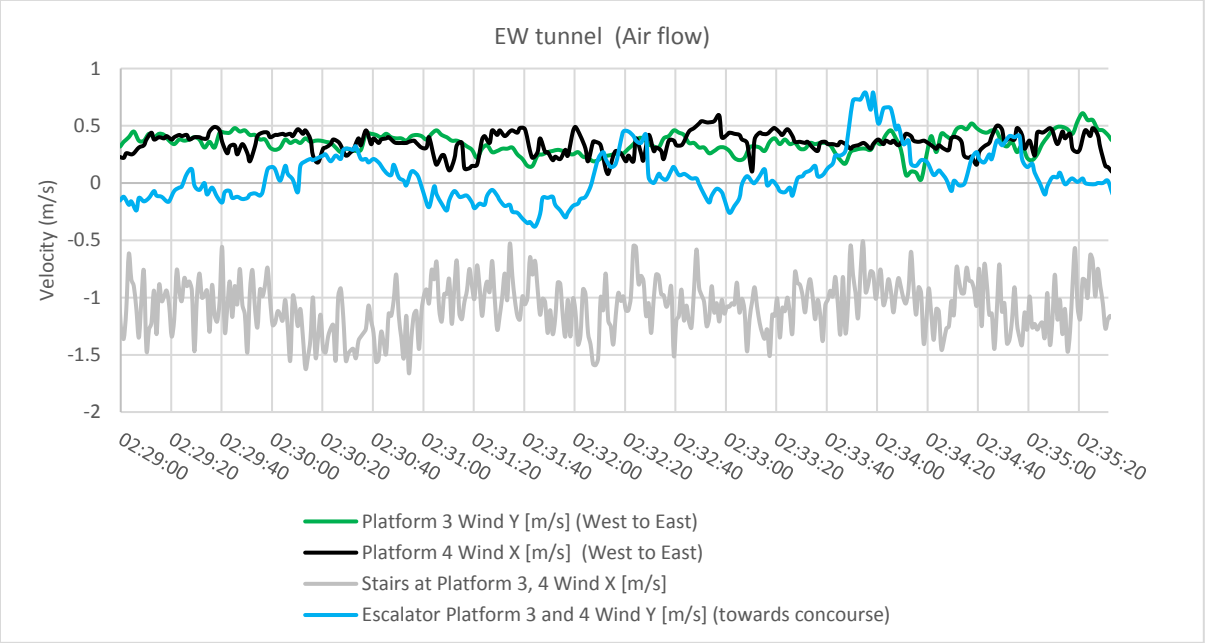

Figure 55: Tracer gas experiment 1 ultrasonic anemometer air flow result at EW tunnel

For compareison with exit air flow, the esclator air flows shown in Figure 56 are the same as the NS and EW tunnel graphs. The exit air flow is variable with a maximum value up to 2m/s flowing from the coucourse to the outside. This is shown over a shorter time range in Figure 56 which indicates that the flow from platform 1 and 2 has the least variability but the flow from the East-West platforms is linked to the flow at Exit 1 in that a higher velocity at the exit produces a reverse flow at the escalators to platform 3 and 4. This is the first indication that the outside weather plays a roll in determining the air flow in the station.

Figure 56: Tracer gas experiment 1 ultrasonic anemometer air flow result at concourse area

The ultrasonic anemometers, indicated as a blue circle in Figure 53 are also measured the temperature throughout the duration of Experiment 1. It was noticed that the ultrasonic anemometers placed on the platforms indicated a different temperature to that recorded by the data logger placed in the tunnel which was discussed in Chapter 5. In addition the data logger measurement step was 10 minutes whereas, the ultrasonic anemometer time step was 1 second resulting in the anemometer output being much more detailed. This can be appreciated by comparing Figure 57 showing the temperature graph from the ultrasonic anemometer with Figure 58 and Figure 59 which show the temperature recorded by the data logger during Experiment 1 at Monument tunnel track 1 and 2 and at track 3 and 4 respectively. The anemometer measurements provided details of the temperature distribution around the station whereas the data logger only measured the tunnel temperature, These results will be used as input data and for validating the CFD modelling of the station in Chapter 7.

It can be seen from the results shown above that the air temperature at the stair case and the escalators are higher than the temperatures at the platforms and in the tunnels. This could be a result of the heat released from the lighting, advertisement illumination and escalator motors. Although there are slight discrepancies from the ultrasonic anemometer and the data logger they both show that the temperature at platform 1 is 4ºC which was 3ºC higher than platform 2 and platform 3 is 1-2ºC higher than platform 4. That could be caused by interference from a ventilation shaft installed in the tunnel.

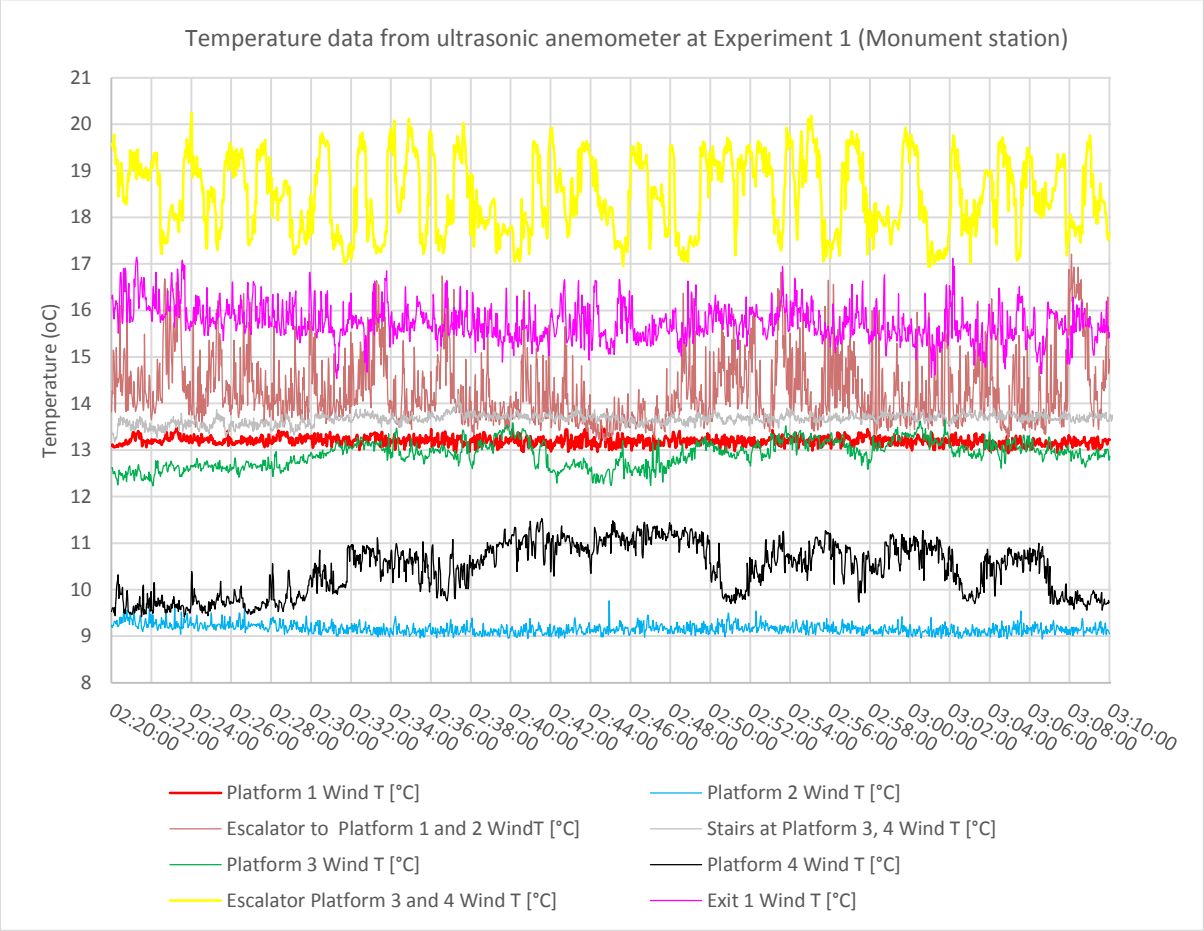

Figure 57: Tracer gas experiment 1 ultrasonic anemometer temperature data at Monument station (50 minutes time range)

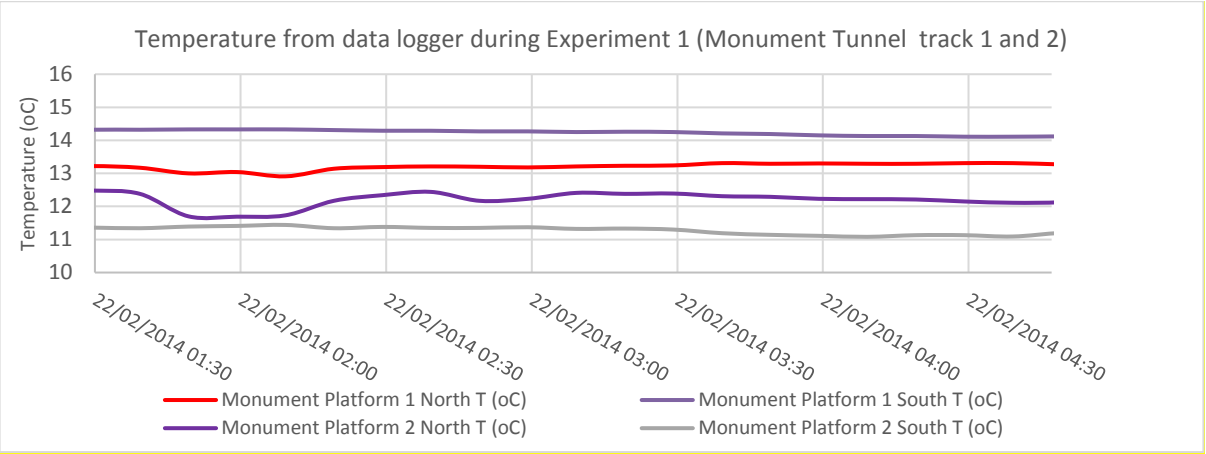

Figure 58: Temperature from data logger during Experiment 1 at Monument tunnel track 1 and 2 (3 hours' time range)

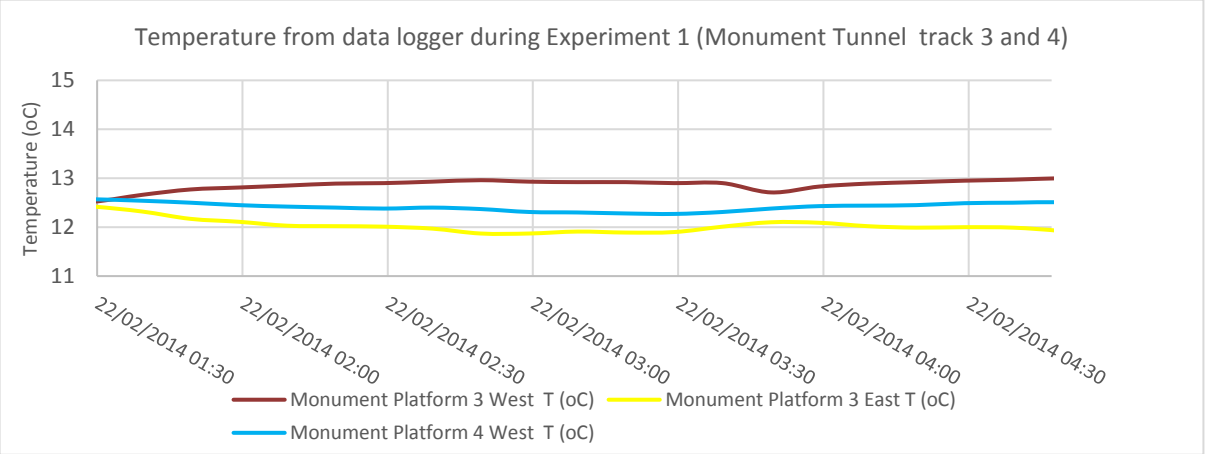

Figure 59: Temperature from data logger during Experiment 1 at Monument tunnel track 3 and 4 (3 hours' time range)

6.4.3 Tracer gas experiment 1 tracer gas concentration results

The results of the tracer gas tests are presented in this section. The location of the gas sensors placed in this expriment are shown in Figure 53.

The temporal development of tracer gas dispersal during the experiment is displayed in Figure 60,Figure 61 and Figure 62. The tracer gas was emitted on the lower platform in the middle of track 1 north of the escalator exit but south of the stairwell linking the different tracks. Within the first minute after discharge the SF_6 was detected on the opposite platform of the lower track, platform 2, the other parts of the station were not affected until 3 minutes after the release. These features can also be appreciated by considering the readings of the SF_6 detectors.

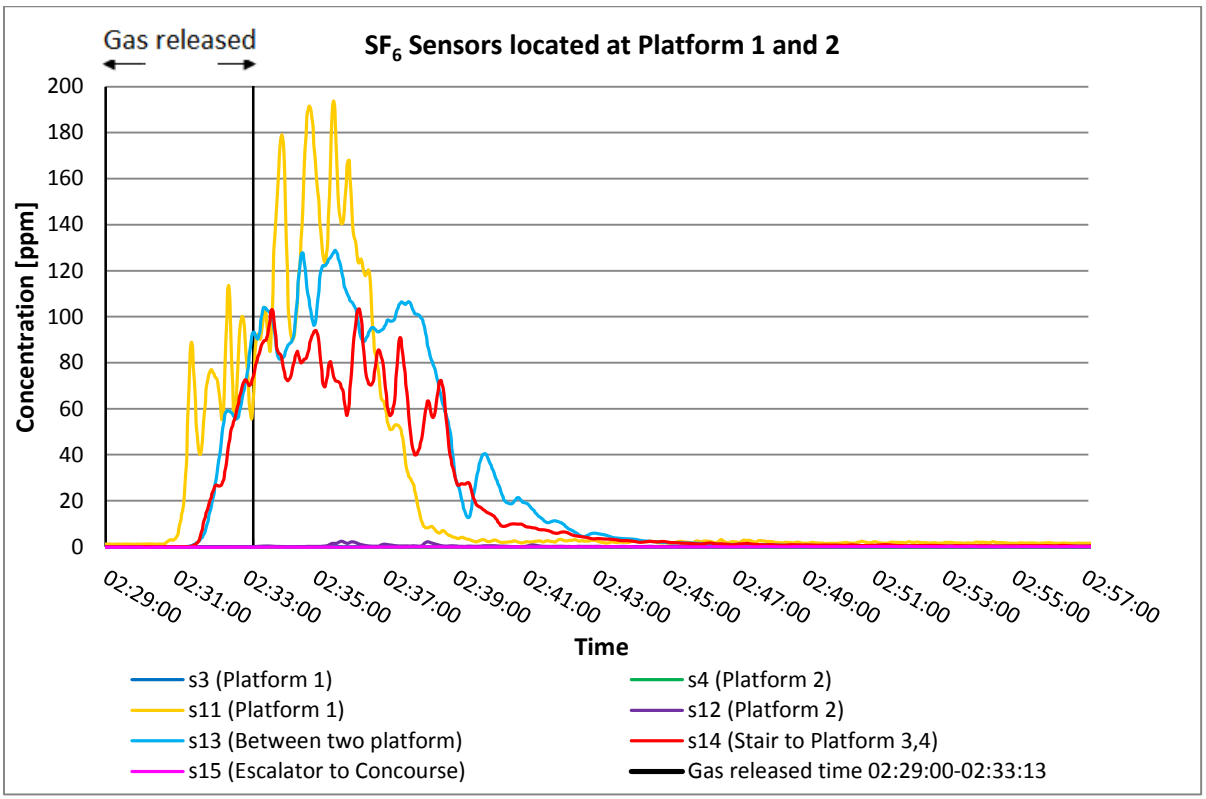

Figure 60: SF_6 concentration at Monument station platform 1 and 2 of tracer gas experiment 1

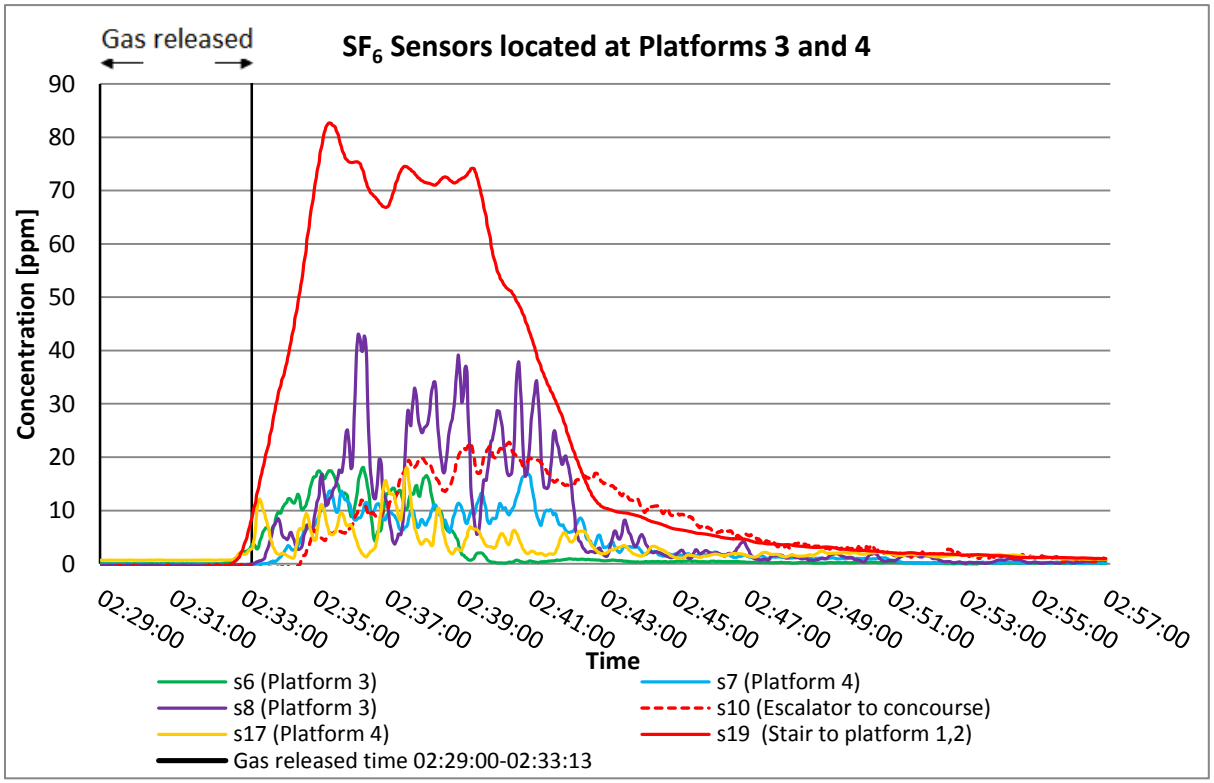

Figure 61: SF_6 concentration at Monument station platform 3 and 4 of tracer gas experiment 1

After three minutes the gas is seen to have spread via the stairway, connecting the two platforms to the EW tunnel platforms 3 and 4, with a very high concentration over 100 ppm. The mechanism that drove the SF_6 up the stair well is unclear as the dominant background air flow on platform 1 is northwards towards the Haymarket station but as can be seen in Figure 60 a significant proportion of the SF_6 detected by sensor 14 is moving up the stair well to platform 3 and 4. The other sensors on platform 1 and 2 that are upstream (in terms of the background air flow) of the gas release point, sensor 3, 4, 9 and 15 do not detect any levels of SF_6 for the duration of the experiment.

After six minutes (Figure 60) only the northern area of the lowest level NS tunnel was affected, while the remaining parts stayed free of SF_6. The upper level was now completely filled with tracer gas while the concourse stayed clear. It is clear from the recordings of sensor 15 at the base of the escalator and sensor 2 at the top. That the SF_6 was entering the concourse area from the escalator from the EW tunnel (platform 3 and 4) as can be seen from the readings of sensors 1 and 10. It is remarkable that the escalator from the lower level to the concourse area, despite the short distance to the release point, stays free of SF_6 over the entire test period. In an emergency, this would be the ideal escape route from the lower level as the concourse shows no contamination until 10 minutes after the gas release. After 19 minutes, the concentration has almost completely disappeared from the lower level. The upper level is still partially affected but with a rather low concentration. However, the tracer gas has moved from the upper level via the central escalator to the concourse and contaminated a large area. All three exits to the surface show a medium concentration of SF_6 however what is surprising is that the exit that shows the highest concentration of SF_6 is Exit 2 that leads into Eldon Square shopping centre whereas the outside exit onto Blackett Street, Exit 1, shows much lower SF_6 concentration.

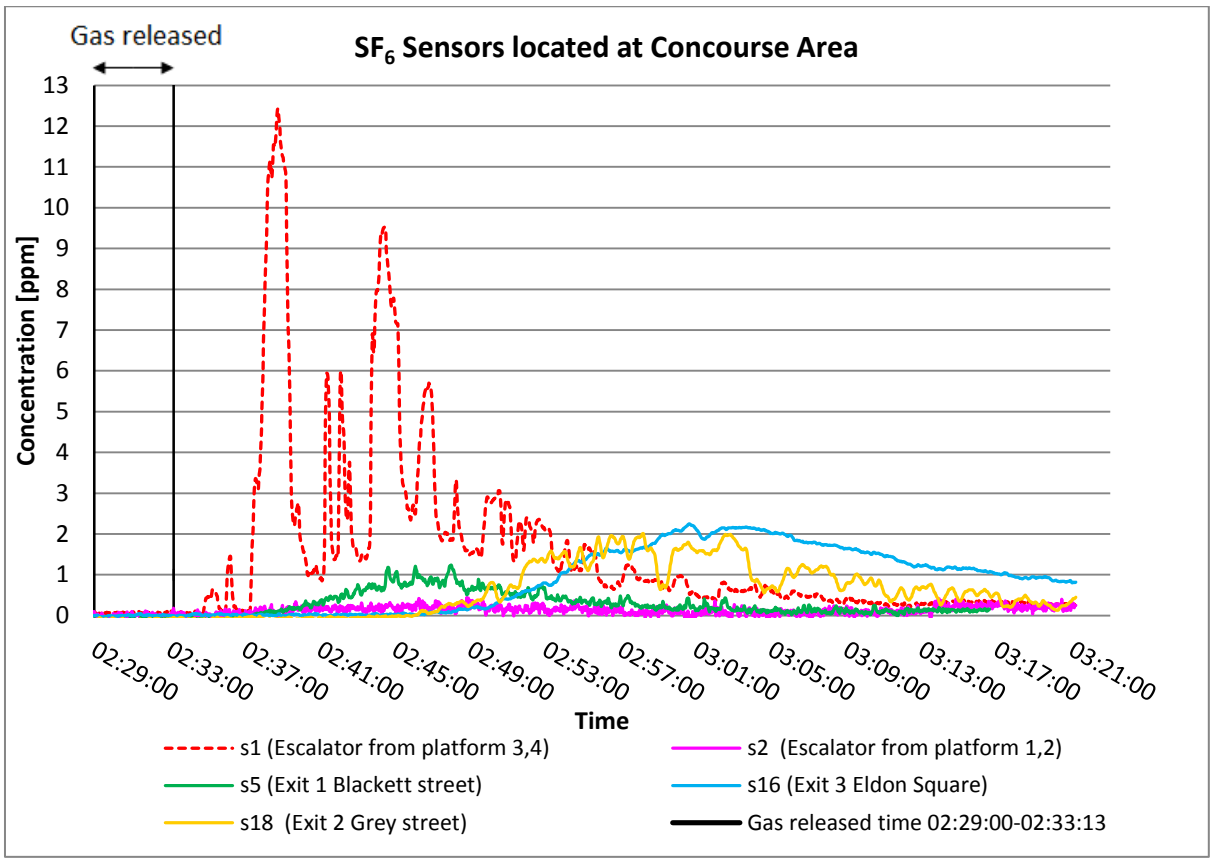

Figure 62: SF_6 concentration at Monument station concourse area of tracer gas experiment 1

The behaviour of the SF_6 in choosing that particular migration path was most unexpected. The most important result is that showing the contamination of the stairwell connection between the two tunnels. This occurs because of a chimney effect from the lower level supported by a clear inflow of warm background air from the south end of the NS tunnel at the lower level. This is shown in Figure 54 as a steady inflow of approximately 1 m/s by the ultrasonic anemometer located at platform 2 and a smaller inflow of 0.25 m/s by the ultrasonic flow meter located at platform 1. The upper level EW tunnel shows a small but steady outflow of 0.4 m/s in the west direction towards St. James station. The ultrasonic flow meter placed in front of the stairway between the upper and lower level shows a strong airflow of 1.25 m/s from the lower to the upper level. The Exit 1 at Blackett Street in the concourse demonstrates a strong airflow to the surface of average 1.5 m/s, interrupted by various dips of cold air. The connection between the concourse and the two platform levels shows different airflow patterns.

The connection from the concourse to platform 1 and 2 shows a steady flow of 1m/s from the lowest level to the concourse while that from platform 3 and 4 shows an

alternating flow with slightly more movement from the EW tunnel (upper level) to the concourse (see Figure 55 and Figure 56). The concourse level with connected shops is relatively warmer than the rest of the station and therefore pulls air out of the lower parts. This could be the source of this chimney effects. The stable background air flow conditions on the NS tunnel (lower level) can be explained by the tunnel geometry. Northwards the tunnel rises up to the next station approximately a total of 25m. The relatively light warm air within the tunnel system is moved through the rising tunnel by a chimney effect. The same situation occurs on the EW tunnel (upper level), where the next station to the west is St. James, which is some 10m higher than the Monument station. The relative magnitude of these chimney effects will determine whether the air flow at the lower level is dominant which will draw air into the station or whether the air flow to Saint James is dominant which will then draw air through and away from the station from the lower level. The unexpected flow of SF_6 into the Exit 3 and shopping centre outside Exit 3 is a point of concern as this could place hundreds of shoppers at risk in the event of a chemical or biological attack.

6.5 Tracer gas experiment 2 and 3

Tracer gas experiment 2 and 3 were performed in order to track the propagation of the SF_6 to the adjacent stations at operational time and during an operation break respectively. Two experiments were performed, one during the operational time of the metro at 20:15:00 on 22/02/2014 when 2.15 kg SF_6 were released over a 10 minute period and the second in the operation break at 00:52:00 on the 22/02/2014 when 2.06 kg SF_6 were released over a period of 8 minutes and 22 seconds. In contrast to experiment 1 the SF_6 was released in the passage linking platform 1 and 2 but north of the escalator to the concourse level as shown in Figure 63. A number of SF_6 sensors were placed at the platform ends in the Monument station and at the end of the platforms of the adjoining stations but the ultrasonic anemometers were not used in this experiment as their presence would have impeded the movement of passengers. The tracer gas release point and the sensor locations in tracer gas experiment 3, as shown in Figure 64, were the same as in experiment 2 but this occurred during an operational break.

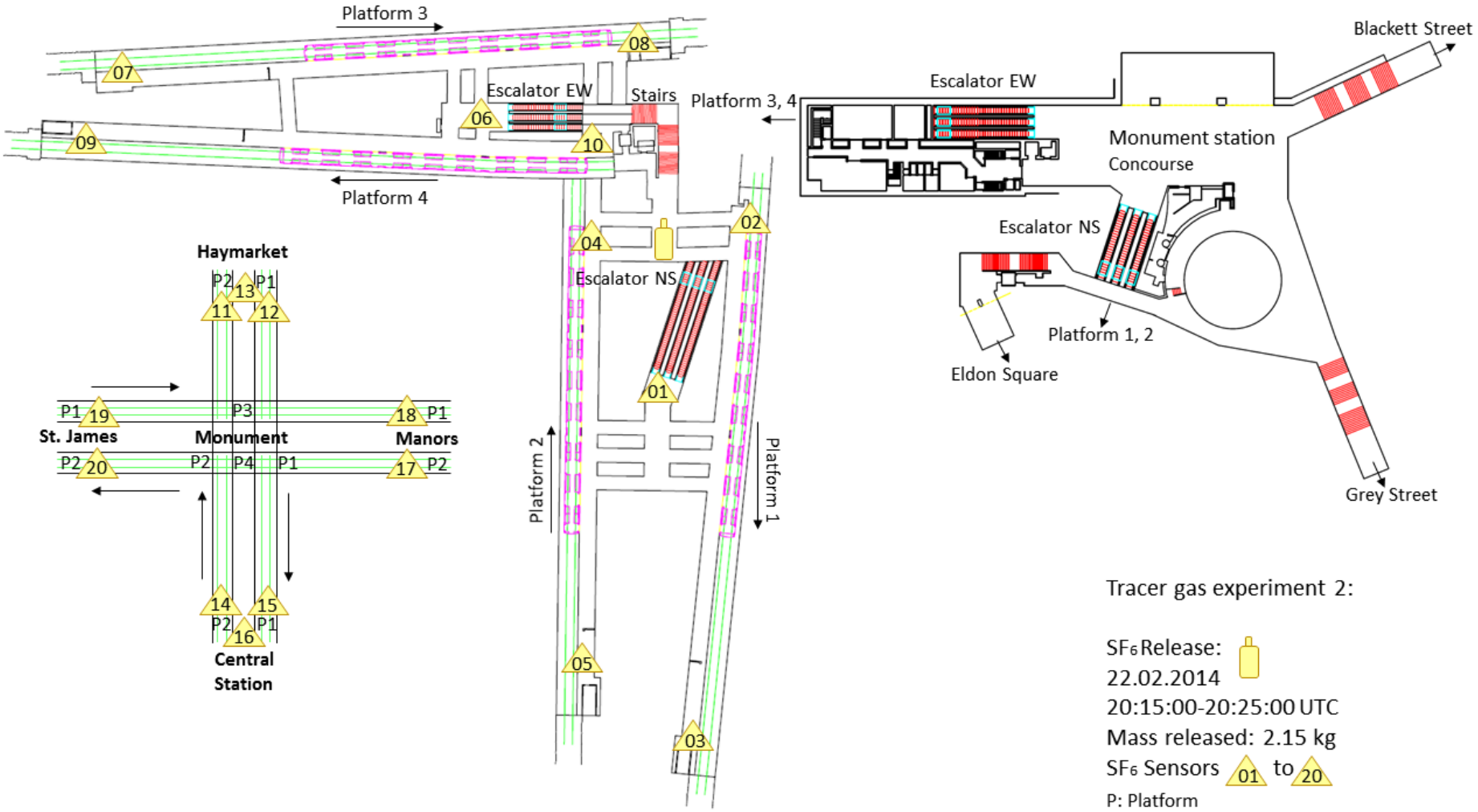

Figure 63: Location of the measurement instruments in Monument Station and neighbouring Stations for Tracer Gas Experiment 2 (operation time)

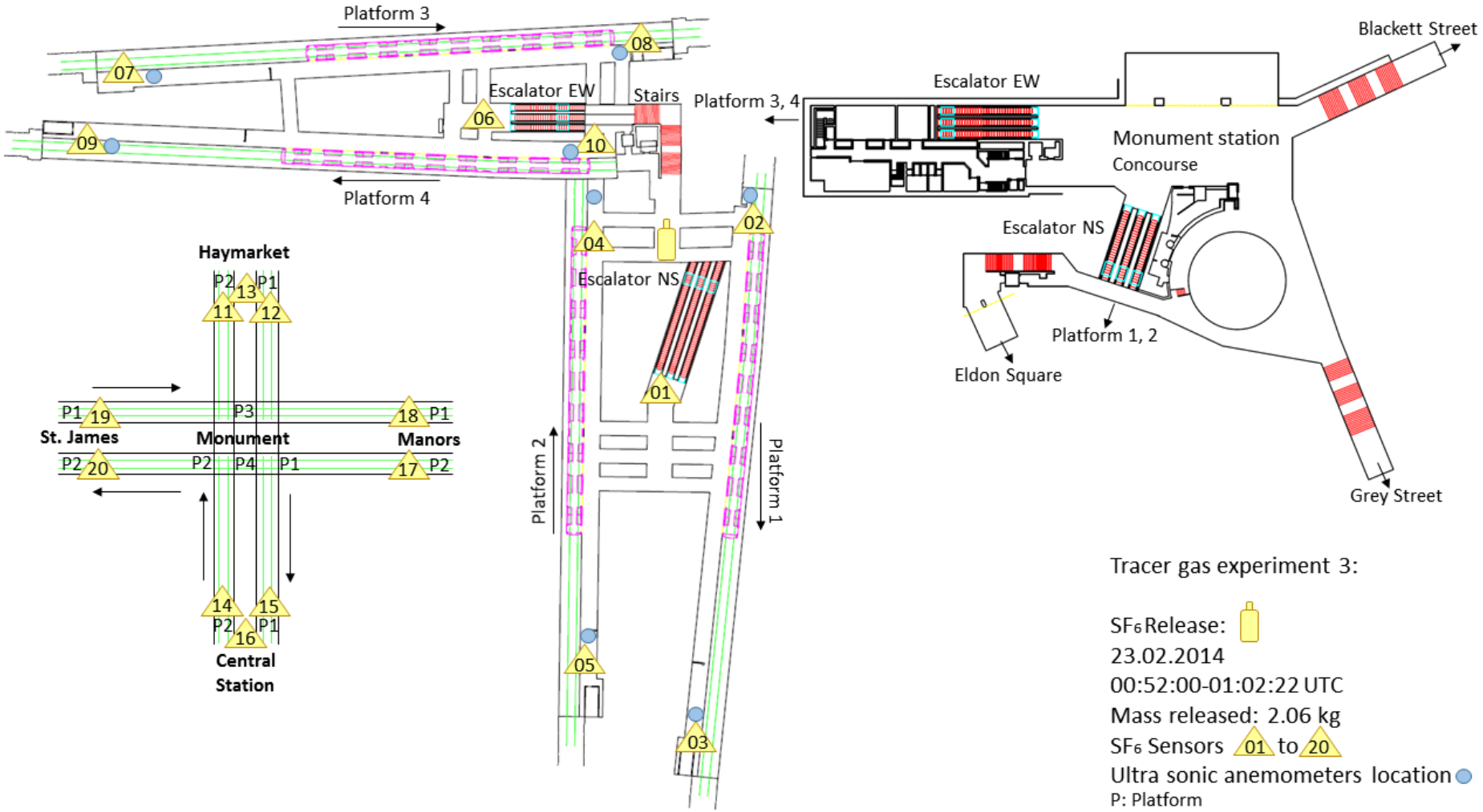

Figure 64: Location of the measurement instruments in Monument Station and neighbouring Stations for Tracer Gas Experiment 3 (operation brake)

6.5.1 Tracer gas experiment 3 ultrasonic anemometer result

In contrast to experiment 2 in which one ultrasonic anemometer was located at one end of each platform and at the concourse area, in this experiment anemometers were also located at each end of the platforms. This allowed the conditions on the platforms to be examined in more detail and gave an indication of the amount of air that was diverted from the tunnels into the station. The air flow direction at the NS tunnel showed the same results as in experiment 1 from south to north but as shown in Figure 65 and Figure 66 the airflow leaving the station at the north end of both platforms was slightly lower and had smaller variability than that entering the platforms from the south.

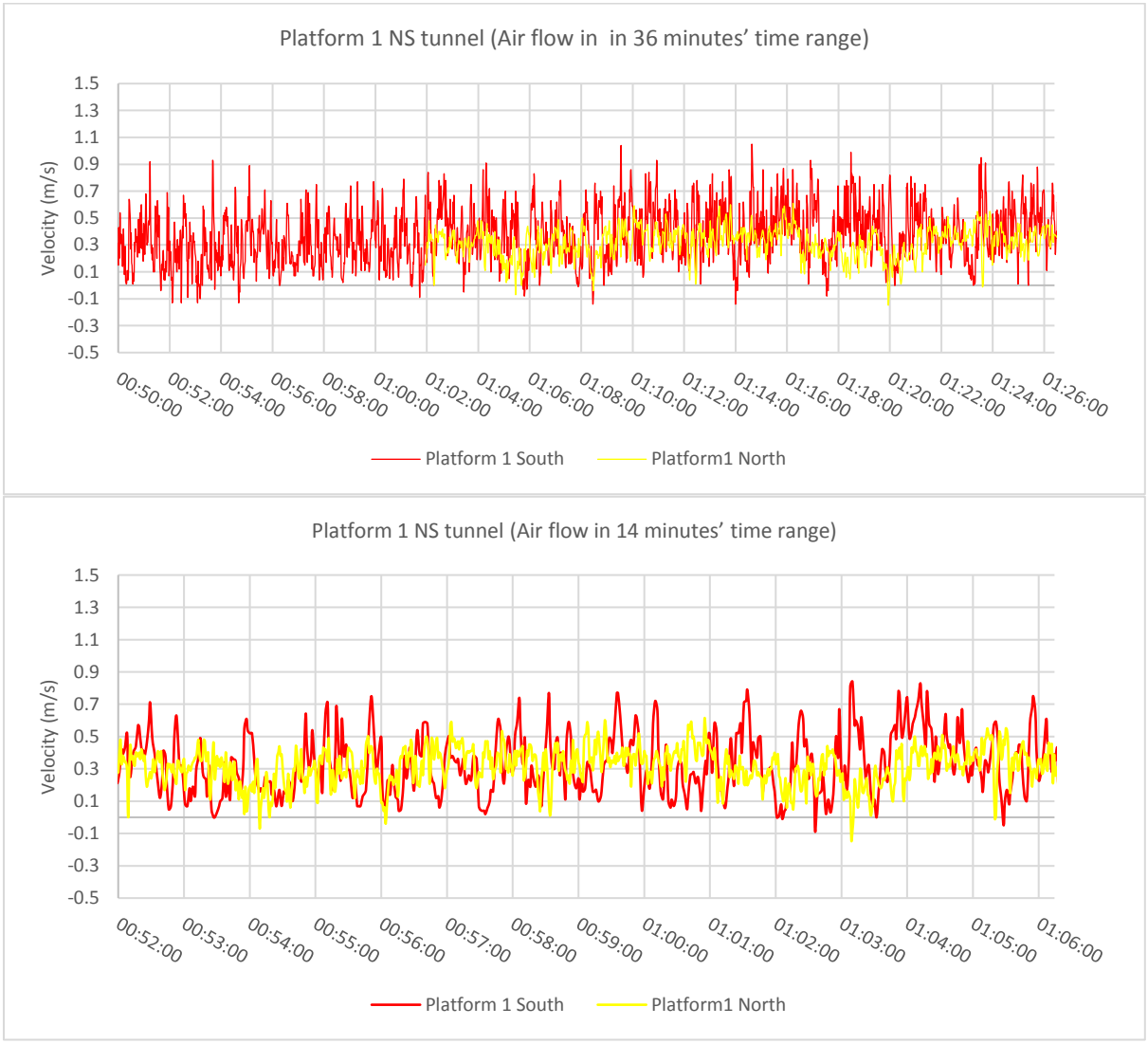

Figure 65: Tracer gas experiment 3 ultrasonic anemometer air flow result at platform 1 NS tunnel

Figure 66: Tracer gas experiment 3 ultrasonic anemometer air flow result at platform 2 NS tunnel

Figure 67 and Figure 68 show the East-West tunnel air flows, the positive flow speed indicate the flow direction to be from east to west, the negative indicate the flow direction from west to east. The flow reverses frequently on both platform 3 and 4 within a small range up to 0.6m/s. The air flow was mainly from the east to west direction with the velocity at the west end of both platforms, leaving the station, being larger than that entering from the east. This air flow speed discrepancy was greater than for the North-South tunnel. These results are the key to set up the boundary conditions for the CFD station simulation and for validating the simulation results in Chapter 7.

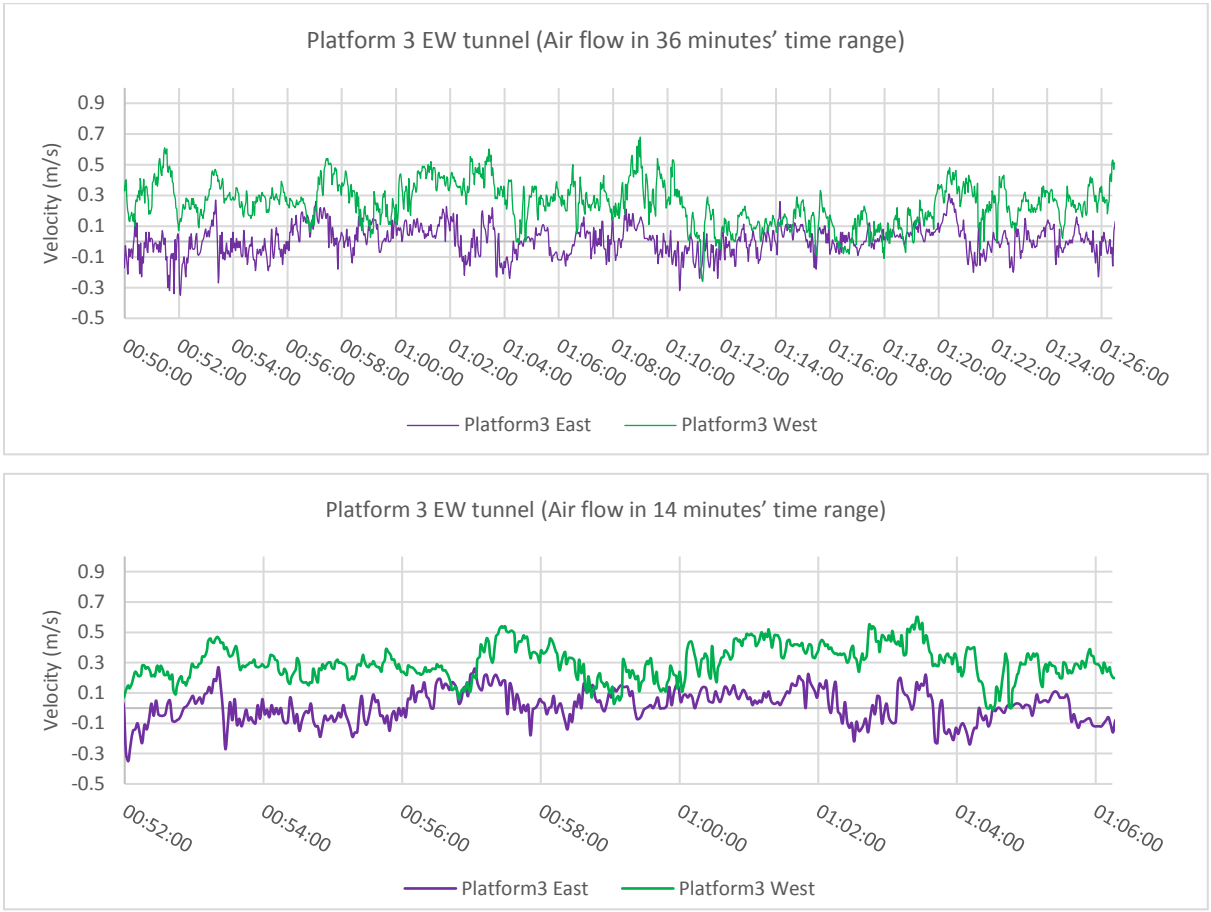

Figure 67: Tracer gas experiment 3 ultrasonic anemometer air flow result at platform 3 EW tunnel

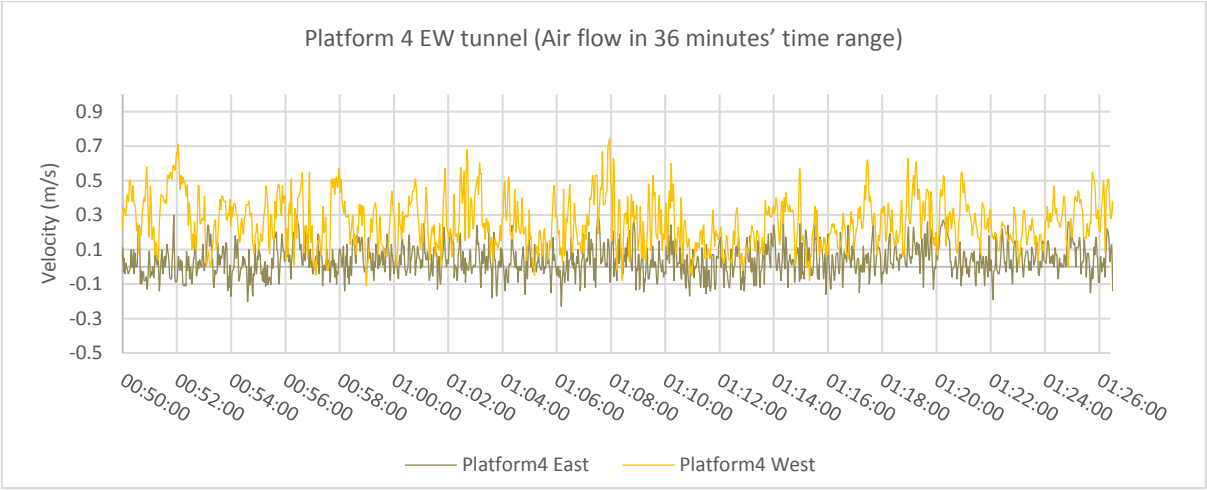

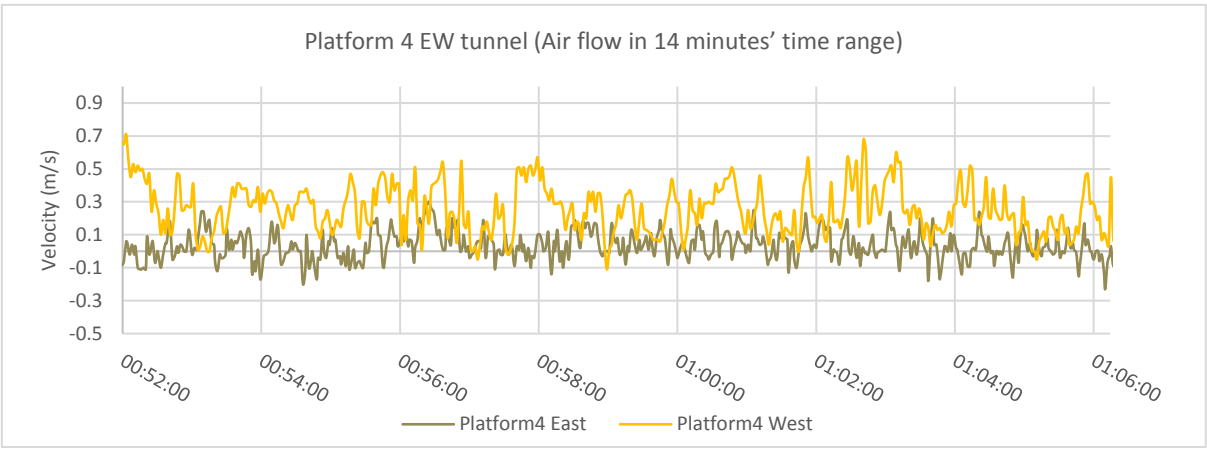

Figure 68: Tracer gas experiment 3 ultrasonic anemometer air flow result at platform 4 EW tunnel

The ultrasonic anemometer also measured the air temperature at each end of each platform thus indicating the temperature change as the air passed through the station. This is shown in Figure 69 and Figure 71. Figure 69 shows that the temperature at the north of platform 1 was 1^{o}C lower than that at the south end and the air temperature at platform 2 was raised by 0.5^{o}C in travelling the length of the platform. A 2^{o}C difference can be seen between platform 1 and 2. A similar situation can be seen for platform 3 and 4 as the temperatures at the east of platform 3 and 4 are lower than those at the west of the platforms as shown in Figure 71 but the difference is larger for platform 4 than platform 3. Comparing the two temperature measurements at the platform with Figure 70 and Figure 72 measured by temperature data logger shows close agreement and similar temperature differences although there are discrepancies as discussed at tracer gas experiment 1.

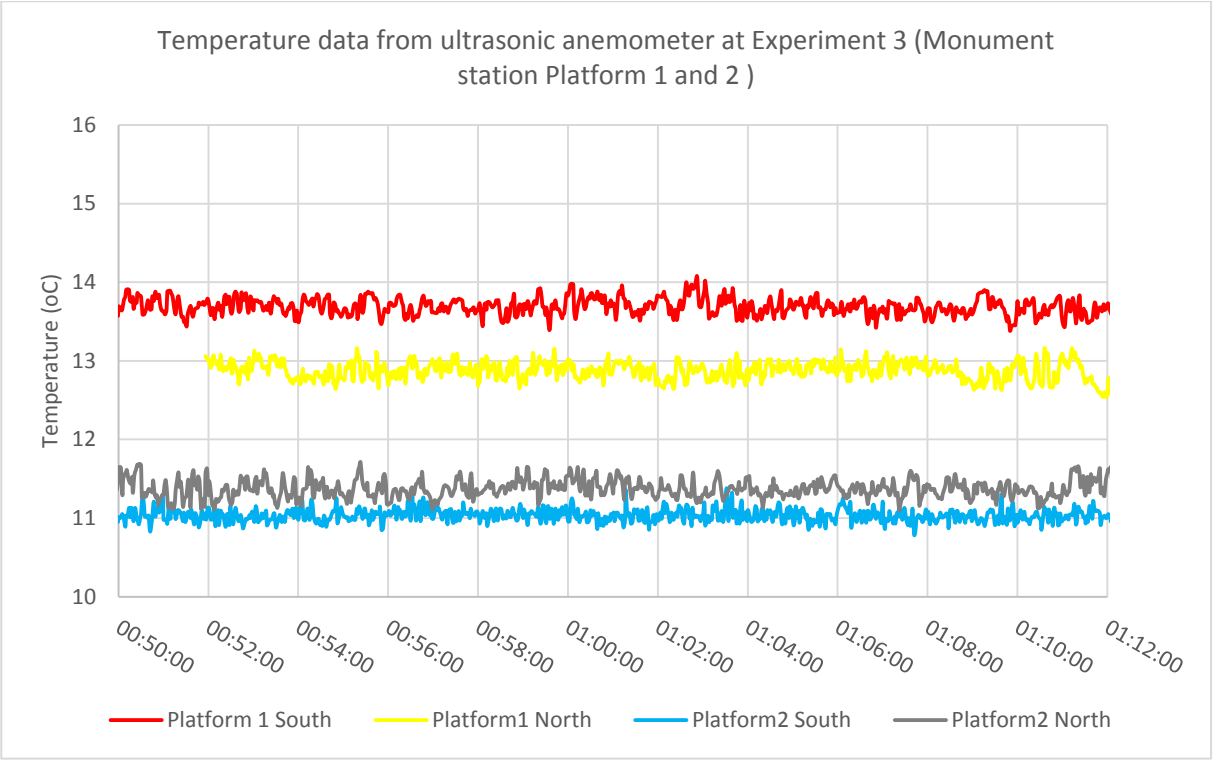

Figure 69: Tracer gas experiment 1 ultrasonic anemometer temperature data at Monument Station (22 minutes' time range)

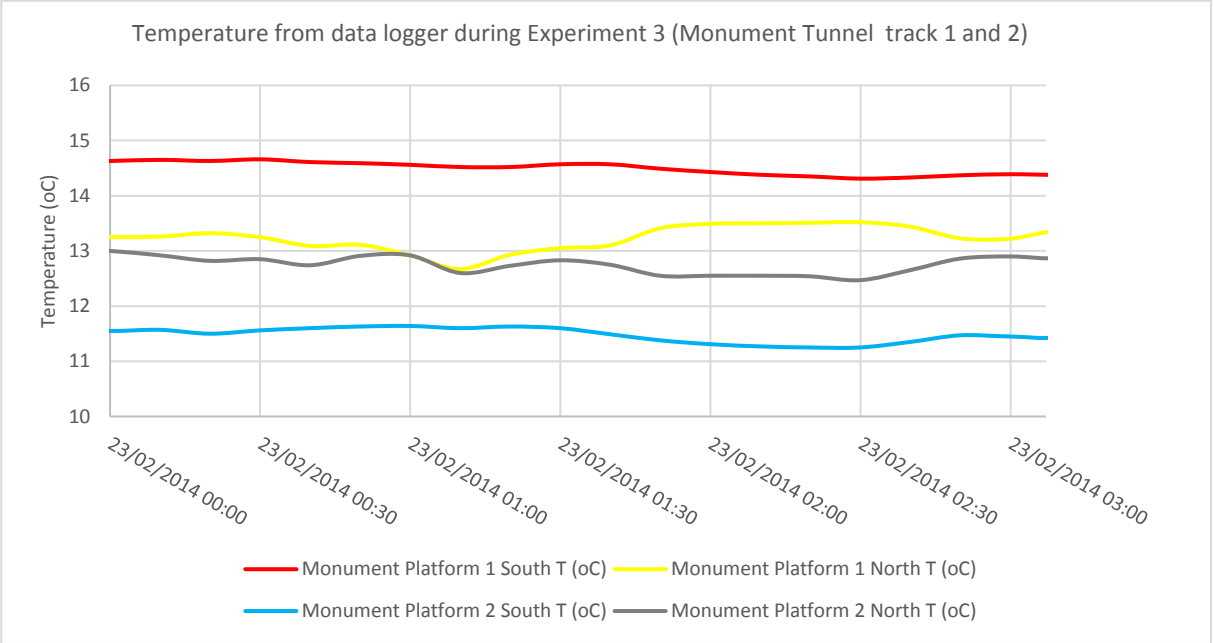

Figure 70: Temperature from data logger during Experiment 1 at Monument Station tunnel track 1 and 2 (3 hours' time range)

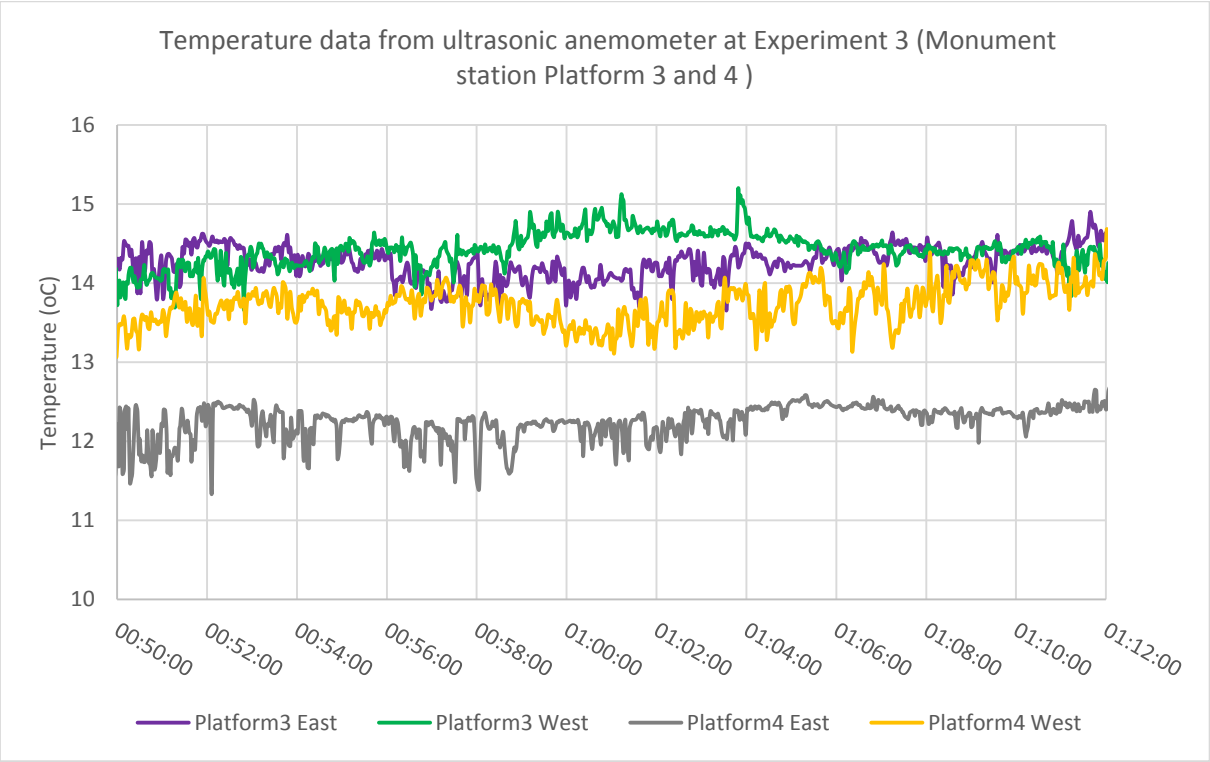

Figure 71: Temperature from data logger during Experiment 1 at Monument Station tunnel track 1 and 2 (22 minutes' time range)

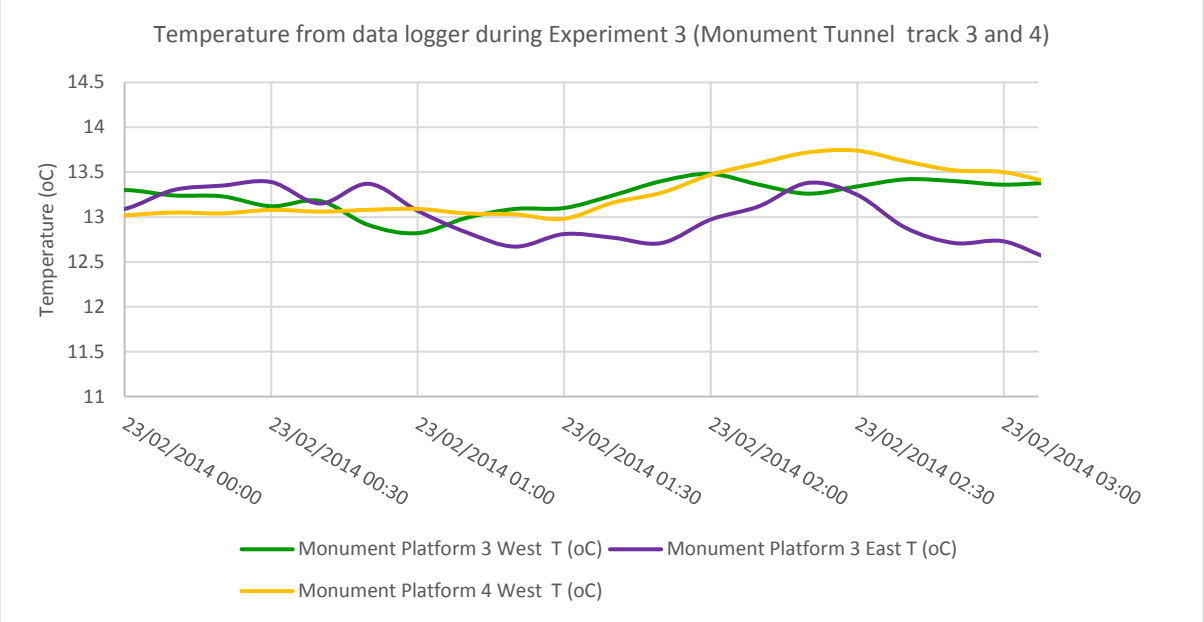

Figure 72: Temperature from data logger during Experiment 1 at Monument Station tunnel track 3 and 4 (3 hours' time range)

6.5.2 Comparing tracer gas experiment 2 and 3 tracer gas concentration result

Tracer gas experiment 2 was conducted at the operation break with the gas released between 00:52:00 01:02:22 on the night of 22.02.2014. The tracer gas experiment 3 was conducted the next day, 23.02.2014, at the operational time between 20:15:00 and 20:25:00. The SF_6 concentration sensors for both experiments were located at the Monument station and the neighbouring stations. The weather conditions were similar and the experimental set up and gas released locations were the same. Therefore, the results from experiment 2 and 3 could indicate the effect of train operation on the air flow and gas dispersion within the station and the tunnels.

The figures below indicated the concentration of SF_6, they are presented in this particular order so that the output from the same sensors but from different experiments can be compared easily. The figures have the same time base and the black vertical line indicates the tracer gas release end time. The location and designation of the SF_6 sensors is as shown in Figure 63 and Figure 64.

Figure 73 shows the level of tracer gas concentration on platform 1 and 2 where the tracer gas was released. Both graphs display the same time range of 30 minutes after the tracer gas release. Generally compared to the operation break experiment 1, experiment 2 shows a much higher SF_6 concentration at the south of platform 1 as shown by sensor S02. This was within 2 minutes of the gas release and must be due to train operation as the results are quite different from those of experiment 1 and 3 which occurred during an operational break.

The situation on the upper level platform 3 and 4, is quite different as shown in Figure 74, during the operational break, experiment 3, the SF_6 concentration is very high compared to the levels detected during the same experiment on platform 1. The sensors at the north end of platform 1 and 2 are beyond the stair case linking the lower platforms to 3 and 4 so it appears that the SF_6 is not progressing beyond the stair case but taking a preferred path to and contaminating the higher platforms. In additional, sensors 06 which was placed at the escalator linking platform 3 and 4 to the concourse, detected the SF_6 1 min 30 seconds after the gas was released at a concentration up to 93 ppm. This was much quicker and at a higher concentration than experiment 2 in which the SF_6 was detected 3 minutes after the gas was released with a lower concentration of up to 65 ppm.

Overall the tracer gas distribution in the Monument station, tracer gas experiment 3, are very similar to those of tracer gas experiment 1. The contamination of the north-south tunnel is highly dependent on the background air flow pattern and the location of tracer gas released point. The contamination of east-west platforms is from the stairs and evenly distribute to the entire tunnel when the trains were not operating.

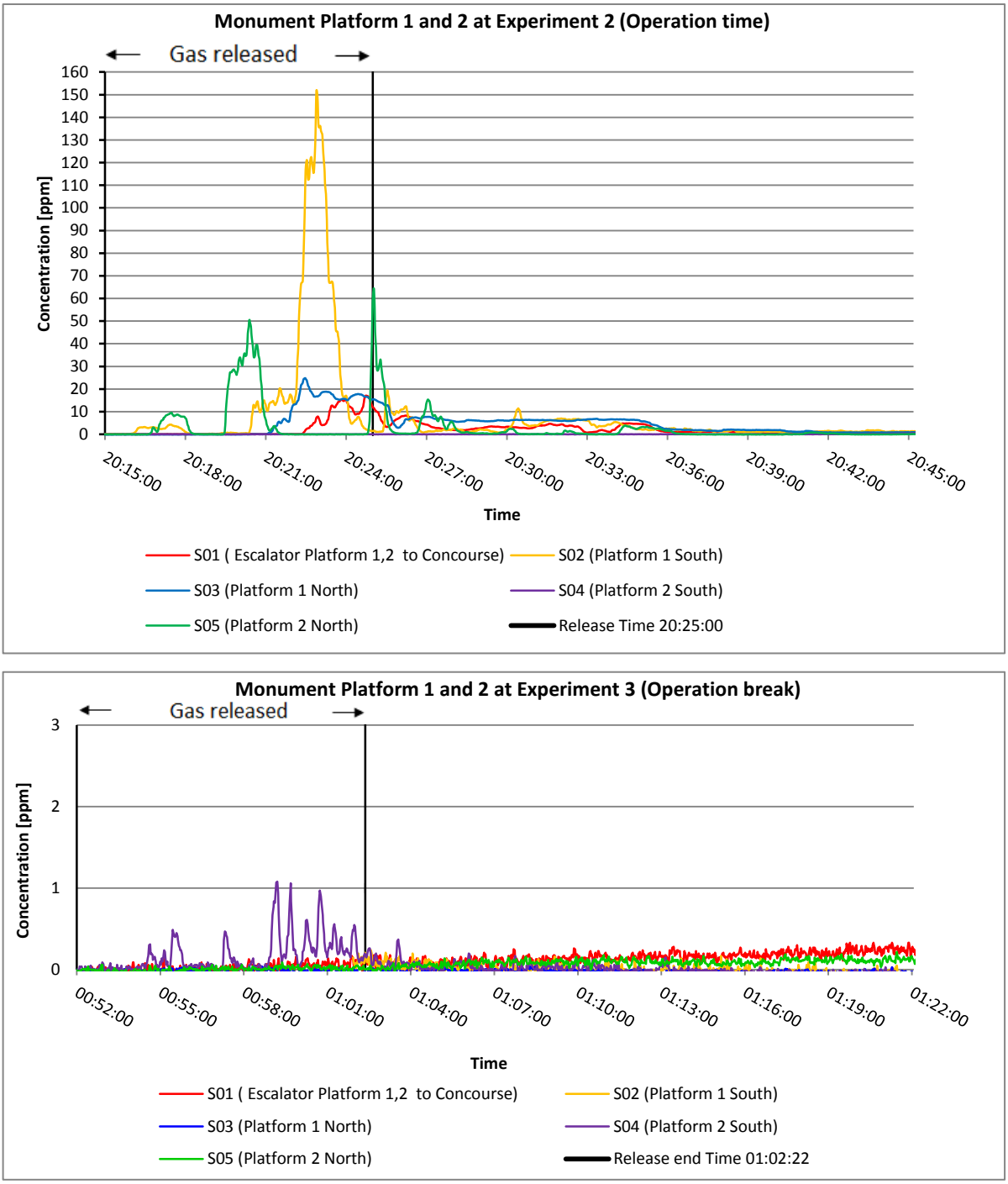

Figure 73: SF_6 concentration at Monument Station platform 1 and 2 of tracer gas experiment 2 and 3

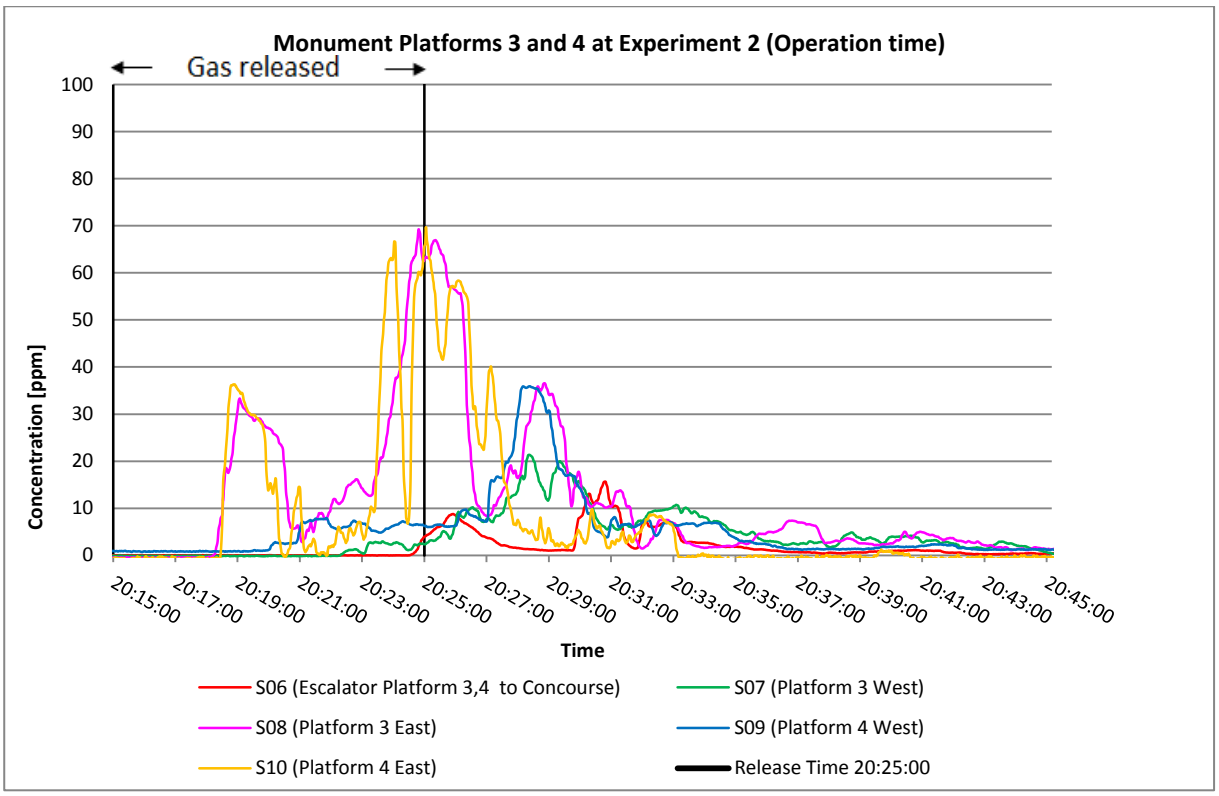

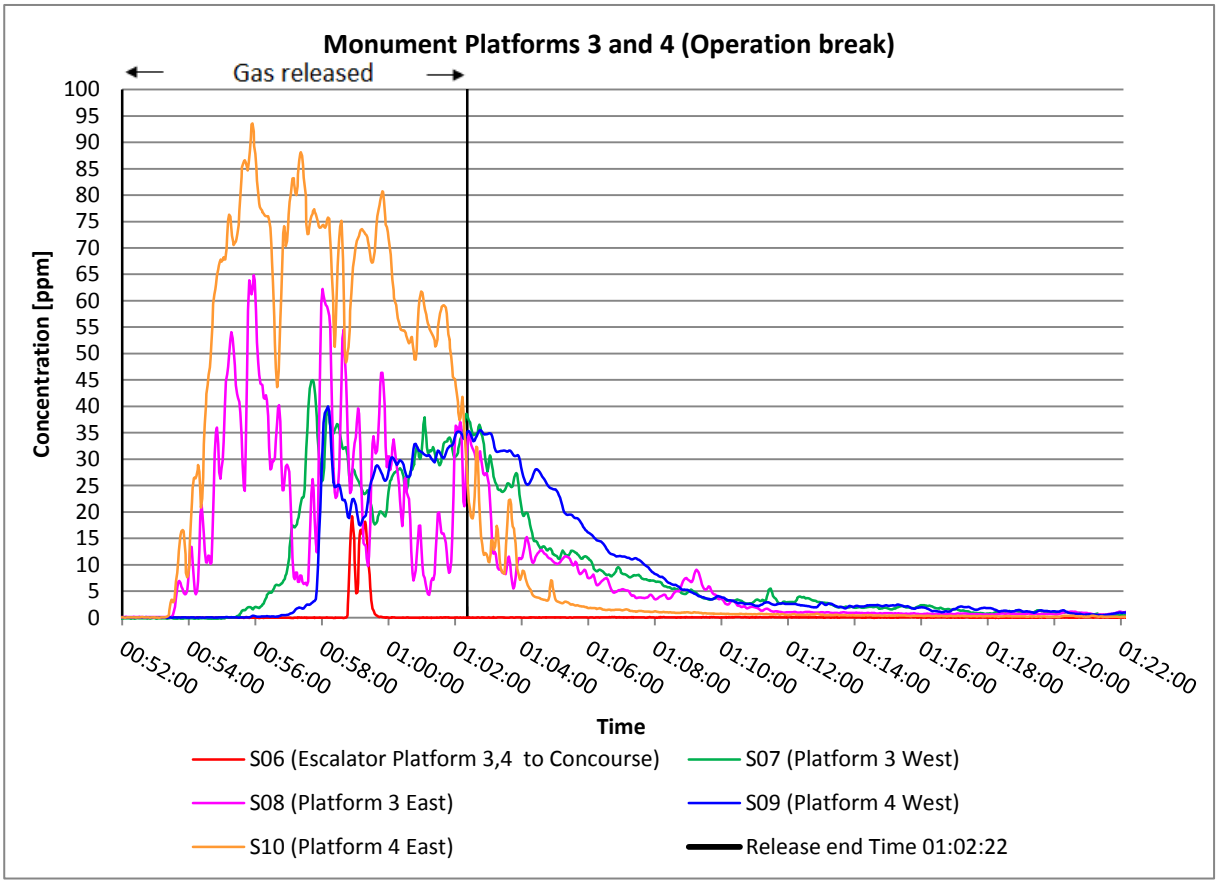

Figure 74: SF_6 concentration at Monument station platform 3 and 4 of tracer gas experiment 2 and 3

The stations north and south of the Monument Station are the Haymarket station and Central Station respectively. Figure 75 shows that with the train operation the SF_6 gas was detected at the Central station 26 minutes after the gas was released. The concentrations were very small but this was against the natural air flow so could only be produced by the movement of trains. As Figure 76 shows with train operation the sensors at the Haymarket Station detected high levels of SF_6 gas only 8 minutes after the gas was released but at the operational break, experiment 3, there was no SF_6 gas detected at the Haymarket Station.

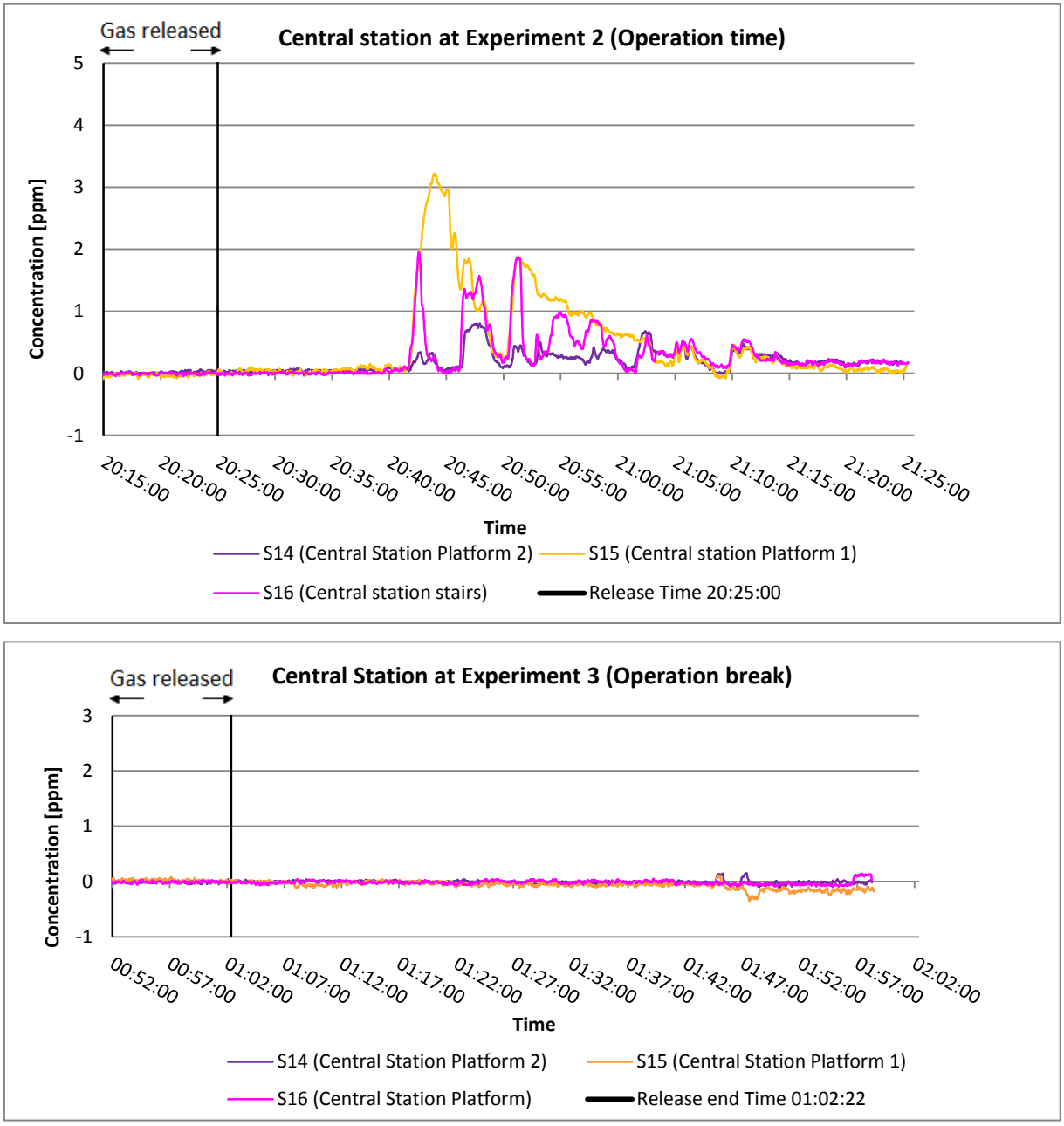

Figure 75: SF_6 concentration at Central Station of tracer gas experiment 2 and 3

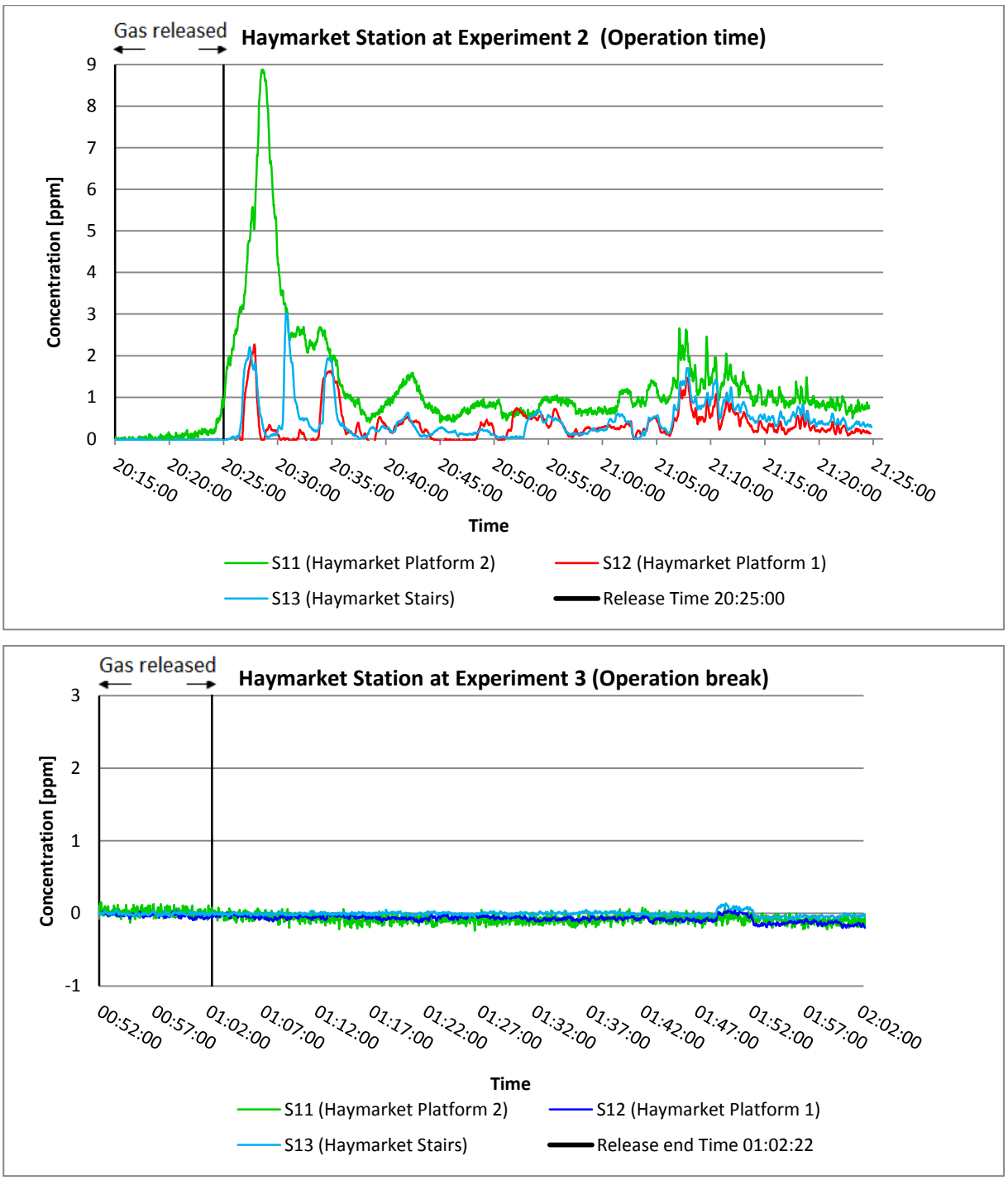

Figure 76: SF_6 concentration at Haymarket Station of tracer gas experiment 2 and 3

The Manors Station and St. James Station are located east and west of the Monument Station EW tunnel respectively. It is possible that any SF_6 gas dispersion at the Monument station platform 3 and 4 will result in the SF_6 being detected at these two neighbouring Stations. As pointed out previously the background airflow is from the east, Manors Station to Monument in the EW tunnel and this has prevented the SF_6 gas from dispersing to the Manors Station as shown in Figure 77 for both experiment 2 and 3.

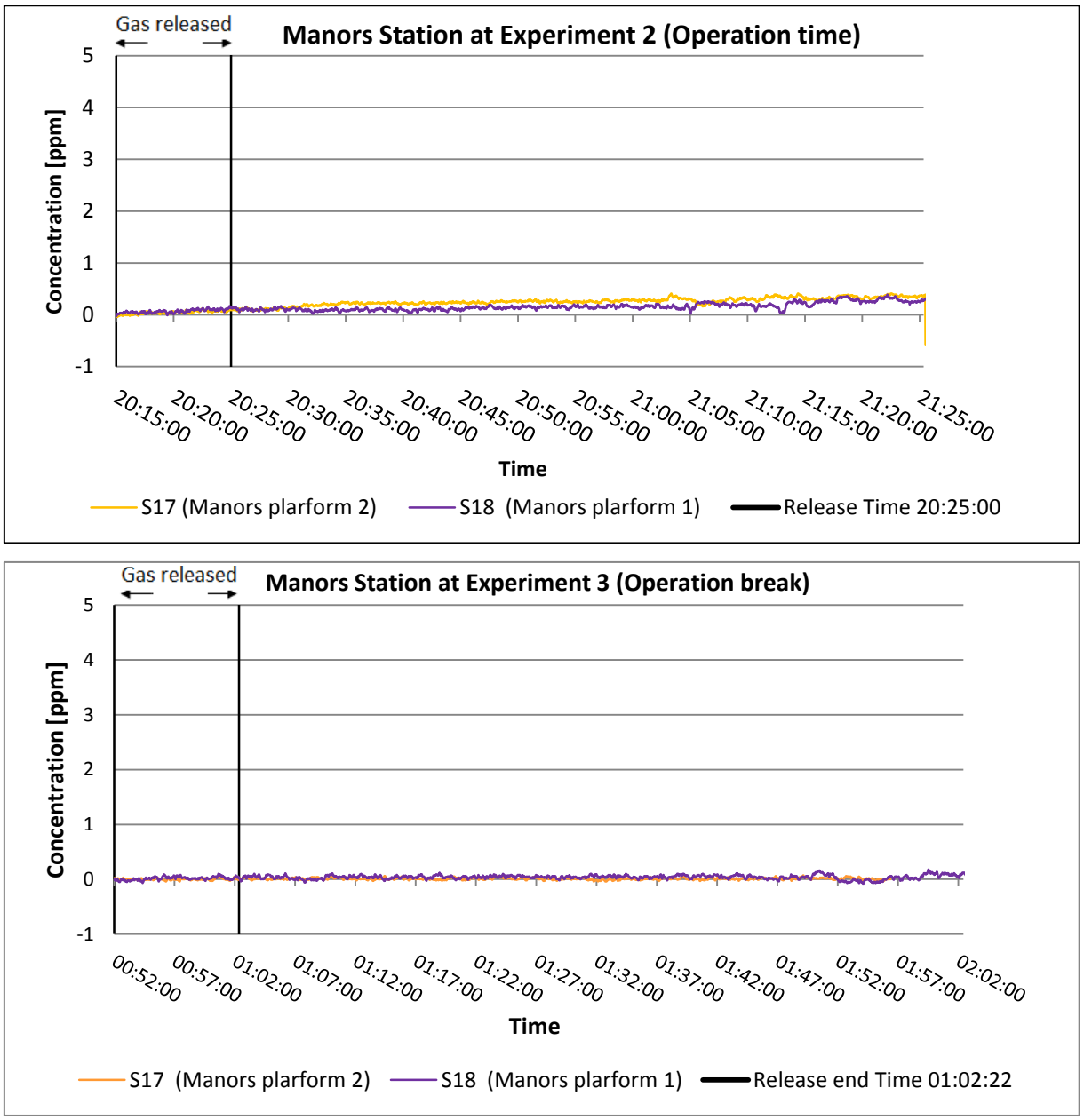

Figure 77: SF_6 concentration at Manors Station of tracer gas experiment 2 and 3

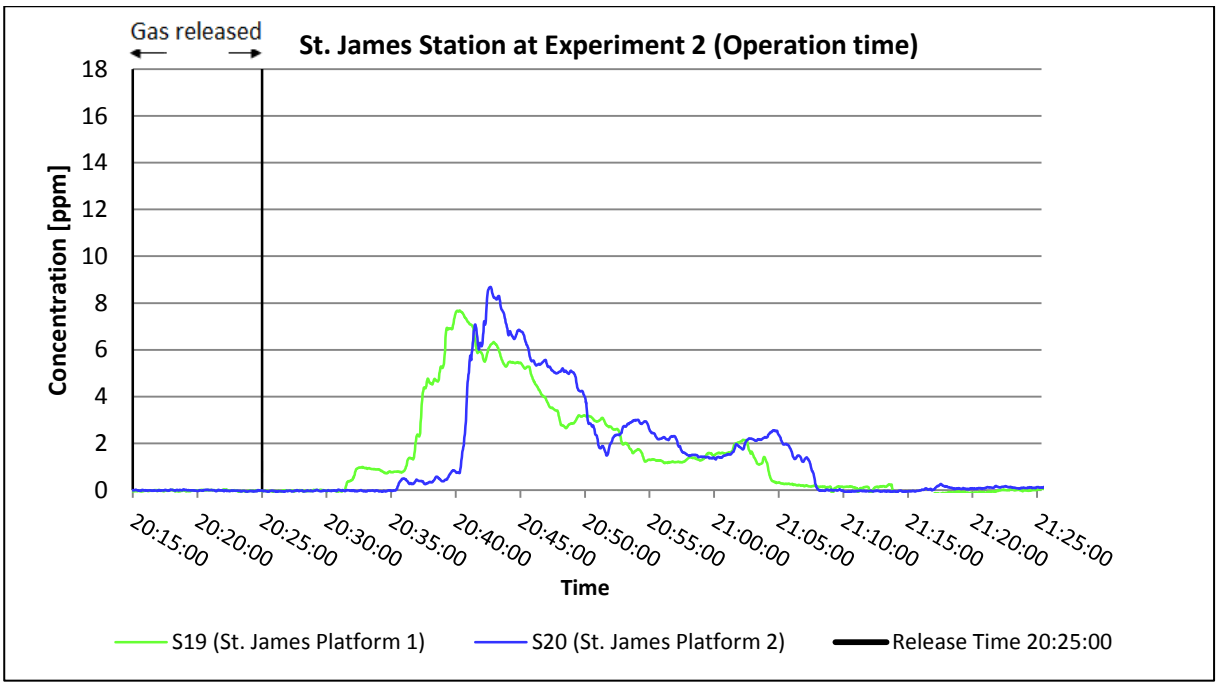

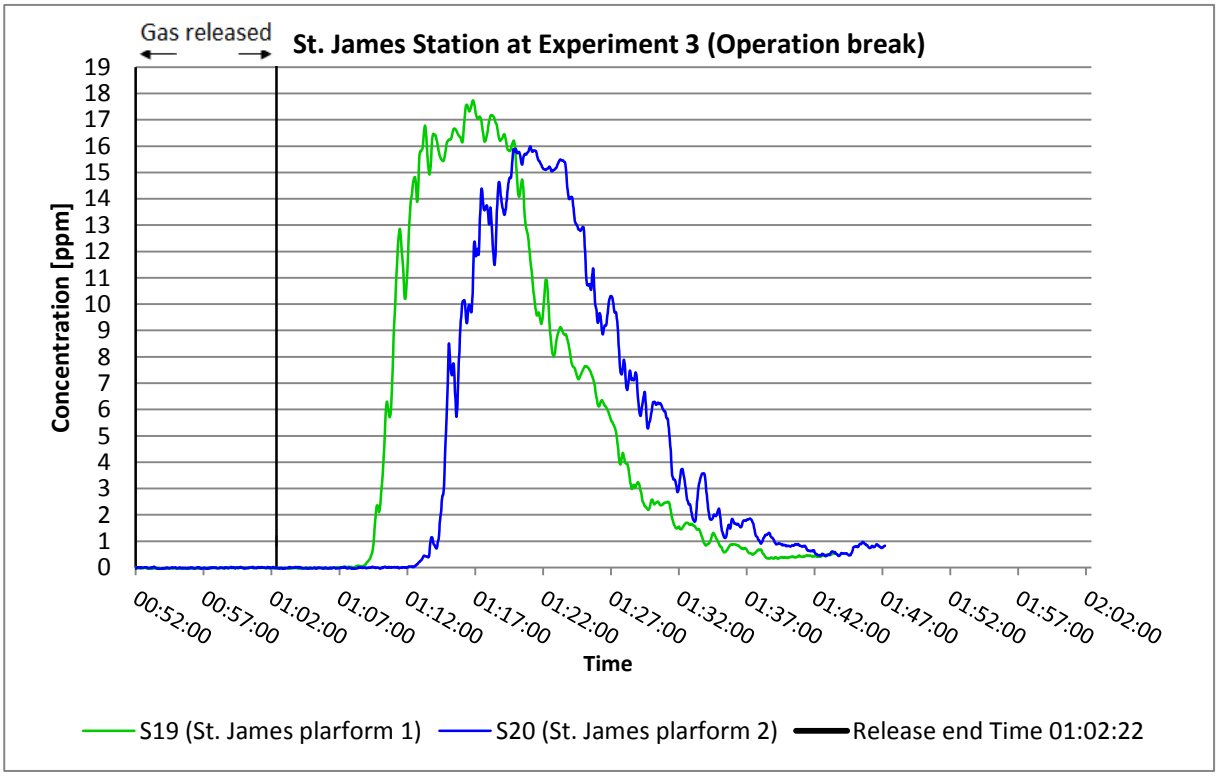

Figure 78: SF_6 concentration at St. James Station of tracer gas experiment 2 and 3

Figure 78 indicates that the sensor number 19 at St. James station detected elevated levels of SF_6 17.5 minutes after the gas release during the operating phase. Sensor 20 on the opposite track responded 3.5 minutes later which coincided with the arrival of a train. The observed concentrations were very low which may indicate that the train movement had an influence on the SF_6 dispersion.

The dispersion of the SF_6 along the north south track was clearly influenced by the train motion. The natural background air flow on this track is produced by a buoyancy effect produced by the gradual elevation of the track from south to north. The SF_6 reached the Haymarket station 10 minutes after the release but took three times longer to reach the Central station against the natural background air flow. This pattern of dispersion must be only caused by the piston effect of the trains.

The recorded tracer gas values were higher during the operational mode and more parts of the platforms were affected. The propagation paths were also more chaotic due to several train movements. A similar picture emerged when the adjacent stations were examined but here the maximum concentrations were found at St James station during the operational break.

6.6 Tracer gas experiment 4 and 5

Tracer gas was released twice inside operational trains running in both directions through the tunnels. 1.49 kg of SF_6 gas was released inside a train travelling from Gateshead station to Jesmond station in experiment 4 between 10:55:55 and 11:02:45 on 24/02/2014. A further 1.91 kg of SF_6 was released inside a train travelling from Ilford Road station to Central station in experiment 5 from 12:33:35 to 12:41:49 on the same day. SF_6 sensors were placed in the train carriage in which the SF_6 was released, in a following train and on the platforms of the stations the train travelled through. These experiments were intended to show how quickly substances disperse and how large an area is contaminated when gas is released in an operational train. The red line on Figure 79 indicates the metro tunnels and the purple lines show the tracer gas release path for these two experiments.

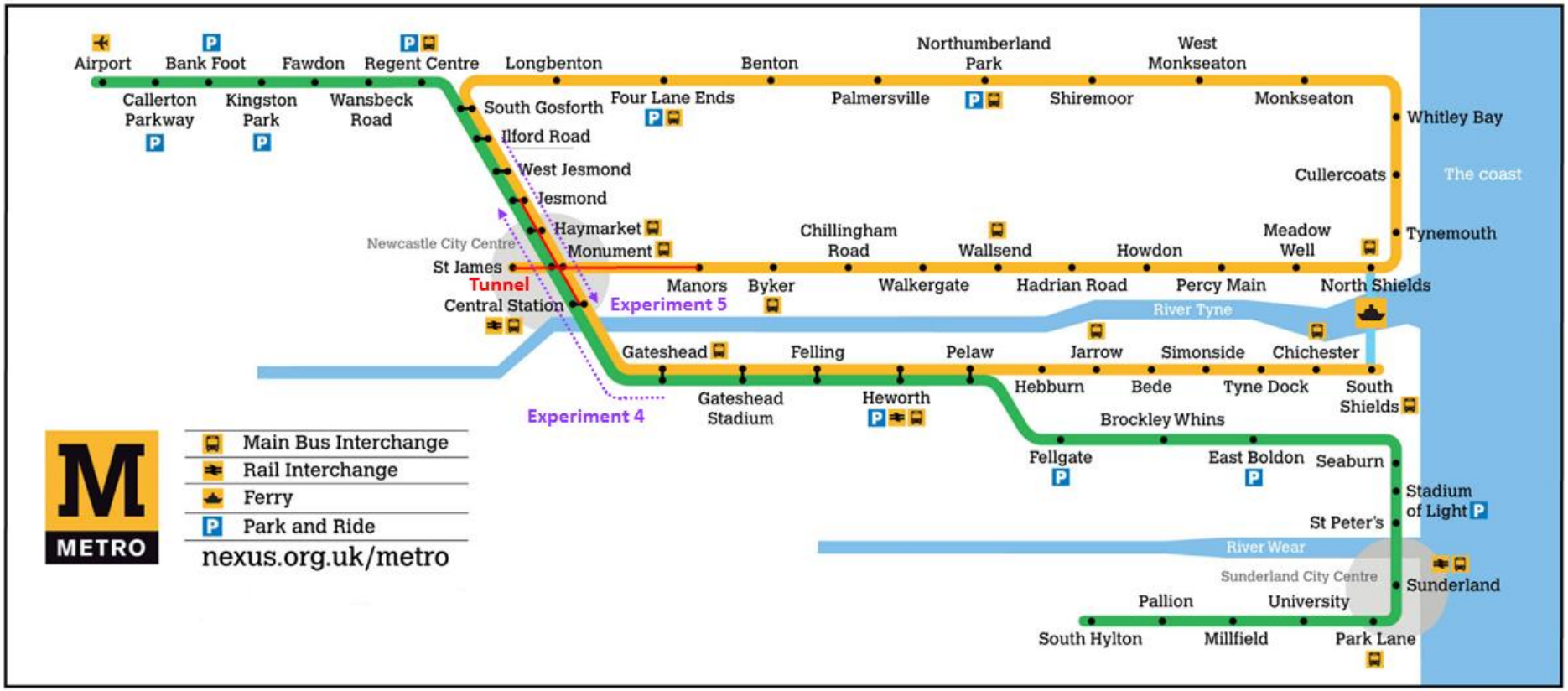

Figure 79: Map of Tyne and Wear Metro system map

6.6.1 Tracer gas experiment 4 and 5 setup and map

Experiment 4 and 5 were concerned with the release of a quantity of tracer gas in an operational train consisting of two carriages. In performing these experiments care was taken not to alarm the travelling public by enclosing the SF_6 gas container in a wooden box so it could not be identified as shown in Figure 80. Also the release point of the gas in the carriage was carefully chosen at the rear end at a location that was slightly obscured by the drivers cab.

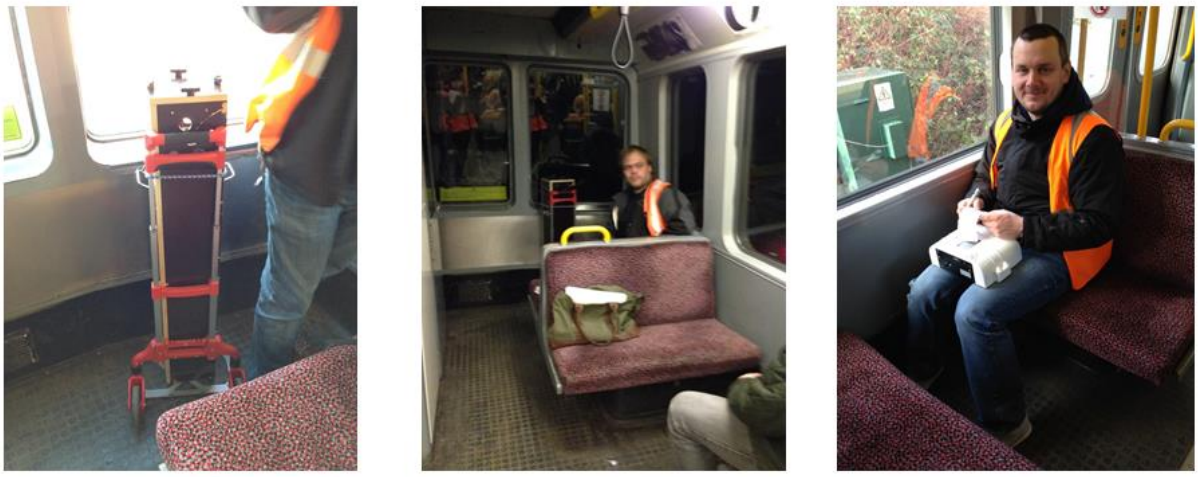

Figure 80: Photos of the disguised gas bottle, gas release point and measurement instruments in the train of tracer gas experiments 4 and 5

The route of train travelled during the tracer gas experiment 4 and 5 are shown in Figure 79. The extent that the tracer gas could contaminate the stations is a function of the gas release rate and the time taken for the train to travel between the stations. The Nexus time table shows that the scheduled time between all the stations on the route is 2 minutes with the exception of the period between West Jesmond and Ilford Road which is 3 minutes. The interval between trains is 6 minutes during the operational time when the gas was released so that by the time the following train had reached the Monument Station the contaminated train would have reached the Haymarket station. All the concentration graphs begin at the time of the gas released with a black vertical line indicating when the gas release stopped. In addition, further vertical lines indicate the operational time for the train to arrive at a station on its route. Full information of the metro operation timetables at the stations are related to this research can be found from Nexus (2014).

6.6.2 Tracer gas experiment 4 gas concentration results.

The concentration of the SF_6 in the first train rear coach where the gas was released is shown in Figure 81. The thick black line indicates when all the gas had been released and the grey vertical lines in Figure 81 and Figure 82 indicate the internals of the train arrival at each subsequent station. The gas was released at 10.55.55 when the doors were closed in readiness for the train to leave Gateshead Station. Within 2 minutes when the train was standing at the Monument Station the concentration had risen from 400 ppm throughout the carriage and continued to rise to between 600 and 900 ppm as more gas was released. Then the concentration reached a peak level of 1050 ppm when the train departed from the Monument Station to the Haymarket station. The concentration declined slightly when the doors were opened at the Central station but continued to increase when the train resumed its journey. The concentration gradually declined between 500 to100 ppm when the train had reached Ilford Road Station and finally became undetectable 25 minutes after the initial discharge. The blue line indicates the concentration of the SF_6 in the first train front coach and the output of the sensors located in a following train are also shown in Figure 82. A low concentration of the SF_6 was detected at the front coach of the contaminated train after it arrived at the stations.

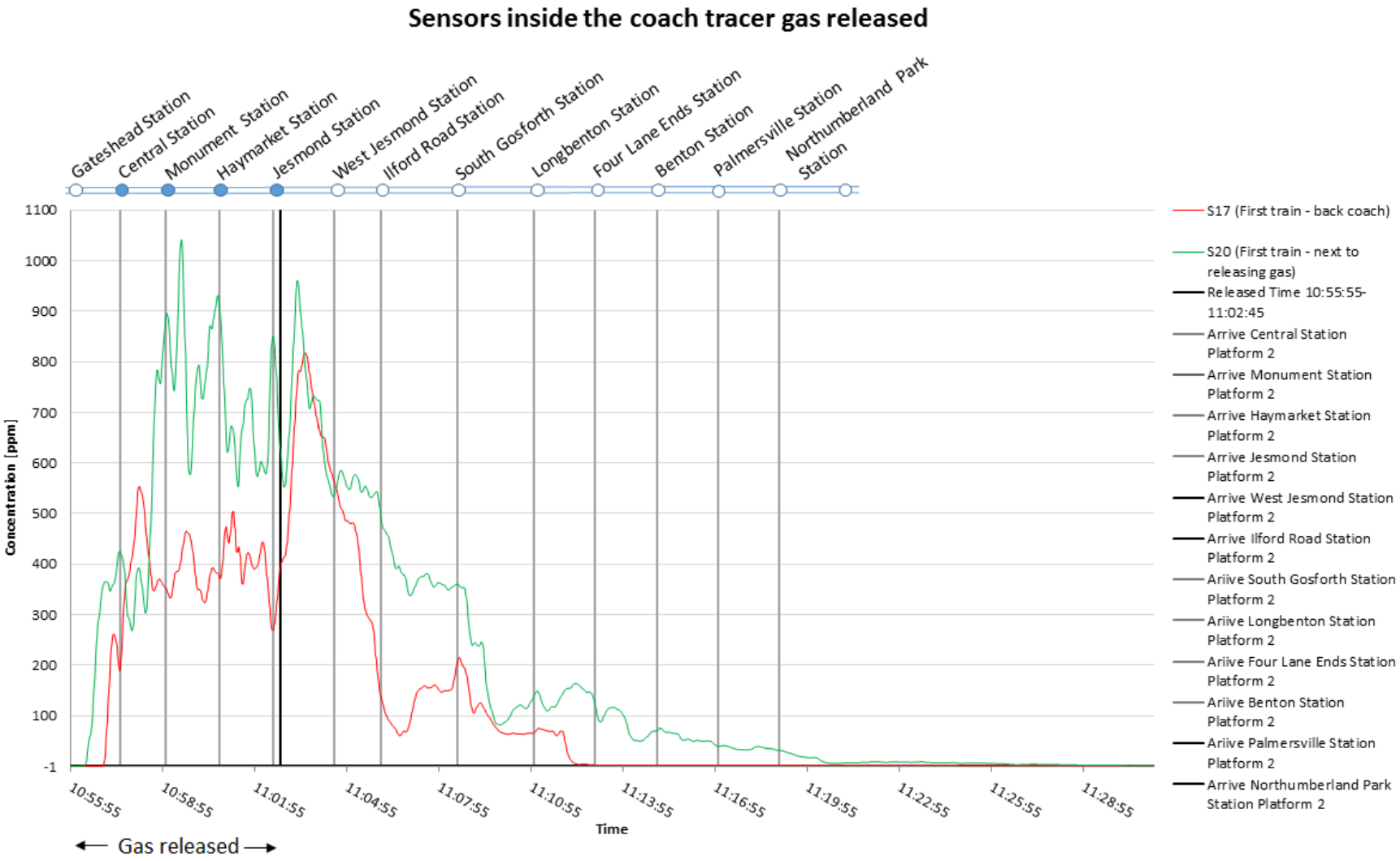

Figure 81: SF_6 concentration in the contaminated train rear coach with time line of train arrival station (Tracer gas experiment 4)

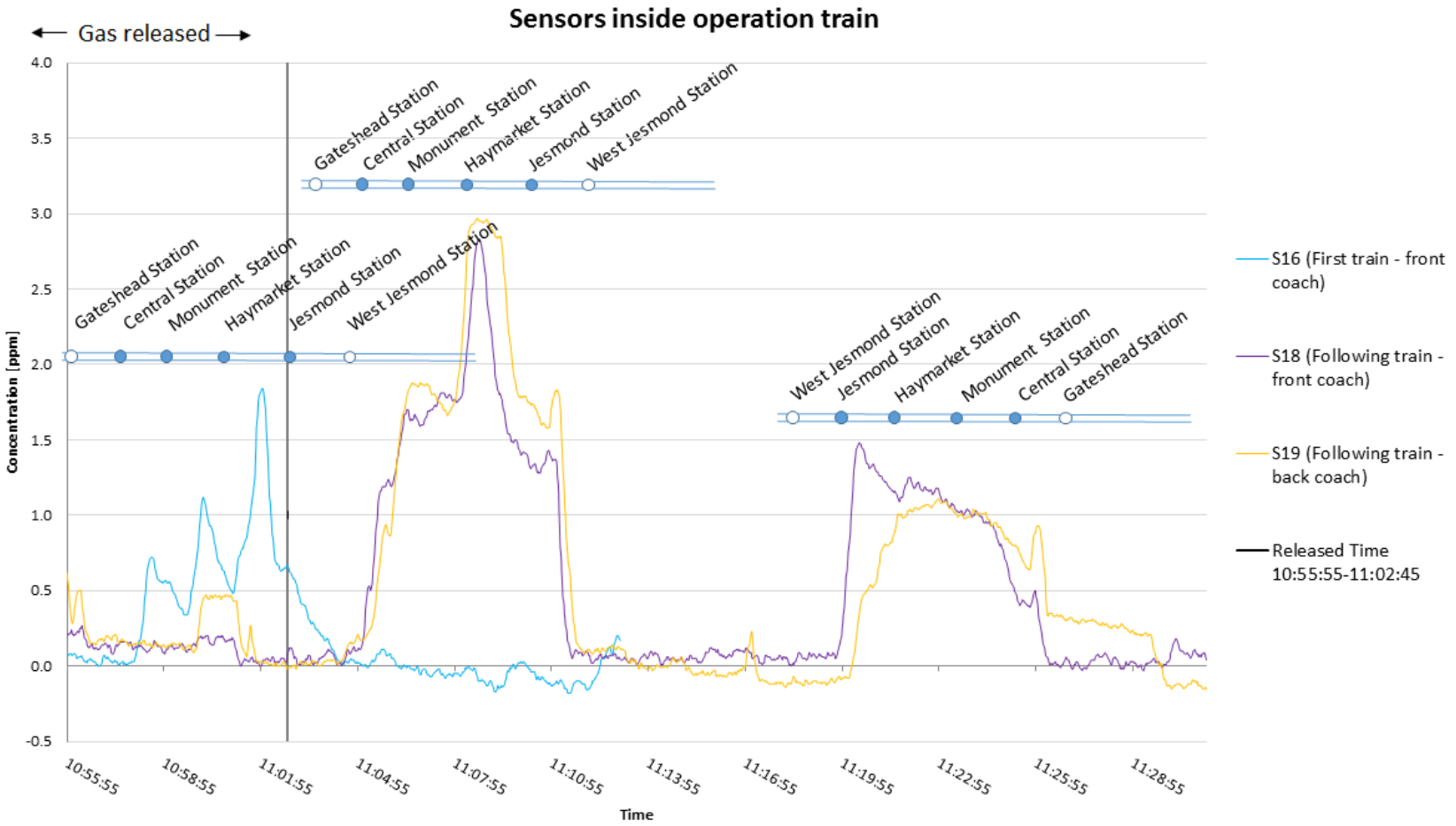

Figure 82: SF_6 concentration in the contaminated train front coach and the following train with time line of train arrival station (Tracer gas experiment 4)

As the train travelled along the route the sensors at the station platforms detected varying level of SF_6 gas immediately. Low levels of tracer gas were detected at the Central station and Jesmond station which are at the two ends of the underground tunnel. The whole of the Monument station was contaminated with a low level of SF_6. But the area contaminated from the moving train was larger than that when the gas was released from the platform in experiment 1. At the Haymarket station extremely high levels of tracer gas were detected and remained for 4 minutes in the station.

The following figures present the SF_6 concentration at each station. The vertical lines in the figures indicate when a train passed through the station in 6 minute intervals. Figure 83 presents the output from the sensors at the platform of the Central station. It can be seen that sensors S8 and S9 indicated a low concentration of SF_6. S9, which was located at platform 2, detected SF_6 immediately when the contaminated train arrived but sensor 8 located on platform 1 did not sense the SF_6 for a further 1 to 2 minutes.

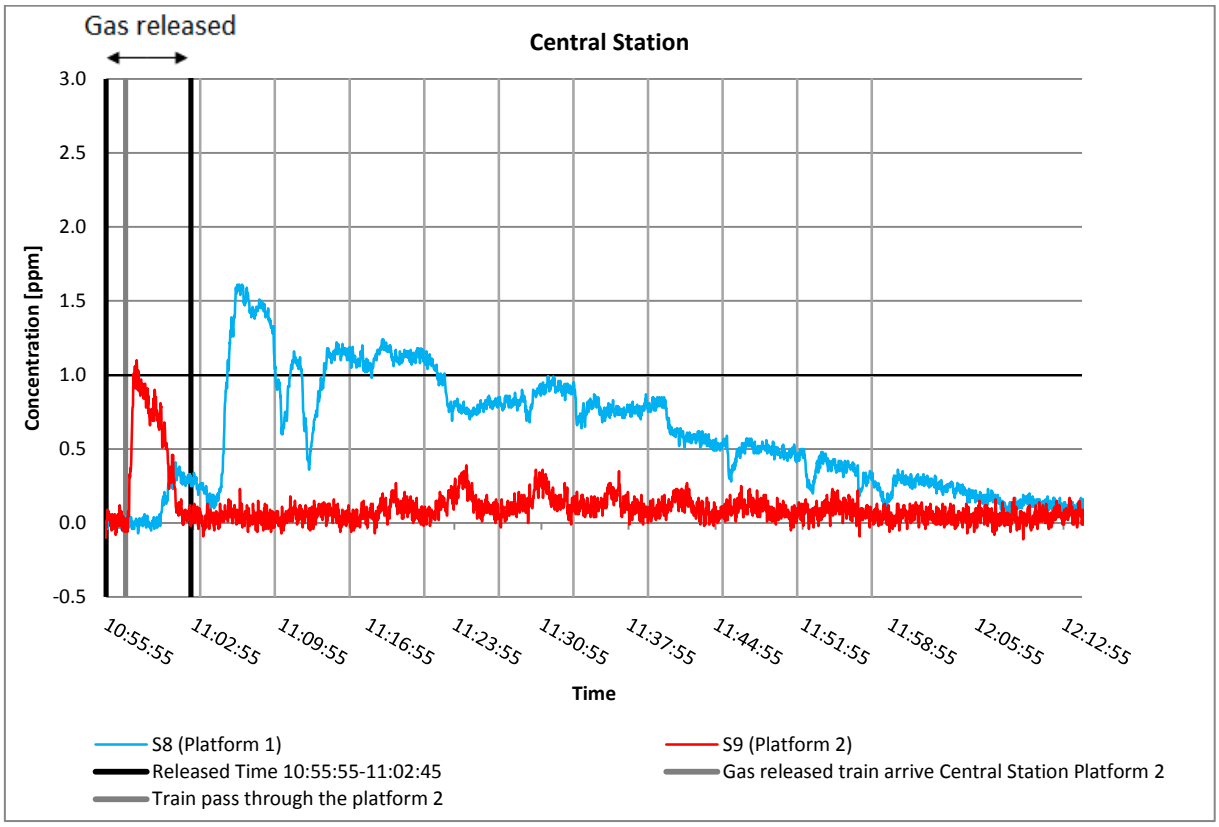

Figure 83: SF_6 concentration at Central Station with train arrival time line through platform 2 (Tracer gas experiment 4)

The contaminated train reached the Central station platform two minutes after leaving the Gateshead station whilst the SF_6 was still being released. The concentration in the back coach of the contaminated train had reached 400 ppm at this stage and spread onto platform 1. The SF_6 was dispersed throughout the platform by the train movement with sensor S8 recording a maximum level of 1.6 ppm at 11.06. The SF_6 lingered at the platform at levels that could be dangerous (depending on the toxin) for an hour before it became undetectable by sensor S8. The movement of trains through the station can be seen to influence the sensor readings and the peaks in the output of sensor S9 indicates that the SF_6 was spread from platform 1 to platform 2.

The Monument station received the contaminated train on the lower level 4 minutes after the gas release and was severely contaminated when the doors opened as shown in Figure 84 and Figure 85. By the time the contaminated train reached the Monument station, platform 1, the SF_6 concentration in the rear coach had risen to 900 ppm near the release point and to 400 ppm in other parts of the rear coach. Figure 84 indicates the time the train passed through both platform 1 and 2. The SF_6 quickly spread into the platforms when the carriage doors were opened and, as can be seen in figures 37, showed a preferential dispersion path through the stair case linking the NS platforms with the EW platforms (Figure 85) and then to the concourse area. The dispersion occurred very quickly with the majority of the gas in the station accumulating in the concourse area leaving a small concentration on the platforms. The subsequant passage of in-service trains through the station, indicated by the purple and green lines on the graphs, has no further effect on the concentration in the concourse area but clearly agitated the SF_6 that remained at the platform levels. Figure 85 also shows that the concentration level was effected by all of the trains passing through the station. This is a good indication that the train movement has an influence on the air flow in the whole station.

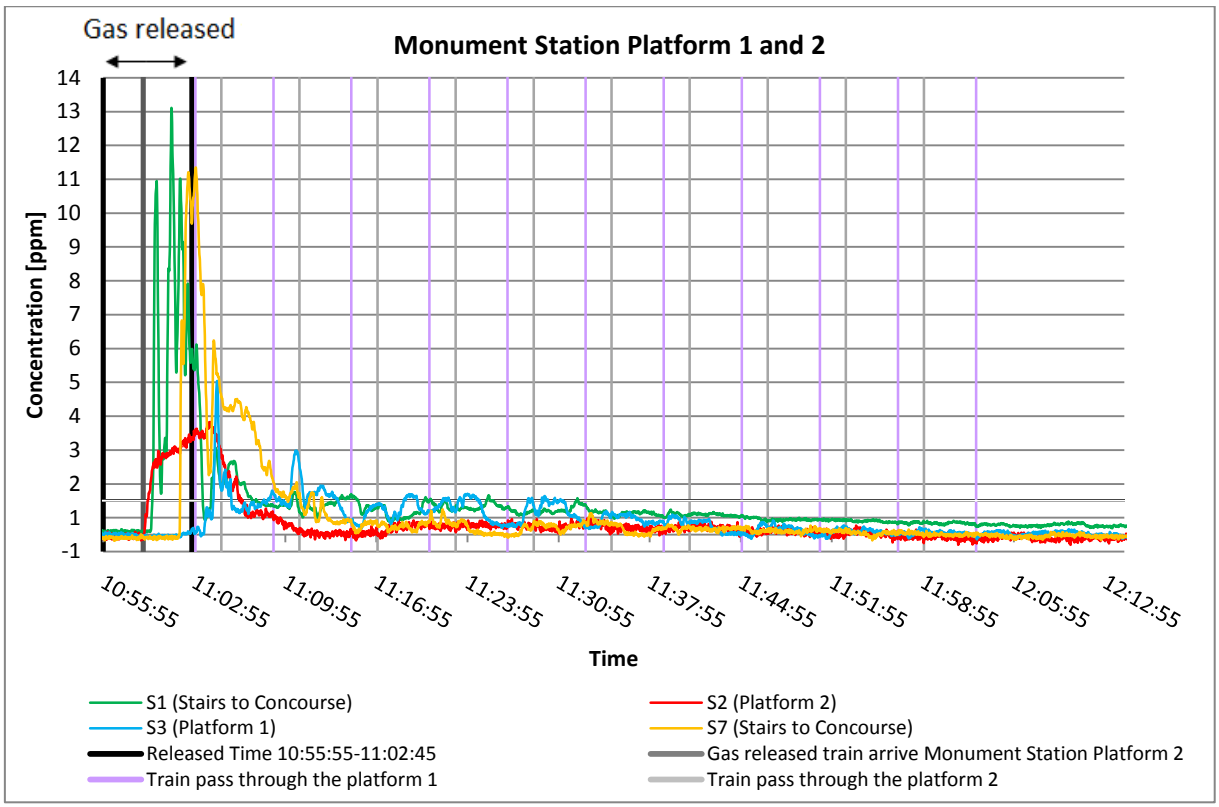

Figure 84: SF_6 concentration at Monument Station platform 1 and 2 with train arrival time line through platform 1 and 2 (Tracer gas experiment 4)

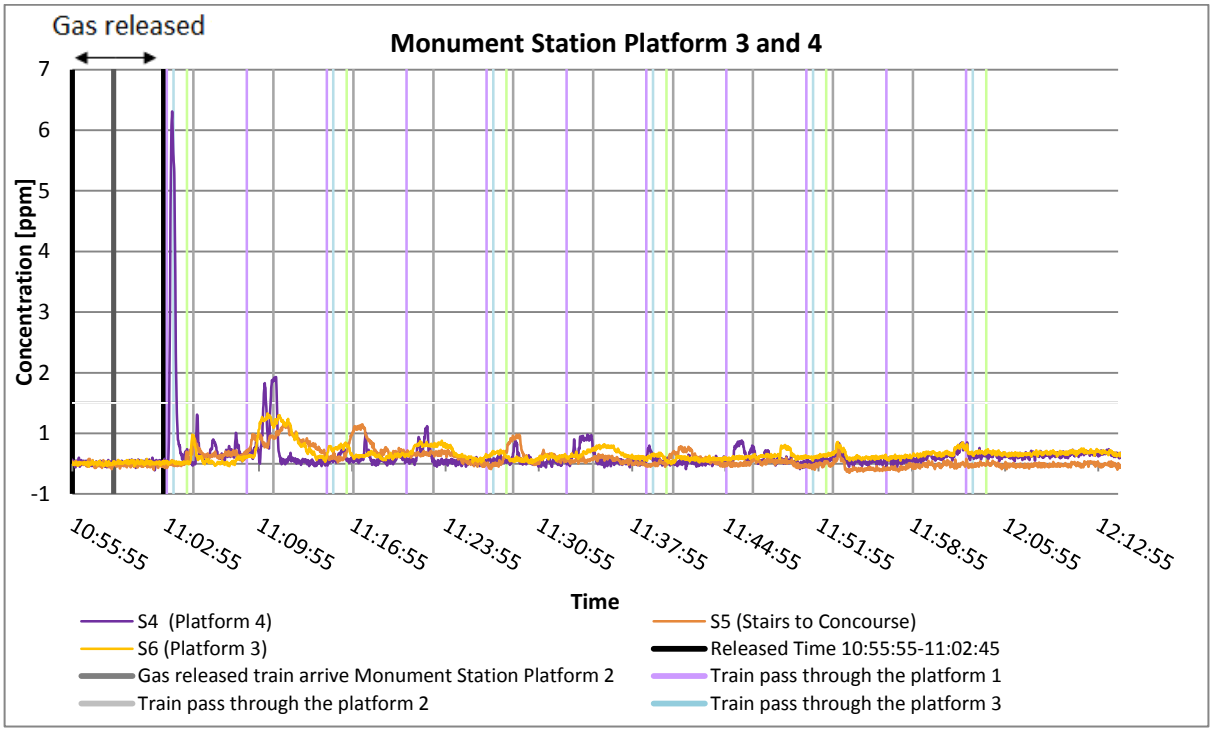

Figure 85: SF_6 concentration at Monument Station platform 3 and 4 with train arrival time line through the Monument Station (Tracer gas experiment 4)

By the time the contaminated train reached the Haymarket station (Figure 86) the concentration in the rear carriage had stabilised at around 800 ppm whilst in the front carriage the concentration continued to rise when the doors were closed. When the train was in the station it can be seen in Figure 81 that the SF_6 left the train and then the concentration continued to rise as the train continued its journey. The high degree of contamination at the Haymarket station lasted for less than 2 minutes with most of the SF_6 migrating to the station concourse area.

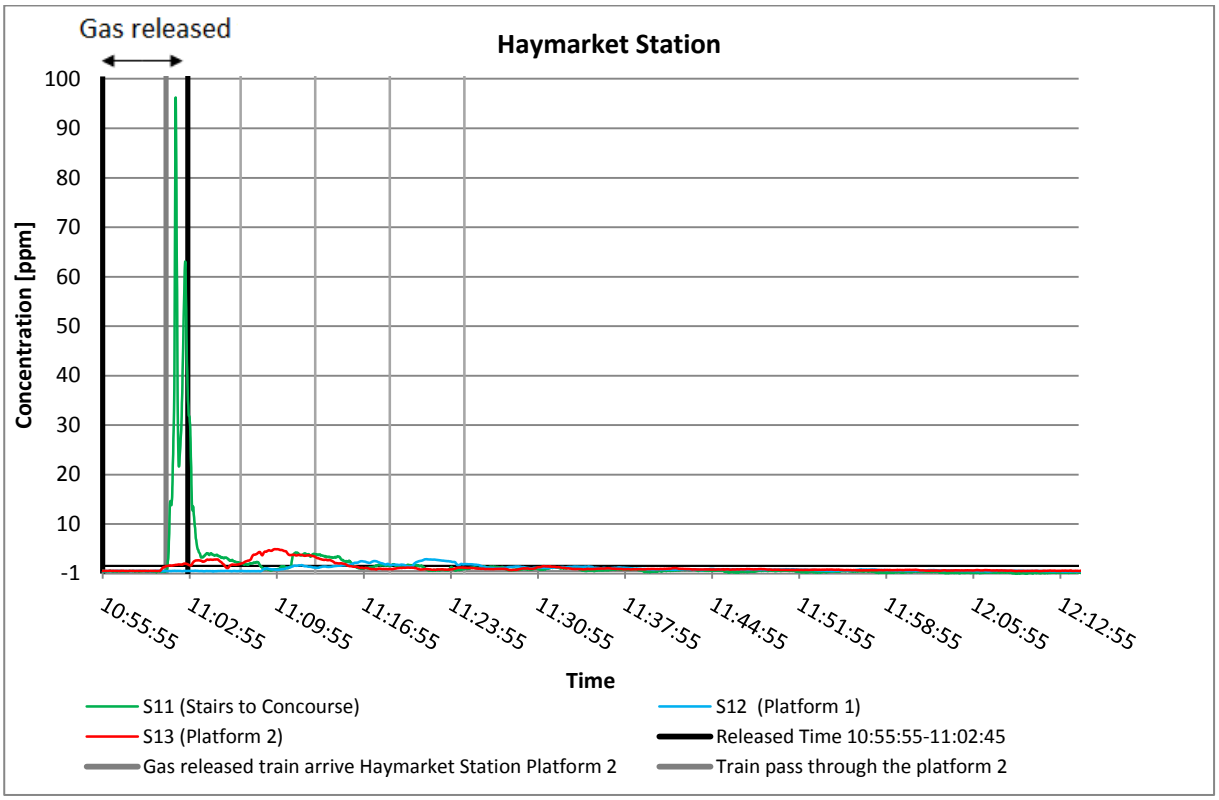

Figure 86: SF_6 concentration at Haymarket Station with train arrival time line through platform 2 (Tracer gas experiment 4)

SF_6 was still being released in the contaminated train when it reached the end of the underground section at Jesmond Station (Figure 87). The concentration levels in the rear coach were still of the order of 800ppm but had begun to decrease in the front carriage. The measured concentrations at the Jesmond Station detected by sensors S14 and S15 were much lower than in the previous stations and quickly reduced to almost undetectable levels. The movement of inservice trains had little influence in this station.

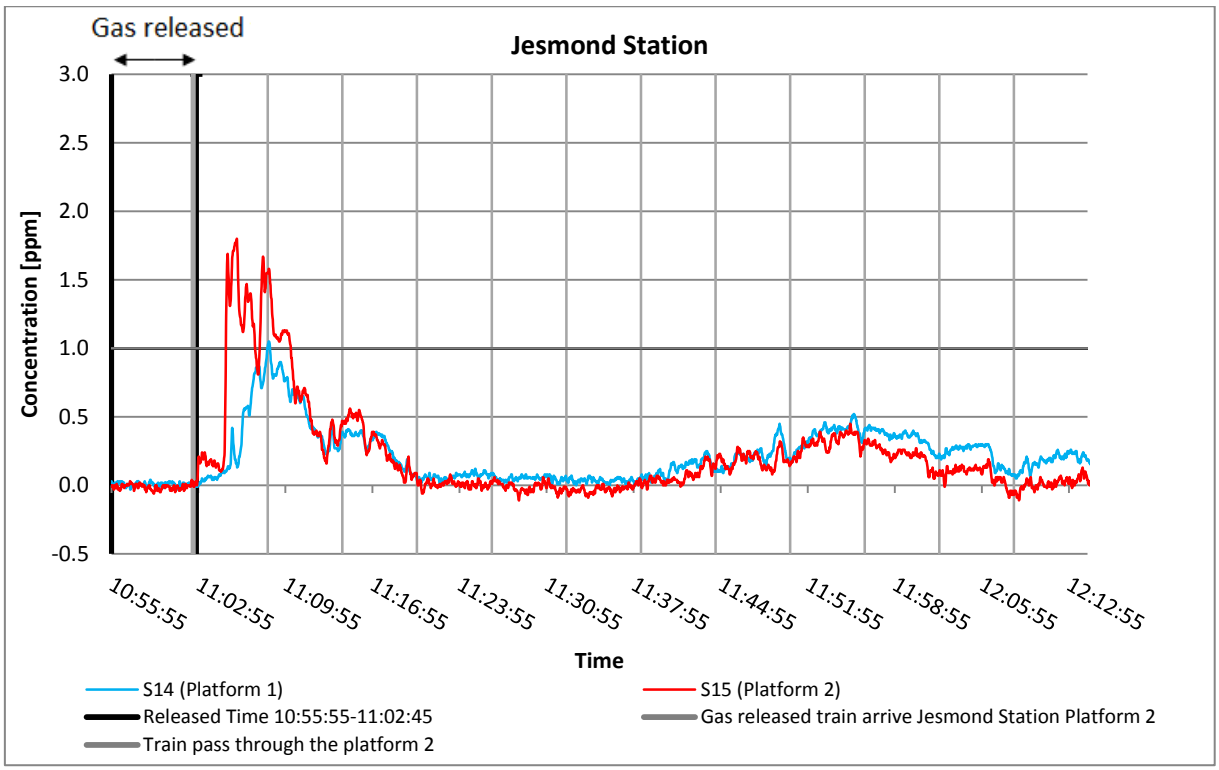

Figure 87: SF_6 concentration at Jesmond Station with train arrival time line through platform 2 (Tracer gas experiment 4)

6.6.3 Tracer gas experiment 5 tracer gas concentration result

Experiment 5 was a repeat of experiment 4 but in this case the train was travelling in the opposite direction and 1.91 kg of SF_6 was released. The dispersion of the SF_6 in the train was the same as in Experiment 4. The train was contaminated immediately on the release of the gas which was available in sufficient concentration to contaminate Jesmond station immediately once the train had arrived at the platform 1 as shown in Figure 88. This phenomenon also appeared at Haymarket Station (Figure 89), Monument Station (Figure 90 and Figure 91) and at the Central Station Figure 92.

The Monument station, platform 3 and 4, were contaminated 6 minutes after platform 1 and 2. It took more than 1 hour for the tracer gas at the Haymarket and Jesmond station to clear as gas was continuously flowing from the southern stations through the tunnel to these stations.

Compared with experiment 4 the concentrations at the stations are generally lower. This could be explained by the train movement which is against the back ground air flow in this case whereas it was in the same direction in the previous experiment.

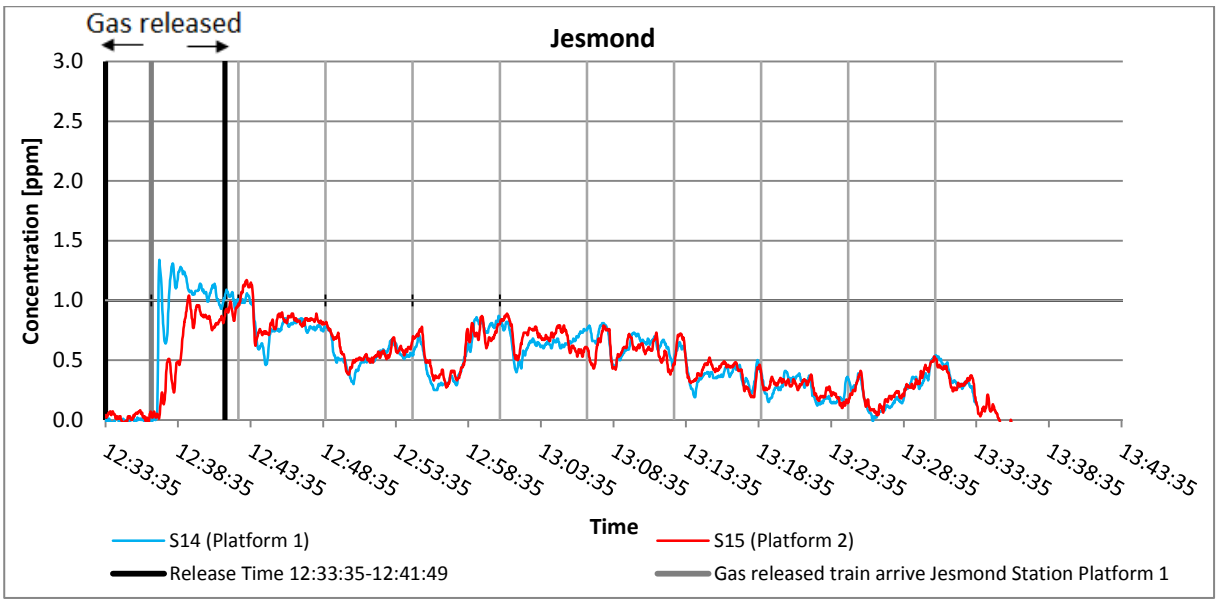

Figure 88: SF_6 concentration at Jesmond Station with train arrival time line through platform 1 (Tracer gas experiment 5)

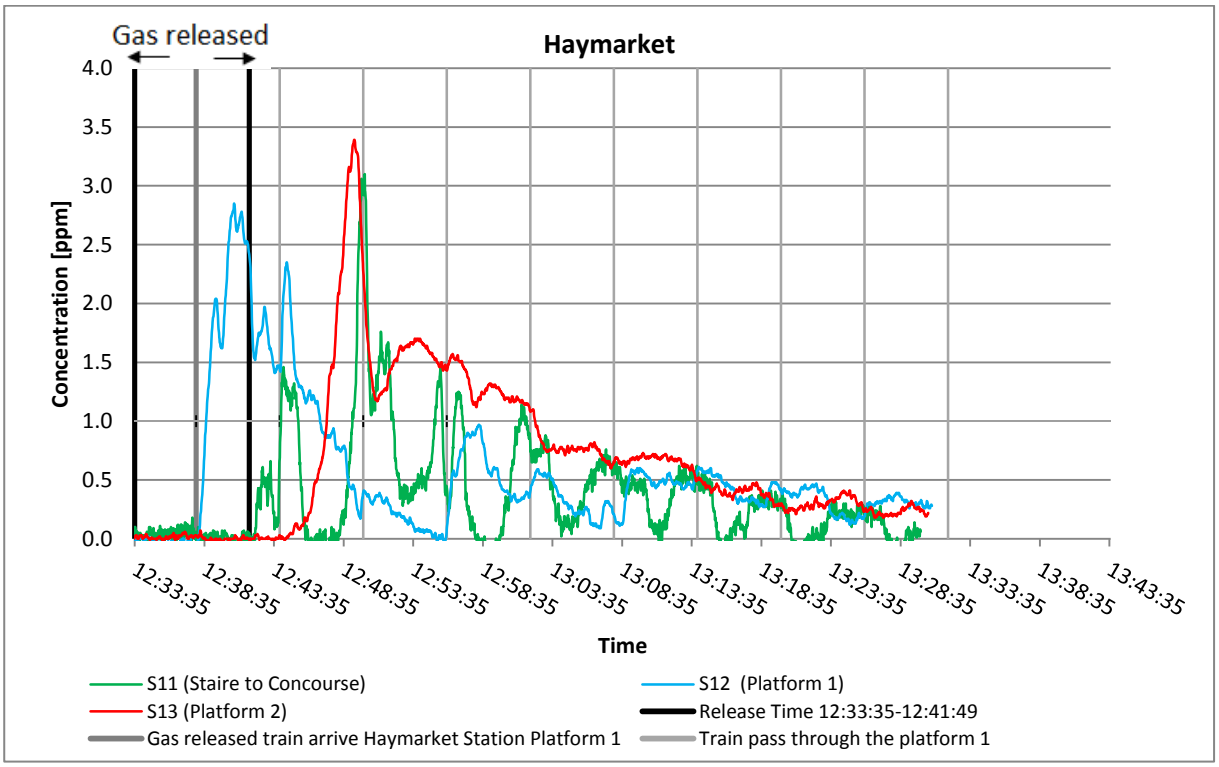

Figure 89: SF_6 concentration at Haymarket Station with train arrival time line through platform 1 (Tracer gas experiment 5)

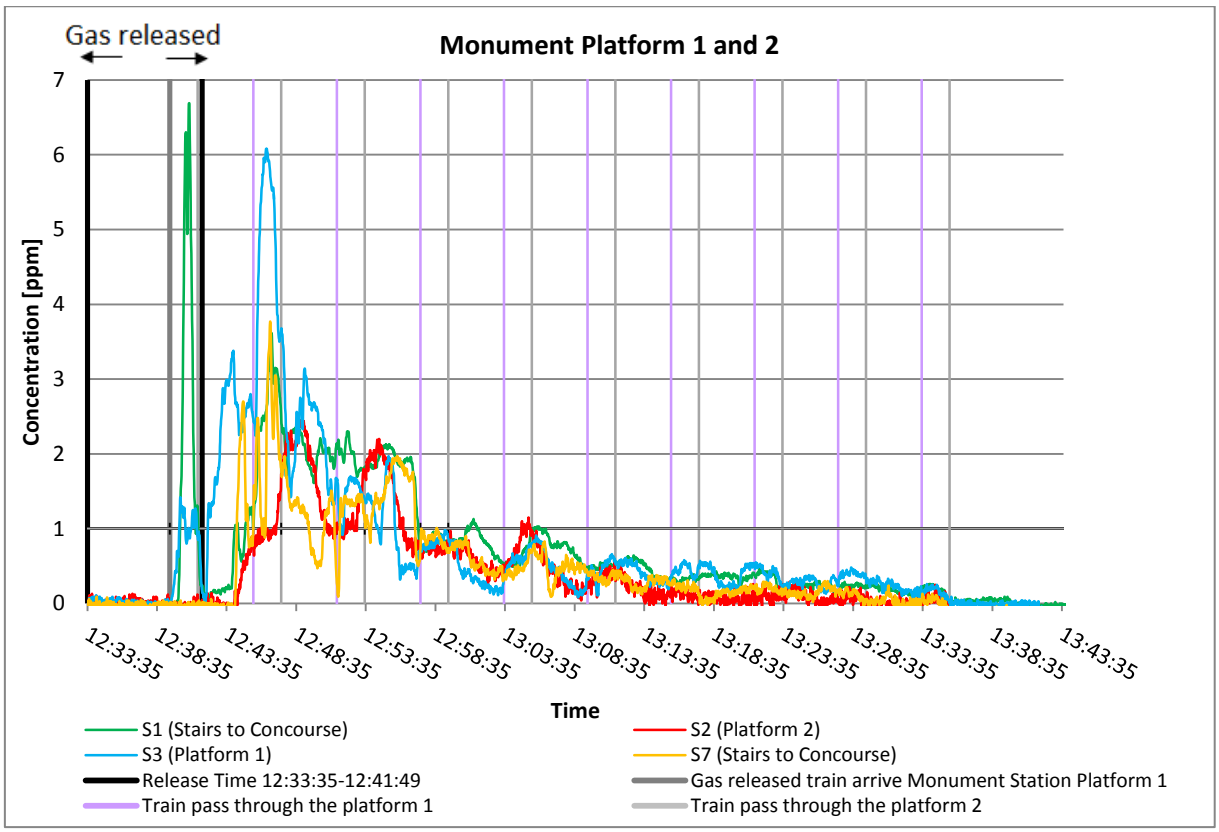

Figure 90: SF_6 concentration at Monument Station Platform 1 and 2 with train arrival time line through platform 1 and 2 (Tracer gas experiment 5)

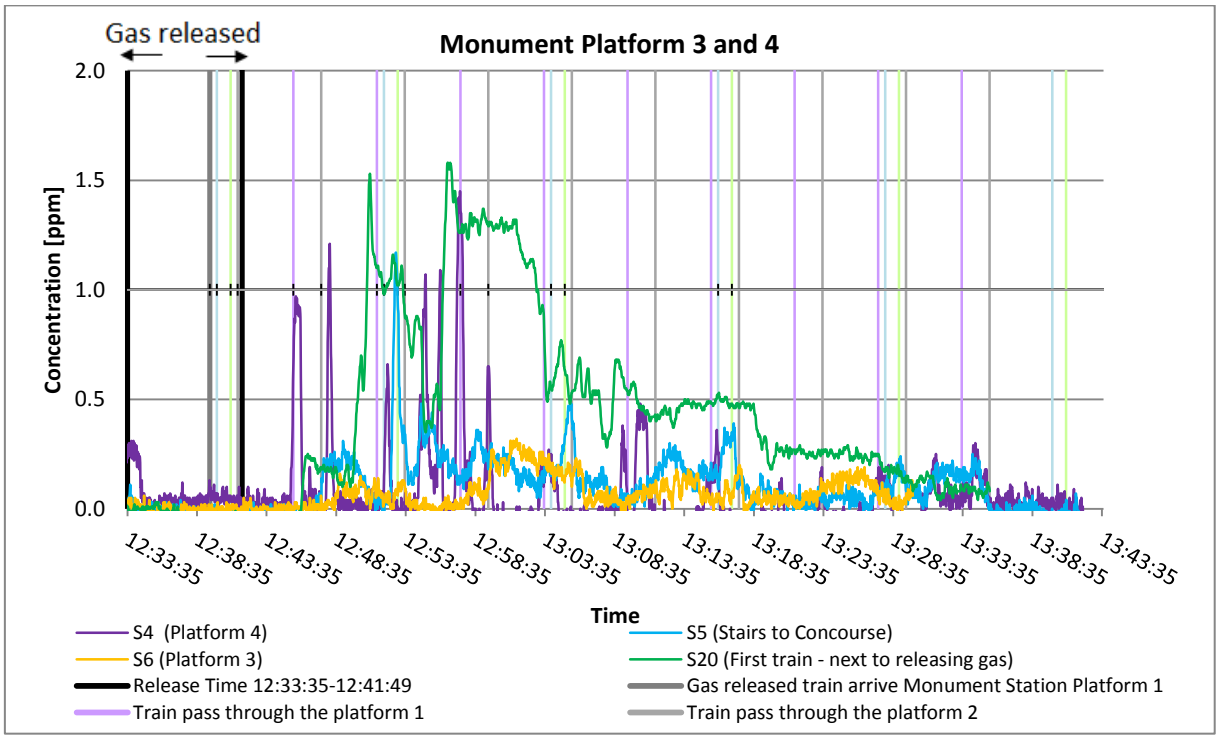

Figure 91: SF_6 concentration at Monument Station platform 3 and 4 with train arrival time line through all platforms at Monument Station (Tracer gas experiment 5)

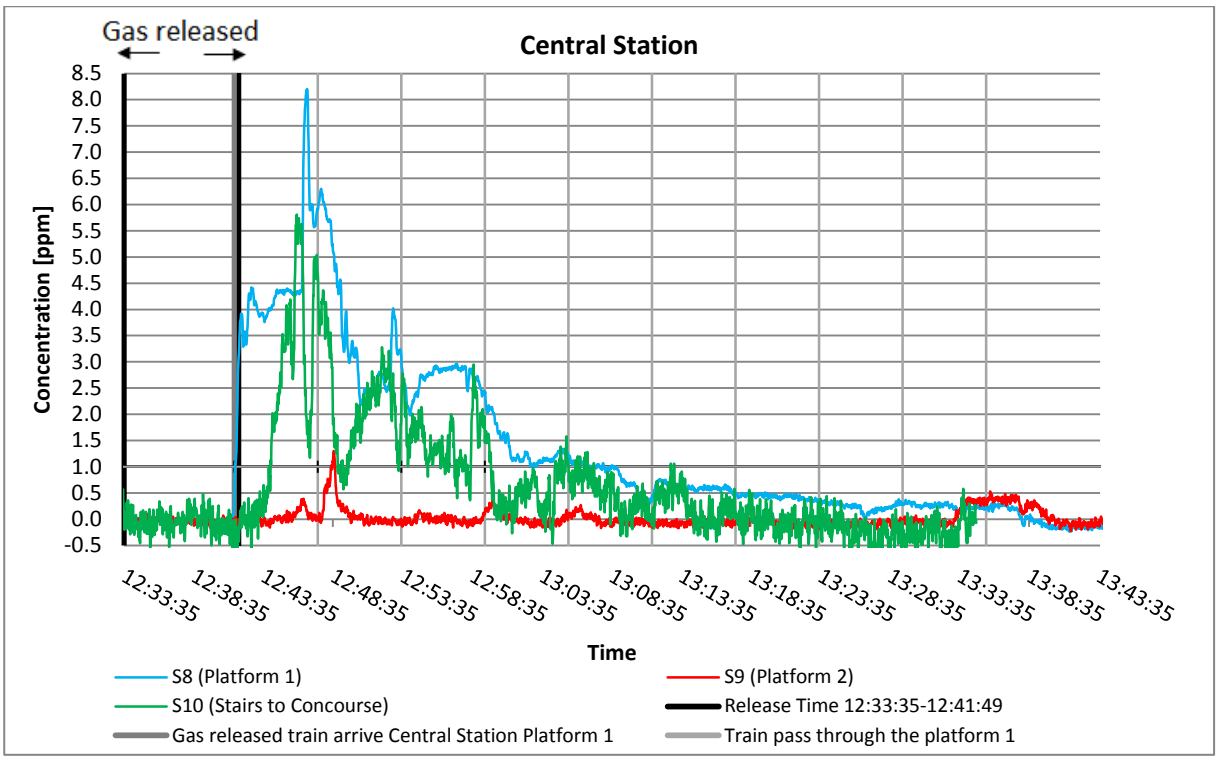

Figure 92: SF_6 concentration at Central Station with train arrival time line through platform 1 (Tracer gas experiment 5)

During these experiments it was found that within 5 minutes most evacuation routes were contaminated with significant levels of SF_6. The tracer gas experiments have shown that a toxic substance can be distributed over a wide area by means of the airflow in a subway system. The natural background air flow is the primary driver for the gas dispersion but the piston effect of the train can force the gas against the background air flow in an unpredictable manner. The maximum dispersion occurred when the gas was released in an operational train and this was seen to contaminate several stations and following trains. The concentration of the gas in some cases was very small of the order of 2 to 3ppm but to put this into perspective consider the effects if the tracer gas had been Phosgene. Phosgene is a highly toxic substance that exists as a gas at room temperature. Owing to its poor water solubility, one of the hallmarks of phosgene toxicity is an unpredictable asymptomatic latent phase before the development of noncardiogenic pulmonary edema (Grainge and Rice, 2010). The degree of toxicity of gases depends on several factors including the concentration, the exposure time and the health and physical capacity of the victim. This is characterised by the Acute Exposure Guideline Levels (AEGL) (Bruckner, 2004). A toxic level of Phosgene that can place a person's life and well-being in jeopardy can be as low as 2 ppm (Grainge and Rice, 2010). Exposure to moderate-to-high concentrations of

phosgene (>3-4 ppm) can produce an immediate irritant reaction that typically lasts 3-30 minutes and includes the following:

• Lacrimation

• Conjunctival irritation/burning

• Burning sensation in mouth/throat

• Throat swelling/changes in phonation - May reflect laryngeal edema

Respiratory manifestations, which can develop relatively early at greater than 4.8 ppm (Grainge and Rice, 2010), usually do not develop until after a latent period lasting 4-24 hours post exposure. Signs and symptoms of this phase, which result primarily from hypoxemia or volume depletion, include the following:

• Lightheadedness

• Palpitations

• Angina

• Headache

• Anorexia

• Nausea, and vomiting

• Weakness

• Anxiety and sense of impending doom

On physical examination, respiratory findings may include the following:

• Crackles on auscultation - Herald the onset of pulmonary edema

• Cyanosis - Late finding

• Thin, frothy white/yellow secretions

• Wheezing

• Tachypnea

• Stridor

• Accessory muscle use for respiratory effort

Cardiovascular findings may include the following:

• Tachycardia

• Hypotension - Late finding secondary to inflammation-mediated fluid diversion out of vascular system and into lung interstitium.

Skin findings may include the following:

• Cyanosis from pulmonary injury and resultant hypoxemia

• Chemical burns from liquefied phosgene (although it also is considered a frostbite hazard in the compressed liquid form)

Sarin gas was used by the Aum Shinriko group when they attacked the Tokyo underground in 1995 killing 12 people and leaving 5000 with temporary vision problems (Ogawa *et al.,* 2000). The sarin was released inside several trains and then leaked into stations. Sarin has a level of toxicity that is 43 times greater than that of Phosgene as a single drop can kill an adult (Sidell, 1996). Sarine is the most volatile of the nerve agents, it evaporates and spreads into the surroundings quickly. To date over 5,000 people have applied for benefits to assist them with the after effects of the attack. Forty-seven have been certified as disabled and 1,077 have received compensation for serious injuries. A survey of the victims in 1998 and 2001 showed that many suffered from post-traumatic stress disorder, 20% of those surveyed said they felt uneasy using the underground and over 60% mentioned eye strain and worsening vision (Ogawa *et al.,* 2000).

The most critical time for the dispersion of toxic substances in the Tyne and Wear Metro can be determined from the station footfall data. With regard to the main stations examined in this study, the Gateshead Station, Central Station and the Monument Station the maximum footfall count occurs between 17.00 and 18.00 at the beginning of the week of 700, 1200, 3000 individuals respectively. The count in the Monument station is made up of the north-south and east-west lines as it is clearly the busiest station in the system. An event involving a toxic agent such as Sarin in an operational train at 17.00 hrs on Monday to Wednesday would inevitably lead to hundreds of causalities that would overwhelm the rescue and health services and result in major disruption in the City Centre.

6.7 Conclusions

The tracer gas experiments have shown how complicated and unexpected the air flow in a subway station can be. The highest concentration inside the station was found in the escalators to the concourse levels and the exits and this occurred very quickly. This is a further verification that escalators in subway stations are sucking air from the lower levels. During the repeat of this experiment, a slightly lower concentration was recorded, but the patterns of the spatial and temporal distribution were confirmed. Subway stations are mostly relatively over-warmed in the temperate climatic zone. With increasing depths of stations, and lengths of staircases, the buoyancy effect, which pushes air upwards, also increases. The experiments have shown that the tracer gas propagates to upper parts within a few minutes. Unfortunately, the propagation path overlaps with escape routes for passengers. The geometry of tunnels has an effect, as differences in elevation drive a natural background air flow. Of immediate concern is the unexpected distribution of the tracer gas into the station by way of the stair case linking the two platform levels that contaminated platform 3 and 4 and subsequently the concourse area. The concourse is the only escape route from the platforms so the fact that this becomes contaminated so quickly before the passengers could exit the station is of concern. Another unexpected feature of the results is shown in Figure 62 as a significant part of the tracer gas does not leave the station through the street exits but travels to the exit that links with the Eldon Square shopping centre. This could have serious consequences in the event of a highly toxic gas being released in the station.

The tracer gas is dispersed more quickly through the station when the trains are in operation and is spread through the tunnels to the adjacent stations more rapidly than in the operational break. The maximum value of recorded tracer gas concentration was higher and larger parts of the platform levels were affected. The propagation paths were chaotic due to several train movements.

The background air flow (south to north) is disturbed by the operating trains (experiment 5). The gas dispersion to the Haymarket station occurred very quickly (within 5 minutes) during operational time with the train travelling in the same direction as the natural flow (experiment 4). At the Central Station, on the other hand, it took three times longer for gas dispersed to the opposite platform, to be transported against the direction of natural flow (experiment 5) by the piston effect of the trains.

In order to measure the concentration over a longer time period, one mobile sensor remained in the contaminated train. Concentrations remained at nearly 950 ppm for three further stops in the tunnel. After Jesmond Station, the train continued over ground such that at 10 minutes after the end of the gas release the concentration of SF_6 had decreased to 500 ppm, and after 18 minutes, after calling at six over ground stations, the levels dropped to 100 ppm. At 25 minutes after the beginning of the gas release and after calling at 14 stations, there were no measurably residues left in the contaminated train (see Figure 81).

The gas release inside an operating trains can affect wide parts of stations and even harm passengers in following trains up to 35 minutes later. The trains of the Tyne and Wear Metro system consist of two separate coaches. At each station the train doors are opened and some contaminated air flows into the coaches. After the first stop, a small contamination was observed in a following train and at the third stop significantly higher values were logged. Consequently, the concentration accumulated up to 3 ppm after the passage of the following train through the Haymarket Station (see Figure 82).

A significant advantage of the mobile sensors was the ability to take measurements in different trains. The sensors that travelled with the first following train after the contaminated train were transferred to trains traveling in the opposite direction as it left the tunnel. The sensor detected concentrations that were slightly lower in the returning train but they showed the tracer gas remained in the system for a long period as 30 minutes after the gas release, a demonstrable concentration was observed in the operational train at the opposite platform.

Chapter 7. Microclimate CFD Modelling

7.1 Microclimate CFD modelling

The tracer gas experiments described in Chapter 6 combined with pedestrian simulation gives a highly accurate overview of evacuation plans but the tracer gas experiment only represents one weather condition so it does not provide a complete picture. In order to fully understand the air flow dynamics in the station it will be necessary to extend this work to account for the seasonal variation of the weather. Previous research by Wilby (2005) shows that the local microclimate in cities is strongly influenced by the so called “heat island effect” in which the temperature and airflow are strongly influenced by the presence of buildings. This has been observed in Newcastle and reproduced by measurements and CFD simulation of the area around the Monument for a limited number of cases.

The microclimate of Newcastle city centre, where the Monument Metro Station is located, has been determined through comparing the measurement data and the weather data from the weather station located at the Ellison Building which is the nearest weather station to Monument. Data is routinely recorded on an hourly basis at the weather station. The yellow probe shown in Figure 28 in Chapter 5.3 indicates the location of the weather station. The measurements performed and shown in chapter 5.4 indicate a loose correlation between the local weather data within the metro system and that recorded by the weather station. The air temperatures of the three Monument Station exits correlate with weather station data according to a logarithmic plot under different weather conditions, although the wind speed and wind direction show a larger influence of the surrounding buildings. A photo of a street view outside Exit 1 is shown in Figure 93. This assessment is not accurate enough to be a reliable estimate of the complete situation at Monument however, to address this issue the weather station data can be used as an input to a CFD model of the area around the station.

Figure 93: A Photo of the Monument Station Exit 1 in Blackett Street

7.2 CFD model development

A Newcastle city centre CFD model has been developed using PHOENICS to ascertain if the wind speed and direction correlations between the Monument station entrances and exits and the weather station can be reproduced in a CFD simulation. Gosman (1999) pointed out that although there are well-known weaknesses in the physics modelling, using commercial CFD codes as a tool for wind engineering application in the built environment, the level of prediction accuracy is already sufficient for some purposes. PHOENICS is a general-purpose commercial CFD code suitable for steady or unsteady, turbulent or laminar, compressible or incompressible flows using Cartesian, cylindrical-polar or curvilinear coordinates (Ludwig and Mortimor, 2010). The code also has a spatial marching integration option to handle parabolic and hyperbolic flows. The numerical procedure is of the finite-volume type in which the original partial differential equations are converted into algebraic finite-volume equations with the aid of discretisation assumptions for the transient, convection, diffusion and source terms. For this purpose, the solution domain is subdivided into a number of control volumes on a mono-block mesh using a conventional staggered-grid approach. All field variables except velocities are stored at the grid nodes, while the

velocities themselves are stored at staggered cell-face locations which lie between the nodes.

The model requires a grid mesh representing a domain, in this case the city streets, to be created. This was done using information from the Northumbria City Model (Figure 97) to produce the PHOENICS image of the city streets in the VR viewer as shown in Figure 98. This was created by using Digimap which is a software designed for modelling city canyons. The domain shape is typically circular or elliptical as this tends to negate edge or vertex effects such as local accelerations or artificial gradients that may occur in cubical domains. The main advantage however lies in the specification of wind conditions during the pre-processing process as an entire array of wind conditions can be set up quickly in using the same CAD and mesh file. This produces a large saving in set up time as the user has only to assign inlet and outlet conditions for the different simulations.

It is crucial that the domain be of such a size to minimise the effect of downwash and interference from the surroundings. The computational domain should be large enough to avoid artificial acceleration of the flow. Its size can be based on the height of the tallest building in the urban configuration and/or on the blockage ratio (Blocken et al., 2012). Consequently, keeping the domain large enough to capture any wake effects (regardless of direction) is crucial. There are many industry guidelines on choosing the diameter and height of the domain, but in reality the domain size is also governed by the computational cost and items of priority (i.e. investigation of wakes or local regions of recirculation). Using the tallest building (of height H) as a guide, the vertical extent of the domain should extend to at least 5H (Wildeanalysis, 2012). In the lateral direction, the choice for domain width is largely dependent on some measure of wind blockage area and how tightly the buildings are packed in the landscape.

• For groups of buildings with a large net aspect ratio (i.e. significant blockage to the wind), the effective width of the collective buildings is taken into account. Using this value the length of the domain in the wake region is typically kept to 4 or more.

• For cases where wake effects are not a high priority (e.g. region of interest is enclosed, taller structures are in immediate surrounding or more commonly where the downstream buildings are not included due to their location or size) or the buildings offer very little blockage, an effective downstream length of 3 to 4 times the collective width will suffice. In using any of the above guidelines, care should be taken to ensure

that the domain edges are a good distance away from the outermost building, in order for the flow field to stabilize before it exits the domain.

• The size of the domain also depends on the velocity field expected within the domain. For higher velocities (which may take longer to stabilize in the wake region) a larger domain might be required.

The asymmetric wind pressure distribution on the windward face, side faces and leeward face can cause torsional vibration. This is due to both wind turbulence and the vortex in the building's wake. The torsional moment induced wind force is subject to the effects of building shape and wind behaviour. While there are a lot of guidelines for domain size based on downstream wake capture, it is important to note that the upstream velocity resolution and terrain definition are just as important. Failure to provide a stable upstream velocity can result in seriously flawed downstream flow patterns, regardless of how well defined the downstream domain is modelled (Wildeanalysis, 2012). Common effects of placing the Inlet boundaries too close to the built-up areas or not adequately defining the velocity in the upstream region include:

• Artificial acceleration of fluid near building surfaces; this occurs because the fluid has to squeeze past the building and the outer edge of the domain. This squeezing effect through a small area increases the velocity in the local region.

• Vortex generation from mundane surfaces: the above effect in combination with the building being in close proximity to the domain boundary leads to artificial vortex shedding due to rapidly changing gradients in this region.

• Non-real velocities been applied at the inlet. This occurs when the stagnation pressure region (upstream of an object) interacts with the Inlet, due to their close proximity. In such cases, there is a danger that the Inlet velocity profile might end up being different to the one manually inputted by the user, due to flow interaction.

An example of mesh generation of flows within and around buildings modelled with a commercial CFD codes is shown in Figure 94 (Alamdari, 1996). Figure 95 and Figure 96 show an example of a terrain model for CFD analysis simulated by ANSYS CFD of flow through a city block (Wildanalysis, 2012) for the purpose of better understanding the airflow around the structure and also to provide recommendations on design improvements. This steady flow (time average calculation method) model simulation utilized a traditional Reynolds Averaged Navier-Stokes (RANS) model. Comparison

with transient Scale Adaptive Shear Stress Transport (SAS-SST) or Large Eddy Simulation (LES) approaches, has shown that the 'average' solution obtained using the RANS method is sufficient for design purposes and steady state has a much low cost in time and computational effort.

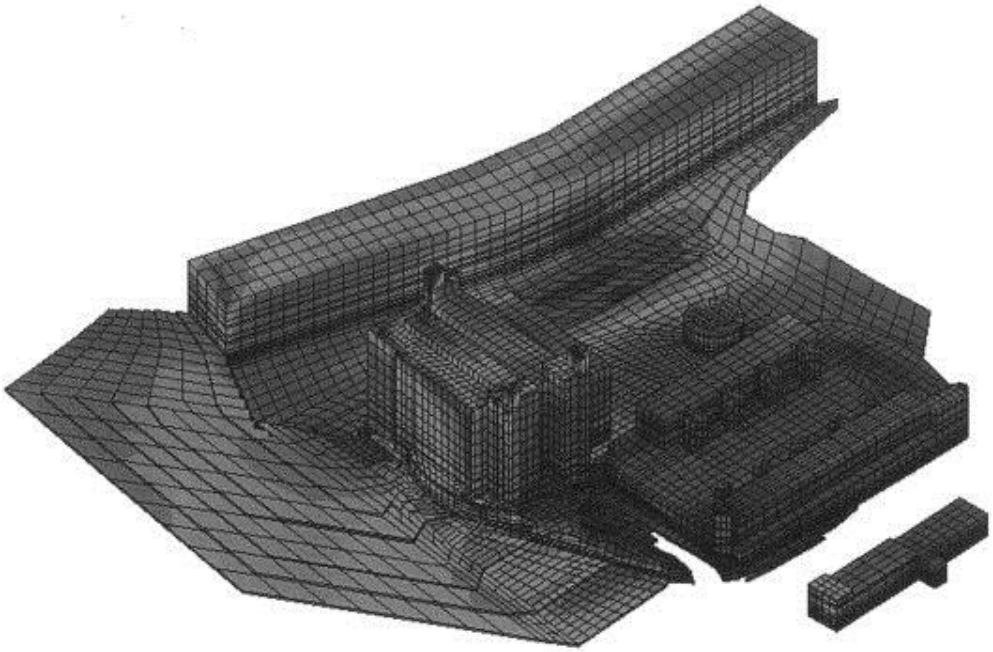

Figure 94: Mesh generation in commercial CFD software for the built environment model (Alamdari, 1996)

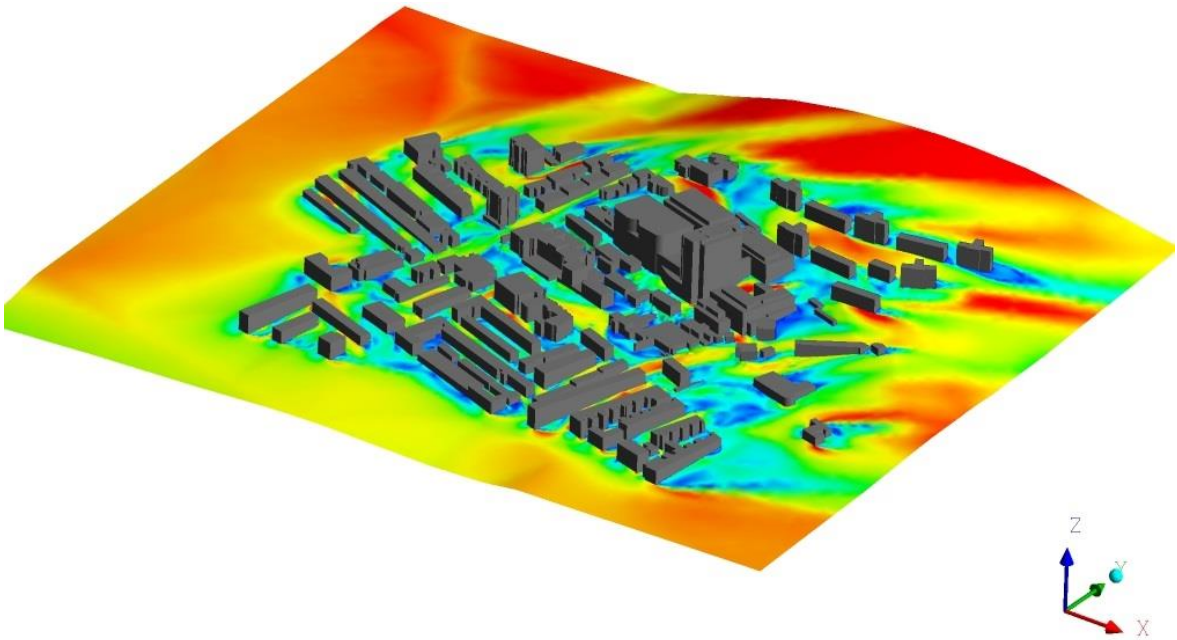

Figure 95: Example of a terrain model for a wind flow analysis (1)

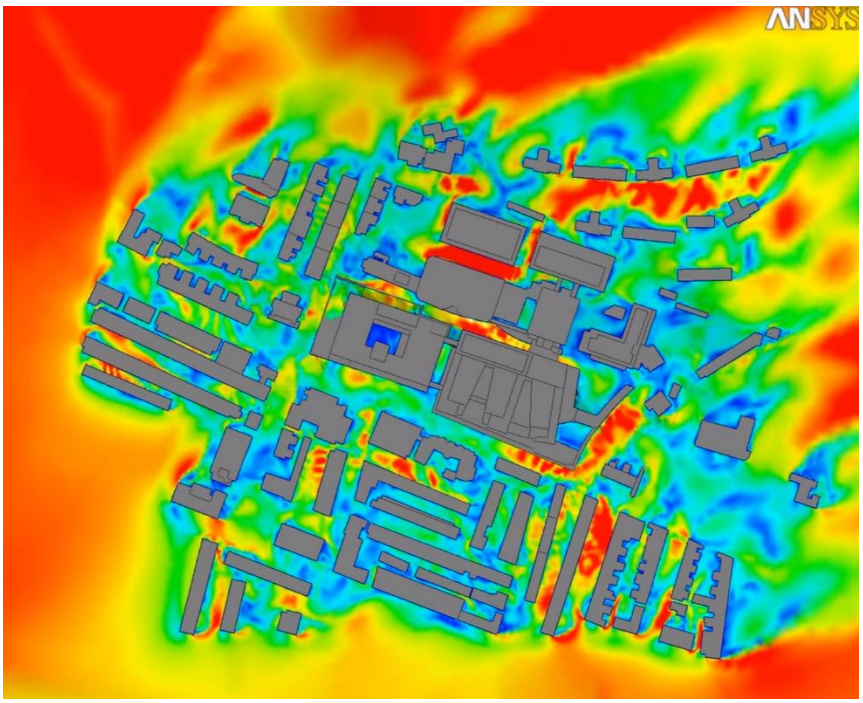

Figure 96: Example of a terrain model for a wind flow analysis (2)

7.3 CFD model settings and results

The CFD model developed from the Virtual Newcastle Gateshead City Model (Figure 97) is shown in Figure 98 and Figure 99. It will be noticed that the PHOENICS image has rotated 40 degrees clockwise compared to the City model in order to provide satisfactory boundary conditions for the simulation. A general boundary condition of wind speed was provided at the edge of the model regime close to the location of the weather station and the PHOENICS image was rotated to extend the extent of the boundary condition.

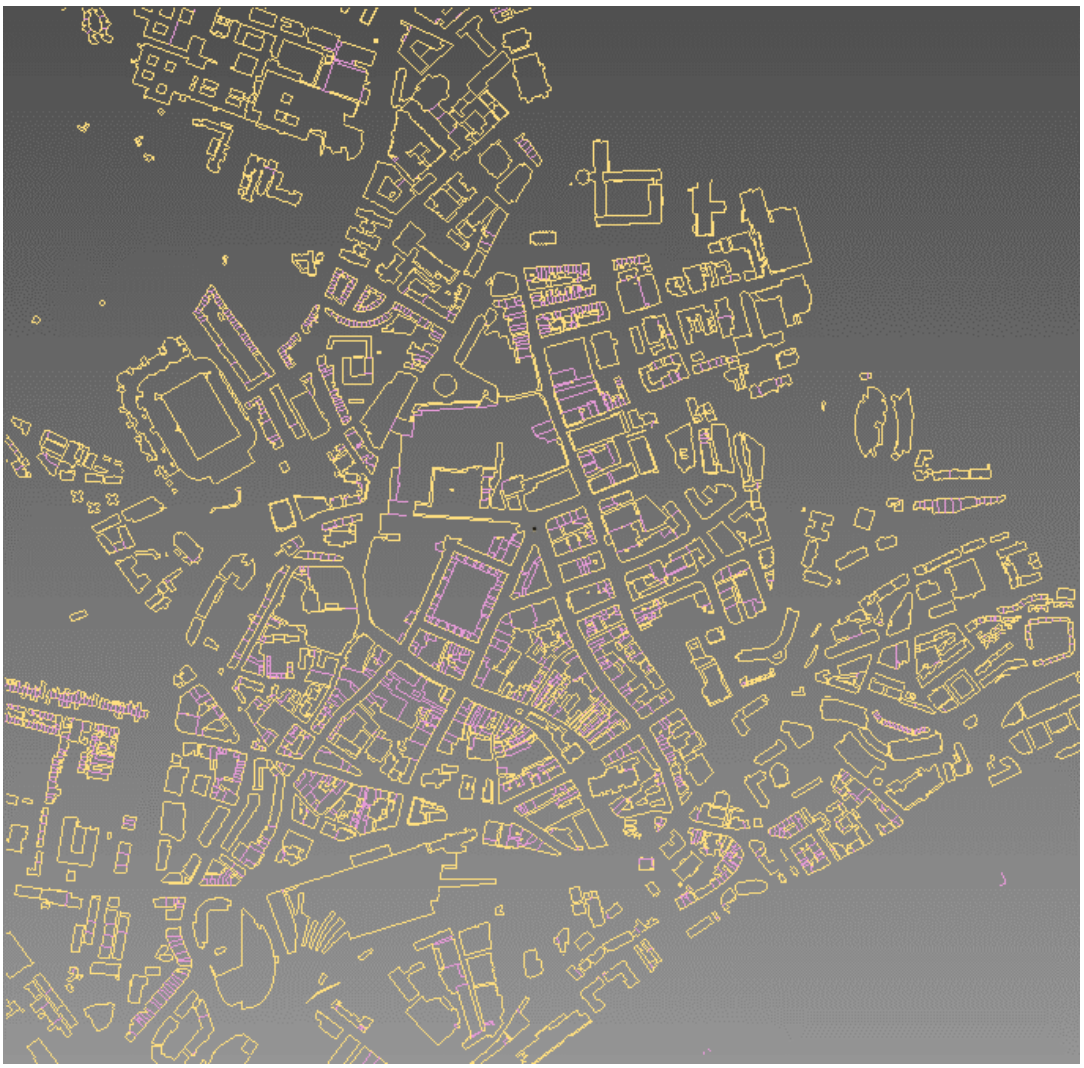

Figure 97: Newcastle City Model used to produce the Microclimate CFD

The microclimate model in PHOENICS has a size in the X direction of 1,400 m, and in the Y direction 1,330 m. The distance from the outer building to the domain boundary is from 100 m to 200 m and the Z direction which represents the height of the computation zone is 100 m. This is more than five times the height of the weather station on the Ellison Building. The location of the Ellison Building and Probe 1 is indicated in Figure 98 and Figure 99. The city centre and the Monument station are located in the central area of the model. The mesh size is 1.5 m-3 m in the regain containing the buildings in the centre part of the Microclimate CFD model as shown in the XY section in Figure 98 and XZ section Figure 99. The wind velocity is shown by the gradation of colour in the streets and the direction is indicated by arrows as shown in the later figures.

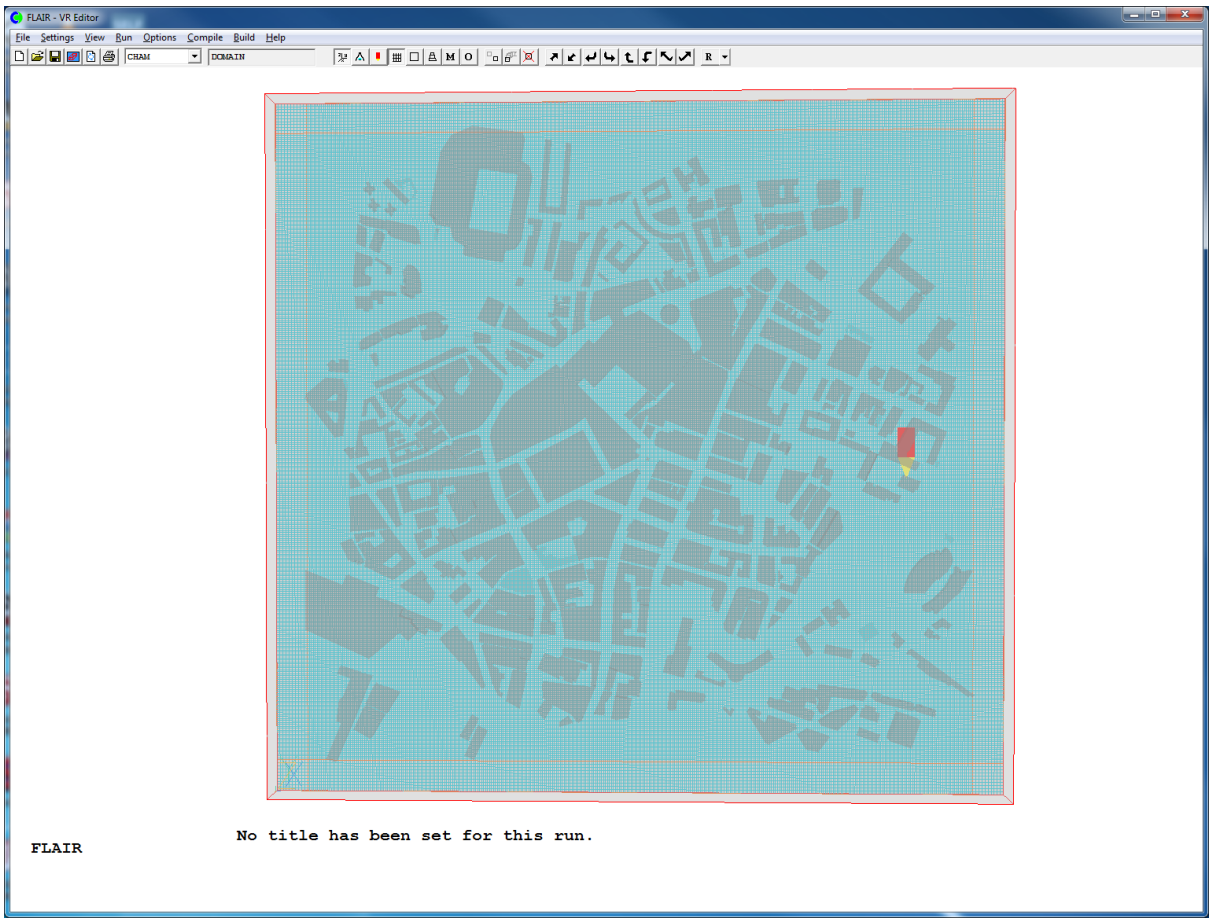

Figure 98: XY section mesh of Microclimate CFD modelling in PHOENICS and Probe 1 (weather station) location

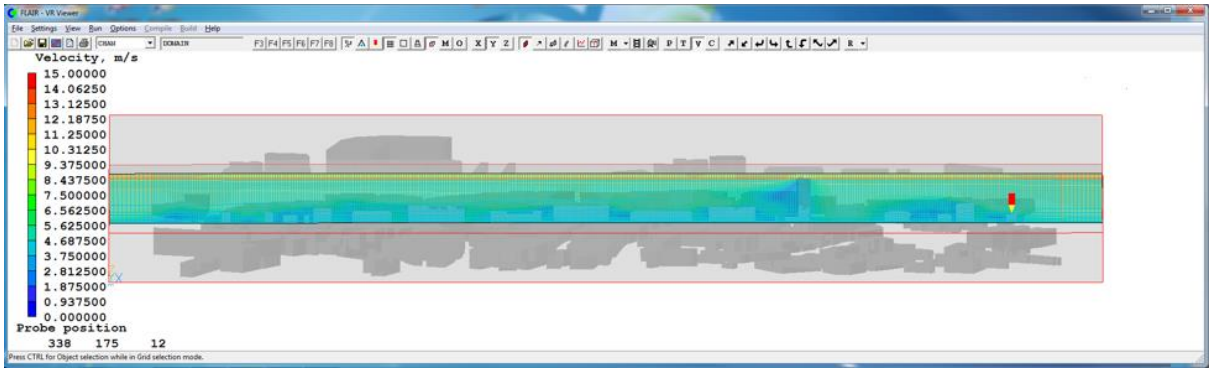

Figure 99: XZ section mesh of Microclimate CFD modelling in PHOENICS and Probe 1 (weather station) location

The simulation has been performed for 16 wind directions with 5 different wind speeds at the general boundary ranging between 2 and 13 m/s in each direction. The directions are shown in Table 16.

Abbreviation of wind direction	Wind direction	Wind direction (degree)	PHOENICS input direction (degree)
N	North	0	40
NNE	North-Northeast	22.5	62.5
NE	Northeast	45	85
ENE	East-Northeast	67.5	107.5
E	East	90	130
ESE	East-Southeast	112.5	152.5
SE	Southeast	135	175
SSE	South-Southeast	157.5	197.5
S	South	180	220
SSW	South-Southwest	202.5	242.5
SW	Southwest	225	265
WSW	West-Southwest	247.5	287.5
W	West	270	310
WNW	West-Northwest	292.5	332.5
NW	Northwest	315	355
NNW	North-Northwest	337.5	377.5

Table 16: List of the wind direction with PHOENICS input direction

The general boundary condition of wind speeds varied in each direction in order to achieve nearly the same speeds at the point representing the weather station irrespective of direction. The inlet boundary conditions of wind was set up as the atmospheric boundary profile as open sky wind entered into the program in the format shown in Figure 100. These values applied to the edge of the domain providing values of the prevailing temperature, wind height, direction and speed. These initial conditions applied to the whole domain and the upper boundary was treated as a fixed pressure boundary. A logarithmic boundary layer at the buildings and on the ground level plane was selected in this case. In meteorology the atmospheric boundary layer (ABL), is the lowest part of the atmosphere. Its behaviour is directly influenced by its contact with a planetary surface. On Earth it usually responds to changes in surface radiative forcing in an hour or less. (Garratt, 1994). This input parameter of wind is not been affected by the urban layout and which is not represent the weather data measured in this research. Therefore, the wind speed is a boundary condition input, the probe 1 value represent the weather data station although there is a minor difference. This can be shown in a simulation example input wind is 2m/s (Figure 100) with Probe 1 weather station value at 2.03m/s (Figure 101).

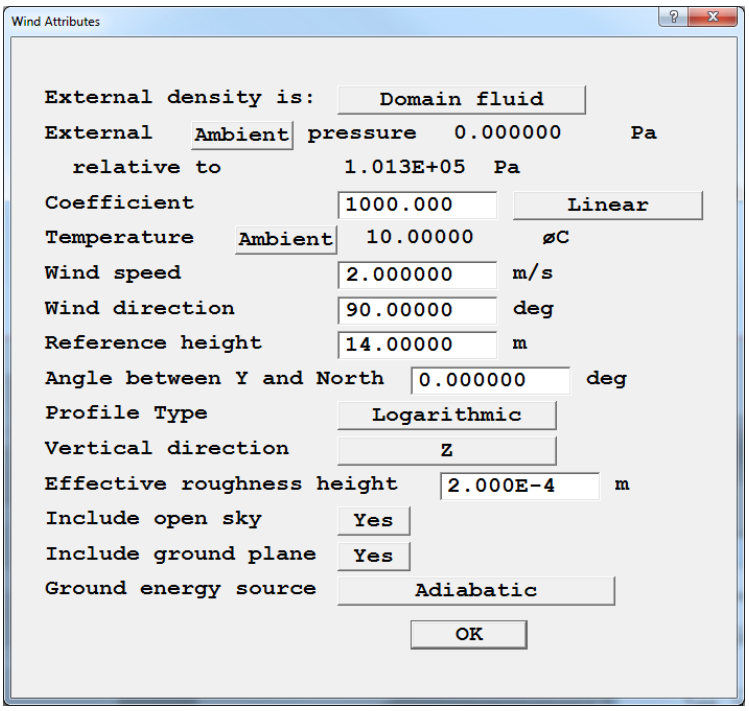

Figure 100: The initial wind profile attributes dialog setting window

Figure 101 and Figure 102 show the format of the output from the PHOENICS program simulated wind input from North with speed at 2m/s, the different colours indicate the wind strength and the velocity distribution on the horizontal plane for the model. Figure 101 represents the XY plane at the height of the weather station and Figure 102 represents the XZ plan at city centre. Figure 103 is the XY plane at street level at the station Exit 2 where is the Probe 2, Exit 1, the difference in the colour range of these figures indicates the attenuation effect of the surroundings on the wind velocity and the influence of the surrounding buildings in modifying the air flow direction.

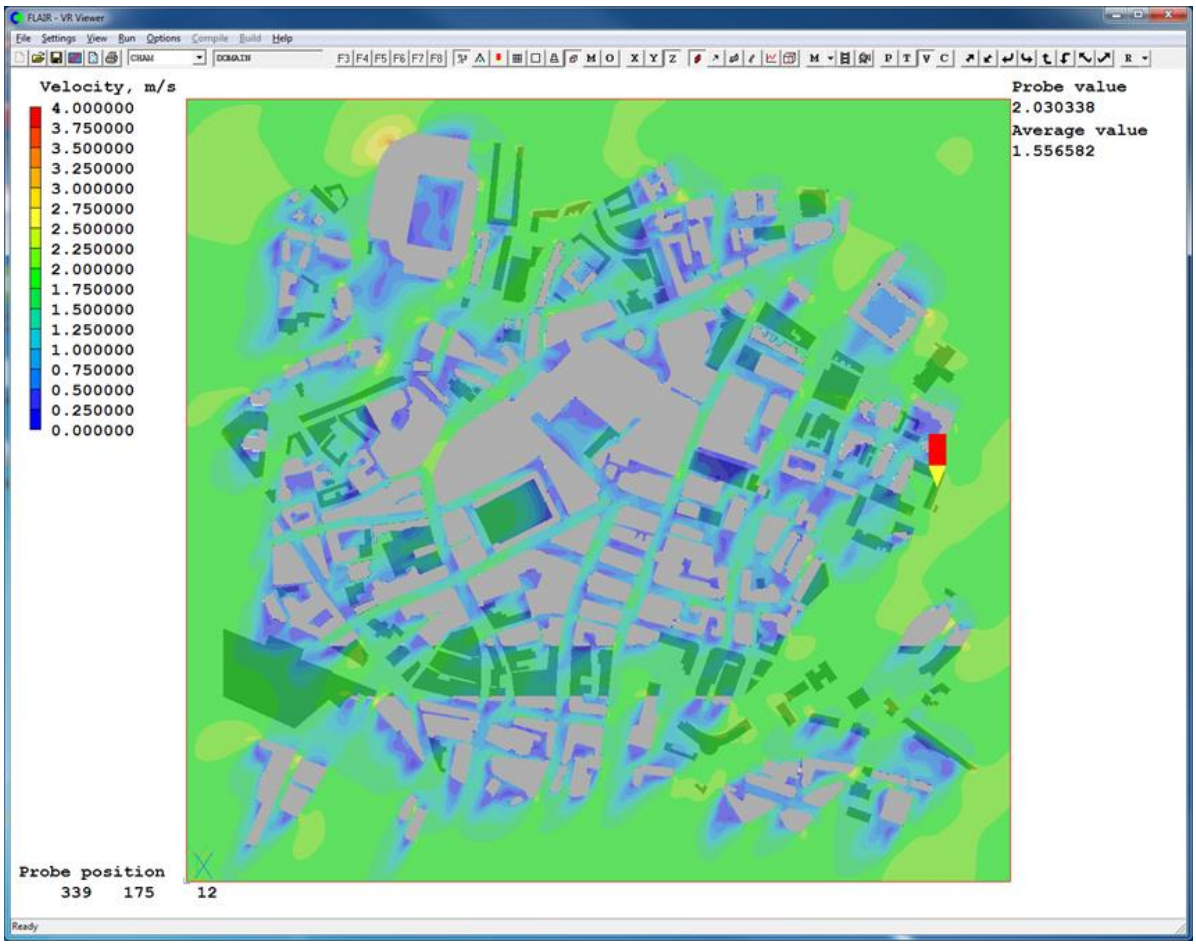

Figure 101: XY section of velocity output from CFD modelling in PHOENICS at height of probe 1

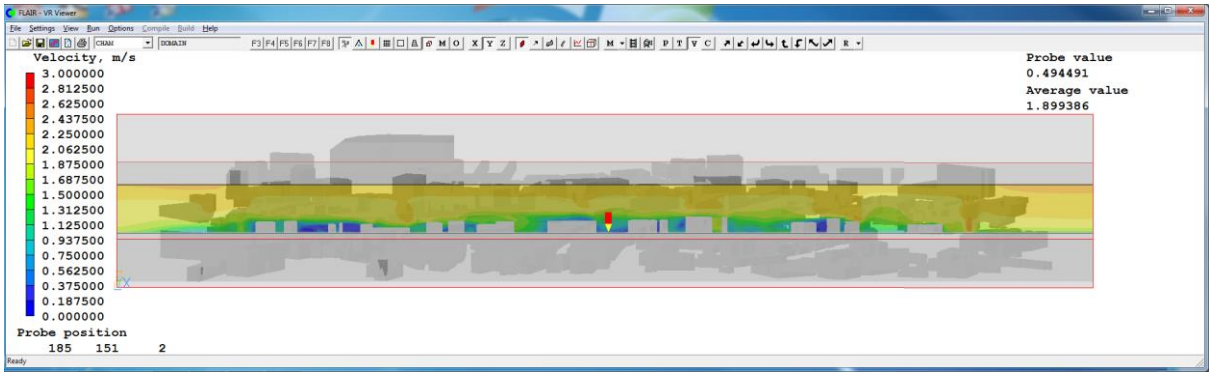

Figure 102: XZ section of velocity output from CFD modelling in PHOENICS at city centre

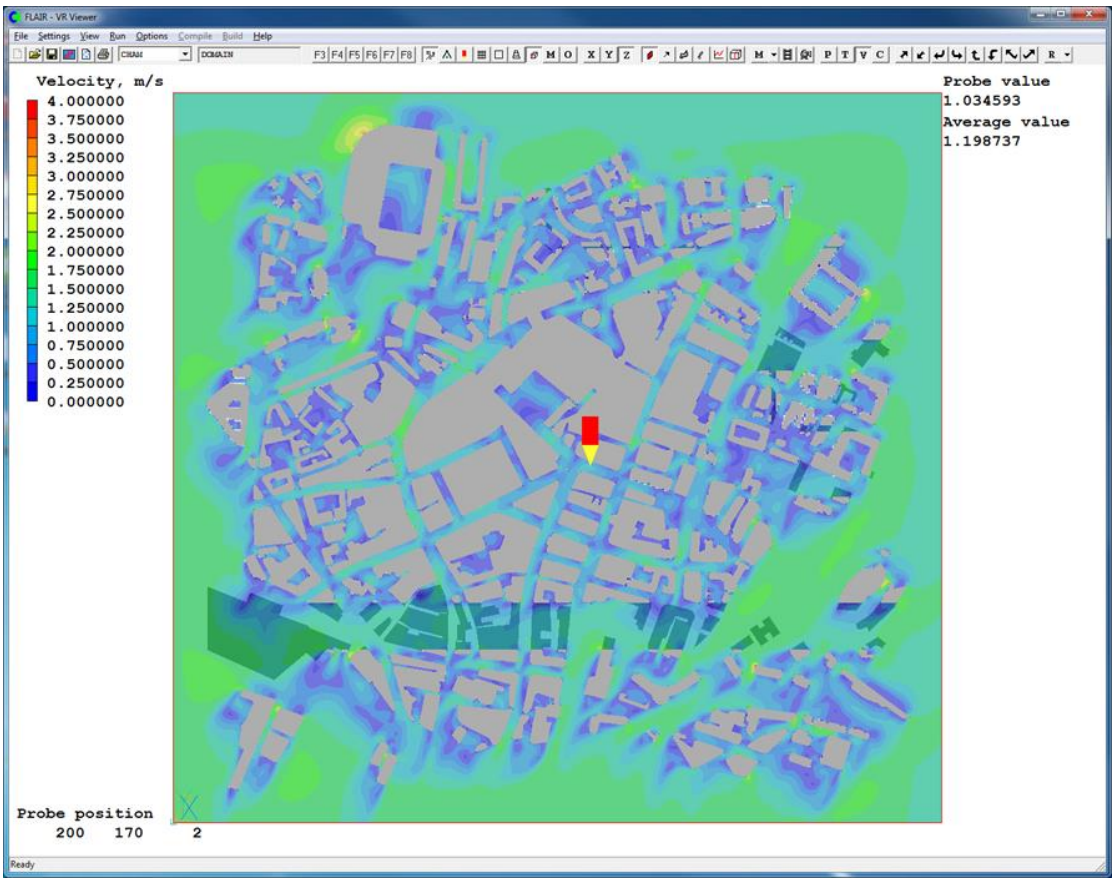

Figure 103: XY section of velocity output at height of probe 2 (Exit 1) in Blackett Street

7.3.1 Sample result of wind direction from North speed at 2 m/s

The influence of overall wind direction as determined at the weather station on the condition at the station Exit 1 in Blackett Street can be seen from Figure 103. When the wind direction was from the North the dominant air flow in Blackett Street was in the east to west direction towards Exit 1 of the station. The velocity at the location of the probe was 1.03m/s as shown in Figure 104. Exit 2 in Grey Street (Figure 105) was subject to a northerly air flow away from the station which could induce an outflow at the station exit. The air flow around the Monument is mainly in the southerly direction. It can be seen that there is a significant amount of recirculation in the rectangular region west of the monument and that the side streets off Grey Street have little influence on the general air flow. Figure 106 shows the Probe 4 location is outside Exit 3 which is inside the Eldon square entrance. It can be seen that the external environment of Exit 3 had a negative wind pressure which could induce outflow at this location. Figure 107 displays the probe values of the weather station and the three exits with all the variable wind speeds that were simulated with a northerly direction input wind profile. The figure

shows a significant correlation between the wind speed at the weather station and that at the three station exits.

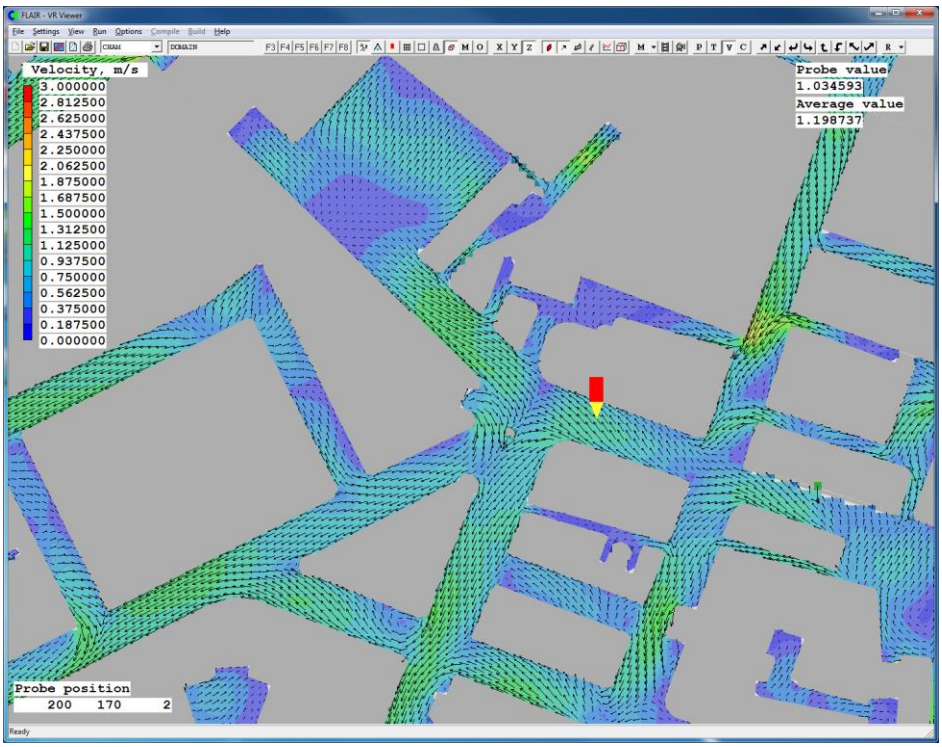

Figure 104: Probe 2 locate at Exit 1 in Blackett Street (Wind input from North, speed at 2 m/s)

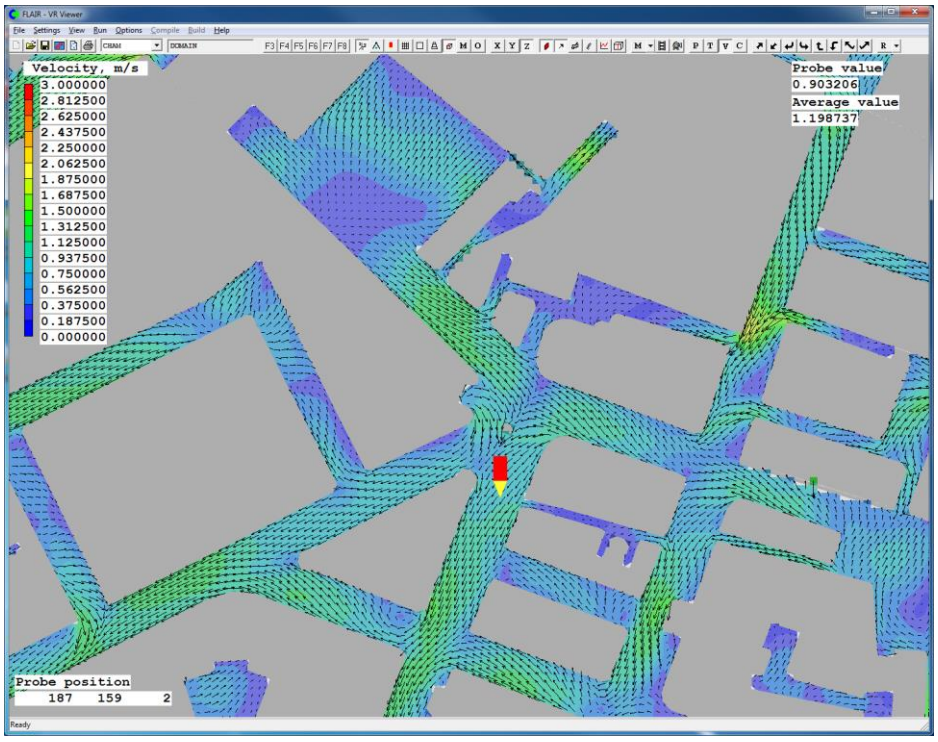

Figure 105: Probe 3 locate at Exit 2 in Grey Street (Wind input from North, speed at 2 m/s)

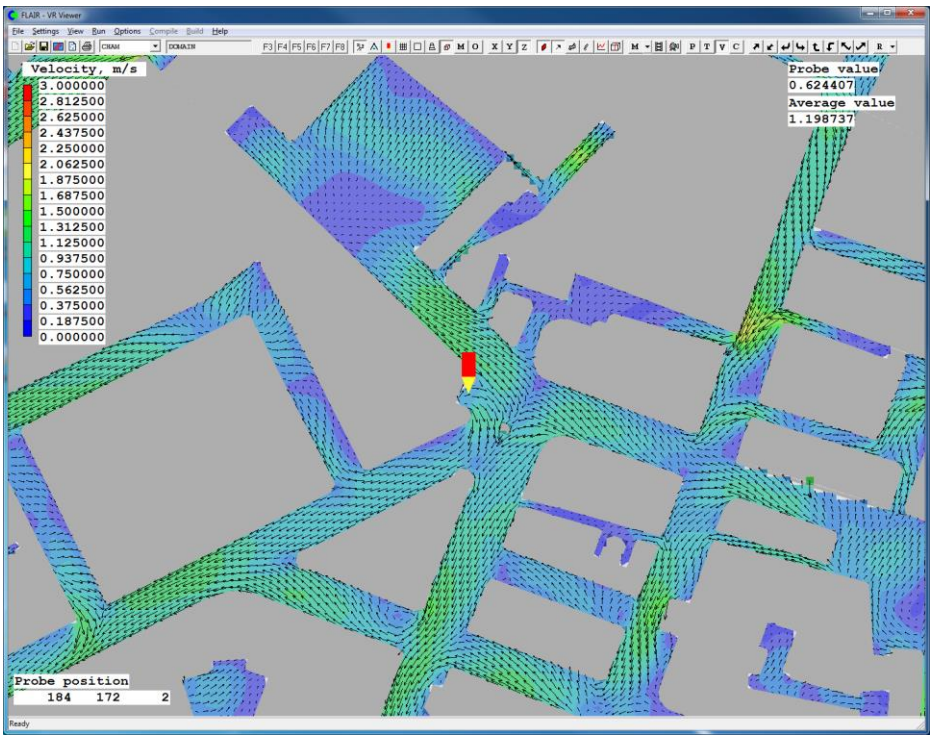

Figure 106: Probe 4 locate at Exit 3 in Elden square (Wind input from North, speed at 2 m/s)

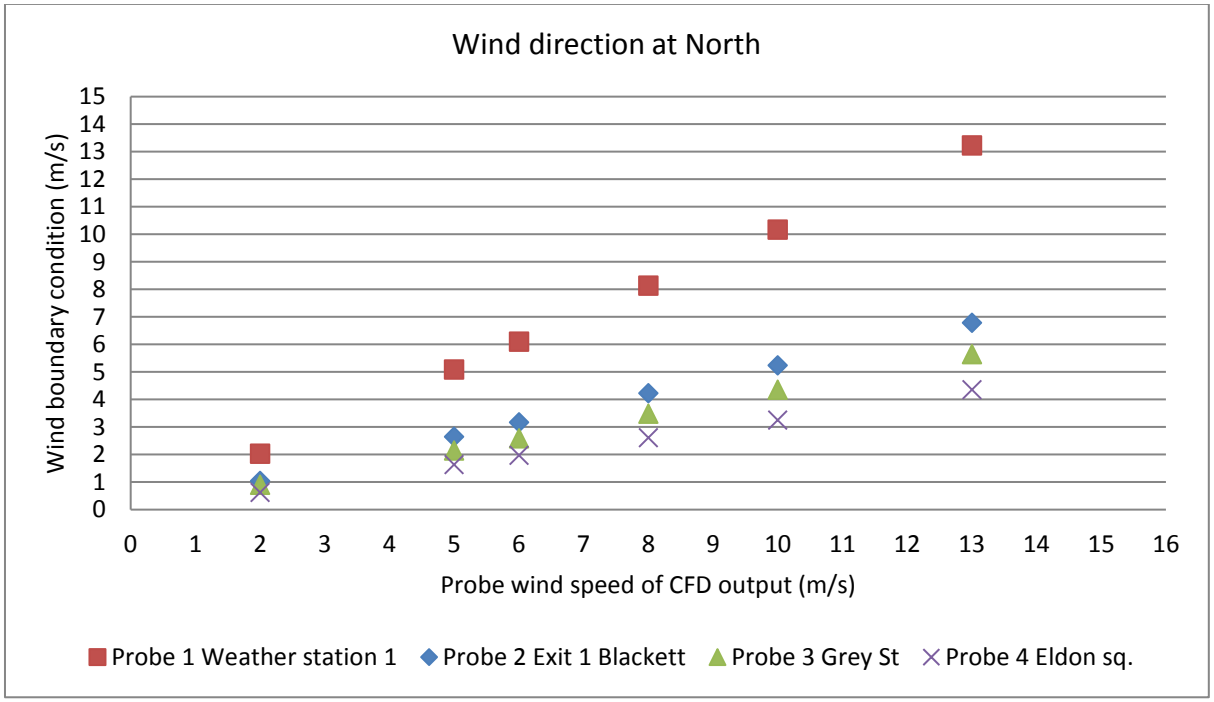

Figure 107: Probe values at weather station and exits in variable wind input speeds from North

7.3.2 Sample result of wind direction from East speed at 1m/s

When the wind direction was from the east the air flow in Blackett Street (Exit 1) was still towards the Exit 1 as shown in Figure 108. Exit 2 in Grey Street (Figure 109) was subject to a southerly air flow toward the exit which produced recirculation in the region effected by the buildings on Grey Street. A stream of air emerging from a side street on Grey Street close to the station also had an impact on the flow at the station. In this condition both Exit 1 and Exit 2 could have inflows. The airflow at Exit 3 was mainly in the windward direction with small recirculation outside the Eldon Square entrance.

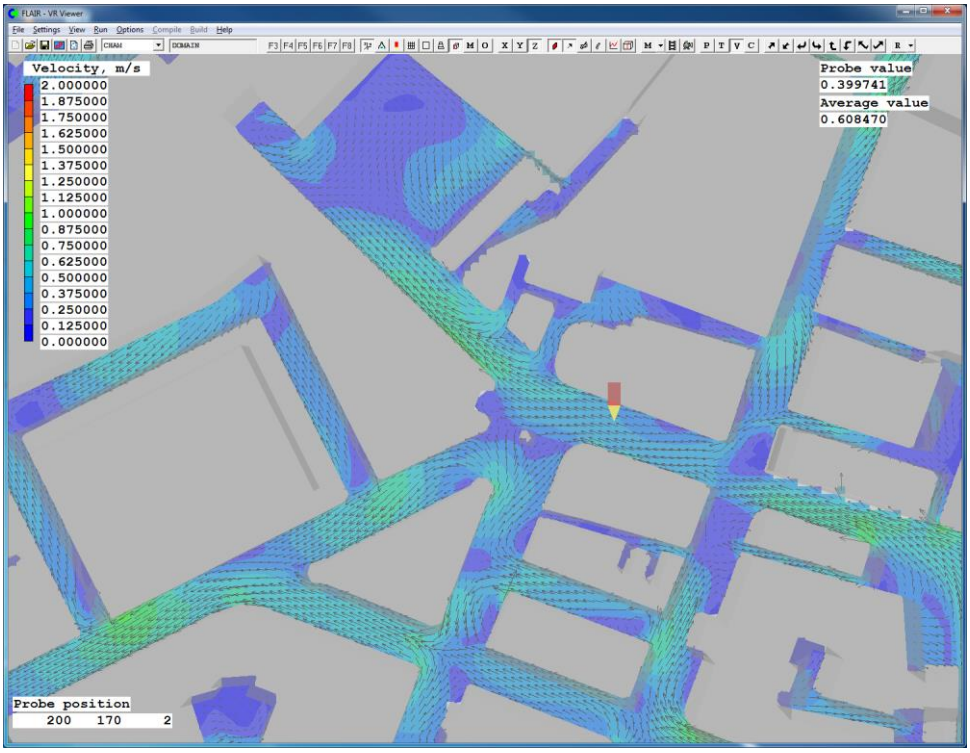

Figure 108: Probe 2 locate at Exit 1 in Blackett Street (Wind input from East, speed at 1 m/s)

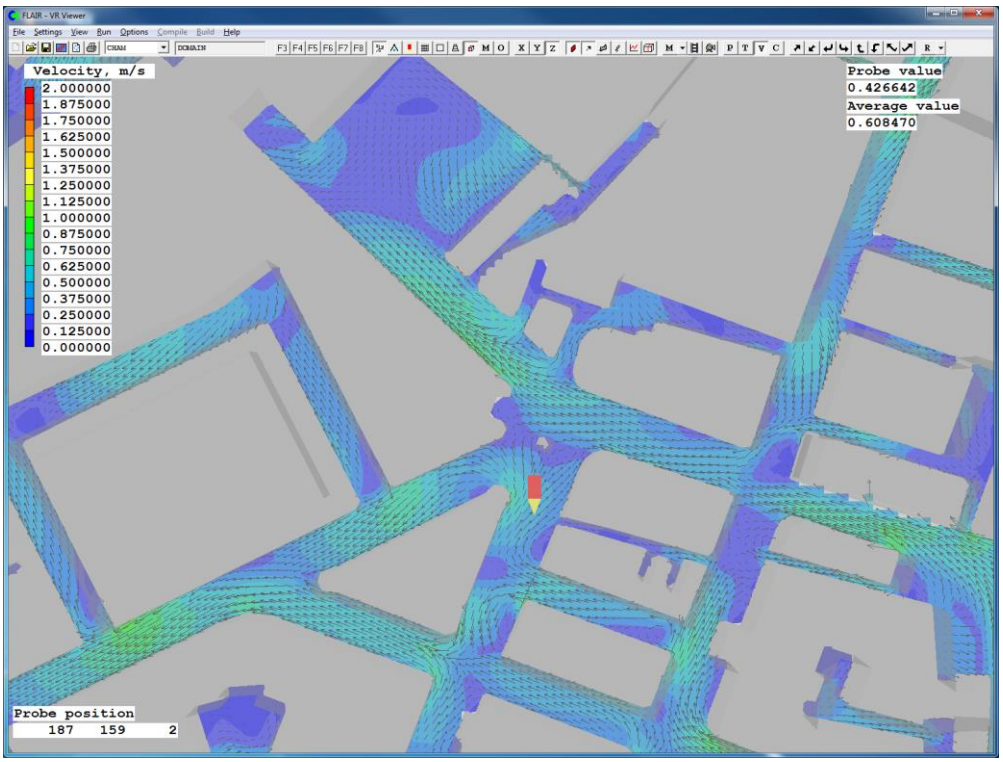

Figure 109: Probe 3 locate at Exit 2 in Grey Street (Wind input from East, speed at 1 m/s)

7.3.3 Sample result of wind direction from South speed at 1 m/s

When the main airflow was from the South a different pattern was apparent at the station as can be seen in Figure 110 and Figure 111. In this case the flow around Exit 2 was mainly from the west in Blackett Street. This would induce an outflow at the station exit. In Grey Street however the air flow was from the south following the street orientation towards Exit 2. This would create a strong inflow to the station. Figure 112 shows the probe value of three exits with weather station in all the variable wind speeds that were simulated.

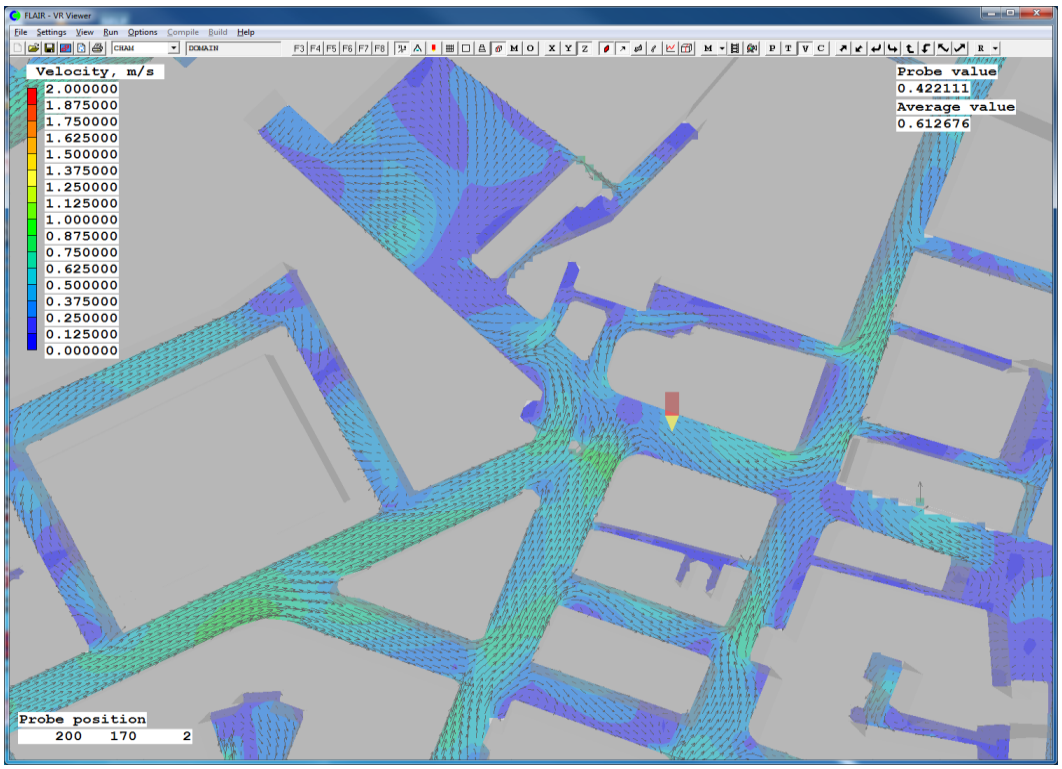

Figure 110: Probe 2 locate at Exit 1 in Blackett Street (Wind input from South, speed at 1 m/s)

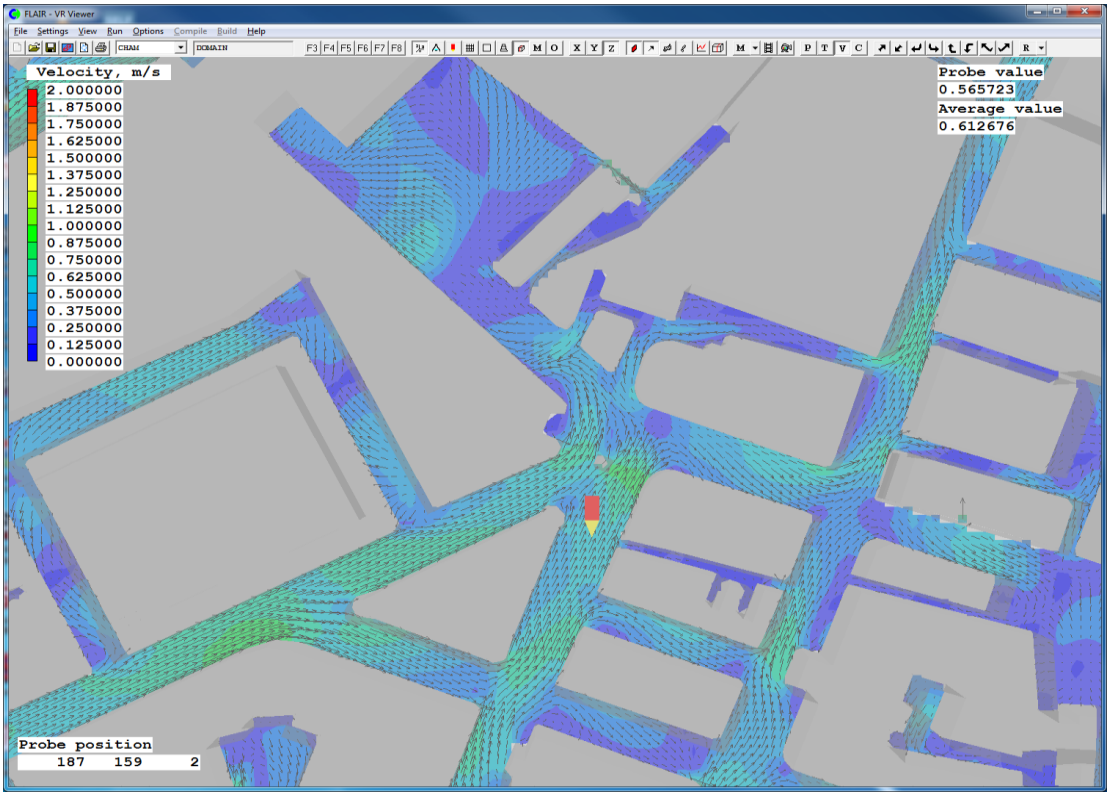

Figure 111: Probe 3 locate at Exit 2 in Grey Street (Wind input from South, speed at 1 m/s)

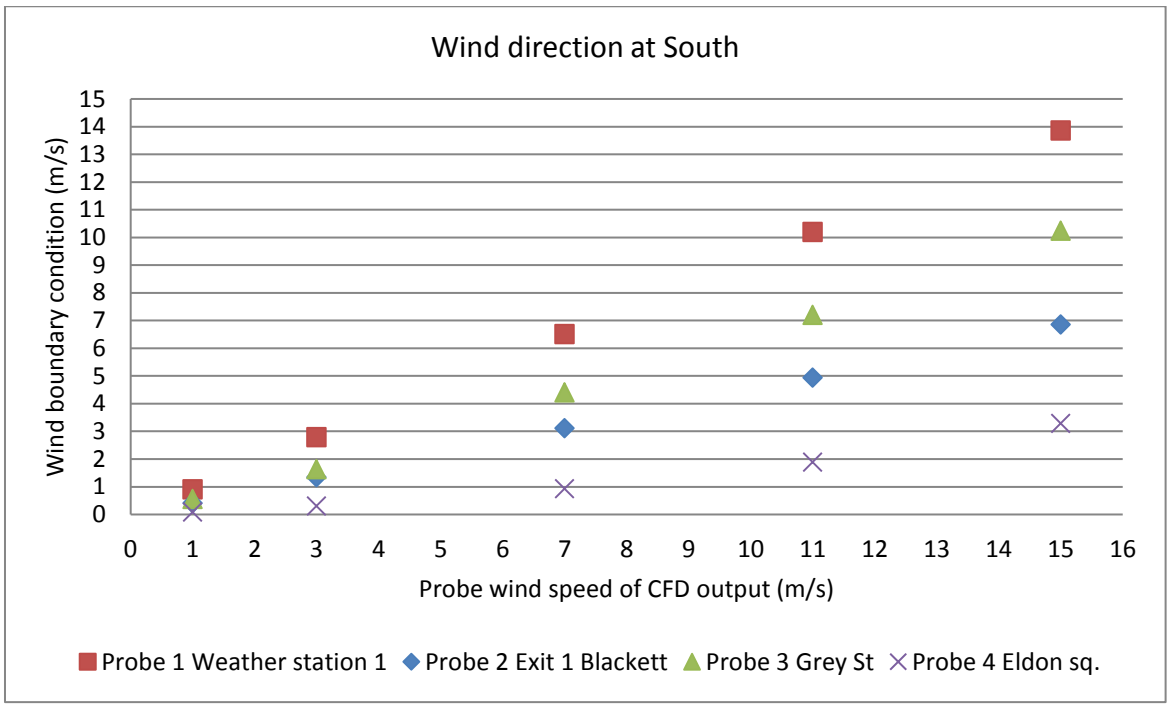

Figure 112: Probe values at weather station and exits in variable wind input speeds from South.

7.3.4 Sample result of wind direction from West speed at 1 m/s

The final sample of simulation results presented in this section is that of a west wind profile at 1m/s. This is as shown in Figure 113 and Figure 114. The main air flow pattern in Blackett Street, Exit 1, still followed the street orientation but the direction changed from west to east with a slight southerly direction affect from Grainger Street. The air flow direction outside Exit 2 was from east to west but exhibited some interference from the buildings of Grey Street and the nearby side street mentioned earlier. In this case the three exits are all in the leeward pressure region which would induce outflow.

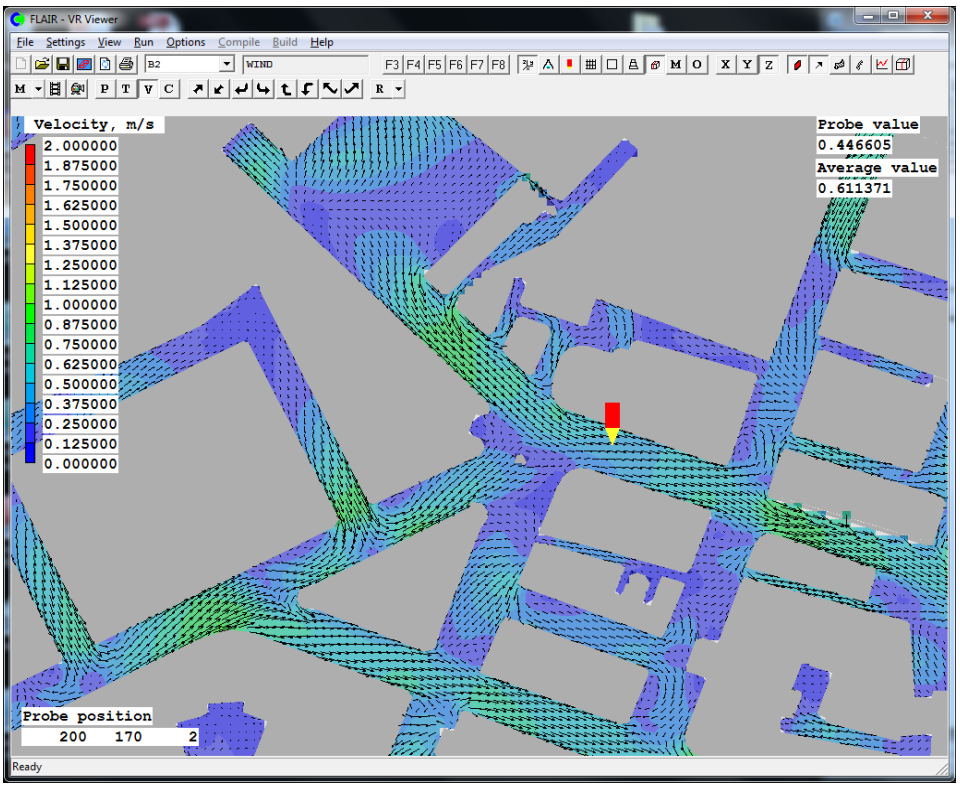

Figure 113: Probe 2 locate at Exit 1 in Blackett Street (Wind input from West, speed at 1 m/s)

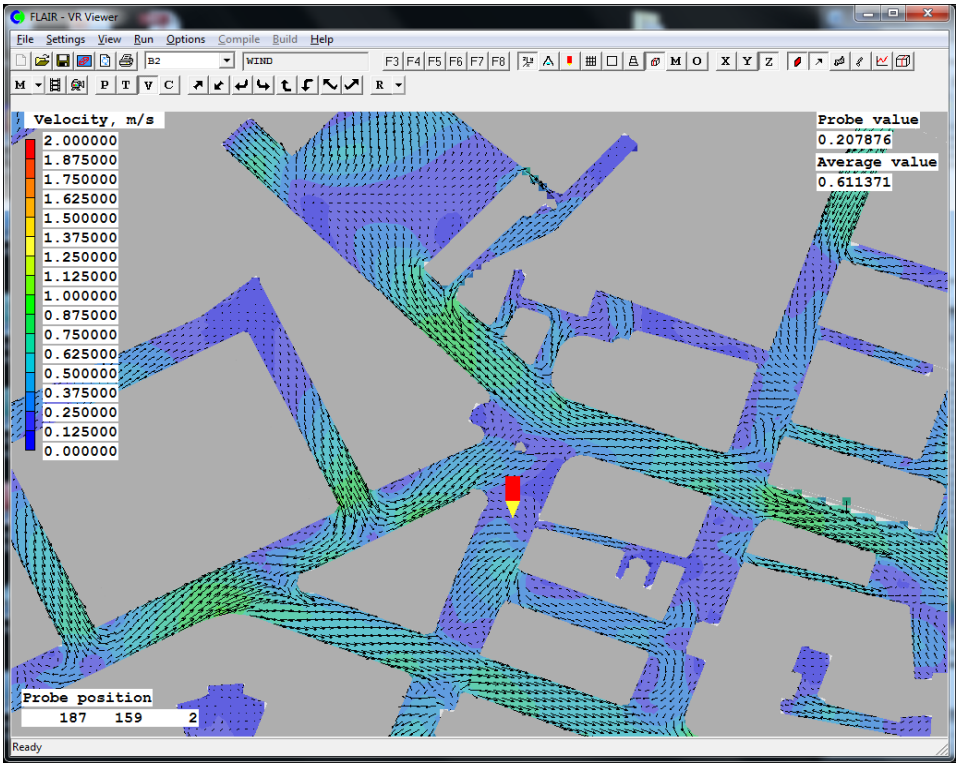

Figure 114: Probe 3 locate at Exit 2 in Grey Street (Wind input from West, speed at 1 m/s)

The outcome of the simulation of the above graphs indicating the microclimate around the Monument station exits is shown in the figures above. Although only a limited range of cases, in terms of wind profile have been described many more cases were examined. All the CFD simulation results with the specified conditions at the weather station and the resulting wind speeds and directions at the station exits are listed in Table 17. A full copy of the CFD simulation results figures can be found in Appendix B.

				Probe 1	Probe 2	Probe 3			Probe 4	
Abbreviation of wind direction	Wind direction (degree)	Phoenics input direction (degree)	Wind speed input (m/s)	Weather station 1 (m/s)	Exit 1 Blackett (m/s)	Exit 2 Direction	Exit 2 Grey St. (m/s)	Exit 3 Direction	Exit 3 Eldon sq. (m/s)	Pressure
N	0	40	2	2.03	1.03	E to W	0.9	N to S	0.62	neg.
			5	5.08	2.64		2.15		1.63	neg.
			6	6.1	3.17		2.59		1.97	neg.
			8	8.14	4.22		3.48		2.61	neg.
			10	10.17	5.23		4.36		3.24	neg.
			13	13.22	6.78		5.65		4.35	neg.
NNE	22.5	62.5	1	1	0.55	E to W	0.47	N to S	0.24	neg.
			3	3	1.54		1.38		0.76	neg.
			7	7.01	3.55		3.19		1.6	neg.
			9	9.03	4.61		4.12		1.97	neg.
			13	13.07	6.6		6.01		2.76	neg.
NE	45	85	2	1.86	0.81	E to W	1.03	N to S	0.28	neg.
			5	4.65	2.01		2.6		0.85	neg.
			8	7.44	3.3		4.17		1.35	neg.
			12	11.16	5.04		6.24		2.02	neg.
			15	13.95	6.36		7.85		2.46	neg.
ENE	67.5	107.5	3	2.68	1.22	E to W	0.68	S to N	0.46	neg.
			5	4.46	1.93		1.26		0.82	neg.
			7	6.24	2.58		1.77		1.15	neg.
			11	9.81	3.94		3.06		1.81	neg.
			13	11.59	4.72	with turbulence	3.74	with turbulence	2.18	neg.
			15	13.4	5.42	with turbulence	4.39	with turbulence	2.49	neg.

E	90	130	1	0.9	0.4	E to W	0.43	S to N	0.14	neg.
			4	3.59	1.8		1.69		0.56	neg.
			7	6.28	2.27		3.02		1.01	neg.
			10	8.95	2.88		4.41		1.49	neg.
			14	12.49	3.6		6.18		2.13	neg.
ESE	112.5	152.5	1	0.91	0.43	E to W	0.31	S to N	0.29	neg.
			2	1.81	0.79		0.61		0.53	neg.
			6	5.44	2.26		1.99		1.69	neg.
			10	9.09	3.73		3.38		2.94	neg.
			14	12.73	5.09		4.75		4.25	neg.
SE	135	175	3	2.75	1.6	E to W	0.43	N to S	0.63	neg.
			6	5.52	3.18		1.21		1.08	neg.
			9	8.28	4.76		1.77		1.59	neg.
			12	11.04	6.35		2.35		1.95	neg.
			15	13.8	7.96		3.08		2.3	neg.
SSE	157.5	197.5	2	1.71	0.97	W to E	0.77	S to N	0.36	neg.
			4	3.35	1.95		0.84		0.76	neg.
			6	4.98	2.97		1.75		1.11	neg.
			10	8.2	4.92		4.83		1.59	neg.
			14	11.25	6.77		7.73		2.19	neg.
S	180	220	1	0.91	0.42	W to E	0.57	S to N	0.1	neg.
			3	2.8	1.35		1.64		0.32	neg.
			7	6.52	3.12		4.41		0.94	neg.
			11	10.21	4.95		7.21		1.89	neg.
			15	13.87	6.87		10.25		3.3	neg.
SSW	202.5	242.5	2	1.93	0.8	W to E	1.28	S to N	0.23	neg.
			5	4.88	1.94		3.53		0.32	neg.
			8	7.78	2.92		5.82		0.82	neg.
			11	10.67	3.9		8.17		1.85	neg.

			14	13.54	5.29		10.67		2.86	neg.
SW	225	265	1	0.85	0.62	W to E	0.69	S to N	0.12	neg.
			4	3.36	2.66		2.96		0.35	neg.
			7	5.89	4.59		5.17		1.18	neg.
			10	8.45	6.96		7.32		1.71	neg.
			13	11.01	9.62		9.46		2.23	neg.
WSW	247.5	287.5	2	1.08	1.11	W to E	0.59	N to S	0.15	neg.
			4	2.32	2.15		1.17		0.22	neg.
			6	3.57	3.21		1.86		0.34	neg.
			10	5.84	5.3		3.55		0.53	neg.
			14	8.13	7.45		4.94		0.75	neg.
W	270	310	1	0.75	0.45	W to E	0.21	E to W	0.1	neg.
			5	3.67	1.95		1.65		0.36	neg.
			9	6.91	3.62		3.06		0.62	neg.
			13	10.04	5.56		4.53		0.94	neg.
			15	11.57	6.45		5.34		1.11	neg.
WNW	292.5	332.5	1	0.86	0.38	W to E	0.49	N to S	0.15	neg.
			4	3.39	1.39		2.03		0.38	neg.
			7	5.89	2.37		3.46		0.6	neg.
			10	8.39	3.3		4.81		0.89	neg.
			13	10.87	4.28		6.21		1.2	neg.
NW	315	355	2	0.98	0.84	W to E	1.15	N to S	0.25	neg.
			5	2.15	2.08		2.86		0.51	neg.
			8	3.49	3.38		4.61		0.85	neg.
			11	4.9	4.68		6.3		1.36	neg.
			14	6.32	5.99		7.99		2.22	neg.
NNW	337.5	377.5	2	1.87	0.56	W to E	1.26	N to S	0.47	neg.
			5	4.7	1.95		3.3		1.08	neg.
			8	7.52	3.28		5.43		1.72	neg.

	11	10.34	4.55	7.63	2.32	neg.
	14	13.15	5.23	9.67	2.91	neg.

Table 17: List of Microclimate CFD simulation results at weather station and three exits of Monument station with variable wind profile inputs

The results shown in Table 17 produced from the microclimate modelling of the city centre around the Monument station were then used to produce a correlation between the weather station data and the condition at the three station exits. The result of this exercise is shown in Figure 115 and Figure 116, Figure 117, Figure 118 are comparisons with measurement data. In these graphs the velocity at the weather station is represented by the x axis. The y axis represents the value of the velocity at exit of the station. Figure 115 is shows the wind speed at three exits correlate to same weather station speed in the same wind direction. In Figure 115 the points are the simulated value and the continuous lines are the velocity values predicted by PHOENICS at the particular station exit point. In Figure 116, Figure 117 and Figure 118 are comparisons of simulated and measured value at three exit in similar weather condition. The red triangles represent the measured wind speed and circle points represent the same velocity as determined from the CFD which shown in the Figure 115 (simulated data). Going further to examine the measured and simulated values at Exit 1 and Exit 2, it can be seen that the measured data (red triangles) exhibits a large degree of scatter and that the values are higher than those predicted by PHOENICS but the values are similar. It would be expected that measured air flow would show a large degree of scatter because of the unsteady nature of natural air flow that can be considered to be a bulk flow with turbulent eddies superimposed. At Exit 3 the measured value are close or smaller than the simulated values, as this exit is inside the Eldon square entrance it is possible that the flow would be less turbulent than that in the open street.

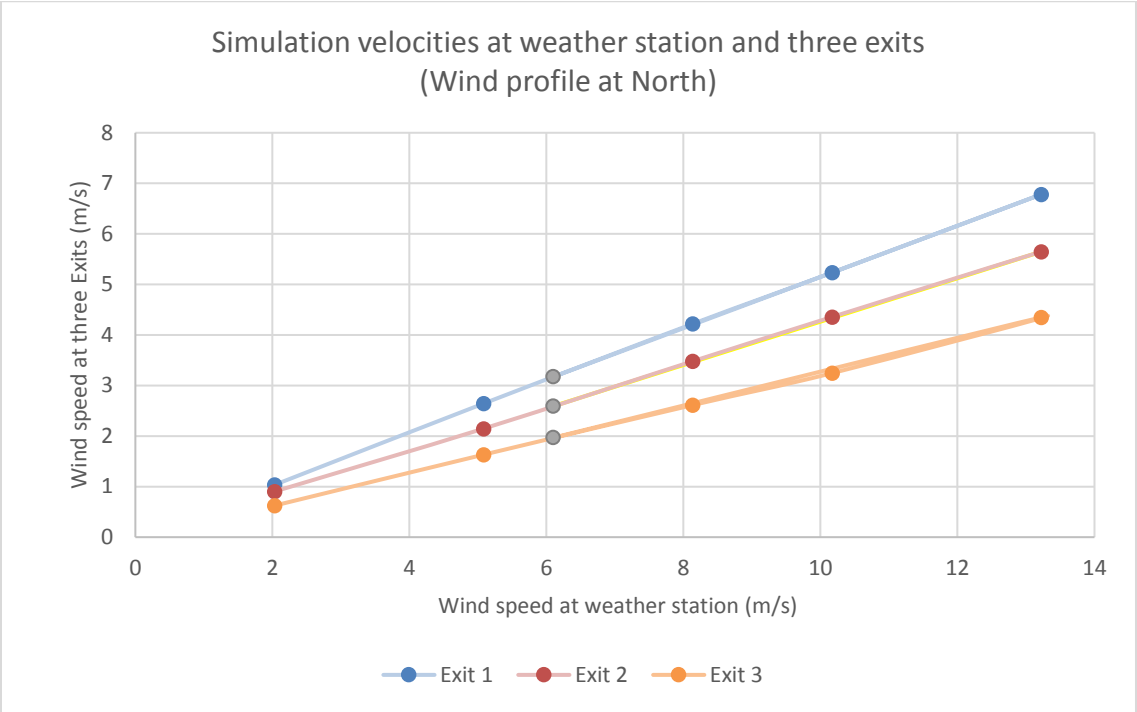

Figure 115: Predicted wind speed based on the simulation input and results at four Probe location

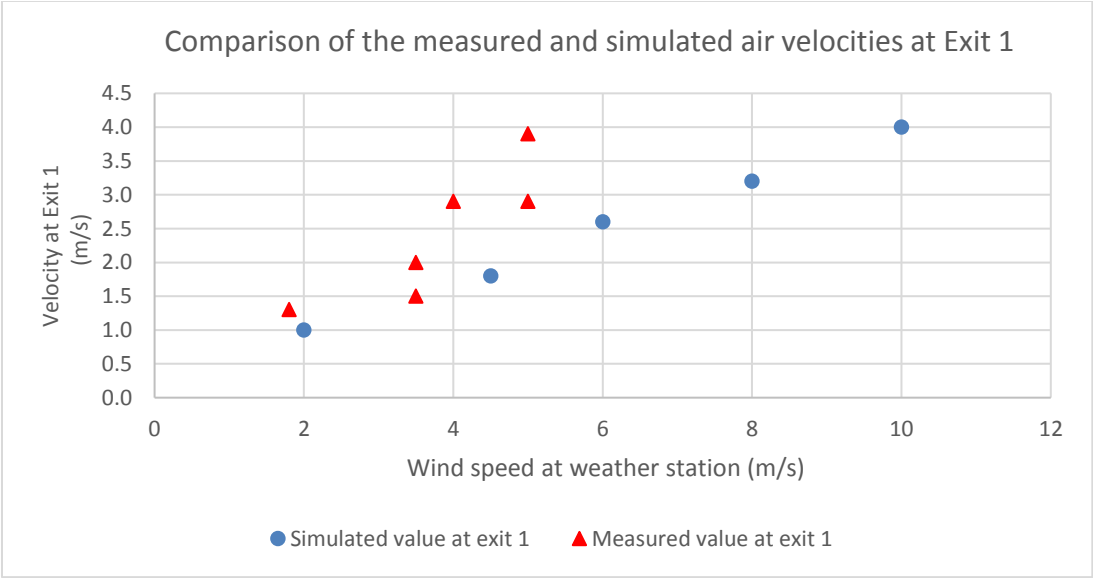

Figure 116: Sample of compare the simulation and measured air flow at Exit 1

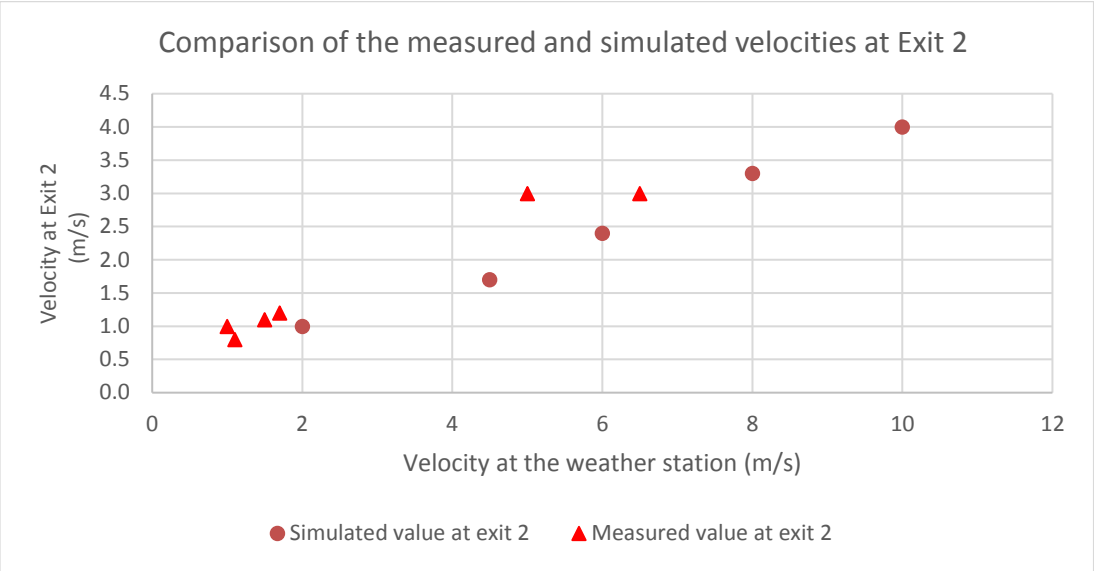

Figure 117: Sample of compare the simulation and measured air flow at Exit 2

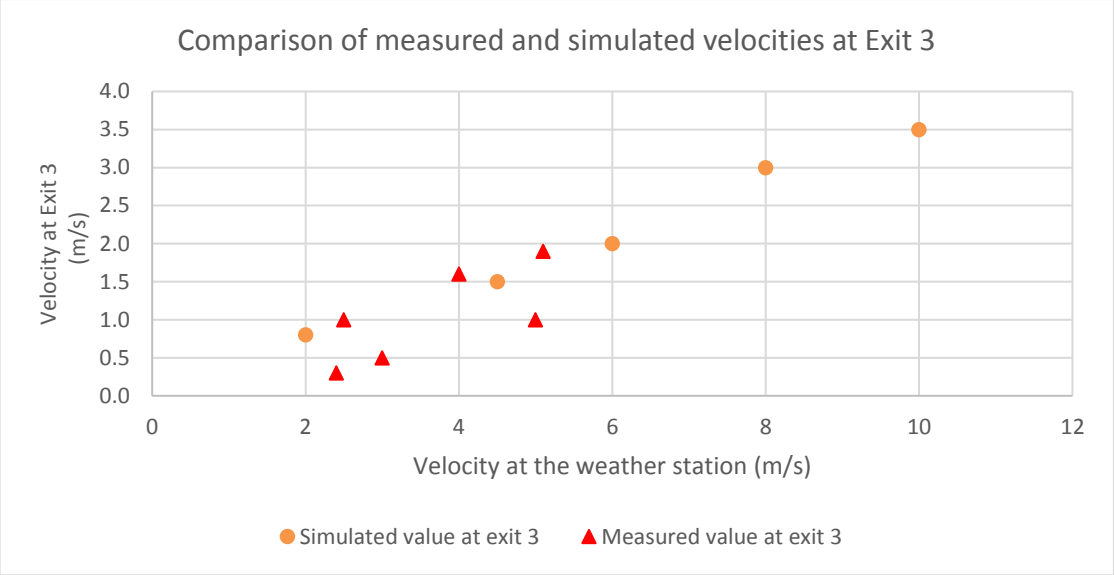

Figure 118: Sample of compare the simulation and measured air flow at Exit 3

7.4 Conclusion of microclimate modelling

This part of the simulation work has indicated that the microclimate simulation is able to reproduce the general air flow situation at the exits of Monument station. The simulated and predicted values of the velocities at the different station exits are very close considering the scatter of the measured data and the uncertainty in the measurements. What is more important however, is that the simulation is able to predict with some confidence the direction of the airflow as this, rather than the absolute magnitude of the air velocity will have the greatest impact on the air flow in

the station. What cannot be neglected however, as has been discussed in Chapter 5 is the impact the train movement and the resulting air movement in the station has on the air flow at the station exits. The next step in this study is to consider the full CFD modelling of the station taking into account the local microclimate and the internal airflow.

Chapter 8. Station CFD Modelling

8.1 Introduction

Microclimate CFD modelling was used to examine the characteristics of wind direction and speed outside the station and the impact variations in these parameters had on the station internal air flow and that through the station exits. These results provided boundary conditions at the three station exits under different weather condition for the station air flow CFD modelling as shown in the research method flow chart in Figure 11 (Chapter 3). This chapter describes the CFD simulation of the station interior using the commercial CFD package ANSYS 16.1. It begins with a discussion of the mesh generating procedure and explains how the model was assembled from different parts. It was necessary to divide the model into different parts to reduce the size and complexity of each model. A number of simplifications, to improve the meshing quality were made to the 3D station model that was modelled from the point cloud data obtained from the laser scanning. The final section demonstrates the detailed procedure used to develop a CFD model using measurement data, evaluating the simulation result and validating the model by the measured data.

8.2 Model development

In developing the CFD model, a mesh was made using the meshing software ANSYS ICEM to produce a suitable mesh model for use with Fluent Work Bench, the CFD solver. ANSYS ICEM (2013) CFD meshing software contains advanced CAD/geometry readers and repair tools to examine complex models to assist in producing a good quality model. It can produce a variety of geometry-tolerant meshes and produce high-quality volume or surface meshes with advanced mesh diagnostics, interactive and automated mesh editing. These can be used in a wide variety of computational fluid dynamics (CFD) and finite element analysis (FEA) solvers and multi-physics post-processing tools.

The polygon station model developed from the point cloud data of the laser scanning was the starting point of the mesh generation. This was exported from 3ds max as an SAT. format and then imported to ANSYS ICEM CFD16.1 for the mesh creation. Figure 119 to Figure 120 illustrate the polygon model of the whole station it shows that the whole area can be meshed but the complexity and level of detail of the model was so extensive that the meshing quality was significantly affected which would have resulted

in a poor CFD model. To overcome this problem, the station was divided into three parts. The first represented the lower tunnel, which is the NS tunnel and platform 1 and 2 with the escalator well to the station concourse area and the stairs linking the NS tunnel with the EW tunnel shown in Figure 121, Figure 122 and Figure 123.

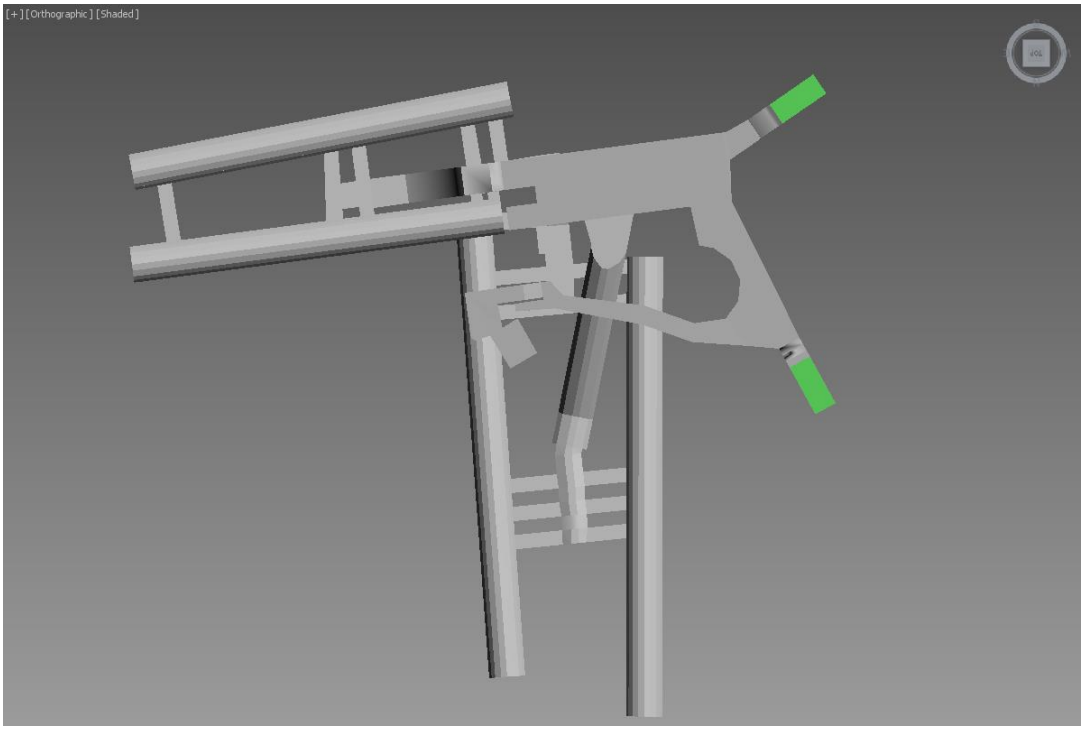

Figure 119: Polygon model of the whole station (plan elevation)

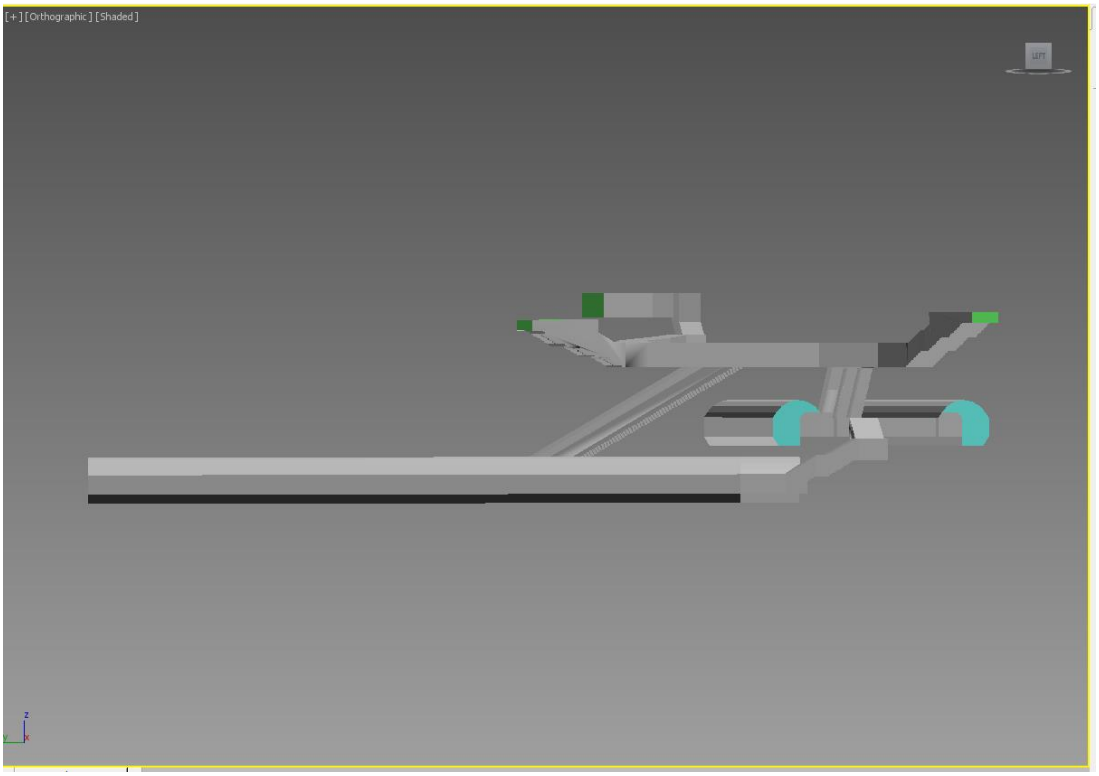

Figure 120: Polygon model of the whole station (side elevation)

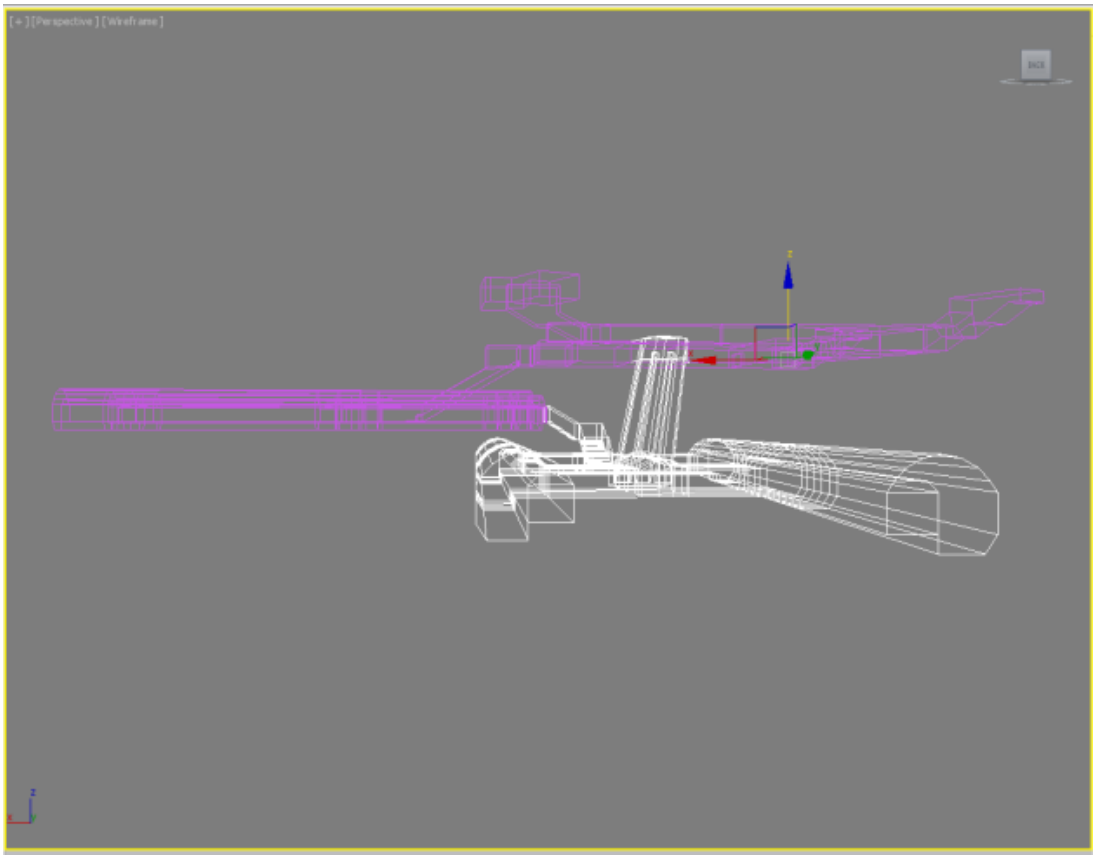

Figure 121: Polygon frame model of the whole station highlight (white) NS tunnel (side elevation)

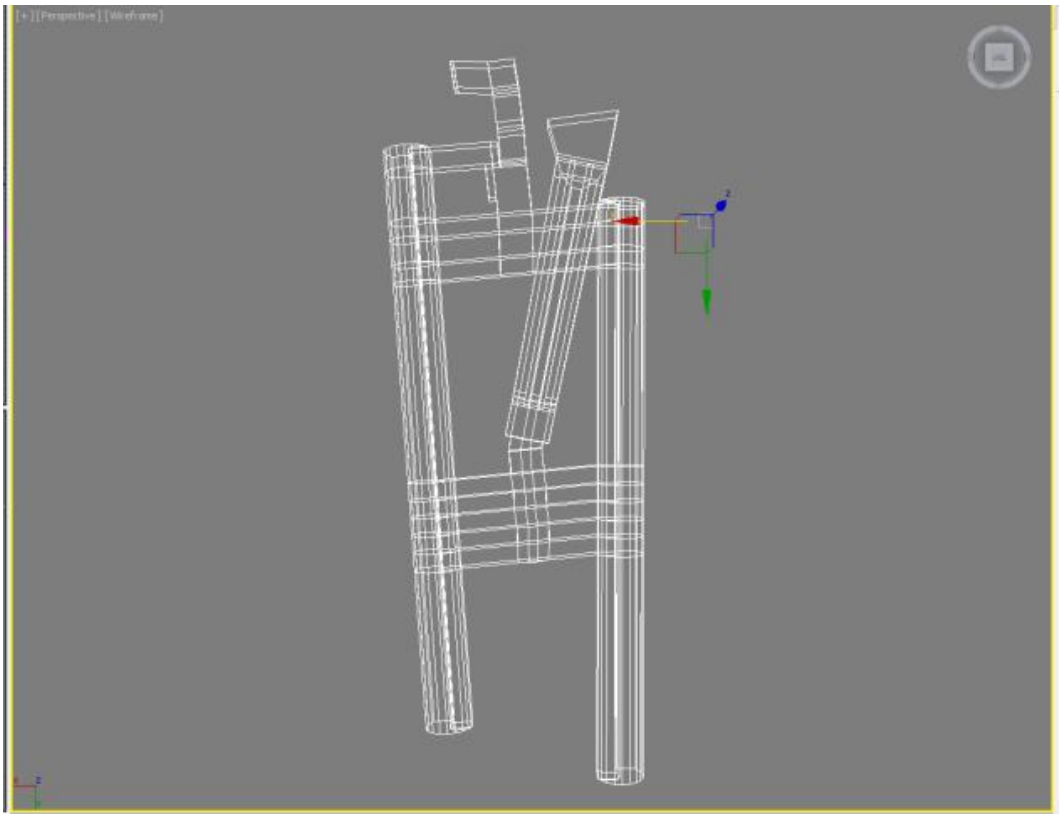

Figure 122: Figure frame Polygon model of NS tunnel (plan elevation)

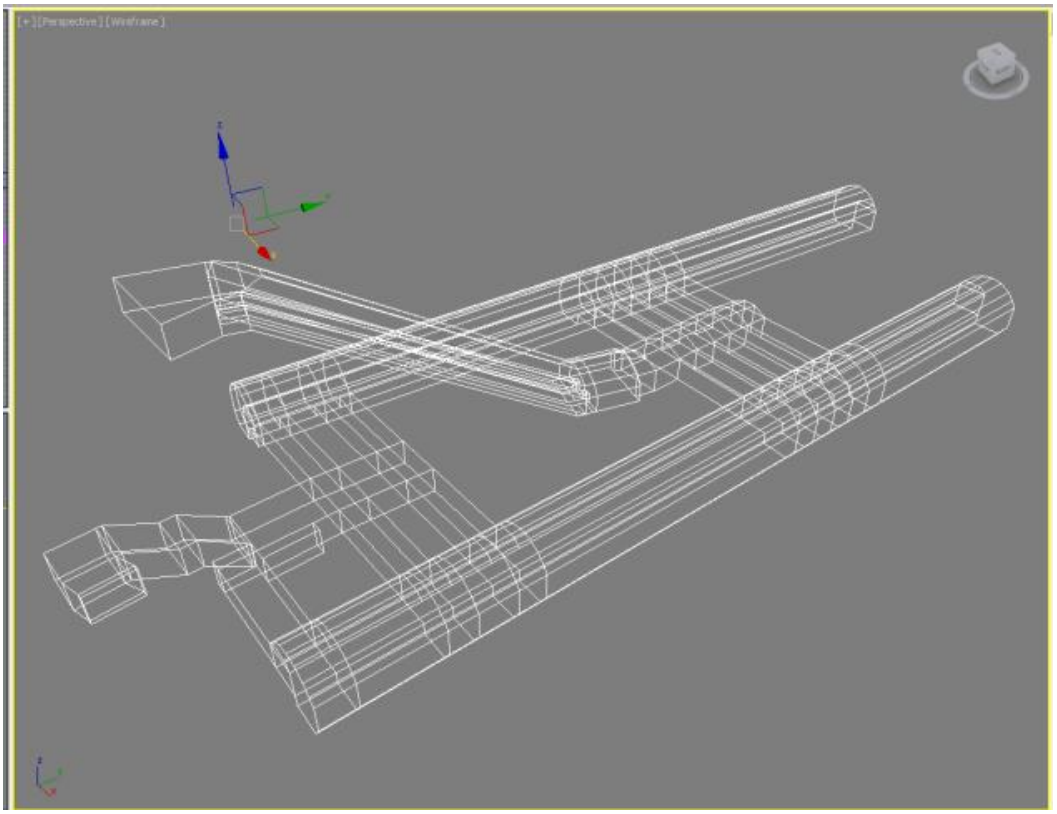

Figure 123: Polygon frame model of the NS tunnel

The second part of the divided model is the East-West (EW) tunnel that contains platform 3 and 4 with the escalator well connecting to the concourse level and the stair linking to the NS tunnel as shown in Figure 124, Figure 125 and Figure 126.

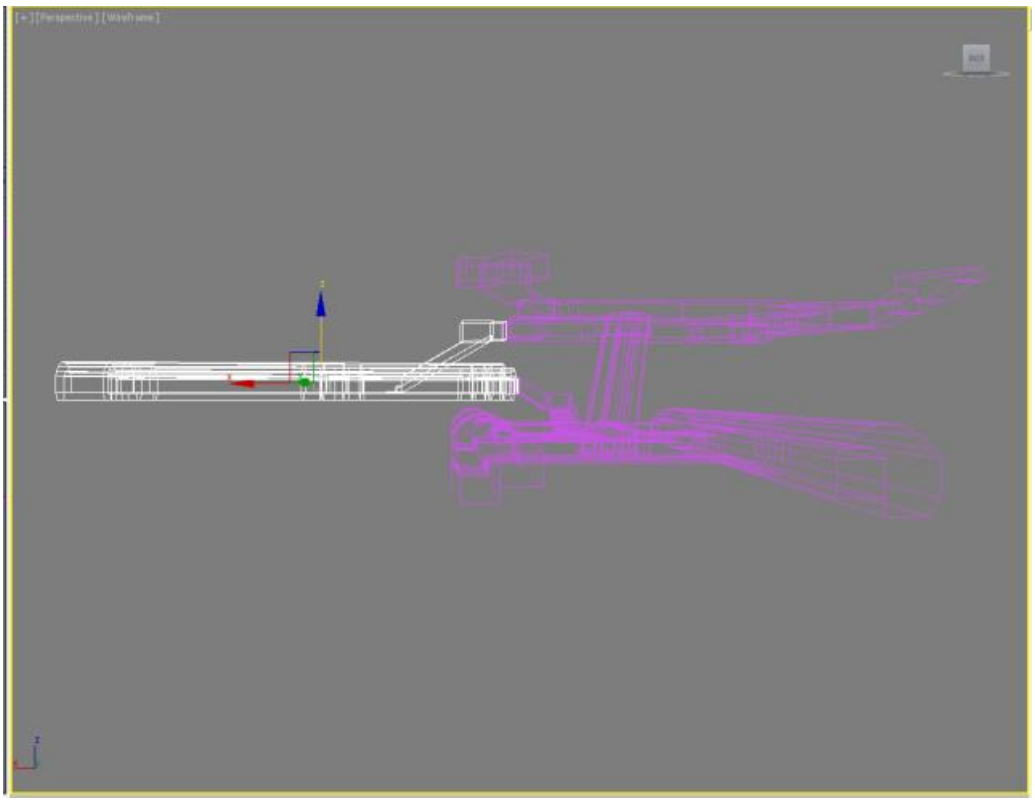

Figure 124: Polygon frame model of the whole station highlight (white) EW tunnel (side elevation)

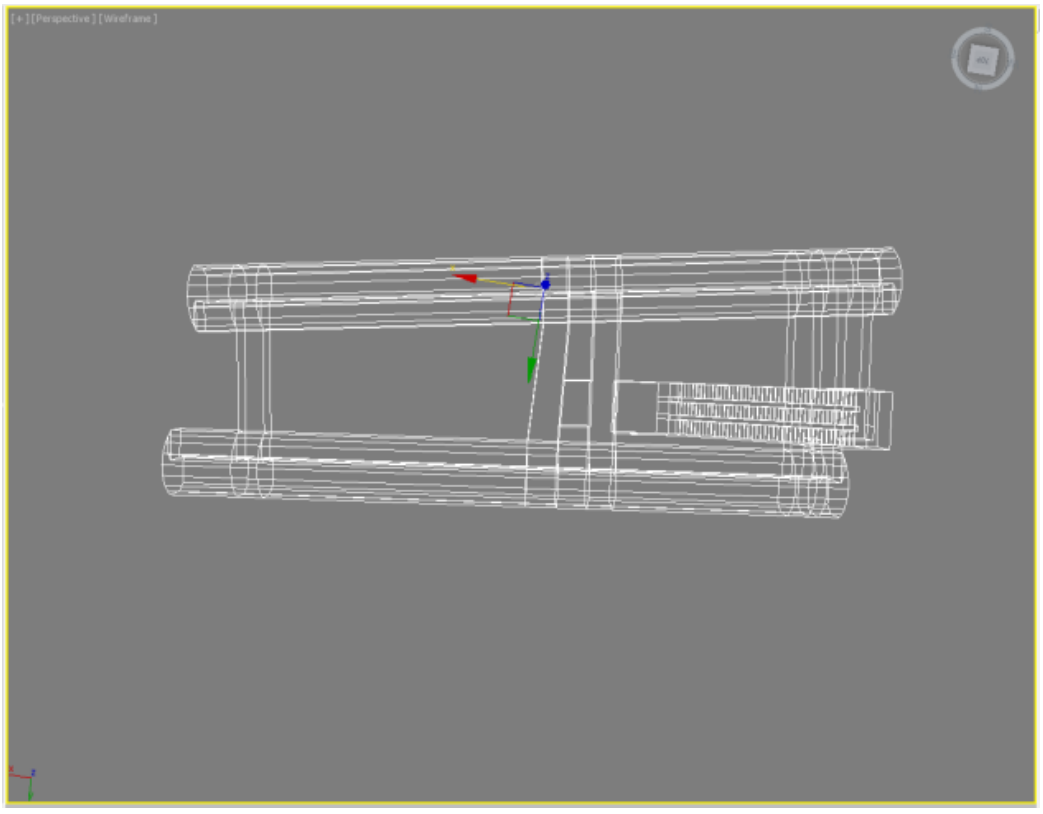

Figure 125: Polygon frame Model of the East-West platforms (plan elevation)

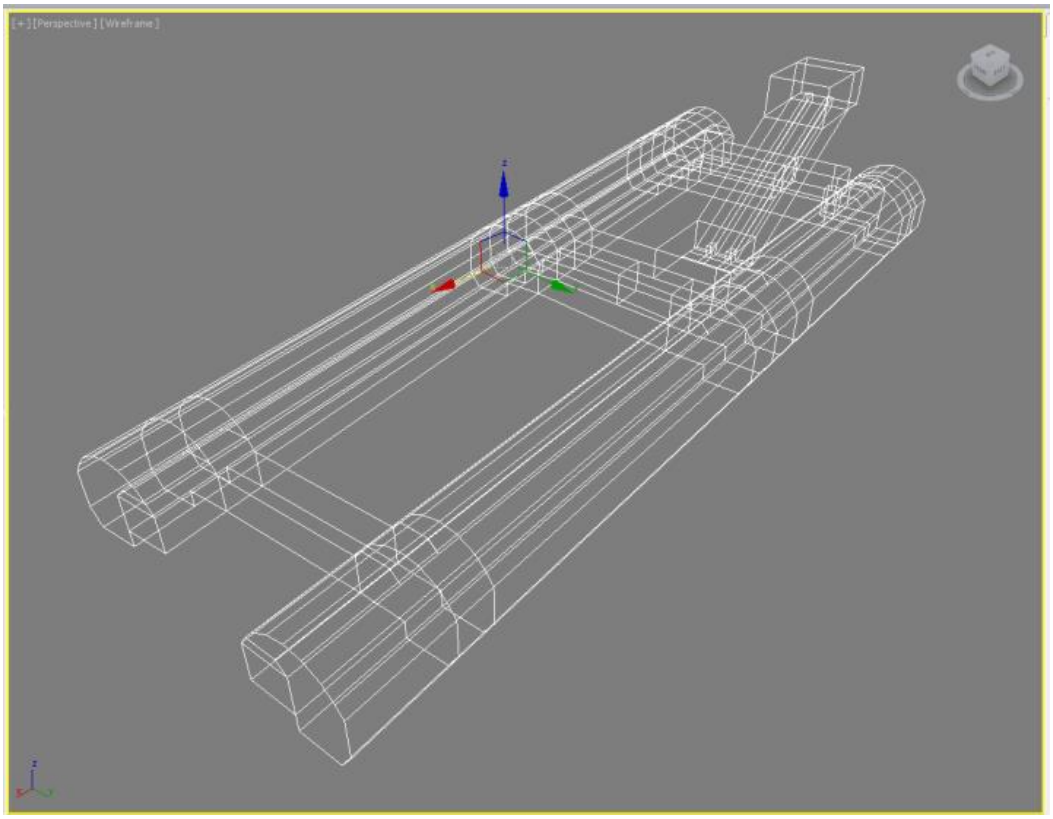

Figure 126: Polygon frame Model of the East-West platforms

The third part of the model is the concourse level with the three exits connecting to the external environment as shown in Figure 127 and Figure 128. The three exits at street level are higher than the concourse area. Two boundaries are the top of the escalators which connect the concourse with the NS and EW tunnels.

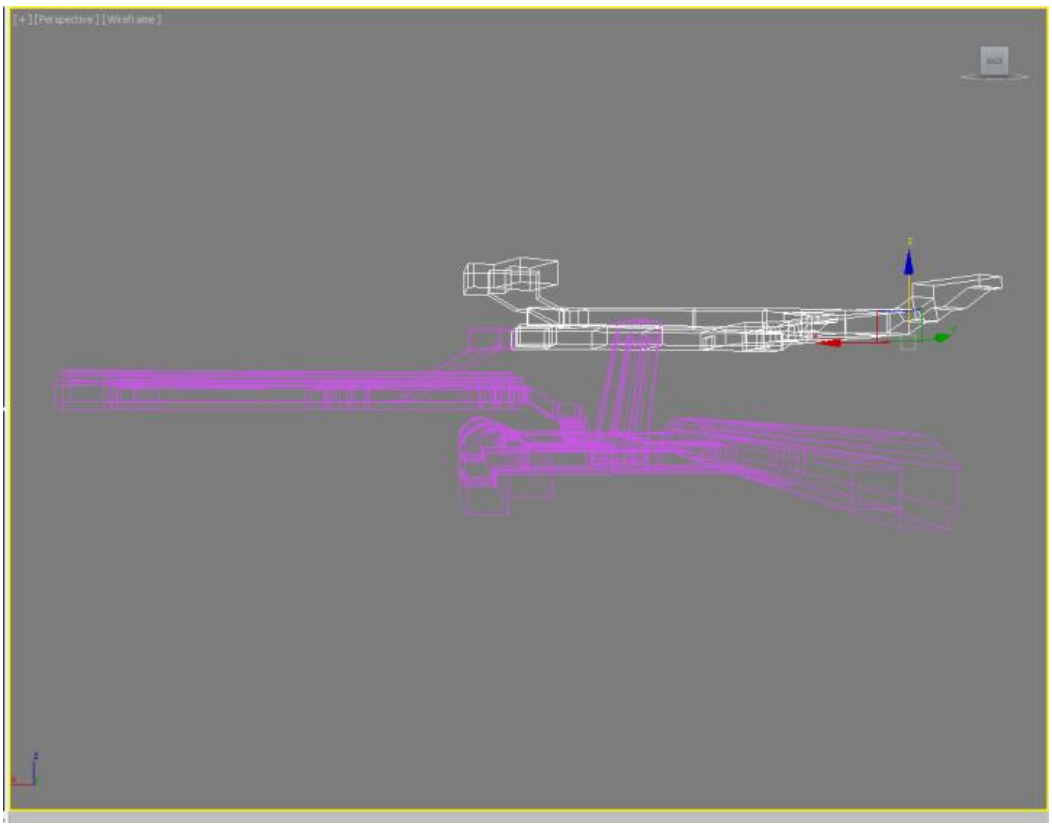

Figure 127: Polygon frame model of the whole station highlight (white) concourse level

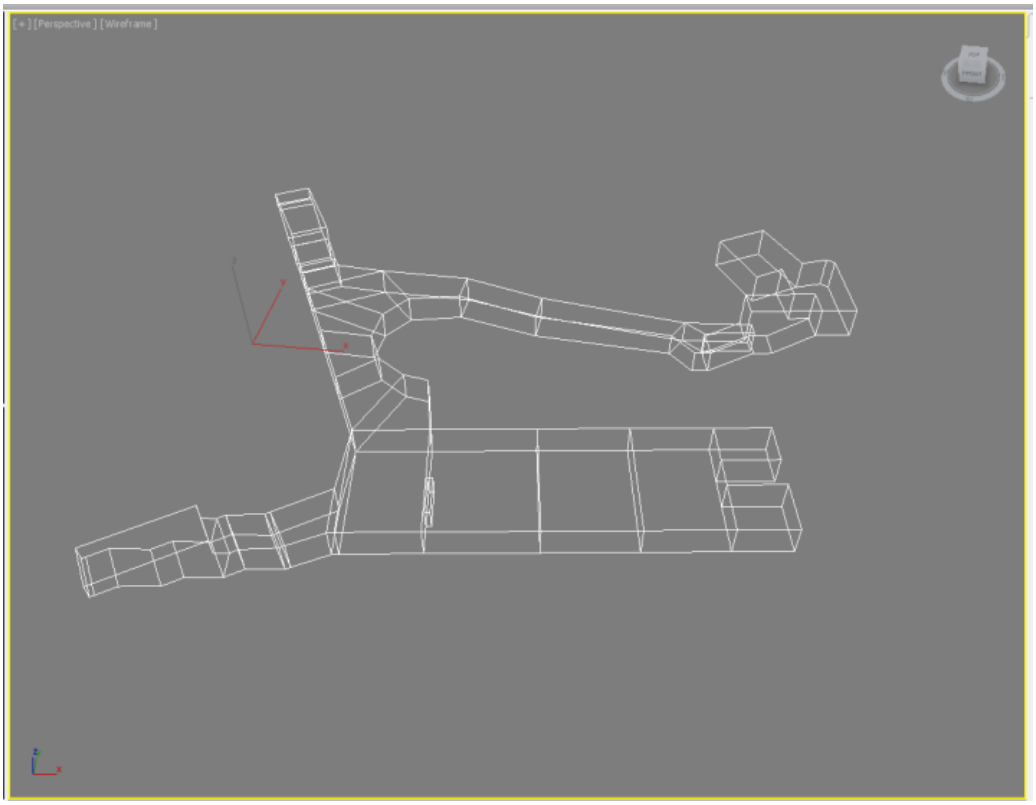

Figure 128: Polygon frame model of the concourse level

8.2.1 Meshing method

A 3D solid mesh has been used in this model, which is generally used for fluid dynamic problems. Different 3D solid mesh types can be used including Tetra (tetrahedron), Pyramid, Penta (prism) and Hexa (hexahedron) as shown in Figure 129.

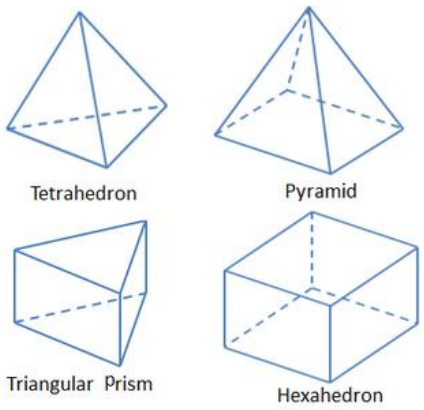

Figure 129: The three-dimensional mesh shapes

In 3D fluid modelling the tetra and hexa meshes are widely used for large size and low speed fluid cases (Gosman, 1999; Pain *et al.,* 2001). The tetra and hexa mesh produces a high degree of accuracy compared to other mesh arrangements for the same number of cells and also produces a better resolution control of the surface contours and the boundaries (Pain *et al.,* 2001; ANSYS ICEM, 2013). The triangular and tetrahedral edge elements have the advantage of being able to model very complex geometries, the tetrahedral edge elements actually produced more accurate solutions than the hexahedral edge elements (Chatterjee *et al.,* 1992). In other words, to solve same case, it can be use a much larger mesh size for the tetrahedral edge elements than the hexahedral edge elements to achieve the same accuracy and it also reduce the number of element/cell at same time. Wu and Lee (1997) also point out, because of the low phase error of the tetrahedral edge elements, it is now possible to use a coarser mesh for tetrahedral edge elements than for other elements as the numerical dispersion error is the dominant factor determining the mesh discretisation. This is especially superior in solve problems involving electrically large structures or low loss cavities. Figure 130 shows the hexa mesh generated to represent the platform level of the station and Figure 131 shows the quality of the mesh which for CFD simulation should generally be higher than 0.3 for good convergence and minimum error. The numbers at the bottom right in Figure 131 represent the mesh size in the mesh model. The ICEM mesh generator repaired, smoothed and fixed unexpected

surface and mesh irregularities. The faulty meshes are highlighted in orange in figure 8.3, they occur at the corner or curved edge of the tunnel. This part of the mesh has a quality lower than 0.3, which is not acceptable although the majority of the mesh had a quality of the order of 0.5.

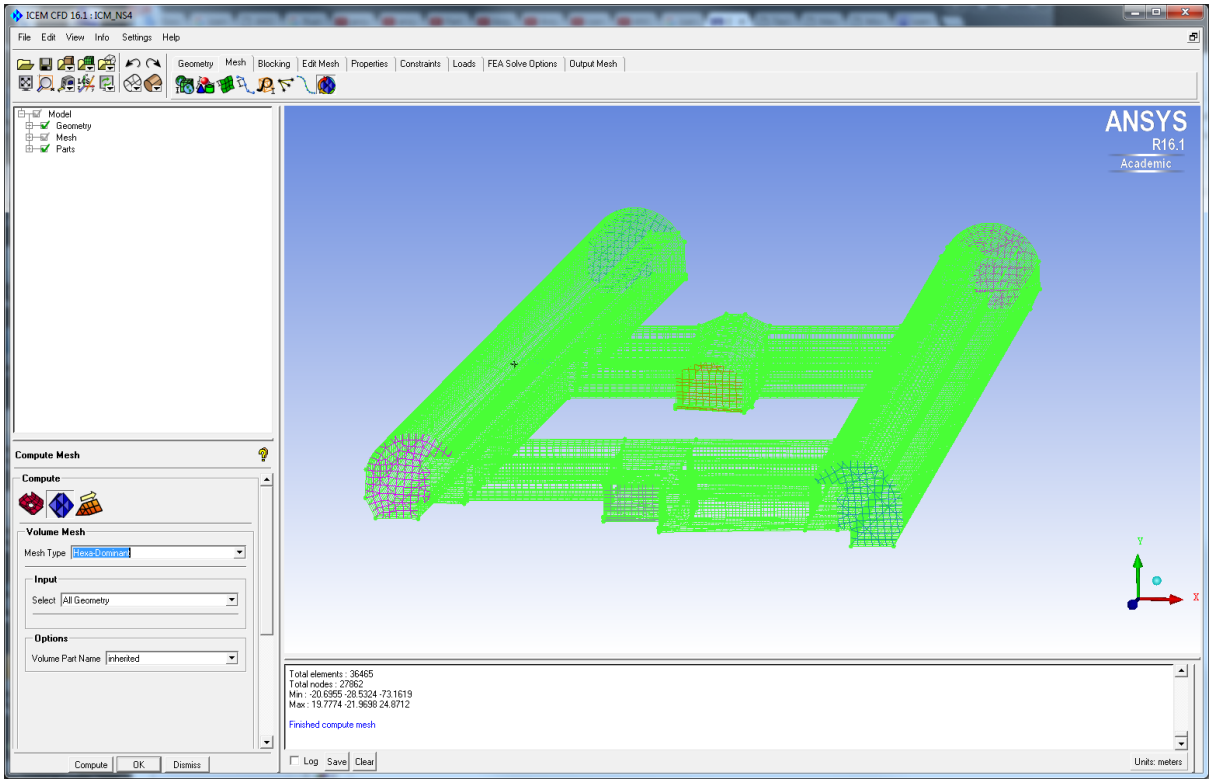

Figure 130: Sample of hexahedron mesh of tunnel and junction area

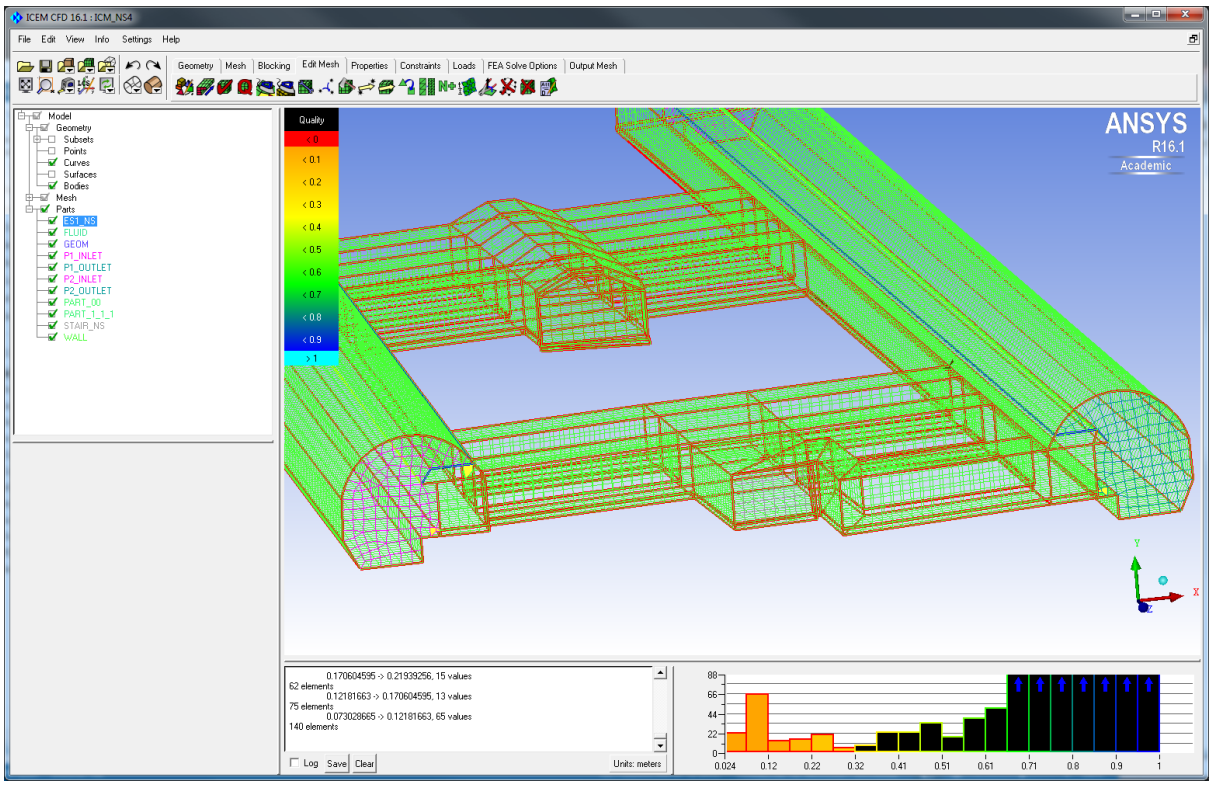

Figure 131: Mesh quality diagnostics for hexahedron mesh of tunnel and junction area

In order to achieve a higher mesh quality a tetra mesh was considered. This is another widely used mesh type which is more suitable for complex geometries and for which the edges of a tetrahedron are better matched to prescribed points and curves. Tetra mesh can be merged into another tetra, hexa or hybrid mesh and then can be smoothed to improve the overall mesh quality. As can be seen in Figure 132, Figure 133 and Figure 134 the good mesh quality has achieved with a tetra mesh. The irregular boundary surface of the escalator in Figure 132 and tunnel boundary in Figure 133 are all showing even distribution and good quality meshes.

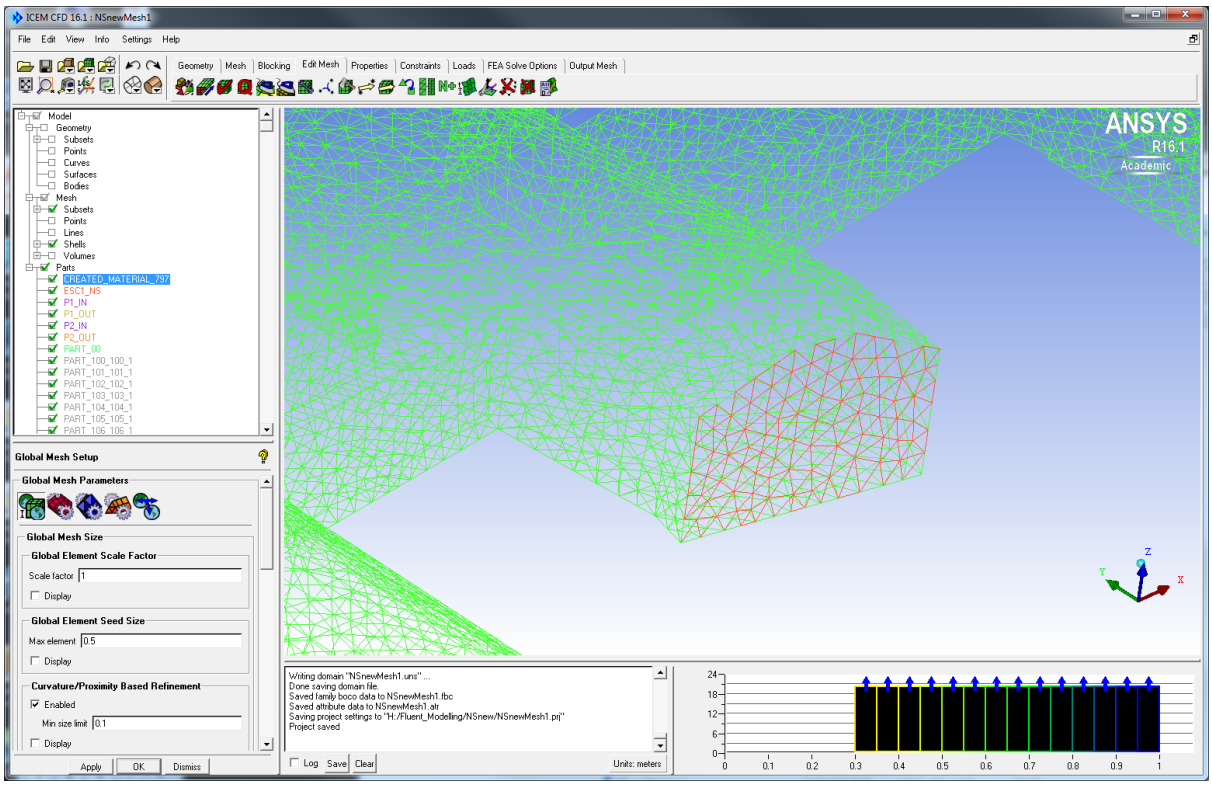

Figure 132: Mesh quality diagnostics for tetrahedron mesh of tunnel and junction area (escalator boundary)

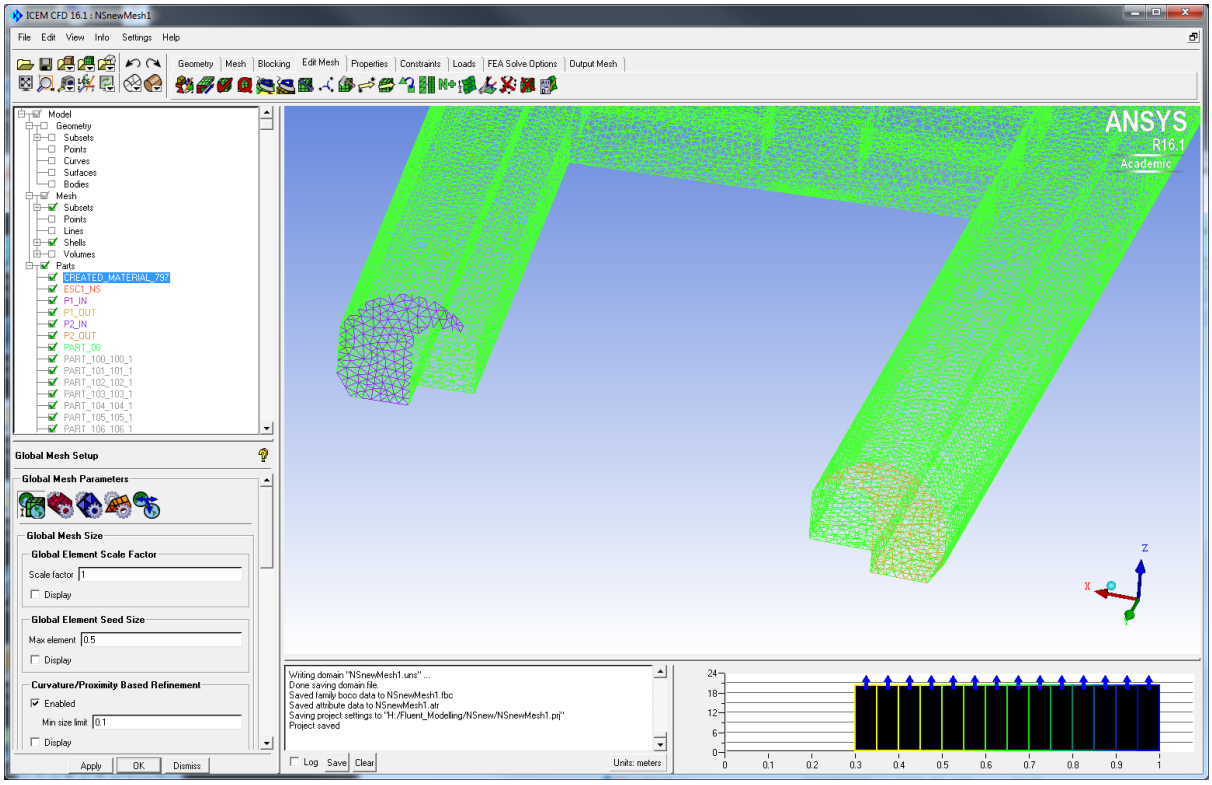

Figure 133: Mesh quality diagnostics for tetrahedron mesh of tunnel and junction area (tunnel boundary)

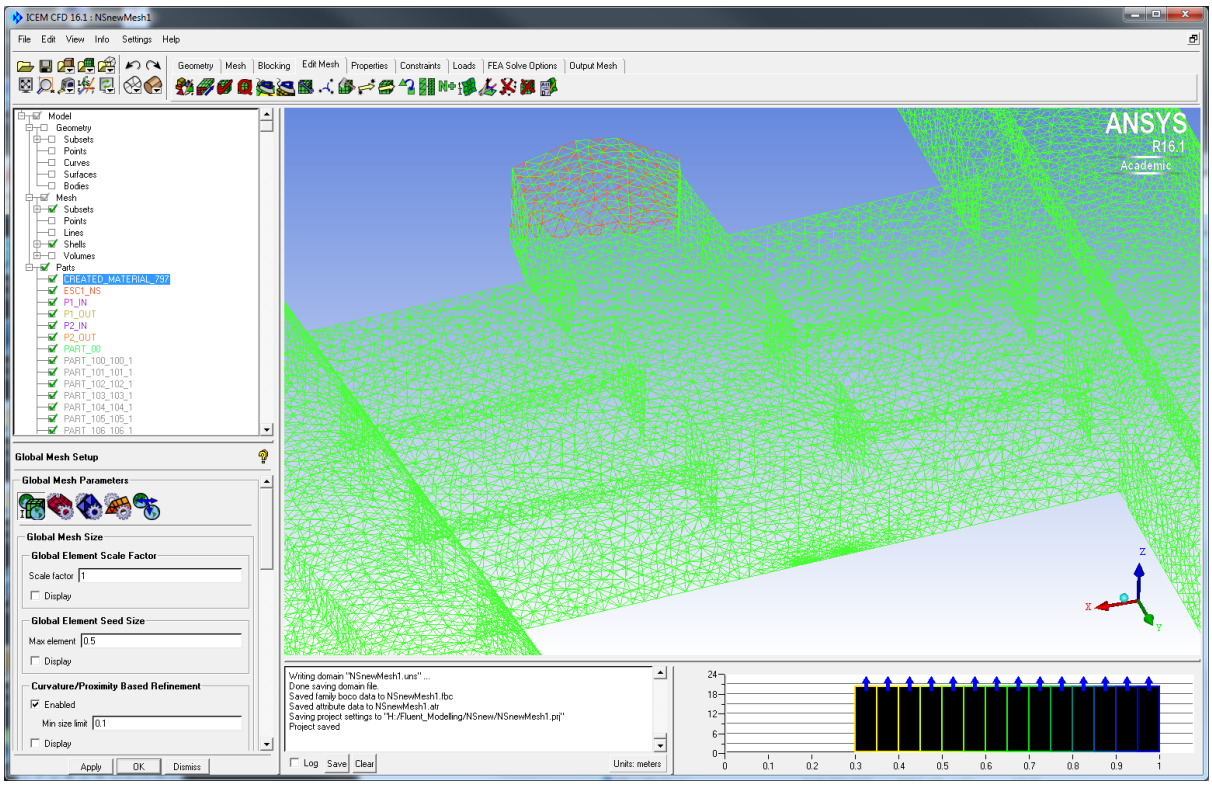

Figure 134: Mesh quality diagnostics for tetrahedron mesh of tunnel and junction area

8.2.2 Simplified model to improve meshing

Generating the mesh proved to be somewhat problematic, this was thought to be due to the size of the model and the presence of very fine details transferred to the mesh generator from the point cloud data that were not necessary for the CFD model. Such details included edges of advertising hoardings on the walls, skirting boards and the footfalls in the staircase and escalators. These fine details resulted in a large variation of the mesh size and a large number of elements resulting in poor mesh quality and large computational errors. Steps were then taken to remove some detail from the model in such a way that the overall accuracy was not compromised. This is illustrated by considering the stairs and the escalators. The staircase was modelled separately in two different ways. In the first the full detail of the steps was included in the model. The mesh was characterised by choosing the maximum and minimum liner scales to be 0.5m and 0.3m respectively. The air inlet velocity was 1 m/s. The model extended only from the bottom to the top of the stairs. This is shown in Figure 135. In the second model, the stair was modelled as a plane slope that allowed a mesh with the same mesh size to be used, as shown in Figure 136. A comparison of the output of these models have shown in Figure 137 to Figure 143, the left figure shows the result of the complete stair with full detail of the steps and the right shows the simplified stair model.

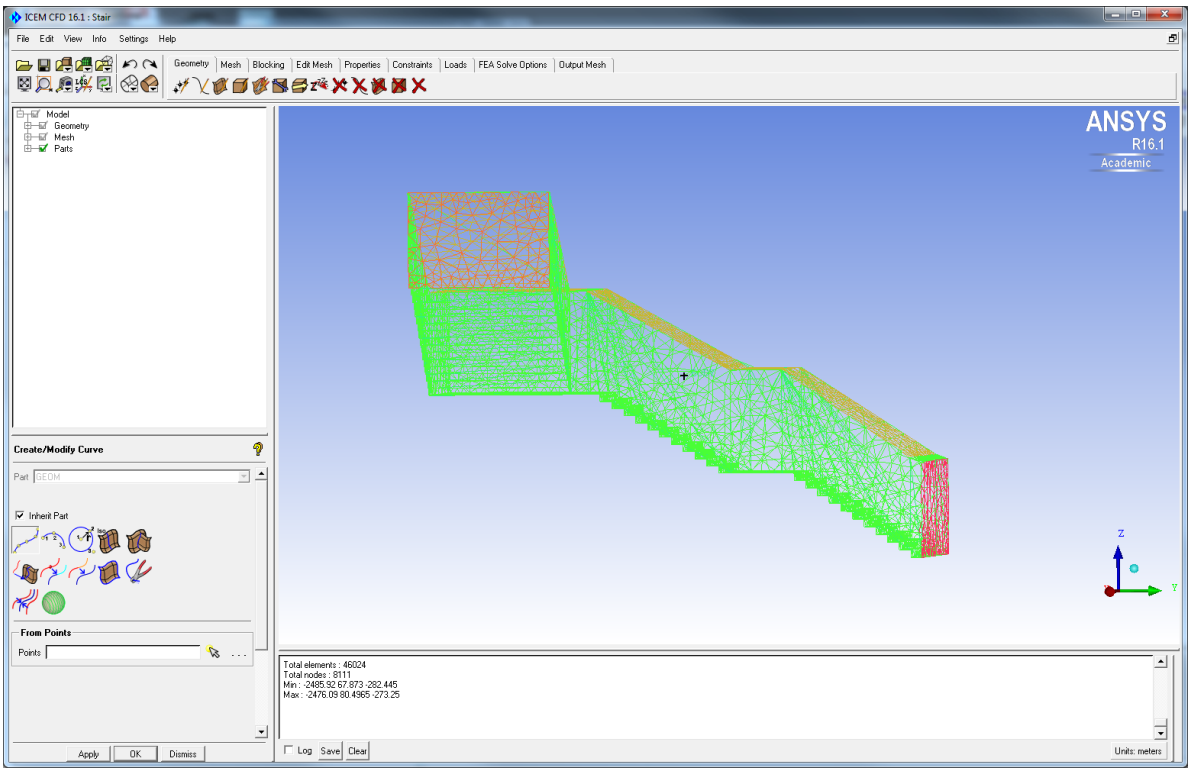

Figure 135: Mesh model of stairs

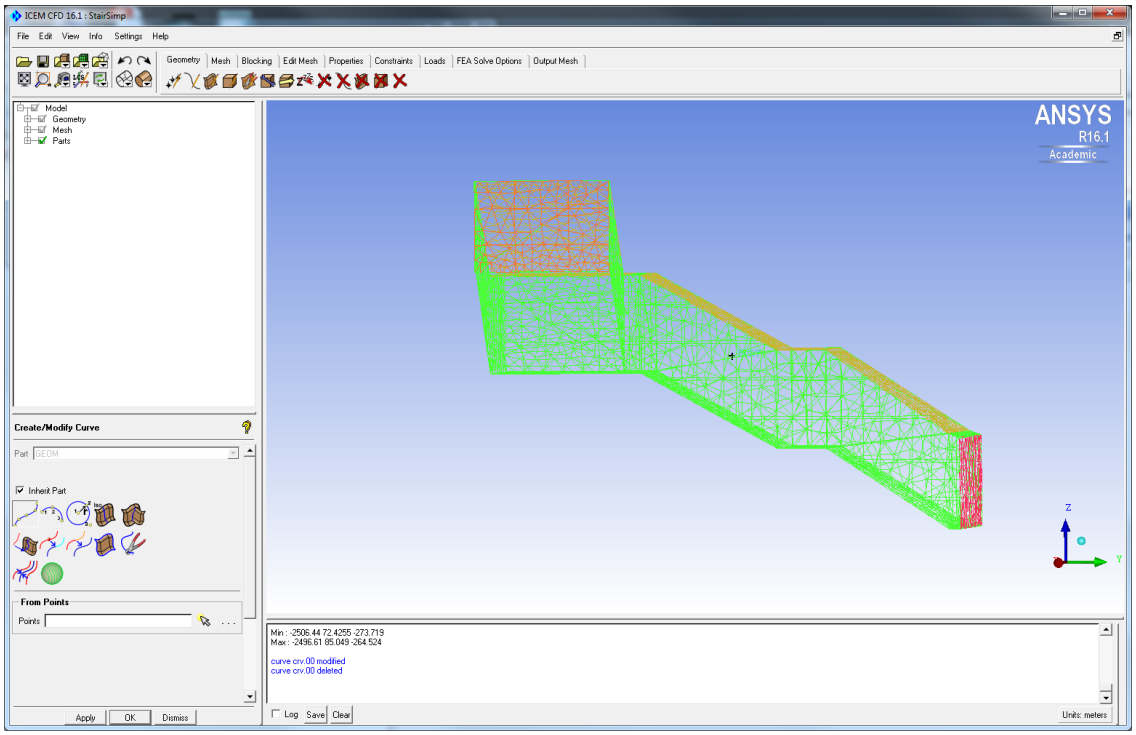

Figure 136: Mesh model of simplified stairs

A comparison of the airflow velocity contour at the upper boundary (outlet) of the stair (left) and the simplified stair model (right) is shown in Figure 137. The maximum air velocity in both cases is between 1.2 m/s to 1.4m/s although the stair with full detail of the steps indicates a higher variable speed distribution up to 1.7 m/s. This has also

demonstrated by Figure 138 in which the graphs plot velocity magnitude show more variation at the outlet section of the stair with full detail of the steps but in genially the velocity differences are minor. Figure 139 indicates the temperature distribution that in general is very close for the two cases.

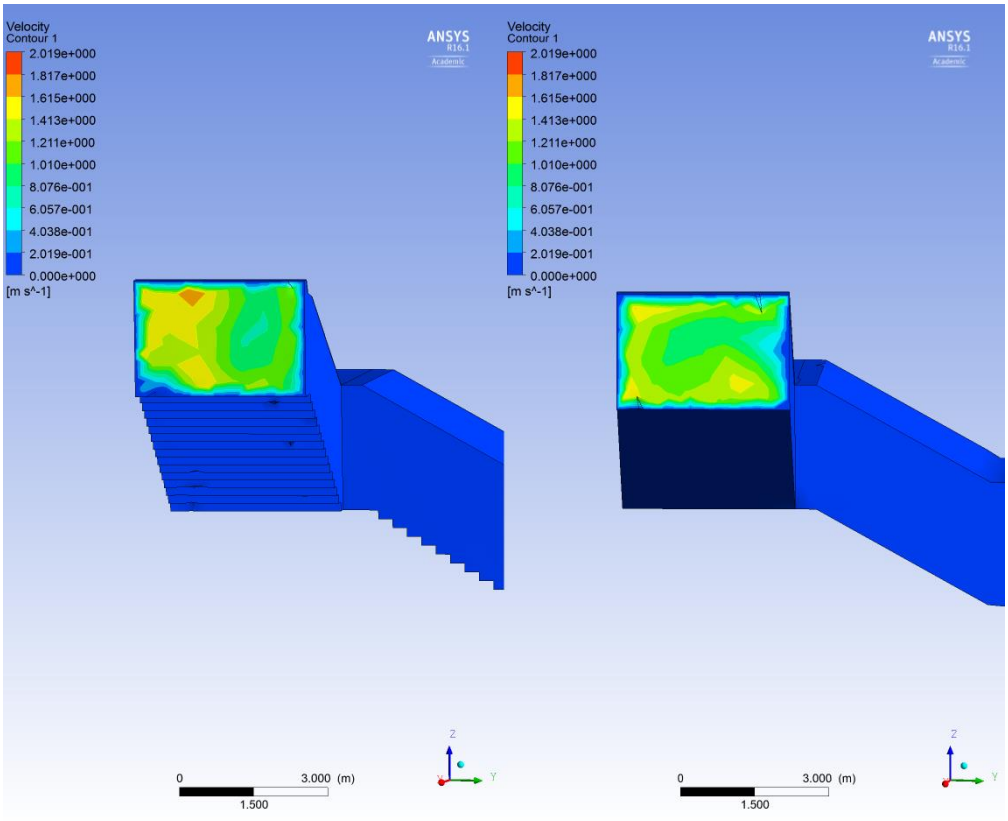

Figure 137: Comparison the velocity contour graphs of the stair and simplified stair model outlet

With stair

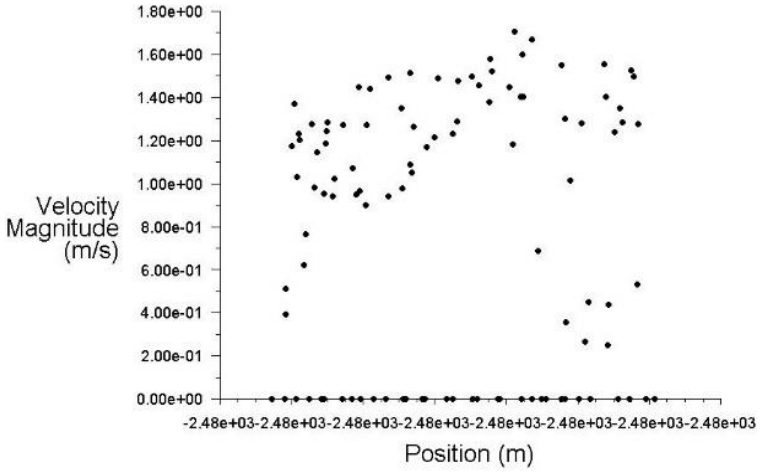

Simplified stair

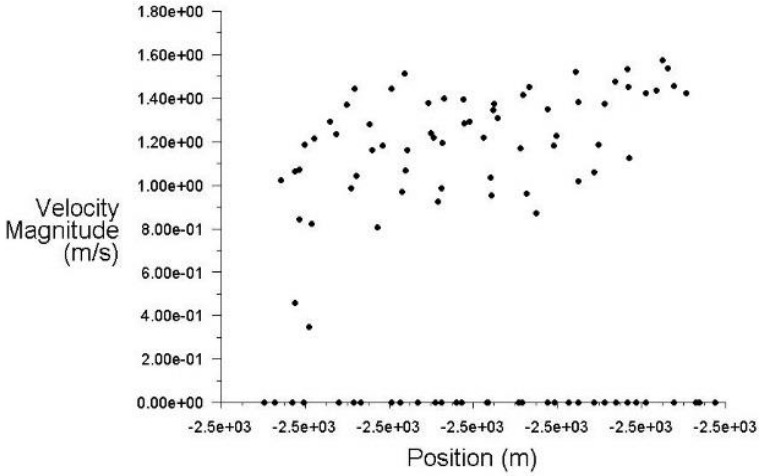

Figure 138: Comparison of the velocity magnitude plot graphs of the stair and simplified stair model at outlet

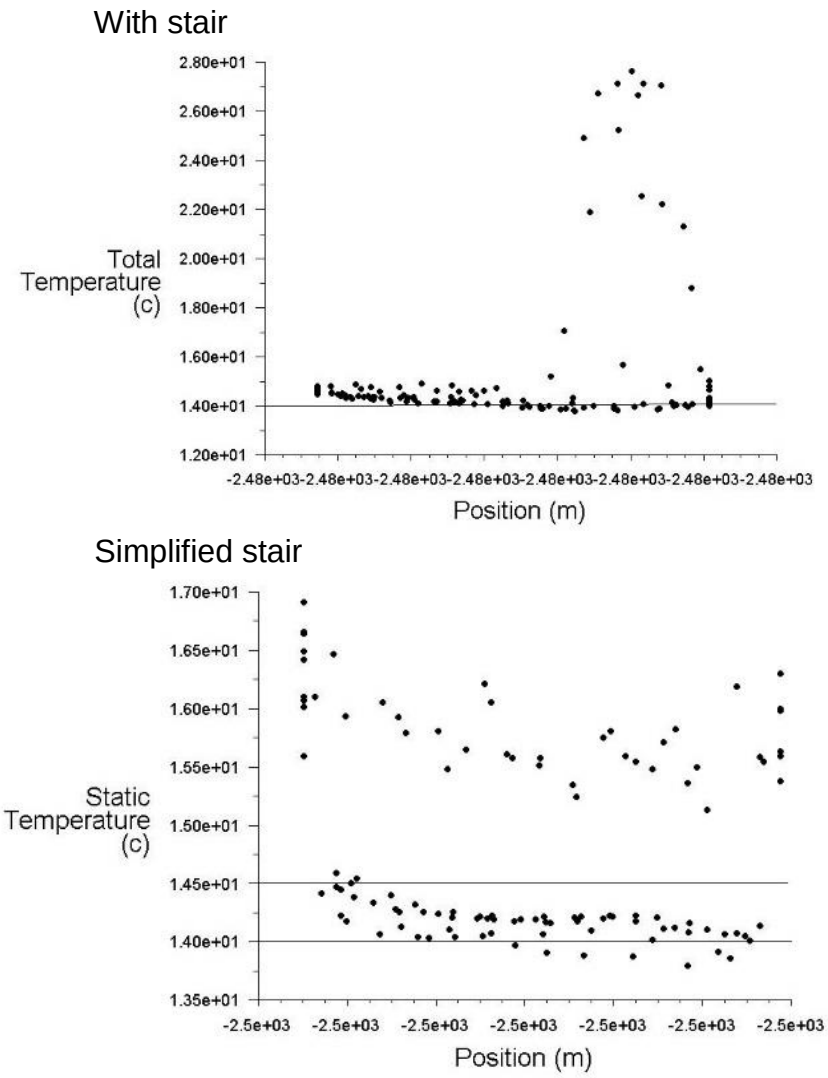

Figure 139: Comparison the velocity magnitude plot graphs of the stair and simplified stair model at outlet

The velocity vector in Figure 140 and Figure 141 indicate both the magnitude and direction of the air flow through the stairs from the bottom inlet to the top outlet. There was significantly more turbulence near the steps in the detailed model than the simplified stair. A comparison of the velocity streamlines, which are path lines of the velocity vector for steady flows, between the stair and simplified stair is shown in Figure 142 and Figure 143. Also shown is the relatively steady airflow in the simplified model. A steady or stationary flow is defined as one whose statistical features do not change in time. Homogeneity implies that, given a number of different spatial points and time, the statistics will remain unchanged if all positions are shifted by the same constant displacement. This is often applied in theoretical studies, since these assumptions simplify the equations and shorten the analysis time. The difference of the velocity vector at the outlet section does not affect the overall trend of airflow through the stairs.

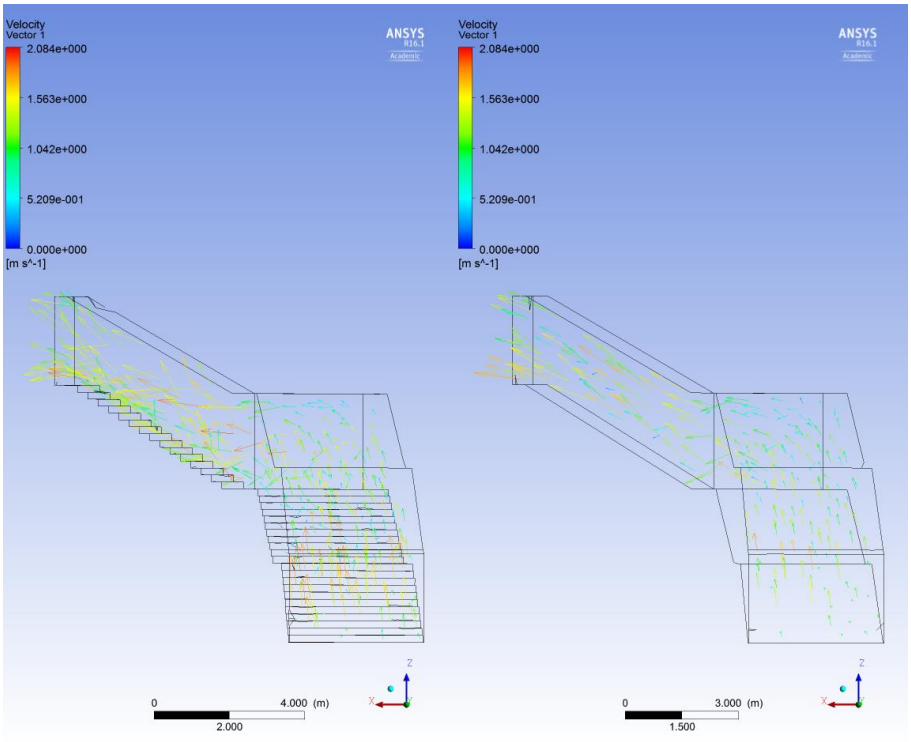

Figure 140: Comparison velocity vector of the stair and simplified stair (side elevation)

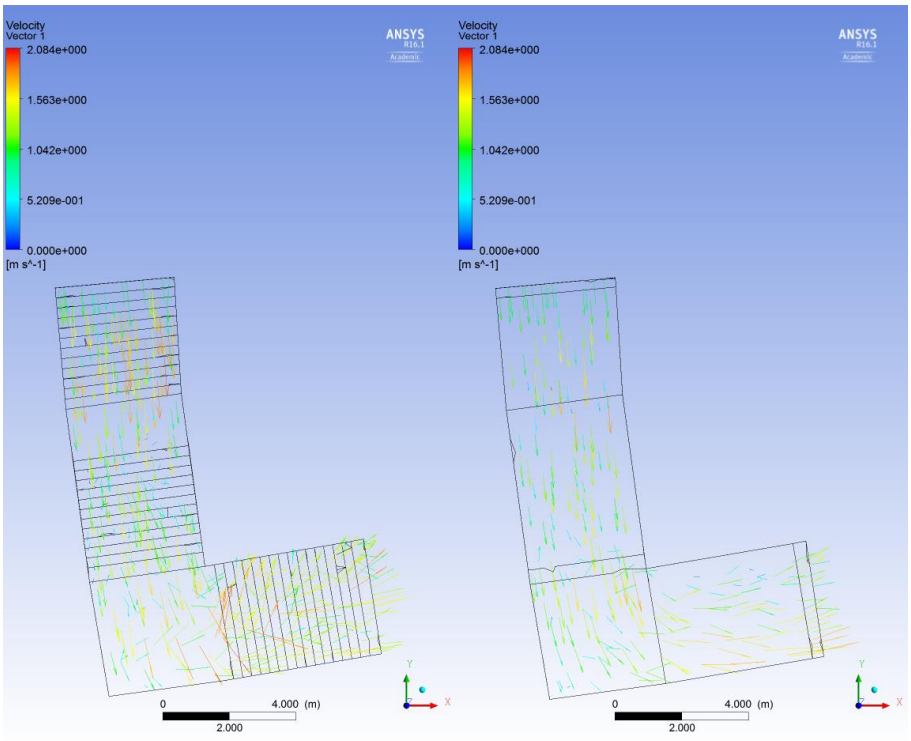

Figure 141: Comparison velocity vector of the stair and simplified stair (plan elevation)

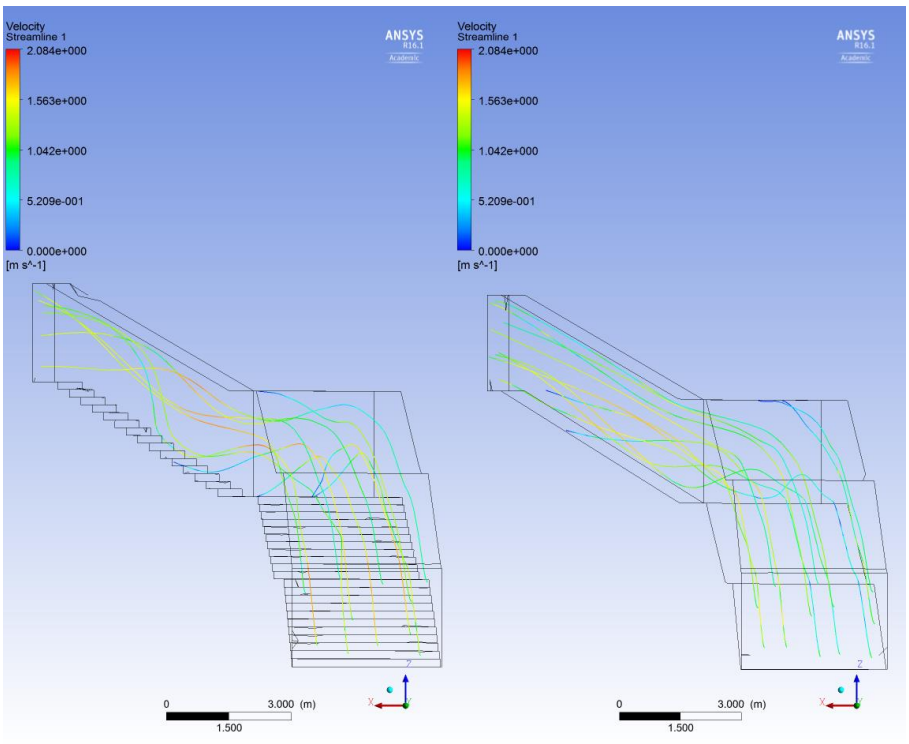

Figure 142: Comparison velocity streamline of the stair and simplified stair (side elevation)

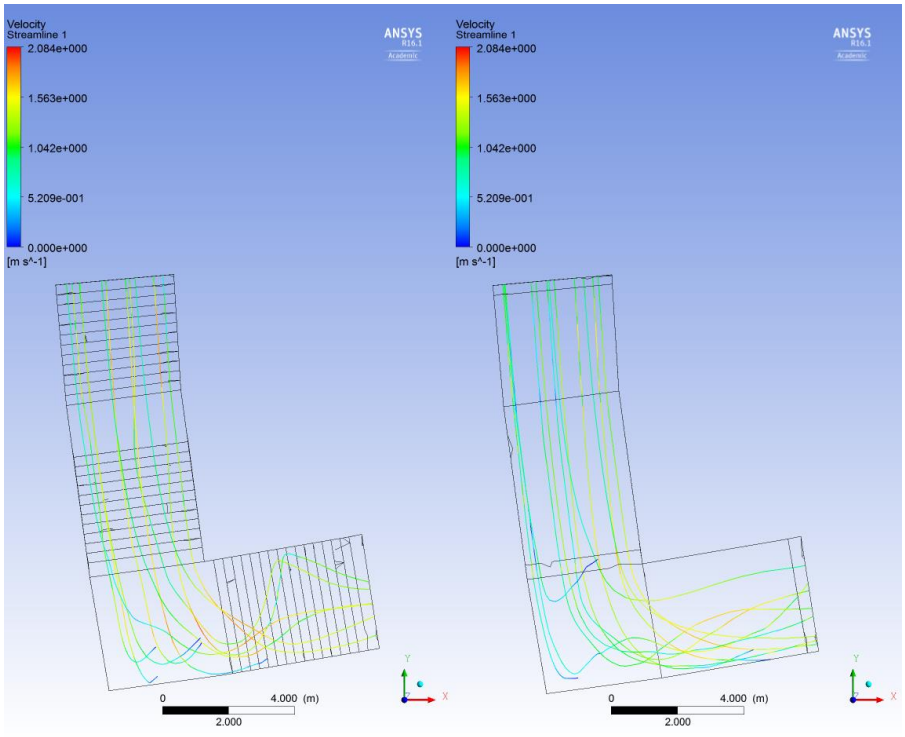

Figure 143: Comparison velocity streamline of the stair and simplified stair (plan elevation)

It can be seen that the simplified model of the stairs behaves in a very similar way to the detailed model in terms of air flow capacity for the conditions examined. This was achieved with the simplified model having the same mesh structure but the simplified model resulted in a higher mesh quality and greater computational accuracy compared with the detailed model. The simplified model produced results that were very close to the detailed model which, within the scale of this overall model, are considered to be acceptable. This resulted in a considerable reduction in mesh complexity, a higher mesh quality and a reduction in computational time. Following this exercise all the stairs and escalators in the station were modelled in the simplified form and other unnecessary detail was removed from the other elements of the station.

8.2.3 Model setup, assumption and boundary conditions

CFD modelling of a building is heavily influenced by the choice of turbulence model and boundary conditions and assumptions regarding the thermal interactions from countless variables between external conditions, and internal conditions. This section is intended to demonstrate the model assumption and boundary conditions used for this simulation.

ANSYS FLUENT is the most common software used in fluid mechanics and wind engineering that uses the RANS turbulence models. Yakhot *et al.* (1992) have improved this RNG k–ε turbulence model over the standard k–ε turbulence model. The RNG-based k-ε turbulence model is derived from the instantaneous Navier-Stokes equations, using a mathematical technique called "renormalization group" (RNG) methods. Additional terms and functions are applied to the standard k-ε model. The refinements have been explained in the ANSYS Fluent manual (2006) as follows:

· The RNG model has an additional term in its k-ε equation that significantly improves the accuracy for rapidly strained flows.

· The effect of swirl on turbulence is included in the RNG model, enhancing accuracy for swirling flows.

· The RNG theory provides an analytical formula for turbulent numbers, while the standard k-ε model uses user-specified, constant values.

· While the standard k-ε model is a high-Reynolds-number model, the RNG theory provides an analytically-derived differential formula for effective viscosity that accounts

for low-Reynolds-number effects. Effective use of this feature does, however depend on an appropriate treatment of the near-wall region.

· These features make the RNG k-ε model more accurate and reliable for a wider class of flows than the standard k-ε model.

It is essentially the standard RNG k-ε model and its variations that are commonly used for FLUENT CFD simulations of wind flow and dispersion (Meroney *et al.,* 1999). Further examples using FLUENT for validation of simulations using data from wind tunnel experiments can been seen in literature (Leitl *et al.,* 1997; Chang and Meroney, 2003). The setup of the turbulence model for this work is shown in Figure 144.

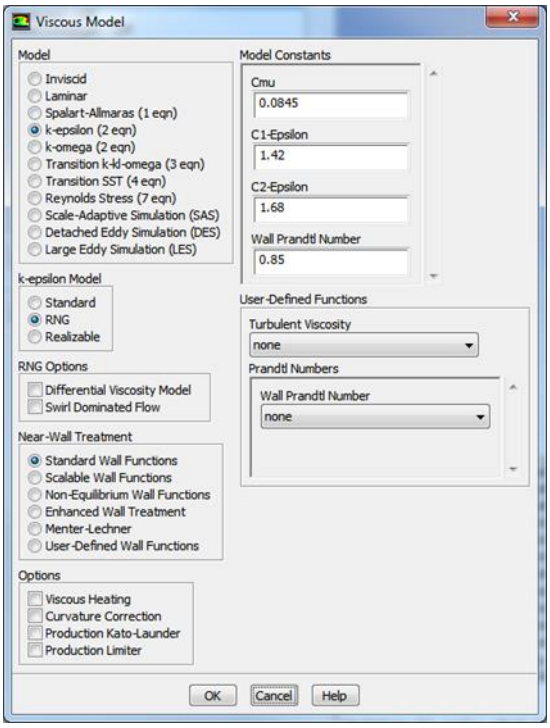

Figure 144: Viscous model setup for CFD simulations

The assumption and boundary conditions made for the NS tunnel model are listed in Table 18. The lighting use in the station had an average Illumination level of 300-400lx according to the London Underground Station Design Idiom (Transport for London, 2015). This specifies that the fluorescent lighting power is between 40w to 80w depending on the location. Due to the setting in Fluent the lighting is positioned flat on the ceiling giving a heat flux on the ceiling of 12W/m^{2}· This is similar to the values used by Yuan *et al.* (2012) in their examination of a subway system ventilation. A slightly lower value of 10w/$m^{2}$was used for the advertising board lighting on the wall at the platform, pedestrian areas and at the escalator as shown in Figure 145 and Figure 146.

The boundary of the escalator linking the NS tunnel and the concourse level is shown in orange, and the boundary of the stair link to the NS tunnel and the EW tunnel is shown in light green. Figure 147 shows the boundary of the tunnel at the end of each of the platforms, these boundaries are setup as velocity inflow or outflow depending on the airflow direction measured. The three parts of the station have been specified for the CFD model as a fluid body filled with air as shown for the NS tunnel model in Figure 148.

Boundary Name:	Location	Boundary character
Wall	All station wall	Solid
Celling lighting	Celling	Heat Flux 12w/m^2
Advertise lighting	Advertise wall	Heat Flux 10w/m^2
Esc_NS	Escalator to NS tunnel	Velocity Inlet/Outflow
Esc_motor	Escalator motor	Heat Flux 5w/m^2
Stair_NS	Stair to NS tunnel	Velocity Inlet/Outflow
P1_S	South of Platform1	Velocity Inlet/Outflow
P1_N	North of Platform1	Velocity Inlet/Outflow
P2_S	South of Platform2	Velocity Inlet/Outflow
P2_N	North of Platform2	Velocity Inlet/Outflow

Table 18: Boundary in the NS tunnel model

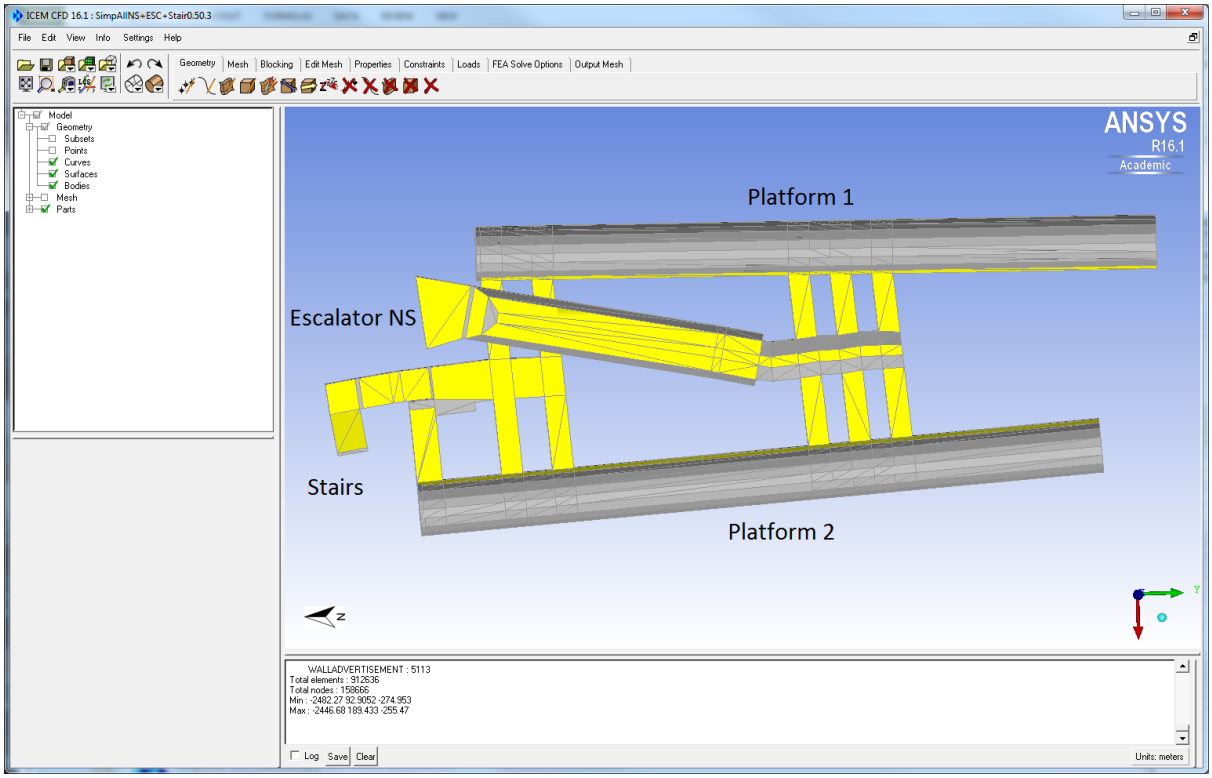

Figure 145: Boundary condition set up for North-South tunnel with stair and escalator model (plan elevation)

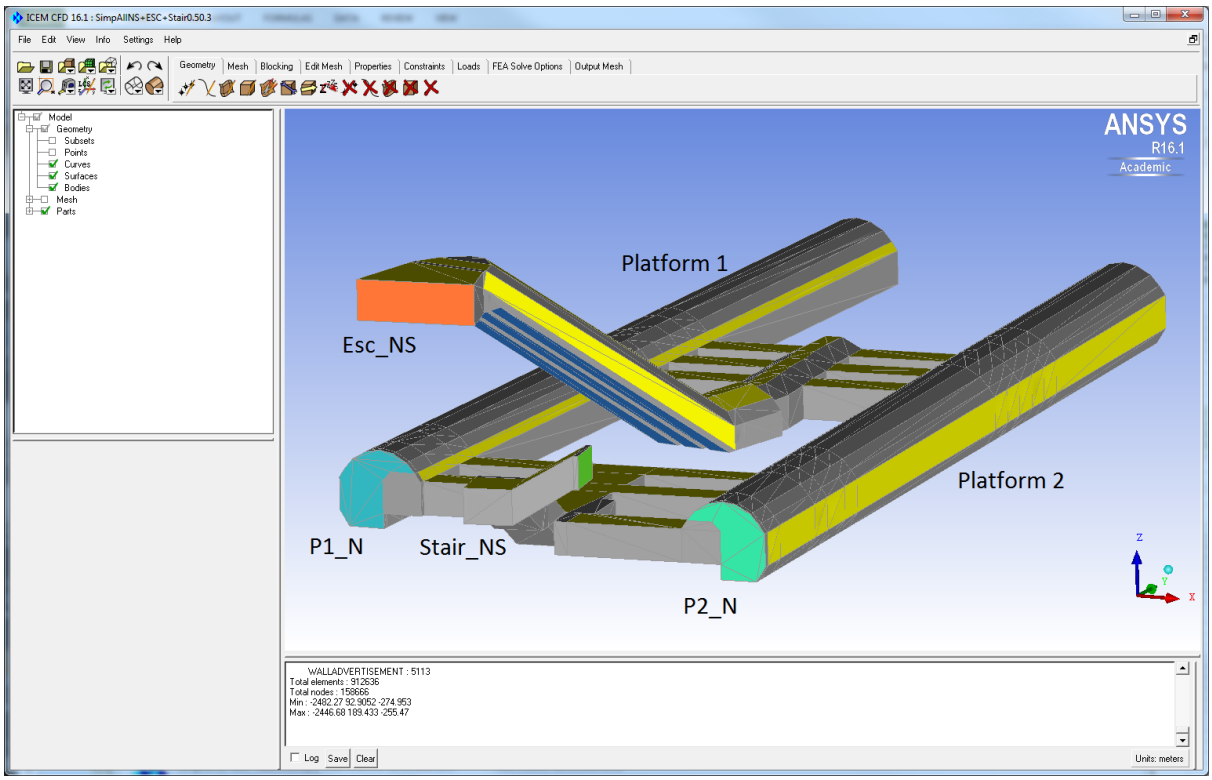

Figure 146: Boundary condition set up for North-South tunnel with stair and escalator model (side elevation from north-west)

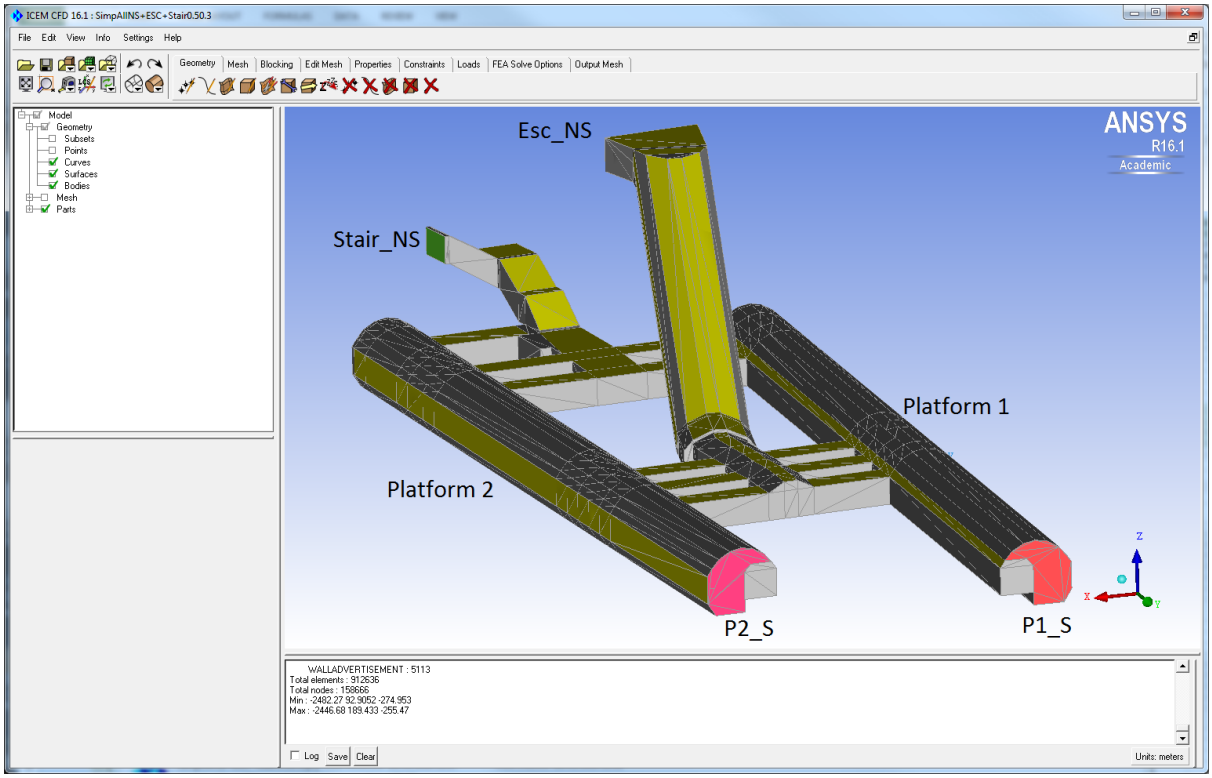

Figure 147: Boundary condition set up for North-South tunnel with stair and escalator model (side elevation from southwest)

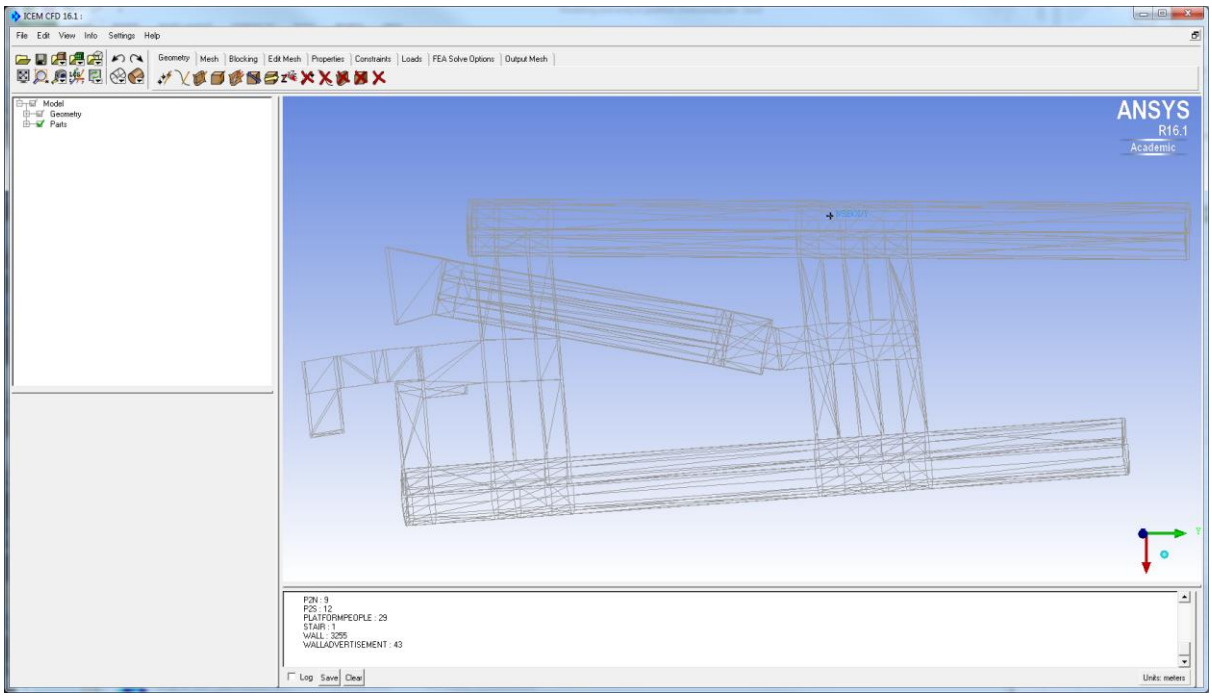

Figure 148: Fluid body set up for North-South tunnel with stair and escalator model (plan elevation)

The assumptions and boundary conditions made for the EW tunnel model are the same as the NS tunnel. These are listed in Table 19 and the model is shown in Figure 149 and Figure 150.

Boundary Name	Location	Boundary character
Wall	All station wall	Solid wall
Celling lighting	Celling	Heat Flux 12w/m^2
Advertise lighting	Advertise wall	Heat Flux 10w/m^2
Esc_EW	Escalator to EW tunnel	Velocity Inlet/Outflow
Esc_motor	Escalator motor	Heat Flux 5w/m^2
Stair_EW	Stair to EW tunnel	Velocity Inlet/Outflow
P3_W	West of Platform4	Velocity Inlet/Outflow
P3_E	East of Platform 3	Velocity Inlet/Outflow
P4_W	West of Platform4	Velocity Inlet/Outflow
P4_E	East of Platform 4	Velocity Inlet/Outflow

Table 19: Boundary in the EW tunnel model

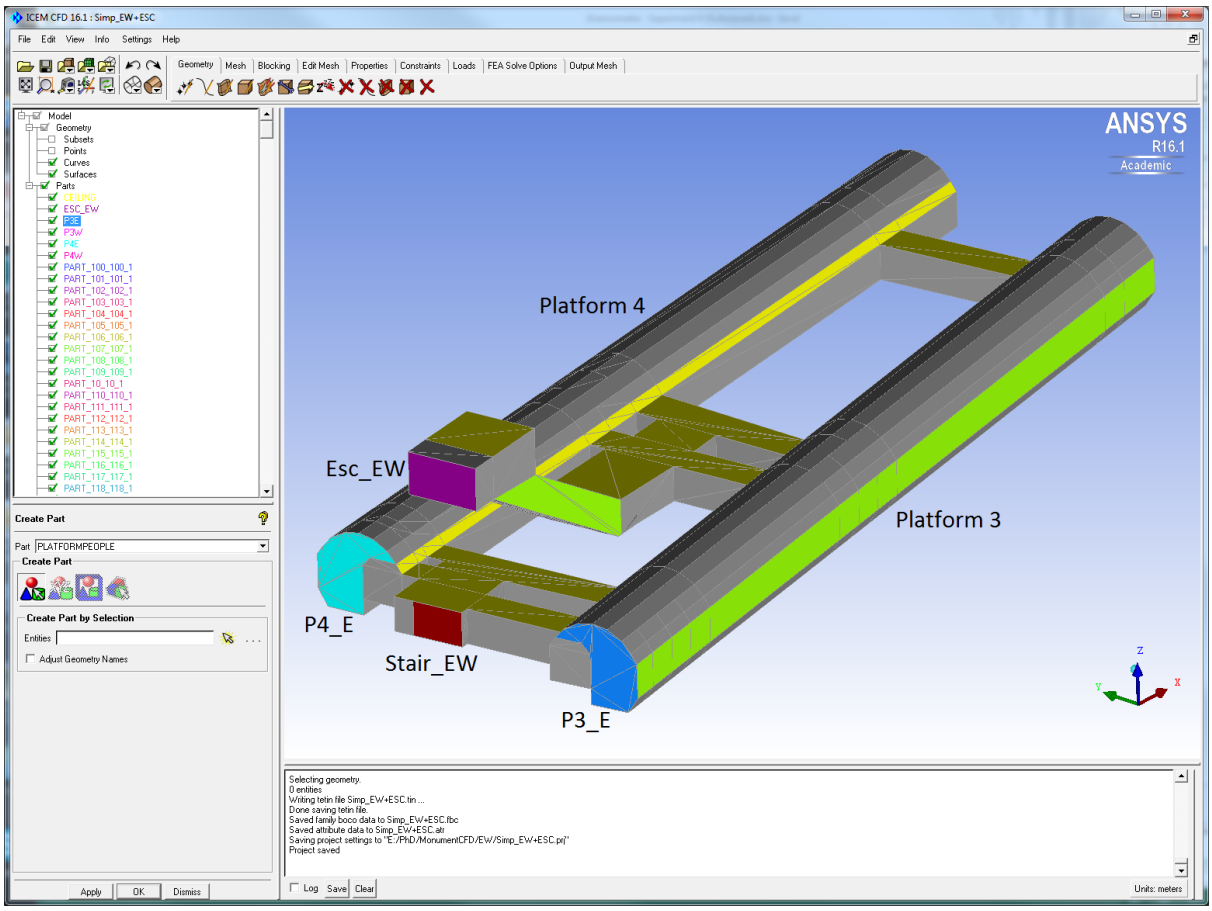

Figure 149: Boundary condition set up for East-West tunnel with stair model (side elevation from southeast)

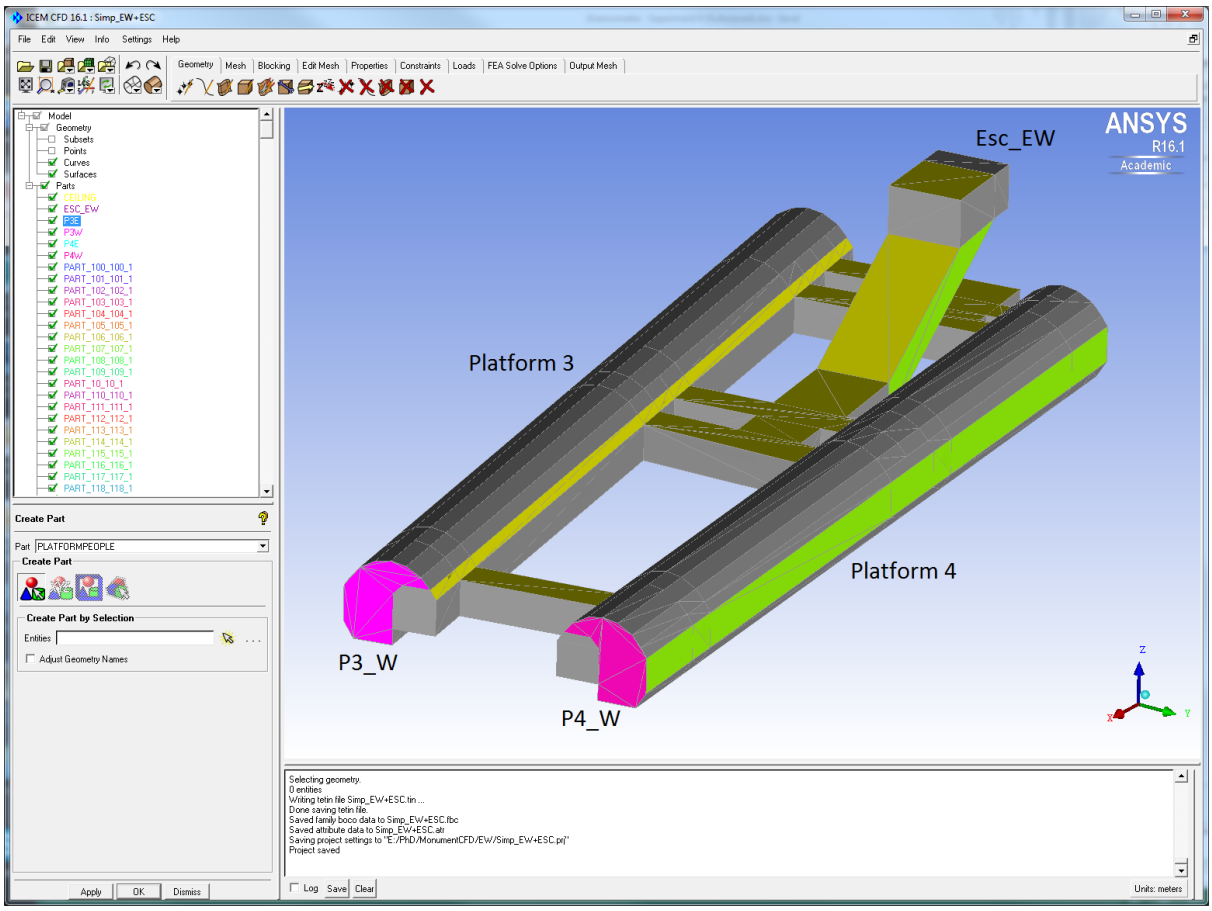

Figure 150: Boundary condition set up for East-West tunnel with stair model (side elevation from south-west)

At the concourse area, the two inner boundaries are the escalators linking the NS tunnel and the EW tunnel to the concourse level. The three station exits are the boundaries to the external environment. The assumptions and boundary conditions made for the concourse are listed in Table 20 and the model is shown in Figure 151 and Figure 152. The boundaries at the exits are setup as velocity inlet or outflow depending on the wind direction and the pressure indicated by the microclimate CFD simulation scenarios in Chapter 7.

Boundary Name	Location	Boundary character
Wall	All station wall	Solid wall
Celling lighting	Celling	Heat Flux 12w/m^2
Advertise lighting	Advertise wall	Heat Flux 10w/m^2
Esc_NS	Escalator to EW tunnel	Velocity Inlet/Outflow
Esc_EW	Escalator to EW tunnel	Velocity Inlet/Outflow
Exit 1	Station Exit 1	Velocity Inlet/Outflow
Exit 2	Station Exit 2	Velocity Inlet/Outflow
Exit 3	Station Exit 3	Velocity Inlet/Outflow

Table 20: Boundary in the EW tunnel model

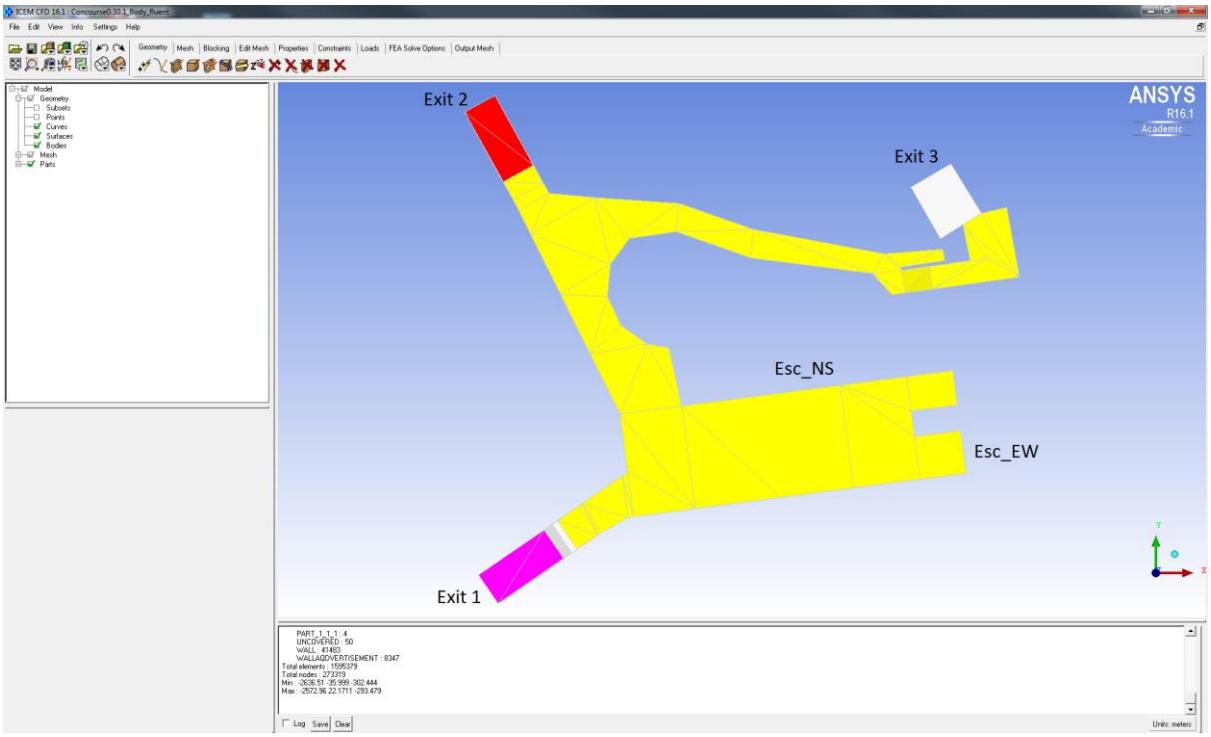

Figure 151: Boundary condition set up for East-West tunnel with stair model (plan elevation)

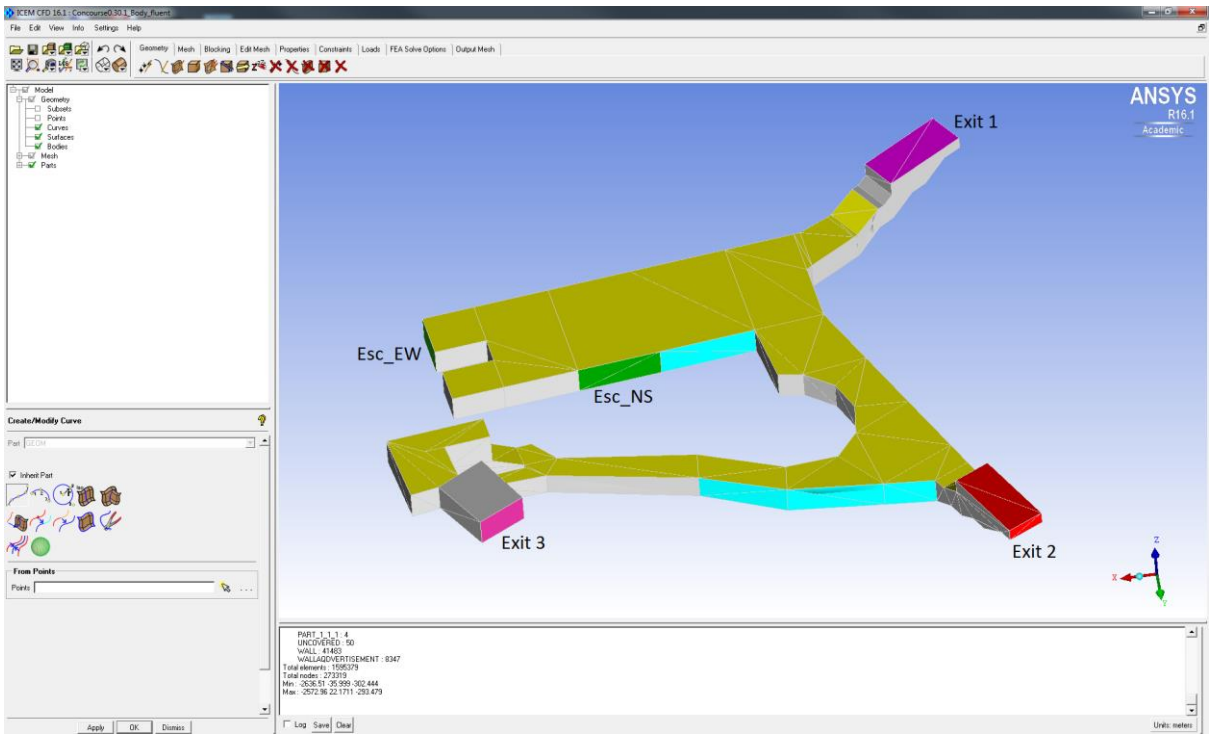

Figure 152: Boundary condition set up for East-West tunnel with stair model (side elevation from south-west)

8.3 Validating the CFD model

The generation of proper meshes to simulate turbulent flows using the RANS model for the three sections of the station and validation of the simulation using experiment data have been discussed in a previous section. A good mesh requires great precision. The mesh should be highly refined at pedestrian level and in areas where strong wind gradients are planned. However, over fine mesh does not always lead to a good mesh. It also depends on the physical problem to be simulated. Adapting the mesh is an effective way to model accurately separation and attachment flow details without too many calculations. The ultimate test of a mesh is the closeness of the simulation is to the experiment (Kim and Boysan, 1999).

The initial considerations in validating the mesh is to ensure that the residual error drops below 10^{-4}, that the monitor points are steady, and that the imbalances are below 1%. If the simulation is run the residual error and the monitor point values for successive cases can be compared and any changes that result from refining the mesh indicate that the solution is not mesh independent. The mesh needs to be further refined until a solution that is independent of the mesh is reached. The goal is to produce the smallest mesh that gives the mesh independent solution as this will reduce the simulation run time. For this research, that is based on simulation and validation

by the experiment, it is important to compare the residual error and the monitor point values but it is equally important to compare the simulation with measured values.

8.3.1 North-South tunnel with escalator and stairs

A comparison of meshing size, CFD simulation time and CFD simulation results has been carried out for the NS tunnel model. In the meshing control option a maximum mesh size and a minimum mesh size were defined. Mesh size input was varied for several cases listed in Table 21. The smallest mesh size that could be generated was maximum 0.2 m and minimum 0.1 m within the computer power available. The simulation time for the different mesh sizes for the NS tunnel with escalator and stairs is listed in Table 21 and Figure 153 to Figure 157 shows the mesh model for this simulation.

	max.	min.	max.	min.	max.	min.	max.	min.
Mesh size (m)	0.5	0.3	0.4	0.2	0.3	0.1	0.2	0.1
Total mesh:	912,636		1,633,217		4,246,201		11,312,055	
Simulation time:	2hr		4hr		7hr30min		20hrs	

Table 21: Mesh and simulation time detail of North-South tunnel

Mesh size: maximum 0.5 minimum 0.3

The mesh model that produced good quality was that in which the maximum size was 0.5 and the minimum 0.3. this is shown in Figure 153 and an exploded view of the tunnel boundary and curve ceiling showing the mesh detail is in Figure 154. The mesh near the surface edge is smaller than the centre.

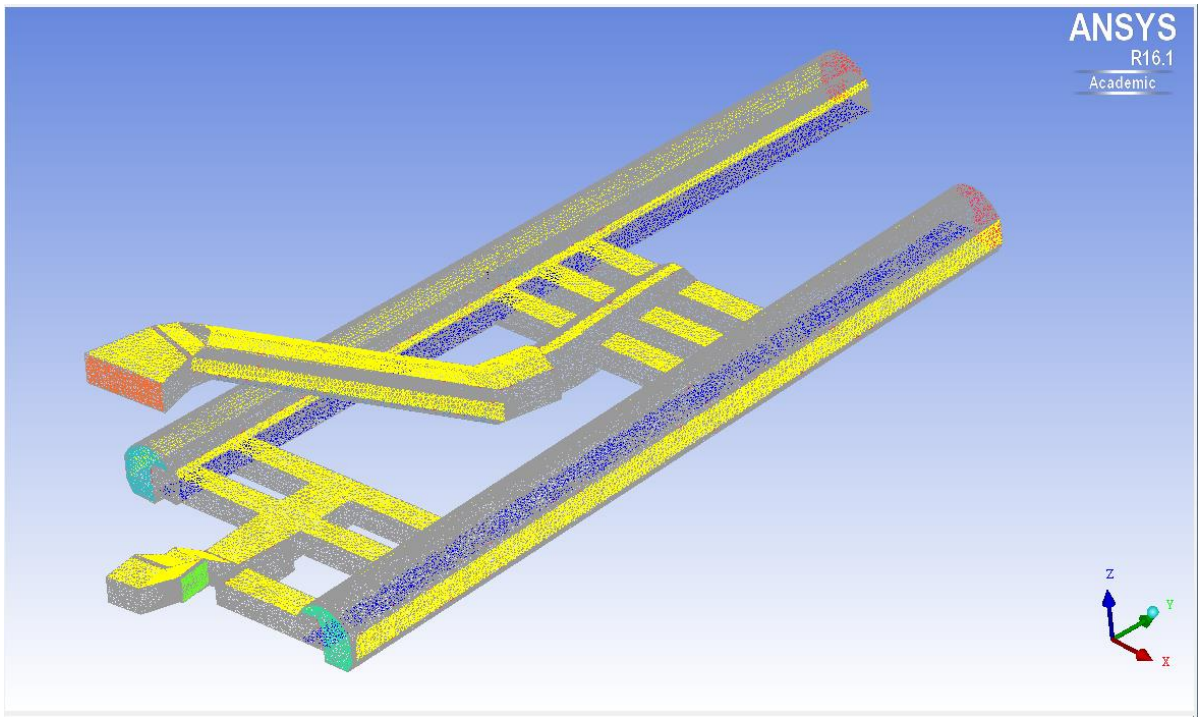

Figure 153: North-South tunnel with escalator and stairs in mesh size maximum 0.5 minimum 0.3

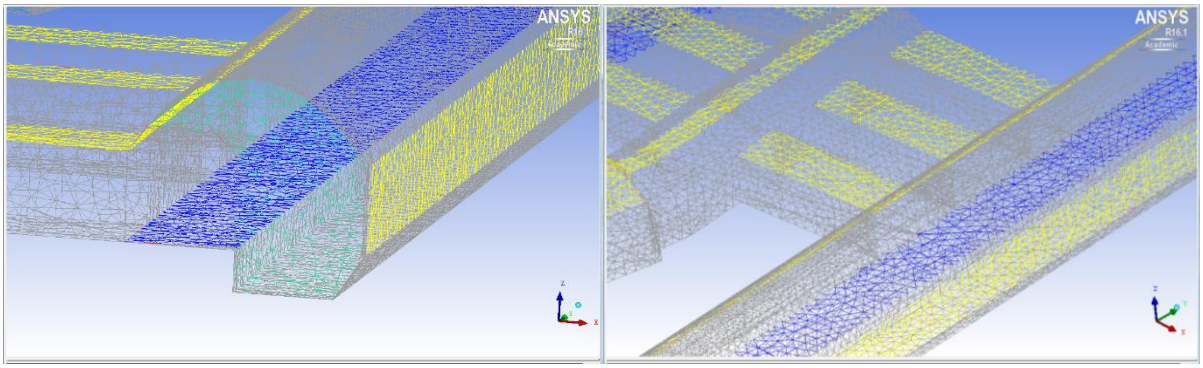

Figure 154: North-South tunnel with escalator and stairs in mesh size maximum 0.5 minimum 0.3 (Detail elevation)

The simulation time was about 2 hours with this mesh size and the residual error was within the acceptable range and the monitor points steady. A further refined mesh of maximum 0.4 and minimum 0.2, shown in Figure 155 required a simulation time of 4 hours with an acceptable range of residual error and steady monitor points. A further refined mesh of maximum 0.3 and minimum 0.1 as shown in Figure 156 required a simulation time of 7 hour and 30 minutes.

Mesh size: maximum 0.4 minimum 0.2

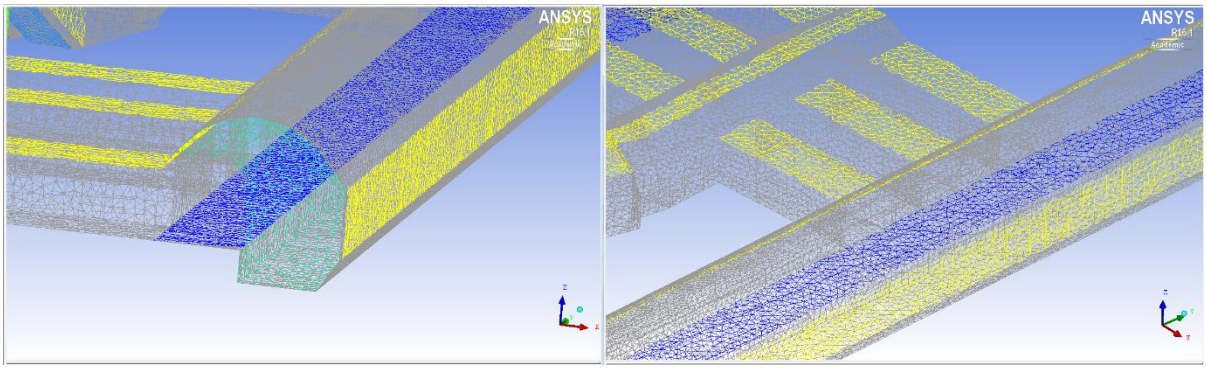

Figure 155: North-South tunnel with escalator and stairs in mesh size maximum 0.4 minimum 0.2 (Detail elevation)

Mesh size: maximum 0.3 minimum 0.1

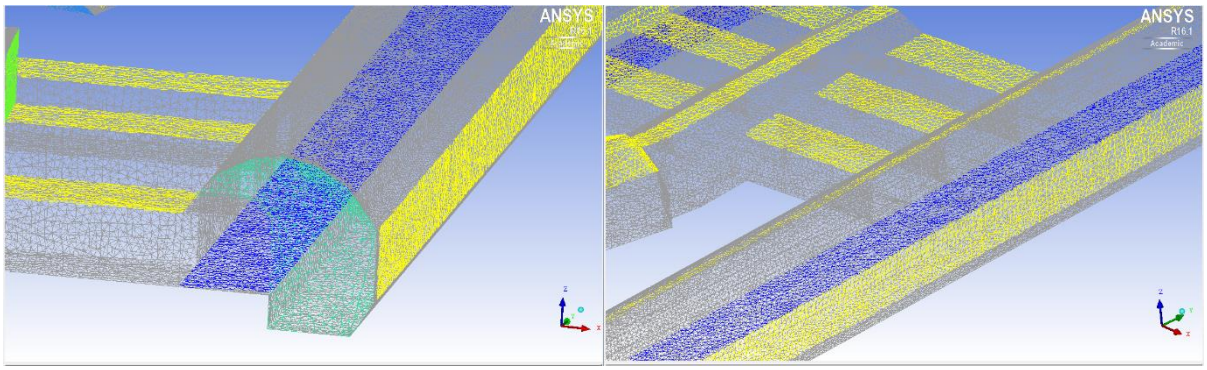

Figure 156: North-South tunnel with escalator and stairs in mesh size maximum 0.3 minimum 0.1 (Detail elevation)

The final mesh considered was maximum 0.2 and minimum 0.1 as shown in Figure 157. This required a simulation time of more than 20 hours. It was felt that the degree of precision produced by this model was not required for this type of work.

Mesh size: maximum 0.2 minimum 0.1

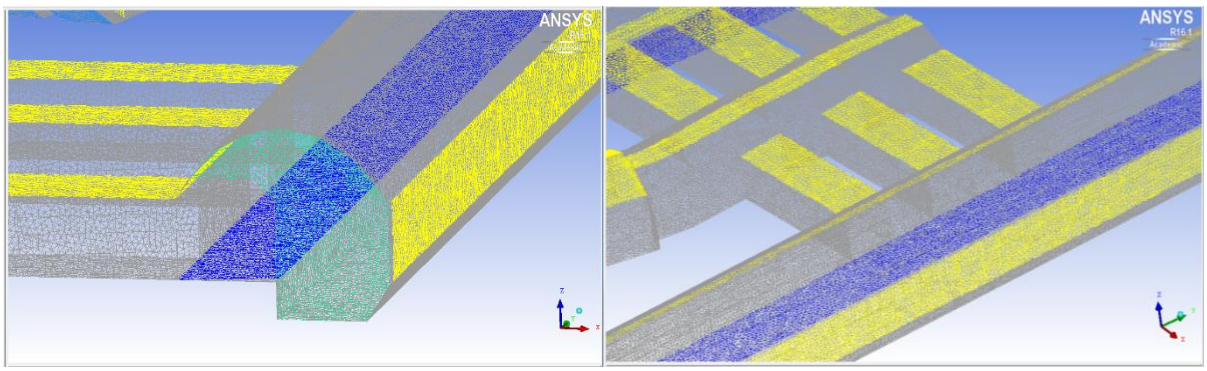

Figure 157: North-South tunnel with escalator and stairs in mesh size maximum 0.2 minimum 0.1 (Detail plan elevation)

For the purpose of this CFD simulation, which is the establishment of a methodology to recreate air flow conditions inside a subway station and produce an early stage design tool to assist architects and building engineers in understanding the air flow in subway systems, establishing the overall air flow pattern is more important than absolute precision in air flow velocity and distribution. The following simulation results are based on input data for the whole station obtained from the tracer gas measurements experiments 1 and 3 (ultrasonic anemometer used for measure air flow direction and speed) that are shown in Table 22 and Table 23 and summarise the tracer gas data. These two sets of data need to be combined together for use in the later sections for determining the input parameters and for validating the output. The measurements taken in the tracer gas experiments were very limited but these two experiments were conducted during very similar weather conditions. It was therefor considered satisfactory to combine the measured data from these two experiments to give an overall picture of the events at the platforms, the escalators and the exits.

Location		Airflow (m/s)	Direction in positive value	Temperature (°C)
NS tunnel	P1_S	0.4 (0.1-0.8)	S to N	14.3
	P2_S	1 (0.5-1.3)	S to N	11.5
	P1_N	-	-	13.3
	P2_N	-	-	12.2
EW tunnel	P3_W	0.4 (0.3-0.5)	E to W	12.9
	P4_W	0.4 (0.3-0.5)	E to W	12.4
	Stair_EW	1 (0.4-1.5)	Up flow	
	P3_E	-	-	12
	P4_E	-	-	-
Concourse	Esc_NS	1 (0.4-1.3)	NS to Con	-
	Esc_EW	0.3 (-0.5-0.8)	EW to Con	-
	Exit 1	1 (0.2-2.4)	Outflow	-
	Exit 2	0.5(-0.3 - 0.9)	Outflow	-
	Exit 3	-	-	-

Table 22: Average data from tracer gas experiment 1 for CFD simulation

Location		Airflow (m/s)	Direction in positive value	Temperature (°C)
NS tunnel	P1_S	0.5 (-0.1-1)	S to N	14.5
	P2_S	0.7 (0-1.1)	S to N	11.5
	P1_N	0.3 (-0.1-6)	S to N	13.2
	P2_N	0.5 (0.1-0.8)	S to N	12.8
EW tunnel	P3_W	0.3 (-0.2-0.7)	E to W	12.8
	P4_W	0.4 (-0.1-0.7)	E to W	13.1
	P3_E	0 (-0.3-0.3)	E to W	12.5
	P4_E	0.1 (-0.2-0.3)	E to W	-

Table 23: Average data measured from tracer gas experiment 3 for CFD simulation and validation

A sub set of the boundary conditions for the input simulation and outflow measurement data used to validate the NS tunnels is shown in Table 24. A three dimensional representation of the output of the CFD simulation model showing the air flow velocity contours on the horizontal plan and the temperature contours on the model surface is shown in Figure 158 and Figure 159 respectively. The initial boundary conditions are marked as “inlet” The outflow values are all determined from the simulation. The closeness of the fit of the simulation with the experimental data can be seen by comparing the same points in Table 24 and Table 25 that show very good agreement. There are around 0.1m/s difference of average value at P1_N, P1_N, P2_N and Stair_NS. Yuan and You (2007) used CFD simulation to evaluate and optimize the velocity and temperature distribution for subway station found about 13.7%–15.9% difference between computation and measurement for air velocity.

Location	Boundary condition	Airflow (m/s)	Direction in positive value	Temperature (°C)
P1_S	Inlet (CFD)	0.4	S to N	14.3
P2_S	Inlet (CFD)	1	S to N	11.5
P1_N	Outflow (Validate)	0.3 (-0.1-6) (Exp 3)	S to N	13.2 (Exp 5) 13.3 (Exp 1)
P2_N	Outflow (Validate)	0.5 (0.1-0.8) (Exp 3)	S to N	12.2 (Exp 4) 12.8 (Exp 3)
Stair_NS	Outflow (Validate)	1 (0.4-1.5) (Exp 1)	Up flow	-
Esc_NS	Outflow (Validate)	1 (0.4-1.3) (Exp 1)	Up flow	-

Table 24: Input simulated and outflow need to be validated for NS tunnel CFD simulation

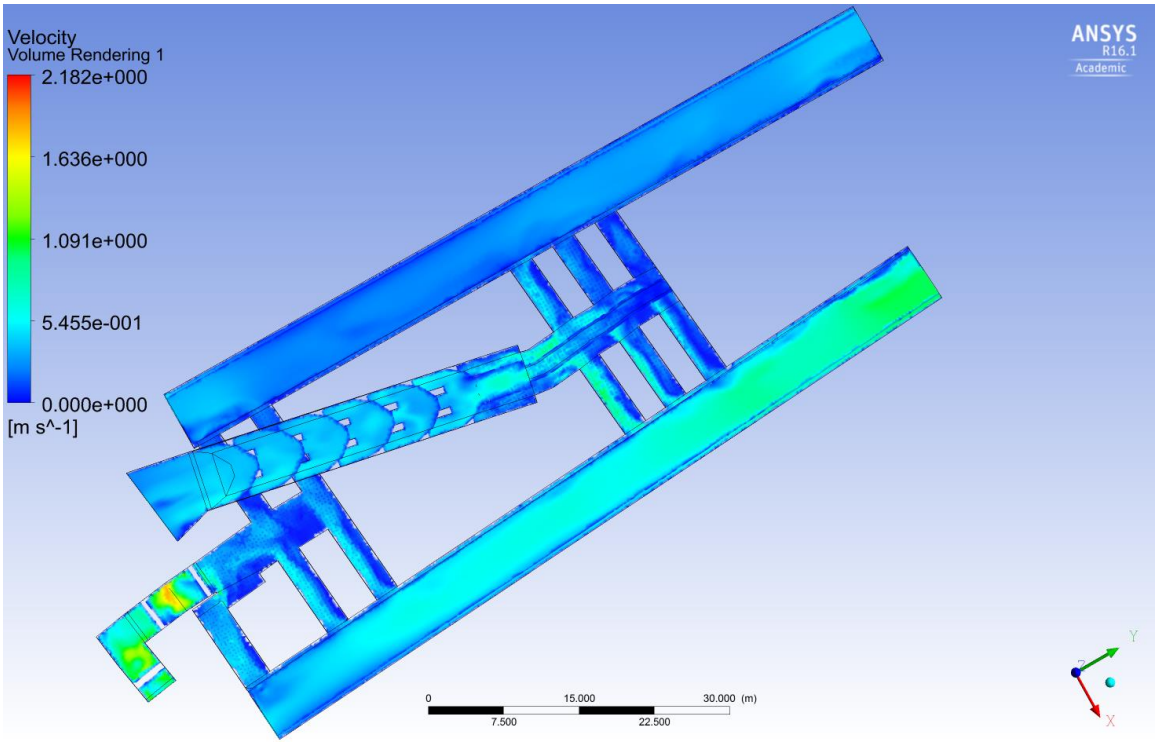

Figure 158: Airflow velocity contour on the horizontal plan of CFD simulation result (plan elevation)

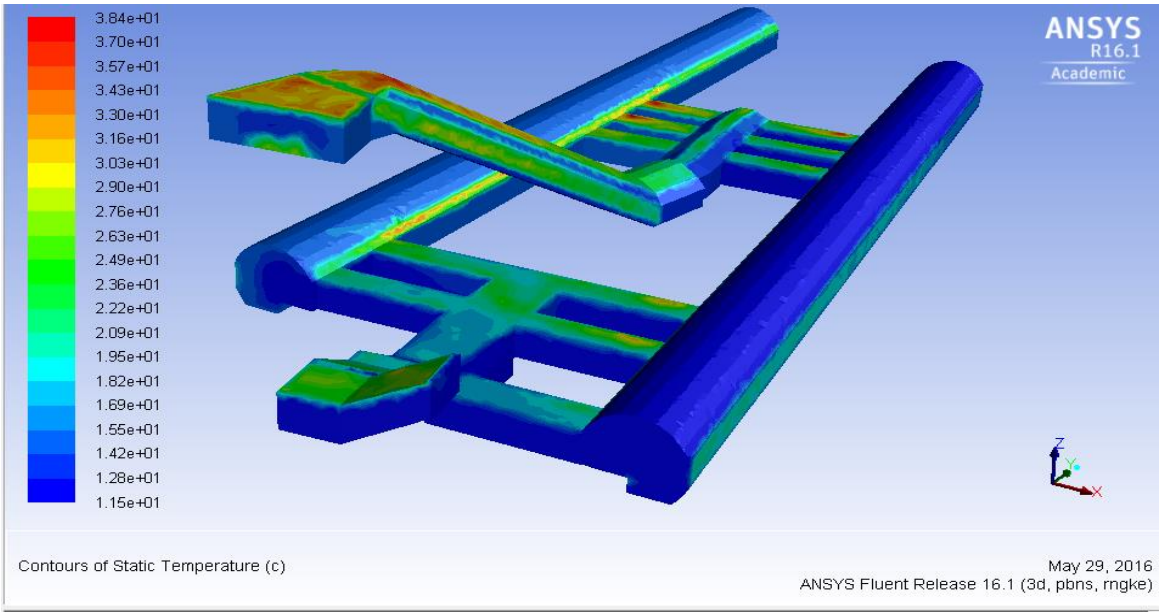

Figure 159: Temperature contour on the model surface of CFD simulation result

Simulations using different mesh sizes have been compared for the NS tunnels in order to ensure that the simulation results agree with the experimental data. Figure 160 to Figure 163 are XY plots of an output variable as a function of position along a specified direction vector, for one particular outlet boundary surface from the simulation result. The point scatter on these graphs is an indication of the mesh sensitivity of the solution. The positions of the points has coordinate values that correspond to the dot product of

either velocity or temperature coordinate with the direction vector. The most suitable mesh is characterised by a minimum average value consistent with an acceptable computational time.

Figure 160 and Figure 161 compare the velocity and temperature profiles respectively with different mesh size for the north tunnel boundary at platform 1 and 2. Figure 162 and Figure 163 compare the velocity and temperature at the stair and the escalator boundary. As the mesh size is reduced the number of dots increases as the mesh is made finer indicating more mesh cells in this boundary surface. Comparing the temperature or velocity on the y axis for the different mesh sizes shows the values to be increasing as the mesh is made finer indicating that the solution is mesh dependent as mentioned earlier.

The CFD simulation carried out in this section used the average value at P1_S and P2_S measured in experiment 1 as velocity inlet. The outlets need to be validated but not all required data was measured in the experiments so measurements taken in experiment 3 at the same location were used instead. This was justified because the input values of experiment 1 and experiment 3 are very similar. A summary of the results displayed graphically is shown in Table 25.

A comparison with Table 24 indicates the best mesh size to be used in the simulation was maximum 0.3 minimum 0.1. The outlet airflow value of P1_N 0.4 m/s, P2_N 0.45m/s and Stair_NS 0.9m/s are very close to the measured average value of 0.3 m/s, 0.5 m/s and 1 m/s. Although the airflow value of the NS escalator at 0.4 m/s is lower than the measured average of 1 m/s, it is still within the range 0.4-1.3 m/s. All the temperatures predicted by the simulation are very well validated by the measurement. A comparison of the streamlines produced using different mesh sizes are shown in Figure 164. The streamlines are also well reproduced in the simulation using a mesh size maximum 0.3 minimum 0.1 and this closely replicate the measured condition.

Mesh size (m)		max.: 0.5, min.: 0.3		max.: 0.4, min.: 0.2	
Boundary		Airflow (m/s)	Temperature (°C)	Airflow (m/s)	Temperature (°C)
P1_N	Outflow	0.36 (0.28-0.45)	12.5-15	0.38 (0.3-0.45)	12.5-15
P2_N	Outflow	0.4 (0.25-0.55)	11.5-12	0.42(0.25-0.57)	11.5-12.2
Stair_NS	Outflow	0.8 (0.2-1.5)	12-12.5	0.9 (0.5-1.5)	12-12.5
Esc_NS	Outflow	0.3 (0.1-0.45)	12.5-14	0.3 (0.1-0.45)	12.5-13.5
Mesh size (m) max., min.		max.: 0.3, min.: 0.1		max.: 0.2, min.: 0.1	
Boundary		Airflow (m/s)	Temperature (°C)	Airflow (m/s)	Temperature (°C)
P1_N	Outflow	0.4 (0.2-0.52)	12.25-15.5	0.42 (0.2-0.58)	12.5-15.5
P2_N	Outflow	0.45 (0.2-0.55)	11.5-12.2	0.48 (0.2-0.55)	11.5-12.4
Stair_NS	Outflow	0.9 (0.1-2)	11.8-12.5	0.9 (0.1-1.7)	11.8-12.5
Esc_NS	Outflow	0.4 (0.1-0.5)	12 - 14	0.4 (0.1-0.5)	11.8-14

Table 25: Summery outflow from NS tunnel CFD simulation

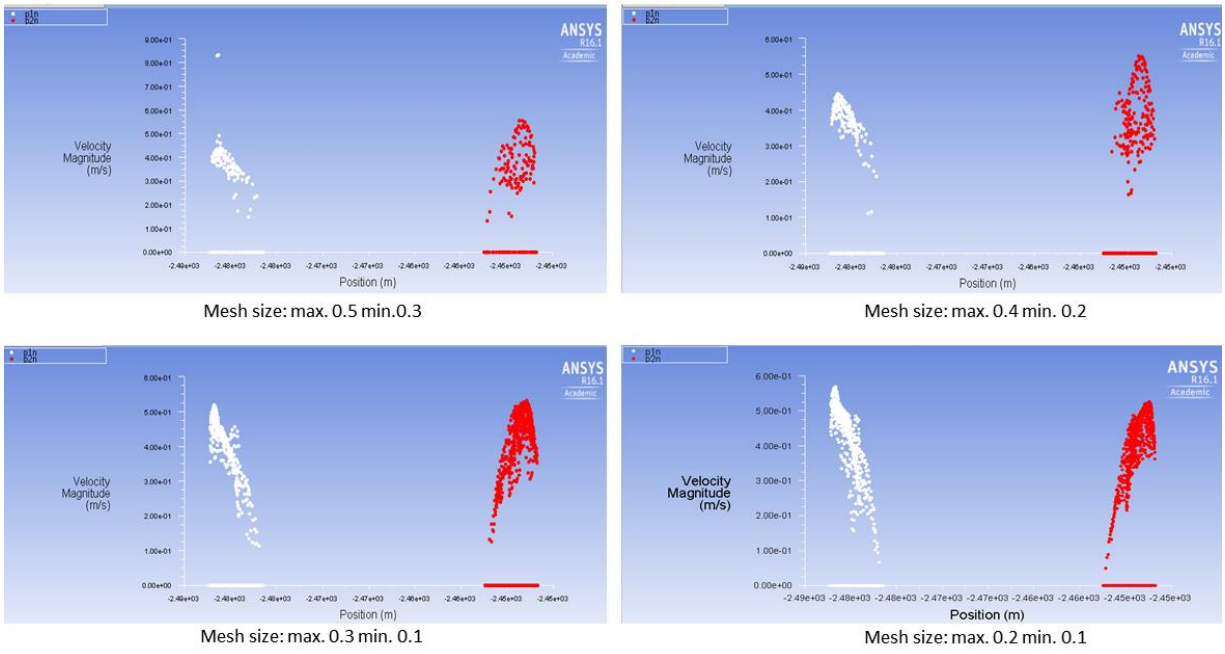

Figure 160: Comparing velocity plot graph at the North of platform 1 and 2 for different mesh sizes

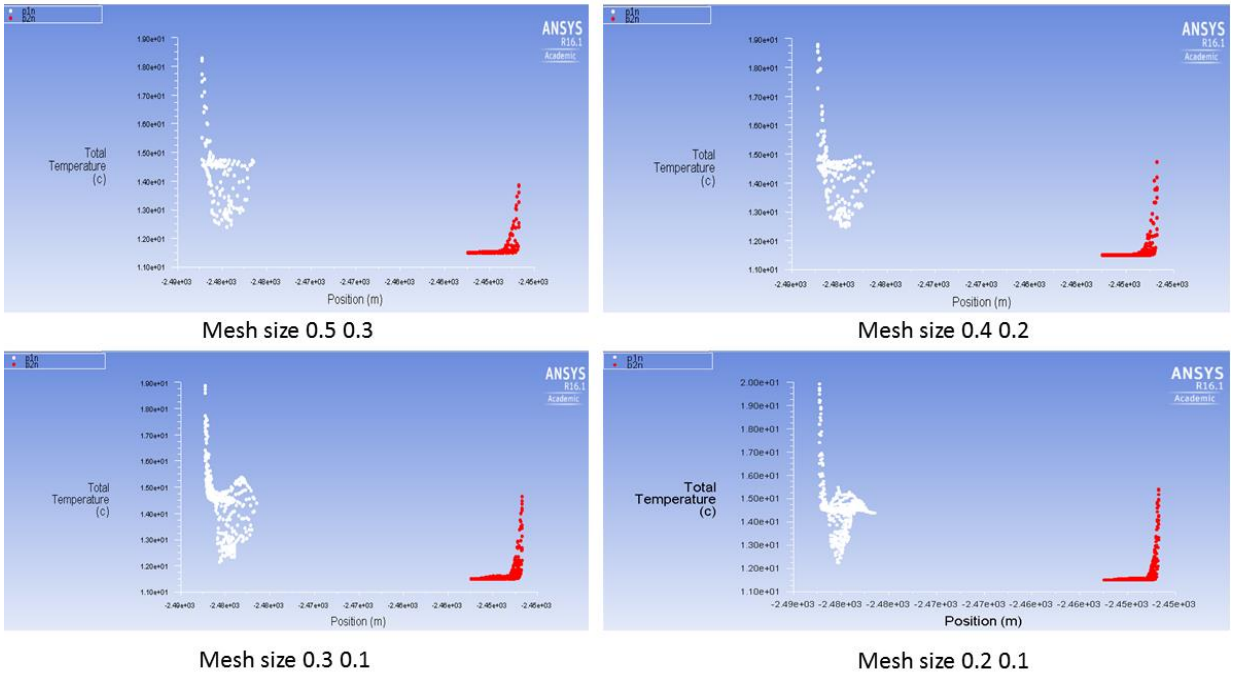

Figure 161: Comparing temperature plot graph at the North of platform 1 and 2 for different mesh sizes

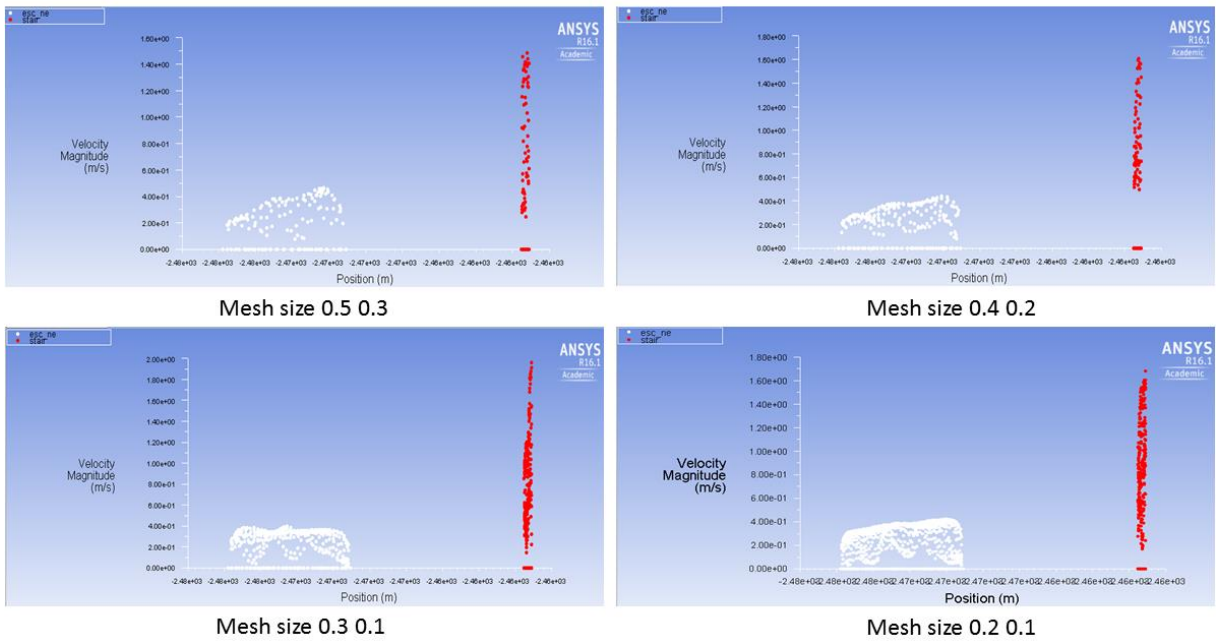

Figure 162: Comparing velocity plot graph at the stairs and the escalator of the NS tunnel for different mesh sizes

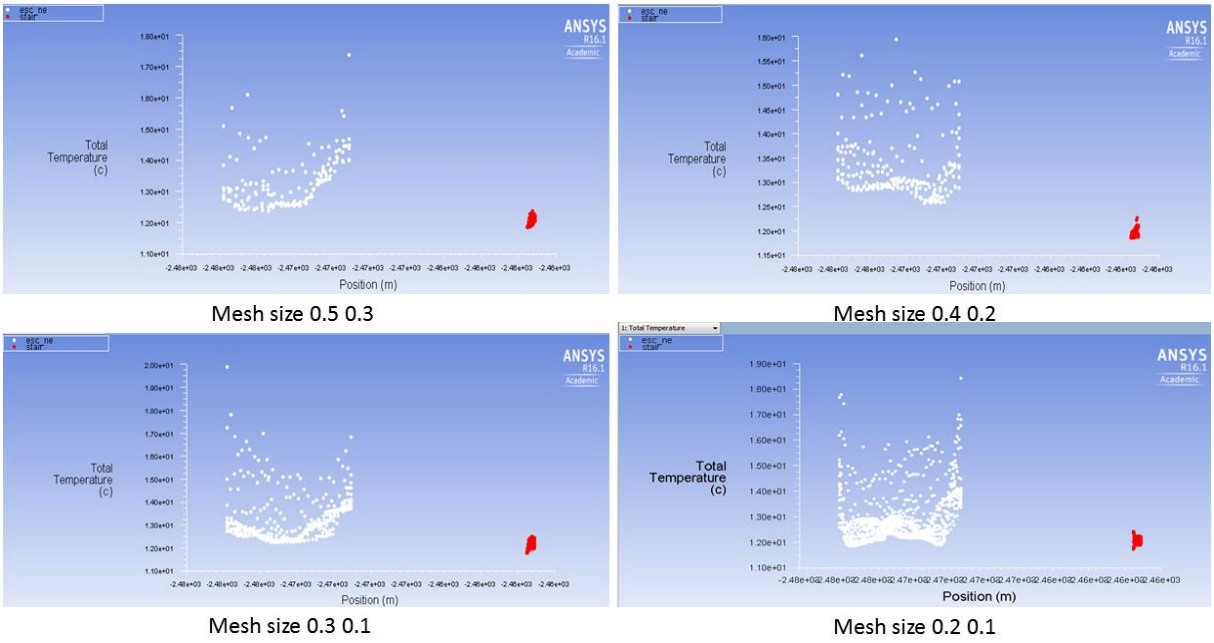

Figure 163: Comparing temperature plot graph at the stairs and the escalator of the NS tunnel for different mesh sizes

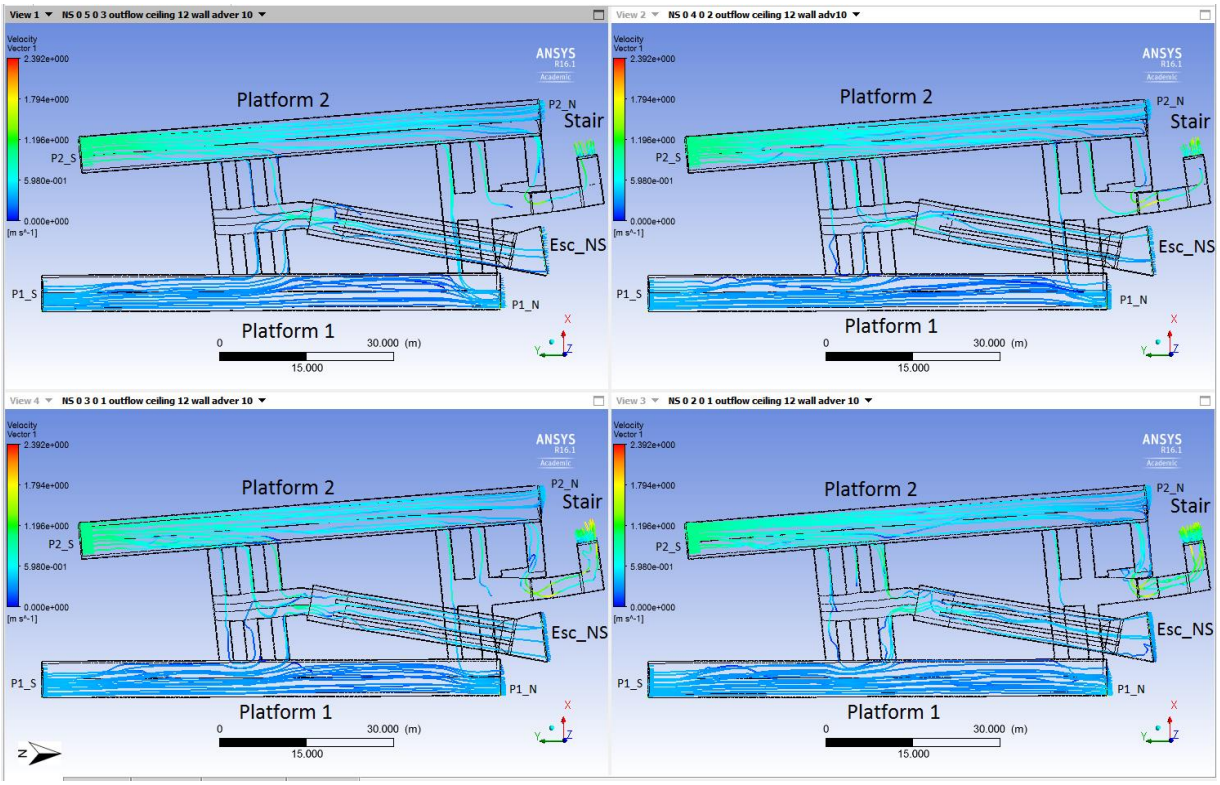

Figure 164: Comparing airflow streamline of the NS tunnel for different mesh sizes (plan elevation)

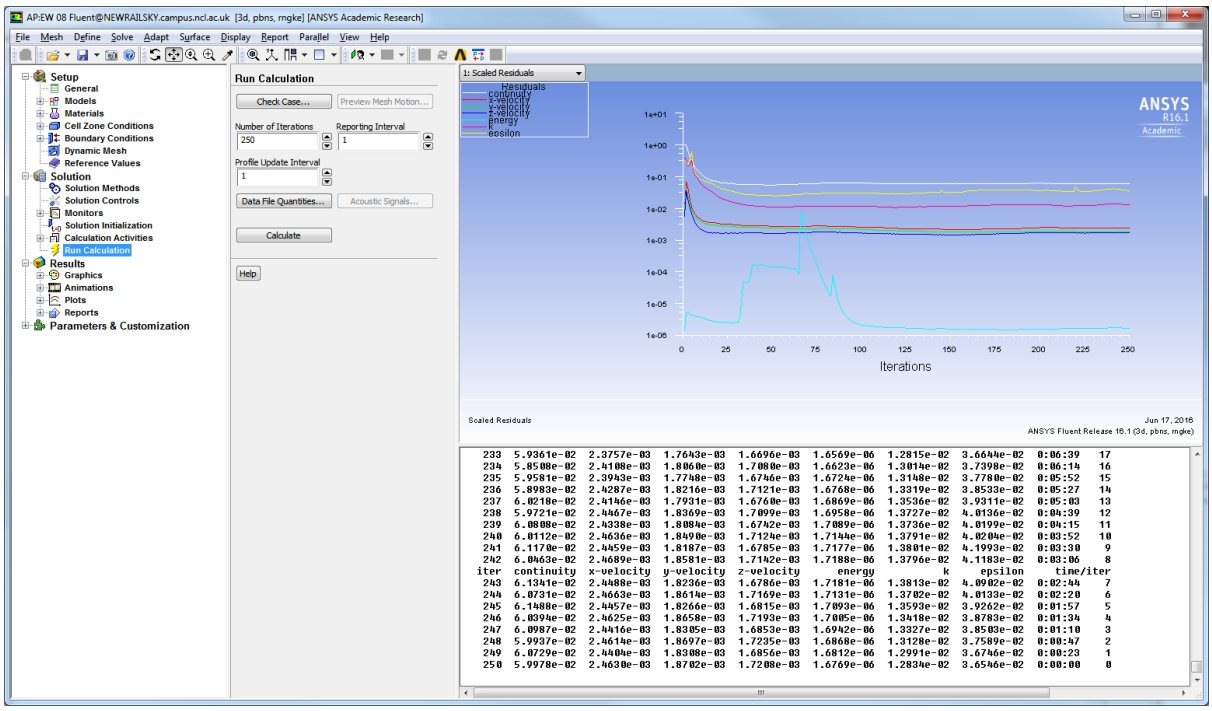

Figure 165: Screenshot of the residuals monitor

Overall, all the simulations reached a stable residual value which indicates the solutions were fully converged and numerically accurate. The residuals were monitored and displayed as shown in Figure 165. In terms of simulation time with simulation time, the mesh size of maximum 0.3 and minimum 0.1 is most appropriate for solving this type of problem so this was applied to the EW tunnel model and the concourse level model in the following section without further verification.

8.3.2 East-West tunnel with escalator

A mesh size of maximum 0.3 m and minimum 0.1 m has been applied to the EW tunnel CFD simulation as shown in Figure 166. Each simulation took 5 hours and the mesh detail is tabulated in Table 26. The airflow measurement conducted in the tracer gas experiments 1 and 3 were used as the boundary conditions for the EW tunnel. These are shown in Table 27 and Table 28 which are subsets of the data shown in Table 22 and Table 23 that are related to simulation of EW tunnel. The boundary condition settings and output values from the simulation are shown in Table 29. The outflow velocities of P3 E of 0.12 m/s, P4 E of 0.12 m/s, Esc EW of 0.2 m/s are very close to the measured average values shown in tables 16 P3 E of 0.1 m/s, P4 E of 0.1 m/s, and Esc_EW of 0.3 m/s. The CFD simulation flow pattern is from the east to west tunnel at 0.4m/s and a strong airflow at the stair of 1m/s was predicted as can be seen from the streamlines shown in Figure 167. The flow direction at platform 3 and 4 is

from east to west is shown in Figure 168. A second outlet from the platform level is from the escalator to the concourse level shown in Figure 169.

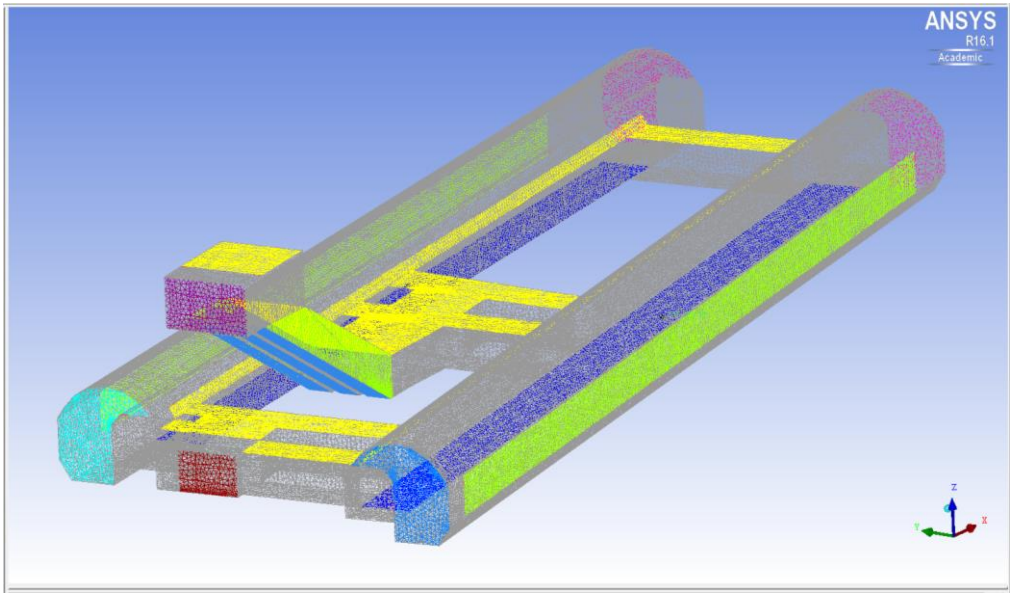

Figure 166: East-West tunnel with escalator in mesh size maximum 0.3 minimum 0.1

Mesh size (m)	max.: 0.5, min.: 0.3
Total mesh:	2,515,061
Simulation time:	5hrs

Table 26: Mesh and simulation time detail of for EW tunnel

Location		Airflow (m/s)	Direction in positive value	Temperature (ºC)
EW tunnel	P3_W	0.4 (0.3-0.5)	E to W	12.9
	P4_W	0.4 (0.3-0.5)	E to W	12.4
	Stair_EW	1 (0.4-1.5)	Up flow	-
	P3 E	-	-	12
	P4 E	-	-	-
	Esc_EW	0.3 (-0.5-0.8)	Up flow	-

Table 27: Average data from tracer gas experiment 1 for EW tunnel CFD simulation

Location		Airflow (m/s)	Direction in positive value	Temperature (ºC)
EW tunnel	P3_W	0.3 (-0.2-0.7)	E to W	12.8
	P4_W	0.4 (-0.1-0.7)	E to W	13.1
	P3_E	0.1/-0.1 (-0.3-0.3)	E to W	12.5
	P4_E	`0.1 (-0.2-0.3)	E to W	-

Table 28: Average data from tracer gas experiment 3 for CFD EW tunnel simulation

Boundary condition in average setting and results:

	Location	Boundary condition	Airflow (m/s)	Temperature (ºC)
EW tunnel	P3_W	Inlet	0.4	12.9
	P4_W	Inlet	0.4	12.4
	Stair_EW	Inlet	1	13
	P3_E	Outflow	0.12	12.7
	P4_E	Outflow	0.12	12.8
	Esc_EW	Outflow	0.2	12.7

Table 29: Simulated inlet and outlet for EW tunnel CFD simulation

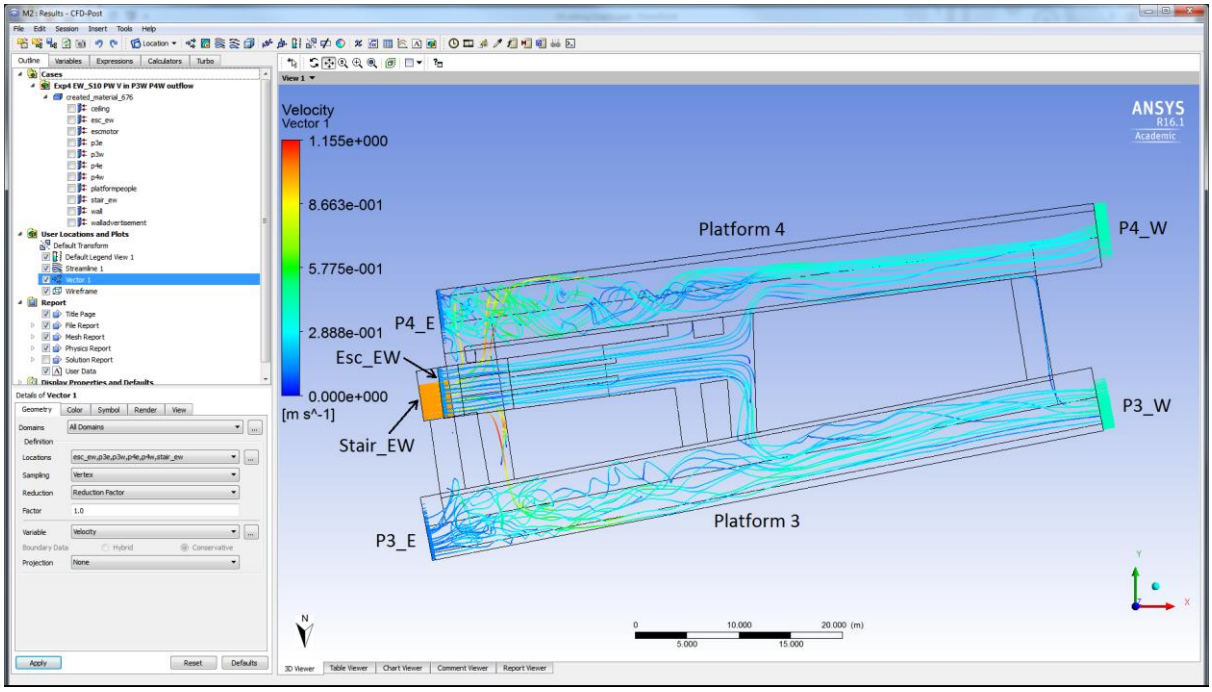

Figure 167: Air flow streamline of East-West tunnel (plan elevation)

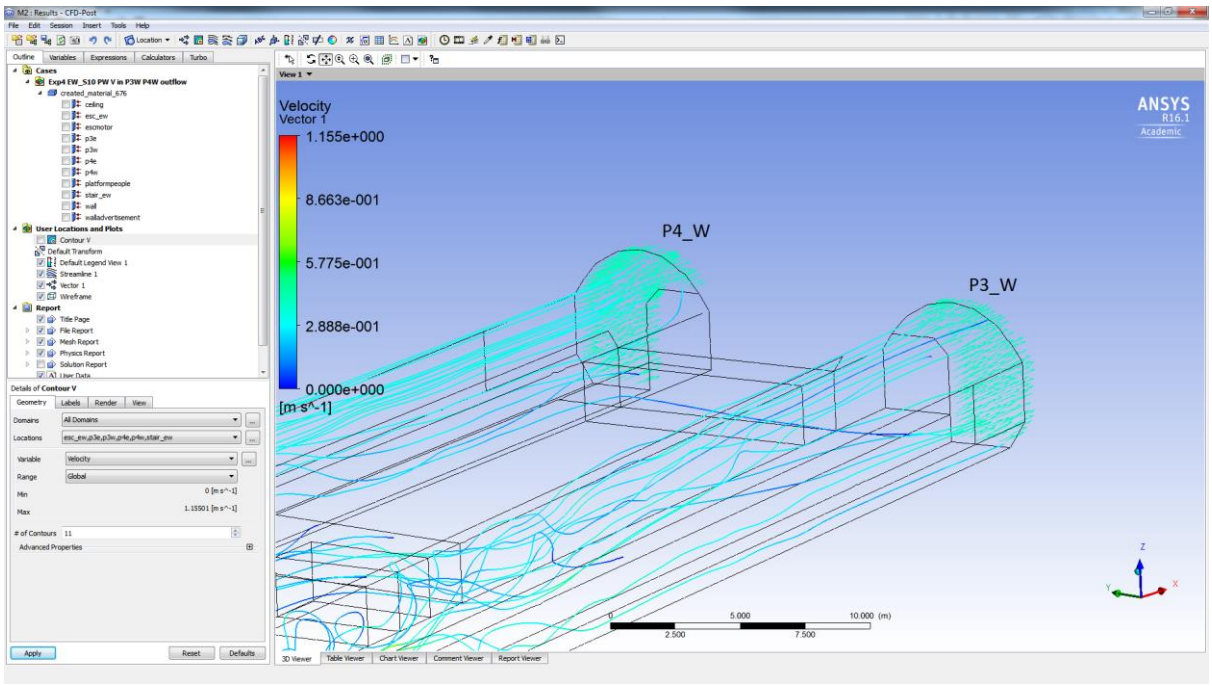

Figure 168: Air flow streamline of East-West tunnel (Inlets: west of platform 3 and 4)

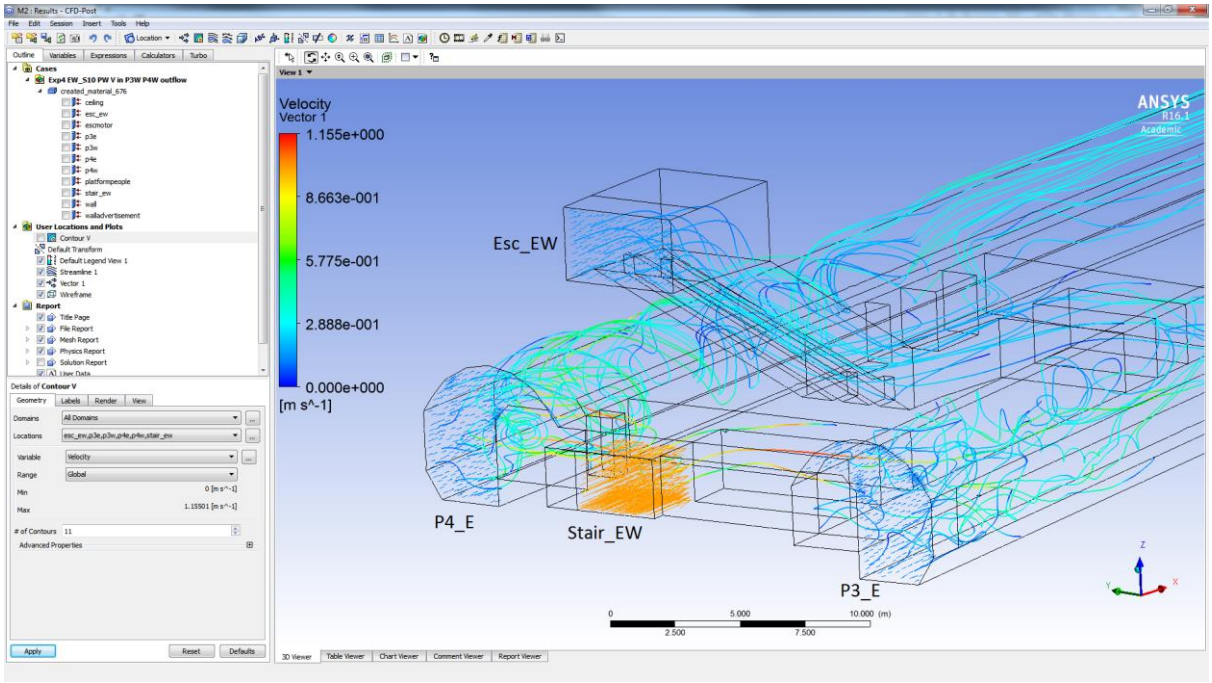

Figure 169: Airflow streamline of East-West tunnel (Inlets: Stair. Outlets: East of platform 3 and 4, escalator)

8.3.3 Concourse level

A single simulation of the concourse took approximately 4 hours with mesh size maximum 0.3 m and minimum 0.1 m. The mesh for this simulation is shown in Figure 170. The mesh detail is listed in Table 30. Table 31 lists the air flow measurements taken during the tracer gas experiment 1 at the concourse level and in Table 32 are listed the simulated inlet and outlet values. This simulation is based on very low air speeds at the station exits. Therefore, this simulation indicates how the exits behave when the main influential factors are from the station and the tunnel. The inlet of this simulation is from the escalators with the outflow through the three exits. These three exits are at a higher level than the concourse, therefor the buoyancy effect and the air flow from the escalators leads the air flow toward the exits as shown in Figure 171. The Exit 1 and Exit 2 have horizontal opening on top of their staircase so the airflow vector is upwards at Exit 1 and 2 as shown in Figure 172. The CFD simulation result at Exit 1 and 2 are all within the measured range and very close to the average of the measurements.

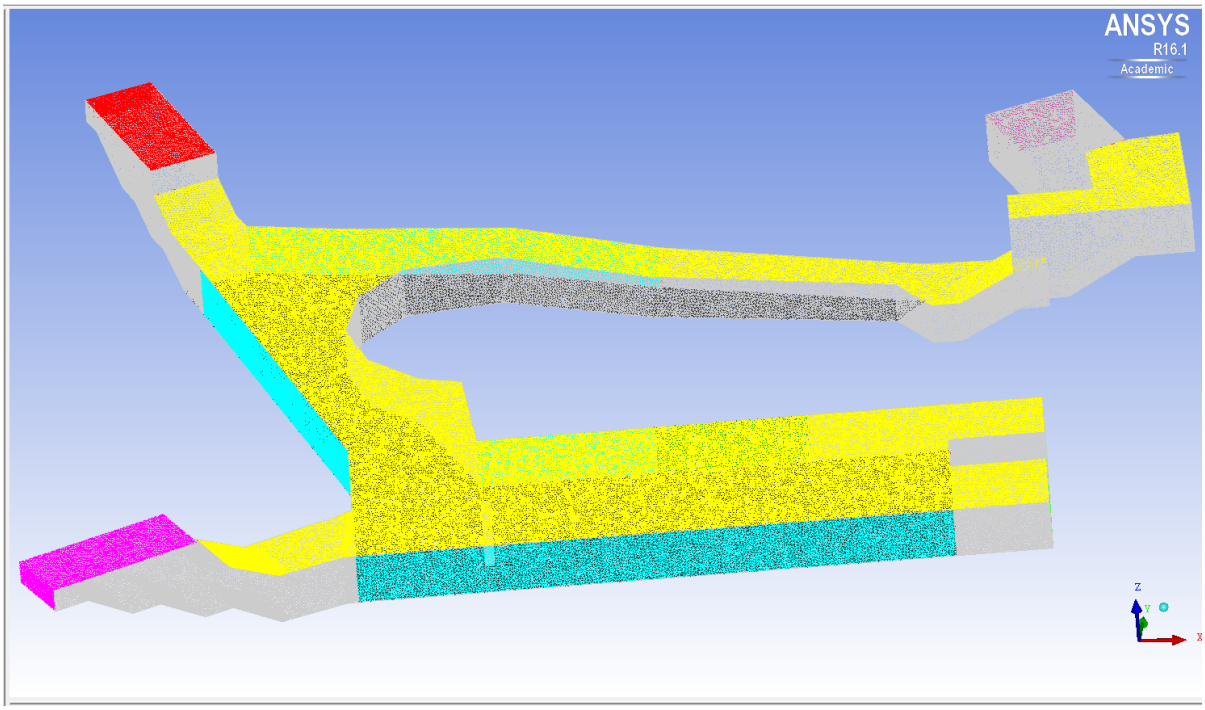

Figure 170: Concourse level with exits in mesh size maximum 0.3 minimum 0.1

Mesh size	max.: 0.3, min.: 0.1
Total mesh:	1,629,881
Simulation time:	4hr

Table 30: Mesh and simulation time detail of for Concourse level

Location		Airflow (m/s)	Direction in positive value	Temperature (°C)
Concourse	Esc_NS	1 (0.5-1.3)	NS to Con	-
	Esc_EW	0.3 (-0.5-0.8)	NS to Con	-
	Exit 1	1 (0.2-2.4)	Outflow	-
	Exit 2	0.5 (-0.3 - 0.9)	Outflow	-
	Exit 3	-	-	-

Table 31: Average data from tracer gas experiment 1 for concourse level

Location		Boundary condition	Airflow (m/s)	Temperature (°C)
Concourse	Esc_NS	Inlet	1	14.5
	Esc_EW	Inlet	0.3	18.5
	Exit 1	outflow	0.5 (0-1.4)	16.5
	Exit 2	outflow	0.4 (0-1)	14.8
	Exit 3	outflow	0.7 (0-1.4)	14.8

Table 32: Simulated inlet and outlet for Concourse level

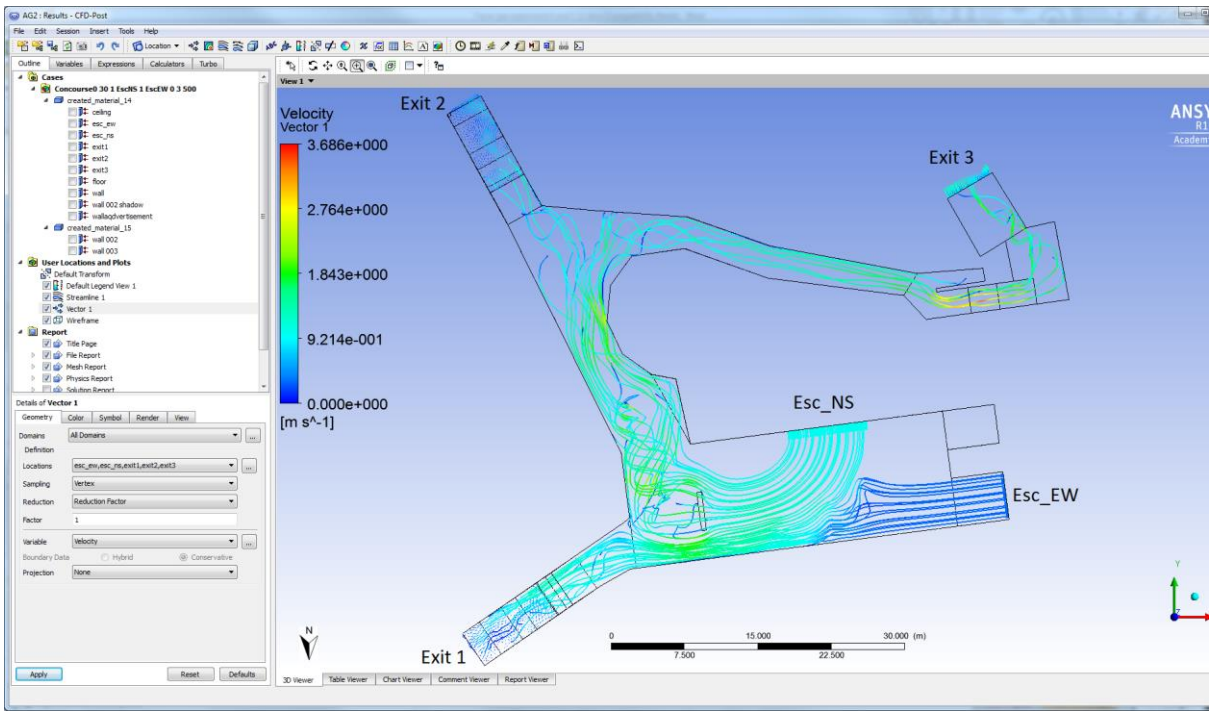

Figure 171: Airflow streamline of Concourse level with exits (plan elevation)

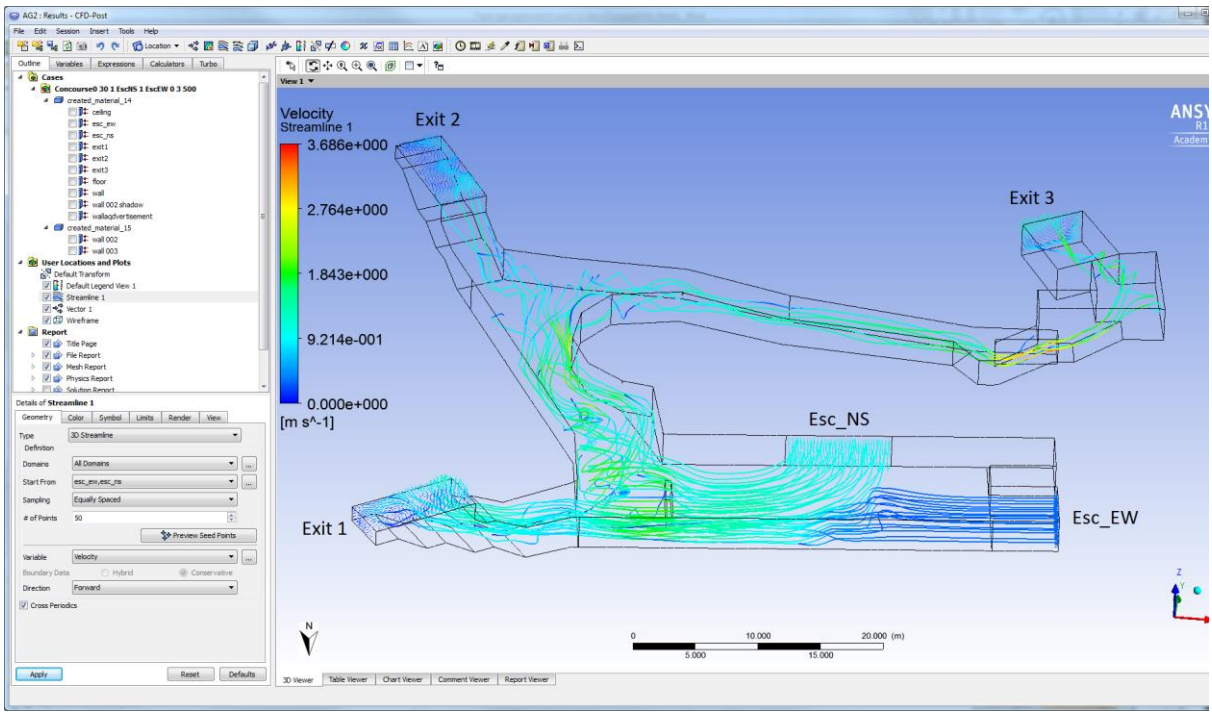

Figure 172: Airflow streamline of Concourse level with exits

8.4 Conclusion

This chapter has presented the preliminary work required to set up a CFD simulation of the Monument station. First, the station was divided into three parts for further simulation based on the geographical level. This division has allowed for the simplification of each model to improve the mesh and CFD simulation quality without unnecessary overlapping at the division boundaries. The value and type of boundary input parameters have been determined and set up as part of this process. This chapter has also shown the method for development of the mesh model and the refinement of the mesh quality which has included defining the mesh size by balancing between mesh quantity, regarding the model size in this research, and the simulation time. The CFD modelling input data was based on the average value obtained from the measurements. Each part of the station CFD model has been validated using the air flow data measured during tracer gas experiments 1 and 3.The outputs are within the range of the measurements and show a good match to the average values hence validating the approach followed. Therefore, it was possible to go to the next step to recreate through simulation the air flow condition when the tracer gas experiment 1 was conducted and to take this further by investigating the sensitivity of the air flow to

train movement and changes in the external weather condition. This is described and discussed in the next chapter.

Chapter 9. Air Flow Sensitivity Analysis and Evacuation Simulation

9.1 Introduction

Three parts of station CFD model have been established and validated using the measurement data as discussed in Chapter 8. As mentioned earlier (Chapter 7.2 and Chapter 8.2), a common strategy used in CFD codes for steady problems is to solve the unsteady equations and march in time as a steady state. A steady flow analysis is performed only when successive unsteady solutions do not change over a very short time range. The steady flow case is usually established by examining the velocity variation from case to case as the air flow in the tunnels and the station is more sensitive to changes than is the temperature variable even in similar weather conditions. This chapter introduces an initial validation of the CFD model, which has been performed by recreating the conditions that existed when the tracer gas tests were performed. To further understand the air flow behaviour in the station over longer time period, further CFD modelling at each part of the station has been performed to determine the degree of sensitivity of the internal air flow to changes in external conditions. The final part of this chapter considers a pedestrian evacuation simulation to establish the degree to which train passengers would be affected by a gas release in the station. Three different scenarios are considered that differ by the number of trains and passengers that are in the station at the beginning of the evacuation.

9.2 Recreating the tracer gas experiment 1 air flow environment

The airflow speed is a very sensitive input parameter as it drives through the station controlling the airflow patterns inside. The airflow velocity measured varied from 0 to 1m/s at the tunnel and 0.5 to 2 m/s at the exits over short time intervals as the ultra-sonic anemometer measurements graphs taken from the tracer gas experiments show in Chapter 6. This is examined in this section in which each part of the station is simulated over a shorter time range typical of the tracer gas release time in order to recreate the air flow conditions when the gas was released. This also acts as a further validation of the CFD model. Location of the measurement instruments in Monument Station for tracer gas Experiment 1 can be found in Figure 53 in Chapter 6.

9.2.1 North-South tunnel with escalator and stairs

The gas was released from 02:29:00 to 02:33:13 on 22.02.2014 at the NS tunnel at platform 1. The assumption of average uniform air flow when the gas was released as an inlet boundary condition and the simulated outflow at other boundaries is listed in Table 33. As Figure 173 shows the air flow is from the south tunnel at both platforms towards the north. The air enters platform 1 at around 0.7m/s and flows out with a velocity around 0.5m/s. The distance between the SF_6 gas release point and sensor 11 is around 40m. The SF_6 sensor 11 stared to detect the presence of the gas around 1 minute 30 seconds after the gas was released. After a very short time sensors 13 and 14 also reacted as shown in Figure 174 (a copy of Figure 60 from Chapter 6). The CFD results of airflow velocity and direction closely follow the measured SF_6 sensor concentration results.

Boundary Name	Boundary condition	Velocity (m/s)
P1_S	Inlet	0.6
P2_S	Inlet	0.9
P1_N	Outflow	0.4
P2_N	Outflow	0.6
Stair_NS	Outflow	1
Esc_NS	Outflow	0.9

Table 33: Simulated inlet and outlet average value of NS tunnel

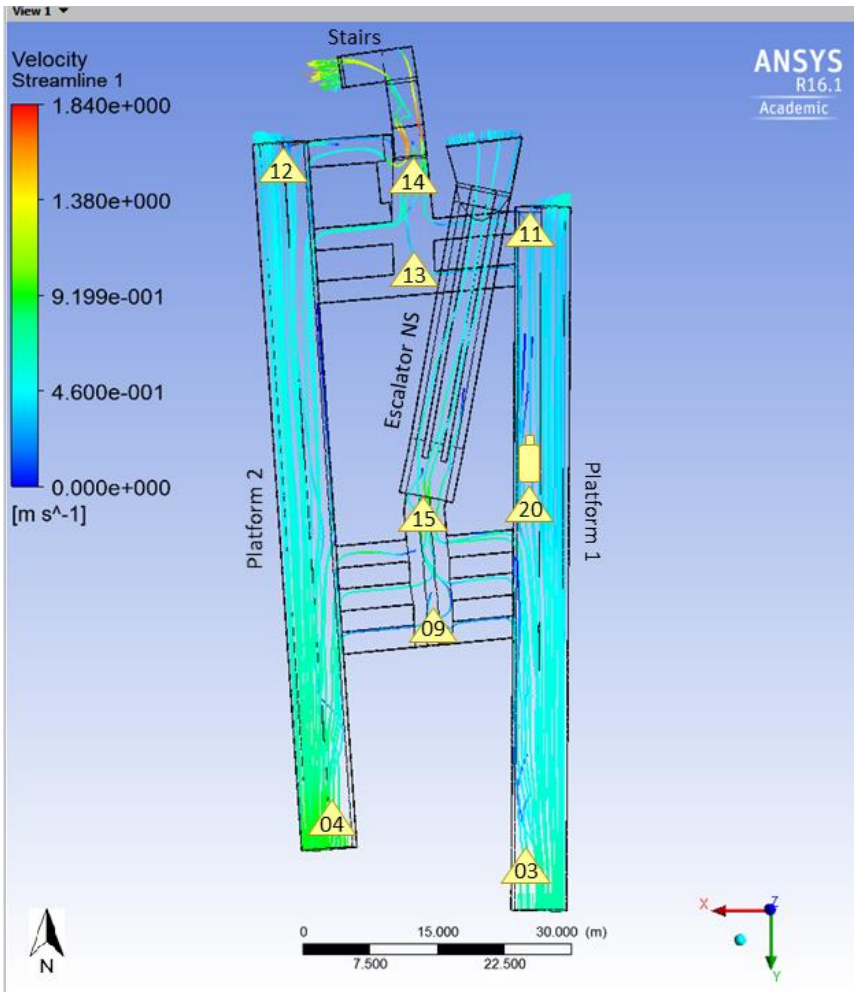

Figure 173: Airflow streamline of NS tunnel

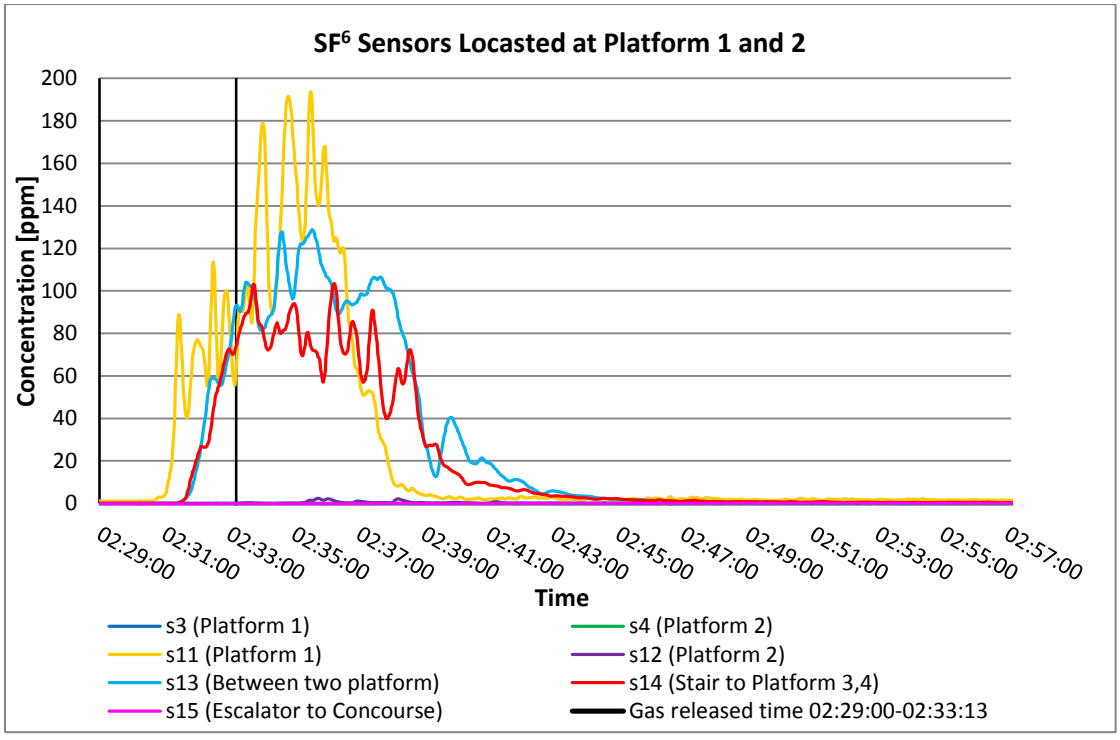

Figure 174: SF_6 concentration at platform 1 and 2 of tracer gas experiment 1 (Copy of Figure 54 from Chapter 6)

9.2.2 East-West tunnel with escalator

After around 1mins 30 seconds the tracer gas was detected at the EW tunnel. As shown in Table 34, air flow from both tunnels was from east to west with similar velocities. Two different scenarios were considered with the velocities close to 0.4m/s (Scenario A) and 0.3m/s (Scenario B) respectively that differed with regard to the air flow at the stair case linking the two platform levels. The airflow from the stair was from the NS tunnel towards the EW tunnel at a speed of 1.5m/s (Scenario A) and 0.5m/s (Scenario B) respectively. As shown in Chapter 6, Figure 55, the air flow at the escalator at the EW tunnel had a reversed flow direction. Therefore, air flow from EW towards the concourse averaged around 0.3 m/s (Scenario A) and the reversed flow upto -0.4 m/s (Scenario B).

The Scenario A flow pattern is shown in the Figure 175 which shows the airflow streamlines alongside the SF_6 sensors concentration graph, Figure 177 (a copy of Figure 61 from Chapter 6). The SF_6 entered the EW level by the staircase and was then distributed through the connecting area to both tunnel and platforms. The Scenario B streamlines are shown in Figure 176. In this case, the stairwell had a lower flow velocity and airflow pattern was reversed at the escalator that now flows from the escalators down to the platforms. This causes the SF_6 concentration fluctuations shown in Figure 173 even though the reverse flow pattern is relatively steady. Table 34 also contains temperature variations in both scenarios at each boundary. As discussed earlier, the variation and differences are very small and the focus is on the air flow velocity and flow pattern in the later discussions.

	Scenario A			Scenario B		
Boundary Name	Boundary condition	Velocity (m/s)	Temperature (°C)	Boundary condition	Velocity (m/s)	Temperature (°C)
P3_W	Inlet	-0.4	12.9	Inlet	-0.3	12.9
P4_W	Inlet	-0.4	12.4	Inlet	-0.3	12.4
Stair_EW	Inlet	1	13	Inlet	0.4	12.6
P3_E	Outflow	0.12	12.7	Outflow	0.02	13.7
P4_E	Outflow	0.12	12.8	Outflow	0.1	12.7
Esc_EW	Outflow	0.3	12.7	Inlet	-0.4	13.2

Table 34: Simulated inlet and outlet average value of EW tunnel

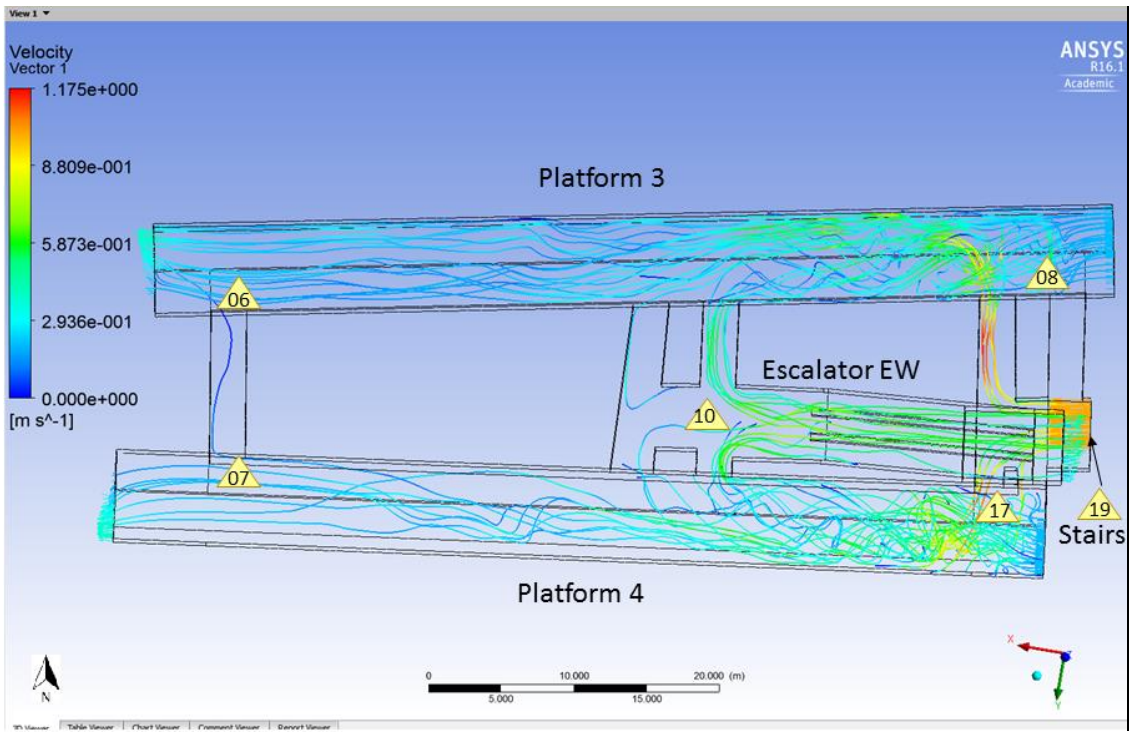

Figure 175: Scenario A air flow streamline of EW tunnel

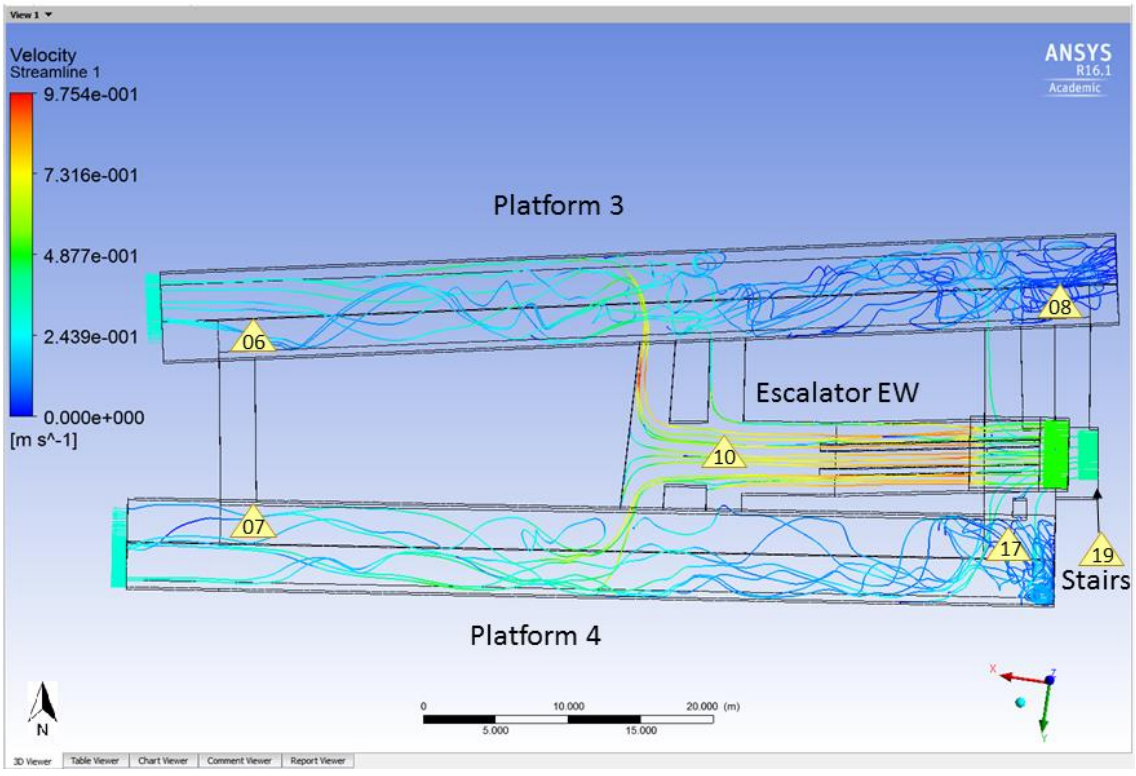

Figure 176: Scenario B air flow streamline of EW tunnel

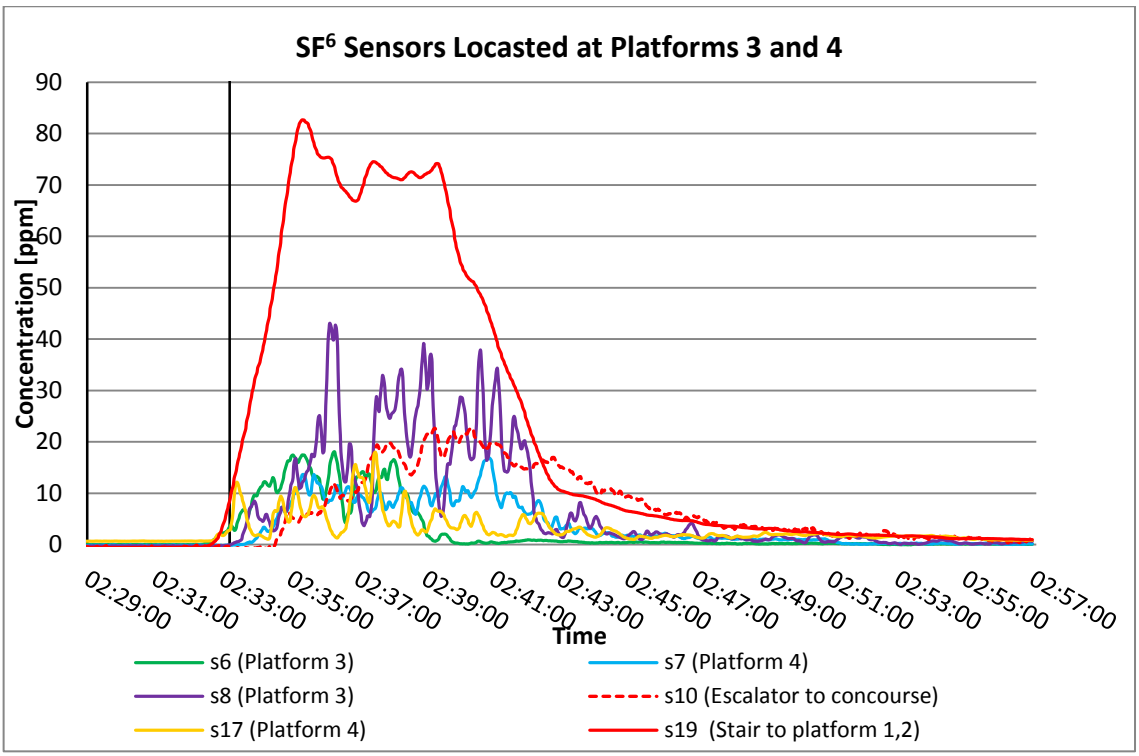

Figure 177: SF_6 concentration at platform 3 and 4 of tracer gas experiment 1 (Copy of Figure 62 from Chapter 6)

9.2.3 Concourse Level

The tracer gas entered the concourse area through the escalator from the EW platforms at around 02:34 2on 2/02/2014. As discussed the airflow was stable from the NS tunnel to the concourse area though the EW escalator airflow was reversed. The CFD simulation at the concourse area also had two possible scenarios of input as shown in Table 35. These two possible airflow patterns were mainly derived by the weather condition outside the station during the gas dispersion. The weather data was obtained from the weather station between 02:30:06 and 02:45:04 on the night of 22/02/2014. This is listed in Table 36.

Scenario A			Scenario B		
Boundary Name	Boundary condition	Velocity (m/s)	Boundary Name	Boundary condition	Velocity (m/s)
Esc_NS	Inlet	1	Esc_NS	Inlet	1
Esc_EW	Inlet	0.3	Esc_EW	Inlet	-0.4
Exit 1	Outflow	0.4	Exit 1	Outflow	0.6
Exit 2	Outflow	0.4	Exit 2	Inlet	-0.4
Exit 3	Outflow	0.6	Exit 3	Outflow	0.3

Table 35: Simulated inlet and outlet average value of concourse level

Date	Time	Wind speed (m/s)	Wind gust (m/s)	Direction (degree)	Air temperature (oC)	Humidity (%rh)	Pressure (mb)
22/02/2014	02:30:06	1.73	3.53	304	6.77	69.34	983.45
22/02/2014	02:45:04	0.59	2.07	230	6.81	69.23	983.54

Table 36: Weather condition during tracer gas experiment 1

The boundary conditions at the station exits were based on the values obtained from the Microclimate CFD simulation described in Chapter 7, Table 17 using the weather station data that was closest to the actual condition on the night of the experiment. These were wind directions of WNW 292.5 degrees (Scenario A) and SW 225 degrees (Scenario B). Figure 178 shows the Microclimate CFD simulation at wind direction WNW 292.5 and Figure 180 simulation at wind direction SW 225. In both cases, the wind speed was 1m/s. However, in the case of Scenario A it can be seen in Figure 178 that the three exits experienced a negative wind pressure when the wind direction was from the WNW resulting in the exits all having outflows. This is in agreement with the results of the tracer gas experiment 1. The airflow direction is consistent with the flow from the station being towards the outside. As Figure 179 shows the air flow at Exit 1 was from the station to the outside at a speed of 0.2 m/s to 2.3 m/s.

In the case of Scenario B, when the airflow was from the SW into Exit 2 the flow was into in Figure 180. The results from the microclimate simulation have been used to define the boundary conditions in this case because the measurements were not taken on the night of the tracer gas experiments. The minimum wind speed was around 0.59 m/s and the maximum speed 2.07 m/s as shown in Figure 181. Therefore, from the results of the microclimate CFD simulation it can be determined that the air flow speed at exit 2 was between 0.4 m/s to 1.6 m/s directed into the station. The airflow at Exit 1 that was measured on the night of the experiment was very close to the value predicted. This is another good validation of the microclimate CFD result.

The airflow at Exit 2 in the real weather condition could be a highly fluctuating flow as mentioned in Chapter 5. Therefore, at Exit 2 a minimum flow velocity of 0.4 m/s was used in both CFD scenarios but in different directions. In Scenario A the flow direction was from the station to the outside and in Scenario B the flow was reversed.

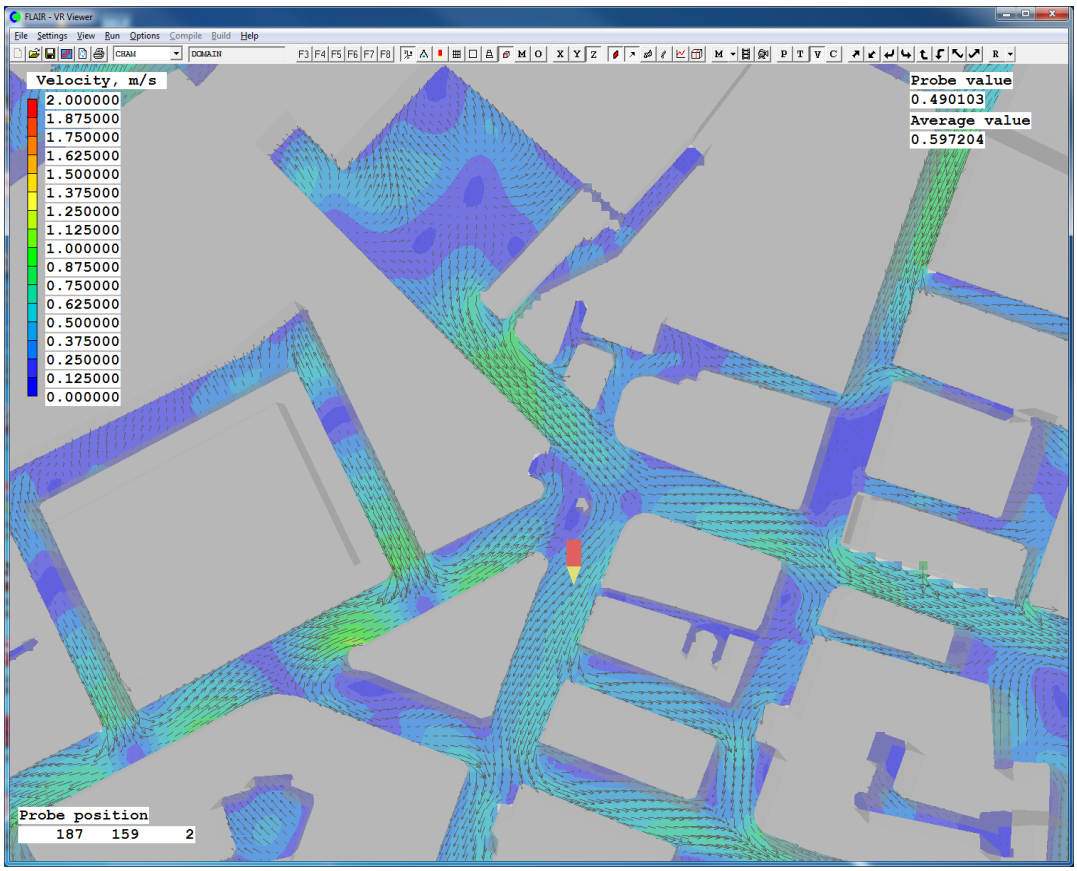

Figure 178: Microclimate CFD results at Exit 2 (Wind input from WNW 292.5 degree, speed at 1 m/s)

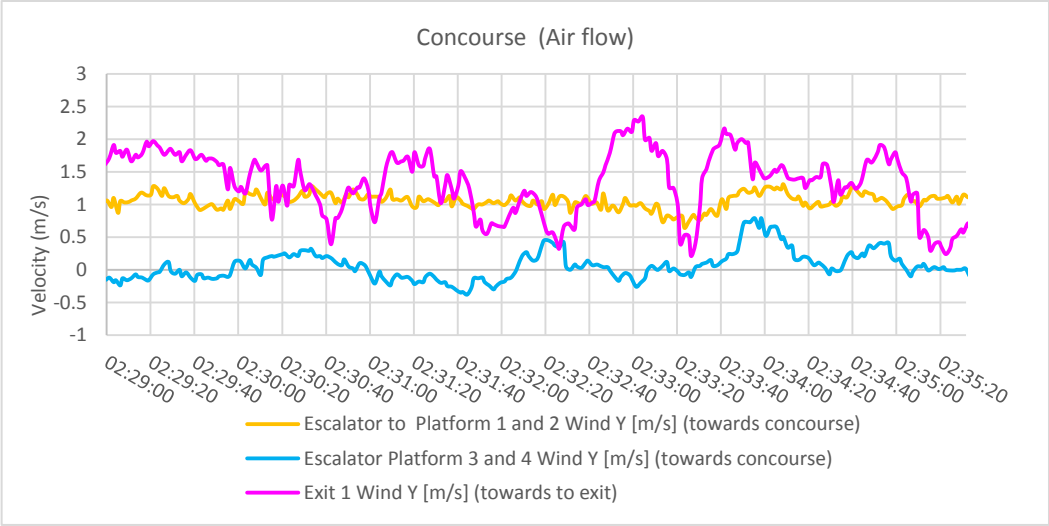

Figure 179: Tracer gas experiment 1 ultrasonic anemometer air flow result at concourse area (copy of Figure 57 from Chapter 6)

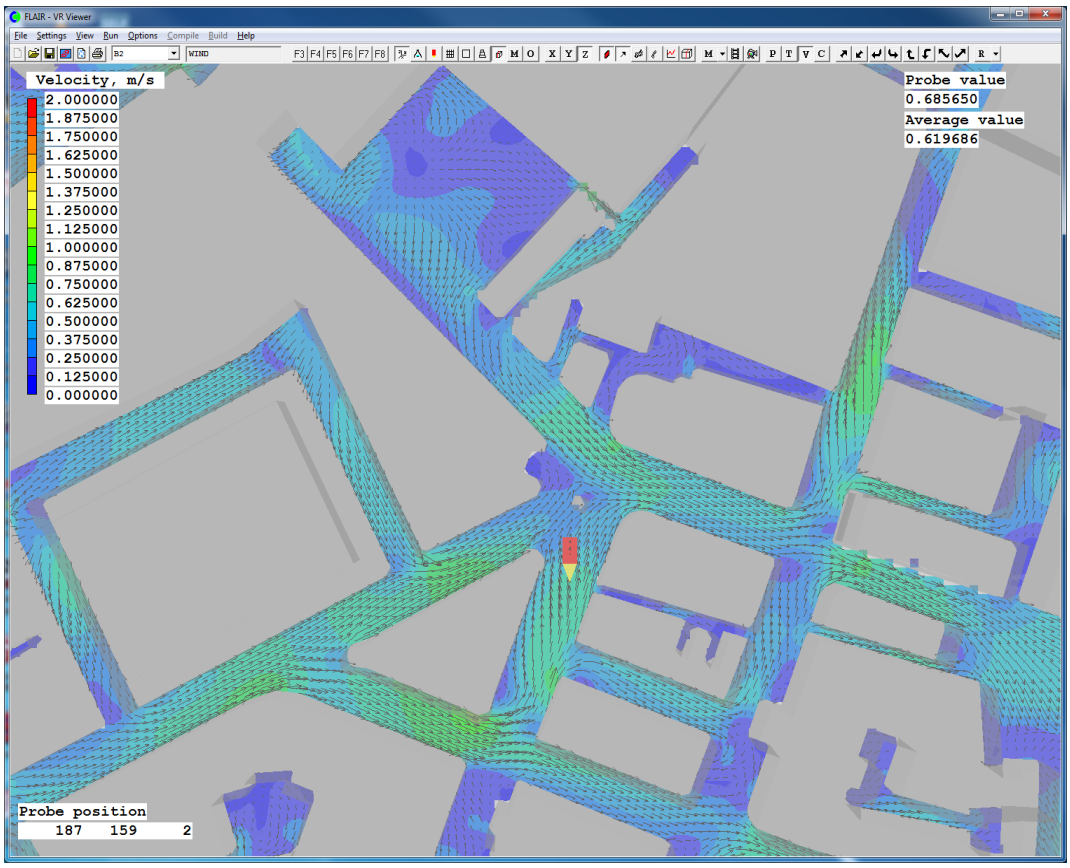

Figure 180: Microclimate CFD results at Exit 2 (Wind input from SW 225 degree, speed at 1 m/s)

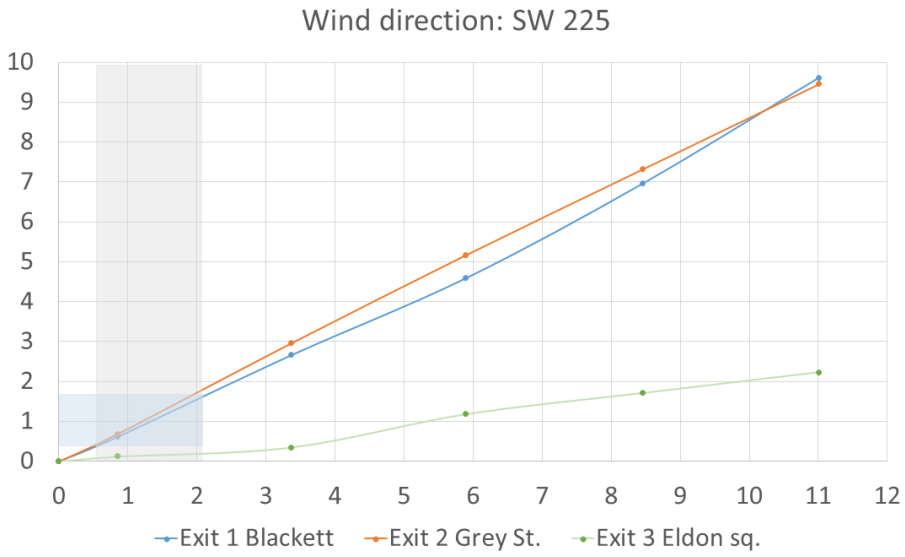

Figure 181: Wind simulation and prediction diagram in wind direction SW 225 from Microclimate CFD simulation

The CFD simulation of these two patterns is shown in Figure 182 and Figure 183. The tracer gas was distributed to all of the concourse area and to the three exits from the escalators when the three exits were all experiencing outflows (Scenario A). The airflow at exit 3 is seen to be disturbed by the reversed flow at exit 2 shown as Scenario

B in Figure 183 but the direction at this exit is still outwards. The tracer gas concertation results are shown in Figure 184. All the sensors at the three exits detected tracer gas but that at exit 2 showed a large variation due to the effect of the reversed flow. The simulated airflow velocities did predict the same SF_6 transit times that were recorded on the night of the tracer gas experiments.

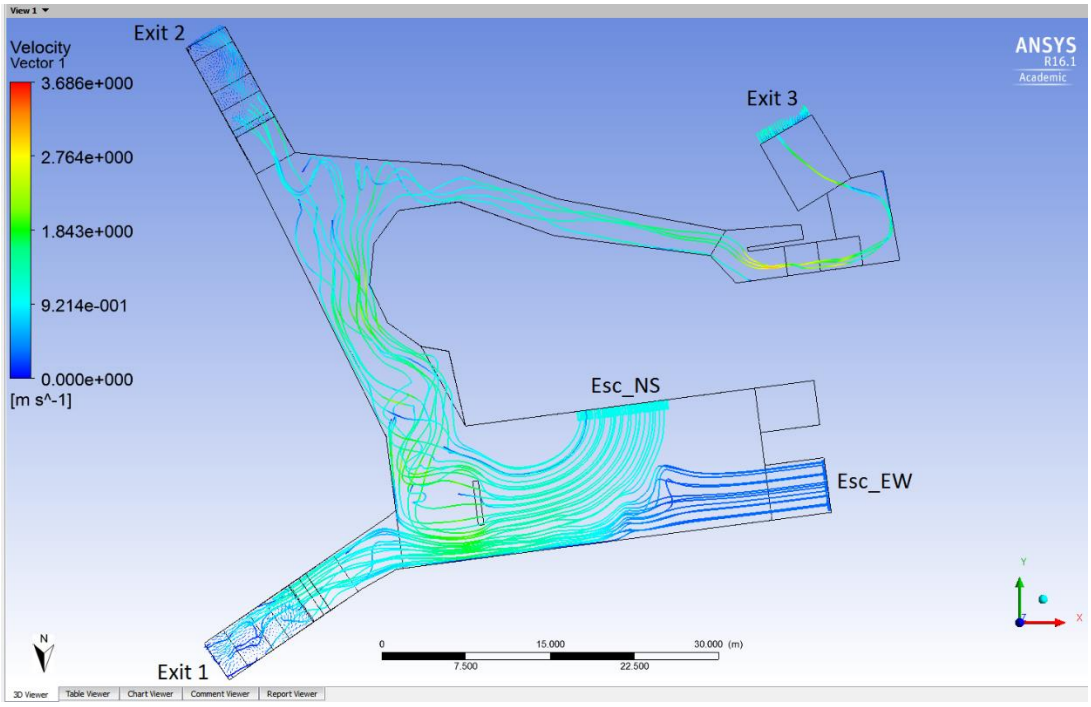

Figure 182: Scenario A air flow streamline at the concourse level

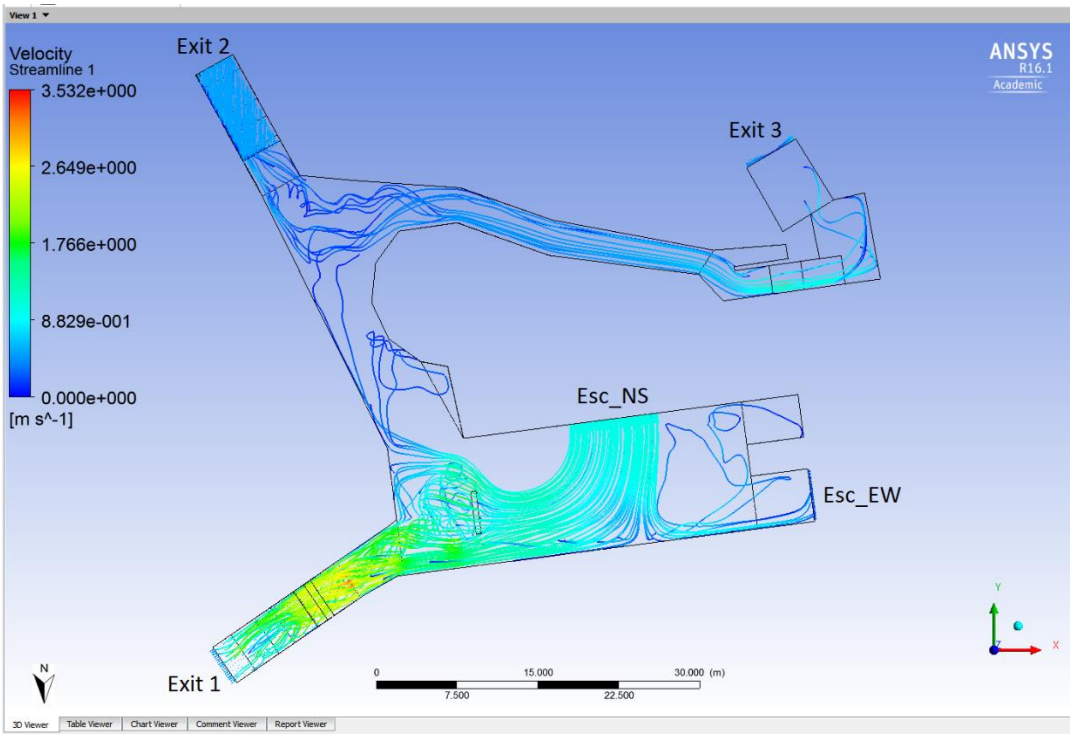

Figure 183: Scenario B air flow streamline of concourse level

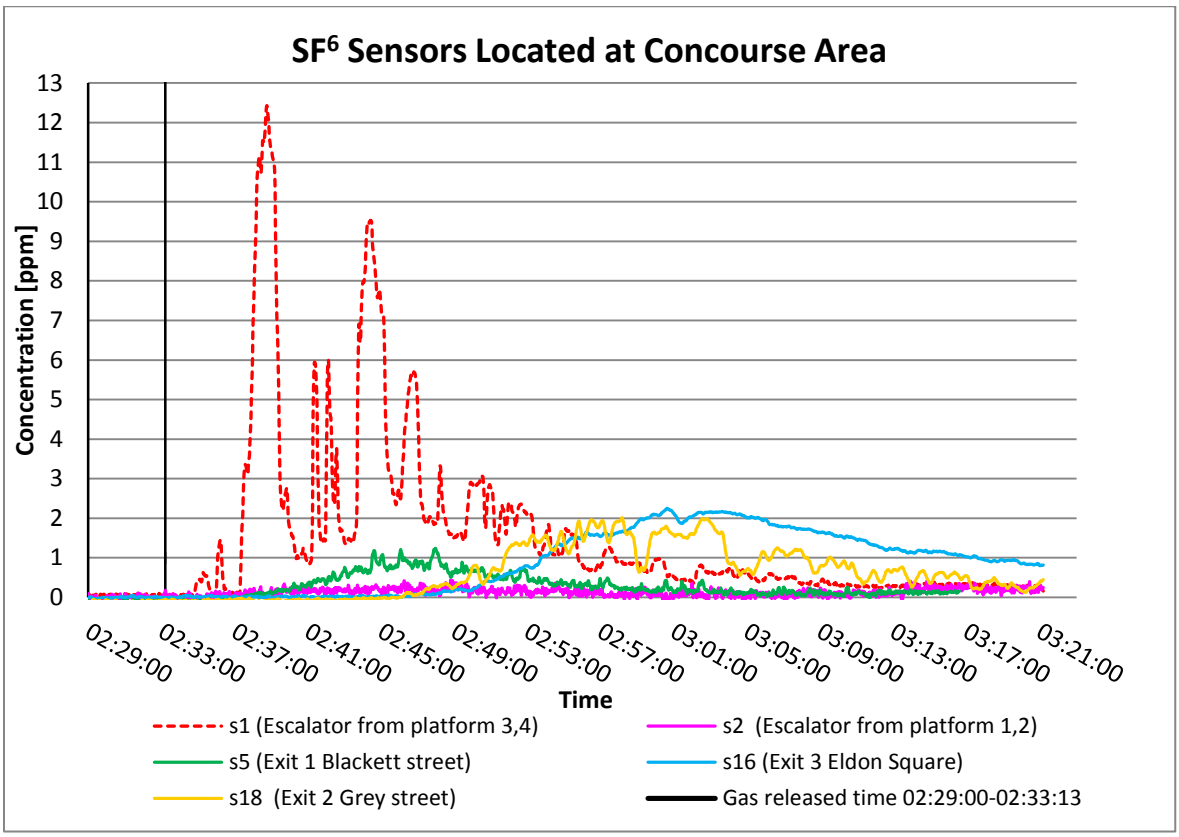

Figure 184: SF_6 concentration at the concourse level for tracer gas experiment 1 (Copy of Figure 63 from Chapter 6)

9.3 Sensitivity CFD simulation

The previous section produced the simulation results with velocity levels determined from the average values of the measured data. The tracer gas experiments were also simulated to produce a general overview model of the station. These models were all produced with steady flow as a boundary condition but throughout the time that the experimental work was being performed it was noticeable that the air velocity exhibited a degree of unsteadiness at the measurement points. The purpose of this section is to consider how sensitive the internal air flow is to variations in the external air velocity i.e. to determine if the internal flow is stable over a wide range of velocity conditions and what these conditions are.

To simulate the possible air flow patterns this section uses data taken from earlier air flow measurements (Pflitsch, 2012) that showed flow reversals in the station. The air flow and gas dispersion could be calculated from the air flow speed and the distance from the source of gas release to each exit. The gas source could be at any point of the station so the dispersion pattern could be totally different depending on the location of the source even in the same overall air flow condition. So the key to the provision of a prevention strategy or ventilation solution is to fully understand the flow pattern in the variable condition.

9.3.1 Sensitivity CFD simulation of North-South tunnel:

In this section, eight different air flow cases that are combinations of the different flow regimes observed in the earlier tests are simulated. The air flows studied consist of five cases having variable inlet velocity at the south of platform 1 and 2 with combinations of maximum and minimum velocities taken from the measurement reported in Chapters 5 and 6 without train operation. The remaining 3 cases simulated the flow pattern during the train operational period. These conditions are shown in Table 37. As discussed earlier the CFD simulation temperature change was very small and the air flow pattern and velocity showed larger variation, therefore this section focus on the air flow pattern and velocity variations. The NS tunnel is approximately 80m long and the EW tunnel approximately 70m. The dispersion time of a toxic agent can be determined from time of flight calculations based on the average air flow speed.

Simulation Case	Condition variables	
NS_S01	At operation break	Both platform at minimum background airflow
NS_S02	At operation break	Both platform at maximum background airflow
NS_S03	At operation break	Platform 1 at min. and platform 2 at max. background airflow
NS_S04	At operation break	Platform 1 at max. and platform 2 at min. background airflow
NS_S05	At operation break	Platform 1 at revere airflow and platform 2 at average background airflow
NS_S06	At operation time	When train come at platform 1 and no train at platform 2
NS_S07	At operation time	When train come at platform 2 and no train at platform 1
NS_S08	At operation time	When train come at both platform 1 and 2 (from opposite direction)

Table 37: Variables of case simulated at the North-South tunnel CFD model

NS_S01 simulated minimum and NS_S02 maximum background airflow at both platform at operation break.

Simulation Case NS_S01 and Case NS_S02 has simulated the air flow from the south tunnel to the north tunnel with different background air flow values from minimum to maximum values as shown in Table 38. The stream line flow patterns resulting from this simulation are shown in Figure 185 and Figure 186 which show similar features. The streamlines which are mainly from the south tunnel to the north tunnel, towards the concourse through the escalator and then through the stairs to the EW platforms are clearly shown in these two cases. The air flow from the south tunnel is very similar although that at platform 2 it is slightly higher than that at platform 1. There is evidence of very small flow between the different platforms. The contaminated area is highly dependent on the location of the source. The streamlines indicate the dispersion path. If the source was on one of the platforms the gas would disperse to the concourse or EW tunnel through escalators and stairs. If the gas was released at the south end of the platform it could be spread to the concourse and EW tunnel after 5 minutes in the case of a minimum velocity and 1.5 minutes at maximum velocity.

Case NS_S01			Case NS_S02		
Boundary Name	Boundary condition	Velocity (m/s)	Boundary Name	Boundary condition	Velocity (m/s)
P1_S	Inlet	0.1	P1_S	Inlet	0.8
P2_S	Inlet	0.5	P2_S	Inlet	1.3
P1_N	Outflow	0.2	P1_N	Outflow	0.74
P2_N	Outflow	0.18	P2_N	Outflow	0.65
Stair_NS	Outflow	0.45	Stair_NS	Outflow	1.3
Esc_NS	Outflow	0.16	Esc_NS	Outflow	0.6

Table 38: Boundary conditions and outflow average value of simulation case NS_S01 and NS_S02

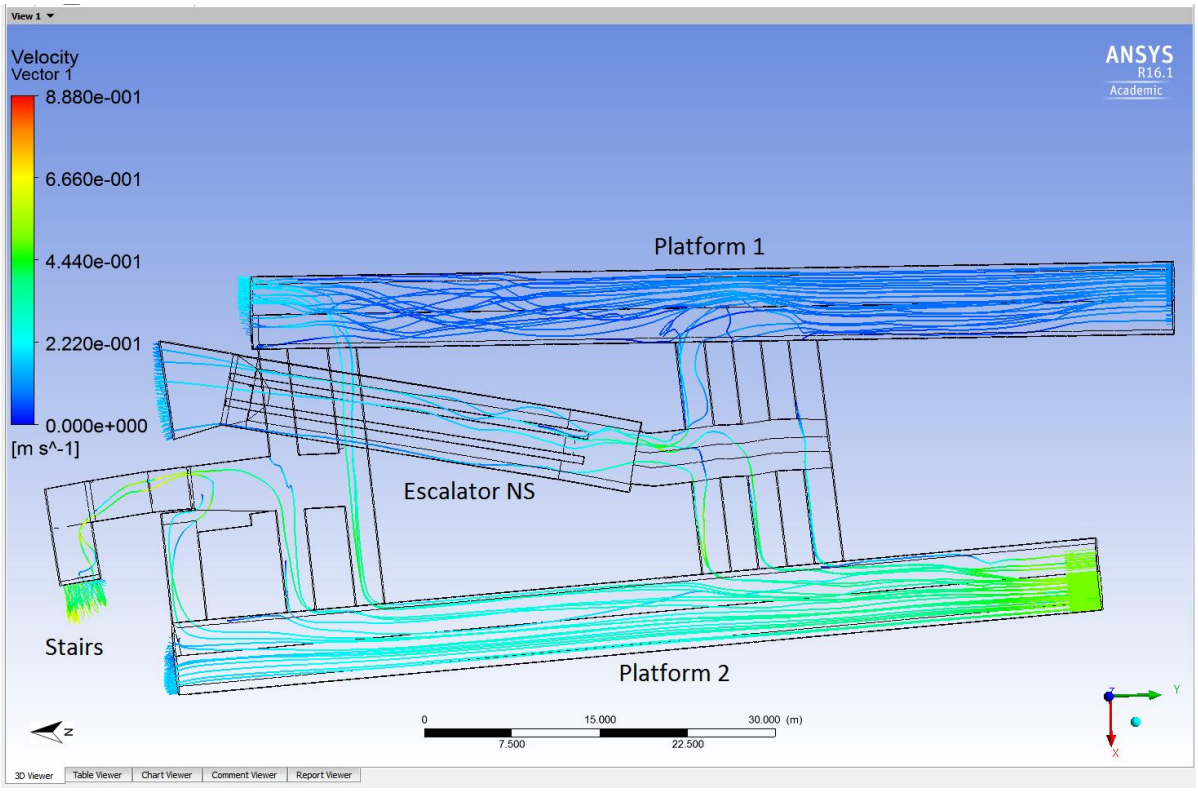

Figure 185: Simulation case NS_S01 air flow streamline of NS tunnel (plan elevation)

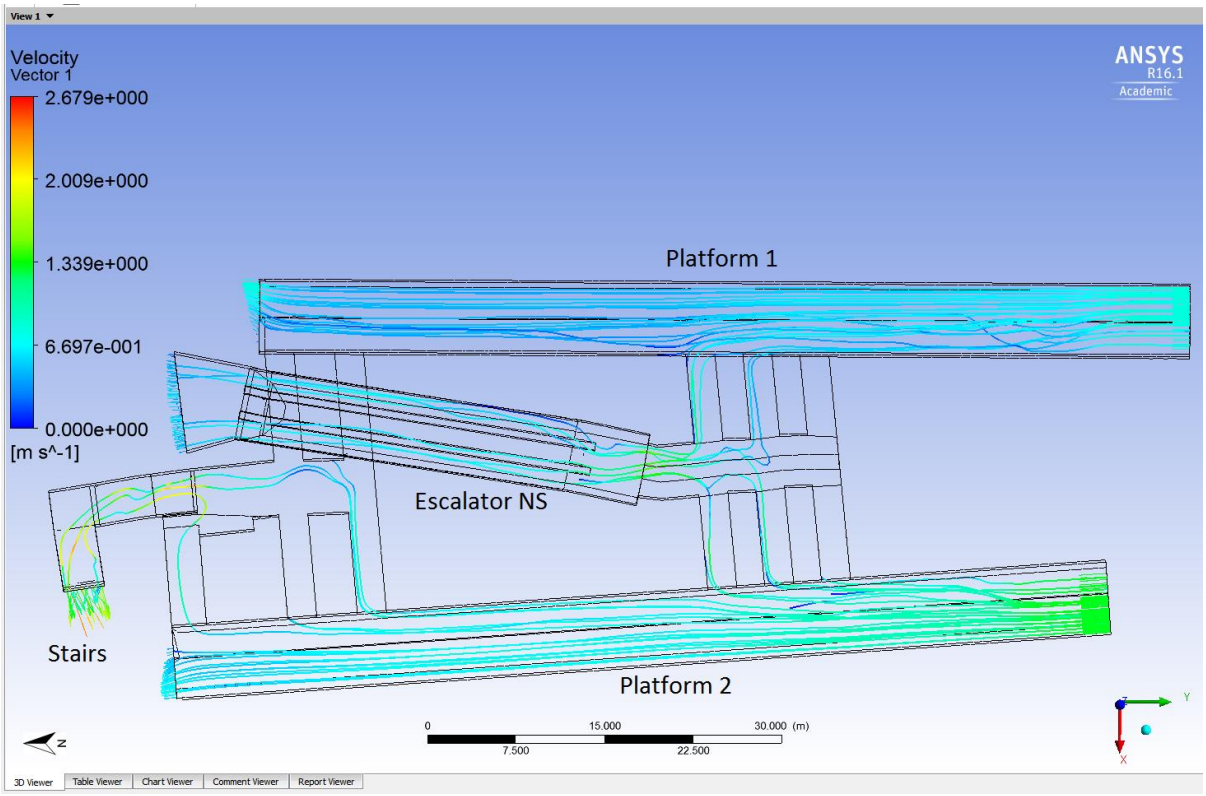

Figure 186: Simulation case NS_S02 air flow streamline of NS tunnel (plan elevation)

NS_S03 and NS_S04 are simulated when platform 1 at maximum/minimum and platform 2 at maximum/minimum background airflow at operation break.

Simulation Case NS_S03 and Case NS_S04 present the case when one tunnel has the minimum and the other have the maximum background velocity as the inlet setting shown in Table 39. In this case there is a stronger exchange between the platforms which is in the reverse direction of the previous cases. Outlet flows at the north of the tunnel are very similar. The flow pattern at the escalator and stairs are the same as the previous case as shown in Figure 187 and Figure 188. In these two case, the gas has the potential to spread to most areas of the tunnel then towards the EW tunnel and the concourse level. The gas will spread throughout the station within 2 minutes if it was released at the platform with the stronger air flow.

Case NS_S03			Case NS_S04		
Boundary Name	Boundary condition	Velocity (m/s)	Boundary Name	Boundary condition	Velocity (m/s)
P1_S	Inlet	0.1	P1_S	Inlet	1.3
P2_S	Inlet	1.3	P2_S	Inlet	0.1
P1_N	Outflow	0.6	P1_N	Outflow	0.6
P2_N	Outflow	0.5	P2_N	Outflow	0.5
Stair_NS	Outflow	1	Stair_NS	Outflow	0.8
Esc_NS	Outflow	0.4	Esc_NS	Outflow	0.5

Table 39: Velocity boundary conditions for NS_S03 and NS_S04

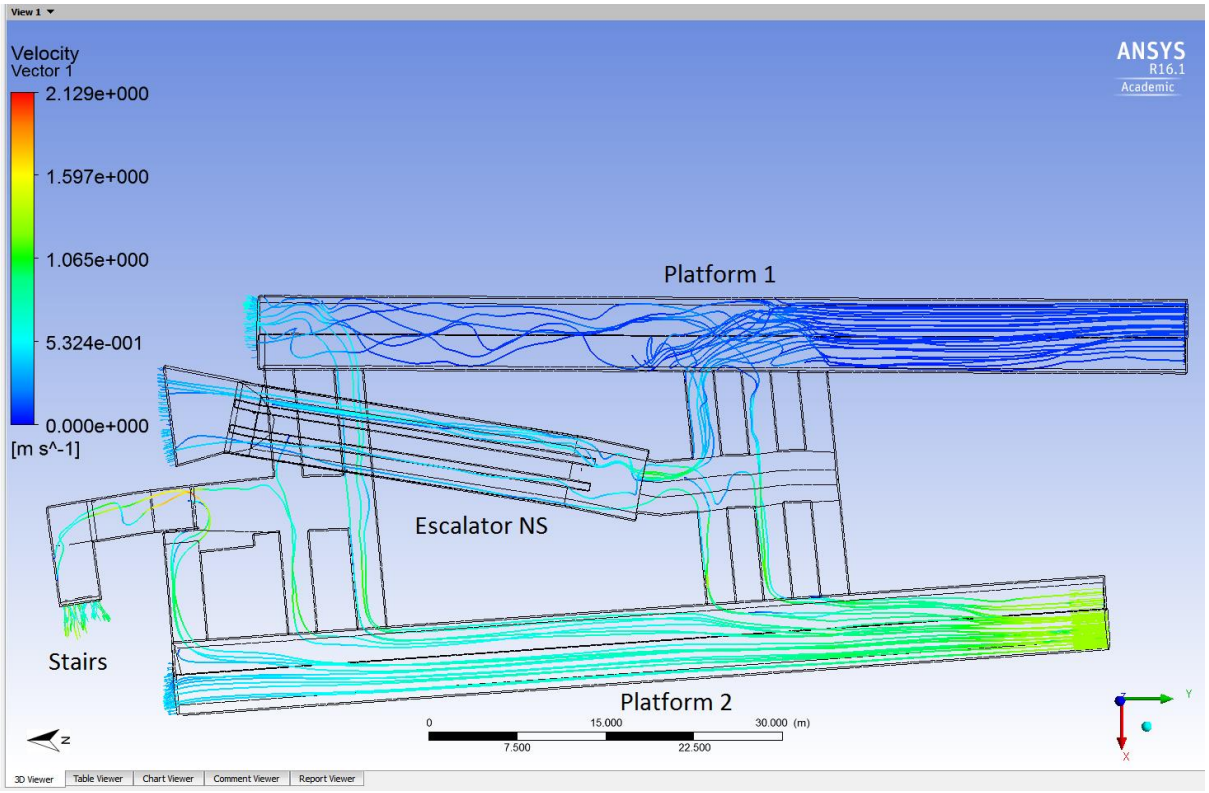

Figure 187: Simulation case NS_S03 air flow streamline of NS tunnel (plan elevation)

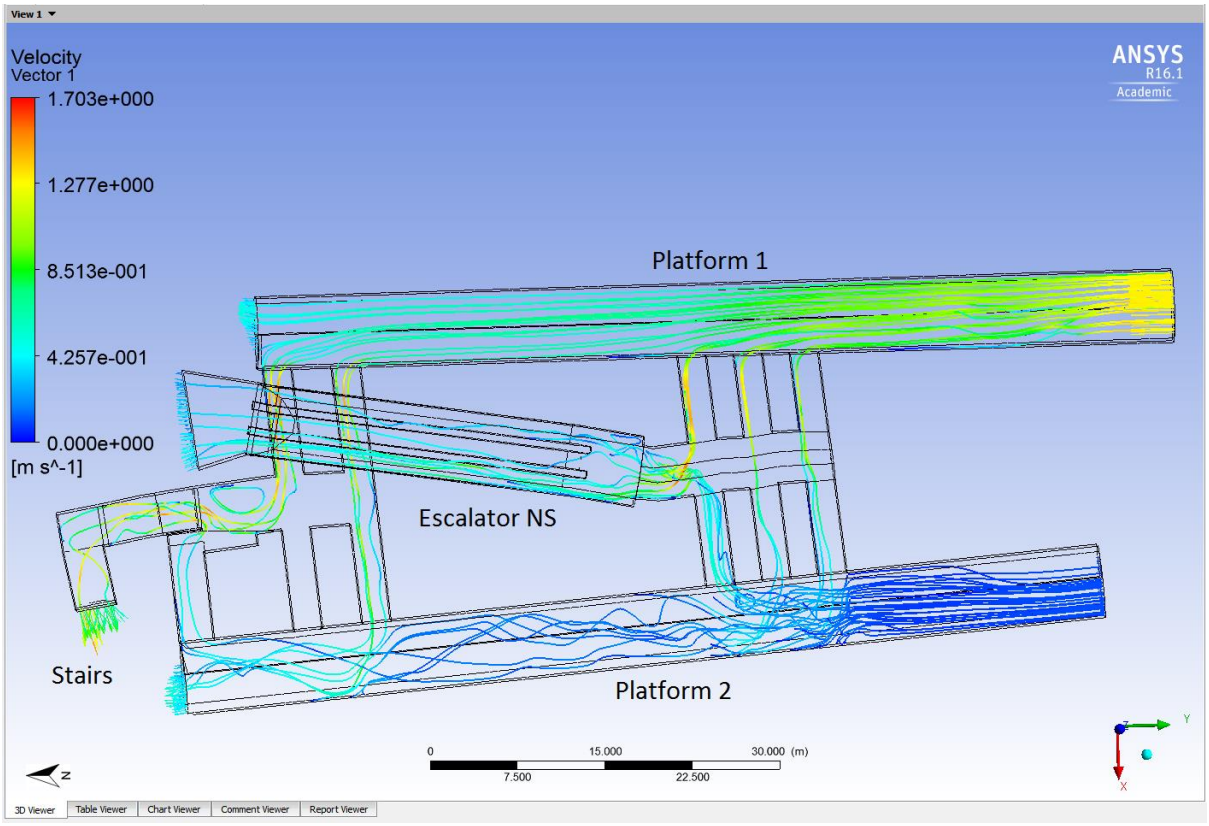

Figure 188: Simulation case NS_S04 air flow streamline of NS tunnel (plan elevation)

NS_S05 simulated when platform 1 had reverse airflow and platform 2 at average background airflow at operation break.

Simulation Case NS_S05 studied the condition that one of the tunnels had a very weak background air flow or reversed flow. These boundary conditions are shown in Table 40 and the resulting streamline in Figure 189. In this case, there was a strong exchange between platform 2 and the south end of platform 1. With this air flow scenario if the gas was released on platform 2 it would migrate to platform 1 and then to the EW tunnel and the concourse area within 2 minutes of being released.

Case NS_S05		
Boundary Name	Boundary condition	Velocity (m/s)
P1_S	Inlet	-0.2
P2_S	Inlet	1
P1_N	Outflow	0.4
P2_N	Outflow	0.2
Stair_NS	Outflow	0.7
Esc_NS	Outflow	0.2

Table 40: Velocity boundary conditions for NS_S05

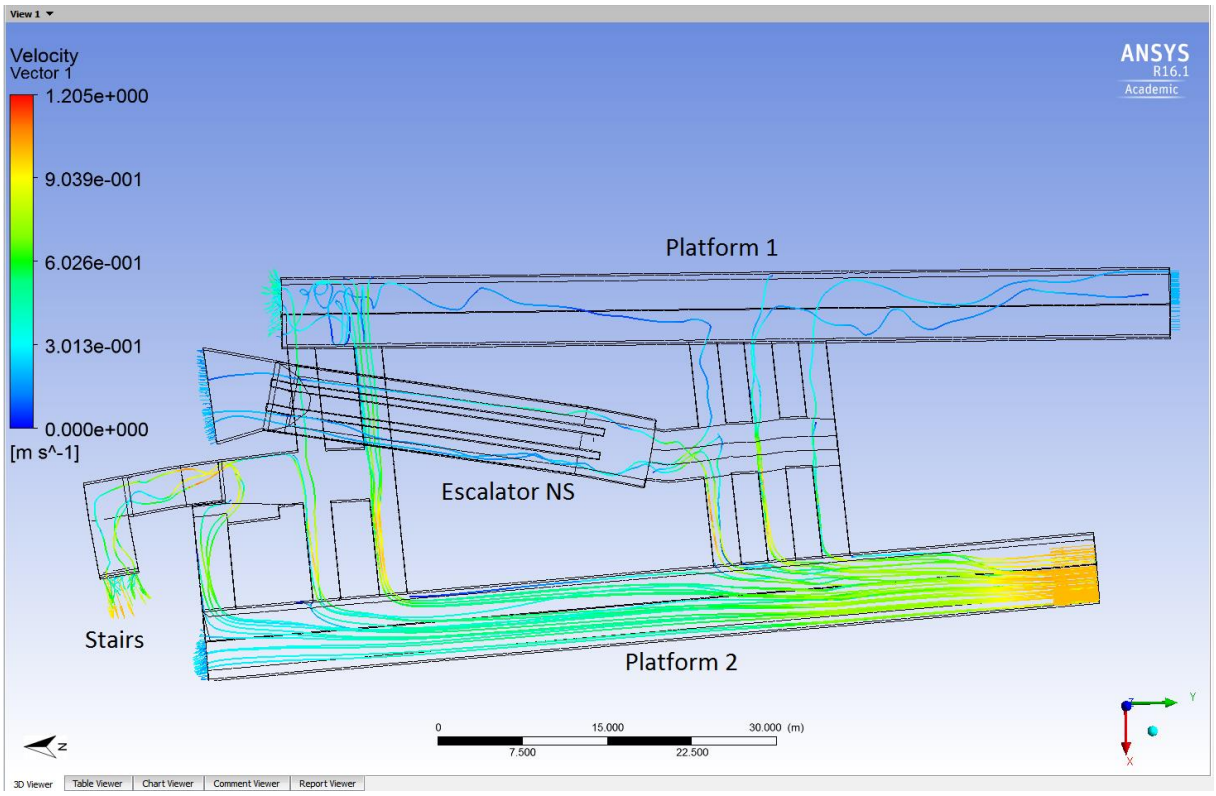

Figure 189: Simulation case NS_S05 air flow streamline of NS tunnel (plan elevation)

NS_S06, NS_S07 and NS_S08 simulated when train operation

The following cases examine the situation when the trains are operational. The air flow is then distorted by the piston effect of the trains which could reach a velocity of 5 m/s. The three cases considered simulated the case when a train was approaching each platform separately, NS_S06 at platform 1 and NS_S07 at platform 2 and finally the case when a train was approaching both platforms at the same time, NS_S08.

Measurements taken earlier indicated that when a train approached platform 1 the piston effect would produce a high air velocity of 5m/s and minimum velocity of 0.1m/s that would persist for some time after the train had left the station. A train approaching platform 2 operating from south to north would produce a similar air flow velocity but in this case the background air flow would assist the piston effect. The boundary conditions for the different parts of the station in this case are shown in Table 41.

In the case of NS_S06, the streamlines in Figure 190 show a strong air flow from the north of platform 1 pushing the air to platform 2 through the connecting corridor. The air enters the escalator only from platform 1 and the flow to the stair from the platform 2 is very strong with a speed of 3 m/s. In this case the gas could be dispersed to the whole of the NS tunnel, the EW tunnel and concourse level within 30 seconds if it were released at the north of platform 1 or from a train standing at platform 1.

The air flow pattern is not reversed as the operational train approaches platform 2 as shown in case NS_S07. The streamlines are shown in Figure 191. A train operating from platform 2 pushes the air to platform 1 and the stairs directly through the connecting corridors and enhances the air flow at platform 1 from north to south. Therefore, the gas or toxic agent could contaminate the EW tunnel as it is dispersed from platform 2 but not platform 1. Air flow towards the escalator is from both platforms in this case.

Case NS_S08 simulated the air flow condition when a train arrived at both platforms at the same time. As the streamlines show in Figure 192 the air flow pattern is very similar with Case NS_S01 and NS_S02. When the air flow at each of the platforms have a similar velocity there is little flow between the two platforms but the angle of the platform to the connecting corridors biases the flow in this region to come from platform 1. The gas or toxic agent could contaminate the NS tunnel and be dispersed to the EW tunnel and concourse level rapidly (within 20seconds) in this condition.

	Case NS_S06		Case NS_S07		Case NS_S08	
Boundary Name	Boundary condition	Velocity (m/s)	Boundary condition	Velocity (m/s)	Boundary condition	Velocity (m/s)
P1_S	Outflow	1.8	Outflow	1.6	Outflow	3.2
P2_S	Inlet	0.1	Inlet	5	Inlet	5
P1_N	Inlet	5	Inlet	0.1	Inlet	5
P2_N	Outflow	1.5	Outflow	2	Outflow	3
Stair_NS	Outflow	3	Outflow	2.5	Outflow	5.7
Esc_NS	Outflow	1.5	Outflow	1.3	Outflow	3.1

Table 41: Velocity boundary conditions for NS_S06, NS_S07 and NS_S08

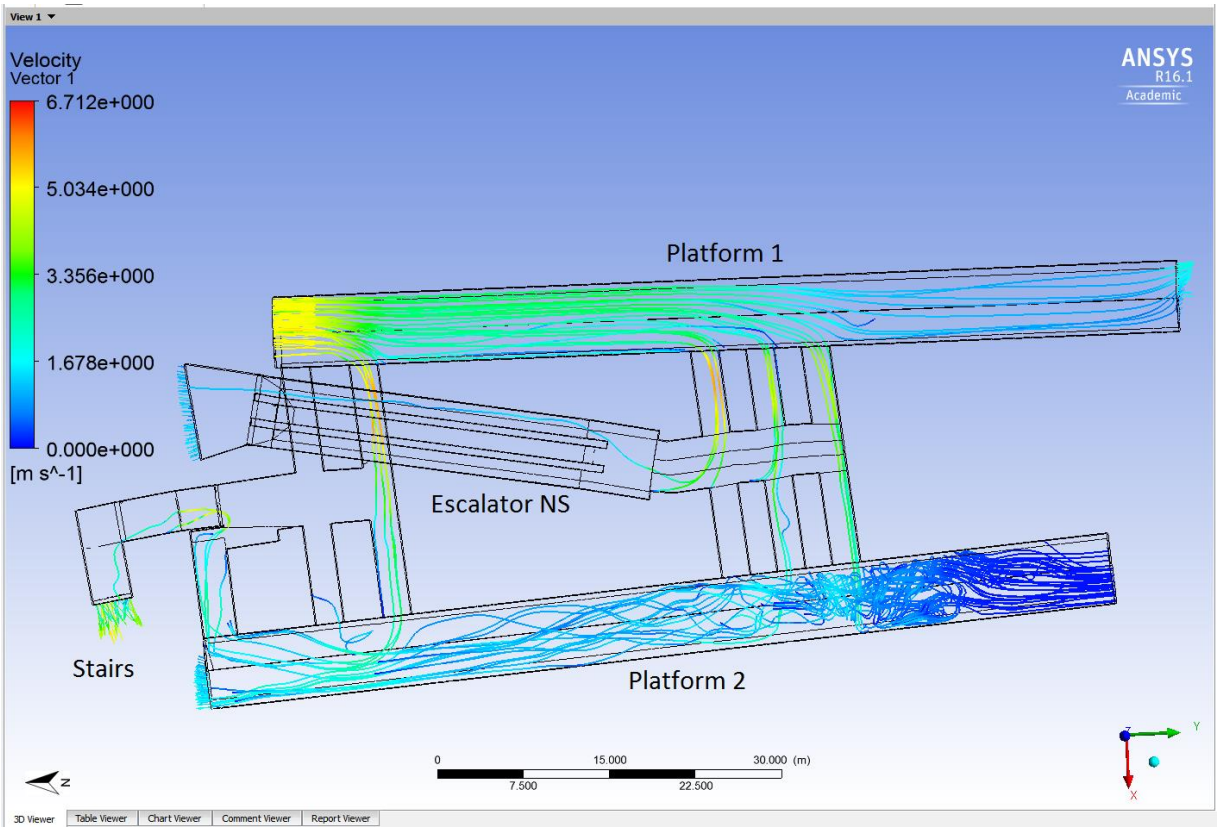

Figure 190: Simulation case NS_S06 air flow streamline of NS tunnel (plan elevation)

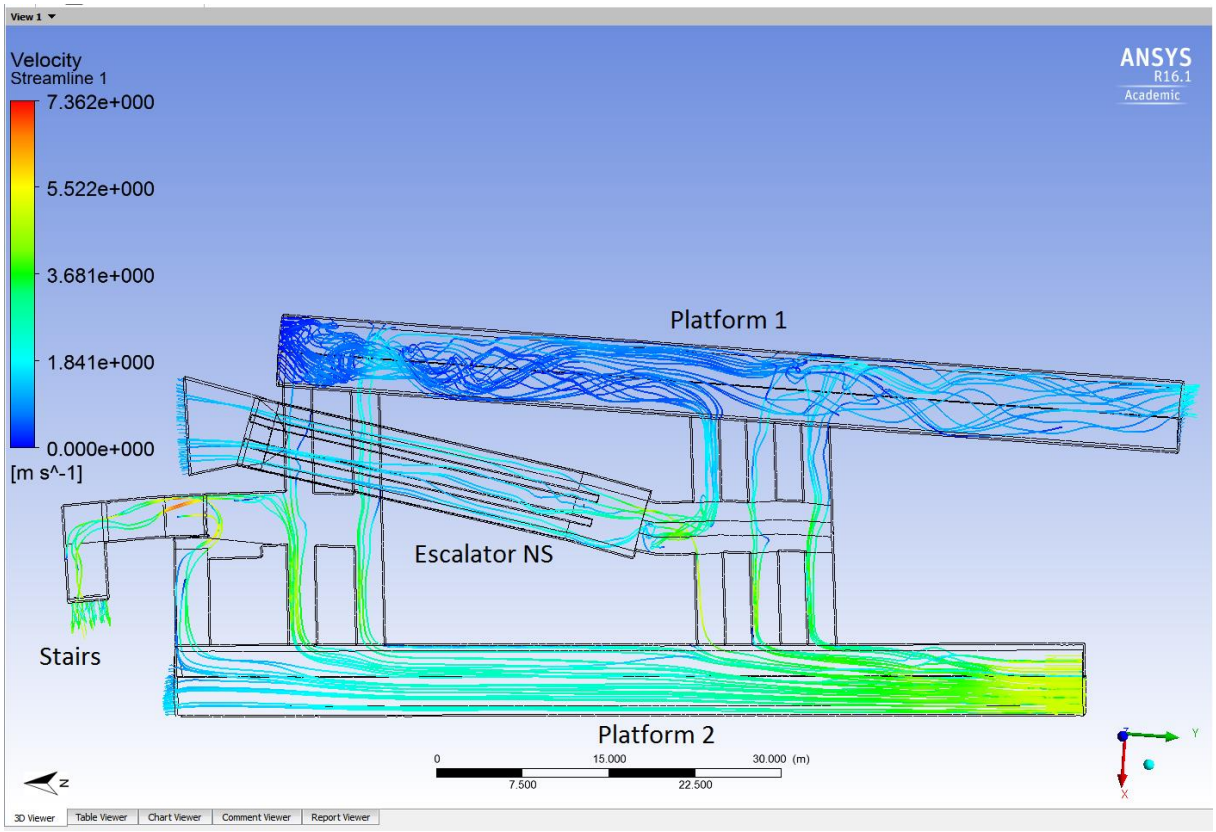

Figure 191: Simulation case NS_S07 air flow streamline of NS tunnel (plan elevation)

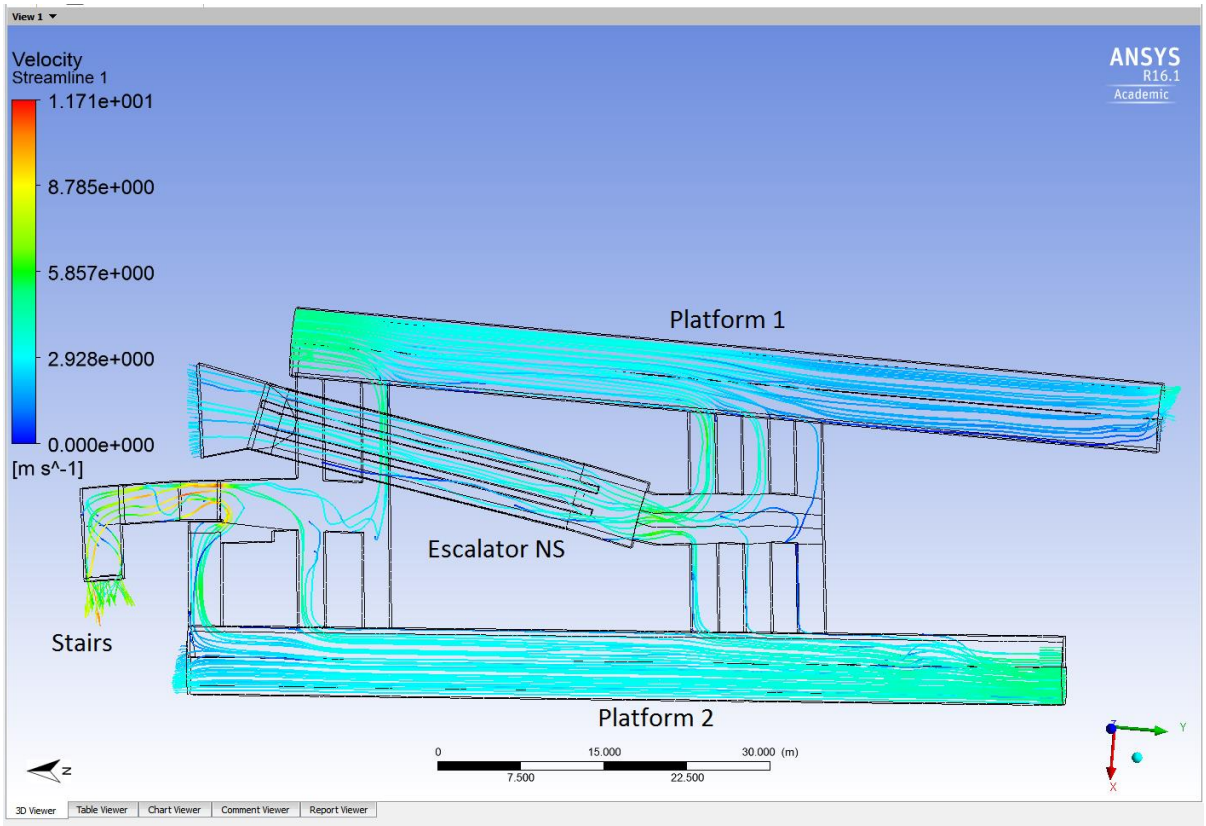

Figure 192: Simulation case NS_S08 air flow streamline of NS tunnel (plan elevation)

9.3.2 Sensitivity simulation of EW:

A similar exercise was performed for the East-West tunnels and platforms. Five simulation case were studied during the operation break. The input data consisted of a combination of maximum and minimum velocity from the tunnel boundary based on measurements reported in Chapter 5 and 6. The air flow at the stair from the NS tunnel was variable. Three further cases were simulated with the train operating in the same manner as with platform 1 and 2 discussed previously. These simulations are listed in Table 42.

In the EW tunnel level the previous measurements indicated the air flow was mainly from East to West at a moderate velocity of 0.3 m/s with very little flow reversal. The background air flow here was weak in comparison with the background flow on the North-South platforms. The air flow from the stairs from the north-south platforms had a large variability up to 1.7 m/s which was mainly from the lower lever to the higher level. This air flow velocity was most noticeable during the operational break and was attenuated by the piston effect of the trains. There was also a noticeable variability of the airflow at the escalator at this level with flow reversals occurring and the velocity ranging from 0.5 to 0.8 m/s during operation break. The piston effect of the trains produced a velocity of up to 3 m/s.

A list and description of the variables at East-West tunnel:

Simulation Case	Condition variables	
EW_S01	At operation break	The max. air flow from stair with background air flow at platform 3 and 4 from E to W. Escalator is outflow
EW_S02	At operation break	The max. air flow from stair with background air flow at platform 3 and 4 from E to W. Escalator reverse
EW_S03	At operation break	The max. air flow at platform 3 and 4 from E to W. With an average flow from stair. Escalator is outflow
EW_S04	At operation break	The maxi. Air flow at platform 3 and 4 from W to E with an avg. flow from stair. Escalator is outflow
EW_S05	At operation break	When only platform 4 at revere air flow and platform 3 is background airflow
EW_S06	At operation time	When train come at platform 3 and no train at platform 4 with an avg. flow from stair
EW_S07	At operation time	When train come at platform 4 and no train at platform 3 with an avg. flow from stair
EW_S08	At operation time	When train come at both platform 3 and 4 (from opposite direction) with an avg. flow from stair

Table 42: Variables of test case simulated at the East West tunnel CFD model

EW_S01 and EW_S02 simulated maximum airflow from stair and reversed flow at escalator at operation break

The cases EW_S01 and EW_S02 simulated the EW tunnel with moderate background air flow velocity from East to West at 0.3 m/s and high inlet air flow 1.7 m/s from the NE tunnel through the stairs. The flow at the EW escalators were different for these two cases as shown in Table 43. The streamlines resulting from analysing these cases are shown in Figure 193 and Figure 194. This air flow reversal at the escalator in case EW_S02 could prevent the gas dispersing to the concourse level when the source was from the NS tunnel or the EW tunnel.

EW_S01			EW_S02		
Boundary Name	Boundary condition	Velocity (m/s)	Boundary Name	Boundary condition	Velocity (m/s)
P3_W	Inlet	-0.3	P3_W	Inlet	-0.3
P4_W	Inlet	-0.3	P4_W	Inlet	-0.3
Stair_EW	Inlet	1.7	Stair_EW	Inlet	1.7
P3_E	Outflow	-0.2	P3_E	Outflow	-0.2
P4_E	Outflow	-0.2	P4_E	Outflow	-0.1
Esc_EW	Inlet	-0.8	Esc_EW	Inlet	0.5

Table 43: Velocity boundary conditions for simulation case EW_S01 and EW_S02

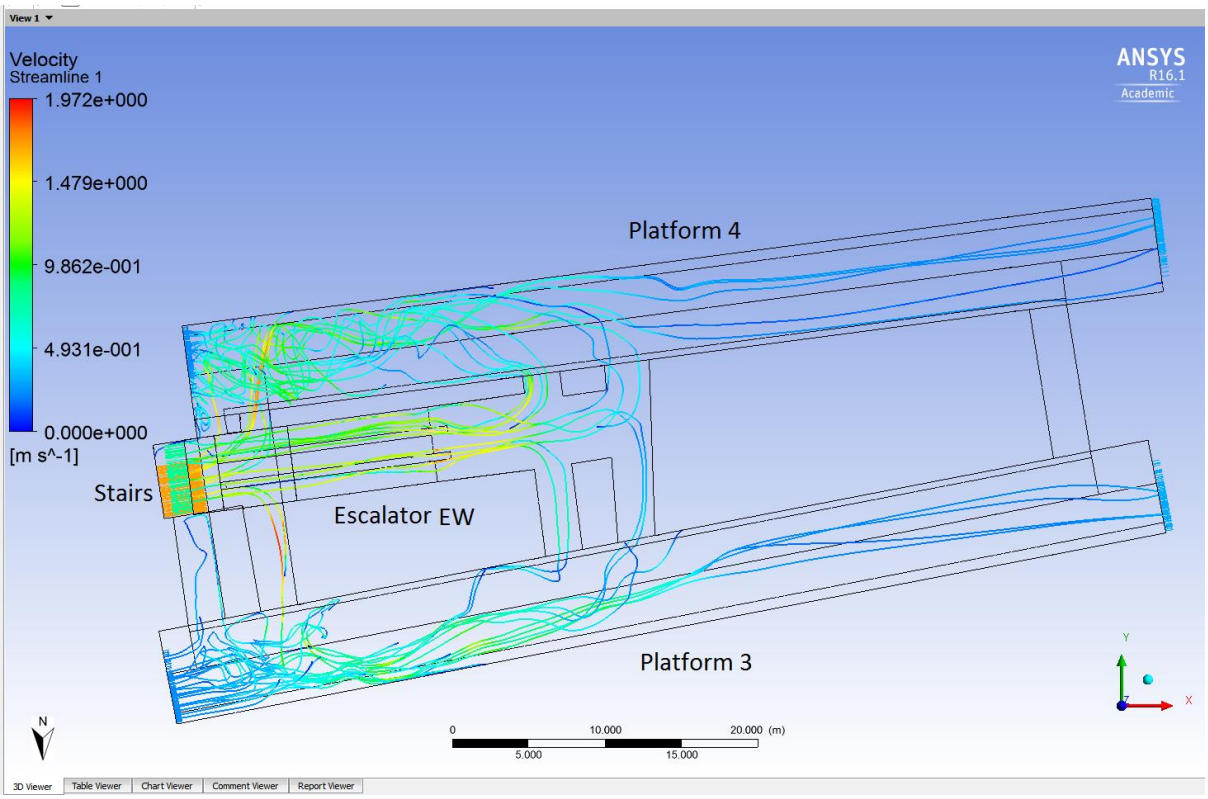

Figure 193: Simulation case EW_S01 air flow streamline of EW tunnel (plan elevation)

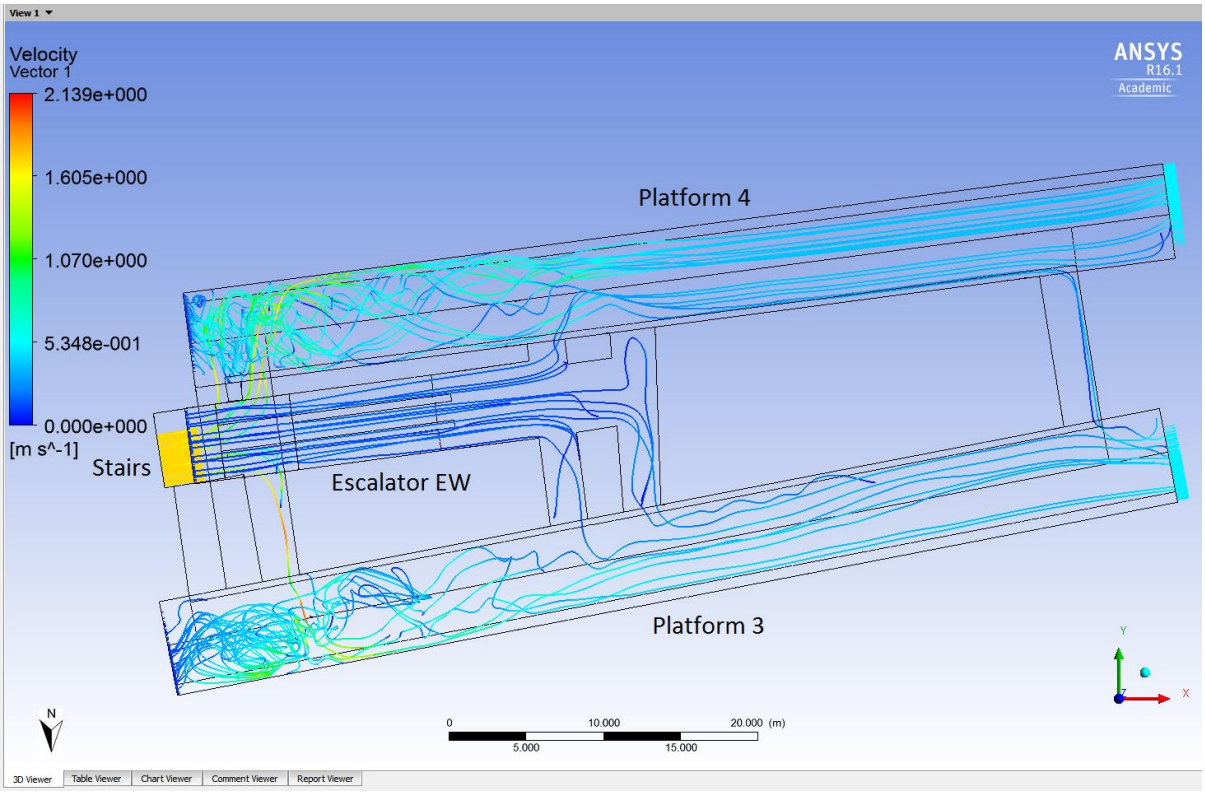

Figure 194: Simulation case EW_S02 air flow streamline of EW tunnel (plan elevation)

EW_S03, EW_S04 and EW_S05 simulated variable of reverse flow at platform 3 and 4

Cases EW_S03 and EW_S04 simulated the situations of maximum airflow from the east of the EW tunnel and small reverse flow from the west as had been measured previously. The average inlet flow at the stair was 1 m/s. Case EW_S05 simulated a moderate airflow from the opposite direction from platform 3 and 4. The boundary conditions are shown in Table 44.

	EW_S03		EW_S04		EW_S05	
Boundary Name	Boundary condition	Velocity (m/s)	Boundary condition	Velocity (m/s)	Boundary condition	Velocity (m/s)
P3_W	Outflow	0.8	Inlet	0.1	Outflow	0.35
P4_W	Outflow	1	Inlet	0.1	Inlet	0.3
Stair_EW	Inlet	1	Inlet	1	Inlet	1
P3_E	Inlet	0.6	Outflow	0.3	Inlet	0.3
P4_E	Inlet	1.2	Outflow	0.3	Outflow	0.55
Esc_EW	Outflow	1.1	Outflow	0.1	Outflow	0.5

Table 44: Velocity boundary conditions for Simulation Case EW_S03, EW_S04 and EW_S05

The streamlines of case EW_S03, shown in Figure 195, indicate the air flow from the East to West tunnel mixed with air from the stair to flow towards the escalator with quite a strong velocity. This was the main pattern at this tunnel level. The results also indicate that the gas dispersed evenly throughout this level and contaminated the concourse area as quickly as indicated by the tracer gas experiment 1. A completely different flow pattern would be caused by a little flow reversal from the West to East tunnel as shown in the case EW_S04 Figure 196. The flow was blocked by the flow from the West tunnel that prevented the gas contaminating the escalator.

In the case EW_S05, as the streamline in Figure 197 show, although the airflow from the platforms are in opposite directions with lower velocity, the outflow pattern at the escalator towards the concourse is at a moderate velocity that still indicates a higher risk of contamination.

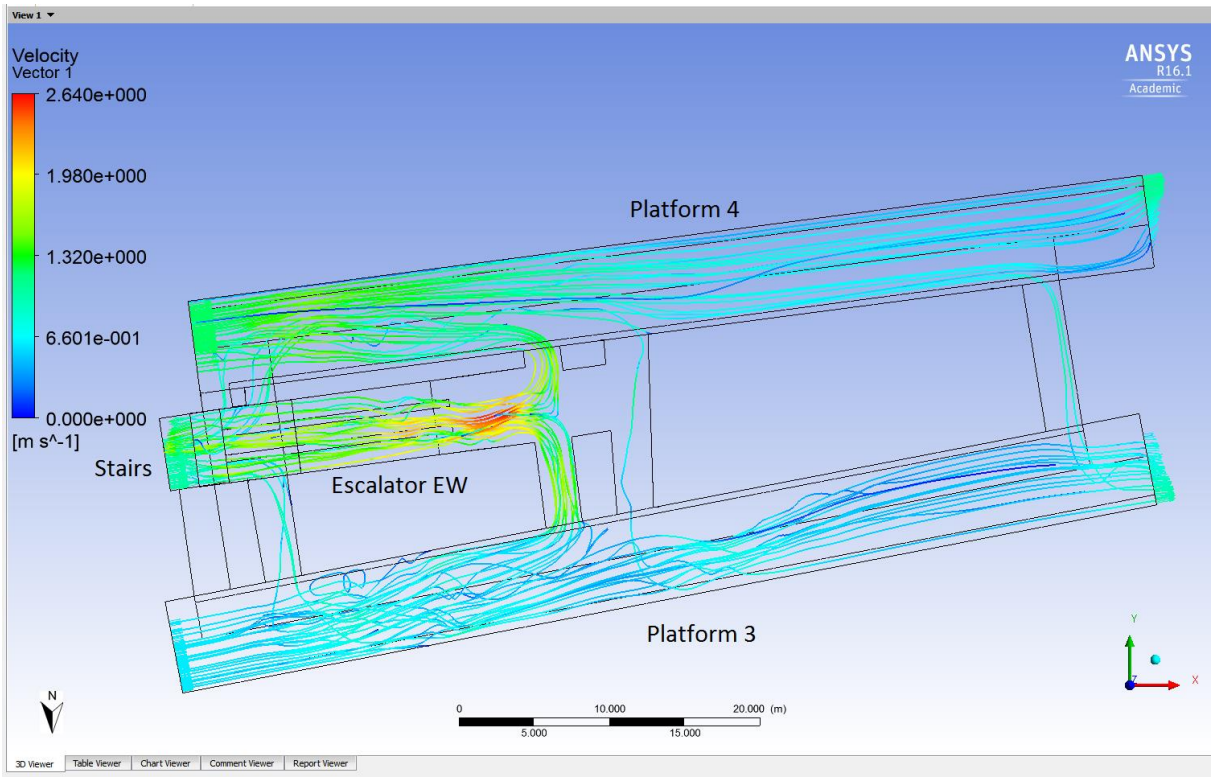

Figure 195: Simulation case EW_S03 air flow streamline of EW tunnel (plan elevation)

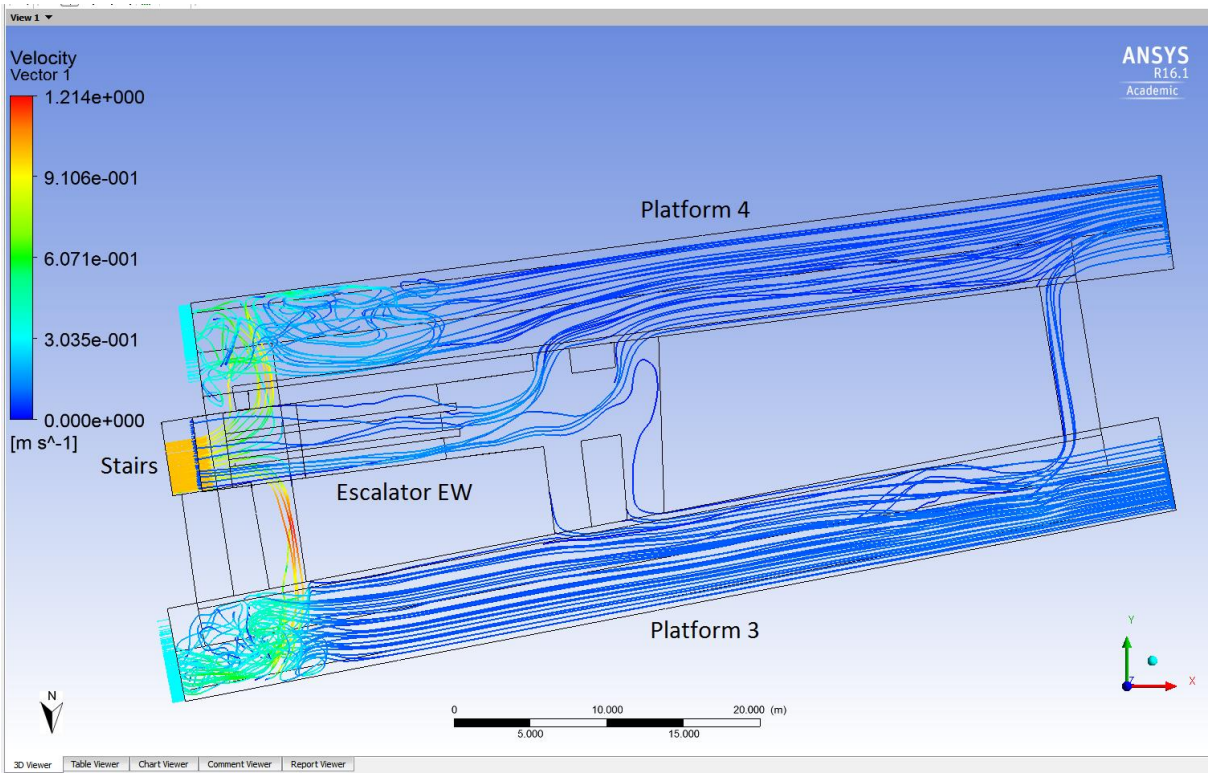

Figure 196: Simulation case EW_S04 air flow streamline of EW tunnel (plan elevation)

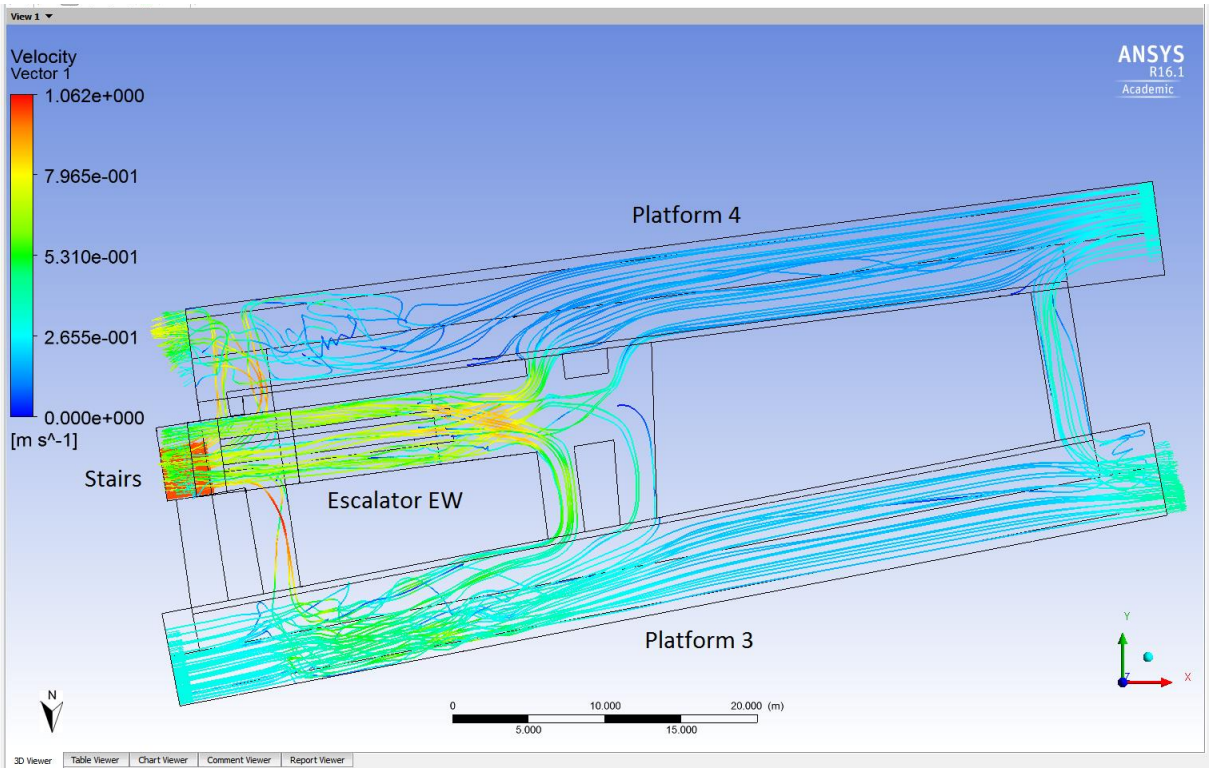

Figure 197: Simulation case EW_S05 air flow streamline of EW tunnel (plan elevation)

EW_S06, EW_S07 and EW_S08 simulated cases when train operation

The last three cases simulated scenarios are with the same flow from the stars at 1 m/s combined with train operation boundary conditions at the EW tunnel as shown in Table 45. The airflow measured when a train arrived at the EW platforms are lower than the NS tunnels. Simulation case EW_S06, had a train at platform 3, EW_S07 had a train at platform 4 and EW_S08 had trains at both platforms at the same time.

	EW_S06		EW_S07		EW_S08	
Boundary Name	Boundary condition	Velocity (m/s)	Boundary condition	Velocity (m/s)	Boundary condition	Velocity (m/s)
P3_W	Inlet	2.3	Outflow	2	Inlet	2.3
P4_W	Outflow	1.2	Outflow	1.5	Outflow	2.2
Stair_EW	Inlet	1	Inlet	1	Inlet	1
P3_E	Outflow	1.3	Inlet	0.3	Outflow	2.5
P4_E	Inlet	0.3	Inlet	3.8	Inlet	3.8
Esc_EW	Outflow	1.5	Outflow	2.3	Outflow	3

Table 45: Velocity boundary conditions for simulation case EW_S06, EW_S07 and EW_S08

The streamlines of case EW_S06 is shown in Figure 198. The effect of the train is to push the air through the whole level and towards the escalator then to the concourse. The air flow from the stairs was pushed to platform 4 before being dispersed to the escalator. A similar flow pattern is shown in Figure 199 for case EW_S07, although the airflow from the stair was mixed flow from both platforms before it flowed up to the escalator. The air flow at the platform with the operational train is a strong forcing exchange of air between the platforms that disrupts the steady background flow. The condition when trains were at both platforms, case EW_S08, is shown in Figure 200. The airflow from platform to platform are a minimum but mixed air flow from the stairs at the corridor is pushed towards the escalator. The air flow pattern with train operation is unstable and quicker at this level which makes it difficult to predict the effect of a toxic gas dispersion at this level. The potential of toxic gas dispersion from stairs to contaminate the majority of the area of the EW tunnel is very high.

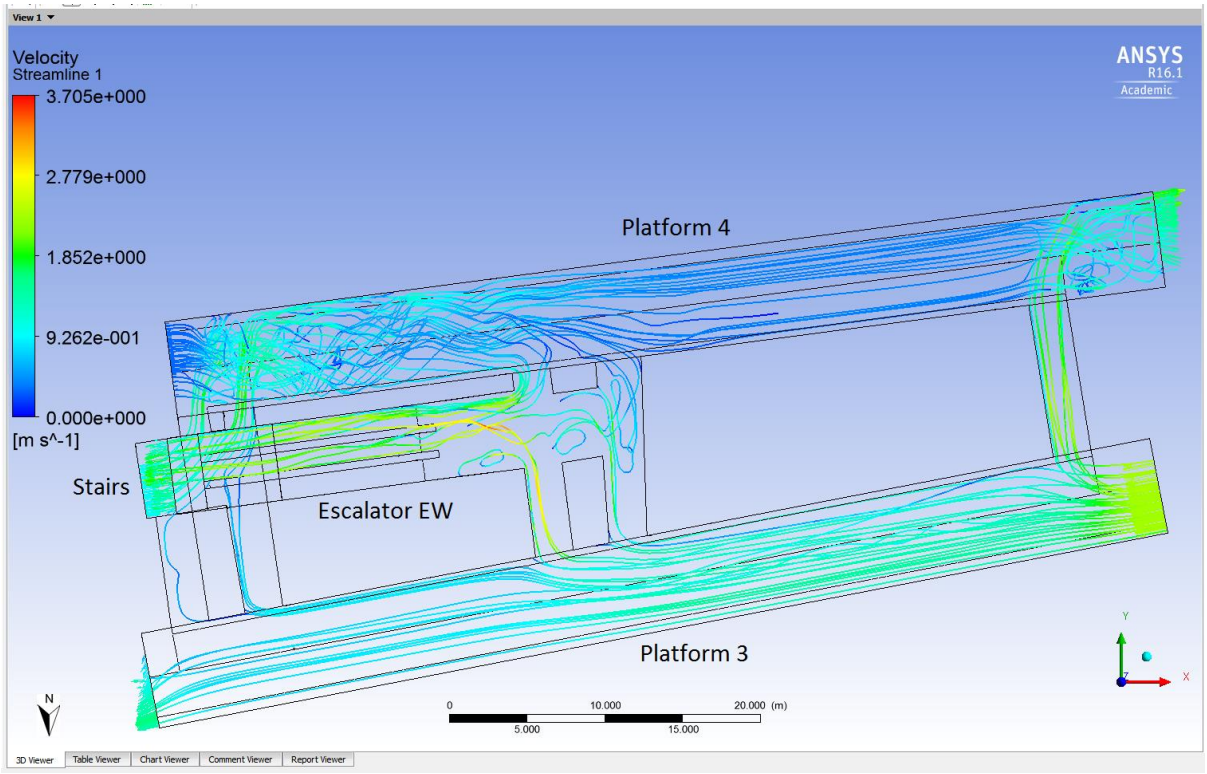

Figure 198: Simulation case EW_S06 air flow streamline of EW tunnel (plan elevation)

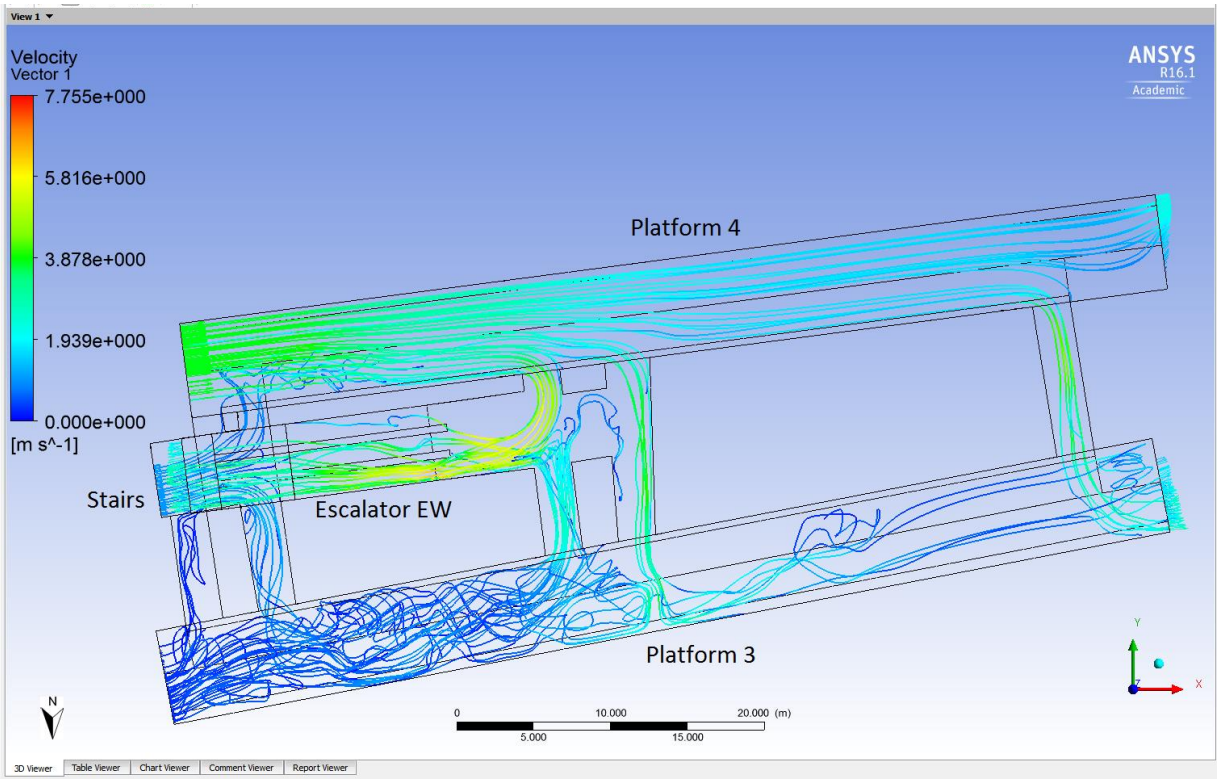

Figure 199: Simulation case EW_S07 air flow streamline of EW tunnel (plan elevation)

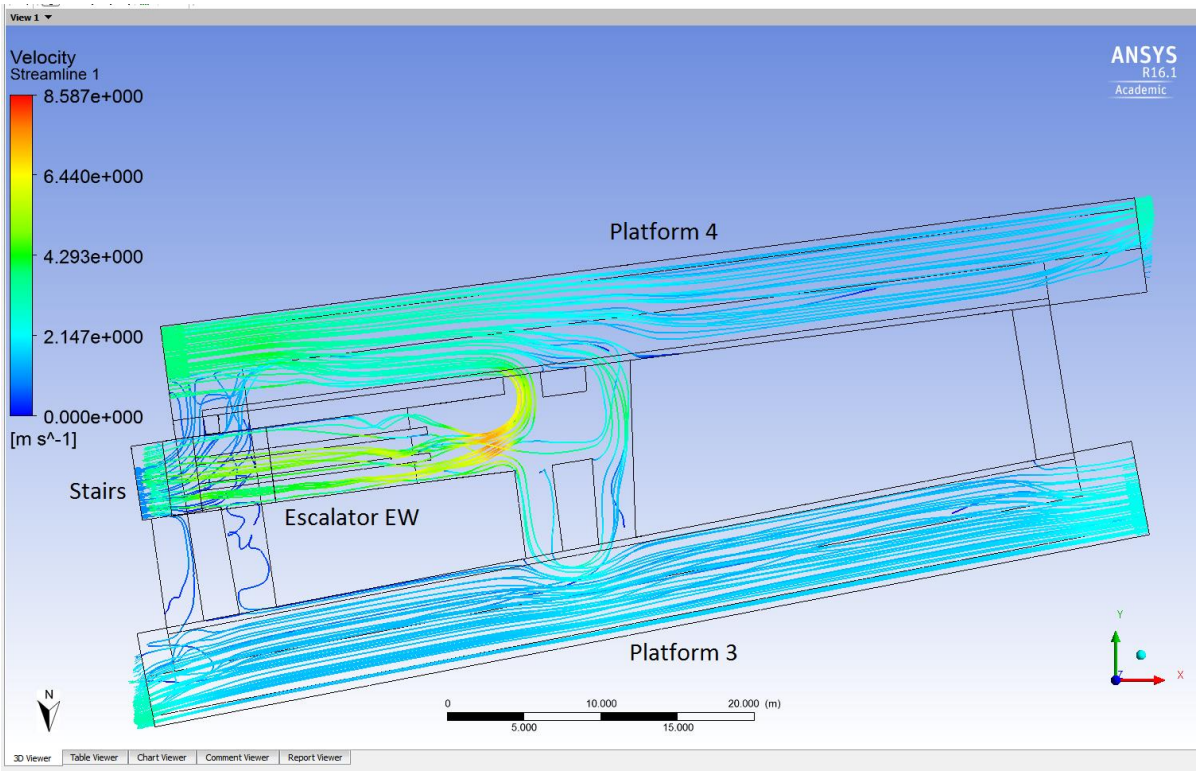

Figure 200: Simulation case EW_S08 air flow streamline of EW tunnel (plan elevation)

9.3.3 Sensitivity simulation of Concourse:

A similar exercise was performed for the station concourse. The CFD models produced earlier showed that the air flow at the station exits has a major influence on the flow pattern in the concourse area. During the day the airflow at Exit 1 was predominantly influenced by the east west street and the local traffic. The airflow into the station at Exit 1 could vary from 0.2 m/s up to 1 m/s. Also the air flow at Exit 2 into the station in the south direction could vary from zero to 1.5 m/s. This has been discussed at Chapter 7 Microclimate CFD modelling. Three simulation cases have been examined focusing on the impact of the air flow at the exits to the station. The boundary conditions for these cases are shown in Table 46.

The list and description of the variables at concourse level:

Simulation Case	Condition variables
Con_S01	Exit 1 max. inlet E to W. Exit 2 and 3 outflows.
Con_S02	Exit 2 max. inlet S to N. Exit 1 and 3 outflow.
Con_S03	Exit 1 min. inlet E to W. Exit 2 min. inlet S to N
Con_S04	Exit 1 max. inlet E to W. Exit 2 max. inlet S to N
Con_S05	Exit 1 and 2 max. inlet E to W. Exit 3 outflow.
Con_S06	Control outflow of Exit 1
Con_S07	Control outflow of Exit 1 and 2 with low velocity
Con_S08	Control outflow of Exit 1 and 2 with higher velocity

Table 46: Variables of test case simulated at the concourse level CFD model

Con_S01 and Con_S02 simulated only one exit have inlet flow at maximum and other two exits are outlet.

Case Con_S01 and Con_S02 simulated the concourse level with moderate inlet air flow velocity inlet at the escalators from the NE tunnel and the EW tunnel at 0.5 m/s with the inlet air flow from Exit 1 and 2 respectively of 1m/s and 1.5 m/s. These two case present the effect of the external environment wind condition only affecting the air flow inside the station through Exit 1 or Exit 2. The boundary conditions are shown in Table 47. The airflow streamlines for these cases are shown in Figure 201 and Figure 202. It can be seen that when one exit acts as an air inlet to the station the other two exits act as outflows. In Figure 201 case Con_S01 the air flow from the two escalators is enhanced by the inlet flow from Exit 1 which would speed up the gas dispersion at the concourse level and spread to contaminate the nearby shopping centre from Exit 3. Although the outflow speed at exit 3 is similar in these two case, the flow pattern in Con_S02, Figure 202, is very different to Con_S01. The inlet flow from Exit2 was distorted and mixed with the out flow from the escalator to Exit 2 and Exit3. In these two cases the potential to contaminate the shopping centre is very high.

Con_S01			Con_S02		
Boundary Name	Boundary condition	Velocity (m/s)	Boundary Name	Boundary condition	Velocity (m/s)
Esc_NS	Inlet	0.5	Esc_NS	Inlet	0.5
Esc_EW	Inlet	0.5	Esc_EW	Inlet	0.5
Exit 1	Inlet E to W	1	Exit 1	Outflow	0.5
Exit 2	Outflow	0.3	Exit 2	Inlet S to N	1.5
Exit 3	Outflow	0.8	Exit 3	Outflow	0.9

Table 47: Velocity boundary conditions for simulation case Con_S01 and Con_S02

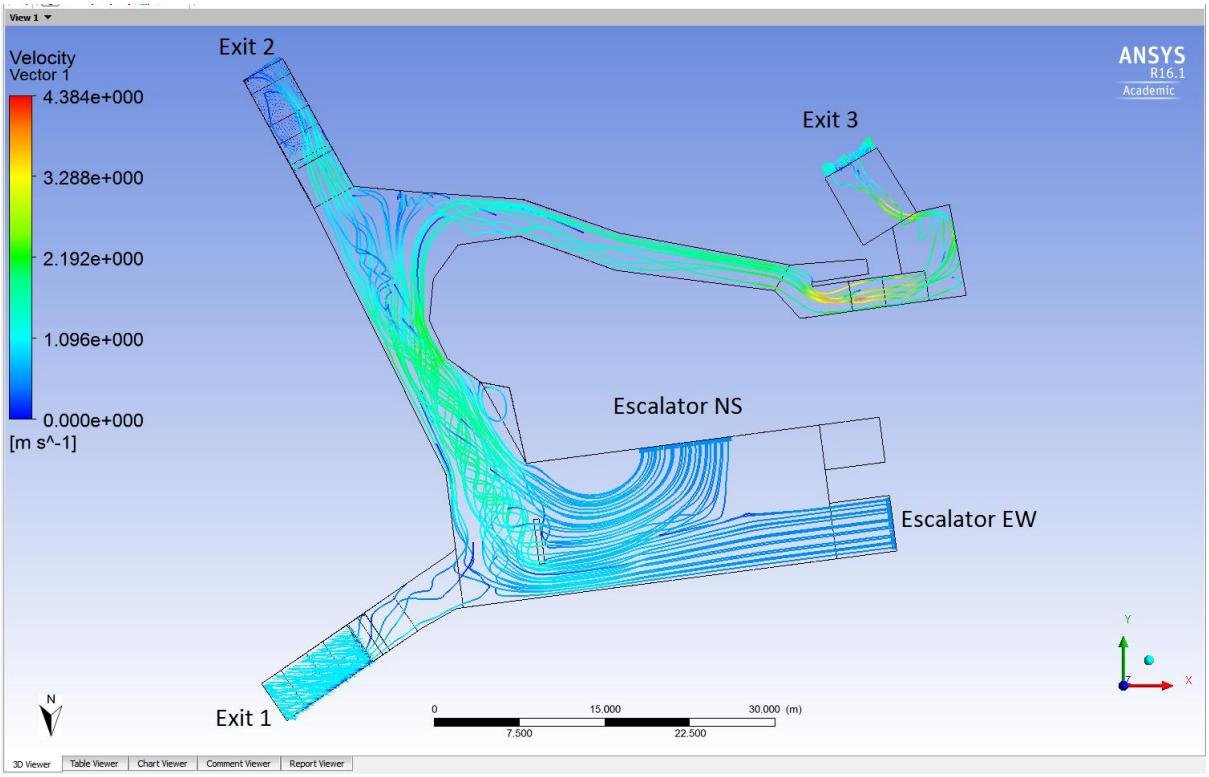

Figure 201: Simulation case Con_S01 air flow streamline of concourse level (plan elevation)

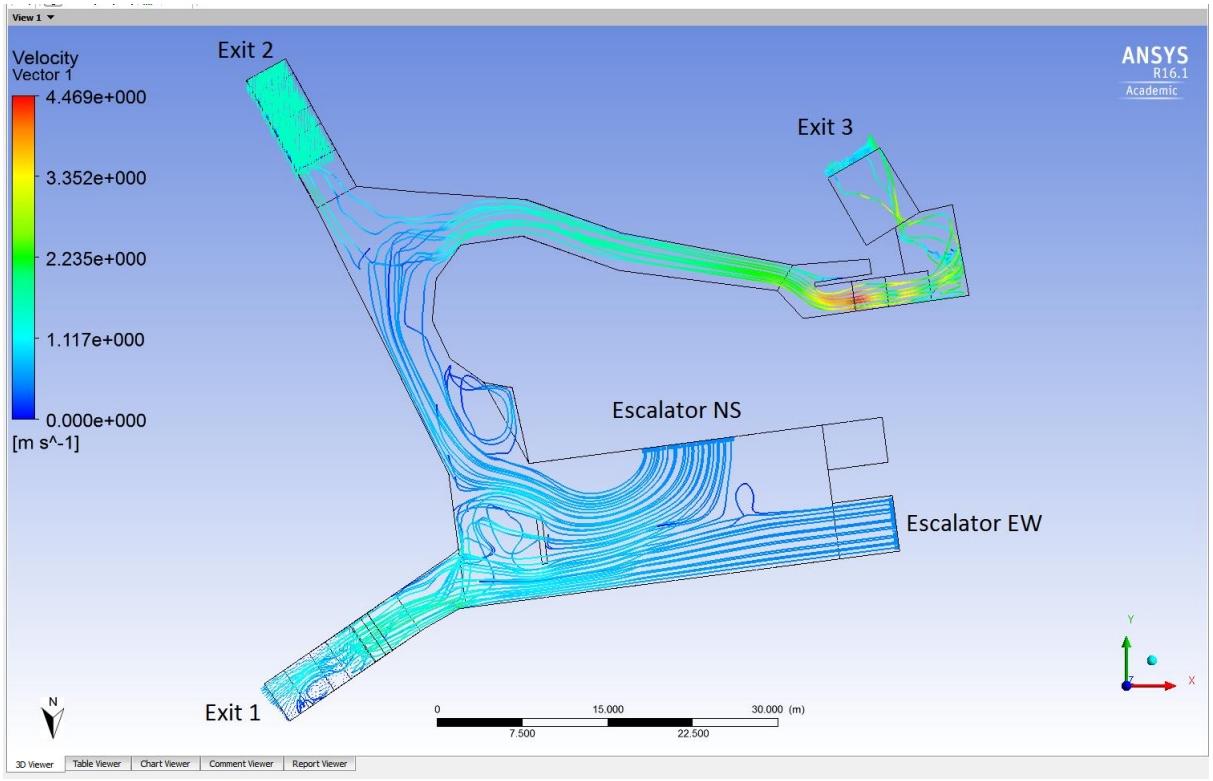

Figure 202: Simulation Case Con_S02 air flow streamline of concourse level (plan elevation)

Con_S03, Con_S04 and Con_S05 simulated Exit 1 and 2 are inlet and Exit 3 is outflow

Cases Con_S03 and Con_S04 simulated the condition of the concourse level with minimum and maximum inlet flow at both Exit 1 and Exit 2. The difference between the two cases being the inlet direction at Exit 2 is from the south in Con_S03 and from the east in Con_S04. This was based on the findings from chapter 7 which indicated that the microclimate outside exit 2 had two major wind directions from the east and from the south. The boundary condition for these three case are listed in Table 48. The streamlines for cases Con_S03 and Con_S04 are shown in Figure 203 and Figure 204. These flow pattern are very similar. The inlet flows at Exit 1 and Exit 2 are mixed with the flow from the two escalators which then migrates towards Exit 3 and the shopping centre. The higher velocity at Exit 1 and Exit 2 resulted in an outflow at Exit 3 with a magnitude up to 2 m/s. In this case the concourse level was contaminated within 1 minute.

When the external flow was from the east at exit 2, Con_S05, this produced a similar flow regime to that which existed with Con_S04 when the flow was from the south. At

a first glance it appears that an inflow at exit 2, irrespective of the external air flow direction will cause the air in the concourse area to flow towards exit 3. The approach angle of the external flow does however influence the flow velocity at exit 3 as shown by the streamlines in Figure 205 and Table 48.

	Con_S03		Con_S04		Con_S05	
Boundary Name	Boundary condition	Velocity (m/s)	Boundary condition	Velocity (m/s)	Boundary condition	Velocity (m/s)
Esc_NS	Inlet	0.5	Inlet	0.5	Inlet	0.5
Esc_EW	Inlet	0.5	Inlet	0.5	Inlet	0.5
Exit 1	Inlet E to W	0.2	Inlet E to W	1	Inlet E to W	1
Exit 2	Inlet S to N	0.3	Inlet S to N	1.5	Inlet E to W	1.5
Exit 3	Outflow	1	Outflow	2	Outflow	1.8

Table 48: Velocity boundary conditions for simulation case Con_S01, Con_S02 and Con_S03

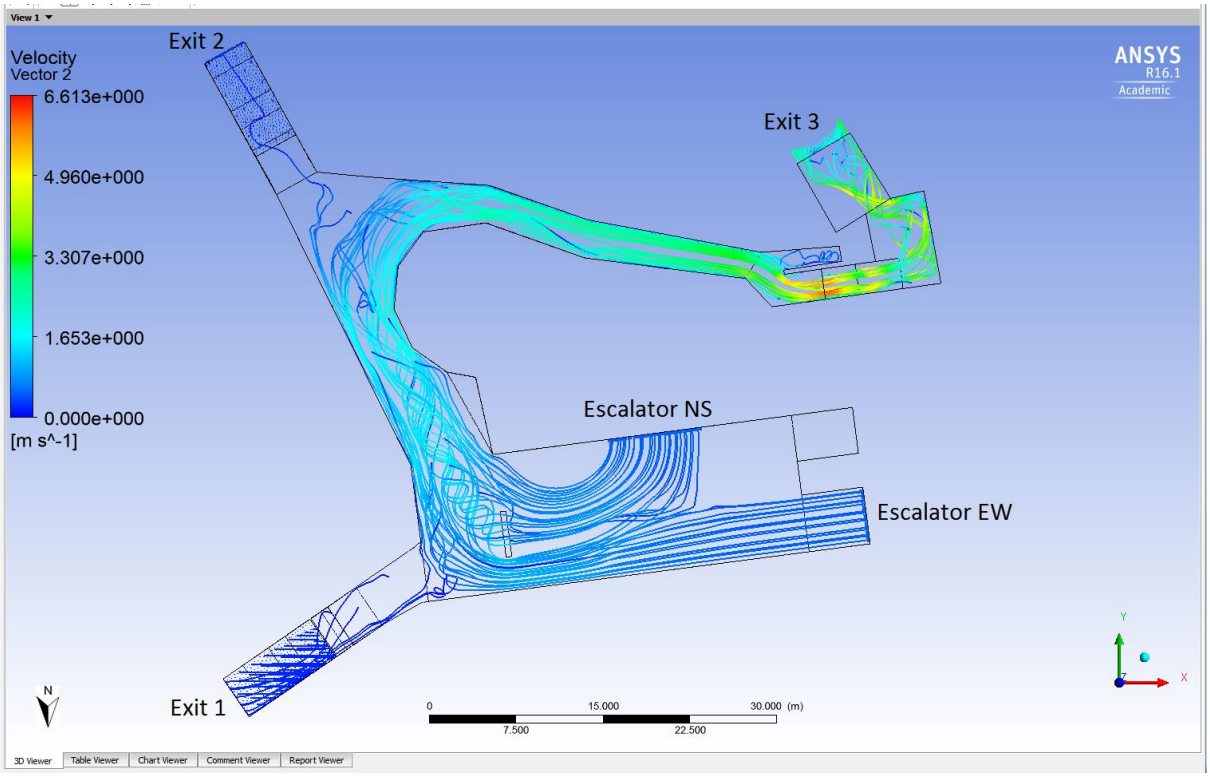

Figure 203: Simulation case Con_S03 air flow streamline of concourse level (plan elevation)

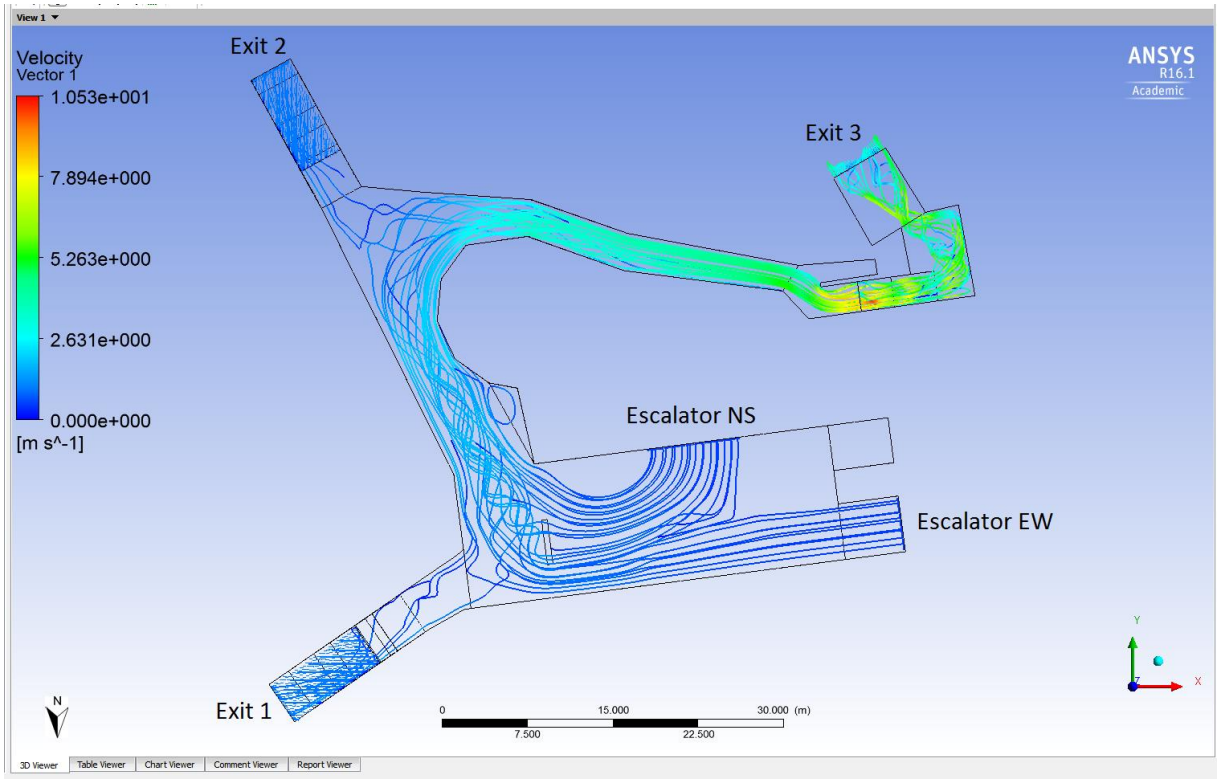

Figure 204: Simulation case Con_S04 air flow streamline of concourse level (plan elevation)

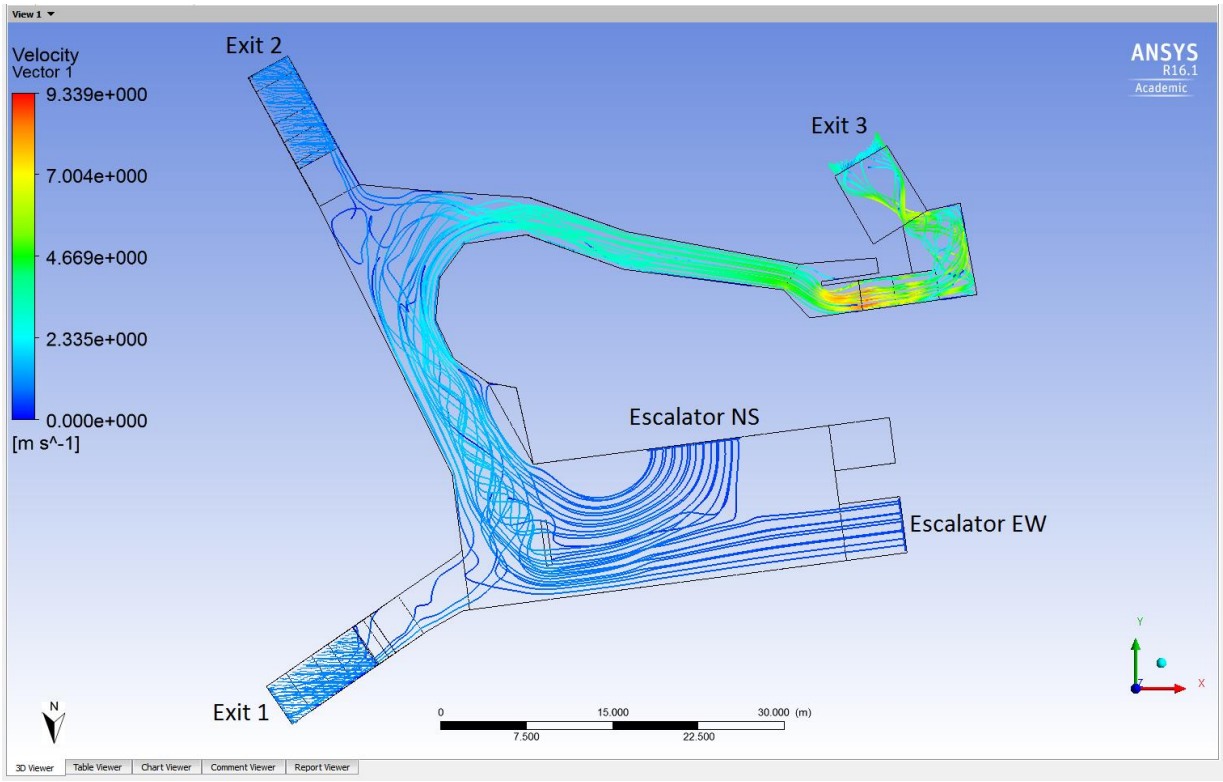

Figure 205: Simulation case Con_S05 air flow streamline of concourse level (plan elevation)

Con_S06, Con_S07 and Con_S08 simulated control ventilation velocity at Exits

It was observed from the microclimate analysis that when Exit 3 was always on the leeward side this lead to an outflow from the station. Therefor in this section are simulated three cases that consider the possibility to control the flow towards Exit 3 to prevent contamination of the shopping centre. The boundary conditions for these three cases are listed in Table 49.

	Con_S06		Con_S07		Con_S08	
Boundary Name	Boundary condition	Velocity (m/s)	Boundary condition	Velocity (m/s)	Boundary condition	Velocity (m/s)
Esc_NS	Inlet	1	Inlet	1	Inlet	1
Esc_EW	Inlet	0.5	Inlet	0.5	Inlet	0.5
Exit 1	Inlet	-1	Inlet	-0.5	Inlet	-1
Exit 2	Inlet	0.5	Inlet	-0.3	Inlet	-0.5
Exit 3	Outflow	1	Outflow	-0.1 in	Outflow	-1.4

Table 49: Velocity boundary conditions for simulation case Con_S06, Con_S07 and Con_S08

Case Con_S06 simulated only control of Exit 1 as an outflow. The simulation results are shown in Figure 206. It can be seen in Figure 207 that the flow at Exit 3 is still towards the shopping centre. The simulated exhaust flow both at Exit 1 (Figure 209) and Exit 2 (Figure 210) was set as a low velocity in case Con_S07 as shown in Figure 208 and a high velocity in case Con_S08 in Figure 212. The flow at Exit 3 was nearly in balance in case Con_S07 as the flow is into the station at 0.1 m/s (Figure 211), which could avoid the dispersion to the shopping centre. Then, with a higher exhaust flow in case Con_S08, the flow velocity could up to 1.4 m/s which is a strong flow pattern from exit 3 into the concourse area as shown by the streamlines in Figure 213.

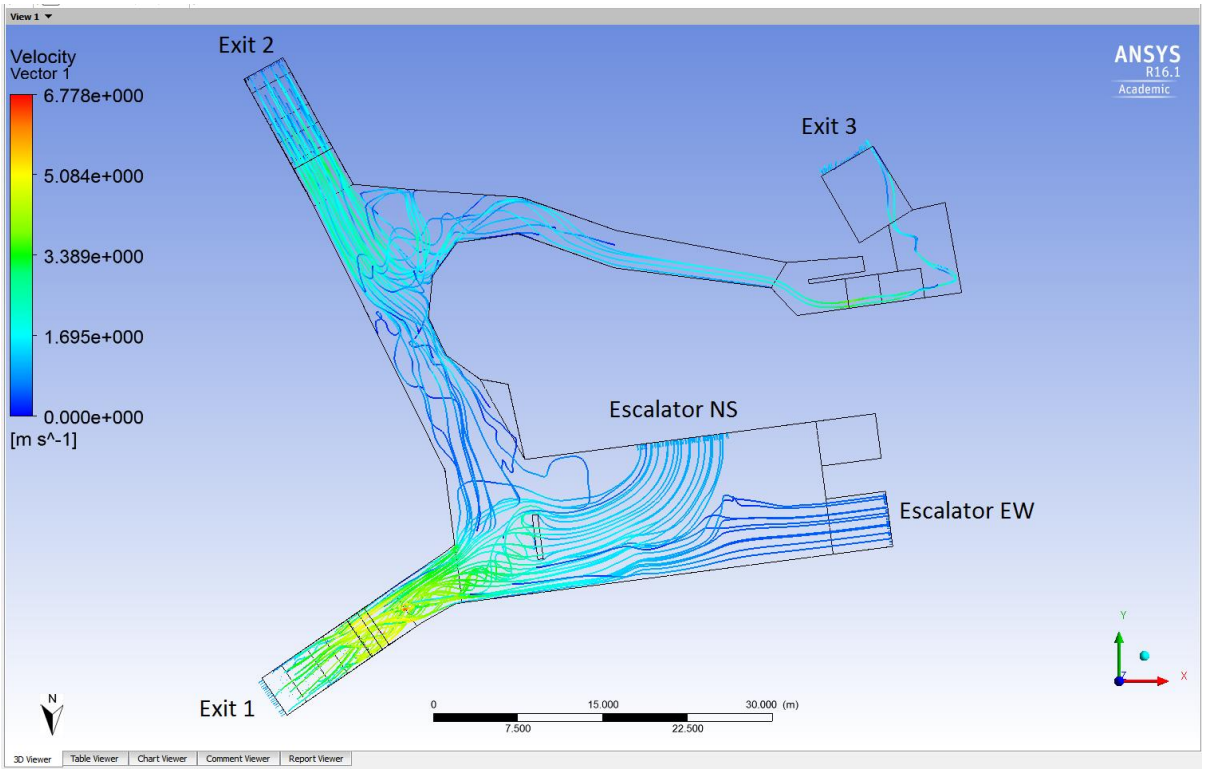

Figure 206: Simulation case Con_S06 air flow streamline of concourse level (plan elevation)

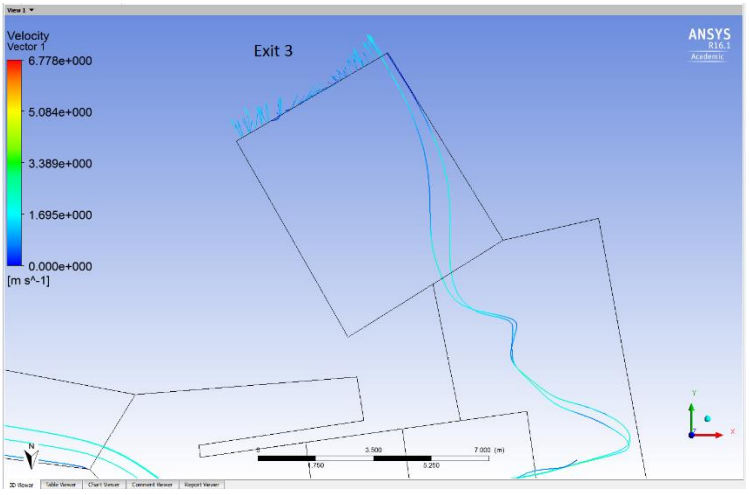

Figure 207: Simulation case Con_S06 air flow streamline of Exit 3 (plan elevation)

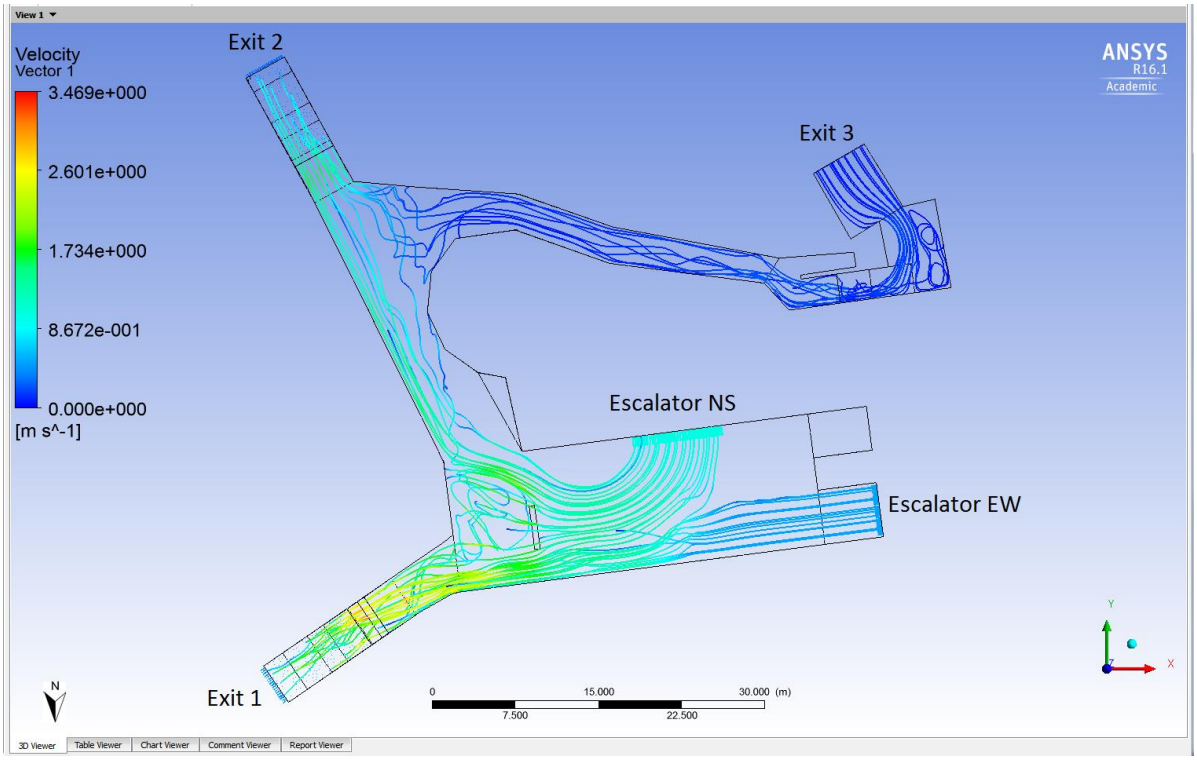

Figure 208: Simulation case Con_S07 air flow streamline of concourse level (plan elevation)

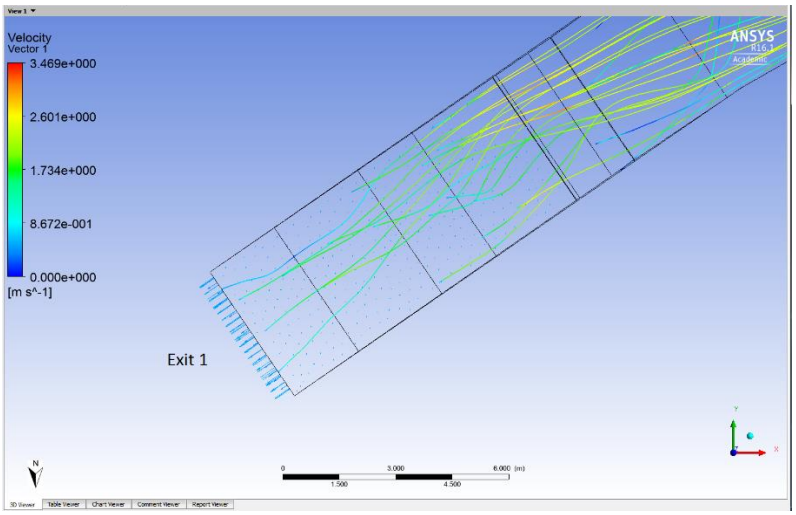

Figure 209: Simulation case Con_S07 air flow streamline of Exit 1 (plan elevation)

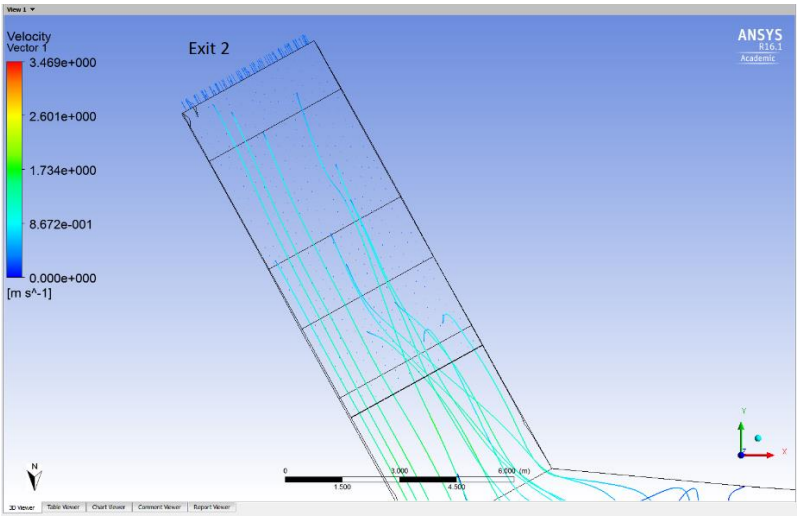

Figure 210: Simulation case Con_S07 air flow streamline of Exit 2 (plan elevation)

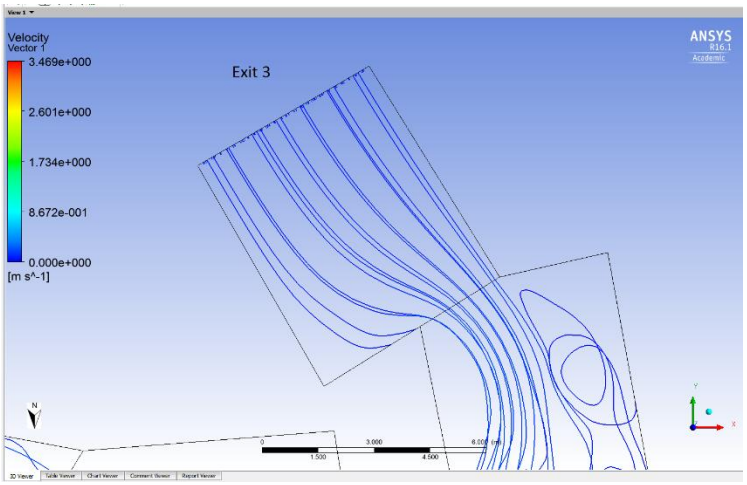

Figure 211: Simulation case Con_S07 air flow streamline of Exit 3 (plan elevation)

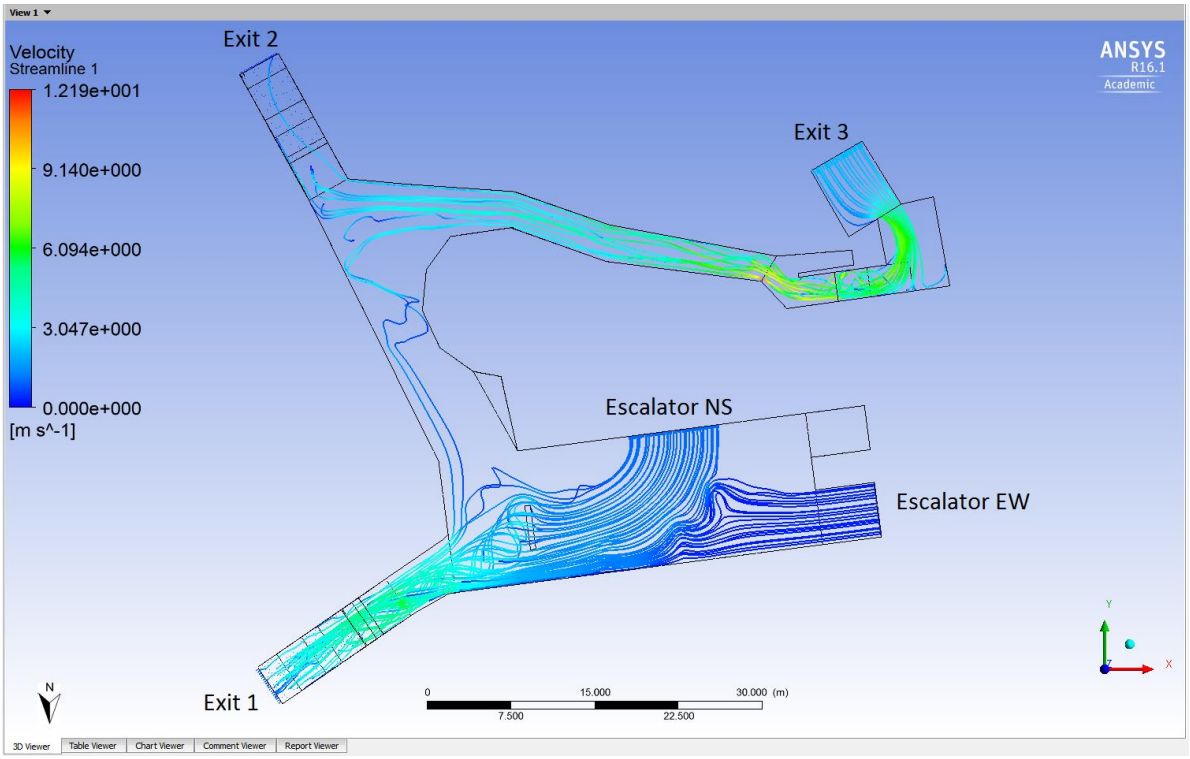

Figure 212: Simulation case Con_S08 air flow streamline of concourse level (plan elevation)

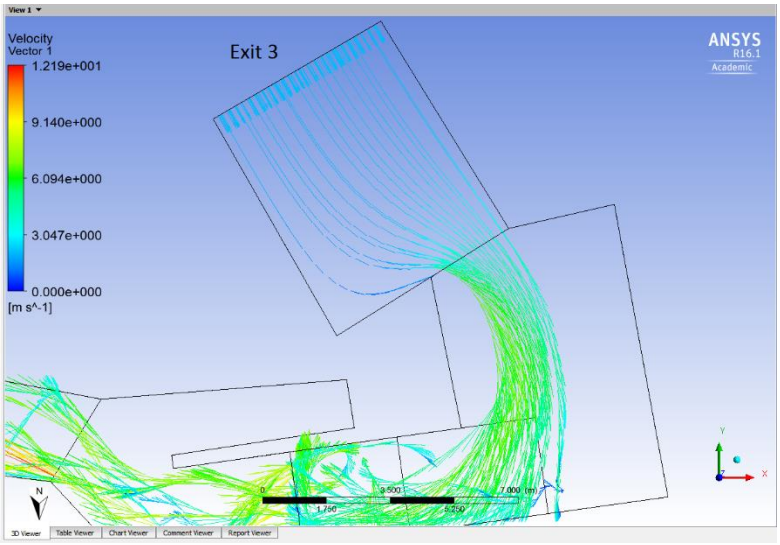

Figure 213: Simulation case Con_S08 air flow streamline of Exit 3 (plan elevation)

9.4 Evacuation simulations

To examine the evacuation capabilities of the Monument station, a simulation of an evacuation has been produced using the pedestrian simulation software Legion Spaceworks. Agent-based pedestrian modelling software is capable of representing the attributes and behaviour of individual agents within given environments (Castle, 2006). For example, entities can be programmed to have varying degrees of prior knowledge regarding a buildings layout (e.g. commuters vs. tourists), different mobility (e.g. children, adults, impaired, runner, etc.), or different global origins (e.g. UK, Asia, North American, etc.). All of these varying options and interactions define the speed and route in which entities will navigate through a space.

The agent based software selected, Legion SpaceWorks, superseded the original Legion Studio, in 2010 (Legion, 2012). Legion Studio was believed to have been the most advanced and realistic simulation model available for micro-level pedestrian analysis (Helgason *et al.,* 2010) and Legion SpaceWorks has continued this innovation. Primarily used by architects and civil engineers, one of the greatest innovations from Legion Studio is that in Legion SpaceWorks users are no longer required to define the paths they take, but instead only define the origin and exit point of the pedestrian. Route modifiers are then added to the model to trigger a change in the movement, activity or destination of the pedestrian, allowing for a more organic and realistic pedestrian flow to be achieved. In the past Legion SpaceWorks has been used to perform virtual experiments on the design and operation for railway stations, sports stadiums, airports, transport hubs, etc. to assess the impact of different physical designs or levels of pedestrian demand.

9.4.1 Pedestrian simulation model of the Monument Station

The simulation exercise was intended to evaluate the effectiveness of the established evacuation route for passengers in the event of an emergency in the station. The point cloud created from laser scanning the station as described in Chapter 4 was imported into Legion and the location of the agents specified. The numbers of train, numbers of passenger and location of escalators, stairs and exits was set up within Legion Spaceworks, the simulation was run to assess the egress from the station with the agents having the free choice to find the shortest route out of the station. Then a simulation showing the movement of the agents in the form of a series of still pictures

is created and from this is calculated the agent cumulative density, the evacuation time based one a 2D map and ingress-egress count over time.

Three possible and realistic scenarios were considered and simulated in the Monument station. The scenarios differ in terms of the number of trains in the station and their location. Scenario 1 is the worst case with a maximum number of passengers in the station represented by the presence of a train at each of the platforms containing 250 passengers each with an additional 50 passengers waiting in the station. The second and third scenarios considered 2 trains in the station, one at each level (Scenario 2) or both at the NS tunnel platforms (Scenario 3). Each train contained 250 passengers. Figure 214 shows how the output map colour indicate the levels of service (LoS) and the correlation between levels of service (LoS) and the quality of the passenger's space. Theoutput of cumulative maximum density (Figure 215, Figure 218 and Figure 221) and 2D evacuation time map (Figure 216, Figure 219 and Figure 222) from these three simulations show the breakdown in evacuation flow with stoppages that occurred at the concourse area and station exits. These are following the same path as the smoke/gas dispersion which is the key to evaluating the pedestrian evacuation. Therefore, the numbers/percentage of potential inhalation can be calculate from the evacuation numbers (Figure 217, Figure 220 and Figure 223) of passengers that have exited the model and the CFD airflow simulation or gas dispersion results. These indicate the potential contaminated pathway and exits. An example shown in Figure 217, indicates the timeline of gas dispersion and the number of agents exiting the model.

Level of service	Description (for queuing areas, walkways and stairways)
A	Free circulation.
B	Uni-directional flows and free circulation. Reverse and cross-flows with only minor conflicts.
C	Slightly restricted circulation due to difficulty in passing others. Reverse and cross-flows with difficulty.
D	Restricted circulation for most pedestrians. Significant difficulty for reverse and cross-flows.
E	Restricted circulation for all pedestrians. Intermittent stoppages and serious difficulties for reverse and cross-flows.
F	Complete breakdown in traffic flow with many stoppages.

Figure 214: Correlation between “levels of service” (LoS) and the quality of the passenger’s space (Transport for London, 2012)

Scenario 1: The input parameter represent realistic worst case as follows:

- 4 trains in the station at 250 people/train
- 50 people on each platform
- Concourse level with 50 people
- Movie picturing evacuation

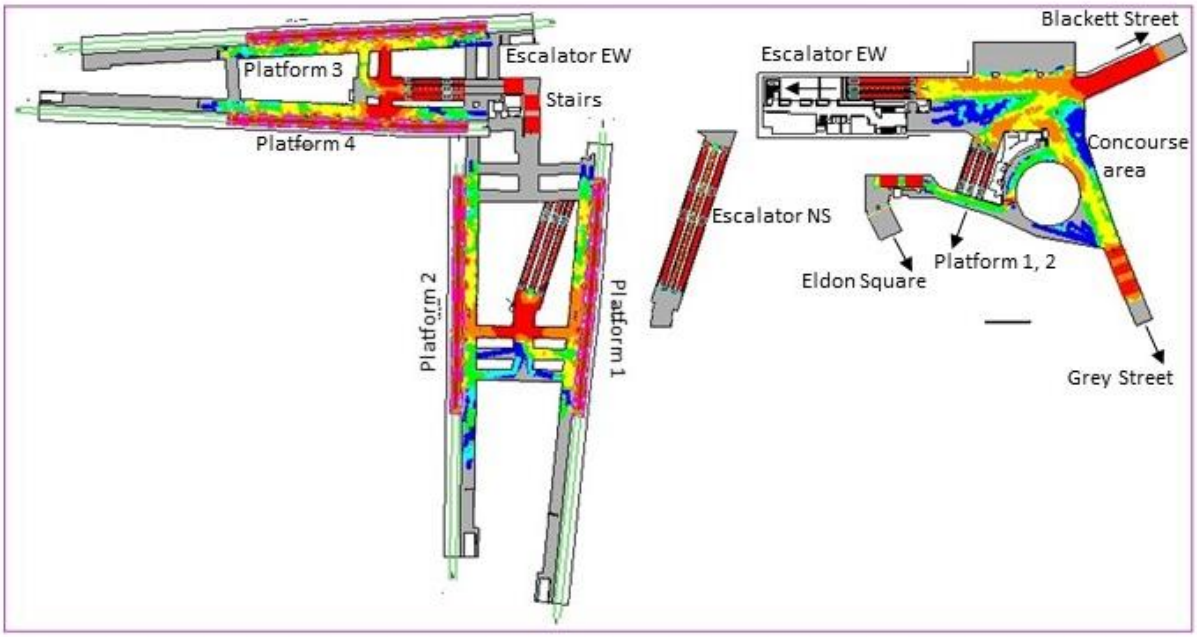

Figure 215: Scenario 1 the realistic worst case cumulative maximum density

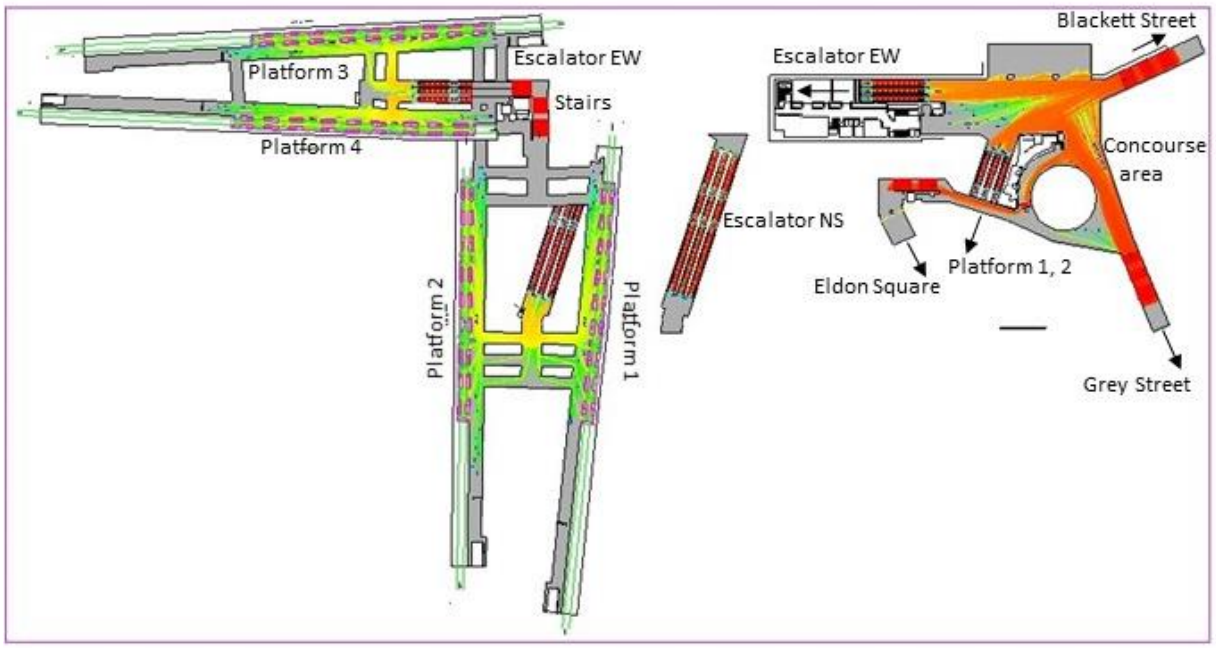

Figure 216: Scenario 1 the worst case evacuation time

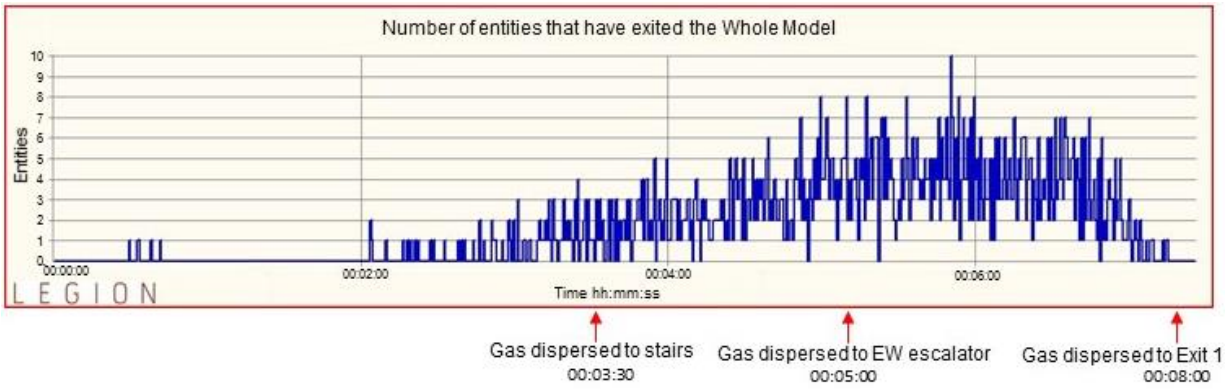

Figure 217: Scenario 1 graph model of ingress-egress count over time

Scenarios 2: The input parameter represent one train arrive at one platform in each tunnel as follows:

- 2 trains in the station at 250 people / train,1 train at platform 2 and 1 train at platform 3
- 50 people on each platform
- Concourse level with 50 people
- Movie picturing evacuation

The simulation results are shown in Figure 218, Figure 219 and Figure 220.

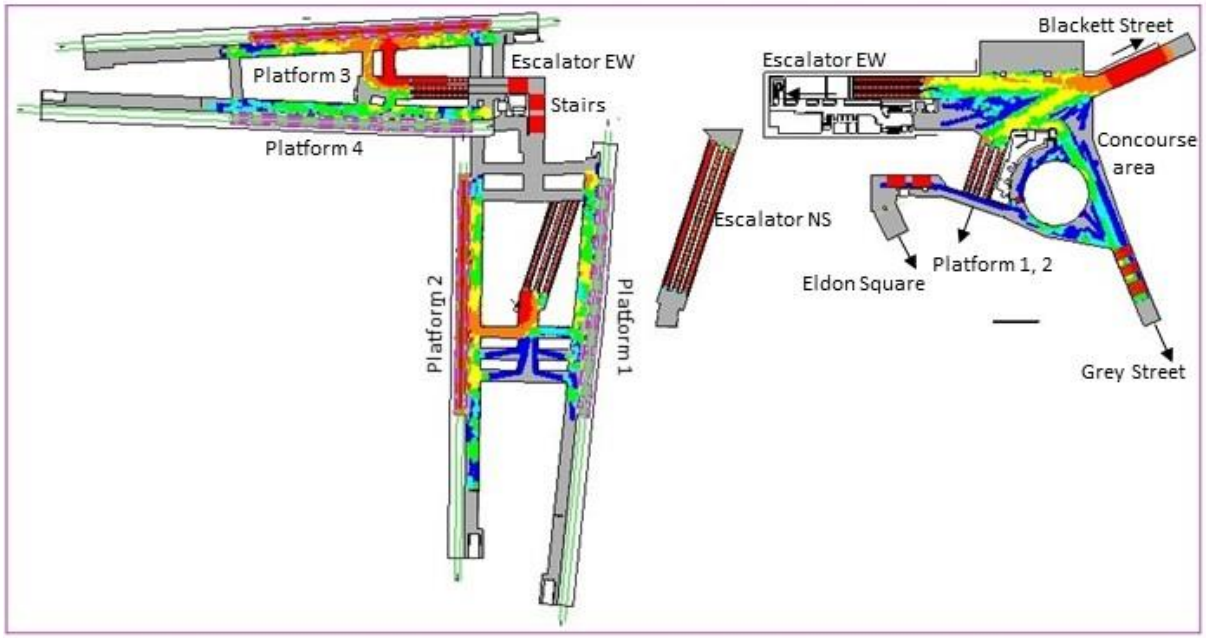

Figure 218: Scenario 2 cumulative maximum density

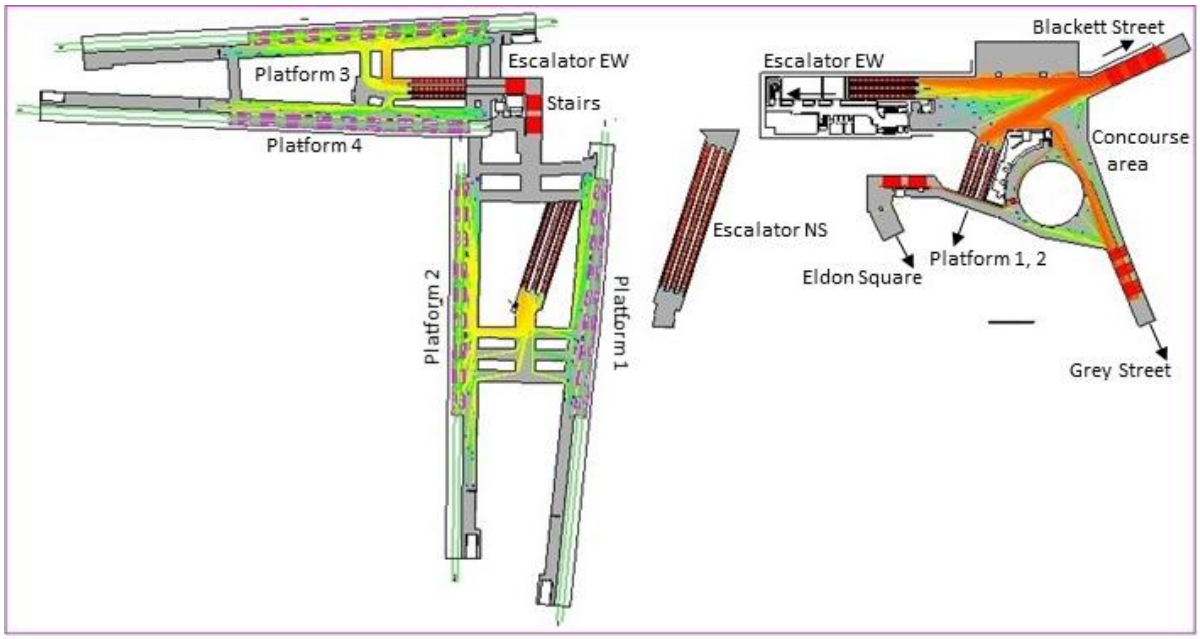

Figure 219: Scenario 2 evacuation time

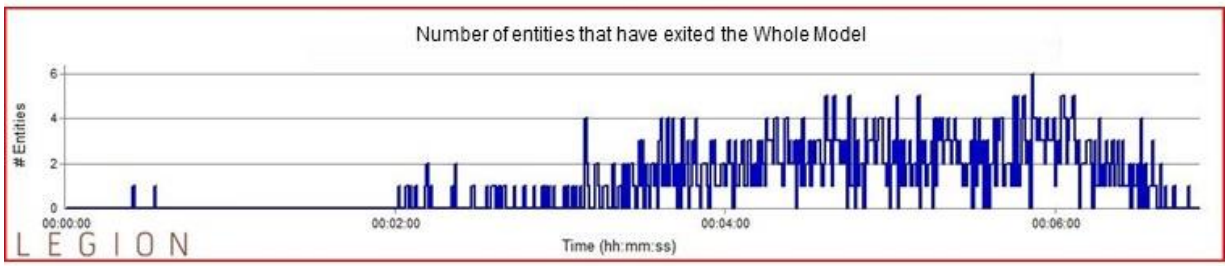

Figure 220: Scenarios 2 graph model of ingress-egress count over time

Scenarios 3: The input parameter represent two trains arrive at same tunnel platforms as follows 2 trains in the station at 250 people / train

- 2 trains on the NS tunnel level (platforms 1 and 2)
- 50 people on each platform
- Concourse level with 50 people
- Movie picturing evacuation

The simulation results are shown in Figure 221, Figure 222 and Figure 223.

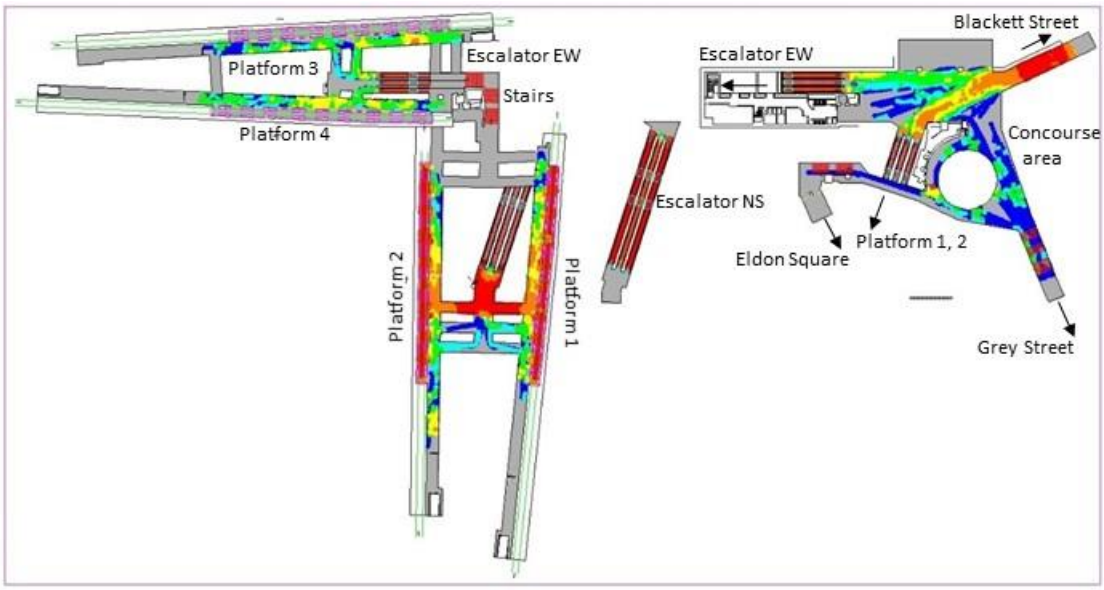

Figure 221: Scenario 3 cumulative maximum density

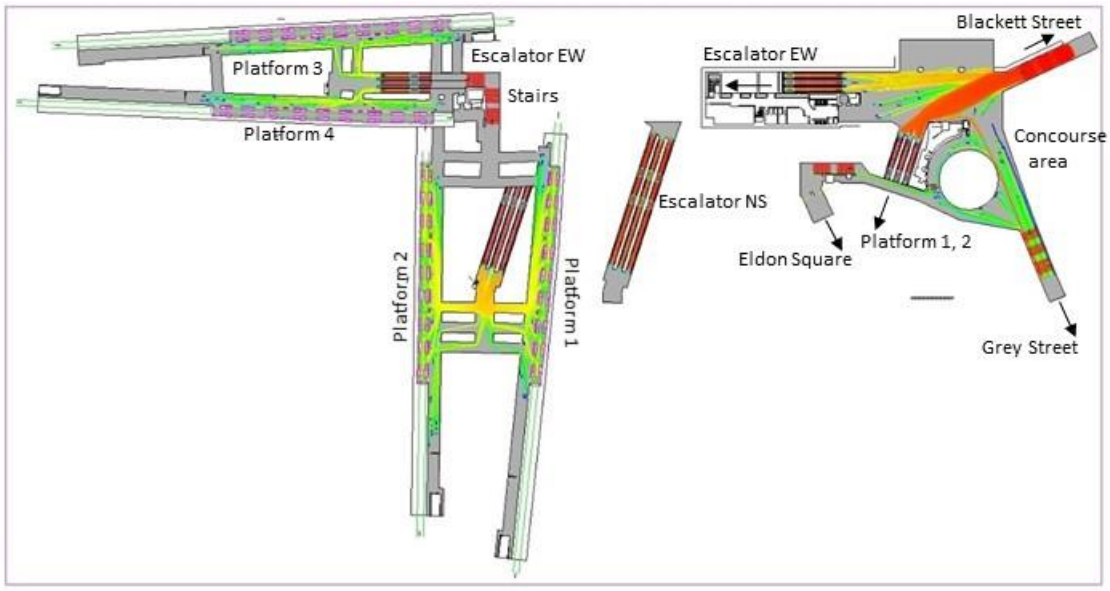

Figure 222: Scenario 3 evacuation time

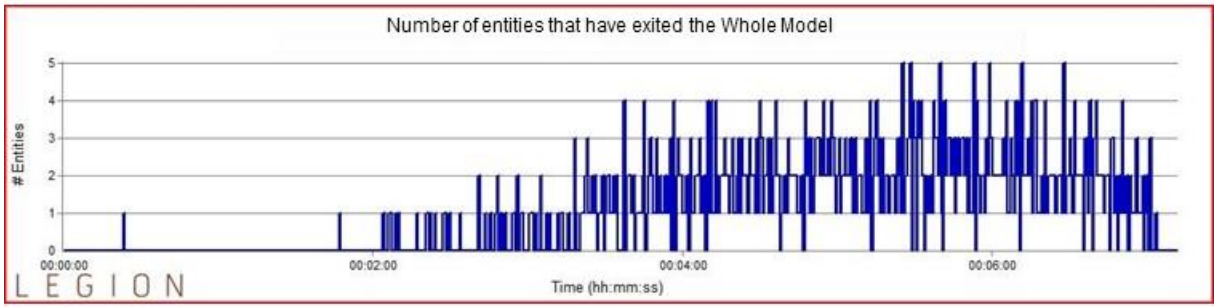

Figure 223: Scenarios 3 graph model of ingress-egress count over time

9.4.2 Results and Discussion

In setting up the simulation it was important to consider the factors most likely to influence the behaviour and movement of the agents as discussed by Sime (Sime, 1994). The speed profiles for each of the agents were configured to represent Northern European commuters. The agent's reaction time to an alarm sounding was defined in accordance with British Standards for a transportation hub (British Standards Institution, 1997) which refers to six key categories of fire evacuation analysis; alertness, familiarity, building type, staff training and alarm type. In accordance with these guidelines, generally in each of the scenarios simulated, no agents reacted to the alarm sounding in the first 30 seconds, the majority of the agents reacted around 90 seconds and all agents had reacted within 240 seconds.

A review the cumulative density result of all the scenarios shows that most congestion occurred at both escalators and exit 1. This is shown in the red color which indicate the level of service to be F, i.e. ‘Complete breakdown in traffic flow with many stoppages’. Passengers in the train and platform used the escalator closest to them into the concourse area. Then they left the station at the nearest exit which was exit 1. This evacuation strategy is based on choosing the shortest route that is the quickest evacuation strategy in practice. But compared with the station CFD simulation of the concourse level, the exit 1 could be the first to be, and the most contaminated, exit when the wind pressure is negative at this point. For example the sensitivity CFD simulation case Con_S02, shows at Exit 1 the airflow is outwards and at Exit 2 there is a strong inflow. The suggested evacuation strategy in this weather condition should be through Exit 2 where the route is less contaminate because of clean air flowing into the station from the outside.

An examination of Figure 216, Figure 219 and Figure 222 of evacuation time on the evacuation route shows that the choice of exit route in the Monument station is very limited as the agents were not allowed to proceed down the rail track and the simulation showed that all of the agents chose to exit using the main escalators to the concourse area from their platforms. None of the agents chose to change platform level before ascending the escalators. The escalators quickly became congested and this continued into the concourse area where the stairs at exits 1 and 2 were severely congested.

The egress times for the different simulations are shown in Figure 217, Figure 220 and Figure 223. It can be seen that the pedestrians are evacuated from 2 minutes to 7 minutes after the beginning of the evacuation. Overlaying the tracer gas results on this data provides an indication of the number of causalities that may be expected from an emergency incident. It can be seen that passengers on platform 1 south of the gas release point can safely exit the platform by way of the escalator to the concourse area. The tracer gas tests mentioned in chapter 6 showed that the SF_6 released on platform 2 migrated through the stair well to platform 3 and 4 in around 4 minutes and then travelled to the concourse area via the escalator in 7 minutes. This means that the passengers on platform 3 and 4 and in the concourse area near the escalators from these platforms are at greatest risk. The evacuation route from platforms 1 and 2 is less hazardous and the egress times indicate that passengers on these platforms experienced the least exposure to the SF_6 if they were amongst the first to leave the

station. Of great concern is the migration of the tracer gas to the Eldon square shopping centre through exit 3 as this was a most unexpected event for which there is currently no strategic planning. The findings from the simulations indicate that an improved evacuation strategy for this station would be for the passengers on platform 3 and 4 to be evacuated as quickly as possible to the concourse area. The passengers on the lower platforms should leave the station by walking down the track southwards against the background air flow. This will take them away from the gas release site in the station and reduce the congestion at the main exits to the station allowing speedier evacuation of the passengers on platform 3 and 4.

9.4.3 Evaluating the effects of gas dispersion on evacuation routes

The simulations performed so far have established the dispersion routes of the SF_6 released in the station and the egress time of the passengers. The next step is to establish the likelihood of passengers being overcome by the gas if the SF6 was replaced by a toxin such as phosgene.

From simply overlaying the outputs from the pedestrian simulation with the contamination maps produced from the tracer gas experiments it is possible to carry out an initial examination into those agents which may have been exposed to high levels of gas. It is clear that the limited choice of exit routes will expose the passengers to high contamination levels.

Phosgene is most commonly used today in the production process of polycarbonate. It gained infamy as a chemical weapon in world war one (Spiers, 2010). The World Health Organisation estimates a world production of up to 3 billion tons in 1997 (World Health Organization, 1997) and due to its toxicity it is produced at the same place where it is used. According to the Acute Exposure Guideline Levels (AEGL) of the US Environmental Protection Agency two values can be used for this case study:

AEGL-2 is the airborne concentration of a substance above which it is predicted that the general population, including susceptible individuals, could experience irreversible or other serious, long-lasting adverse health effects or an impaired ability to escape. AEGL-3 is the airborne concentration of a substance above which it is predicted that the general population, including susceptible individuals, could experience life-threatening health effects or death (National Research Council NRC, 2001). Phosgene AEGL-2 and AEGL-3 have a value of 600 ppb and 3,600 ppb, respectively, validated

for an exposure period of 10 min (National Research Council NRC, 2001). Each of the agents in the simulation was assigned an equivalent concentration level to 10 minutes of phosgene exposure. Based on the egress time and the interpolated SF_6 concentration along the route. This process allowed for the cumulative amount of inhaled phosgene to be calculated for each agent and for this to be compared with the cumulative value to the validated AEGL-2 and AEGL-3 exposure periods. In doing so, the number of passengers reaching and surpassing these values could be established and a safety assessment of the evacuations can be made from the total numbers of passengers reaching the different levels. Table 50 summarizes these results and indicates the number of passengers that exceed the two levels.

Concentration	Simulation 1 four trains	Simulation 2 two trains
< 600 ppb	38 agents	38
AEGL-2 (>600 to 3600 ppb)	4	2
AEGL-3 (>3600 ppb)	0	0

Table 50: AEGL Level Agents reach in different simulation

The passengers that were exposed to low concentrations of <600 ppb were those in the concourse area at the start of the evacuation so could exit the station very quickly. The egress times show that the station was fully evacuated in less than ten minutes so the exposure level of the passengers with the exception of the very slow moving did not reach AEGL-2. Those agents that were slow to respond were caught in the congestion that built up on the escalators and the staircases at the station exits. Overall however the station is well designed in terms of evacuation as the transit time for the passengers is very short compared to other stations elsewhere. From the completed study, the results show that no passengers exceeded the AGEL-3 level and therefore none would have died during their evacuation but 4 may have long-lasting health issues. This study could not take into account the possibility of passengers who exceed AEGL-2 level of contamination evacuating slower and consequently increasing the congestions build up. This may lead to a higher causality rate.

9.5 Conclusion of sensitivity modelling

This chapter has presented the results from the simulation of a variety of air flow patterns and strength based on the extended measurement and experiment results described earlier in the thesis. The simulation results are shown as steady flow streamlines which indicate the pattern and strength of the air flow. The air flow or gas dispersion speed has been calculated from the flow speed and the distance from the source of gas or toxic gas release point. The source could be at any point in the station or in a passing train, therefore, to improve evacuation strategy or to improve the station ventilation it is necessary to fully understand the flow pattern in the station under several different conditions.

The CFD sensitivity simulations show the flow pattern at the NS tunnel is relatively simple compared with the rest of the station. The flow is mainly towards the NS tunnel and the concourse level. The background airflow at the EW tunnel is lower than the NS tunnel, but here additional factors such as the stairs from the NS tunnel complicates the situation. This flow from the stairs has a significant influence to the flow pattern to

the EW tunnel that drives gas or toxic dispersion on a large scale. In the concourse simulation cases, the results indicate the air flow pattern is highly sensitive to the exit flow condition. Therefore, control of the flow direction and velocity at the exits could efficiently improve the station ventilation and control the dispersion of gas or toxic agents.

It has been demonstrated that the evacuation capabilities of the station and the efficiency of an evacuation strategy can be established by considering together the CFD analysis and an agent based evacuation simulation. A safety assessment of the evacuation strategy can be evaluates as indicated by the example given and an estimate of potential causalities can be determined by considering the cumulative exposure time for each agent and comparing this with the values based on AEGL-2 and AEGL-3. This study has only shown an example of the potential hazard of inhalation phosgene gas, but the impact of more toxic chemicals such as the nerve agent Sarin can be determined by reference to the AEGL exposure guidelines, concentrate level, exposure and cumulative periods for these chemicals. This method could also be extended to fires or events that involve the release of smoke which will introduce another factor into the evacuation simulation, that of reduced visibility, which will inhibit the movement of the agents.

Chapter 10. Conclusions and Recommendations for Further Work

10.1 Overview of this research

This chapter presents an overview and discussion of the experimental and theoretical work described in this thesis. Each of the main objectives are discussed and the main conclusions drawn from this work stated. Recommendations for further work are considered.

The literature review in chapter 2 established that subway systems have become a potential target for acts of terrorists since 9/11 and the bombings in London in 2005. Acts of terrorism against subway systems are quite frequent but not routinely reported. It is also clear that fires or similar events such as electrical faults that put the travelling public at risk are also quite frequent. In spite of the high incidence of potentially hazardous events the subway operators have a poor understanding of the potential dangers to the traveling public and have ill thought out evacuation strategies. One reason for this is the lack of understanding of the dispersion routes of smoke or toxic agents inside a station or tunnel system.

It is evident from the literature review that the air flow in a subway system is very complex and unpredictable. An initial attempt to understand this has been undertaken by the research team at the Ruhr University Bochum who based their work on studies of caves. They established a new area of research which they called “Subway Climatology” and likened the airflow in subways to that in caves in as much as it exhibits a background air flow that also showed a seasonal variability created by interaction with the outside environment.

The studies reported here showed that there existed a strong background air flow in the underground section of the Newcastle Metro that influenced the airflow within the stations. The seasonality of this was not established however and there are question marks about this aspect due to the subway being in an urban not a rural environment and being subject to the so called “Heat Island Effect” from the surrounding buildings and from elevated ground water temperatures.

It was clear from previous studies that the subway operators and the Fire and Rescue agencies are poorly informed about the risks involved in a terrorist attack in a subway system and that they need information to be presented to them in a non-technical way that they can readily understand and assimilate. As virtual environment is a format

familiar to the Fire and Rescue agencies it was sensible to develop a computing and dissemination platform based on VR. This had additional advantages in that the VR platform could share files with CFD packages, smoke and visibility software and pedestrian evacuation simulation software. It has been shown that an integrated computational environment can be created to encompass all of these aspects and further more can be extended to include air quality assessment, energy audits of stations, heating and ventilation of stations and training programs for the subway maintenance crews and the Fire and Rescue personnel.

The series of tests shown in Chapter 5 performed to measure the micro-climate in the vicinity of the station revealed that the climate was very much influenced by the presence of the surrounding buildings compared with that at a nearby weather station. There was a very loose correlation between the weather station data and the physical measurements taken at the station. A CFD analysis using the package Phoenix however based on boundary conditions at the weather station was able to predict the measured values of air flow temperature and velocity with acceptable accuracy in Chapter 7. Of particular interest is the impact of wind direction on the air flow at the station exits. When the wind was from the north air was forced into the station exit at Blackett Street and the exit at Grey Street exhibited a discharge of air. When the wind was from the south however the air entered the station at the Grey Street exit and the Blackett street exit. When the wind was from other directions the flow at the station exits was confused. What happens at the station exits has a significant effect on the airflow in the station so controlling the air flow at the station exits removes one level of uncertainty and will help to remove doubt in the minds of the station operating staff with regard to the air flow direction.

The tracer gas experiments in Chapter 6 showed that the tracer gas propagates to the upper parts of the station very quickly emerging at the station concourse within a few minutes after the release. The propagation path of the SF_6 released on the station platform was most unexpected as in addition to travelling down the subway tunnel to the Haymarket station, a significant proportion traversed the stairway linking platform 1 and 2 to platforms 3 and 4 contaminating the east-west platforms. The SF_6 then travelled up the escalator from platform 3 and 4 to the station concourse before exiting the concourse into Eldon Square shopping centre. Unfortunately, the propagation path overlapped with the main exit and evacuation routes for passengers.

The new integrated analysis and measuring system used in this work opens new opportunities, as more complex field tests can be conducted with less effort than previously producing more reliable and accurate results. During the measurement campaign five tracer gas experiments were conducted. Collecting this amount of data with the previous methods such as taking air samples using syringes required over 6000 samples to cover the same measuring time, with a sample rate of only 1 min. The new sensors could measure with a sample rate of 2 s, which is a big advantage. Experiment costs are reduced to a tenth with the method used in this work. The tracer gas test results have proved to be very valuable in validating the CFD simulation results.

Observation of the two tracer gas tests in which SF_6 was released in the operating train shows the tracer gas filled the coach in which the gas was released with a very high concentration. It took more than 25 minuses with 13 stops at stations to circulate the air in the coach and finally eject the gas. When the train arrived at a station the gas quickly transferred to the second coach and dispersed quickly into the station due to the strong air movement produced by the train entering the station. The gas remained longer in the station when the train operation was in the opposite direction to the natural background direction. The tracer gas could last in the station more than an hour and it could contaminate all the trains that travelled through the station. The air motion created by the piston effect of the train as it passed through the station affected all levels in the station. The piston effect could push air through the station and also cause reverse flows as the train left the station. It could also contaminate other trains that passed through the station. The concentration of tracer gas was much lower and the contamination time much shorter when the train travelled in the same direction as the natural background air flow in the tunnel.

This work has shown that it is possible to set up a computational environment encompassing aspects from virtual environment and CFD in Chapter 8. The common computational platforms that are available for these two distinct disciplines allows data to be shared between different source codes and platforms. As this is a rapidly developing area it may be that in the future different platforms, such as gaming platforms, may be used to engage with this work. The reasons behind this are related to the degree of detail and accuracy that is warranted in modelling large scale structures such as a subway station. The information that was produced from the point cloud data generated from the laser scans was far too detailed such that when it was used to generate a CFD mesh in an unrefined state, the mesh was far too complicated.

Accommodating the fine detail from the laser scan resulted in a very large CFD mesh with a large number of elements of numerous sizes especially near the walls to accommodate the boundary layer details. Such features as skirting boards and wall mounted display cabinets, for example, required small and detailed meshing in order to accommodate them. This resulted in vary large set up times and long computational times. Removing these items and simplifying other features such as stairs and escalators simplified the meshing considerable and reduced the set up time. Comparing the predicted airflow after taking out the details and simplifying the mesh with the original predictions showed no significant difference in the factors of interest in this work which are the direction of travel, the bulk velocity and the flow rate. There is then scope for examining the type of computing platform that could be used for this work. There is clearly a compromise to be met between detail and cost (CPU time and set up time) which may be met by choosing a more appropriate CFD package.

The CFD predictions were compared against the results of the tracer gas tests and proved to be in good agreement in Chapter 9. In addition to performing a CFD analysis of the actual conditions when the tracer gas tests were performed, a sensitivity analysis examining the response of the station air flow to external factors was also performed. This was important because it was possible to show the conditions or factors that influenced the internal air flow and how these can be controlled. The migration of the SF_6 in the concourse level is arguable the most important aspect of this work as this has the potential of resulting in a large loss of life if an aggressive and highly potent toxin is released in the station. The sensitivity analysis showed that this flow pattern is reached when there is an inflow of air from the Grey street exit of the station. This then forces the air entering the concourse from the escalators to go to the Eldon square exit and enter the shopping area. As mentioned earlier removing the variability of the air flow at the station exits will lead to a better understanding of the air flow in the station and lead to higher confidence in an evacuation strategy.

An integrated modelling and information distribution platform has been created encompassing elements of virtual environment model, CFD, and pedestrian evacuation simulation that can be further developed to include smoke dispersion, air quality, heating and ventilation and training activities. This has been done by choosing packages such as FARO SCENE, Autodesk 3ds Max, PHOENICS, ANSYS ICEM, ANSYS Fluent and LEGION that can exchange data files in a common format. It will be possible to include other files such as SOFIA in this activity. One important aspect

that has emerged from this work is that it is important to be aware of the level of detail required in the simulation tools so that acceptable accuracy is achieved without requiring excessive set up and CPU time. In the future it may be advisable to consider the use of alternative platforms such as gaming based as developments are moving ahead very quickly in this field and they offer a readily understood (by lay people) user interface and display.

10.2 Contribution of this thesis

1. The airflow in a subway system is extremely complex and is influenced by the system design and by an interaction with the over ground weather. The hypothesis that a subway system behaves like a cave in exhibiting a seasonal variability in air flow has not been fully established. The research has proved the airflow pattern in subway stations is affected by the external environment and the subways behaves like caves in this respect. Although it is considered that the urban heat island effect, urban microclimate and the activities in the subway system are attenuating the seasonal variability of the airflow and more airflow patterns are created in a shorter time range compare to the caves.
2. The ventilation systems of the Monument Station was poorly specified and when coupled with an inadequate understanding of the station internal airflow produced a most unexpected air flow pattern in the station including flow reversals and recirculation. Such factors could compromise evacuation strategies in the event of the release of a toxic agent in the station and result in passengers being directed to areas in the station with a greater risk of danger.
3. A method of analysing subway systems has been established in this work which can be used for existing stations and tunnels which are not accessible to other analysis methods due to the lack of CAD files or architectural drawings. This method would be very applicable to the analysis of existing stations that may be due for improvement or as an early stage design tool for the architect or designer. It will allow the station to be analysed before construction has got underway and can also be used to assess the efficacy of proposed changes in the station decoration and signage. The virtual output of this methodology provides information that can be understood by lay people and can be extended to provide further information such as the dispersion of smoke in the event of a fire, or the assessment of the air quality in a station. This methodology could also be used in an energy audit or environmental analysis of a subway station

where air quality has an important impact on the performance of air handling units.

4. CFD is a powerful tool for examining the air flow in stations. The software package used in this work, ANSYS-Fluent which is a well-established CFD package can produce very detailed flow patterns which have proved to be is very informative. However ANSYS-fluent may not be the best package to use for this type of work. It is better suited for simulating very detailed flows such as the high speed secondary flows in an axial compressor rather than the low speed, incompressible bulk flows in this work. A better suited package needs to be found that has the required degree of accuracy for this type of work and has short set up time and computational times. This may be a more attractive platform for civil engineering companies and architects to use.
5. Tracer gas experiments using SF_6 are a very effective way of examining the air flow in a subway system. The sensors used in this work can accurately detect SF_6 contamination from 0.05 to 50 ppm and are a low cost method of performing these experiments. A very low detection limit is warranted due to the high greenhouse potential of SF_6. The threshold limit of SF_6 is 1,000 ppm for an average eight hour working day, so it is possible to conduct such tracer gas experiments during operational times without harming the passengers.
6. The over ground external climate, especially the wind direction had a significant influence on the station airflow. It was established that changes in the strength and direction of the air flow at the station exits produced significant changes to the internal air flow strength and migration path. The control of the air flow strength and direction at the exits would stabilise the air flow in the station and allow evacuation routes to be developed with a high level of confidence.
7. The manner in which the SF_6 tracer gas dispersed in the station and the evacuation simulation performed using Legion showed that the current evacuation strategy of the Monument Station will lead passengers into danger The SF_6 followed the passenger exit routes but was able to overtake many subjects due to the high chimney effects in the escalator shafts. The safest evacuation route is to travel away from the source of contamination and against the background air flow. In the case of the Newcastle system which has an overhead power feed, the best choice of evacuation route following an incident at the Monument station is to move down the track in the southerly direction

towards the Central Station for passengers on platform 1 and 2 and eastwards towards Manors Station for passengers on platform 3 and 4.

10.3 Recommendations for further work

It has been established in this work that virtual environment offers a very appropriate platform for examining fluid dynamic and related activities in a subway system. This can be used at several different levels, to provide information that can be easily assimilated and understood to people without a technical background such as subway operators and the Fire and Rescue personnel to people that understand very sophisticated CFD modelling. The platform can be used for several different activities from a training tool for Fire and Rescue personnel and maintenance teams to an early stage design tool to assist building engineers and architects in the design of stations. For instance, combining of fire modelling and smoke dispersion with the models developed in this research could form the basis of future studies seeking efficiency of operational aspects of evacuation procedures. The rapid development of the graphics of gaming platforms has now reached the stage that they may be a viable alternative to the traditional form VR presentation.

The results from the air flow modelling have shown that the interface between the station and the outside environment has a significant impact on the air flow in the station. Whenever the wind outside Exit 2 in Grey Street had a component from the south this entered the concourse area of the station and drove air entering the concourse area from the platforms into Eldon Square. The unsteadiness of the external environment at the exit on Blackett Street, produced mainly by the frequent passage of busses was also an issue of concern. It is felt that controlling the air flow velocity conditions at the station exits is fundamental to controlling the air flow in the station. Essentially, open exits emerging directly onto a street promote unsteadiness in the station air flow. This type of exit has not changed since the construction of the first subway system in 1863. We now have the tools to investigate through modelling the impact on the internal air flow of the station of isolating the exits from the external environment and examining the type of air flow at the exits that offers the safest regime in the station. This may then lead to the exits being contained within a structure with ventilation fans that remove air from the concourse area. It may be that a recommendation from this work is that these types of exits are no longer used and that all station exits are placed within buildings.

Further modelling can be performed to examine the possibility of using the natural air flow in a subway system to assist environmental control. Certainly any consideration of environmental and energy control within a station should take the background air flow into account. The computer platform that has been produced in this work can be extended to include energy audit modelling.

APPENDIX A

Full transcript of portable measurements in Chapter 5 on the CD enclosed with this thesis.

APPENDIX B

Full screenshot of the Microclimate CFD simulation results in Chapter 7 on the CD enclosed with this thesis.

REFERENCES

Ampofo, F., Maidment, G., & Missenden, J. (2004) 'Underground railway environment in the UK Part 2: Investigation of heat load'. Applied Thermal Engineering, 24(5), 633-645.

ANSYS Fluent. (2006) *FLUENT 6.3 User's Guide - 12.4.2 RNG – Model*. [online] Available at: https://www.sharcnet.ca/Software/Fluent6/html/ug/node479.htm [Accessed 19 Jan. 2015].

ANSYS ICEM. (2013) 'CFD User's Manual'. *Ansys Inc.*

Apte, V., Green, A., & Kent, J. (1991) 'Pool fire plume flow in a large-scale wind tunnel'. Fire Safety Science—Proc. 3rd Int. Symposium.

Autodesk.co.uk. (2013) *3ds Max* | *3D Modelling & Rendering Software* | *Autodesk*. [online] Available at: http://www.autodesk.co.uk/products/3ds-max/overview [Accessed 8 Sep. 2013].

Banlaoi, R. C. (2009) 'Counter Terrorism Measures in Southeast Asia: How Effective Are They?'. Manila: Yuchengco Center, De La Salle University.

Barnes E., (1998) 'Protecting Public Transport from Terrorists'. Inst. of Justice Journal. 1998.

Batty M., (2003), *Agent Based Pedestrian Modelling*, CASA paper 61.

Beard, A. N. (2009) 'Fire safety in tunnels'. *Fire Safety Journal*, 44(2), 276-278.

Beard, A., & Cope, D. (2007) 'Assessment of the Safety of Tunnels. Study. Final Report for the STOA'. *Science and Technology Options Assessment*. European Parliament.

Bendelius. A. G. (1976) 'Aerodynamic and thermodynamic evaluation for the Atlanta subway system'. *In: Proceedings of the 2nd international symposium on aerodynamics and ventilation of vehicle tunnels*, C1, p. C1-1– 20.

Berrou, J. L., Beecham, J., Quaglia, P., Kagarlis, M. A., & Gerodimos, A. (2007) 'Calibration and validation of the Legion simulation model using empirical data'. *In Pedestrian and Evacuation Dynamics 2005* (pp. 167-181). Springer Berlin Heidelberg.

Blue V., Adler J. (1998) ‘Emergent Fundamental Pedestrian Flows from Cellular Automata Micro simulation’, *Transportation Research Board,* 1664, 1998.

Boes C., Kies C., Massen A., Schintgen F., Singer E, Waringo G., (1997) The Moestroff Cave, A Study in the Geology and Climate of Luxembourg’s Largest Maze Cave. Centre de Recherches Public Centre Universitaire, pp 200, Luxembourge.

Borth J., (1989) ‘Numerical Simulation of Air Flows in Rooms’, *ERCOFTAC Bulletin*, Vol. 6.

Borth, J. (1990) ‘Numerical simulation of air flows in rooms’, *ERCOFTAC Bulletin*, 5, 9-14.

Brandies, J., & Bergmann, D. J. (1983) ‘A numerical study of tunnel fires’, *Combustion science and technology*, 35(1-4), 133-155.

Breuer, M., Lakehal, D., & Rodi, W. (1996) Flow around a surface mounted cubical obstacle: comparison of LES and RANS-results Computation of Three-Dimensional Complex Flows (pp. 22-30): Springer.

British Standards Institution. (1997) Draft British Standard BS DD240 fire safety engineering in buildings, Part 1: guide to the application of fire safety engineering principles. British Standards Institution.

Brown, W. G. (1966). ‘Basic Theory of Rapid-Transit Tunnel Ventilation’, *Journal of Engineering for Industry*, 88(1), 1-7.

Bruckner, J. V., Keys, D. A., & Fisher, J. W. (2004) ‘The Acute Exposure Guideline Level (AEGL) program: applications of physiologically based pharmacokinetic modeling’, *Journal of Toxicology and Environmental Health*, Part A, 67(8-10), 621-634.

Brune M., Charlton J., Pflitsch A., Agnew B., (2016) ‘The Influence of subway climatology on gas dispersion and the effectiveness of guided evacuations in a complex subway station’, *Meteorologische Zeitschrift*, Vol. 25 No. 4, p. 489 – 499.

Bullister, J. L., Wisegarver, D. P., & Sonnerup, R. E. (2006). Sulfur hexafluoride as a transient tracer in the North Pacific Ocean. Geophysical Research Letters, 33(18).

Castle, C. J. E. (2006) *Developing a prototype agent-based pedestrian evacuation model to explore the evacuation of King' s Cross St Pancras underground station*.

Castle, C. J. E. (2006) *Developing a prototype agent-based pedestrian evacuation model to explore the evacuation of King's Cross St Pancras underground station.* UCL Centre for Advanced Spatial Analysis (Ed.), Working Paper Series. Working Paper 108, London.

Certainty3d.com. (2013) *Certainty 3D*. [online] Available at: http://www.certainty3d.com/ [Accessed 8 Sep. 2013].

Chang, C. H., & Meroney, R. N. (2003) 'Concentration and flow distributions in urban street canyons: wind tunnel and computational data', *Journal of Wind Engineering and Industrial Aerodynamics*, 91(9), 1141-1154.

Charlton, J. (2011) *An integrated approach to the design of city centre squares, using three-dimensional computer representations* (Doctoral dissertation, Northumbria University).

Chasse, P. (1993) 'Sensitivity study of different modelling techniques for the computer simulation of tunnel fires, comparison with experimental measures', *First CFDS International User Conference*.

Chen, F., Chien, S. W., Jang, H. M., & Chang, W. J. (2003) 'Stack effects on smoke propagation in subway stations'. Continuum Mechanics and Thermodynamics, 15(5), 425-440.

Chen, F., Guo, S.-C., Chuay, H.-Y., & Chien, S.-W. (2003) 'Smoke control of fires in subway stations', *Theoretical and Computational Fluid Dynamics*, 16(5), 349-368.

Chen, X., & Zhan, F. B. (2008) 'Agent-based modelling and simulation of urban evacuation: relative effectiveness of simultaneous and staged evacuation strategies', *Journal of the Operational Research Society*, 59(1), 25-33.

Chow, T. T., Lin, Z., & Tsang, C. F. (2006) 'Applying large eddy simulation in the study of fire and smoke spread at underground car park', *International Journal on Architectural Science*, 7(2), 35-46.

Chow, W.K., (1996) 'Simulation of tunnel fires using a zone model', *Tunnelling and Underground Space Technology*, 11(2), pp.221-236.

Chu, J. (2004) Glance at world subway, Railway Knowledge, no. 2, pp. 20.

Cignoni, P. (2013) *MeshLab*. [online] Available at: Meshlab.sourceforge.net. Available at: http://meshlab.sourceforge.net/ [Accessed 8 Sep. 2013].

Coke, L., Sanchez, J., & Policastro, A. (2000) A model for dispersion of contaminants in the subway environment: Argonne National Lab., IL (US).

eBIM. (2011a) Existing Building Information Modeling, [online] Available at: http://www.ebim.co.uk/what-is-ebim/ [2 November 2012]

eBIM. (2011b) 'Pointcloud intergration into Revit: A few thoughts', eBIM Existing Building Information Modeling.

Ergin-Özkan, S., Mokhtarzadeh-Dehghan, M., & Reynolds, A. (1995) 'Experimental study of natural convection between two compartments of a stairwell', *International journal of heat and mass transfer*, 38(12), 2159-2168.

Faro.com. (2013) *FARO Laser Scanner Software - SCENE - Overview*. [online] Available at: http://www.faro.com/products/faro-software/scene/overview [Accessed 8 Sep. 2013].

Ferziger, J. H. (1985) 'Large eddy simulation: its role in turbulence research'*. In Theoretical approaches to turbulence* (pp. 51-72). Springer New York.

Fletcher, D., Kent, J., Apte, V., & Green, A. (1994) 'Numerical simulations of smoke movement from a pool fire in a ventilated tunnel', *Fire Safety Journal*, 23(3), 305-325.

Fureby, C., & Grinstein, F. (1998). Towards large eddy simulations of flows in complex geometries. AIAA Paper (98-2806).

Gao, P., Liu, S., Chow, W., & Fong, N. (2004) 'Large eddy simulations for studying tunnel smoke ventilation', *Tunnelling and Underground Space Technology*, 19(6), 577-586.

Geomagic.com. (2014). 3D scanning, design and reverse engineering software from 3D Systems Geomagic. [online] Available at: http://www.geomagic.com/en/ [Accessed 8 Sep. 2013].

Giddings, B., Charlton, J., & Horne, M. (2011). Public squares in European city centres. Urban Design International, 16(3), 202-212.

GoogleMaps. (2013). *Monument Metro station Retrieved* 07 January 2013, 2013, from https://maps.google.co.uk/maps?rls=com.microsoft:en-gb:IE-Address&q=Monument%20Metro%20station&um=1&ie=UTF-8&hl=zh-CN&sa=N&tab=wl&authuser=0. [Accessed 8 Sep. 2013].

Gosman, A. (1999) 'Developments in CFD for industrial and environmental applications in wind engineering', *Journal of Wind Engineering and Industrial Aerodynamics*, 81(1), 21-39.

Gousseau, P., Blocken, B., Stathopoulos, T., & van Heijst, G. J. F. (2011) 'CFD simulation of near-field pollutant dispersion on a high-resolution grid: A case study by LES and RANS for a building group in downtown Montreal', *Atmospheric Environment*, 45(2), 428-438. doi: 10.1016/j.atmosenv.2010.09.065

Grainge, C., & Rice, P. (2010). Management of phosgene-induced acute lung injury. Clinical toxicology, 48(6), 497-508.

Greater London Authority. (2006) 'London's urban heat island: a summary for decision makers'. London: Greater London Authority.

Greenwood, D., Horne, M., Thompson, E. M., Allwood, C. M., Wernemyr, C., & Westerdahl, B. (2008) S*trategic perspectives on the use of virtual reality within the building industries of four countries.* Architectural engineering and design management, 4(2), 85-98.

Gwynne, S., Galea, E. R., Owen, M., Lawrence, P. J., & Filippidis, L. (1999) ‘A review of the methodologies used in the computer simulation of evacuation from the built environment’, *Building and environment*, 34(6), 741-749.

Hagenah, B., Reinke, P., & Vardy, A. (2006) ‘Effectiveness of pressure relief shafts–full scale assessment’, *In 12th International Symposium on Aerodynamics and Ventilation of Vehicle Tunnels*, Portoroz, Slowenien.

Hamil, S. (2011). *Point cloud surveys' NBS Retrieved* 15 November 2012, from http://www.thenbs.com/topics/bim/articles/pointCloudSurveys.asp

Han, Y., Zhao, L., and L. Xing, Y., (2010) *Research on the form of air shaft upon tunnel ventilation*. Railway Standard Design, no. 2, pp. 62–64.

He, J. B.,Wu, X. P., and Bian, Z.M., (2007) ‘Influence factors of the piston wind in single line tunnel’, *UrbanMass Transit*, no. 3,pp. 46–50.

Helgason, Ó., Kouyoumdjieva, S. T., & Karlsson, G. (2010) ‘Does mobility matter?. In Wireless On-demand Network Systems and Services (WONS)’, *2010 Seventh International Conference* (pp. 9-16). IEEE.

Horne, M., & Thompson, E. M. (2008) ‘The role of virtual reality in built environment education’, *Journal for Education in the Built Environment*, 3(1), 5-24.

Horne, M., Thompson, E. M., & Charlton, J. (2014) Towards a multifunctional virtual city model. *Technologies for Urban and Spatial Planning: Virtual Cities and Territories: Virtual Cities and Territories*, 154-172.

Hu, L., Wu, L., Lu, K., Zhang, X., Liu, S., & Qiu, Z. (2014) ‘Optimization of emergency ventilation mode for a train on fire stopping beside platform of a metro station’, *In Building Simulation* (Vol. 7, No. 2, pp. 137-146). Tsinghua University Press.

Huang, Y., Hong, T. H., & Kim, C. N. (2012) ‘A numerical simulation of train-induced unsteady airflow in a tunnel of Seoul subway’. *Journal of mechanical science and technology*, 26(3), 785-792.

Ingason, H., Hägglund, B. and Werling, P., (1999) ‘Effects of ventilation on smoke spread in tunnels’, *In Proceedings of the first international conference on tunnel fires and one day seminar on escape from tunnels*, Lyon, France (pp. 407-46).

Jenkins, B. M. (2001) ‘Protecting public surface transportation against terrorism and serious crime: An executive overview’. (No. FHWA/CA/OR-2001-29,). Mineta Transportation Institute, College of Business, San José State University.

Jones, W., & Launder, B. (1972) ‘The prediction of laminarization with a two-equation model of turbulence’, *International journal of heat and mass transfer*, 15(2), 301-314.

Junfeng, X. U. (2010) ‘Application of Passenger Simulation in Design of Metro Transfer Stations [J]’, *Tunnel Construction*, 1, 007.

Kato S., Murakami S., Shoya S., Hanyu F., Zeng J., (1995) *CFD Analysis of Flow and Temperature Fields in Atrium with Ceiling Height of 130m*, ASHRE Trans vol 101.

Kim, J., & Kim, K. (2007) ‘Experimental and numerical analyses of train-induced unsteady tunnel flow in subway’, *Tunnelling and Underground Space Technology*, 22(2), 166-172.

Kim, S. E., & Boysan, F. (1999) ‘Application of CFD to environmental flows’, *Journal of Wind Engineering and Industrial Aerodynamics*, 81(1), 145-158.

Kimpton, G., Horne, M., & Heslop, D. (2010) ‘Terrestrial laser scanning and 3D imaging: Heritage case study–The Black Gate, Newcastle upon Tyne’, *International Archives of the Photogrammetry, Remote Sensing and Spatial Information Sciences*, 325-330.

Kuligowski, E. D. (2016) ‘Computer evacuation models for buildings’, *InSFPE Handbook of Fire Protection Engineering* (pp. 2152-2180). Springer New York.

Lateb, M., Masson, C., Stathopoulos, T., & Bédard, C. (2011). Effect of stack height and exhaust velocity on pollutant dispersion in the wake of a building. Atmospheric Environment, 45(29), 5150-5163.

Law, C. S., Watson, A. J., & Liddicoat, M. I. (1994) ‘Automated vacuum analysis of sulphur hexafluoride in seawater: derivation of the atmospheric trend (1970–1993) and potential as a transient tracer’. *Marine Chemistry*, 48(1), 57-69.

Le Glatin, N., Milford, I., & Hutton, A. (2014) ‘London Bridge: The Role Pedestrian Modelling Played in Designing the New Station’, *In Pedestrian and Evacuation Dynamics 2012* (pp. 21-37). Springer International Publishing.

Lee, S.R. and Ryou, H.S., (2006) ‘A numerical study on smoke movement in longitudinal ventilation tunnel fires for different aspect ratio’, *Building and Environment*, 41(6), pp.719-725.

Legion, (2012) *Legion Studio*. [online] Available at: http://www.legion.com/software/studio-2006.php. [Accessed 8 Jun. 2014].

Legion.com. (2013) *Legion* | *Science in Motion*. [online] Available at: http://www.legion.com [Accessed 25 Sep. 2013].

Leitl, B. M., Kastner-Klein, P., Rau, M., & Meroney, R. N. (1997) ‘Concentration and flow distributions in the vicinity of U-shaped buildings: wind-tunnel and computational data’, *Journal of Wind Engineering and Industrial Aerodynamics*, 67, 745-755.

Leonard, J. J., Feddes, J. J. R., & McQuitty, J. B. (1984) ‘Measurement of ventilation rates using a tracer gas’, *Canadian Agricultural Engineering*, 26(1), 49-51.

Levy, C. J. (2010). Moscow attack a test for Putin and his record against terror. New York Times.

Li, W.-l., Yan, X.-p., & Wang, F. (2003) ‘Relation between the mrt building and underground space exploitation’, *Chinese Geographical Science*, 13(4), 364-369.

Lin, W. (2010). Large-Eddy Simulation of Premixed Turbulent Combustion Using Flame Surface Density Approach. University of Toronto.

Litman, T. (2005) ‘Terrorism, transit and public safety: evaluating the risks’. *Journal of Public Transportation*, 8(4), 3.

Liying, H. (2010). Evacuation Simulation of Atrium Metro Station in Fire Accidents. Chinese *Journal of Underground Space and Engineering*, 4, 861-866.

Loukaitou-Sideris, A., Taylor, B. D., & Fink, C. N. (2006) 'Rail transit security in an international context lessons from four cities'. *Urban Affairs Review,* 41(6), 727-748.

Ludwig, J. C., & Mortimor, S. (2010). PHOENICS-VR reference guide.*London: CHAM*.

Mendonca, F., & Drake, S. (1996). Computational fluid dynamics (CFD) analysis of a decelerating train entering an underground station. Paper presented at the Proc. 1st Int. Conf. on Computer Application in Transportation Systems.

Meng, N., Hu, L., Wu, L., Yang, L., Zhu, S., Chen, L., & Tang, W. (2014). Numerical study on the optimization of smoke ventilation mode at the conjunction area between tunnel track and platform in emergency of a train fire at subway station. *Tunnelling and Underground Space Technology*, 40, 151-159.

Meroney, R. N., Leitl, B. M., Rafailidis, S., & Schatzmann, M. (1999). Wind-tunnel and numerical modeling of flow and dispersion about several building shapes. *Journal of Wind Engineering and Industrial Aerodynamics*, 81(1), 333-345.

Metraux, D. A. (1995). Religious terrorism in Japan: The fatal appeal of Aum Shinrikyo. Asian Survey, 35(12), 1140-1154.

Monaghan, A. (2010). The Moscow metro bombings and terrorism in Russia. *NATO Defence College.*

Moore G.W., Sullivan G.N., 1964, Speleology – the Study of Caves. Zephrus Press, USA, 1964.

Morton, P. J., Horne, M., Dalton, R., & Thompson, E. M. (2012). Virtual City Models: avoidance of obsolescence. *Digital Physicality-Proceedings of the 30th eCAADe Confer-Comparative evaluation of the two methodologies*.

Murakami, H. (2010). Underground: The Tokyo gas attack and the Japanese psyche: Random House LLC.

Murakami, S., Kato, S., Chikamoto, T., Laurence, D., & Blay, D. (1996). New low-Reynolds-number k-ε model including damping effect due to buoyancy in a stratified flow field. *International journal of heat and mass transfer,* 39(16), 3483-3496.

Murakami, S., Mochida, A., & Ooka, R. (1993). Numerical simulation of flowfield over surface-mounted cube with various second-moment closure models. *9th Symposium on Turbulent Shear Flow*.

Murphy, P. (2006). Report into the London terrorist attacks on 7 July 2005. Intelligence and Security Committee.

National Research Council NRC, (2001). *Standing Operating Procedures for Developing Acute Exposure Guideline Levels for Hazardous Chemicals*. National Academy Press, Washington, DC (2001).

Network Rail (2011), Guide to Station Planning and Design, Issue 1, 1-110.

Nexus. (2013) Nexus. [online] Available at: http://www.nexus.org.uk/metro/ [Accessed 1 Oct. 2013].

Nexus. (2014) Nexus. [online] Available at: http://www.nexus.org.uk/metro/timetables-stations [Accessed 7 Feb. 2014].

Ogawa, Y., Yamamura, Y., Ando, H., Kadokura, M., Agata, T., Fukumoto, M. & Nonaka, H., (2000). An attack with sarin nerve gas on the Tokyo subway system and its effects on victims.

Palmer A.N., (2007) Cave Geology, *Cave Books*, pp 454, Dayton Ohio, 2007.

Pan, S., Fan, L., Liu, J., Xie, J., Sun, Y., Cui, N., Zhang, L. and Zheng, B., (2013) 'A review of the piston effect in subway stations', *Advances in Mechanical Engineering*, 5, p.950205.

Park, N., Kobayashi, T., & Taniguchi, N. (1997) 'Investigation on Large Eddy Simulation of Flows Around a Cubical Obstacle Mounted on a Surface Channel', *International Conference on Fluid Engineering*, Tokyo, Japan.

Patel, V. C., Rodi, W., & Scheuerer, G. (1985) 'Turbulence models for near-wall and low Reynolds number flows-a review', *AIAA journal*, 23(9), 1308-1319.

Pflitsch A., Piasecki J., (2003) 'Detection of an Airflow System in Niedzwiedzia (Bear) Cave, Kletno, Poland', *Journal of Cave and Karst Studies*, 65, 3, pp. 160 – 173, 2003.

Pflitsch A., Piasecki J., Ringeis J, (2005) Untersuchun gen zur Klimatologie Barometrischer Hohlen am Beispiel von Jewel Cave and Wind Cave in Sud Dakota USA, In: Verein fur Hohlenkunde in West-falen (ed.) *Spelaologisches Jahrbuch*. 2005-06.

Pflitsch, A., (2001a) 'Investigations on air currents in underground public transportation systems', *Meteorologische Zeitschrift*, 10(4), 239-246.

Pflitsch, A. (2001b) 'Subway von New York City: Stadtklima im Untergrund', *Geographische Rundschau,* 53(1), 34-41.

Pflitsch, A., & Flick, B. (2000) 'Proof and characterization of slowest air currents using sonic anemometers in urban and topographical climatology research: Sensors', *Journal of Applied Sensing Technology*, 17, 75-82.

Pflitsch, A., & Geppert, C. (2000) 'Comparison of airflow in two different passively ventilated subway systems-New York City (USA) and Dortmund (Germany)', *Proceedings of the Third Symposium on the Urban Environment*.

Pflitsch, A., & Küsel, H. (2003) 'Subway-Climatology–New research Field for the Management of possible Catastrophes in subway systems', *Man and Climate in the 20th Century, Studia Geograficzne*, 75, 384-394.

Pflitsch, A., (2003) 'Climatic Measurements in Barometric Cave Systems in South Dakota USA', *1st Int. Workshop on Cave Climatology*, Wroclaw.

Pflitsch, A., Arnold, U., & Combs, P. (2000) 'An initial study of linkages between subterranean and street-level climate in New York City', *Paper presented at the Biometeorology and Urban Climatology at the Turn of the Millennium: Selected Papers from the Conference ICB-ICUC*.

Pflitsch, A., Brüene, M., & Küsel, H. (2002) 'Spatial Variability and Dynamic Changes in Air Temperature Distribution within Different Subway Station', *15th Conf. on Biometeorology/Aerobiology and 16th International Congress of Biometeorology*.

Pflitsch, A., Bruene, M., Steiling, B., Killing-Heinze, M., Agnew, B., Irving, M., & Lockhart, J. (2012) 'Air flow measurements in the underground section of a UK light rail system', *Applied Thermal Engineering*, 32, 22-30.

Pflitsch, A., Brüne, M., Killing-Heinze, M., Ringeis, J., Agnew, B., & Steiling, B. (2013) 'Natural Ventilation as a Factor Controlling the Dispersal of Airborne Toxins in Subway Systems in a Disaster Situation', *Journal of Transportation Safety & Security*, 5(1), 78-92.

Pflitsch, A., Brüne, M., Ringeis, J., & Killing-Heinze, M. (2010) 'OrGaMIR"– Development of a safety system for reaction to an event with emission of hazardous airborne substances-like a terrorist attack or fire-based on subway climatology', *In 4th International Symposium on Tunnel Safety and Security*, Frankfurt (pp. 451-462).

Pflitsch, A., Wiles, M., Horrocks, R., Piasecki, J., & Ringeis, J. (2010) 'Dynamic climatologic processes of barometric cave systems using the example of Jewel Cave and Wind Cave in South Dakota', USA. Acta carsologica, 39(3).

Policastro, A., & Coke, L. (1998) 'Protecting US subway systems from chemical/biological terrorism', *Transit Policing*, 8(1), 5-20.

Potje-Kamloth, K. (2014) *Finding the ideal escape and emergency route.* [online] Available at: http://www.imm.fraunhofer.de/content/dam/imm/de/documents/pdfs/PD_MAusKat_final.pdf [Accessed 9 Mar. 2014].

Proulx, G. (1991) 'Passengers' behaviour during an underground evacuation',*EDRA-22*, 11-15.

Rasmus, W., & Brock, E. (1944) 'Train piston action ventilation and atmospheric conditions in Chicago subways', *Heating, Piping and Air Conditioning*, 16(8), 495-504.

Ren, A., Chen, C., & Luo, Y. (2008) 'Simulation of emergency evacuation in virtual reality', *Tsinghua Science & Technology*, 13(5), 674-680.

Ren, A., Chen, C., Shi, J., & Zou, L. (2006) 'Application of Virtual Reality Technology to Evacuation Simulation In Fire Disaster', *In CGVR* (pp. 15-21).

Reynolds, A. (1986) 'The scaling of flows of energy and mass through stairwells', *Building and Environment*, 21(3), 149-153.

Ribot, B., Chasse, P. and Gay, B., (1999) Numerical simulations of smoke extraction by roof vents in a tunnel: comparison with experimental tests analysis of

physical phenomena', *In Proceedings of the first international conference on tunnel fires and one day seminar on escape from tunnels*, Lyon, France (pp. 169-79).

Rose, W., Murphy, R., & Abrahms, M. (2007) 'Does terrorism ever work? The 2004 Madrid train bombings'. *International Security,* 32(1), 185-192.

Rudolf, A. (1997) 'Simulation of compressible flow phenomena in the Swissmetro tunnel network', *BHR GROUP CONFERENCE SERIES PUBLICATION*.

Shaw, C. Y. (1984) 'The effect of tracer gas on the accuracy of air-change measurements in buildings', *ASHRAE transactions*, 90, 212-25.

Shi, C., Zhong, M., Nong, X., He, L., Shi, J., & Feng, G. (2012) 'Modelling and safety strategy of passenger evacuation in a metro station in China', *Safety Science*, 50(5), 1319-1332.

Sidell, F. R. (1996). Chemical agent terrorism. Annals of emergency medicine, 28(2), 223-224.

Simcox, S., Wilkes, N., & Jones, I. (1992) 'Computer simulation of the flows of hot gases from the fire at King's Cross underground station', *Fire Safety Journal*, 18(1), 49-73.

Sime J.D., (1994) Escape behaviour in fires design against fire: an introduction to fire safety engineering design, London: Chapman & Hall.

Soulhac, L., & Salizzoni, P. (2010) 'Dispersion in a street canyon for a wind direction parallel to the street axis', *Journal of Wind Engineering and Industrial Aerodynamics*, 98(12), 903-910.

Spiegel, J., Brüne, M., Dering, N., Pflitsch, A., Qian, Z., Agnew, B., Palacin, R. and Irving, M., (2014) 'Propagation of tracer gas in a subway station controlled by natural ventilation'. *Journal of Heat Island Institute International* Vol, 9, p.2.

Spiegel, J., Letzel, M., Flassak, T., & Pflitsch, A. (2014) 'Dispersion of Airborne Toxins in a highly complex Subway Station', *In Proceedings of the 6th International Symposium on Tunnel Safety and Security* (Vol. 1214).

Spiers, E. M. (2010) A history of chemical and biological weapons. Reaktion Books.

Stathopoulos, T. (2004) *The Effect of Stack Height, Stack Location and Rooftop Structures on Air Intake Contamination, a Laboratory and Full-scale Study*. IRSST.

Systèmes, D. (2002-2014) *Dassault Systemes*. Retrieved 19 June 2013, 2013, from http://www.3ds.com/products-services/catia

Tahry, S. E., & Gosman, A. (1981) 'The two-and three-dimensional dispersal of a passive scalar in a turbulent boundary layer', *International journal of heat and mass transfer*, 24(1), 35-46.

Transport for London (2012) *London Underground Station planning standards and guidelines 2012 edition.* [Online]. Available at: http://www.persona.uk.com/nle/B-Core_docs/G/NLE-G1.pdf (Accessed:3 Sep 2015).

Transport for London, (2015). *London Underground Station Design Idiom*. London Underground.

THE EUROPEAN RAIL RESEARCH ADVISORY COUNCIL (ERRAC) (2009). *Metro, light rail and tram systems in Europe*.

Tao, L., (2005) *Influence of Piston Wind on the Subway Environment,* Tianjin University, Tianjin, China.

Teodosiu, C., Ilie, V., Dumitru, R., & Teodosiu, R., (2016) 'Numerical Evaluation of Ventilation Efficiency in Underground Metro Rail Transport Systems', *Energy Procedia*, 85, 539-549.

Thompson, P. A., & Marchant, E. W. (1995) 'A computer model for the evacuation of large building populations', *Fire safety journal*, 24(2), 131-148.

Ting, Y. S., Eckford, D. C., Dinsdale-Young, O. R., Liang, H., & Bowman, I. N. (2012) 'Crossrail Fire Safety Designs'. *6th International Conference Tunnel Safety and Ventilation*, Graz.

Turk, A., Edmonds, S. M., Mark, H. L., & Collins, G. F. (1968) 'Sulfur hexafluoride as a gas-air tracer', *Environmental Science & Technology*, 2(1), 44-48.

van Hooff, T., & Blocken, B. (2012) ‘Full-scale measurements of indoor environmental conditions and natural ventilation in a large semi-enclosed stadium: possibilities and limitations for CFD validation’. Journal of Wind Engineering and Industrial Aerodynamics, 104, 330-341.

Vrmesh.com. (2013) *VRMesh - 3D point cloud and mesh processing software*. [online] Available at: http://www.vrmesh.com/ [Accessed 8 Sep. 2013].

Wang, L. H., Shi, K., Song, J., and Zheng, Y. (2010) ‘Velocity fields characteristics research on the piston air shaft and the bypass duct in subway’, *Fluid Machinery*, 3, 006.

Wen, J. X., Kang, K., Donchev, T., & Karwatzki, J. (2007) ‘Validation of FDS for the prediction of medium-scale pool fires’, *Fire Safety Journal*, 42(2), 127-138.

Wilby, R. (2005) *Urban heat island and air quality of London*, UK.

Wildeanalysis. (2012) *Wind Flow Analysis through City Block for WSP to Assess Pedestrian Comfort within Built Environment*. [online] Available at: http://wildeanalysis.co.uk/casestudies/cfd-wind-flow-pedestrian-comfort-built-environment [Accessed 12 Mar. 2014].

Woodburn, P., & Britter, R. (1996a) ‘CFD simulations of a tunnel fire—Part I’, *Fire Safety Journal*, 26(1), 35-62.

Woodburn, P., & Britter, R. (1996b) ‘CFD simulations of a tunnel fire—Part II’, *Fire Safety Journal*, 26(1), 63-90.

Woolley, W. D., & Raftery, M. M. (1975) ‘Smoke and toxicity hazards of plastics in fires’. Journal of Hazardous Materials, 1(3), 215-222.

World Health Organization, (1997) Phosgene: Health and Safety Guide, *The International Programme on Chemical Safety (IPCS)*. World Health Organization, Geneva, 70 pp.

Xiaojun, C. (2008) ‘Simulation of temperature and smoke distribution of a tunnel fire based on modifications of multi-layer zone model’, *Tunnelling and Underground Space Technology*, 23(1), 75-79.

Yakhot, V. S. A. S. T. B. C. G., Orszag, S. A., Thangam, S., Gatski, T. B., & Speziale, C. G. (1992) 'Development of turbulence models for shear flows by a double expansion technique. Physics of Fluids A', *Fluid Dynamics* (1989-1993), 4(7), 1510-1520.

Yakhot, V., Orszag, S.A., Thangam, S., Gatski, T.B. & Speziale, C.G. (1992) 'Development of turbulence models for shear flows by a double expansion technique', *Physics of Fluids A*, Vol. 4, No. 7, pp1510-1520.

Yuan, D.-P., Jin, X.-S., Zhang, X.-L., Wang, C.-J., Jiang, L.-R., Wang, X.-B., & Shen, J. Y. (2012) 'Design and implementation of immersive environment for firefighting tactical training', *Xiaofang Kexue yu Jishu,* 31(2), 162-165.

Yuan, F.D. and You, S.J., (2007) 'CFD simulation and optimization of the ventilation for subway side-platform', *Tunnelling and Underground Space Technology*, 22(4), pp.474-482

Zhou, R., & Zhang, W. (2012) 'Analysis and optimization of ventilation mode of smoke control system in subway station fires', *Journal of Theoretical & Applied Information Technology*,44(2).

Zhou, Y. D., (2006) 'Little knowledge about development of urban rail transit', *Railway Operation Technology*, no. 4, pp. 19–21.